Advances in Quantum Chemistry

Volume 49

ADVANCES IN

QUANTUM CHEMISTRY

VOLUME 49

ADVANCES IN
QUANTUM CHEMISTRY

EDITORS

JOHN R. SABIN
QUANTUM THEORY PROJECT
UNIVERSITY OF FLORIDA
GAINESVILLE, FLORIDA

ERKKI BRÄNDAS
DEPARTMENT OF QUANTUM CHEMISTRY
UPPSALA UNIVERSITY
UPPSALA, SWEDEN

FOUNDING EDITOR

PER-OLOV LÖWDIN
1916–2000

VOLUME 49

AMSTERDAM • BOSTON • HEIDELBERG • LONDON • NEW YORK • OXFORD
PARIS • SAN DIEGO • SAN FRANCISCO • SINGAPORE • SYDNEY • TOKYO

Academic Press is an imprint of Elsevier

Academic Press is an imprint of Elsevier
84 Theobald's Road, London WC1X 8RR, UK
Radarweg 29, PO Box 211, 1000 AE, Amsterdam, The Netherlands
30 Corporate Drive, Suite 400, Burlington, MA 01803, USA
525 B Street, Suite 1900, San Diego, California 92101-4495, USA

This book is printed on acid-free paper ♾

ISBN-13: 978-0-12-034849-7
ISBN-10: 0-12-034849-7
ISSN: 0065-3276

For information on all Academic Press publications visit our web site at http://books.elsevier.com

Printed and bound in USA

05 06 07 08 09 10 10 9 8 7 6 5 4 3 2 1

Contents

This page intentionally left blank

Contributors

Alán Aspuru-Guzik, Kenneth S. Pitzer Center for Theoretical Chemistry, Department of Chemistry, University of California, Berkeley, CA 94720-1460, USA, alan@aspuru.com

James Avery, Departments of Computer Science and Chemistry, University of Copenhagen, Denmark

John Avery, Departments of Computer Science and Chemistry, University of Copenhagen, Denmark

Salvatore Capozziello, Dipartimento di Scienze Fisiche and INFN (sez. di Napoli), Università di Napoli "Federico II", Complesso Universitario di Monte S. Angelo, Via Cinthia, I-80126, Napoli, Italy, capozziello@sa.infn.it

Ramon Carbó-Dorca, Department of Inorganic and Physical Chemistry, Ghent University, Krijgslaan 281, B-9000 Gent, Belgium and Institut de Química Computacional, Universitat de Girona, Girona 17071, Catalonia, Spain

Erik Deumens, Quantum Theory Project, Gainesville, FL 32611-8435, USA

Alessandra Lattanzi, Dipartimento di Chimica, Università di Salerno, Via S. Allende, I-84081 Baronissi, Salerno, Italy, lattanzi@unisa.it

William A. Lester, Jr., Chemical Sciences Division, Lawrence Berkeley National Laboratory, Berkeley, CA 94720, USA, walester@lbl.gov

David Masiello, Quantum Theory Project, Gainesville, FL 32611-8435, USA

Marcel Nooijen, Department of Chemistry, University of Waterloo, Waterloo, Ontario, Canada, N2L 3G1

Jens Oddershede, Kemisk Institut, Syddansk Universitet, Odense, Denmark

Yngve Öhrn, Quantum Theory Project, Gainesville, FL 32611-8435, USA

John R. Sabin, Departments of Physics and Chemistry, University of Florida, Gainesville, FL, USA

Mark Wladyslawski, Department of Chemistry, Princeton University, Princeton, NJ 08544, USA

This page intentionally left blank

Preface

Serials such as *Advances in Quantum Chemistry* have traditionally been a forum for articles that can be slightly longer, more review like, or more speculative than those found in journals. This gives us an advantage in attracting in depth studies that are, perhaps, less suitable for space limited journals. In this issue we continue this tradition with seven articles on a variety of topics.

The first article in the volume, by Wladyslawski and Nooijen, is an extended and in depth discussion of the calculation of analytical first derivatives of the energy in a similarity transformed equation-of-motion couples-cluster method, and explicit, algebraic formulae are given for the analytic first derivatives of excitation energies, double ionization potentials, and double electron affinities. They utilize the automated symbolic algebra package to accomplish this, and give some emphasis to that implementation.

The father and son team of John and James Avery, frequent contributors to Advances over the past few years, author the second article in this volume, which deals with calculation of energies of energies of doubly excited, autoionizing states of atoms. This is done using generalized Sturmians. Several general properties and approximations with more wide ranging applicability are discussed.

The third contribution, by Carbó-Dorca, treats the formal structure and mathematical properties of electronic density functions (eDF's). In this paper it is demonstrated that they connect to a rich source of problems leading up to an imaginative set of algorithms and techniques. The discussion reports on recent developments from the author's laboratory. Even though this paper might appear highly abstract and mathematical, some surprising links and unforeseen relationships are revealed.

Capozziello and Lattanzi address the problem of molecular chirality from an algebraic point of view in the fourth article in this volume. Starting from a tetrahedral model, they derive a chirality index from a general O(4) algebra, then predict chirality of tetrahedral chains using a molecular aufbau principle.

Molecular Quantum Monte Carlo calculations are the subject of the fifth contribution to this volume. Aspuru-Guzik and Lester compare the computational resources necessary for molecular calculations carried out using Quantum Monte Carlo methods with more conventional methods, and rehearse the advantages of Quantum Monte Carlo in terms of resources and accuracy of the results.

Masiello and colleagues present methods for dealing with the coupled non-linear Maxwell–Schrödinger partial differential equations in our sixth contribution. A solution to the Maxwell–Schrödinger equations is presented, and the dynamics of a single spinless hydrogen atom interacting with the electromagnetic field in a cavity is discussed.

In the final contribution to this volume, Sabin and Oddershede discuss the state of the art of computation and experiment for the problem of energy deposition by swift ions in

materials. They suggest several places where the physics has not yet been fully explored and where further work could produce interesting results.

This volume thus addresses a diverse set of topics which will, we hope, make it of interest to a large audience. Have a good read!

Erkki Brändas and John R. Sabin
Editors

Analytical Energy Gradients for Excited-State Coupled-Cluster Methods: Automated Algebraic Derivation of First Derivatives for Equation-of-Motion Coupled-Cluster and Similarity Transformed Equation-of-Motion Coupled-Cluster Theories

Mark Wladyslawski[1] and Marcel Nooijen[2]

[1]*Department of Chemistry, Princeton University, Princeton, NJ 08544, USA*
[2]*Department of Chemistry, University of Waterloo, Waterloo, Ontario, Canada, N2L 3G1*

Abstract

The equation-of-motion coupled-cluster (EOM-CC) and similarity transformed equation-of-motion coupled-cluster (STEOM-CC) methods have been firmly established as accurate and routinely applicable extensions of single-reference coupled-cluster theory to describe electronically excited states. An overview of these methods is provided, with emphasis on the many-body similarity transform concept that is the key to a rationalization of their accuracy. The main topic of the paper is the derivation of analytical energy gradients for such non-variational electronic structure approaches, with an ultimate focus on obtaining their detailed algebraic working equations. A general theoretical framework using Lagrange's method of undetermined multipliers is presented, and the method is applied to formulate the EOM-CC and STEOM-CC gradients in abstract operator terms, following the previous work in [P.G. Szalay, *Int. J. Quantum Chem.* **55** (1995) 151] and [S.R. Gwaltney, R.J. Bartlett, M. Nooijen, *J. Chem. Phys.* **111** (1999) 58]. Moreover, the systematics of the Lagrange multiplier approach is suitable for automation by computer, enabling the derivation of the detailed derivative equations through a standardized and direct procedure. To this end, we have developed the *SMART* (Symbolic Manipulation and Regrouping of Tensors) package of automated symbolic algebra routines, written in the *Mathematica* programming language. The *SMART* toolkit provides the means to expand, differentiate, and simplify equations by manipulation of the detailed algebraic tensor expressions directly. The Lagrangian multiplier formulation establishes a uniform strategy to perform the automated derivation in a standardized manner: A Lagrange multiplier functional is constructed from the explicit algebraic equations that define the energy in the electronic method; the energy functional is then made fully variational with respect to all of its parameters, and the symbolic differentiations directly yield the explicit equations for the wavefunction amplitudes, the Lagrange multipliers, and the analytical gradient via the perturbation-independent generalized Hellmann–Feynman effective density matrix. This systematic automated derivation procedure is applied to obtain the detailed gradient equations for the excitation energy (EE-), double ionization potential (DIP-), and double electron affinity (DEA-) similarity transformed equation-of-motion coupled-cluster singles-and-doubles (STEOM-CCSD) methods. In addition, the derivatives of the closed-shell-reference excitation energy (EE-), ionization potential (IP-), and electron affinity (EA-) equation-of-motion coupled-cluster singles-and-doubles (EOM-CCSD) methods are derived. Furthermore, the perturbative EOM-PT and STEOM-PT gradients are obtained. The algebraic derivative expressions for these dozen methods are all derived here uniformly through the automated Lagrange multiplier process and are expressed compactly in a chain-rule/intermediate-density formulation, which facilitates a unified modular implementation of analytic energy gradients for CCSD/PT-based electronic methods. The working equations for these analytical gradients are presented in full detail, and their factorization and implementation into an efficient computer code are discussed.

ADVANCES IN QUANTUM CHEMISTRY, VOLUME 49
ISSN: 0065-3276 DOI: 10.1016/S0065-3276(05)49001-2

Contents

1. INTRODUCTION

Similarity transformed equation-of-motion coupled-cluster (STEOM-CC) theory [1–20] has recently emerged as a powerful and accurate method for calculating a large number of singly excited electronic states simultaneously at moderate cost. The STEOM-CC method has its roots in the early "transform-then-diagonalize" formulation of Fock-space coupled-cluster (FSCC) theory by Stolarczyk and Monkhorst [21–24]. Reference [25] resolved some long-standing difficulties (with the inverse of the normal-ordered exponential operator) and elucidated the fundamental relationship between the conventional Bloch-equation wave-operator formulation [26–29] of FSCC and the alternative similarity transformation approach. The STEOM-CC method brings to fruition the similarity transformation methodology and yields an elegant and independent formulation that is equivalent to conventional FSCC for the lowest sectors (singly ionized or attached) and is somewhat different for the higher sectors [3]. Formulated in terms of independent eigenvalue calculations rather than the numerically less stable solution of coupled non-linear equations, the STEOM method avoids the intruder state problem [30,31] that earlier plagued FSCC, and the conceptual

simplicity of the theory rationalizes difficult aspects of Bloch-equation-based FSCC theory.

The STEOM-CC method builds on equation-of-motion coupled-cluster (EOM-CC) theory [32–42]. The EOM-CC method presents a unified approach to extend single-reference ground-state coupled-cluster (CC) theory (*e.g.* references [43–46]) to excited, ionized, and electron-attached states. An alternative derivation of EOM-CC theory is provided by coupled-cluster linear response theory (CCLRT) [47–50], and the methods are fully equivalent for excitation energies. Likewise, the coupled-cluster Green's function method [51–53] starts from a Green's function *ansatz* but eventually reaches the same equations using diagrammatic re-summation techniques. The symmetry-adapted-cluster configuration-interaction (SAC-CI) approach [54–57] by Hirao and Nakatsuji is also closely related, although some additional approximations are invoked compared to EOM-CC and CCLRT. More approximate methods related to EOM-CC include QCISD linear response [58,59] and CIS(D) [60–62]. The STEOM-CC method rivals EOM-CC in accuracy and improves upon EOM-CC in efficiency and generality in the types and number of states that can be treated.

The philosophy underlying the EOM and STEOM methods is rather different than many conventional electronic structure approaches, which focus on optimizing the wavefunction. In the EOM and STEOM methods, instead, a sequence of many-body similarity transformations [25] is performed on the Hamiltonian itself, with the purpose of simplifying the transformed eigenvalue problem. In this work, we take a simple and (we think) intuitive viewpoint to understand the effects of these similarity transformations, namely in terms of the modification of the second-quantized Hamiltonian elementary operator amplitudes and the resulting change in the block structure of the Hamiltonian matrix elements (over singly, doubly, triply, and quadruply excited determinants). This perspective in terms of second-quantized many-body elementary operators is perhaps somewhat different and less well known than more familiar approaches to EOM-CC theory, which can be phrased completely in terms of the projected CC equations and the associated parameterization of the wavefunction.

In the EOM and STEOM methods, the electronic states are obtained by standard truncated configuration-interaction-like diagonalization, but of a correlated effective Hamiltonian created through a many-body similarity transformation. By means of these similarity transformations, elementary operators in the transformed Hamiltonian are eliminated that couple determinants *out of the truncated diagonalization subspace*, that is, operators that connect the *included* lower-excitation-level determinants to the higher-excitation-level determinants, which are *excluded*. The effects of these eliminated elementary operators are implicitly incorporated into the lower-level transformed Hamiltonian amplitudes/matrix-elements, thereby providing increased accuracy with smaller diagonalization subspaces.

The EOM-CCSD method diagonalizes the similarity transformed Hamiltonian $\hat{\bar{H}}$ generated from a coupled-cluster singles-and-doubles (CCSD) reference treatment [43,44], where the one- and two-body pure-excitation operators ($1h1p$ and $2h2p$) are eliminated. The two-body pure-excitation operator is the primary elementary operator that would couple singly excited determinants to triply excited determinants (*i.e.* the leading elementary operator that would participate in the $\langle \mathbf{\Phi}^{\mathbf{bcd}}_{\mathbf{jkl}} | \hat{\bar{H}} | \mathbf{\Phi}^{\mathbf{a}}_{\mathbf{i}} \rangle$ singles-to-triples matrix elements). This same two-body pure-excitation operator also represents a significant portion of the coupling from doubly to quadruply excited determinants. By eliminating these operator

components, the similarity transformation implicitly incorporates the associated higher-excitation contributions into the singles- and doubles-level transformed Hamiltonian matrix elements. The EOM-CCSD method thus gives greatly improved results compared to the corresponding configuration-interaction (CI) diagonalization of the *bare* Hamiltonian in the same singles-and-doubles basis [33–35,50,63,64].

Furthermore, EOM-CCSD excitation energies are additively separable [50,65,66] for a localized single excitation, an important feature absent in truncated-CI approaches (with the exception of CI singles). This additive separability means that the excitation energy obtained for an isolated system separated from non-interacting ground-state systems is identical whether the calculation is performed on the components separately or performed on the combined supersystem. The lack of this property artifactually degrades the accuracy of excitation energies with increasing molecular size, even if the added units are well removed from the excitation region. Additionally, Stanton [67] analyzed the superiority of EOM-CC (and by analogy STEOM-CC) over traditional CC and other methods for treating strongly interacting potential energy surfaces, such as in pseudo-Jahn–Teller interactions and conical intersections.

The accuracy and ease of use of the EOM-CCSD method has facilitated its widespread utilization in a variety of interesting systems. The excitation energy (EE-) EOM-CCSD variant [34] has recently been applied, for example, to exciton formation rates in conjugated polymer LEDs [68], to NMR spin–spin coupling constants as a function of dihedral angle in model peptides [69], and to a novel treatment of bond breaking in terms of spin-flipping EE-EOM excitations [70,71]. The ionization potential (IP-) EOM-CCSD variant [39,52] has recently been applied to resolve some discrepancies in the vertical ionization potentials of the prototypical molecule ethylene [72] and to examine the geometry and vibrational frequencies of the ground state of the vinyl radical by deletion of an electron from the closed-shell anion reference [73]. The electron affinity (EA-) EOM-CCSD variant [36] has been applied, for example, to core-excitation spectra [74] by adding an extra electron to the core-ionized state and to the excitation spectrum of Al_3 in terms of single electron attachment to the closed-shell Al_3^+ reference determinant [75].

In STEOM-CCSD theory, a *second* similarity transformation is employed to eliminate the chief remaining net-excitation operators ($3h1p$ and $3p1h$) and thereby allow further reduction in the size of the approximate diagonalization subspace, while at the same time maintaining or even improving accuracy. For "singly excited" physical states, the STEOM-CCSD transformed Hamiltonian is diagonalized accurately and efficiently in a subspace of *singly* promoted determinants only, rather than triples as would be appropriate for CI or doubles for EOM-CC. The excitation operators in the transformed Hamiltonian coupling the singly excited determinants to more highly excited configurations have mostly been eliminated and their effects incorporated implicitly into the singles-level matrix elements. In fact, the STEOM-CCSD method can be considered a rigorous correlated equivalent [1] of the CI-singles (CIS) method, but using a fully correlated and connected effective Hamiltonian. Conceptually, the method offers immediate interpretation of excited states in terms of single excitations in a correlated molecular-orbital picture. Practically, the cost of the final CIS-like diagonalization is trivial compared to the rest of the calculation, and a large number of eigenstates can thus be computed simultaneously, and in a balanced manner, for little additional cost. In one of its earliest applications, for example, the STEOM-CCSD method was used to compute a staggering $\sim$200 excited states of free base porphin us-

ing a large ANO basis set extended in two different ways with diffuse and polarization functions [5].

Although the diagonalization subspace includes only singly excited determinants, through the similarity transformations, the STEOM-CCSD method incorporates a selection of connected doubly and triply excited configurations implicitly. (Moreover, if these higher configurations are very prominent, as in "doubly excited" systems, the diagonalization subspace can be expanded to include doubly promoted determinants *explicitly*—and *implicitly* more triples and even quadruples—as is done in the extended-STEOM-CCSD approach [12,13].) Connected triples contributions are absent from standard EOM-CCSD, and such corrections can be particularly important in valence excited states [76–79]. Note that standard EOM-CCSD theory can be augmented to incorporate connected triples contributions in various ways, such as through a dressing of the states [65], or by extending the method to include triples corrections approximately, such as in the EOM-CCSDT-3 or EOM-CCSD($\tilde{\mathrm{T}}$) methods [80] (or the closely related linear response CC3 method [78]), or even by including triply promoted determinants completely, in the full EOM-CCSDT method [81–83]. These expanded EOM approaches, however, are quite expensive.

Also related to triples, STEOM-CCSD, unlike standard EOM-CCSD, satisfies the complete definition of additive separability for single excitations [3,65,66]. In addition to the separability of a *local* excitation on a single subsystem, STEOM-CCSD also possesses charge-transfer separability, meaning that the energy of a charge-transfer excitation *between* two otherwise non-interacting closed-shell subsystems is equal to the ionization potential of one plus the electron affinity of the other. The STEOM-CCSD theory is fully linked in a diagrammatic sense and is rigorously size-extensive [3,65,66]. These separability properties are not needed simply for the treatment of such separated systems, but rather their inclusion ensures proper behavior for all systems and increases the accuracy of the method. A careful overview of such scaling properties and the extension to a concept of generalized-extensivity is presented in the recent *festschrift* celebrating the work of Rodney J. Bartlett on the occasion of his 60th birthday [66].

The STEOM method incorporates both dynamic and non-dynamic correlation effects and can be applied to certain systems that have traditionally required a multi-reference description [3,4,14–17], such as many difficult classes of transition states and biradicals. In addition to singlet and triplet excited states of a single-determinant closed-shell reference system by the excitation energy (EE-) STEOM variant [1,3], states related to a closed-shell parent by the removal or addition of two electrons can be considered by the double ionization potential (DIP-) STEOM or the double electron affinity (DEA-) STEOM variants [3], respectively. (The STEOM-CCSD treatment of states with one less or one more electron than the closed-shell reference has been shown to be equivalent to the corresponding IP- or EA-EOM-CCSD treatment [3].) For example, the DIP-STEOM-CCSD method has been straightforwardly applied to such difficult cases as the vibrational frequencies of ozone [3] and the symmetry-breaking states in the NO_3^+ cation [15], while DEA-STEOM-CCSD has recently been applied to the weakly interacting and highly multi-configurational ground and low-lying excited states of the dimer $(NO)_2$ [17]. For such systems, the STEOM method is appealing for accurate blackbox-type calculations by non-specialists because it is single reference (in the sense that it is based on one reference determinant), treats the open-shell configurations on a balanced footing, is automatically spin-adapted, and involves relatively few choices on the part of the user, unlike other highly accurate, but user-input intensive, multi-reference based methods.

Because of the efficiency with which a large number of eigenstates can be computed, the STEOM-CCSD method also offers several advantages for tracking electronic states. In vibrational frequency calculations, the small geometrical distortions typically cause the state of interest as well as other nearby states to fall into lower symmetry groups. Calculating the manifold of nearby states of a variety of symmetries allows the state of interest to be picked out based on a nearest-in-energy, rather than symmetry, criterion. Furthermore, due to the general proximity of excited states, it is common to encounter state crossings during the geometry optimization of an excited state. Rather than specifying an excited state by its symmetry and (ill-defined) energy ordering, the desired diabatic state of a particular orbital character can instead be followed through a crossing by computing its approximate overlap with the set of *all* nearby states (of appropriate symmetry) at the next step in the optimization. We have implemented this electronic state-tracking algorithm into our local version of the ACES II suite [84] of electronic structure programs, and the procedure was applied in examining the conical intersection regions in the NO_3^+ excited-state manifold by the DIP-STEOM-CCSD method [15].

Lastly, the computational cost of the STEOM-CCSD methods can be reduced substantially by replacing one of the most intensive steps, the calculation of the reference CCSD amplitudes, by the first-order perturbative treatment (*e.g.* reference [45]), yielding the STEOM-PT methods [3]. The perturbative reference amplitudes also lead to simplifications in the analytical derivative expressions, and thus the STEOM-PT method can be useful as a cheaper "pre-optimization" tool, which can subsequently be improved upon by a more-accurate STEOM-CCSD gradient calculation if so desired.

The utilization of analytical formulations for the energy gradient began some decades ago with the pioneering work of Pulay on self-consistent-field (SCF) gradients [85]. While it is conceivable that the energy landscape can be explored through numerical differentiation, it is quite inefficient and only feasible for small systems. For a variety of fundamental as well as technical reasons, single-point energy calculations of excited states have lagged behind ground-state treatments, and even more so for excited-state analytical gradients. Yet excited-state gradients play a critical role in explaining the adiabatic and dynamic features of experimental spectra and in understanding photochemical processes.

The most familiar use of gradients is the determination of stationary points on electronic potential energy surfaces. The location (nuclear configuration and energy) of minima and transition states is essential for examining structures, adiabatic 0–0 transitions, intermediates, and barriers and provides insight into stability and reaction pathways. Less familiar features of potential energy surfaces that nonetheless play critical roles in excited-state and photochemical processes are avoided crossings and conical intersections. Since the noncrossing rule only applies to diatomics, the closely-spaced excited states of polyatomics can become degenerate along selected hypersurfaces in nuclear coordinate space, and the orbital character of the states can change rapidly in regions of genuine and avoided crossings. To study these ubiquitous features, it is important that the electronic structure method provide a number of excited states straightforwardly, efficiently, accurately, and in a balanced manner. The ability to calculate a manifold of economical but accurate excited states is valuable in the development of intelligent search procedures on the excited-state surfaces, in order to avoid missing the features of interest. With the ability to monitor the system during the course of an optimization, such as with the state-tracking algorithm described above, the STEOM method is well-suited to these tasks.

In addition to simply (!) locating the interesting features on potential energy surfaces, gradients also play a vital role in the description of the dynamics on the surface(s) and their spectroscopic consequences. The most familiar example is their use in basic vibrational frequency calculations through the second derivative (typically calculated as numerical derivatives of the analytical gradient). The gradient is essential in treating the dynamics of photochemical processes, where the reactants start and evolve on the excited-state manifold. In a recent review, Robb *et al.* [86] considered some practical computational strategies to investigate photochemical processes, and the importance of surface features such as conical intersections and gradients is clear. The use of gradients is evident in the "direct dynamics" methods (*e.g.* reference [87]), where dynamical quantities are calculated without explicit construction of the surfaces but rather on-the-fly from the electronic structure computations directly. The dynamics are often non-Born–Oppenheimer and require calculations on multiple surfaces simultaneously, such as the "multiple spawning" method of Martinez *et al.* [88,89]. The strength of the non-adiabatic coupling between surfaces can be computed from matrix elements of the differentiated Hamiltonian between the interacting adiabatic states, a concept closely related to the analytical gradient. In our own recent work, the STEOM and EOM methods are being employed to tackle complicated electronic absorption spectra in conjunction with either sophisticated Franck–Condon approaches [20] or a non-adiabatic vibronic coupling methodology [18,19].

In an even more general application, appropriate derivatives of the energy can be used to calculate first-order properties through the generalized Hellmann–Feynman (GHF) theorem [90–92]. In contrast to the standard Hellmann–Feynman theorem [93–95] for exact and fully variational formulations, for *non-variational* electronic structure methods the energy gradient and the expectation value of the Hamiltonian response are *not* identical; the gradient additionally contains "relaxation" terms accounting for the response of the non-variational wavefunction parameters. The gradient therefore typically represents first-order properties more accurately [96]. In particular for CC-based methods, the gradient approach to property calculations is generally preferred because an expectation value approach [97–99] does not have a simple natural truncation.

In their raw form, however, the derivatives contained in the gradient of the non-variational wavefunction parameters would be rate limiting in a calculation, since they must be recomputed separately for each perturbation and degree of freedom. These expensive terms can be avoided, however, if a GHF relation can be constructed: For non-variational wavefunctions, the GHF theorem is said to apply if the gradient can be written as the trace of the Hamiltonian derivatives with an effective (relaxed) density matrix [41,100–104]. This elegant form of the gradient completely separates the perturbation dependence from the electronic structure approximation of the wavefunction. The perturbation dependence is isolated in the response of the Hamiltonian amplitudes only. The relaxation terms that account for the response of the non-variational wavefunction parameters are contained in the effective density matrix. The effective density matrix is *independent* of the perturbation; its expression is completely defined by the electronic structure method, and it in turn determines the method's analytical gradient.

The problem of course is how to derive the expression for the effective density matrix, namely how to restructure the raw analytical gradient expressions to avoid the perturbation-dependent non-variational parameter derivatives. A major bottleneck in the derivation of practical analytical gradient expressions for new electronic structure methods has been the difficulty and tedium of this elimination. Traditionally, the non-variational parameter

derivatives have often been eliminated through the Dalgarno–Stewart interchange [105], also called the Z-vector method. The method was first applied to eliminate the molecular-orbital coefficient derivatives in CI gradients by Handy and Schaefer [106]. This technique was also used, for example, in the original derivation of the EOM-CCSD/PT analytical gradients [37–42], the gradient for SAC-CI theory [56,57], and the gradient for ground-state CC theory [103,104,107–110]. The procedure can be quite cumbersome, however, and the details depend greatly on the particular electronic structure method being considered.

In the present work instead, the non-variational parameter derivatives are eliminated systematically through Lagrange's method of undetermined multipliers [111–115]. In this well-defined procedure for obtaining the derivative of an expression subject to constraints, a functional is first constructed from the electronic method's energy expression together with all supplementary equations that define the non-variational energy parameters, each supplementary equation multiplied by an undetermined coefficient. These so-called Lagrange multipliers are then determined by *defining the functional* to be variational with respect to the *non-variational energy* parameters. The Lagrange multipliers provide exactly the flexibility needed to impose this remaining stationarity. The expensive perturbation-dependent parameter derivatives are thereby avoided and are replaced by this coupled set of linear equations that is independent of the perturbation and degrees of freedom. With their solution, the energy functional becomes stationary with respect to *all* its wavefunction parameters, and the simplifications associated with fully variational energy formulations then apply [113]. In particular, the variational $2n + 1$ rule [112–114] implies that the expensive non-variational parameter derivatives will be avoided and that the first derivative of the energy can be obtained through the GHF relation, in terms of a perturbation-independent effective density matrix that contains all the parameter response. Indeed, the Lagrange multiplier method incorporates the Dalgarno–Stewart interchange to all orders of derivative, eliminating the unnecessary non-variational parameter derivatives wherever possible. The Lagrange multiplier approach has been applied, for example, to write the analytical gradient expressions for CI [113,116], MP-MBPT [114], CC [117–120], EOM-CC [111], P-EOM-MBPT(2) [121], and other methods [111].

In addition to its elegance and generality, the Lagrange multiplier formulation defines a systematic derivation procedure that can be adapted to computer automation. Traditionally, equations for the analytical energy gradient are first derived by hand in abstract operator terms. Through algebraic [122,123] or diagrammatic [26,27,124–126] expansion, the abstract derivative expressions are subsequently translated into explicit algebraic working equations. This expansion is also often performed by hand. The explicit expansion procedure is relatively straightforward but can be subtle, for example, in the symmetries and permutations (numerical factors, signs, *etc.*). As the number of possible terms increases, the process quickly becomes tedious and error-prone. It would be desirable, instead, to take the (much simpler) algebraic expressions that define the electronic method and differentiate them by computer to obtain the explicit derivative expressions *directly* in algebraic terms.

This direct algebraic manipulation has been hindered by the lack of a suitable computer package capable of handling the detailed algebraic expressions, particularly in treating symmetry and the so-called "dummy" summation indices. To this end, we have created the *SMART* (Symbolic Manipulation and Regrouping of Tensors) package of automated symbolic algebra tools. Beginning with the Lagrange multiplier energy functional in algebraic terms as input, the *SMART* toolkit is used to expand, differentiate, and simplify the algebraic expressions to obtain the explicit derivative equations directly and systematically.

Although developed with the specific case of STEOM-CCSD/PT gradients for the present work, this general package can treat a variety of tensor algebraic expressions originating from second-quantized methods. The toolkit is written in the *Mathematica* programming language [127], and its features will be considered here.

To be clear, the primary function of the *SMART* package is deriving and manipulating the algebraic derivative equations, whereas their implementation into the computer code of an electronic structure program is still performed here by hand. The fledgling field of automated equation derivation and implementation has progressed rapidly since a prototype of the *SMART* package was first presented in a poster at the 1999 Sanibel Symposium. For instance, Kállay *et al.* have cleverly adapted string-based CI algorithms and diagrammatic many-body perturbation theory to automate the derivation and implementation of single-reference [128] and state-selective multi-reference [129] CC and CI equations of arbitrary truncation; the methods have even recently been extended with analytical first [130] and second [131] derivatives. An important area of research is devising efficient factorization and optimization algorithms, particularly taking into account computer resources and the requirements of the chemical system being examined. (Truly *optimal* factorization is an NP-complete problem.) In recent work in our group, the Automatic Program Generator (APG) package [132,133] was developed to construct the algebraic formulas for general many-body methods, efficiently factorize them employing a heuristic algorithm, and produce FORTRAN code for compilation into the ACES II program. The APG work has been superseded by our fruitful multi-disciplinary collaboration with the groups of Sadayappan and Baumgartner at The Ohio State University, Bernholdt and Harrison at Oak Ridge National Laboratory, Ramanujam at Louisiana State University, Hirata formerly at Pacific Northwest National Laboratory and now at the Quantum Theory Project of the University of Florida, and others in the development of the general-purpose Tensor Contraction Engine (TCE) [134–141]. The TCE work endeavors to develop a high-level language for the automated symbolic derivation of many-body electronic structure theory formulas and an optimizing compiler to implement the resulting equations in high-performance parallel computer code. A first generation TCE has been created by Hirata and applied to the automated derivation of a range of CI, MBPT, and CC energy expressions and their automated implementation in operation- and memory-efficient serial and parallel computer codes [134] (interfaced with the UTChem [142,143] and NWChem [144,145] computational chemistry suites). Development continues on this first generation TCE, with the recent automated implementation of EOM-CC excitation energies and properties, the related CC $\boldsymbol{\Lambda}$ equation solvers, and various combined CC and MBPT theories, in codes that take advantage of spin, spatial (real Abelian), and permutation symmetries simultaneously [135, 136]. Moreover, work progresses on the automated *optimization* of the implemented computer code (the so-called optimizing TCE), in order to maximize performance and parallel scalability over a broad range of computer system architectures by tailoring to the specific platform's speed, communication, and resource characteristics; for a recent overview, see reference [141]. The power of these automated derivation and implementation programs is that rapid progress can be made, once the overhead of developing the general toolkit has been paid. Modifying an electronic method to incorporate additional/different corrections, arbitrary-order derivatives, new computer architectures/algorithms, *etc*. may be a matter of simply pressing a button, allowing quantum chemists and physicists to shift focus to the theoretical approximations rather than the tedious details of equation expansion, factorization, and implementation.

Returning our focus to the *SMART* package, the symbolic differentiation can be performed here with respect to a single term or can be performed as a chain rule using the bare (**H**) or transformed ($\bar{\mathbf{H}}$) Hamiltonian amplitudes as intermediate variables. These chain rules respectively lead to a natural definition of the GHF effective density matrix (**D**) and an intermediate density matrix ($\bar{\mathbf{D}}$). Unlike the full effective density matrix **D**, which contains *all* of the electronic method's GHF gradient information, the intermediate density matrix $\bar{\mathbf{D}}$ removes the common parts associated with the underlying CC/PT reference treatment, which are shared by all CC- or PT-based methods. The intermediate density matrix contains just the post-CC/PT information that is unique to each method. Thus, after computing the appropriate $\bar{\mathbf{D}}$, the gradient calculations can otherwise proceed identically for nearly any electronic method based on, for example, a CCSD reference treatment. Moreover, these same $\bar{\mathbf{D}}$ define the gradients for the PT-based variants, as the simplifications associated with a perturbative reference treatment are isolated outside of $\bar{\mathbf{D}}$.

In the present work, the general automated *SMART* derivation toolkit is applied to derive the specific spatial-orbital equations for the EE-, DIP-, and DEA-STEOM-CCSD/PT analytical first derivatives in explicit algebraic terms. These detailed gradient expressions are derived systematically in the Lagrange multiplier formulation and directly through the straight symbolic algebraic treatment. Moreover, the gradient equations for these various methods are expressed compactly and uniformly in the chain-rule/intermediate-density formulation, allowing reuse of much computer code in implementation. Although the derivation procedure here is fully algebraic (starting from the input algebraic Lagrange multiplier energy functionals), for completeness and to thoroughly understand the process, the abstract STEOM-CCSD/PT energy theory is reviewed, as well as Lagrange multiplier theory in abstract terms. Furthermore, Lagrange multiplier theory is applied to write the STEOM-CCSD/PT analytic gradient expressions in abstract operator form, expanding on the previous abstract derivation by Gwaltney, Bartlett, and Nooijen [10].

Since (besides the method-dependent $\bar{\mathbf{D}}$) the remaining expressions needed for STEOM-CCSD/PT gradients are identical and since STEOM theory builds on the theory of EOM, it is convenient to first derive the EOM-CCSD/PT gradient expressions in the present chain-rule/intermediate-density formulation. We note that analytical EOM-CCSD/PT gradients were first derived by Stanton and Gauss [37–42] in abstract operator form through the Z-vector method and subsequently in explicit algebraic terms through diagrammatic expansion. A Lagrange multiplier formulation for the abstract gradient expressions was presented soon after by Szalay [111]. In the present work, the EE-, IP-, and EA-EOM-CCSD/PT explicit algebraic gradient expressions are obtained *directly* by automated symbolic differentiation of the input algebraic energy expressions that define these methods. These EOM gradient expressions are presented here to unify their implementation with the STEOM-CCSD/PT gradients. The differences between the original and current EOM gradient formulations are discussed.

The algebraic STEOM-CCSD/PT gradient expressions were implemented by hand into a local version of the ACES II suite, and the existing program for EOM-CCSD/PT gradients was revised to conform to the present intermediate-density formulation. The modular chain-rule construction systematizes all these methods, as well as any future additions of CCSD/PT-based methods, to otherwise use the same unified computer code for the analytical gradient, once the particular method's $\bar{\mathbf{D}}$ is calculated. The implementation was tested thoroughly against numerical gradients for a variety of test cases as well as at intermediate points in the evaluation. There is one small part of the STEOM gradient that

has not been treated in the current work, which relates to the rotation between active and inactive orbitals. In practice, inclusion of the active/inactive orbital response would lead to very minor changes in the gradient, and in most cases the omission is not expected to be numerically relevant.

In the first example of their use, the analytical gradient of the DIP-STEOM-CCSD method was applied in examining the photoelectron spectrum of the NO_3 radical [15]. The STEOM method avoids artifactual symmetry breaking of the wavefunctions by starting from the symmetry-correct closed-shell nitrate anion (NO_3^-) orbitals as the reference. By deleting two electrons in all possible ways, the approach provides a balanced treatment of the multi-configurational character of the cation (NO_3^+) states. In addition to geometry optimizations and vibrational frequency calculations of the ground and several singlet and triplet excited states of NO_3^+, regions of conical intersection in the excited-state manifold were pinpointed by minimizing the energies on the two intersecting surfaces simultaneously. Additionally, the above-described electronic state-tracking algorithm was implemented to correctly follow an individual diabatic state through regions of intersection. This first example is illustrative of many of the potential advantages of the STEOM method and its analytical gradient, namely the accurate and balanced treatment of dynamical and non-dynamical correlation effects in some difficult multi-configurational problems and the ease and efficiency with which a large number of states can be calculated and tracked. As part of a comparative study of multi-configurational methods, the analytical gradient in the DEA-STEOM-CCSD method was also recently applied to geometry optimizations and vibrational frequency calculations in the prototypically difficult $(NO)_2$ dimer system [17].

For completeness, we note that an analytic linear response theory [47] has been available for some years in the closely-related FSCC method due to Pal and co-workers [146–148], but in the basic formulation where the non-variational wavefunction response terms are included explicitly and must be re-solved for each mode of the perturbation. The approach may be sufficient for molecular electronic properties, where there are only three independent degrees of freedom, but it is less practical for nuclear gradients. Applications have been restricted primarily to dipole moment calculations in the IP [149,150], EA [151], and EE [152] sectors. Additionally, the analytic molecular-orbital relaxation response was not included, although by comparison to numerical gradients was shown at times to be substantial. A Z-vector construction was later applied [153,154] that was only partly successful; the elimination relied on certain approximations and only removed the response of the highest-order amplitudes. In the IP-sector example considered, the $(0, 1)$-amplitude derivatives were successfully eliminated, whereas the lower, ground-state, $(0, 0)$-amplitude derivatives were not. Independently and some years before the Z-vector treatment, Szalay [111] examined the structure of FSCC gradients using a Lagrange multiplier approach and in principle eliminated both the ground as well as higher-order amplitude responses in the abstract expressions. Just recently, during review of the present manuscript, Pal and coworkers published [155] a generalization of Szalay's treatment and in particular presented diagrammatic "equations" for the Lagrange multipliers of the $(0, 1)$, $(1, 0)$, and $(1, 1)$ sectors, a large step towards implementing fully simplified analytical gradient expressions for FSCC theory.

To summarize, the principal objectives of the current paper are:

1. to review carefully the EOM- and STEOM-CCSD/PT excited-state energy theories, the general theory of deriving analytical energy gradients through Lagrange's method of

undetermined multipliers, and the application of Lagrange multiplier theory to EOM- and STEOM-CCSD/PT gradients, all in abstract terms;
2. to discuss the automation of a systematic fully algebraic derivation procedure through our new *SMART* toolkit of symbolic manipulation routines;
3. to apply the *SMART* package to derive in full detail the spatial-orbital working equations for the closed-shell-reference EE-, DIP-, and DEA-STEOM-CCSD/PT, and also the EE-, IP-, and EA-EOM-CCSD/PT, analytic first derivatives in explicit algebraic terms;
4. to describe the general chain-rule/intermediate-density formulation, facilitating a uniform and compact organization of the explicit gradient equations for CCSD/PT-based electronic methods.

The material of this paper is divided roughly into two halves, the *abstract* analysis (Sections 2 and 3) and the *explicit algebraic* analysis (Sections 4 and 5). In the first half, the EOM- and STEOM-CCSD/PT energy theories are reviewed in Section 2, the general theory of the energy gradient and Lagrange multipliers is introduced in Section 3.1, and the formulation is applied in Sections 3.2 and 3.3 to obtain the EOM-CC/PT and STEOM-CCSD/PT intermediate and effective density matrices for the analytical gradient in abstract operator form. The second half of the paper, Sections 4 and 5, somewhat parallels the abstract gradient derivations of Section 3, but in explicit algebraic terms. In Section 4, an overview of the *SMART* package is presented, along with extensive examples of the automated derivation procedure. Section 5 presents and examines the individual components of the explicit EOM- and STEOM-CCSD/PT gradient equations. Much of the discussion in Section 5 explains detailed features that arise in the algebraic expressions, which might be difficult to organize manually but here are handled automatically in the direct algebraic derivation. Also described are the factorization approach and certain general efficiency aspects applicable to the implementation of the working equations. The full set of algebraic derivative expressions, contained in the tables of Section 5, were generated and checked using our *SMART* package and should thus be free of mathematical and typographical errors. Additionally, the extensive captions of the tables in Section 5 provide a synopsis of the current work. In Section 6, the main features of this work are summarized.

2. THE EOM-CCSD/PT AND STEOM-CCSD/PT ENERGY METHODS

Let us first establish the notation. In the abstract expressions of Sections 2 and 3, all indices refer to *spin* molecular orbitals; in the explicit algebraic expressions of Sections 4 and 5, all indices refer to *spatial* molecular orbitals. The molecular orbital space is partitioned into occupied (also called hole or h) and unoccupied (also called virtual, particle, or p) subspaces, based on a closed-shell reference determinant. Generic occupied orbitals are labeled i, j, k, l, k_1, k_2, k_3, and k_4, while generic virtual orbitals are labeled a, b, c, d, c_1, c_2, c_3, and c_4. Each occupation subspace is further divided into active and inactive subspaces. Occupied orbitals that are explicitly active are labeled m, n, and m_1; virtual orbitals that are explicitly active are labeled e, f, and e_1. Explicitly inactive orbitals are given primed labels, such as i' for occupied inactive and a' for virtual inactive. The labels p, q, r, s, t, and u are used when neither the occupation nor the active character is specified, and these labels run over the entire molecular orbital space. Groups of indices are denoted by the Greek characters μ, ν, and γ. In the *spin*-orbital expressions only, so as to minimize the

appearance of numerical factors and signs, indices related by antisymmetry are restricted (*e.g.* $i < j$), and the Greek group indices should likewise be interpreted as including restrictions to unique indices. Terms are written in x^{12}_{12} notation, where upper indices usually refer to creation operators and lower indices refer to annihilation operators with respect to the true vacuum; expressions obtained by differentiation, such as D_μ and $\bar{D}_\mu$, follow the opposite convention, in the sense that the upper and lower indices are exchanged relative to the differentiating term. This standard facilitates a consistent tensor notation where summed indices appear once above and once below. In case of typographical arbitrariness, all three-index terms have the paired indices in the second position. Bold capital letters refer to the set of elementary coefficients/amplitudes of the associated second-quantized operator, *e.g.* $\bar{\mathbf{H}}$ refers to the set of coefficients $\bar{h}_\mu$ of the normal-ordered elementary operators of $\hat{\bar{H}}$ in second quantization. (Note that the amplitudes of the bare Hamiltonian $\hat{H}$ are denoted as h_0, f_μ, and V_μ but are collectively referred to as h_μ and $\mathbf{H}$.) In this work, clear distinction is made between these second-quantized elementary operator amplitudes and the associated matrix elements of the total operator between determinants. Although often interchangeable, the difference will be apparent for the perturbative variants, where certain matrix elements are not precisely the same as the "associated" elementary coefficients, due to the participation of residual pure-excitation terms in the matrix elements. Lastly, symbols with an under-tilde, such as $\underset{\sim}{F}$ or $\underset{\sim}{\mathbf{R}}$, are temporary quantities needed briefly to further the discussion.

2.1. The (ST)EOM-CCSD methods

The EOM and STEOM methods, collectively referred to here as (ST)EOM, can be based on any truncated coupled-cluster (CC) [45,46] or many-body perturbation theory [45] treatment of the reference state. In this discussion, we will focus on a coupled-cluster singles-and-doubles (CCSD) treatment [43] of the reference, but the analysis can be extended to other CC truncation schemes. The reference system may instead be treated perturbatively, and the perturbative amplitudes used in the CC-based (ST)EOM expressions. In particular, we will consider the simplifications associated with using first-order Møller–Plesset [156] amplitudes in place of the full CCSD amplitudes, yielding the (ST)EOM-PT methods.

We begin with a single closed-shell Slater determinant $|\Phi_0\rangle$ as the reference determinant. Although $|\Phi_0\rangle$ is typically taken to be comprised of Hartree–Fock (HF) or canonical HF orbitals, the CC-based expressions will be derived here for the general case of non-HF orbitals; the PT-based (ST)EOM methods will instead employ only canonical HF orbitals, and the simplifications will be discussed in Section 2.2. The normal-ordered spin-orbital electronic Hamiltonian is given in second quantization (*e.g.* reference [46]) by

$$\hat{H} = h_0 + \sum_{p,q} f^p_q \{\hat{p}^\dagger \hat{q}\} + \sum_{p<q,\, r<s} V^{pq}_{rs} \{\hat{p}^\dagger \hat{r} \hat{q}^\dagger \hat{s}\}, \tag{1}$$

where the constant $h_0 = \langle \Phi_0 | \hat{H} | \Phi_0 \rangle$ is the energy of the reference determinant, the f^p_q are the amplitudes of the corresponding Fock operator, the V^{pq}_{rs} are antisymmetrized two-electron integrals, and the curly brackets { } denote normal-ordering [27] with respect to the reference determinant.

Note that the Hamiltonian of expression (1) contains two-electron pure-excitation operators $\{\hat{a}^\dagger \hat{i} \hat{b}^\dagger \hat{j}\}$. Such operators excite a given determinant to determinants *two excitation*

levels higher, and their participation implies that at least *two* additional excitation levels above the state of interest must be included in a reasonable truncated-CI description. In particular, to adequately approximate states dominated by single excitations in CI, the Hamiltonian should be diagonalized in a subspace including at least up to (a selection of) *triply* excited determinants. To better understand these statements, the block structure of the matrix obtained by mapping $\hat{H}$ over the reference determinant and singly, doubly, triply, and quadruply excited determinants is presented in Fig. 1. The $\{\hat{a}^\dagger \hat{i} \hat{b}^\dagger \hat{j}\}$ operators yield sizeable matrix elements in the singles-to-triples block $\langle \mathbf{\Phi}^{\mathbf{abc}}_{\mathbf{ijk}} | \hat{H} | \mathbf{\Phi}^{\mathbf{a}}_{\mathbf{i}} \rangle$ of the Hamiltonian, and thus a diagonalization subspace of $\hat{H}$ for singly excited states should include (the most important of) these matrix elements, *i.e.* should include triply excited determinants, as indicated by the dashed line in Fig. 1.

In (ST)EOM-CC theory, a many-body similarity transformation [25] ($\hat{X}^{-1} \hat{H} \hat{X}$) is first performed on the so-called "bare" Hamiltonian $\hat{H}$ above, with the purpose of eliminating the major elementary operators that couple between different excitation levels and thereby reducing the minimum reasonable subspace needed in the approximate diagonalization. A similarity transformation changes the matrix elements and eigenfunctions of an operator but, in the (impractical) case of a *complete* diagonalization space, leaves the eigenvalues unchanged. In a *truncated* diagonalization subspace, the transformation can be chosen to eliminate the most important (net-) excitation operators that excite *out of the diagonalization subspace*. At the same time, the effects from the higher-level matrix elements (excluded from the diagonalization) are incorporated implicitly into the lower-level matrix

$\hat{H}$	$\lvert \Phi_0 \rangle$	$\lvert \mathbf{\Phi}^{\mathbf{a}}_{\mathbf{i}} \rangle$	$\lvert \mathbf{\Phi}^{\mathbf{ab}}_{\mathbf{ij}} \rangle$	$\lvert \mathbf{\Phi}^{\mathbf{abc}}_{\mathbf{ijk}} \rangle$	$\lvert \mathbf{\Phi}^{\mathbf{abcd}}_{\mathbf{ijkl}} \rangle$
$\langle \Phi_0 \rvert$	h_0	$\mathbf{X}$	$\mathbf{X}$	$\mathbf{0}$	$\mathbf{0}$
$\langle \mathbf{\Phi}^{\mathbf{a}}_{\mathbf{i}} \rvert$	$f^a_i \{\hat{a}^\dagger \hat{i}\}$	$\mathbf{X}$	$\mathbf{X}$	$\mathbf{X}$	$\mathbf{0}$
$\langle \mathbf{\Phi}^{\mathbf{ab}}_{\mathbf{ij}} \rvert$	$V^{ab}_{ij} \{\hat{a}^\dagger \hat{i} \hat{b}^\dagger \hat{j}\}$	$f^a_i \{\hat{a}^\dagger \hat{i}\},\ V^{kb}_{ij} \{\hat{k}^\dagger \hat{i} \hat{b}^\dagger \hat{j}\},\ V^{ab}_{cj} \{\hat{a}^\dagger \hat{c} \hat{b}^\dagger \hat{j}\}$	$\mathbf{X}$	$\mathbf{X}$	$\mathbf{X}$
$\langle \mathbf{\Phi}^{\mathbf{abc}}_{\mathbf{ijk}} \rvert$	$\mathbf{0}$	$V^{ab}_{ij} \{\hat{a}^\dagger \hat{i} \hat{b}^\dagger \hat{j}\}$	$\mathbf{X}$	$\mathbf{X}$	$\mathbf{X}$
$\langle \mathbf{\Phi}^{\mathbf{abcd}}_{\mathbf{ijkl}} \rvert$	$\mathbf{0}$	$\mathbf{0}$	$\mathbf{X}$	$\mathbf{X}$	$\mathbf{X}$

Fig. 1. *Block structure of the bare Hamiltonian $\hat{H}$ matrix elements*. The matrix elements are partitioned intuitively in blocks $\langle \mathbf{\Phi}_{\boldsymbol{\nu}} | \hat{H} | \mathbf{\Phi}_{\boldsymbol{\mu}} \rangle$, where the left- and right-hand determinants are of a particular excitation level. An **X** indicates sizeable matrix elements, while **0** indicates rigorously vanishing matrix elements (since $\hat{H}$ is at most a two-body operator). Certain **X** of interest have been replaced by the actual second-quantized elementary operators that participate in the block. Diagonalization of the $\hat{H}$ matrix over up-to a particular excitation level is the truncated-CI method. In order to reasonably approximate "singly excited" electronic states, that is to say, states dominated by singly excited determinants $|\Phi^a_i\rangle$, a truncated-CI diagonalization subspace should include at least up to (a selection of) triply excited determinants. This up-to-triples diagonalization subspace is indicated by the dashed line, and its necessity is a simple consequence of the sizeable matrix elements $\langle \mathbf{\Phi}^{\mathbf{abc}}_{\mathbf{ijk}} | (V^{ab}_{ij} \{\hat{a}^\dagger \hat{i} \hat{b}^\dagger \hat{j}\}) | \mathbf{\Phi}^{\mathbf{a}}_{\mathbf{i}} \rangle$ that couple singly excited determinants to triply excited determinants. (To avoid confusion, note that all index labels in the three parts of the preceding expression should be considered as dissimilar.)

elements (that *are* included in the diagonalization). The transformed Hamiltonian matrix can then be diagonalized approximately in a smaller, more economical, subspace with increased accuracy. Equivalently, for a given diagonalization subspace (say up-to-doubles), diagonalization of an appropriately similarity transformed Hamiltonian should yield better results than diagonalization of the bare Hamiltonian over the same subspace.

The similarity transformation of CC and EOM-CC theory is performed through the exponential operator $e^{\hat{T}}$ and defines a new, transformed, Hamiltonian $\hat{\bar{H}}$,

$$\begin{aligned}\hat{\bar{H}} &\equiv e^{-\hat{T}}\hat{H}e^{\hat{T}} \\ &= \bar{h}_0 + \sum_{p,q}\bar{h}_q^p\{\hat{p}^\dagger\hat{q}\} + \sum_{p<q,\,r<s}\bar{h}_{rs}^{pq}\{\hat{p}^\dagger\hat{r}\hat{q}^\dagger\hat{s}\} \\ &\quad + \sum_{p<q<r,\,s<t<u}\bar{h}_{stu}^{pqr}\{\hat{p}^\dagger\hat{s}\hat{q}^\dagger\hat{t}\hat{r}^\dagger\hat{u}\} + \cdots,\end{aligned} \tag{2}$$

with new elementary amplitudes $\bar{h}_\mu$ that are (diagrammatically connected) tensor products of the original bare-Hamiltonian amplitudes with the $\hat{T}$ operator amplitudes; as seen above, these $\bar{h}_\mu$ are defined as the coefficients of the second-quantized elementary operators of $\hat{\bar{H}}$ written in normal-ordered form. The $\hat{T}$ operator is composed of connected pure-excitation operators and, in the CCSD method, contains only one- and two-body components,

$$\hat{T} = \hat{T}_1 + \hat{T}_2 = \sum_{i,a} t_i^a\{\hat{a}^\dagger\hat{i}\} + \sum_{i<j,\,a<b} t_{ij}^{ab}\{\hat{a}^\dagger\hat{i}\hat{b}^\dagger\hat{j}\}. \tag{3}$$

The explicit algebraic expressions for the CCSD one- and two-body $\bar{h}_\mu$ amplitudes are well documented in the literature, as spin-orbital (*e.g.* reference [110]) or spatial-orbital (*e.g.* reference [157]) quantities; the spatial-orbital $\bar{h}_\mu$ expressions needed in this work are collected in expanded form in Tables 5 and 6 of Section 5. (These expressions can be obtained by diagrammatic evaluation [26,27,124–126] of the definition $e^{-\hat{T}}\hat{H}e^{\hat{T}}$ in conjunction with the Hausdorff expansion [158] or by algebraic evaluation [122,123] of Wick's theorem [124,159] to combine the product of the three normal-ordered operators—actually many more elementary normal-ordered operators due to the Taylor-series expansion of the exponentials—into a *single* normal-ordered operator, followed by collection of like elementary coefficients.) In contrast to the bare Hamiltonian $\hat{H}$ in expression (1), the transformed Hamiltonian $\hat{\bar{H}}$ now contains three- and higher-body operators, up to six in the case of CCSD, but their amplitudes are typically small (*e.g.* references [3,6]). Moreover, the limited determinantal subspaces employed here in the diagonalizations and supplementary equations will prevent all four- and higher-body terms from contributing to the (ST)EOM-CCSD/PT methods. Finally, since the $e^{\hat{T}}$ operator is not unitary, the similarity transformed Hamiltonian $\hat{\bar{H}}$ is non-Hermitian.

So far, we have done little more than rearrange the elementary coefficients in the Hamiltonian. The simplification of the eigenvalue problem arises by setting some of these coefficients to vanish, thereby eliminating their associated elementary operators. In CCSD, the one- and two-body pure-excitation operators $\{\hat{a}^\dagger\hat{i}\}$ and $\{\hat{a}^\dagger\hat{i}\hat{b}^\dagger\hat{j}\}$ in $\hat{\bar{H}}$ are eliminated by setting their associated coefficients $\bar{h}_i^a$ and $\bar{h}_{ij}^{ab}$ to zero. This yields the familiar CCSD

equations [110,157]

$$\bar{h}_i^a = \langle \Phi_i^a | \hat{\bar{H}} | \Phi_0 \rangle \equiv 0 \quad \forall\, i, a,$$
$$\bar{h}_{ij}^{ab} = \langle \Phi_{ij}^{ab} | \hat{\bar{H}} | \Phi_0 \rangle \equiv 0 \quad \forall\, i < j,\ a < b \tag{4}$$

that determine the amplitudes $\mathbf{T}$. The $\hat{T}$ transformation operators in expression (3) were intentionally chosen to have the exact same form as the excitation operators in the transformed Hamiltonian that would be made to vanish, and there are an equal number of (non-linear) equations above as there are $\mathbf{T}$-amplitude unknowns. With the solution of the CCSD equations (4), the reference determinant becomes the ground-state eigenfunction of $\hat{\bar{H}}$ truncated at doubles, with the CCSD energy given by

$$\bar{h}_0 = \langle \Phi_0 | \hat{\bar{H}} | \Phi_0 \rangle. \tag{5}$$

While the CCSD method focuses on the ground state, the EOM-CCSD method [32–35] considers excited states by matrix diagonalization of the transformed $\hat{\bar{H}}$ Hamiltonian (or more precisely, by iterative solution for individual eigenvectors). With the removal of the pure-excitation $\{\hat{a}^\dagger \hat{i}\}$ and $\{\hat{a}^\dagger \hat{i} \hat{b}^\dagger \hat{j}\}$ elementary operators, through the vanishing CCSD equations, the transformed $\hat{\bar{H}}$ matrix attains the approximate block structure presented in Fig. 2. The two-body pure-excitation $\{\hat{a}^\dagger \hat{i} \hat{b}^\dagger \hat{j}\}$ operators would have been the primary operators in $\hat{\bar{H}}$ that coupled singly excited determinants to triply excited determinants, *i.e.* the most important participants in the singles-to-triples $\langle \mathbf{\Phi}_{\mathbf{ijk}}^{\mathbf{abc}} | \hat{\bar{H}} | \mathbf{\Phi}_{\mathbf{i}}^{\mathbf{a}} \rangle$ block of matrix elements. With their removal, the only remaining couplings in this singles-to-triples block are due to new three- and four-body operators, whose coefficients tend to be small in magnitude. The vanishing of the two-body pure-excitation operators thus implies that the diagonalization subspace of $\hat{\bar{H}}$ need extend only *one* excitation level beyond the level of interest to achieve adequate accuracy. For states dominated by single excitations, the excitation energy (EE-) EOM-CCSD method [34] yields accurate results with a diagonalization subspace including singly ($1h1p$) and doubly ($2h2p$) excited determinants only. This moderately sized diagonalization subspace is indicated by the dashed line in Fig. 2 and is in contrast to the much less practical up-to-triples subspace appropriate in CI (*cf.* Fig. 1). This alternative many-body-operator viewpoint—and the subsequent simplification of the block structure before matrix diagonalization—is a straightforward, though perhaps less familiar, explanation of the accuracy of the EOM-CCSD and related methods, whose *ansätze* are often phrased in terms of just the wavefunction parameterization and Hilbert-space projections over determinants, or the action of a wave operator.

Furthermore, in this second-quantized many-body-operator formalism, the approximate (*i.e.* incomplete) decoupling in the transformed Hamiltonian applies immediately to all sectors of Fock space [21,25,29] involving determinants with a different number of electrons. In the ionization potential (IP-) EOM-CCSD variant [39,52], $\hat{\bar{H}}$ is diagonalized over the subspace of $1h$ and $2h1p$ configurations, giving principal ionizations relative to the closed-shell reference system. Conversely, $\hat{\bar{H}}$ is diagonalized over $1p$ and $2p1h$ configurations in the electron affinity (EA-) EOM-CCSD variant [36]. As in the EE- diagonalization, elimination of the two-body pure-excitation $\{\hat{a}^\dagger \hat{i} \hat{b}^\dagger \hat{j}\}$ operators greatly reduces the coupling to determinants outside of the diagonalization subspace, in particular the IP- or EA- "singles"-to-"triples" matrix elements, $\langle \mathbf{\Phi}_{\mathbf{ijk}}^{\mathbf{bc}} | \hat{\bar{H}} | \mathbf{\Phi}_{\mathbf{i}} \rangle$ or $\langle \mathbf{\Phi}^{\mathbf{abc}}_{\mathbf{jk}} | \hat{\bar{H}} | \mathbf{\Phi}^{\mathbf{a}} \rangle$, respectively.

$\hat{\bar{H}}$	$\lvert\Phi_0\rangle$	$\lvert\mathbf{\Phi_i^a}\rangle$	$\lvert\mathbf{\Phi_{ij}^{ab}}\rangle$	$\lvert\mathbf{\Phi_{ijk}^{abc}}\rangle$	$\lvert\mathbf{\Phi_{ijkl}^{abcd}}\rangle$
$\langle\Phi_0\rvert$	$\bar{h}_0$	$\bar{\mathbf{X}}$	$\bar{\mathbf{X}}$	$\mathbf{0}$	$\mathbf{0}$
$\langle\mathbf{\Phi_i^a}\rvert$	$\bar{h}_i^a \equiv 0$	$\bar{\mathbf{X}}$	$\bar{\mathbf{X}}$	$\bar{\mathbf{X}}$	$\mathbf{0}$
$\langle\mathbf{\Phi_{ij}^{ab}}\rvert$	$\bar{h}_{ij}^{ab} \equiv 0$	$\bar{h}_i^a \equiv 0,\ \bar{h}_{ij}^{kb}\{\hat{k}^\dagger\hat{i}\hat{b}^\dagger\hat{j}\},\ \bar{h}_{cj}^{ab}\{\hat{a}^\dagger\hat{c}\hat{b}^\dagger\hat{j}\},\ \sim$	$\bar{\mathbf{X}}$	$\bar{\mathbf{X}}$	$\bar{\mathbf{X}}$
$\langle\mathbf{\Phi_{ijk}^{abc}}\rvert$	$\sim$	$\bar{h}_{ij}^{ab} \equiv 0,\ \sim$	$\bar{\mathbf{X}}$	$\bar{\mathbf{X}}$	$\bar{\mathbf{X}}$
$\langle\mathbf{\Phi_{ijkl}^{abcd}}\rvert$	$\sim$	$\sim$	$\sim$	$\bar{\mathbf{X}}$	$\bar{\mathbf{X}}$

Fig. 2. *Block structure of the singly transformed Hamiltonian* $\hat{\bar{H}}$ *matrix elements*. A similarity transformation changes the matrix elements of an operator but, in the complete diagonalization limit, leaves the eigenvalues rigorously unchanged. In a *truncated*-subspace diagonalization, the similarity transformation can be chosen to eliminate the major elementary operators that couple between the included and the excluded configurations, thereby allowing increased accuracy with a smaller diagonalization subspace. In the CCSD and EOM-CCSD methods, the $\hat{\bar{H}} \equiv e^{-\hat{T}}\hat{H}e^{\hat{T}}$ similarity transformation is performed with the purpose of eliminating the $\{\hat{a}^\dagger\hat{i}\}$ and $\{\hat{a}^\dagger\hat{i}\hat{b}^\dagger\hat{j}\}$ elementary operators. These pure-excitation operators couple a given determinant to determinants respectively one and two excitation levels higher. The operators are eliminated by setting their associated elementary coefficients $\bar{h}_i^a \equiv 0$ and $\bar{h}_{ij}^{ab} \equiv 0$, and the $\mathbf{T}$ amplitudes introduced by the similarity transformation provide exactly the free parameters needed to perform this elimination. With their removal, $\langle\mathbf{\Phi_i^a}|\hat{\bar{H}}|\Phi_0\rangle = \mathbf{0}$, $\langle\mathbf{\Phi_{ij}^{ab}}|\hat{\bar{H}}|\Phi_0\rangle = \mathbf{0}$, and $\langle\Phi_0|\hat{\bar{H}}|\Phi_0\rangle = \bar{h}_0$, yielding CCSD theory for ground states. In the EOM-CCSD method, $\hat{\bar{H}}$ is then matrix diagonalized over singly and doubly excited determinants, to approximate singly excited electronic states. The eliminated two-body pure-excitation $\{\hat{a}^\dagger\hat{i}\hat{b}^\dagger\hat{j}\}$ operators provided the primary coupling between singly and triply excited determinants, and with their removal, the singles-to-triples block $\langle\mathbf{\Phi_{ijk}^{abc}}|\hat{\bar{H}}|\mathbf{\Phi_i^a}\rangle$ of the matrix is greatly reduced. Singly excited electronic states are thereby obtained accurately in this diagonalization that is up-to-*doubles* only. This smaller, more economical, diagonalization subspace is indicated by the dashed line and is in contrast to the up-to-*triples* subspace reasonably required in CI (*cf.* Fig. 1). The individual matrix elements are changed by the similarity transformation, indicated by the bar over the normal-magnitude elements, $\bar{\mathbf{X}}$; moreover, three- and higher-body elementary operators are introduced, but these terms are typically small and are indicated by the $\sim$. In this second-quantized approach, the same one- and two-body pure-excitation elementary operators also couple between determinants of a different fixed number of electrons, and so this same approximate block structure applies in the IP- and EA- variants of EOM-CCSD as well.

Recently, we have reported the first results of a *double* ionization potential (DIP-) EOM-CCSD variant [15], where $\hat{\bar{H}}$ is diagonalized over $2h$ and $3h1p$ configurations, giving doubly ionized states relative to the closed-shell reference system.

In the STEOM-CCSD method [1–3], the process is pushed one step further. A *second* similarity transformation is performed in order to eliminate the primary net-excitation operators that couple between singly and *doubly* excited determinants and thereby further reduce the minimum size of the approximate diagonalization subspace. This second trans-

formation is performed through a normal-ordered exponential operator $\{e^{\hat{S}}\}$ [25,26]. The doubly transformed STEOM-CCSD Hamiltonian becomes

$$\begin{aligned}\hat{G} &\equiv \{e^{\hat{S}}\}^{-1}\hat{\bar{H}}\{e^{\hat{S}}\} \\ &= \mathsf{g}_0 + \sum_{p,q}\mathsf{g}_q^p\{\hat{p}^\dagger\hat{q}\} + \sum_{p<q,\,r<s}\mathsf{g}_{rs}^{pq}\{\hat{p}^\dagger\hat{r}\hat{q}^\dagger\hat{s}\} + \cdots,\end{aligned} \tag{6}$$

with new elementary coefficients g_μ and $\mathsf{g}_0 = \bar{h}_0$. The $\hat{S}$ operator consists of two parts, $\hat{S} = \hat{S}^- + \hat{S}^+$, with

$$\begin{aligned}\hat{S}^- &= \hat{S}_1^- + \hat{S}_2^- = \sum_{i',m} s_{i'}^m\{\hat{m}^\dagger\hat{i}'\} + \sum_{m,b,i<j} s_{ij}^{mb}\{\hat{m}^\dagger\hat{i}\hat{b}^\dagger\hat{j}\}, \\ \hat{S}^+ &= \hat{S}_1^+ + \hat{S}_2^+ = \sum_{a',e} s_e^{a'}\{\hat{a}'^\dagger\hat{e}\} + \sum_{e,j,a<b} s_{ej}^{ab}\{\hat{a}^\dagger\hat{e}\hat{b}^\dagger\hat{j}\}.\end{aligned} \tag{7}$$

These elementary operators in $\hat{S}$ have precisely the same form as the elementary operators in the doubly transformed Hamiltonian $\hat{G}$ that will be made to vanish. For the double ionization potential (DIP-) STEOM variant [3], the $\hat{S}^+$ operator is not used, as the matching elementary operators in the Hamiltonian cannot participate in the $(2h)$ diagonalization; contrariwise, for the double electron affinity (DEA-) STEOM variant [3], the $\hat{S}^-$ operator is not used; for the excitation energy (EE-) STEOM method [1,3], both $\hat{S}^-$ and $\hat{S}^+$ are needed. Unlike the pure-excitation $\hat{T}$ in the first transformation, the $\hat{S}$ operators do not commute, due to their $\hat{m}^\dagger$ or $\hat{e}$ q-annihilation components (annihilation operators with respect to the quasi-particle vacuum $|\Phi_0\rangle$), but the overall normal-ordering is included in $\{e^{\hat{S}}\}$ to prevent the non-commuting components from contracting among themselves and thereby streamline the resulting **G** expressions. Note that contractions are still possible between the $\{e^{\hat{S}}\}$ operator and its inverse in the similarity transformation.

Again, this second similarity transformation *by itself* does little more than rearrange the elementary coefficients in the doubly transformed Hamiltonian. But it does serve to introduce the free parameters **S**, which are then used to eliminate the coefficients of the unwanted net-excitation operators in $\hat{G}$. To begin with, this second similarity transformation preserves the zeros of the first [25], so that the decoupling due to the CCSD equations remains true,

$$\begin{aligned}&\mathsf{g}_i^a = \bar{h}_i^a = 0 \qquad \forall\ i, a, \\ &\mathsf{g}_{ij}^{ab} = \bar{h}_{ij}^{ab} = 0 \quad \forall\ i<j,\ a<b\end{aligned} \tag{8}$$

(where the first equation has been used in the second). These zeros are independent of the value of the **S** coefficients, and so the $\hat{G}$ similarity transformation does not interfere with the pure-excitation $\{\hat{a}^\dagger\hat{i}\}$ and $\{\hat{a}^\dagger\hat{i}\hat{b}^\dagger\hat{j}\}$ eliminations achieved in the preceding $\hat{\bar{H}}$ transformation. The equations that determine the STEOM-CCSD **S** amplitudes are analogous to those of the CCSD and EOM-CCSD **T** amplitudes, namely they set the matching operator coefficients of the resulting transformed Hamiltonian to zero. The equations that determine $\mathbf{S}^-$ for EE- and DIP-STEOM-CCSD are

$$\begin{aligned}&\mathsf{g}_{i'}^m = -\langle\Phi_{i'}|\hat{G}|\Phi_m\rangle \equiv 0 \qquad \forall\ i', m, \\ &\mathsf{g}_{ij}^{mb} = -\langle\Phi_{ij}^{\ b}|\hat{G}|\Phi_m\rangle \equiv 0 \quad \forall\ m, b,\ i<j,\end{aligned} \tag{9}$$

and these vanishing $\mathsf{g}_{i'}^{m}$ and g_{ij}^{mb} coefficients eliminate the associated $\{\hat{m}^\dagger \hat{i}'\}$ and net-excitation $\{\hat{m}^\dagger \hat{i} \hat{b}^\dagger \hat{j}\}$ elementary operators in $\hat{G}$. Likewise, the equations that determine $\mathbf{S}^+$ for EE- and DEA-STEOM-CCSD are

$$\begin{aligned} \mathsf{g}_{e}^{a'} &= \langle \Phi^{a'} | \hat{G} | \Phi^{e} \rangle \equiv 0 \quad \forall\ a', e, \\ \mathsf{g}_{ej}^{ab} &= \langle \Phi^{ab}_{\ j} | \hat{G} | \Phi^{e} \rangle \equiv 0 \quad \forall\ e, j,\ a < b, \end{aligned} \tag{10}$$

and these vanishing $\mathsf{g}_{e}^{a'}$ and g_{ej}^{ab} coefficients eliminate the associated $\{\hat{a}'^\dagger \hat{e}\}$ and net-excitation $\{\hat{a}^\dagger \hat{e} \hat{b}^\dagger \hat{j}\}$ operators in $\hat{G}$. (Note that satisfaction of the pure-excitation equations (8) is needed to simplify the matrix elements in equations (9) and (10) to be the same as the associated elementary operator coefficients, an issue to which we will return later in the PT-based discussion.) These eliminated elementary operators in $\hat{G}$ have precisely the same form as the $\hat{S}$ operators of expressions (7), and there are an equal number of equations as there are **S**-amplitude unknowns. Additionally we note that in equations (9) and (10), only a selection of the g_{μ} operator coefficients are made to vanish, and this selection defines the active partitions m and e of the orbital spaces, respectively. The role of the active space in STEOM will be examined in detail later in this section.

Besides the pure-excitation $\{\hat{a}^\dagger \hat{i}\}$ operators eliminated in the first transformation, the eliminated two-body $\{\hat{m}^\dagger \hat{i} \hat{b}^\dagger \hat{j}\}$ and $\{\hat{a}^\dagger \hat{e} \hat{b}^\dagger \hat{j}\}$ net-excitation operators are the primary operators that would couple singly excited determinants to doubly excited determinants. In the EE-STEOM-CCSD method, these are the most important operators that would participate in the singles-to-doubles $\langle \mathbf{\Phi}^{\mathbf{ab}}_{\mathbf{ij}} | \hat{G} | \mathbf{\Phi}^{\mathbf{a}}_{\mathbf{i}} \rangle$ block of matrix elements. To be completely explicit, the only possible contributions to this block of the $\hat{G}$ matrix are of the form $\langle \Phi^{ab}_{ij} | \{\hat{b}^\dagger \hat{j}\} | \Phi^{a}_{i} \rangle$, $\langle \Phi^{ab}_{ij} | \{\hat{k}^\dagger \hat{i} \hat{b}^\dagger \hat{j}\} | \Phi^{a}_{k} \rangle$, $\langle \Phi^{ab}_{ij} | \{\hat{a}^\dagger \hat{c} \hat{b}^\dagger \hat{j}\} | \Phi^{c}_{i} \rangle$, or $\langle \Phi^{ab}_{ij} | \{\hat{k}^\dagger \hat{i} \hat{a}^\dagger \hat{c} \hat{b}^\dagger \hat{j}\} | \Phi^{c}_{k} \rangle$. Eliminating the $\{\hat{a}^\dagger \hat{i}\}$ operators eliminates the first contribution above, and eliminating the $\{\hat{m}^\dagger \hat{i} \hat{b}^\dagger \hat{j}\}$ and $\{\hat{a}^\dagger \hat{e} \hat{b}^\dagger \hat{j}\}$ operators greatly reduces the magnitude of the second and third contributions above, leaving only $\langle \Phi^{ab}_{ij} | \{\hat{k}'^\dagger \hat{i} \hat{b}^\dagger \hat{j}\} | \Phi^{a}_{k'} \rangle$ and $\langle \Phi^{ab}_{ij} | \{\hat{a}^\dagger \hat{c}' \hat{b}^\dagger \hat{j}\} | \Phi^{c'}_{i} \rangle$ involving an inactive orbital and the final three-body term above. (These remaining three-body and inactive two-body couplings from singly to doubly excited determinants are part of the residual contributions that are neglected by the singles-only diagonalization subspace.) Analogously, the same $\{\hat{a}^\dagger \hat{i}\}$ and $\{\hat{m}^\dagger \hat{i} \hat{b}^\dagger \hat{j}\}$ operators present the primary eliminated coupling in the DIP- "singles"-to-"doubles" $\langle \mathbf{\Phi}^{\mathbf{c}}_{\mathbf{ijk}} | \hat{G} | \mathbf{\Phi}_{\mathbf{ij}} \rangle$ matrix elements, and the $\{\hat{a}^\dagger \hat{i}\}$ and $\{\hat{a}^\dagger \hat{e} \hat{b}^\dagger \hat{j}\}$ operators are the primary eliminated participants in the DEA- "singles"-to-"doubles" $\langle \mathbf{\Phi}^{\mathbf{abc}}_{\mathbf{k}} | \hat{G} | \mathbf{\Phi}^{\mathbf{ab}} \rangle$ matrix elements. Note that these eliminated second-quantized operators also reduce a large portion of the couplings between higher excitation blocks (*e.g.* doubles-to-triples) as well.

With the removal of the most important pure-excitation and net-excitation operators through equations (8), (9), and (10)—and the implicit incorporation of their contributions into the lower-level matrix elements through the transformed amplitudes of the Hamiltonian—the doubly transformed STEOM-CCSD $\hat{G}$ Hamiltonian matrix attains the approximate block upper-triangular structure presented in Fig. 3. Each subblock on the diagonal corresponds to a particular excitation level and is approximately decoupled from all more highly excited determinants. As discussed above, the only remaining couplings that can excite out of a subblock involve inactive or three- and higher-body operators. Most notably, singly excited electronic states can now be obtained accurately by diagonalizing $\hat{G}$ over the subspace of *single excitations only*, as indicated by the dashed lined in Fig. 3. Moreover, this same block structure applies in the DIP- or DEA-STEOM-CCSD variants,

$\hat{G}$	$\lvert\Phi_0\rangle$	$\lvert\mathbf{\Phi}^{\mathbf{a}}_{\mathbf{i}}\rangle$	$\lvert\mathbf{\Phi}^{\mathbf{ab}}_{\mathbf{ij}}\rangle$	$\lvert\mathbf{\Phi}^{\mathbf{abc}}_{\mathbf{ijk}}\rangle$	$\lvert\mathbf{\Phi}^{\mathbf{abcd}}_{\mathbf{ijkl}}\rangle$
$\langle\Phi_0\rvert$	$\mathsf{g}_0 = \bar{h}_0$	$\bar{\bar{\mathbf{X}}}$	$\bar{\bar{\mathbf{X}}}$	$\mathbf{0}$	$\mathbf{0}$
$\langle\mathbf{\Phi}^{\mathbf{a}}_{\mathbf{i}}\rvert$	$\mathsf{g}^a_i \equiv 0$	$\bar{\bar{\mathbf{X}}}$	$\bar{\bar{\mathbf{X}}}$	$\bar{\bar{\mathbf{X}}}$	$\mathbf{0}$
$\langle\mathbf{\Phi}^{\mathbf{ab}}_{\mathbf{ij}}\rvert$	$\mathsf{g}^{ab}_{ij} \equiv 0$	$\mathsf{g}^a_i \equiv 0,\ \mathsf{g}^{mb}_{ij} \equiv 0,\ \mathsf{g}^{ab}_{ej} \equiv 0,\ \approx$	$\bar{\bar{\mathbf{X}}}$	$\bar{\bar{\mathbf{X}}}$	$\bar{\bar{\mathbf{X}}}$
$\langle\mathbf{\Phi}^{\mathbf{abc}}_{\mathbf{ijk}}\rvert$	$\approx$	$\mathsf{g}^{ab}_{ij} \equiv 0,\ \approx$	$\approx$	$\bar{\bar{\mathbf{X}}}$	$\bar{\bar{\mathbf{X}}}$
$\langle\mathbf{\Phi}^{\mathbf{abcd}}_{\mathbf{ijkl}}\rvert$	$\approx$	$\approx$	$\approx$	$\approx$	$\bar{\bar{\mathbf{X}}}$

Fig. 3. *Block structure of the doubly transformed Hamiltonian $\hat{G}$ matrix elements*. In STEOM-CCSD, a second similarity transformation, $\hat{G} \equiv \{e^{\hat{S}}\}^{-1}\hat{\bar{H}}\{e^{\hat{S}}\}$, is performed to eliminate the major remaining elementary operators that couple from singly to *doubly* excited determinants and thereby further reduce the size of the approximate diagonalization subspace. This second transformation preserves the zeros of the $\hat{\bar{H}}$ transformation (Fig. 2), and furthermore, the introduced **S** amplitudes set the $\hat{G}$ elementary coefficients $\mathsf{g}^{mb}_{ij} \equiv 0$ and $\mathsf{g}^{ab}_{ej} \equiv 0$ (with m and e indicating active orbitals). These new zeros respectively eliminate the net-excitation $\{\hat{m}^\dagger\hat{i}\hat{b}^\dagger\hat{j}\}$ and $\{\hat{a}^\dagger\hat{e}\hat{b}^\dagger\hat{j}\}$ operators, the primary remaining participants in the singles-to-doubles $\langle\mathbf{\Phi}^{\mathbf{ab}}_{\mathbf{ij}}|\hat{G}|\mathbf{\Phi}^{\mathbf{a}}_{\mathbf{i}}\rangle$ block. The only residual operators left in this block are the corresponding inactive two-body operators and typically-small three-body operators. With the elimination of the primary singles-to-doubles and singles-to-triples coupling operators (and the implicit incorporation of their effects into the singles-level matrix elements through the transformed Hamiltonian amplitudes), singly excited electronic states can now be obtained accurately by diagonalizing $\hat{G}$ over the subspace of *singly excited determinants only*, indicated by the dashed line. This reduction represents an enormous savings over the reasonable diagonalization subspace in CI (up-to-triples, Fig. 1), or even EOM (up-to-doubles, Fig. 2), and allows a large number of singly excited states to be computed at essentially no additional cost. The STEOM-CCSD method can be considered a rigorous correlated equivalent of the CI-singles method, using the fully correlated effective Hamiltonian $\hat{G}$. Additionally, due to the second-quantized nature of the eliminated elementary operators, this same approximate block upper-triangular structure applies in the DIP- and DEA- variants of STEOM-CCSD as well. Finally note that the matrix elements are again changed by the second similarity transformation, indicated by the additional overbar in $\bar{\bar{\mathbf{X}}}$, as are the typically-small residual elements $\approx$.

and the methods can accurately describe open-shell systems with two less or two more electrons respectively (than a closed-shell parent) with a singles-like $2h$ or $2p$ diagonalization subspace only. The cost of these final CI-singles-like diagonalizations is trivial, and a large number of eigenstates can thus be computed simultaneously for essentially no additional cost.

We now consider some detailed features of STEOM-CCSD theory. In equations (9) and (10) that define the eliminated $\hat{G}$ components, it is in fact not necessary that the one-body $\mathsf{g}^m_{i'}$ and $\mathsf{g}^{a'}_e$ coefficients be made to vanish, since the associated $\{\hat{m}^\dagger\hat{i}'\}$ and $\{\hat{a}'^\dagger\hat{e}\}$ operators do not increase the excitation level of a determinant and thus their removal does not aid in decoupling excitation blocks of $\hat{G}$. However, doing so exploits the relationship [3,25,

160,161] between STEOM-CC, EOM-CC, and FSCC [21–24,26–29] theories, allowing the coupled set of non-linear (in **S**) equations (9) and (10) to be re-cast into a series of independent EOM-CCSD eigenvector problems (one for each active orbital m or e), which is numerically more stable. The STEOM-CCSD $\mathbf{S}^-$ and $\mathbf{S}^+$ amplitudes have been shown to be the same as the amplitudes obtained in the FSCC solution for the IP and EA sectors, respectively, and can in turn be computed by solving for a selection of active IP- and EA-EOM-CCSD eigenvectors, along with an additional normalization condition that depends on the size of the STEOM active space [3].

Although needed to calculate the **S** amplitudes, the diagonalization of $\hat{G}$, on the other hand, does not require the one-body $\hat{S}_1$ components. The eigenvalues of $\hat{G}$ can equivalently be obtained from

$$\hat{G}_2 \equiv \{e^{\hat{S}_2}\}^{-1}\hat{\bar{H}}\{e^{\hat{S}_2}\}. \tag{11}$$

As long as the diagonalization is performed over the full set of orbitals (active plus inactive) in the chosen truncation, the eigenvalue spectrum of $\hat{G}_2$ is identical [3] to that of the full $\hat{G}$: Since

$$\{e^{\hat{S}}\} = \{e^{\hat{S}_2+\hat{S}_1}\} = \{e^{\hat{S}_2}\}\{e^{\hat{S}_1}\} \tag{12}$$

by Wick's theorem [124,159] and the fact that the *inactive* q-creation operators (diagrammatically at the top) of $\hat{S}_1$ cannot contract with the explicitly *active* q-annihilation operators (at the bottom) of $\hat{S}_2$, then

$$\begin{aligned}\hat{G} &= \{e^{\hat{S}_2+\hat{S}_1}\}^{-1}\hat{\bar{H}}\{e^{\hat{S}_2+\hat{S}_1}\} = \{e^{\hat{S}_1}\}^{-1}\{e^{\hat{S}_2}\}^{-1}\hat{\bar{H}}\{e^{\hat{S}_2}\}\{e^{\hat{S}_1}\} \\ &\equiv \{e^{\hat{S}_1}\}^{-1}\hat{G}_2\{e^{\hat{S}_1}\},\end{aligned} \tag{13}$$

and thus $\hat{G}$ and $\hat{G}_2$ are related by a similarity transformation and have the same eigenvalues. To summarize therefore, the equations for the **S** amplitudes require the full $\hat{G}$, whereas the diagonalization only requires $\hat{G}_2$. Amplitudes of $\hat{G}_2$ will be denoted typographically as g_μ, whereas amplitudes of the full $\hat{G}$ will be denoted as $\mathfrak{g}_\mu$. In this work, nearly all the explicit algebraic expressions will be written in terms of the $\mathbf{G_2}$ amplitudes, unless noted otherwise.

The explicit algebraic expressions for the **G** (and $\mathbf{G_2}$) amplitudes in terms of $\bar{\mathbf{H}}$ and **S** amplitudes cannot readily be obtained from the definition of $\hat{G}$ in expression (6), though, due to the unknown inverse $\{e^{\hat{S}}\}^{-1}$. In a key development, it was shown [25] that the linear (in **G**) set of equations $\{e^{\hat{S}}\}\hat{G} = \hat{\bar{H}}\{e^{\hat{S}}\}$ can be organized into a block form soluble by backward substitution and leads to

$$\hat{G} = (\hat{\bar{H}}\{e^{\hat{S}}\})_C - (\{e^{\hat{S}} - 1\}\hat{G})_C, \tag{14}$$

where the subscript C means that, in diagrammatic language, the terms must be connected (share one or more summation indices through contractions in Wick's theorem such that the terms cannot be factored into disjoint pieces). Expression (14) has been evaluated diagrammatically for the needed **G** and $\mathbf{G_2}$ amplitudes, and reference [3] lists their explicit spatial-orbital formulas, which are reproduced here in expanded form in Tables 5 and 7 of Section 5 (with some typographical corrections).

Once the **S** amplitudes are obtained and the $\mathbf{G_2}$ amplitudes are calculated (*i.e.* the second similarity transformation is performed), the final transformed Hamiltonian $\mathbf{G_2}$ is

diagonalized over the appropriate singles determinants to compute the energies of interest. Despite this small singles-only diagonalization subspace, however, through the second similarity transformation the STEOM-CCSD method includes implicit "connected" doubles and triples contributions in the wavefunction. To make this statement more concrete, Table 1 compares the individual excitation levels of the EOM-CCSD and STEOM-CCSD approximate final wavefunctions (of the bare $\hat{H}$) in relation to the straightforward CI parameterization. The $\hat{C}$, $\hat{\mathcal{R}}$, and $\hat{R}$ in Table 1 represent operators corresponding to the CI, EOM-CCSD, and STEOM-CCSD diagonalization subspaces of $\hat{H}$, $\hat{\tilde{H}}$, and $\hat{G}_2$, respectively (as well as include the reference element), and the individual excitation levels of these diagonalization operators (constant, singles, doubles, triples, or quadruples) are indicated by their subscripted number (0, 1, 2, 3, or 4, respectively). The diagonalization operators can be taken as pure excitations ($1h1p, 2h2p, \ldots$), as ionizations ($1h, 2h1p, \ldots$), as attachments ($1p, 2p1h, \ldots$), as double ionizations ($2h, 3h1p, \ldots$), or as double attachments ($2p, 3p1h, \ldots$), and the "excitation" level ("singles", "doubles", ...) likewise redefined. Note that the EOM-CCSD method explicitly includes the $\hat{\mathcal{R}}_1$ and $\hat{\mathcal{R}}_2$ operators in its diagonalization, whereas the STEOM-CCSD method only explicitly includes $\hat{R}_1$. To facilitate comparison within a given CI excitation level, the analogous components between the EOM-CCSD and STEOM-CCSD methods are written on the same line. The table entries can be obtained through abstract examination of the (ST)EOM-CCSD wavefunctions by Taylor-series expanding the exponentials and collecting operators of equal excitation rank. (For the most part, the information is also contained algebraically in the full expansion of the EOM- and STEOM-CCSD energy expressions of Section 5.)

We shall now examine the excitation levels in Table 1 individually. Both the EOM-CCSD and STEOM-CCSD wavefunctions include the reference element, and both methods give a total treatment of the singles contributions, through the inclusion of the $\hat{\mathcal{R}}_1$ or $\hat{R}_1$ singles operators in their diagonalization subspaces, respectively. The first difference between the two methods occurs in the doubles-level components. Whereas the EOM-CCSD method includes the doubly excited determinants *explicitly* through the $\hat{\mathcal{R}}_2$ operator in the diagonalization, the STEOM-CCSD method incorporates the doubles contributions *implicitly* through the second similarity transformation. In other words, rather than the full, independent treatment of doubles as in EOM-CCSD, the STEOM-CCSD method approximates the doubles contributions as the connected products of $\hat{R}_1$ with $\hat{S}_2$. The connected $(\hat{S}_2\hat{R}_1)_C$ plays the role of an approximate connected "$\hat{R}_2$" in STEOM, and as previously discussed, the STEOM $\hat{S}$ amplitudes can be computed from the IP- and EA-EOM-CCSD $\hat{\mathcal{R}}_1$ and $\hat{\mathcal{R}}_2$ amplitudes.

The most important difference between the EOM-CCSD and STEOM-CCSD treatments occurs in the triples-level components. In the EOM-CCSD method, all the triples components are diagrammatically "disconnected" products (meaning the $\hat{T}$ and $\hat{\mathcal{R}}$ share no summation indices). In contrast, the STEOM-CCSD method includes the connected $(\{\frac{1}{2}\hat{S}_2{}^2\}\hat{R}_1)_C$ contribution, which acts as an approximate connected "$\hat{R}_3$" triples component in STEOM. This implicit inclusion of *connected* triples typically favors the STEOM approach, particularly for valence excited states [3,6,12,13]. Discarding these connected triples terms from STEOM-CCSD often gives valence results more similar to EOM-CCSD [3]. For Rydberg states, where the effects of triples are less important, STEOM-CCSD offers little if any improvement over EOM-CCSD energies, but transition moments can be sensitive to these included triples effects [3]. As noted in the Introduction, accurate connected triples corrections to EOM-CCSD, such as through EOM-CCSD($\tilde{\mathrm{T}}$) [80]

Table 1. *Individual excitation levels in the EOM-CCSD and STEOM-CCSD approximate $\hat{H}$ final wavefunctions*. The $\hat{C}$, $\hat{\mathcal{R}}$, and $\hat{R}$ correspond to the CI, EOM-CCSD, and STEOM-CCSD diagonalization subspaces of $\hat{H}$, $\hat{\bar{H}}$, and $\hat{G}_2$, respectively. The EOM-CCSD method explicitly includes the singles and doubles $\hat{\mathcal{R}}_1$ and $\hat{\mathcal{R}}_2$ operators in its diagonalization, whereas the STEOM-CCSD method only explicitly includes $\hat{R}_1$. Despite this singles-only diagonalization subspace, the STEOM-CCSD method implicitly includes "connected" doubles $(\hat{S}_2\hat{R}_1)_C$ and triples $(\{\frac{1}{2}\hat{S}_2{}^2\}\hat{R}_1)_C$ contributions in the wavefunction. This implicit inclusion of *connected* triples typically favors the STEOM-CCSD approach over EOM-CCSD, particularly for valence excited states [3,6,12,13]. Separately, note the implicit approximate inclusion of configurations beyond the truncation level (in fact all the way up to the fully excited determinants) favors the EOM-CC and STEOM-CC methods over the like-truncated CI method.

CI $\lvert\underset{\sim}{\Psi}\rangle = \hat{C}\lvert\Phi_0\rangle$	EOM-CCSD $\lvert\underset{\sim}{\Psi}\rangle = e^{\hat{T}}\hat{\mathcal{R}}\lvert\Phi_0\rangle$	STEOM-CCSD $\lvert\underset{\sim}{\Psi}\rangle = e^{\hat{T}}\{e^{\hat{S}_2}\}\hat{R}\lvert\Phi_0\rangle$
$\hat{C}_0$	$\hat{\mathcal{R}}_0$	$\hat{R}_0$
$\hat{C}_1$	$\hat{T}_1\hat{\mathcal{R}}_0$ $+\hat{\mathcal{R}}_1$	$\hat{T}_1\hat{R}_0$ $+\hat{R}_1$
$\hat{C}_2$	$\left(\hat{T}_2+\frac{1}{2}\hat{T}_1^2\right)\hat{\mathcal{R}}_0$ $+\hat{T}_1\hat{\mathcal{R}}_1$ $+\hat{\mathcal{R}}_2$	$\left(\hat{T}_2+\frac{1}{2}\hat{T}_1^2\right)\hat{R}_0$ $+\hat{T}_1\hat{R}_1$ $+(\hat{S}_2\hat{R}_1)_C$
$\hat{C}_3$	$\left(\hat{T}_2\hat{T}_1+\frac{1}{3!}\hat{T}_1^3\right)\hat{\mathcal{R}}_0$ $+\left(\hat{T}_2+\frac{1}{2}\hat{T}_1^2\right)\hat{\mathcal{R}}_1$ $+\hat{T}_1\hat{\mathcal{R}}_2$	$\left(\hat{T}_2\hat{T}_1+\frac{1}{3!}\hat{T}_1^3\right)\hat{R}_0$ $+\left(\hat{T}_2+\frac{1}{2}\hat{T}_1^2\right)\hat{R}_1$ $+\hat{T}_1(\hat{S}_2\hat{R}_1)_C$ $+\left(\{\frac{1}{2}\hat{S}_2{}^2\}\hat{R}_1\right)_C$
$\hat{C}_4$	$\left(\frac{1}{2}\hat{T}_2^2+\frac{1}{2}\hat{T}_2\hat{T}_1^2+\frac{1}{4!}\hat{T}_1^4\right)\hat{\mathcal{R}}_0$ $+\left(\hat{T}_2\hat{T}_1+\frac{1}{3!}\hat{T}_1^3\right)\hat{\mathcal{R}}_1$ $+\left(\hat{T}_2+\frac{1}{2}\hat{T}_1^2\right)\hat{\mathcal{R}}_2$	$\left(\frac{1}{2}\hat{T}_2^2+\frac{1}{2}\hat{T}_2\hat{T}_1^2+\frac{1}{4!}\hat{T}_1^4\right)\hat{R}_0$ $+\left(\hat{T}_2\hat{T}_1+\frac{1}{3!}\hat{T}_1^3\right)\hat{R}_1$ $+\left(\hat{T}_2+\frac{1}{2}\hat{T}_1^2\right)(\hat{S}_2\hat{R}_1)_C$ $+\hat{T}_1\left(\{\frac{1}{2}\hat{S}_2{}^2\}\hat{R}_1\right)_C$
$\vdots$	$\vdots$	$\vdots$

or CC3 [78], can be quite expensive. For many non-trivial organic molecules, the singly excited states given by STEOM-CCSD are found to be comparable in accuracy to the EOM-CCSD($\tilde{\mathrm{T}}$) or CC3 results, but for a fraction of the computational cost [6,12,13]. To give some perspective, an entire EE-STEOM-CCSD calculation, yielding a large number of singly excited states, ionization potentials, and electron affinities of the system, even including property calculations and the analytical gradient, is cheaper than calculating just *one* excitation energy in EE-EOM-CCSD($\tilde{\mathrm{T}}$).

For the quadruples-level components and higher, both the EOM-CCSD and STEOM-CCSD methods include only disconnected contributions. Because of the exponential operators in the similarity transformations, the EOM and STEOM wavefunctions include such disconnected contributions all the way up to the fully excited determinants (given by the total number of electrons). It is this approximate treatment of *all* excited determinants that makes ground-state truncated CC theory superior to the like-truncated CI treatment (which does not include any contributions beyond the truncation). Ground-state CCSD theory is recovered from Table 1 by keeping only the components involving the reference configuration (the first line in each excitation level). We should note that if all levels of $\hat{T}$ were included, this ground-state "full" CC theory would be equivalent to full CI (but computationally more expensive). Furthermore, even for *truncated* $\hat{T}$, due to the exact nature of similarity transformations, a full diagonalization space (all levels of $\hat{\mathcal{R}}$ or $\hat{R}$) would make EOM-CC or STEOM-CC equivalent to full CI for excited states.

The quality of the STEOM-CCSD approximations for singly excited states can be explored through comparison with the extended-STEOM-CCSD approach [12,13]. By extending the diagonalization subspace to include *doubly* excited determinants *explicitly*, through the inclusion of $\hat{R}_2$ in the $\hat{G}$ diagonalization, the extended method gives a full treatment of doubles and a more complete treatment of implicit connected triples (as well as implicit connected quadruples if desired). In general, *for states dominated by single excitations*, the original STEOM-CCSD results are typically unchanged in going to extended-STEOM-CCSD, with shifts often less than 0.05 eV [12,13]. This convergence substantiates the approximation of using a singles-only diagonalization subspace of $\hat{G}$ for singly excited states, indicating that the remaining non-vanishing three-body and inactive two-body operators that couple singles to doubles (the $\approx$ in the $\langle \mathbf{\Phi}^{\mathbf{ab}}_{\mathbf{ij}} | \hat{G} | \mathbf{\Phi}^{\mathbf{a}}_{\mathbf{i}} \rangle$ block in Fig. 3 and given explicitly several paragraphs above) are indeed negligible, in such typical applications. Furthermore, the STEOM-CCSD results for dominantly singly excited states are usually accurate to within 0.1 eV or so compared to experimental or full CI results [3,6,12,13]. (This same 0.1 eV accuracy is generally also found for doubly excited states in extended-STEOM-CCSD [12,13].) However, convergence of the STEOM and extended-STEOM results *alone* does not necessarily guarantee accuracy relative to full CI. Just as in CCSD and EOM-CCSD, large amplitudes in the similarity transformation can indicate that significant contributions are present outside of the treatment. For example [12], the first $^1\Pi_g$ state of N_2 or the first $^1B_2$ state of CH_2 are found to involve an orbital whose corresponding IP- or EA-EOM-CCSD eigenvector has a significant double-excitation character, yielding large associated $\mathbf{S_2}$ amplitudes. Although the STEOM and extended-STEOM results for these particular singly excited states are found to agree, the results do not agree especially well with full CI ($\sim$0.3 eV errors), implying that the large $\hat{S}_2$ may have induced a substantial *direct* singles-to-*triples* coupling through the similarity transformation, by inflating the three- and higher-body (net-double-excitation) operators in $\hat{G}$ (the $\approx$ in the $\langle \mathbf{\Phi}^{\mathbf{abc}}_{\mathbf{ijk}} | \hat{G} | \mathbf{\Phi}^{\mathbf{a}}_{\mathbf{i}} \rangle$ block in Fig. 3). To better understand and identify when results should be

considered suspect or reliable, let us examine the accuracy indicators in STEOM in more detail, in particular with regard to the selection of the active space.

As seen in equations (9) and (10), the active space defines the selection of two-body net-excitation operators that are eliminated through the second similarity transformation, and the selection that are not. The inactive two-body net-excitation operators comprise part of the remaining coupling that is disregarded by the truncated diagonalization. But the active space also determines the extent of the three- and higher-body operators that are modified/created in the second transformation, which too are neglected in the truncated diagonalization. The active space thus plays a dual role in STEOM. Certainly, it serves to reduce computational expense by reducing the number of amplitudes/equations in expressions (9) and (10). But it also enables the restriction of the transformation amplitudes $\mathbf{S_2}$ to those that are relatively small in magnitude. This warrants some further discussion.

An underlying assumption of the STEOM-CCSD approach is that the $\mathbf{S_2}$ and $\mathbf{T}$ amplitudes are small and account primarily for dynamical correlation effects. If these transformation amplitudes are indeed small, then the resulting higher-rank operators in the transformed Hamiltonian can also be expected to be small, and the approximation in STEOM to neglect these operators, through the limited diagonalization subspace, is valid. If the transformation amplitudes are large, however, the accuracy of the results becomes rather unpredictable. In such cases, there will likely be higher-rank operators in $\hat{G}$ that attain large amplitudes, and they may well be important for the excited states of interest. In practice, we find that results from STEOM-CCSD calculations can be trusted if

1. the $\mathbf{T}$ and $\mathbf{S_2}$ transformation amplitudes are relatively small,
2. the %active character in the STEOM eigenvectors is sufficiently high,
3. the STEOM states of interest are predominantly singly excited, and
4. the basis set is adequate, in agreement with standard considerations.

If any of these criteria cannot be met (to be defined more precisely below), results should be regarded with suspicion. In particular, as in the N_2 or CH_2 states mentioned above, it may be that some specific orbital is important for the excited state of interest, but the corresponding $\mathbf{S_2}$ amplitudes (IP/EA-EOM eigenvector) have some large values. In such a case, the STEOM approach simply breaks down, and there is no easy way to circumvent the problem. This is a relatively rare occurrence for well-behaved Hartree–Fock molecules at their ground-state equilibrium geometry, but it can readily become apparent as the geometry is distorted. Let us consider the individual criteria more carefully.

The $\mathbf{T}$ amplitudes will be small (in absolute value) if the reference state is qualitatively well described by a single Hartree–Fock determinant. The requirement that the parent state is well described at the single-reference level is essential for both the EOM and STEOM methods. As a rule of thumb, $\mathbf{T}$ amplitudes are small enough if there are a limited number of them between 0.1 and 0.15 in magnitude. If such amplitudes are plentiful, or if some amplitudes exceed 0.15 in absolute value, the results are suspicious (the permanganate anion is an example of a situation where many intermediately large $\mathbf{T}$ amplitudes are present, and EOM and in particular STEOM are not very accurate [12]).

The $\mathbf{S_2}$ amplitudes in STEOM will be small when the associated IP/EA-EOM states are well described by the principal configurations, *i.e.* when the doubles components of the included IP/EA-EOM eigenvectors are small. For the IP-EOM situation, this is generally the case for the valence ionized states, but the deeper-lying ionized states are typically poorly described by just the $1h$ determinants, or in other words, Koopmans' approximation

progressively breaks down. Typically, the deeper-lying $1h$ and certain $2h1p$ determinants will approach degeneracy, which leads to configurational mixing between the two and a concomitant rise of the associated $\mathbf{S_2}$ amplitudes. For the EA-EOM amplitudes, the situation is somewhat less straightforward. Valence attached states typically have significant $2p1h$ character, whereas Rydberg attached states often revert back to $1p$ descriptions. The coupling between the diffuse Rydberg $1p$ determinants and spatially more-compact $2p1h$ determinants is often minor, and a breakdown of the one-particle picture is only observed for relatively high attachment energies (*e.g.* higher than 10 eV). Eventually the breakdown does occur, and this defines a clear limit to the extent of the virtual active space that should be used in STEOM. Let us emphasize that all of these attached states are usually unbound states, and they would at best approximate resonances in electron scattering experiments. For both the IP- and EA-EOM eigenvectors, there is typically an energy window in which all states are relatively well described by the principal configurations. This is how the active space is chosen in STEOM, usually with about 10–20 occupied and 20–30 virtual orbitals, extending from about -20 to $+10$ eV orbital energies. The quality of the active space (the magnitude of the $\mathbf{S_2}$ amplitudes) is monitored by the %singles character in the IP/EA-EOM eigenvectors. Ideally, all EOM eigenvectors included in the second similarity transformation would have a %singles character above 90%. By default, EOM states that have a %singles character below 70% are discarded from the second transformation, as they may deteriorate the accuracy of the results rather than improve it. Certainly the accuracy would not be predictable if they were included.

Somewhat opposing the %singles character of the included EOM states is the %active character of the resulting STEOM eigenvectors. (The STEOM diagonalization is performed over all orbitals active plus inactive.) The convergence of the energy with the size of the STEOM active space has been observed in practice (*e.g.* reference [3]), and ideally the active space component of the STEOM eigenvectors should exceed 98%, although in actuality we often may need to be satisfied with something like 95%. The STEOM %active character cannot be improved indefinitely as the %singles character of the included IP/EA-EOM eigenvectors would drop too low, and this is considered more of a liability.

As a final check on the accuracy of the results, we calculate the %singles character of the STEOM excited states (in the EOM picture). In other words, we calculate the singles and doubles vector, $\hat{R}_1$ plus $(\hat{S}_2\hat{R}_1)_C$, and monitor the singles component. The %singles character of a STEOM state is considered satisfactory, *i.e.* the state is truly dominated by single excitations, if the character lies above 90%. If not, it is an indication that the state's correlation is not quite "dynamical", and the user should regard the STEOM results with a healthy suspicion. In particular, the system may have low-lying doubly excited states that interfere, and as long as the other indicators are all adequate, results should improve by moving to the extended-STEOM method, although at a substantial increase in computational cost versus regular STEOM. A new and useful intermediate approach is to use a perturbative correction to the STEOM energies, called STEOM+D (unpublished), which incorporates the dominant doubles corrections and which is only slightly more expensive than STEOM itself. The STEOM+D approach cannot access "true" doubly excited states as it is simply a perturbative correction to regular STEOM, but the method does provide a convenient gauge for the accuracy of the STEOM results. For well-behaved singly excited states, STEOM and STEOM+D tend to deviate by less that 0.05 eV, and if the deviation is larger, it provides a fair indication that a more extended treatment may be warranted. The

only published results on the STEOM+D correction at present can be found in Table IV of reference [66].

All of the criteria discussed above can only be guidelines; it is a gray boundary between reliable and suspect. Giving robust error bounds or reliability criteria in this field is difficult, but it is appropriate to say that the STEOM-CCSD method provides an efficient means to calculate a large number of singly excited states with a substantial degree of accuracy. However, the method is not highly systematic, in the sense that it is hard to systematically improve results. On the other hand, there are good, albeit somewhat complicated, internal estimators to judge the resultant accuracy. If the indicators are all clear-cut (all **T** amplitudes smaller than 0.1 in absolute value, %singles in IP/EA-EOM $>$ 90%, %active in STEOM $>$ 98%, and %singles in STEOM $>$ 90%), it is safe to trust the result. If some of the indicators are questionable, the user must exercise judgment, depending on the degree of accuracy needed to provide a reasonable understanding of experimental results. There is only one knob to turn in STEOM-CCSD, the number of states included in the active space, and the results are not especially sensitive to this choice (within reason). Moreover, the knob typically has a clear limit, as the %singles character in the EOM eigenvectors will go down rapidly if too many states are included. In this sense, the lack of systematic improvement in STEOM has its advantages for the user. Most often, it is easy to obtain reliable results. If not, there is no need for endless experimentation with parameters in the calculation. Try another method (or another project) instead.

In general, then, for the manifold of states dominated by singly excited determinants and whose reference state is reasonably well described at the single-reference CCSD level, which comprises a large number of typical systems of interest to quantum chemists, the STEOM-CCSD method is expected to give results accurate to within a few tenths of an eV, often less than 0.1 eV errors, relative to the full CI results. The magnitude of the transformation amplitudes, percent active character, and STEOM percent singles character are useful internal criteria in evaluating the reliability of the STEOM-CCSD results [3,6,12,13].

The STEOM method is most suitable for excitation energies, and this has been the focus of our discussion. The approach can also be used to describe certain multi-reference situations using the DIP- and DEA- variants of STEOM [3,4,14–17]. However, the orbitals used in these approaches are optimized for the parent state having two more or two less electrons than the actual states of interest, and therefore orbital relaxation effects can be expected to be quite important. These are not treated particularly well in STEOM, as the **T** and **S** amplitudes are obtained for states with a different number of electrons, while the diagonalization space in STEOM is too small to include relaxation effects. It typically does not help to redefine the reference orbitals such that they are more suitable for the final states of interest. The preliminary CCSD calculation would then typically yield large $\mathbf{T_1}$ amplitudes, effectively rotating the orbitals back to describe the parent state, and this is generally more deleterious than using orbitals optimized for the parent state in the first place. Despite their clear drawbacks, the DIP- and DEA-STEOM approaches can give easy access to a manifold of multi-configurational states and can be expected to yield semi-quantitative accuracy. This type of approach is typically most suitable if the parent state is neutral or carries one unit of charge. In such instances, the parent state itself is generally a physical state, and the DIP- and DEA- methods can be expected to work satisfactorily if the STEOM criteria discussed above are satisfied. For example, various states of the NO_3^+ cation and their potential energy surfaces have been studied using the DIP-STEOM approach, starting from the well-

behaved ground state of the NO_3^- anion as the parent [15]. In addition, some applications of DIP-STEOM have been presented in which the parent state is a *di*-anion (*e.g.* the vibrational frequencies of ozone have been obtained in this fashion [3]). Such an approach can only work in relatively small basis sets that do not have much diffuse character. Otherwise, the orbitals for the di-anion would describe free electrons at infinity, *i.e.* auto-ionization, and the DIP-STEOM approach would break down. Such problems do not occur for the DEA-STEOM approach, but our experience with this method has been very limited [3,17]. Often, di-cation parents are highly correlated as they typically have compact low-lying virtual valence orbitals. In such cases, the $\mathbf{T_2}$ amplitudes can be large, again deteriorating the results. Even though the DIP-STEOM and DEA-STEOM methods are of somewhat limited use in studies that require spectroscopic accuracy, they are important precursor methods to multi-reference approaches that use similar parameterizations, or generalizations thereof, but in which the orbitals and transformation amplitudes are optimized precisely for the states of interest. The theoretical framework for such approaches has been discussed in reference [162], and initial promising applications of these "internally contracted state-selective multi-reference coupled-cluster" methods have been presented [132,133]. These internally contracted multi-reference theories tend to be rather complicated, although they can be made quite efficient computationally. The need to develop these methods triggered our use of computer-aided implementations, and these methods have been implemented largely in an automated fashion using the Automatic Program Generator (APG) developed by Lotrich and Nooijen (see, for example, reference [132]).

2.2. The (ST)EOM-PT methods

We end this energy discussion by considering the simplified EOM-PT and STEOM-PT methods. In constructing the first similarity transformation that generates $\hat{\bar{H}}$, solving the reference CCSD equations for $\mathbf{T}$ comprises a significant portion of the overall computational cost in a (ST)EOM-CCSD energy calculation (scaling as iterative o^2v^4; see Section 3.3.1). The full-order CCSD $\mathbf{T}$ amplitudes can instead be approximated and replaced by the *first-order* $\mathbf{T}^{(1)}$ amplitudes obtained from Møller–Plesset (MP) [156] many-body perturbation theory (MBPT) (*e.g.* reference [45]), which are much cheaper to calculate. These first-order perturbative $\mathbf{T}^{(1)}$ amplitudes are then used in the $\hat{\bar{H}}$ similarity transformation,

$$\hat{\bar{H}} \equiv e^{-\hat{T}^{(1)}} \hat{H} e^{\hat{T}^{(1)}}, \tag{15}$$

i.e. rather than the $\mathbf{T}$ values obtained from solving the CCSD equations, the perturbative $\mathbf{T}^{(1)}$ values are instead plugged into the detailed CCSD $\bar{\mathbf{H}}$ expressions. Note that *any* similarity transformation preserves the eigenvalues (in the complete diagonalization limit), and choosing the perturbative $\mathbf{T}^{(1)}$ values yields a sound compromise between efficiency and the accuracy of the full CCSD $\mathbf{T}$ solution. Unlike the CCSD method, though, the perturbative $\mathbf{T}^{(1)}$ values do not *fully* eliminate the pure-excitation amplitudes of $\hat{\bar{H}}$ in expression (15); instead, the $\mathbf{T}^{(1)}$ are defined by (*i.e.* eliminate) only the *strictly first-order* component of the CCSD equations. Additionally, the (ST)EOM-PT energy definition is reformulated in terms of a commutator, to exclude the non-vanishing residual pure-excitation components of expression (15) and thereby make the PT-based expressions consistent with the CCSD-based formulation. These modifications will be examined thoroughly below.

Besides these changes to the numerical values of the $\bar{\mathbf{H}}$ amplitudes and the defining equations for $\mathbf{T}^{(1)}$ (and the energy), all other parts of (ST)EOM-PT theory are the same as the (ST)EOM-CCSD theory already described.

This perturbative replacement of the $\mathbf{T}$ amplitudes in $\hat{\bar{H}}$ is of course not the only way to impose simplifying perturbative approximations on the (ST)EOM-CCSD methods. But the approach yields accurate results and is quite simple. For pyridine [1,6], for example, the (ST)EOM-PT excited-state energies are typically within a few tenths of an eV of the corresponding (ST)EOM-CCSD energies. Moreover, the difference between the CCSD-based and PT-based (ST)EOM treatments tends to be highly systematic, meaning that all states shift by a similar amount [1,6]. In free base porphin, whose reference state is more highly correlated and thus whose first-order $\mathbf{T}^{(1)}$ amplitudes differ more substantially from the full-order CCSD $\mathbf{T}$ amplitudes, the differences are found to be somewhat larger and less systematic but are nevertheless reasonable, yielding essentially the same ordering of states in the dense excitation spectrum [2]. Rather than replacing *all* the CCSD amplitudes by their first-order analogs, hybrid (ST)EOM methods can also be devised [11], where the less important $\mathbf{T}$ amplitudes are treated perturbatively while the more important amplitudes are treated to full order, although such methods will not be considered here.

More formal perturbative expansions are also possible, but the additional rigor does not necessarily translate into the same consistent accuracy as above. The CIS(D) method [60, 61], for instance, can be viewed as a second-order perturbative approximation to the EOM-CCSD method. Despite the formal purity, geometry optimizations and frequency calculations have shown [62] that the CIS(D) method can yield erratic results.

Stanton and Gauss have described a general order-by-order hierarchy of MBPT-based EOM methods by submitting $\hat{\bar{H}}$ to a rigorous perturbative expansion [42]. The simplest and most practical of these EOM-CCSD(n) methods, the EOM-CCSD(2) method, employs the same first-order MP $\mathbf{T}^{(1)}$ amplitudes as here. The singles-and-doubles EOM-PT formulation of the present work is in fact equivalent to this EOM-CCSD(2) method [42]: Although the $\bar{h}_0$ element of the present work is given precisely to second order (the MP2 energy), the rest of the $\bar{\mathbf{H}}$ amplitudes of expression (15) are formally of mixed order here; on the other hand, the EOM-CCSD(2) $\bar{\mathbf{H}}$ amplitudes are all strictly up-to second-order. Despite this apparent difference, the singles and doubles matrix elements in the energy expressions of the two methods are identical [42] (using the commutator formulation for the energy here). Admittedly, the extension of the present approach to higher perturbation orders of the reference treatment is not completely clear, but neither is the need for such extensions.

We now consider the first-order equations that define the perturbative $\mathbf{T}^{(1)}$ amplitudes. In MBPT, the bare Hamiltonian, expression (1), is partitioned such that the constant and one-body Fock operator are taken as the zeroth-order Hamiltonian $\hat{H}^{(0)}$ and the two-body component $\hat{V}$ is taken as the perturbing operator. Although this exact partitioning of the electronic Hamiltonian does not require any particular style of orbitals, in this work we will restrict ourselves to canonical Hartree–Fock orbitals in the perturbative variants, and this choice defines the canonical or Møller–Plesset variant of MBPT. For Hartree–Fock (HF) orbitals, the Brillouin condition $f_i^a = f_a^i = 0$ is satisfied, and furthermore, for *canonical* HF orbitals, the Fock matrix is diagonal $f_q^p = \varepsilon_p \delta_{pq}$ (no summation implied on p), where the ε_p are the orbital energies.

The equations $\bar{h}_i^{a(1)}$ and $\bar{h}_{ij}^{ab(1)}$ that determine the first-order $\mathbf{T_1^{(1)}}$ and $\mathbf{T_2^{(1)}}$ amplitudes are the first-order perturbative analogs of the CCSD equations, *i.e.* are the subset of terms in the full-order CCSD $\bar{h}_i^a$ and $\bar{h}_{ij}^{ab}$ expressions that are strictly first-order in the perturbation $\hat{V}$. In the one-body CCSD $\bar{h}_i^a$ expression, all the first-order terms vanish automatically for HF orbitals due to the Brillouin condition, and thus the first-order $\bar{h}_i^{a(1)} = 0$ always. For HF orbitals, then, the $\mathbf{T_1^{(1)}}$ singles amplitudes are not needed (and are discarded everywhere from all the CCSD-based $\bar{\mathbf{H}}$ expressions). In the two-body equation, the first-order component is given by

$$\begin{aligned}
&\bar{h}_{ij}^{ab(1)} \equiv 0 \quad \forall\ i < j,\ a < b, \\
&\bar{h}_{ij}^{ab(1)} = \langle \Phi_{ij}^{ab} | \hat{\bar{H}}_{\mathrm{MP}}^{(1)} | \Phi_0 \rangle = \langle \Phi_{ij}^{ab} | \big[\hat{H}^{(0)}, \hat{T}_2^{(1)} \big] + \hat{V} | \Phi_0 \rangle,
\end{aligned} \tag{16}$$

where the square brackets denote a commutator. Rather than iteratively solving the coupled non-linear CCSD equations for ($\mathbf{T_1}$ and) $\mathbf{T_2}$, the two-body first-order MP analog, equation (16), has an immediate solution for $\mathbf{T_2^{(1)}}$,

$$\begin{aligned}
0 &= V_{ij}^{ab} + \sum_c \big(f_c^a t_{ij}^{cb(1)} + f_c^b t_{ij}^{ac(1)} \big) - \sum_k \big(f_i^k t_{kj}^{ab(1)} + f_j^k t_{ik}^{ab(1)} \big) \\
&= V_{ij}^{ab} + (\varepsilon_a + \varepsilon_b - \varepsilon_i - \varepsilon_j) t_{ij}^{ab(1)}, \\
t_{ij}^{ab(1)} &= \frac{-V_{ij}^{ab}}{(\varepsilon_a + \varepsilon_b - \varepsilon_i - \varepsilon_j)} \quad \forall\ i < j,\ a < b,
\end{aligned} \tag{17}$$

where the diagonal Fock matrix for canonical HF orbitals has been employed. Solution for the MP $t_{ij}^{ab(1)}$ amplitudes thus amounts to simple division by an energy denominator. (This same dramatic simplification will also occur in the analytical gradient equations, in the solution for the $\mathbf{Z_2}$ Lagrange multipliers associated with the $\mathbf{T_2^{(1)}}$.)

Note that in this formulation, only the first-order $\bar{h}_i^{a(1)}$ and $\bar{h}_{ij}^{ab(1)}$ expressions are made to vanish, whereas the actual $\bar{h}_i^a$ and $\bar{h}_{ij}^{ab}$ amplitudes of the (ST)EOM-PT $\hat{\bar{H}}$, defined by the similarity transformation in expression (15), do not completely vanish. In other words, the CCSD equations, equations (4) or (8), are no longer rigorously satisfied, and thus by using the perturbative $\mathbf{T}^{(1)}$ values, $\hat{\bar{H}}$ does *not* have its pure-excitation amplitudes fully eliminated. The residual one-body $\bar{h}_i^a$ amplitudes would then in principle allow the pure-excitation $\{\hat{a}^\dagger \hat{i}\}$ operators to participate in the $\hat{\bar{H}}$ and $\hat{G}_2$ energy diagonalizations; likewise, these residual pure-excitation operators would also in principle participate in the $\mathbf{S}^{\pm}$ equations (9) and (10). These potential complications, however, are avoided by formally introducing commutators everywhere that the residual pure-excitation operators would contribute. The commutators have *no* numerical effect in the CCSD-based formulation, as the pure-excitation amplitudes that they exclude are always rigorously vanishing anyway. In the PT-based methods, these formal commutators allow one to simply ignore the residual $\bar{h}_i^a$ and $\bar{h}_{ij}^{ab}$ amplitudes of the perturbative $\hat{\bar{H}}$, expression (15). The commutator formulation is equivalent to the assumption that these residual pure-excitation amplitudes are actually fully vanishing and need not be included in the detailed algebraic expressions. The commutator form makes the PT-based expressions consistent with the CCSD-based

expressions, by mutually forcing the absence of the pure-excitation terms, and the formulation will be examined carefully in conjunction with the Lagrange multiplier functionals later (Sections 3.2 and 5.3.1).

The use here of the commutator form gives (singles and doubles) EOM-PT expressions identical to the order-by-order treatment of the EOM-CCSD(2) method [42]. The commutator formulation also arises in other perturbative derivations, such as in diagrammatic Green's function CC theory [51–53], where the pure-excitation terms cannot participate as they would lead to diagrammatically disconnected contributions. The commutator arises naturally in such theories that focus on the excitation energy, although these do not provide an unambiguous definition of the *total* energy, which is needed for the gradient. Excluding the residual pure-excitation amplitudes yields consistent CCSD/PT-based expressions and moreover *maintains size-extensivity*. We note, however, that by ignoring these residual operators, the rigorous connection to the full CI limit is lost for the PT-based methods, in the sense that diagonalizing over the full Hilbert space no longer gives the exact result. This choice is made in the definition of (ST)EOM-PT, as the value of maintaining size-extensivity upon truncated diagonalization of the transformed Hamiltonian is considered far more important than the formal exactness of the theory upon (a hypothetical) full diagonalization.

To summarize the present PT-based (ST)EOM energy formulation: Rather than solving the expensive iterative CCSD equations for $\mathbf{T}$, the perturbative $\mathbf{T}^{(1)}$ values are used instead, where $\mathbf{T}_\mathbf{1}^{(1)} = \mathbf{0}$ (with HF orbitals) and $\mathbf{T}_\mathbf{2}^{(1)}$ is given by equation (16), the first-order MP component of the CCSD $\bar{h}_{ij}^{ab}$ equation, which has an instant solution, expression (17). Additionally, the residual pure-excitation amplitudes in the transformed Hamiltonian are assumed to vanish fully and are ignored (or rather are formally excluded by introducing commutators); disregarding these residual pure-excitation amplitudes keeps the PT-based expressions consistent with the CCSD-based expressions and maintains size-extensivity. Equivalently, the pure-excitation amplitudes of $\hat{\bar{H}}$ are taken as the strictly first-order perturbative $\bar{h}_i^{a(1)}$ and $\bar{h}_{ij}^{ab(1)}$ expressions, whereas the rest of the $\bar{\mathbf{H}}$ amplitudes are defined in the standard way according to the similarity transformation of expression (15).

From a practical standpoint relative to the CCSD-based (ST)EOM formulation, the above (ST)EOM-PT summary thus amounts to

1. a simplification of the detailed $\bar{\mathbf{H}}$ expressions by removing all terms involving $\mathbf{T_1}$,
2. the elimination of the one-body $\bar{h}_i^a$ equation, and
3. the substantial reduction of the $\bar{h}_{ij}^{ab}$ equation and its solution by expressions (16) and (17).

Besides these simplifications to the CCSD $\bar{\mathbf{H}}$ formulas, and the procedural bypass of the expensive solution for $\mathbf{T}$, all other parts of the (ST)EOM-PT energy theory are the same as that of (ST)EOM-CCSD energy theory. (The PT-based $\bar{\mathbf{H}}$ simplifications will also lead to simplifications in the analytical gradient expressions, and a straightforward prescription for identifying the (ST)EOM-PT components in the detailed (ST)EOM-CCSD gradient equations will be described in Section 5.1.1.)

In closing, we mention that throughout the paper, we have been careful to distinguish between the general truncation of the CC equations and $\hat{\bar{H}}$ diagonalization and the particular singles-and-doubles truncation. Unambiguously, EOM-CCSD, STEOM-CCSD, and CCSD-based refer to the singles-and-doubles truncation both in the coupled-cluster equa-

tions and in the diagonalization of $\hat{\tilde{H}}$. When we refer to EOM-PT, STEOM-PT, and PT-based, we will always mean first-order MP-based MBPT to obtain the singles and doubles $\mathbf{T}^{(1)}$ amplitudes, and also a single-and-doubles diagonalization of $\hat{\tilde{H}}$. Finally, when we refer to CC/PT, EOM-CC/PT, or STEOM-CC/PT, we are leaving unspecified the reference CC truncation scheme (*e.g.* CCSD, CCSDT, *etc.*) and the details of the perturbative variant. The EOM-CC/PT diagonalization of $\hat{\tilde{H}}$ would be of the same truncation level as the reference CC/PT equations, and the classic truncation for the STEOM diagonalization would be one excitation level less than the EOM-CC/PT treatment, but other truncations (and additional net-excitation-operator eliminations) may also be reasonable [12,13,63,64].

3. THE ENERGY GRADIENT AND LAGRANGE MULTIPLIERS (ABSTRACT EXPRESSIONS)

3.1. Lagrange's method of undetermined multipliers

Given the energy expression for a particular electronic structure method, $E(\mathbf{H}, \mathbf{C}, \mathbf{T})$, which depends on the set of Hamiltonian amplitudes $\mathbf{H}$ (with elements h_μ), the variational wavefunction parameters $\mathbf{C}$ (with elements c_γ), and the non-variational wavefunction parameters $\mathbf{T}$ (with elements t_ν), a direct expression for the first derivative of the electronic energy with respect to a perturbation χ would be

$$\frac{\partial E(\mathbf{H}, \mathbf{C}, \mathbf{T})}{\partial \chi} = \sum_\mu \frac{\partial E}{\partial h_\mu} \frac{\partial h_\mu}{\partial \chi} + \sum_\gamma \underbrace{\frac{\partial E}{\partial c_\gamma}}_{0} \frac{\partial c_\gamma}{\partial \chi} + \sum_\nu \frac{\partial E}{\partial t_\nu} \frac{\partial t_\nu}{\partial \chi}. \tag{18}$$

(Note that the derivative of the *total* energy also includes the nuclear contributions, in the Born–Oppenheimer approximation.)

By definition, the energy is stationary with respect to the variational parameters $\mathbf{C}$, or more precisely, the variational parameters $\mathbf{C}$ are determined by making the energy stationary with respect to these parameters. The derivatives $\partial E/\partial \mathbf{C}$ (and thus $\partial \mathbf{C}/\partial \chi$) vanish immediately from the gradient.

The non-variational wavefunction parameters $\mathbf{T}$ are determined from an equal number of supplementary equations

$$q_\nu(\mathbf{H}, \mathbf{T}) \equiv 0 \quad \forall\ \nu, \tag{19}$$

which do not depend on the variational parameters $\mathbf{C}$. The gradient expression (18) requires the derivatives of the non-variational parameters, $\partial \mathbf{T}/\partial \chi$, which in principle could be obtained by differentiating equations (19) with respect to the perturbation. However, the resulting coupled set of linear equations would need to be re-solved separately for each degree of freedom, and such a complication would be rate limiting and must be avoided. A general technique to eliminate the obstacle of computing $\partial \mathbf{T}/\partial \chi$ is through Lagrange's method of undetermined multipliers [111–115].

An energy functional is created

$$F(\mathbf{H}, \mathbf{C}, \mathbf{T}, \mathbf{Z}) \equiv E(\mathbf{H}, \mathbf{C}, \mathbf{T}) + \sum_\nu z_\nu q_\nu(\mathbf{H}, \mathbf{T}), \tag{20}$$

consisting of the energy expression plus all the supplementary equations that determine the non-variational parameters $\mathbf{T}$, each constraint equation q_ν tensor-multiplied by a single undetermined parameter z_ν called a Lagrange multiplier. Note there are precisely an equal number of Lagrange multipliers z_ν as there are non-variational parameters t_ν. The derivatives of the functional with respect to these new parameters simply yield the constraint equations (19), which vanish when satisfied. When the non-variational parameter equations (19) are solved, therefore, the functional is automatically stationary with respect to the Lagrange multipliers, regardless of their numerical values. Likewise, the numerical value of the functional is simply the energy itself. Finally, both the functional and the energy have numerically equal perturbation derivatives,

$$\frac{\partial F}{\partial \chi} = \frac{\partial E}{\partial \chi} + \sum_\nu \frac{\partial z_\nu}{\partial \chi} \underbrace{q_\nu}_{0} + \sum_\nu z_\nu \underbrace{\frac{\partial q_\nu}{\partial \chi}}_{0}, \tag{21}$$

where the last term is zero by definition and determines $\partial \mathbf{T}/\partial \chi$ (*i.e.* the constraint equations are defined to vanish for all perturbations, thereby determining the perturbed $\mathbf{T}$ parameters).

The so-far undetermined Lagrange multipliers can be chosen such that they precisely eliminate the factors in the original gradient expression (18) that multiply the troublesome derivatives $\partial \mathbf{T}/\partial \chi$. In other words, the Lagrange multipliers provide the precise freedom to define the energy *functional* to be variational with respect to the non-variational *energy* parameters. The equations that determine the Lagrange multipliers $\mathbf{Z}$ are thus chosen as

$$\frac{\partial F(\mathbf{H}, \mathbf{C}, \mathbf{T}, \mathbf{Z})}{\partial t_\nu} \equiv 0 \quad \forall\ \nu. \tag{22}$$

Importantly, this coupled set of linear equations is *independent* of the perturbation and the number of degrees of freedom of the system. The troublesome $\partial \mathbf{T}/\partial \chi$ are thus excluded, and the energy gradient becomes [111]

$$\begin{aligned} \frac{\partial F(\mathbf{H}, \mathbf{C}, \mathbf{T}, \mathbf{Z})}{\partial \chi} &= \sum_\mu \frac{\partial F}{\partial h_\mu} \frac{\partial h_\mu}{\partial \chi} + \sum_\gamma \underbrace{\frac{\partial F}{\partial c_\gamma}}_{0} \frac{\partial c_\gamma}{\partial \chi} + \sum_\nu \underbrace{\frac{\partial F}{\partial t_\nu}}_{\equiv 0} \frac{\partial t_\nu}{\partial \chi} + \sum_\nu \underbrace{\frac{\partial F}{\partial z_\nu}}_{q_\nu = 0} \frac{\partial z_\nu}{\partial \chi} \\ &= \sum_\mu \frac{\partial F}{\partial h_\mu} \frac{\partial h_\mu}{\partial \chi}, \end{aligned} \tag{23}$$

where the first zero $\partial F/\partial c_\gamma$ reduces to $\partial E/\partial c_\gamma = 0$ because the constraint equations (19) are independent of $\mathbf{C}$, the second zero determines the Lagrange multipliers by equations (22), and the third zero is given by the satisfaction of the constraint equations (19).

Although equivalent, as shown in expression (21), the gradient of the energy functional, expression (23), is a very different expression than the gradient of the bare energy, expression (18). The complication of calculating the perturbation-dependent derivatives $\partial \mathbf{T}/\partial \chi$ of the non-variational parameters (as well as the $\partial \mathbf{Z}/\partial \chi$ of the Lagrange multipliers) has been avoided, at the cost of solving a single set of linear perturbation-independent equations (22). (It might also be argued that, in some sense, the variational parameters $\mathbf{C}$ act as their own mutual Lagrange multipliers, eliminating the need to calculate $\partial \mathbf{C}/\partial \chi$. This interpretation will be considered explicitly in the next section for the EOM functional.)

With the solution of the Lagrange multiplier equations, the functional becomes variational with respect to all of its wavefunction parameters, and the generalized Hellmann–Feynman (GHF) theorem [90–92] applies. Expression (23) for the gradient is the GHF relation

$$\frac{\partial F(\mathbf{H},\mathbf{C},\mathbf{T},\mathbf{Z})}{\partial \chi} = \frac{\partial h_0}{\partial \chi} + \sum_{p,q} D_p^q(\mathbf{C},\mathbf{T},\mathbf{Z}) \frac{\partial f_q^p}{\partial \chi} + \sum_{p<q,\, r<s} D_{pq}^{rs}(\mathbf{C},\mathbf{T},\mathbf{Z}) \frac{\partial V_{rs}^{pq}}{\partial \chi}, \tag{24}$$

where the effective (relaxed) density matrix elements [41,100–104]

$$D_p^q(\mathbf{C},\mathbf{T},\mathbf{Z}) \equiv \frac{\partial F}{\partial f_q^p} \quad \text{and} \quad \big(D_{pq}^{rs}(\mathbf{C},\mathbf{T},\mathbf{Z})\big)_{p<q,\, r<s} \equiv \frac{\partial F}{\partial V_{rs}^{pq}} \tag{25}$$

and $D_0 = 1$ are obtained as the derivatives of the Lagrange multiplier energy functional with respect to the (bare) Hamiltonian amplitudes. Note that the upper and lower indices on D_μ (and also $\bar{D}_\mu$ later) are exchanged relative to the Hamiltonian amplitude h_μ (or $\bar{h}_\mu$) with respect to which the functional was differentiated. These $\partial F/\partial \mathbf{H}$ derivatives do not contain *any* dependence on the perturbation; their expressions depend only on the definition of the energy functional for the particular method. The effective density matrix is not a true density; it contains *both* the fundamental (biorthogonal-) wavefunction density (often called the reduced density) and the response contributions from the non-variational parameters, through the Lagrange multipliers.

The GHF expression (24) has enormous appeal in that the analytical gradients of a variety of electronic structure methods have been formulated in this unified way and can subsequently use the same computer code for evaluation. In particular, the $\partial \mathbf{H}/\partial \chi$ derivatives, which isolate all of the degree-of-freedom dependence, are treated efficiently by a general procedure [100,101] that evaluates the GHF expression (24) in the atomic orbital (AO) basis. The process is identical for all SCF-based electronic methods, as it only depends on the underlying Hartree–Fock equations. An overview of the conversion of expression (24) to the efficiently calculated AO-based expression is presented in Section 5.7.1, and its three major steps are outlined here. The preliminary step is the combination of the reference-determinant contributions contained in h_0 and f_q^p with the above D_μ correlated contributions from the electronic method into a *total* effective density matrix, which is contracted with the fundamental Hamiltonian-integral derivatives. Next, the Hamiltonian derivative expressions are converted to the AO basis, eliminating the expensive molecular orbital (MO) coefficient derivatives [163] by a Z-vector [101,108–110] or Lagrange multiplier [118,120] construction. Finally, the MO-based total effective density matrix, after addition of the remaining MO-response contribution, is transformed to the AO basis and is traced directly with the Hamiltonian-integral derivatives in their native AO form. This AO-based evaluation of expression (24) avoids the perturbation-dependent MO-coefficient derivatives, the associated transformation of the AO Hamiltonian-integral derivatives to the MO basis, and the storage of the Hamiltonian-integral derivatives. The above general procedure has been implemented, for instance, in the ACES II package by Gauss, Stanton, and Bartlett [110] in conjunction with CCSD gradients, and the same module of computer code is immediately applicable here. Likewise, for instance, the code available in ACES II for dropped-core gradients [164,165] can be utilized directly as well.

Except for the construction of the MO-based effective density matrix **D** for each electronic method, the remainder of a (ST)EOM-CCSD/PT gradient calculation then proceeds essentially identically in ACES II to a ground-state CC/MBPT gradient. As will be shown in the next two sections, the construction of the effective density matrix itself for each method will also be formulated to maximize uniformity and the reuse of computer code, through the definition of an intermediate density matrix.

3.2. The EOM-CC/PT intermediate and effective density matrices

In this section, we apply the Lagrange multiplier formalism to write the EOM-CC/PT intermediate and effective density matrices in *abstract operator* form. The corresponding *explicit algebraic* spatial-orbital expressions for the closed-shell-reference EE-, IP-, and EA-EOM-CCSD/PT variants are presented in Section 5. Rather than by expanding the abstract derivative expressions presented in this section, however, we emphasize that the algebraic derivative expressions of Section 5 were instead obtained directly, by automated symbolic differentiation of the algebraic energy functionals in *SMART*.

In the present formulation, chain-rule derivatives are constructed through the common, transformed Hamiltonian $\bar{\mathbf{H}}$ amplitudes and yield a compact and uniform structure where the EOM-variant dependence is isolated sooner in an intermediate density matrix $\bar{\mathbf{D}}$, prior to the full effective density matrix **D**. The chain-rule/intermediate-density formulation separates out the parts of the gradient expressions that depend only on the underlying CC or PT reference treatment, establishing otherwise method-independent (**Z**) Lagrange multiplier equations and method-independent conversion expressions to the final GHF **D** that are the same for all the EOM variants. Besides the method-dependent $\bar{\mathbf{D}}$, which isolate the unique post-CC/PT information of each electronic method, these other components of the EOM-CCSD/PT gradients will be identical to those needed for STEOM-CCSD/PT gradients.

We begin with a definition for the EOM-CC/PT Lagrange multiplier energy functional and will show that all of the equations that define the energy and the gradient are obtained from appropriate derivatives. The (general excitation-level) EOM-CC/PT energy functional can be constructed as

$$F \equiv \bar{h}_0 + \langle \Phi_0 | \hat{L} [\hat{\bar{H}}, \hat{R}] | \Phi_0 \rangle + \lambda \big(1 - \langle \Phi_0 | \hat{L} \hat{R} | \Phi_0 \rangle\big) + \langle \Phi_0 | \hat{Z} \hat{\bar{H}} | \Phi_0 \rangle, \tag{26}$$

where the particular EE-, IP-, or EA- variant is determined by the diagonalization operator $\hat{R}$. Differentiating with respect to the Lagrange multipliers (**L**, λ, and **Z**) yields all the supplementary constraint equations that define the energy parameters (**R** and **T**). Conversely, differentiating with respect to the energy parameters yields the equations that determine the associated Lagrange multipliers. When all equations are solved, the functional becomes stationary with respect to first-order variations in any of its parameters, and its perturbation derivative is obtained through the GHF effective density matrix and the response of the Hamiltonian amplitudes only.

Before considering the gradient equations, let us first examine individually the pieces that make up the energy functional. In the EOM-CC methods, an electronic state is obtained as an eigenvector of the non-Hermitian, singly transformed Hamiltonian $\hat{\bar{H}}$, and its energy

is given by

$$E = \frac{\langle \Phi_0 | \hat{L} \hat{\bar{H}} \hat{R} | \Phi_0 \rangle}{\langle \Phi_0 | \hat{L} \hat{R} | \Phi_0 \rangle}, \tag{27}$$

consisting of the state's biorthogonal expectation value and the normalizing denominator. For now, we will keep this familiar representation of the energy and will later discuss the reason for rewriting it as the commutator form that appears in the functional (26).

If we restrict ourselves to normalized eigenvectors, this supplementary constraint on the energy parameters can be incorporated through a Lagrange multiplier. Namely, the Lagrange multiplier functional of the energy (27) under the constraint that the eigenvectors are normalized is

$$\underset{\sim}{F} \equiv \langle \Phi_0 | \hat{L} \hat{\bar{H}} \hat{R} | \Phi_0 \rangle + \lambda \big(1 - \langle \Phi_0 | \hat{L} \hat{R} | \Phi_0 \rangle \big) \tag{28}$$

(where the denominator $\langle \Phi_0 | \hat{L} \hat{R} | \Phi_0 \rangle = 1$ has been removed). This same Lagrange multiplier procedure was used, for instance, to incorporate the normalization condition in the linear variational (CI) problem by Szabo and Ostlund [116]. Enforcing stationarity of the functional with respect to the Lagrange multiplier λ yields

$$\frac{\partial \underset{\sim}{F}}{\partial \lambda} = 1 - \langle \Phi_0 | \hat{L} \hat{R} | \Phi_0 \rangle \equiv 0, \tag{29}$$

and thus, if the eigenvectors are normalized, the functional is automatically stationary with respect to first-order variations in λ.

Both the energy expression (27) and the energy functional (28) are stationary with respect to the (bi-) variational wavefunction parameters **L** and **R**, and this stationarity determines the value of the Lagrange multiplier λ. The energy expression (27) is automatically variational with respect to **L** and **R**, as making these derivatives vanish yields the right- and left-hand eigenvector equations, respectively. Likewise, stationarity of the energy functional (28) with respect to the **L** amplitudes yields the eigenvector equations for the right-hand **R** amplitudes,

$$\frac{\partial \underset{\sim}{F}}{\partial l_\mu} = \langle \Phi_\mu | \hat{\bar{H}} \hat{R} | \Phi_0 \rangle - \lambda \langle \Phi_\mu | \hat{R} | \Phi_0 \rangle \equiv 0 \quad \forall\ \mu, \tag{30}$$

with the identification that the Lagrange multiplier λ is the energy eigenvalue E (the compound index μ will be defined below). Conversely, stationarity with respect to the **R** amplitudes returns the left-hand eigenvector equations that define **L**,

$$\frac{\partial \underset{\sim}{F}}{\partial r_\mu} = \langle \Phi_0 | \hat{L} \hat{\bar{H}} | \Phi_\mu \rangle - \lambda \langle \Phi_0 | \hat{L} | \Phi_\mu \rangle \equiv 0 \quad \forall\ \mu. \tag{31}$$

Thus, if the EOM-CC eigenvector equations are solved for the **L** and **R** amplitudes, the functional (28), like the energy expression (27), is variational with respect to these parameters.

The variational parameters **L** and **R** can be viewed to act as mutual Lagrange multipliers. The **L** amplitudes can be considered as Lagrange multipliers for the eigenvector constraint that determines the **R** amplitudes, equations (30). Vice versa, the **R** amplitudes can be considered as Lagrange multipliers for the constraint that determines the **L** amplitudes, equations (31). This interpretation of **R** as the wavefunction parameters and **L** as the

associated Lagrange multipliers (or vice versa) is appealing, since determining the energy by itself requires only one set of amplitudes, in contrast to expression (27) which seems to imply that both sets are needed.

We now define the compound index μ. In contrast to the Z-vector formulation for the EOM-CC/PT gradient [37–42], the Lagrange multiplier formulation has no need to consider the multitude of determinants that have higher excitation level than the diagonalization space $|\mathbf{\Phi_\mu}\rangle$. For EE-EOM-CCSD/PT, the diagonalization space $|\mathbf{\Phi_\mu}\rangle$ is taken as the set of all determinants related to the reference configuration by promotion of one or two electrons from occupied to virtual orbitals; the associated wavefunction operators have $1h1p$ and $2h2p$ components and the spin-orbital form

$$\hat{R} = \sum_{i,a} r_i^a \{\hat{a}^\dagger \hat{i}\} + \sum_{i<j,\, a<b} r_{ij}^{ab} \{\hat{a}^\dagger \hat{i} \hat{b}^\dagger \hat{j}\} \tag{32}$$

and

$$\hat{L} = \sum_{i,a} l_a^i \{\hat{i}^\dagger \hat{a}\} + \sum_{i<j,\, a<b} l_{ab}^{ij} \{\hat{j}^\dagger \hat{b} \hat{i}^\dagger \hat{a}\}. \tag{33}$$

Note that in this diagonalization, we choose not to consider the components of the Hamiltonian or the eigenvector along $|\Phi_0\rangle$, as these are not needed to determine the excited-state energies. Examining the EE-EOM-CCSD right-hand *full* eigenvector equation $\bar{\mathbf{H}}\underset{\sim}{\mathbf{R}} = E\underset{\sim}{\mathbf{R}}$ schematically,

$$\begin{pmatrix} \bar{h}_0 & \bar{\mathbf{H}}_{0;\boldsymbol{\mu}} \\ \mathbf{0}_{\boldsymbol{\mu};0} & \bar{\mathbf{H}}_{\boldsymbol{\mu};\boldsymbol{\mu}} \end{pmatrix} \begin{pmatrix} r_0 \\ \mathbf{R} \end{pmatrix} = E \begin{pmatrix} r_0 \\ \mathbf{R} \end{pmatrix} = \begin{pmatrix} \bar{h}_0 r_0 + \bar{\mathbf{H}}_{0;\boldsymbol{\mu}} \mathbf{R} \\ \bar{\mathbf{H}}_{\boldsymbol{\mu};\boldsymbol{\mu}} \mathbf{R} \end{pmatrix}, \tag{34}$$

where the matrices are partitioned into blocks $|\Phi_0\rangle$ and $|\mathbf{\Phi_\mu}\rangle = |\mathbf{\Phi_i^a}\rangle \oplus |\mathbf{\Phi_{ij}^{ab}}\rangle$, shows that the excited-state energies can be obtained from the "singles-and-doubles" eigenvector equation $\bar{\mathbf{H}}_{\boldsymbol{\mu};\boldsymbol{\mu}}\mathbf{R} = E\mathbf{R}$. As a result, the vectors defined by operators (32) and (33) are not true eigenvectors of the transformed Hamiltonian truncated at doubles and including the $|\Phi_0\rangle$ column and row, as they are missing the $|\Phi_0\rangle$ element, but these eigenvectors of the singles-and-doubles submatrix $\bar{\mathbf{H}}_{\boldsymbol{\mu};\boldsymbol{\mu}}$ are sufficient to define the excited-state energy and the energy gradient. (Tangentially, we note that the energy functional for the reference CC/PT state $|\Phi_0\rangle$ *can* in fact be obtained from the EOM-CC/PT functional (26) by excluding all dependence on $\hat{L}$ and $\hat{R}$.)

For the IP-EOM-CCSD/PT variant, the $\hat{R}$ operator contains $1h$ and $2h1p$ components, and for the EA-EOM-CCSD/PT variant, $\hat{R}$ contains $1p$ and $2p1h$ components; the $\hat{L}$ is the corresponding conjugate operator in each variant. For the IP- and EA- methods, the $|\Phi_0\rangle$ block of $\bar{\mathbf{H}}$ is completely decoupled, as $\bar{\mathbf{H}}_{0;\boldsymbol{\mu}} = \mathbf{0}$ and $\mathbf{0}_{\boldsymbol{\mu};0} = \mathbf{0}$ automatically in expression (34) because the number of electrons is different than that of $|\mathbf{\Phi_\mu}\rangle$ and $\hat{H}$ is a particle-conserving operator.

For the PT-based methods, however, the pure-excitation operators as previously discussed are not eliminated *fully*. Thus for the EE-EOM-PT variant, the $\mathbf{0}_{\boldsymbol{\mu};0}$ subvector of $\bar{\mathbf{H}}$ in expression (34), which justifies the exclusion of the r_0 element, does not vanish completely, and for all the PT-based variants, the residual one-body pure-excitation $\bar{h}_i^a$ amplitude would also in principle contribute to the $\bar{\mathbf{H}}_{\boldsymbol{\mu};\boldsymbol{\mu}}$ submatrix. These difficulties can be alleviated by rewriting the total energy, the biorthogonal expression (27), as the sum of the reference energy $\bar{h}_0$ plus the excitation energy formulated in terms of a commutator.

This commutator purposefully excludes the residual pure-excitation terms from appearing in the energy expressions.

Let us compare the biorthogonal and commutator formulations of the energy in more detail. Although the following discussion is phrased in terms of the abstract expressions, the ultimate focus is on the slight difference that results *in the detailed algebraic expressions*, that is, the presence or not of pure-excitation terms. Without assumption,

$$\langle\Phi_0|\hat{L}\hat{\bar{H}}\hat{R}|\Phi_0\rangle = \langle\Phi_0|\hat{L}[\hat{\bar{H}},\hat{R}]|\Phi_0\rangle + \langle\Phi_0|\hat{L}\hat{R}\hat{\bar{H}}|\Phi_0\rangle. \tag{35}$$

The only components of $\hat{\bar{H}}$ that can contribute in the last term above are those that do not annihilate $|\Phi_0\rangle$ in normal-order (*i.e.* do not contain any q-annihilation operators), namely the constant $\bar{h}_0$ and the pure-q-creation (pure-excitation) part

$$\langle\Phi_0|\hat{L}\hat{R}\hat{\bar{H}}|\Phi_0\rangle = \bar{h}_0\langle\Phi_0|\hat{L}\hat{R}|\Phi_0\rangle + \langle\Phi_0|\hat{L}\hat{R}\hat{\bar{H}}_{\text{pure-excitation}}|\Phi_0\rangle. \tag{36}$$

Therefore, assuming normalized eigenvectors, expression (35) becomes

$$\langle\Phi_0|\hat{L}\hat{\bar{H}}\hat{R}|\Phi_0\rangle = \bar{h}_0 + \langle\Phi_0|\hat{L}[\hat{\bar{H}},\hat{R}]|\Phi_0\rangle + \langle\Phi_0|\hat{L}\hat{R}\hat{\bar{H}}_{\text{pure-excitation}}|\Phi_0\rangle, \tag{37}$$

strictly. *The biorthogonal energy expression* $\langle\Phi_0|\hat{L}\hat{\bar{H}}\hat{R}|\Phi_0\rangle$ *thus technically contains pure-excitation* $\bar{\mathbf{H}}$ *contributions according to the last term of expression* (37).

In the CCSD-based EOM variants, the only pure-excitation $\hat{\bar{H}}$ operators that can fully contract with $\hat{L}\hat{R}$ in the last term of expression (37) involve the one-body $\bar{h}_i^a$ amplitudes (and the resulting algebraic terms are given in expression (97) of Section 5.3.1). But since $\bar{h}_i^a$ is rigorously set to zero by the CCSD equations, these vanishing pure-excitation terms can in fact be discarded from the detailed algebraic expansion, with no *numerical* effect on the energy. In other words, since the last term of expression (37) is rigorously zero for CCSD-based methods, the commutator representation of the energy is ultimately equivalent to the biorthogonal representation, but the *detailed algebraic expressions* differ slightly by the removed pure-excitation terms.

For the PT-based methods, on the other hand, the pure-excitation $\bar{h}_i^a$ amplitudes are only eliminated to first-order, and thus the last term of expression (37) does not vanish fully. However, excluding this residual term is advantageous for maintaining size-extensivity, as discussed in Section 2.2. Thus this residual term is discarded, as is normally done, and the commutator form of the energy,

$$\langle\Phi_0|\hat{L}\hat{\bar{H}}\hat{R}|\Phi_0\rangle = \bar{h}_0 + \langle\Phi_0|\hat{L}[\hat{\bar{H}},\hat{R}]|\Phi_0\rangle, \tag{38}$$

while rigorously equivalent for the CCSD-based methods, is also assumed applicable to the PT-based methods. In this way, the commutator formulation allows for a unified EOM-CC/PT functional, expression (26).

While excluding the pure-excitation terms from the CC-based algebraic expressions has no effect on the final *energy*, it may not immediately be apparent that this exclusion also has no effect on the final *gradient*. Fundamentally, if the gradient were obtained numerically, then the perturbed pure-excitation coefficients would be made to vanish for every perturbation, *e.g.* $\bar{h}_i^a(\chi) \equiv 0 \;\forall\; \chi$, and therefore inclusion/exclusion of these rigorous zeros for all perturbations can affect neither the final numerical nor analytical gradient. The detailed algebraic expressions for the gradient, however, *are* slightly different; but this difference amounts to a repartitioning of the intermediate quantities, which cancels itself in

the end to yield numerically identical GHF effective density matrices. This property will be demonstrated explicitly for the EOM-CCSD gradient (Section 5.3.1). For the PT-based methods, as expected, only the exclusion of the pure-excitation terms, through the formal commutator above, is consistent with the gradients that would be obtained numerically.

Having considered the energy and normalization terms, the EOM-CC/PT functional (26) contains another Lagrange multiplier term $\langle \Phi_0 | \hat{Z} \hat{\bar{H}} | \Phi_0 \rangle$ associated with the underlying CC/PT constraint that determines the non-variational reference-state parameters $\mathbf{T}$. By construction, differentiating the functional with respect to the associated Lagrange multipliers $\mathbf{Z}$ and setting the results to zero yields the CC/PT equations for $\mathbf{T}$,

$$\frac{\partial F}{\partial z_\nu} = \langle \Phi_\nu | \hat{\bar{H}} | \Phi_0 \rangle = \bar{h}_\nu \equiv 0 \quad \forall\ \nu, \tag{39}$$

where the compound index ν is implicitly defined below. As with all Lagrange multipliers, solving the constraint equations ensures by design that the functional is stationary with respect to the associated Lagrange multipliers (and regardless of their numerical values). For CCSD-based methods, the $\hat{Z}$ operator has one- and two-body components and the spin-orbital form

$$\hat{Z} = \sum_{i,a} z_a^i \{\hat{i}^\dagger \hat{a}\} + \sum_{i<j,\, a<b} z_{ab}^{ij} \{\hat{i}^\dagger \hat{a}\, \hat{j}^\dagger \hat{b}\}. \tag{40}$$

Note that the Lagrange multiplier operator (40) is the pure *de-excitation* analog of the pure-*excitation* components of the transformed Hamiltonian that are made to vanish through the CCSD equations (4). For the PT-based methods, the one-body term in $\hat{Z}$ is not present (since there are no associated $\mathbf{T}_\mathbf{1}^{(1)}$), and the first-order $\hat{\bar{H}}_{\mathrm{MP}}^{(1)}$ that defines $\mathbf{T}_\mathbf{2}^{(1)}$, in equation (16), is used in the $\langle \Phi_0 | \hat{Z} \hat{\bar{H}} | \Phi_0 \rangle$ Lagrange multiplier term,

$$\langle \Phi_0 | \hat{Z} \hat{\bar{H}}_{\mathrm{MP}}^{(1)} | \Phi_0 \rangle = \langle \Phi_0 | \hat{Z}_2 \big(\big[\hat{H}^{(0)}, \hat{T}_2^{(1)} \big] + \hat{V} \big) | \Phi_0 \rangle; \tag{41}$$

this simplification of the pure-excitation expressions is the only difference between the (ST)EOM-CCSD and (ST)EOM-PT functionals.

Table 3 of Section 5 presents the Lagrange multiplier energy functionals of the closed-shell-reference EE-, IP-, and EA-EOM-CCSD/PT variants in explicit spin-adapted spatial-orbital algebraic terms. These relatively simple expressions can be obtained by algebraic or diagrammatic expansion of the abstract functional, expression (26), and are little more than the defining equations of these EOM methods. The explicit algebraic functionals serve as the input to the *SMART* differentiation package, and *all* subsequent derivative expressions in Section 5 are obtained directly by symbolic algebraic differentiation. We emphasize the contrast with more traditional techniques, where an expansion might instead be performed algebraically or diagrammatically on the (more complicated) abstract derivative expressions, which follow in the remainder of this section.

We see above that by solving the appropriate EOM eigenvector and CC/PT equations, the EOM-CC/PT functional (26) is automatically stationary with respect to first-order variations in *all* parameters *except* the reference-state $\mathbf{T}$ amplitudes. Moreover, the $\mathbf{Z}$ Lagrange multipliers are still unspecified. Forcing this remaining stationarity with respect to $\mathbf{T}$ determines the associated Lagrange multipliers $\mathbf{Z}$ and excludes the expensive derivatives $\partial \mathbf{T} / \partial \chi$ from appearing in the final gradient expression (see expression (23)). The resulting set of

linear equations for the $\mathbf{Z}$ amplitudes is given by

$$\begin{aligned}
&\frac{\partial}{\partial t_\nu} F(\mathbf{T}, \mathbf{Z}, \ldots) \equiv 0 \quad \forall\ \nu, \\
&\frac{\partial}{\partial t_\nu} \langle \Phi_0 | \hat{Z} \hat{\bar{H}} | \Phi_0 \rangle = -\frac{\partial}{\partial t_\nu} \underbrace{\big(\bar{h}_0 + \langle \Phi_0 | \hat{L} [\hat{\bar{H}}, \hat{R}] | \Phi_0 \rangle + \lambda \big(1 - \langle \Phi_0 | \hat{L} \hat{R} | \Phi_0 \rangle \big) \big)}_{\equiv\ F^{inh}},
\end{aligned} \tag{42}$$

and these equations are solved only *once* for *all* perturbations and degrees of freedom of the system. Furthermore, this equation for the $\mathbf{Z}$ Lagrange multipliers associated with the underlying CC/PT treatment can be cast into a form that is identical for EOM, STEOM, and all other methods based on a given CC/PT truncation through a chain-rule derivative in the common, transformed Hamiltonian $\bar{\mathbf{H}}$ amplitudes.

The homogeneous left side of equation (42) depends only on the CC or PT truncation scheme (and the parameterization of the associated $\mathbf{Z}$ Lagrange multipliers). Its explicit algebraic spatial-orbital expressions for CCSD-based methods are given in Table 8 of Section 5. These homogeneous-side expressions are the same for all EOM-CCSD and STEOM-CCSD variants, as well as for any electronic method based on a CCSD reference. In fact, these algebraic expressions, as well as all terms in the (ST)EOM-CCSD gradients involving $\mathbf{Z}$ amplitudes, are equivalent in form to those of ground-state CCSD gradient theory [109,118], with $\mathbf{Z}$ replacing $\mathbf{\Lambda}$. For the PT-based methods, the one-body equation is not present, and the two-body homogeneous side reduces to a tiny subset of the terms in the full CCSD-based expression; like the solution of the perturbative $\mathbf{T}_2^{(1)}$ equation (17), solution for the associated $\mathbf{Z_2}$ Lagrange multipliers amounts to simple division by an energy denominator. This economical bypass of the iterative solution of the $\mathbf{Z}$ equations is the only procedural difference between the PT-based and CCSD-based gradients; all other simplifications amount to straightforward skipping of unneeded terms (summarized by the PT-based prescription to be discussed in Section 5.1.1).

The inhomogeneous right side of equation (42) *does* depend on the particular EOM (or STEOM) variant but can be organized in an elegant form that separates out the method dependence, isolating it in an intermediate density matrix $\bar{\mathbf{D}}$. This separation is achieved by performing the differentiation as a chain rule through the $\bar{\mathbf{H}}$ amplitudes as the intermediate variables, which are common to all the methods:

$$\frac{\partial F^{inh}}{\partial t_\nu} = \sum_\mu \frac{\partial F^{inh}}{\partial \bar{h}_\mu} \frac{\partial \bar{h}_\mu}{\partial t_\nu} \equiv \sum_\mu \bar{D}_\mu \frac{\partial \bar{h}_\mu}{\partial t_\nu}, \tag{43}$$

where only $\bar{\mathbf{H}}$ is an explicit function of $\mathbf{T}$ and where μ runs over all the $\bar{\mathbf{H}}$ amplitudes, including $\bar{h}_0$. The derivatives seen above, of the inhomogeneous (non-$\mathbf{Z}$) part of the functional with respect to the *transformed* Hamiltonian amplitudes,

$$\bar{D}_\mu \equiv \frac{\partial F^{inh}}{\partial \bar{h}_\mu}, \tag{44}$$

define the *intermediate* density matrix for the particular electronic method. In contrast to the full effective density matrix $D_\nu \equiv \partial F / \partial h_\nu$, expression (25), which contains *all* of the particular method's GHF response, the intermediate density matrix isolates just the unique post-CC/PT component beyond the underlying reference treatment. In this chain-rule formulation, all remaining parts of the gradient expressions then depend solely on

the $\bar{\mathbf{H}}$ formulas, which are the same for all like-truncated-CC or like-truncated-PT based methods. The $\bar{\mathbf{H}}$ chain-rule formulation thus systematizes the **Z** equations (and later the expressions to convert to the full GHF **D**) by separating the common $\bar{\mathbf{H}}$ parts from the intermediate density matrix $\bar{\mathbf{D}}$, which contains all of the "post-$\bar{\mathbf{H}}$" information that is unique to each electronic method.

For methods based on a CCSD/PT reference truncation, the explicit algebraic spatial-orbital expressions for the inhomogeneous-side chain rule (43) are presented in Table 8 of Section 5. Written in terms of the intermediate density matrix, this convenient method-independent formulation thus allows solution of equation (42) for the **Z** Lagrange multipliers using the same computer code for all (ST)EOM-CCSD/PT variants, once the particular $\bar{\mathbf{D}}$ for the method is calculated.

In practice, due to a passive expansion of the three-body terms, we deviate slightly from the strict formal definition of the intermediate density matrix implied by expression (44). Nevertheless, the consistent algebraic definition $\bar{D}_\mu \equiv \partial F^{inh}/\partial \bar{h}_\mu$ *is maintained*. Whereas the resulting modifications described below might be somewhat tricky to organize by hand, they are all treated automatically here by the mathematics, when dealing with the algebraic expressions directly in *SMART*. For computational storage efficiency, all algebraic expressions in this work are left written in terms of only zero-, one-, and two-body amplitudes. Consequently, the intermediate density matrix elements are computed as derivatives with respect to only the zero-, one-, and two-body amplitudes of $\bar{\mathbf{H}}$. The components associated with the expanded three-body $\bar{\mathbf{H}}$ amplitudes, which formally would lead to three-body $\bar{\mathbf{D}}$, are instead distributed among the rest of the chain rule automatically. First, a small number of method-dependent three-body terms contribute explicitly to the t_{ij}^{ab} chain-rule derivative, and these are collected in Table 9 of Section 5. Second, certain (two-body) $\bar{\mathbf{D}}$ elements are modified to additionally contain the contributions that formally belong in the absent three-body $\bar{\mathbf{D}}$. The modified two-body $\bar{\mathbf{D}}$ correctly carry these three-body contributions throughout the remainder of the gradient calculation. These modifications arise and are all handled automatically here in the fully algebraic treatment, and a more detailed discussion of these three-body contributions is presented in Section 5.2.3.

The (modified) zero-, one-, and two-body $\bar{\mathbf{D}}$ elements for the EE-, IP-, and EA-EOM-CCSD/PT gradients are presented in Table 10 of Section 5. In addition to their use in the now method-independent **Z** Lagrange multiplier equations, the intermediate density matrix $\bar{\mathbf{D}}$ can be related to the full effective density matrix **D** by another chain rule that depends only on the reference CC/PT treatment (*i.e.* the $\bar{\mathbf{H}}$ amplitudes). Thus the intermediate density matrix contains all that is unique to each (ST)EOM variant and, along with the shared expressions involving **Z**, completely defines the gradient for each method.

The final bare-Hamiltonian effective density matrix **D** is related to the transformed-Hamiltonian intermediate density matrix $\bar{\mathbf{D}}$ by another chain rule similar to expression (43),

$$\begin{aligned} D_\mu \equiv \frac{\partial F}{\partial h_\mu} &= \frac{\partial}{\partial h_\mu}\left(F^{inh} + \langle \Phi_0 | \hat{Z}\hat{\bar{H}} | \Phi_0 \rangle\right) \\ &= \sum_\nu \bar{D}_\nu \frac{\partial \bar{h}_\nu}{\partial h_\mu} + \frac{\partial}{\partial h_\mu}\langle \Phi_0 | \hat{Z}\hat{\bar{H}} | \Phi_0 \rangle, \end{aligned} \tag{45}$$

where only $\bar{\mathbf{H}}$ is an explicit function of **H**. The derivatives in expression (45) depend only on the $\bar{\mathbf{H}}$ formulas, and thus the expressions are the same for all methods of a given CC or PT reference treatment. The explicit spatial-orbital expressions relating all one- and two-

body **D** to $\bar{\mathbf{D}}$ elements for CCSD-based methods are given in Table 15 of Section 5; a large number of terms drop out for the PT-based methods, and the simplified $\bar{\mathbf{D}}$ to **D** expressions for PT-based methods are reproduced separately as Table 16. Once the bare-Hamiltonian effective density matrix **D** has been computed, the first derivative of the electronic energy with respect to an arbitrary perturbation is obtained exactly as in a ground-state CC/MBPT gradient calculation by the GHF expression (24).

The explicit EOM-CCSD/PT gradient equations presented in Section 5 are equivalent to those originally derived by Stanton and Gauss [37–42], but the method of derivation, details, and organization are different. In the original treatment, abstract derivative expressions, like those above, were first derived with some effort through the Z-vector method. Subsequently, the abstract derivative expressions were converted into explicit algebraic expressions manually by diagrammatic expansion. In the present work, the detailed algebraic gradient expressions are generated by differentiating the defining algebraic energy equations (functionals) directly and in an automated fashion; see Section 4. Next, the previous EOM gradients were expressed more generally in spin-orbital terms, which are applicable to both open- and closed-shell references, whereas in the present working equations, spin-adapted spatial-orbital quantities and a closed-shell reference are chosen for computational efficiency. Furthermore, the present formulation is somewhat different, as we choose not to include the reference determinant in our diagonalization subspace; relatedly, our $\hat{Z}$ Lagrange multiplier operator is analogous to Stanton's composite operator $\hat{\Delta} \equiv \hat{\mathcal{Z}} + r_0\hat{\mathcal{L}}$, defined in expression (46) of reference [40]. The definition of the energy functional is not unique, as long as the definitions lead to numerically identical GHF effective density matrices in the end, and this flexibility will make our equations look slightly different than those derived previously. Lastly, in the original EOM gradient formulation, no explicit connection is drawn between the inhomogeneous side of the **Z** equations and the final effective density matrix **D**, and both sets of expressions are obtained separately. In the present $\bar{\mathbf{H}}$ chain-rule formulation, all the unique information of the particular (ST)EOM method is isolated sooner in the intermediate density matrix $\bar{\mathbf{D}}$. This allows construction of otherwise method-independent **Z** Lagrange multiplier equations and method-independent conversions of $\bar{\mathbf{D}}$ to the full effective density matrix **D** that are identical for all methods based on a given CC or PT reference treatment. For the CCSD/PT-based methods considered here, the existing code in ACES II for EOM-CCSD/PT gradients was revised to the present chain-rule/intermediate-density formulation as a first step to implementing STEOM-CCSD/PT gradients.

3.3. The STEOM-CCSD/PT intermediate density matrix

The STEOM-CCSD/PT energy functional is similar in form to that of EOM-CCSD/PT, with the addition of another set of Lagrange multiplier terms associated with the supplementary equations that determine the $\mathbf{S}^{\pm}$ amplitudes,

$$F \equiv \bar{h}_0 + \langle \Phi_0|\hat{L}[\hat{G}_2, \hat{R}]|\Phi_0\rangle + \lambda\big(1 - \langle \Phi_0|\hat{L}\hat{R}|\Phi_0\rangle\big) + \langle \Phi_0|\hat{Z}\hat{\bar{H}}|\Phi_0\rangle + \sum_m \langle \Phi_m|\hat{Z}^-[\hat{G}, \hat{m}]|\Phi_0\rangle + \sum_e \langle \Phi^e|\hat{Z}^+[\hat{G}, \hat{e}^\dagger]|\Phi_0\rangle. \tag{46}$$

For the EE-STEOM variant, both new terms are employed, since both the $\hat{S}^+$ and $\hat{S}^-$ amplitudes are needed, whereas for DIP-STEOM, the $\hat{Z}^+$ term is not included and for DEA-STEOM, the $\hat{Z}^-$ term is not included (see discussion after expression (7)).

As in EOM-CCSD, the energy of an electronic state is given by a biorthogonal expectation value, but now of the doubly transformed STEOM-CCSD Hamiltonian $\hat{G}_2$ (defined in expression (11)),

$$E = \frac{\langle \Phi_0 | \hat{L} \hat{G}_2 \hat{R} | \Phi_0 \rangle}{\langle \Phi_0 | \hat{L} \hat{R} | \Phi_0 \rangle}. \tag{47}$$

For simplicity, we will consider the normalization and eigenvector expressions in terms of this customary representation of the energy and will subsequently discuss the same adjustments introduced by the commutator for the PT-based variants. The restriction to normalized eigenvectors is again incorporated through the Lagrange multiplier construction involving the energy eigenvalue λ,

$$\underset{\sim}{F} \equiv \langle \Phi_0 | \hat{L} \hat{G}_2 \hat{R} | \Phi_0 \rangle + \lambda \big(1 - \langle \Phi_0 | \hat{L} \hat{R} | \Phi_0 \rangle\big). \tag{48}$$

The variational parameters **R** and **L** are determined by the eigenvector equations, recovered by enforcing the stationarities,

$$\frac{\partial \underset{\sim}{F}}{\partial l_\mu} = \langle \Phi_\mu | \hat{G}_2 \hat{R} | \Phi_0 \rangle - \lambda \langle \Phi_\mu | \hat{R} | \Phi_0 \rangle \equiv 0 \quad \forall\ \mu \tag{49}$$

and

$$\frac{\partial \underset{\sim}{F}}{\partial r_\mu} = \langle \Phi_0 | \hat{L} \hat{G}_2 | \Phi_\mu \rangle - \lambda \langle \Phi_0 | \hat{L} | \Phi_\mu \rangle \equiv 0 \quad \forall\ \mu, \tag{50}$$

with $|\Phi_\mu\rangle$ defined below. As before, the **L** amplitudes can be viewed as Lagrange multipliers for the eigenvector constraint equations that determine the **R** amplitudes, or vice versa. Equivalently, if the STEOM eigenvector equations are solved for the **R** and **L** amplitudes, the functional is automatically stationary with respect to these variational energy parameters.

As discussed, the STEOM-CCSD/PT diagonalization subspaces are significantly reduced compared to that of EOM-CCSD/PT. In contrast to EE-EOM-CCSD/PT, for example, the EE-STEOM-CCSD/PT n-electron diagonalization subspace $|\boldsymbol{\Phi_\mu}\rangle$ now consists of all singly excited determinants ($1h1p$) only. The doubly excited configurations ($2h2p$) are no longer included in $|\boldsymbol{\Phi_\mu}\rangle$. The EE-STEOM-CCSD/PT eigenvector operators have the spin-orbital forms

$$\hat{R} = \sum_{i,a} r_i^a \{\hat{a}^\dagger \hat{i}\} \quad \text{and} \quad \hat{L} = \sum_{i,a} l_a^i \{\hat{i}^\dagger \hat{a}\}. \tag{51}$$

For the DIP- variant of STEOM-CCSD/PT, the diagonalization subspace $|\boldsymbol{\Phi_\mu}\rangle$ consists of all $(n-2)$-electron states related to the reference determinant by deletion of two electrons ($2h$ configurations), and the operators have the form

$$\hat{R} = \sum_{i<j} r_{ij} \{\hat{i}\,\hat{j}\} \quad \text{and} \quad \hat{L} = \sum_{i<j} l^{ij} \{\hat{j}^\dagger \hat{i}^\dagger\}. \tag{52}$$

For the DEA- variant of STEOM-CCSD/PT, the diagonalization subspace $|\boldsymbol{\Phi_\mu}\rangle$ consists of all $(n+2)$-electron states related to the reference determinant by the addition of two

electrons ($2p$ configurations), and the operators have the form

$$\hat{R} = \sum_{a<b} r^{ab}\{\hat{a}^\dagger \hat{b}^\dagger\} \quad \text{and} \quad \hat{L} = \sum_{a<b} l_{ab}\{\hat{b}\hat{a}\}. \tag{53}$$

As noted earlier, if the sums in expressions (51) through (53) range over the full orbital subspaces, active plus inactive, the eigenvalue spectra of the doubly transformed Hamiltonians $\hat{G}$ and $\hat{G}_2$ are identical, and thus for convenience we choose to neglect the $\hat{S}_1$ components of $\hat{G}$ in the energy expression. This neglect simply amounts to an implicit redefinition of the $\hat{L}$ and $\hat{R}$ amplitudes compared to that of diagonalizing the full $\hat{G}$,

$$\langle\Phi_0|\underset{\sim}{\hat{L}}\hat{G}\underset{\sim}{\hat{R}}|\Phi_0\rangle = \langle\Phi_0|\underset{\sim}{\hat{L}}\{e^{\hat{S}_1}\}^{-1}\hat{G}_2\{e^{\hat{S}_1}\}\underset{\sim}{\hat{R}}|\Phi_0\rangle \equiv \langle\Phi_0|\hat{L}\hat{G}_2\hat{R}|\Phi_0\rangle. \tag{54}$$

Since the remaining constraint equations are independent of the variational **R** and **L** parameters (*cf.* equations (19)), this redefinition has no effect on the form of the rest of the expressions.

The biorthogonal expectation-value energy (47) is again rewritten in terms of the commutator to deliberately exclude the pure-excitation amplitudes from the algebraic expressions and thereby make the functional (46) consistent for both the CCSD-based and PT-based methods. Although the one-body pure-excitation operator cannot contribute in these "singles"-only diagonalization subspaces, its exclusion is still necessary to justify the removal of the r_0 reference component from the EE-STEOM-PT eigenvector (*cf.* the discussion after expression (34)). Lastly, the equivalence of the $\hat{G}$ and $\hat{G}_2$ diagonalizations for the commutator form of the energy can be proven through an expression analogous to expression (54) (although the proof involves a slightly different redefinition of $\hat{L}$ and $\hat{R}$, namely a full $\{e^{\hat{S}_1}\}$ similarity transformation).

We now turn our attention to the remaining Lagrange multiplier terms in the energy functional. Through the $\langle\Phi_0|\hat{Z}\hat{\bar{H}}|\Phi_0\rangle$ term, solving the reference CC/PT equations that determine the **T** parameters makes the functional automatically stationary with respect to the associated **Z** Lagrange multipliers, exactly as in EOM-CC/PT (equation (39)). In STEOM, there are two additional sets of constraint equations, which determine the $\mathbf{S}^{\pm}$ amplitudes. The equations (9) that determine $\mathbf{S}^-$ are recovered from the functional by differentiating with respect to the associated Lagrange multipliers $\mathbf{Z}^-$,

$$\frac{\partial F}{\partial d_m^\mu} = \frac{\partial}{\partial d_m^\mu}\left(\sum_n \langle\Phi_n|\hat{Z}^-[\hat{G},\hat{n}]|\Phi_0\rangle\right) = \mathsf{g}_\mu^m \equiv 0 \quad \forall\, m,\mu, \tag{55}$$

where the $\hat{Z}^-$ amplitudes are denoted d_m^μ ("detachment") and μ is a compound label defined implicitly in expression (57) below. Likewise, equations (10) that determine $\mathbf{S}^+$ are recovered by differentiating with respect to the associated Lagrange multipliers $\mathbf{Z}^+$,

$$\frac{\partial F}{\partial a_\mu^e} = \frac{\partial}{\partial a_\mu^e}\left(\sum_f \langle\Phi^f|\hat{Z}^+[\hat{G},\hat{f}^\dagger]|\Phi_0\rangle\right) = \mathsf{g}_e^\mu \equiv 0 \quad \forall\, e,\mu, \tag{56}$$

where the $\hat{Z}^+$ amplitudes are denoted a_μ^e ("attachment") and μ is defined implicitly in expression (58) below. Thus, solving the $\mathbf{S}^-$ and $\mathbf{S}^+$ equations ensures that the STEOM-CCSD/PT functional is automatically stationary with respect to variations in the $\mathbf{Z}^-$ and $\mathbf{Z}^+$ Lagrange multipliers, respectively. The operators associated with these Lagrange multipliers are, in spin-orbital form,

$$\hat{Z}^- = \hat{Z}_1^- + \hat{Z}_2^- = \sum_{i',m} d_m^{i'}\{\hat{i}'^\dagger \hat{m}\} + \sum_{m,b,\,i<j} d_{mb}^{ij}\{\hat{i}^\dagger \hat{m}\,\hat{j}^\dagger \hat{b}\} \tag{57}$$

and

$$\hat{Z}^+ = \hat{Z}_1^+ + \hat{Z}_2^+ = \sum_{a',e} a_{a'}^{e} \{\hat{e}^\dagger \hat{a}'\} + \sum_{e,j,a<b} a_{ab}^{ej} \{\hat{e}^\dagger \hat{a} \hat{j}^\dagger \hat{b}\}. \tag{58}$$

These Lagrange multiplier operators are the de-excitation analogs of the $\hat{G}$ excitation operators that are made to vanish in equations (9) and (10) (or equivalently, the $\hat{S}^-$ and $\hat{S}^+$ operators, which by definition have the same form as the eliminated $\hat{G}$ components).

A commutator formulation is again employed to make these Lagrange multiplier terms correct for the PT-based methods. For the CCSD-based STEOM methods, the last two terms in the energy functional (46) might instead be written more compactly as

$$+ \sum_m \langle \Phi_m | \hat{Z}^- \hat{G} | \Phi_m \rangle + \sum_e \langle \Phi^e | \hat{Z}^+ \hat{G} | \Phi^e \rangle. \tag{59}$$

These expressions, however, technically contain contributions from the pure-excitation amplitude $\mathfrak{g}_i^a$. As in the EOM-CC/PT discussion, inclusion of such pure-excitation terms can have no numerical effect on the gradient *for the CC-based methods*, since these terms are rigorously made zero for all perturbations, but *for the PT-based methods*, such terms do not vanish completely and should not be included. This struggle with the pure-excitation terms arises somewhat artifactually here by phrasing everything in "matrix-element" notation. In a "many-body" formulation, the second-quantized operators and their elementary coefficients are treated directly. The $\mathbf{S}^-$ amplitudes, for example, are in fact defined to set the $\mathfrak{g}_{i'}^m$ and $\mathfrak{g}_{ij}^{mb}$ *operator coefficients* to zero; the matrix elements written in equations (9) are only equivalent to these operator coefficients if the pure-excitation $\mathfrak{g}_i^a = 0$. The many-body Lagrange multiplier terms would look like $\sim d_m^{i'} \mathfrak{g}_{i'}^m$ and $\sim d_{mb}^{ij} \mathfrak{g}_{ij}^{mb}$, and the pure-excitation coefficients would not show up, in a natural way.

The explicit algebraic expansions of the energy functional in terms of spin-adapted spatial-orbital quantities for the EE-, DIP-, and DEA-STEOM-CCSD/PT variants are presented in Table 4 of Section 5. These expressions are obtained by diagrammatic or algebraic expansion of the abstract operator functional (46) and are the defining equations of these STEOM methods. As before, the algebraic functional comprises the input to our *SMART* package (see Section 4), and all subsequent derivative expressions given explicitly in Section 5 are obtained directly by symbolic algebraic differentiation.

As in the EOM discussion, the Lagrange multipliers are determined by making the energy functional stationary with respect to all of its wavefunction parameters. Once the STEOM-CCSD/PT energy (and left-hand eigenvector $\mathbf{L}$) equations are solved, the functional is automatically stationary with respect to variations in the $\mathbf{R}$, $\mathbf{L}$, λ, $\mathbf{Z}^-$, $\mathbf{Z}^+$, and $\mathbf{Z}$ parameters, but it is not yet stationary with respect to the non-variational $\mathbf{S}^-$, $\mathbf{S}^+$, or $\mathbf{T}$ parameters. Moreover, the associated $\mathbf{Z}^-$, $\mathbf{Z}^+$, and $\mathbf{Z}$ Lagrange multipliers are still unspecified. By construction, enforcing stationarity with respect to the $\mathbf{S}^-$ amplitudes yields the equations that determine the associated $\mathbf{Z}^-$ Lagrange multipliers,

$$\begin{aligned} &\frac{\partial F}{\partial s_\mu^m} \equiv 0 \quad \forall\, m, \mu, \\ &\frac{\partial}{\partial s_\mu^m} \left(\sum_n \langle \Phi_n | \hat{Z}^- [\hat{G}, \hat{n}] | \Phi_0 \rangle \right) = -\frac{\partial}{\partial s_\mu^m} \langle \Phi_0 | \hat{L} [\hat{G}_2, \hat{R}] | \Phi_0 \rangle, \end{aligned} \tag{60}$$

and similarly, setting to vanish the derivatives of the functional with respect to the $\mathbf{S}^+$ amplitudes yields the equations that determine the associated $\mathbf{Z}^+$ Lagrange multipliers,

$$\frac{\partial F}{\partial s_e^\mu} \equiv 0 \quad \forall\, e, \mu,$$
$$\frac{\partial}{\partial s_e^\mu}\left(\sum_f \langle \Phi^f | \hat{Z}^+[\hat{G}, \hat{f}^\dagger] | \Phi_0 \rangle\right) = -\frac{\partial}{\partial s_e^\mu} \langle \Phi_0 | \hat{L}[\hat{G}_2, \hat{R}] | \Phi_0 \rangle, \tag{61}$$

where μ is a compound label for the four classes of $\mathbf{S}$ indices in expressions (7) and only $\mathbf{G}$ and $\mathbf{G_2}$ are explicit functions of $\mathbf{S}$.

The results of differentiating the algebraic functionals to obtain the $\mathbf{Z}^-$ Lagrange multiplier equations (60) for EE- and DIP-STEOM-CCSD/PT are presented in Table 11 of Section 5. The explicit $\mathbf{Z}^+$ Lagrange multiplier equations (61) for EE- and DEA-STEOM-CCSD/PT are presented in Table 12. The homogeneous left sides of equations (60) and (61) depend only on the eliminated $\hat{G}$ coefficients and are therefore identical for both variants in each table. The inhomogeneous right sides depend on the definition of the energy expression (*i.e.* the diagonalization subspace of $\hat{G}_2$) and thus depend on the STEOM variant. Since the $\hat{S}_1$ components of the energy expressions have been eliminated, the right-hand sides vanish for $\mathbf{S_1}$ derivatives, leaving the one-body equations completely homogeneous. The linear $\mathbf{Z}^-$ and $\mathbf{Z}^+$ Lagrange multiplier equations can be decoupled into separate equations for each active orbital index m and e, respectively, aiding numerical convergence and computational efficiency. The details of this decoupling will be considered in Section 5.4.1.

After the solution for the $\mathbf{Z}^-$ and $\mathbf{Z}^+$ Lagrange multipliers that account for the $\mathbf{S}^-$ and $\mathbf{S}^+$ response, the functional is finally made stationary with respect to the remaining reference-state $\mathbf{T}$ parameters, and this determines the associated $\mathbf{Z}$ Lagrange multipliers. Exactly as in the EOM discussion,

$$\frac{\partial}{\partial t_\nu} F(\mathbf{T}, \mathbf{Z}, \ldots) \equiv 0 \quad \forall\, \nu,$$
$$\frac{\partial}{\partial t_\nu} \langle \Phi_0 | \hat{Z} \hat{\bar{H}} | \Phi_0 \rangle = -\frac{\partial F^{inh}}{\partial t_\nu} = -\sum_\mu \frac{\partial F^{inh}}{\partial \bar{h}_\mu} \frac{\partial \bar{h}_\mu}{\partial t_\nu} \equiv -\sum_\mu \bar{D}_\mu \frac{\partial \bar{h}_\mu}{\partial t_\nu}, \tag{62}$$

but now with

$$F^{inh} \equiv \bar{h}_0 + \langle \Phi_0 | \hat{L}[\hat{G}_2, \hat{R}] | \Phi_0 \rangle + \lambda\big(1 - \langle \Phi_0 | \hat{L}\hat{R} | \Phi_0 \rangle\big)$$
$$+ \sum_m \langle \Phi_m | \hat{Z}^-[\hat{G}, \hat{m}] | \Phi_0 \rangle + \sum_e \langle \Phi^e | \hat{Z}^+[\hat{G}, \hat{e}^\dagger] | \Phi_0 \rangle. \tag{63}$$

Equation (62), written in terms of the chain rule, depends only on the derivatives of the transformed Hamiltonian $\bar{\mathbf{H}}$ amplitudes and is therefore *identical* to the $\mathbf{Z}$ Lagrange multiplier equations (42) and (43) already discussed for the EOM-CCSD/PT method. The transformed-Hamiltonian intermediate density matrix elements $\bar{D}_\mu \equiv \partial F^{inh}/\partial \bar{h}_\mu$ however are different, and these contain all of the (ST)EOM-variant dependence. The algebraic zero-, one-, and two-body $\bar{\mathbf{D}}$ elements, which (along with the explicit three-body terms) completely determine the gradient, for the EE-, DIP-, and DEA-STEOM-CCSD/PT variants are presented in Table 14 of Section 5. These $\bar{\mathbf{D}}$ contain all of each method's unique post-CCSD/PT response information, which in STEOM consists of the bivariational $\mathbf{L}$ and $\mathbf{R}$ contributions and the response contributions of the non-variational $\mathbf{S}^\pm$ parameters through the $\mathbf{Z}^\pm$ Lagrange multipliers.

With the construction of $\bar{\mathbf{D}}$, the solution of the **Z** Lagrange multiplier equations and the remainder of the STEOM-CCSD/PT gradient calculation then proceed identically to that of EOM-CCSD/PT. The chain-rule **Z** equations (62) are identical for all CCSD-based methods and have already been considered in the EOM discussion of the preceding section (with explicit expressions in Table 8 of Section 5). For the PT-based methods, the same dramatic simplifications to the homogeneous sides of the **Z** equations arise. There are a pair of method-dependent three-body terms that contribute to the t_{ij}^{ab} chain rule explicitly, and these are presented in Table 9 in Section 5.

With the solution for the final **Z** Lagrange multipliers associated with the underlying CCSD/PT reference treatment, the transformed-Hamiltonian intermediate density matrix $\bar{\mathbf{D}}$ is converted to the bare-Hamiltonian effective density matrix **D** by another method-independent chain rule given previously by expression (45) or explicitly as Table 15/Table 16 in Section 5. The first derivative of the electronic energy with respect to an arbitrary perturbation is then obtained from the GHF relation (24). All expensive perturbation derivatives of the non-variational $\mathbf{S}^-$, $\mathbf{S}^+$, and **T** parameters have been avoided by solution of the associated $\mathbf{Z}^-$, $\mathbf{Z}^+$, and **Z** Lagrange multiplier equations (60), (61), and (62), respectively.

There is one small part of the STEOM-CC/PT gradient that has not yet been treated in the current work. The missing piece relates to rotation between the active and inactive orbitals. By comparison to numerical gradients, if the active space is sufficiently large, the effect is typically very small and its neglect is not significant. The effect is slightly larger when examining conical intersection regions due to the small differences in energy being considered. The omitted part is to some extent analogous to the problem of frozen/dropped-core gradients [101,118,164,165], and we expect this feature can be incorporated with a suitable addition to the Lagrange multiplier functional.

3.3.1. Summary of steps in a STEOM gradient calculation

The following summarizes the sequence of steps in a STEOM-CCSD/PT analytical gradient calculation. The individual steps are presented in Table 2 (Section 5.8), along with the operation-count scaling and the storage of the most expensive terms in each step. The energy and gradient calculations proceed sequentially according to the first column of Table 2 as follows: First, the closed-shell reference determinant is established (usually) through an SCF calculation, to obtain the MO coefficients and to convert the AO-based one- and two-electron Hamiltonian integrals into the MO-based **H** amplitudes of expression (1). The standard STEOM-CCSD/PT energy calculation then begins by solving the reference-state CCSD equations (4) or PT (first-order MP) equation (16), respectively, to yield the **T** amplitudes. The **T** amplitudes define the first similarity transformation, expression (2), yielding $\bar{\mathbf{H}}$. Next, a selection of active IP-EOM-CCSD/PT and EA-EOM-CCSD/PT eigenvectors are determined by diagonalizing $\hat{\bar{H}}$ over $1h \oplus 2h1p$ and $1p \oplus 2p1h$ configurations, and the eigenvector amplitudes are converted into $\mathbf{S}^-$ and $\mathbf{S}^+$, respectively; this procedure is equivalent to solving the $\mathbf{S}^\pm$ equations (9) and (10). (Note that $\mathbf{S}^-$ is not needed for DEA-STEOM, and $\mathbf{S}^+$ is not needed for DIP-STEOM. Both are needed for EE-STEOM.) The $\mathbf{S}^\pm$ amplitudes define the second similarity transformation, expression (11), yielding $\mathbf{G_2}$. The doubly transformed Hamiltonian $\hat{G}_2$ is diagonalized (inexpensively) over $1h1p$, $2h$, or $2p$ configurations to yield **R**, **L**, and energy eigenvalues λ for the individual EE-, DIP-, or DEA-STEOM-CCSD/PT eigenvectors, respectively. (**L** is not needed for the energy

but is needed for the gradient.) The gradient calculation begins by (decoupling in m or e and then) solving the Lagrange multiplier equations (60) and (61) associated with the $\mathbf{S}^-$ and $\mathbf{S}^+$ constraint equations, yielding the $\mathbf{Z}^-$ and $\mathbf{Z}^+$ Lagrange multipliers, respectively. With these amplitudes, the one- and two-body intermediate density matrix elements $\bar{\mathbf{D}}$ are then constructed. (The $\mathbf{R}$ and $\mathbf{L}$ are no longer needed and can now be discarded. The $\mathbf{S}^\pm$ and $\mathbf{Z}^\pm$ could also in principle be discarded, except for the method-dependent three-body terms in the upcoming $\mathbf{Z}$ equations.) The one- and two-body $\bar{\mathbf{D}}$ (along with the explicit three-body terms) are plugged into the method-independent chain-rule equation (62) for the Lagrange multipliers associated with the underlying CCSD or PT $\mathbf{T}$ constraint equations, and solving yields $\mathbf{Z}$. (The $\bar{\mathbf{H}}$ (and $\mathbf{S}^\pm$ and $\mathbf{Z}^\pm$) can now be discarded.) Finally, the method-independent chain-rule expression (45) converts the transformed-Hamiltonian intermediate density matrix $\bar{\mathbf{D}}$ to the bare-Hamiltonian effective density matrix $\mathbf{D}$. (The $\mathbf{Z}$ and $\mathbf{T}$ can now be discarded.) The derivatives of the bare Hamiltonian $\mathbf{H}$ amplitudes with respect to the perturbation are computed in the AO basis (along with the MO coefficient response), and $\mathbf{D}$ is backtransformed into the AO basis. The full derivative of the electronic-state energy with respect to the perturbation is then given by the AO-based expression equivalent to the GHF relation (24) (see Section 5.7.1).

In this formulation, the computational cost of the STEOM-CCSD/PT analytical gradient portion is comparable to that of the single-point energy calculation and does not scale deleteriously with the degrees of freedom of the system. The most expensive steps involve iterative o^2v^4I and ov^4eI operations (see Table 2), and the EE- and DEA-STEOM-CCSD methods each have four such steps: the reference-state CCSD equations for $\mathbf{T}$ and the active EA-EOM-CCSD eigenvector equations for $\mathbf{S}^+$ in the energy calculation, and the associated $\mathbf{Z}$ and $\mathbf{Z}^+$ Lagrange multiplier equations in the analytical gradient. The total cost is thus approximately four times that of the CCSD reference-state calculation. The EE- and DEA-STEOM-PT methods eliminate the two o^2v^4I operations associated with the iterative solution for $\mathbf{T}$ and $\mathbf{Z}$. Finally, the DIP-STEOM-CCSD method is very economical, with only the two o^2v^4I $\mathbf{T}$ and $\mathbf{Z}$ equations. These again are eliminated in the DIP-STEOM-PT variant, and only non-iterative o^3v^3 terms remain. Additionally, the DIP-STEOM-CCSD method does not require the large $\bar{D}^{cd}_{ab}$, $\bar{D}^{bc}_{ia}$, and $\bar{D}^{ic}_{ab}$ matrices, and moreover, for the DIP-STEOM-PT method, the V^{ab}_{cd}, $\bar{h}^{ab}_{cd}$, D^{cd}_{ab}, V^{ab}_{ic}, $\bar{h}^{ab}_{ic}$, and D^{ic}_{ab} are not needed. Of the three methods, the DIP-STEOM variants are thus the most suited for application to larger systems, both in terms of timing and storage. For comparison, the CCSD and EOM-CCSD gradients also involve the two o^2v^4I $\mathbf{T}$ and $\mathbf{Z}$ equations; additionally, computing each $\mathbf{R}$ or $\mathbf{L}$ eigenvector scales as ov^4I in EA-EOM-CCSD/PT and as o^2v^4I in EE-EOM-CCSD/PT.

4. THE *SMART* SYMBOLIC ALGEBRA PACKAGE

Having now completed the discussion of analytical energy gradients in terms of abstract operator expressions, this section marks the start of the second half of the paper in terms of the fully algebraic derivation of the explicit working equations. In this section, an overview is presented of our general *SMART* package, created to manipulate, differentiate, and thereby derive the algebraic gradient expressions directly. The specific (ST)EOM-CCSD/PT derivative equations themselves are presented and examined in full detail in Section 5.

Since a closed-shell reference determinant is employed, the spin integration is straightforward to carry out, and all explicit algebraic expressions in Sections 4 and 5 are given in

terms of *spatial*-orbital indices. Note that the same index labels are used as the *spin*-orbital indices of the previous abstract discussion in Sections 2 and 3. Most expressions are now written in Einstein's summation convention. All two-body terms have vertex-interchange symmetry, *e.g.* $\bar{h}^{pq}_{rs} = \bar{h}^{qp}_{sr}$. Permutations on external (non-summed) indices are denoted as P_{ij} for the permutation that exchanges $i \leftrightarrow j$ and P^{ab}_{ij} for the permutation that exchanges $i \leftrightarrow j$ and $a \leftrightarrow b$ simultaneously. Terms involving the Kronecker delta and a dummy active/inactive summation index only contribute if the non-summed index is of the same active/inactive character (for example, in Table 7, the δ_{im} in $\delta_{im} V^{kl}_{ac} \tilde{s}^{mc}_{kl} \in g^{i}_{a}$ causes the term to contribute only if the external index i is active). The notation $(\,)^{\text{singlet}}_{\text{only}}$ denotes that the quantity enclosed in parentheses is present only for singlet EE-STEOM states and is not included for triplet EE-STEOM states.

4.1. Overview of *SMART*

Traditionally, to obtain *explicit algebraic* expressions for an analytical energy gradient, the *abstract operator* form of the gradient expressions is usually first derived (for (ST)EOM-CCSD/PT: expressions (60), (61), (42) to (44) or (62) to (63), and (45)), which might then be expanded algebraically or diagrammatically to the detailed working equations, and all typically done by hand. While the algebraic expansion procedure could be made automated, even the hand derivation of the abstract gradient expressions themselves is often quite complex. Rather than embark on such a tedious and error-prone undertaking to derive the detailed gradient equations for each new electronic structure method, we instead developed the general *SMART* (Symbolic Manipulation and Regrouping of Tensors) package of automated symbolic algebra tools, written in the *Mathematica* [127] programming language. Bypassing the need to consider the abstract gradient expressions, the algebraic gradient expressions are instead derived *directly*, by explicit *symbolic differentiation* of the algebraic *energy expressions* that define the electronic method. The Lagrange multiplier formulation establishes a uniform framework in which to perform the derivation in a standard manner. The *SMART* toolkit provides the resources to expand, differentiate, and simplify directly, by automated symbolic manipulation of the detailed algebraic tensor expressions themselves. Through a fully symbolic algebraic treatment, the package was used to generate and check all the explicit gradient expressions presented in the tables of Section 5.

To sketch the procedure, we begin as input with the Lagrange multiplier energy functional for each electronic method in explicit algebraic terms. As discussed, the component expressions of the energy functional are simply the defining equations of the electronic structure method. For the (ST)EOM-CCSD/PT methods, the defining algebraic expressions (see Tables 3 and 4) are relatively straightforward and well known, *e.g.* references [3,34,36,52]. As is often the case, these algebraic expressions were originally defined first in abstract operator terms and subsequently expanded by hand using diagrammatic techniques to explicit algebraic terms. The algebraic form of the energy expressions might also in principle be obtained automatically from the abstract operator definitions, such as by automation of Wick's Theorem or diagrams. For recent examples of automated expansion procedures, see for instance Kállay *et al.* [128,129] or Hirata [134,135]. The algebraic functionals, along with the algebraic definitions of any intermediate quantities (in particu-

lar the common $\bar{\mathbf{H}}$, $\mathbf{G}$, and $\mathbf{G_2}$ expressions of Tables 5, 6, and 7), serve as the input to the *SMART* package.

Using the custom symbolic algebra routines, intermediates can be fully expanded such that all parts of the expressions are written in terms of the basic parameters. For example, any transformed Hamiltonian $\bar{\mathbf{H}}$ or doubly transformed $\mathbf{G_2}$ amplitudes can be expanded into their bare Hamiltonian $\mathbf{H}$ expressions (and vice versa, see below). The fully expanded expressions can then be differentiated symbolically with respect to a particular amplitude by proper replacement with Kronecker deltas, for example,

$$\frac{\partial}{\partial t_i^a}\left(\sum_{k,c} f_c^k t_k^c\right) = \sum_{k,c} f_c^k \delta_{ac}\delta_{ik} = f_a^i. \tag{64}$$

Above, the symbolic derivative picks out the corresponding terms whose indices precisely match those of the differentiating amplitude. The symbolic differentiation can also be performed as a chain rule, with the transformed Hamiltonian $\bar{\mathbf{H}}$ amplitudes as the intermediate variables, to automatically construct the derivative in terms of the intermediate density matrix $\bar{\mathbf{D}}$ (see below). The *SMART* routines can reasonably manipulate terms of up to five-body rank or so and can treat common term symmetries, such as antisymmetry or specific vertex-interchange (only two-body vertex-interchange symmetry is needed in this work).

A canonical ordering/reindexing algorithm puts all amplitudes and tensor multiplications into a preferred unique form, treating the symmetry of the individual amplitudes and re-labeling the dummy summation indices in a unique order. All mathematically equivalent forms of a given tensor multiplication are thus converted to the same unique form and then combine automatically. For example,

$$\left.\begin{aligned} V_{cd}^{kl} t_{ik}^{ac} t_l^d &= V_{dc}^{kl} t_{ik}^{ad} t_l^c = V_{cd}^{lk} t_{il}^{ac} t_k^d = V_{dc}^{lk} t_{il}^{ad} t_k^c \\ &= V_{cd}^{kl} t_{ki}^{ca} t_l^d = V_{dc}^{kl} t_{ki}^{da} t_l^c = V_{cd}^{lk} t_{li}^{ca} t_k^d = V_{dc}^{lk} t_{li}^{da} t_k^c \\ &= V_{dc}^{lk} t_{ik}^{ac} t_l^d = V_{cd}^{lk} t_{ik}^{ad} t_l^c = V_{dc}^{kl} t_{il}^{ac} t_k^d = V_{cd}^{kl} t_{il}^{ad} t_k^c \\ &= V_{dc}^{lk} t_{ki}^{ca} t_l^d = V_{cd}^{lk} t_{ki}^{da} t_l^c = V_{dc}^{kl} t_{li}^{ca} t_k^d = V_{cd}^{kl} t_{li}^{da} t_k^c \\ &= V_{bc}^{kl} t_{ik}^{ab} t_l^c = \cdots = V_{cd}^{jk} t_{ij}^{ac} t_k^d = \cdots = V_{bc}^{jk} t_{ij}^{ab} t_k^c \\ &= \cdots \end{aligned}\right\} \rightarrow V_{cd}^{kl} t_{ik}^{ac} t_l^d. \tag{65}$$

In essence, for a given tensor multiplication, the individual amplitudes are sorted, based on a pre-defined canonical ordering of their external index labels and, for amplitudes with no external indices, based on their relation to the preceding ordered amplitudes through their summation indices. For the case of no external indices (*i.e.* scalars), for instance the energy expressions, the indices of the single Hamiltonian amplitude start the process. Besides sorting the amplitudes, each amplitude itself is put in a preferred symmetry form, defined either by its particle-hole type (*e.g.* $\bar{h}_{ic}^{ab}$ vs. $\bar{h}_{ci}^{ba}$), or in the case of symmetric amplitudes (*e.g.* $\bar{h}_{cd}^{ab}$ vs. $\bar{h}_{dc}^{ba}$), based on the same method of following the touched indices used above to sort the amplitudes. Dummy summation indices are then assigned to the uniquely ordered list of preferred-form amplitudes. The ordering algorithm is designed to yield a unique result for the general types of algebraic tensor multiplications considered here. At present, in cases with arbitrariness (in this work, the case of no external indices with a symmetric Hamiltonian amplitude to start), all (*i.e.* both) arbitrary orderings are enumerated and a preferred final reindexed result is chosen uniquely (based on a dictionary-type ordering); the number of arbitrary orderings is larger for more flexible symmetries, such as antisymmetry, and

other more efficient schemes could perhaps be devised, but the current implementation for dealing with arbitrariness has proven sufficient. The canonical reindexing routine is a central feature, and its design represented an important challenge in the development of the *SMART* package. In subsequent applications, the procedure has been generalized to treat a variety of symmetry types, index spaces, and arbitrary number of indices in the amplitudes. The canonical ordering procedure is described in detail in reference [166].

Permutations on external indices can be extracted through another canonical ordering scheme that selects a preferred permuted form [166]. Routines are available to perform some factorization and to aid in the collection and substitution of intermediates. The factorization, extracted permutations, and intermediates can be checked easily by expansion. More discussion of the factorization scheme appears in later sections (in particular, Sections 4.4 and 5.6). The *SMART* code is internally well documented and checks the consistency of the manipulated expressions at numerous points in the evaluation. In addition to the (ST)EOM gradient work presented here, the rather general *SMART* package was also applied to investigate the cumulant expansion of the Contracted Schrödinger Equation [167] and in unpublished work to manipulate a variety of other tensor algebraic expressions directly.

4.2. Example derivations in *SMART*

The above discussion of the *SMART* derivation process is more concretely understood through example. In the following, the *Mathematica* input expressions have been modified slightly for clarity and have been drawn out to reveal the individual substeps. As discussed, the *SMART* package takes as input the algebraic Lagrange multiplier energy functionals, comprised of the defining equations for each electronic method. For example, in singlet EE-STEOM-CCSD, the defining expressions are given by (from Table 4)

```
energyEESinglet[] = hbar0[] + 2l[i,a]((2g2[k,a,c,i]
  - g2[a,k,c,i])r[c,k] + g2[a,c]r[c,i] - g2[k,i]r[a,k]),
Z$equationT[] = 2z[i,a]hbar[a,i]
  +(2z[i,j,a,b]-z[i,j,b,a])hbar[a,b,i,j],
ZMinus$equationSMinus[] = 2d[iPrime,m]g[m,iPrime]
  +(2d[i,j,m,b]-d[j,i,m,b])g[m,b,i,j],
ZPlus$equationSPlus[] = 2a[e,aPrime]g[aPrime,e]
  +(2a[e,j,a,b]-a[e,j,b,a])g[a,b,e,j]                    (66)
```

and the energy functional is defined as

```
functionalEESinglet[] = energyEESinglet[]+ Z$equationT[]
  + ZMinus$equationSMinus[] + ZPlus$equationSPlus[]
    // wellFormed.                                       (67)
```

(The `wellFormed` function above checks the consistency of the algebraic expressions, for example, that the orbital space of each index is defined or that in a tensor multiplication, summation indices appear twice and external indices only once.) The above expressions for the EE-STEOM-CCSD energy functional, along with the common algebraic expansions of the `hbar[`μ`]`, `g[`μ`]`, and `g2[`μ`]` amplitudes (Tables 5, 6, and 7), comprise the

input to *SMART*. All subsequent derivative expressions for the analytical EE-STEOM-CCSD gradient (in Tables 8, 9, 11, 12, 13, 14, and 15) are obtained directly by symbolic differentiation.

Consider the two-body **Z** equation (Table 8), given by the derivative of the energy functional with respect to t_{ij}^{ab}. In order to obtain the homogeneous left side, $\partial\langle\Phi_0|\hat{Z}\bar{\hat{H}}|\Phi_0\rangle/\partial t_{ij}^{ab}$, the following steps are carried out in *SMART*:

```
Z$equationT[]
  /. toBareHamiltonian
  // derivative[#,t[a,b,i,j]]&
  // reindex,
```
(68)

namely, in the **Z** component of the functional the $\bar{\mathbf{H}}$ amplitudes are first expanded to the basic "bare" **H** and **T** amplitudes to allow differentiation, direct symbolic differentiation is performed with respect to t_{ij}^{ab} (by proper replacement of all t_{rs}^{pq} with Kronecker deltas, in the manner of expression (64)), and the result is canonically reindexed to combine the mathematically equivalent terms by putting them each in a uniquely defined form. The result of these operations is 224 distinct terms

$$\begin{aligned} &2z_a^i f_b^j - z_b^i f_a^j - z_a^j f_b^i + 2z_b^j f_a^i + 4z_a^i t_k^c V_{bc}^{jk} \\ &\quad + 4z_b^j t_k^c V_{ac}^{ik} - 2z_a^i t_k^c V_{cb}^{jk} - 2z_b^i t_k^c V_{ac}^{jk} - 2z_a^j t_k^c V_{bc}^{ik} \\ &\quad - 2z_b^j t_k^c V_{ca}^{ik} + z_b^i t_k^c V_{ca}^{jk} + z_a^j t_k^c V_{cb}^{ik} + 2z_c^j V_{ab}^{ic} + \cdots \quad \text{(224 terms).} \end{aligned} \tag{69}$$

As will be examined in Section 5.2.1, re-expressing this fully expanded derivative expression *back* in terms of the transformed $\bar{\mathbf{H}}$ amplitudes leads to a substantial factorization, reducing the above to 56 distinct terms,

```
% /. toTransformedHamiltonian
  // reindex,
```
(70)

$$\begin{aligned} &2z_a^i \bar{h}_b^j - z_b^i \bar{h}_a^j - z_a^j \bar{h}_b^i + 2z_b^j \bar{h}_a^i + 4z_{ac}^{ik} \bar{h}_{bk}^{jc} - 2z_{ca}^{ik} \bar{h}_{bk}^{jc} \\ &\quad - 4z_{ad}^{kl} t_{kl}^{cd} V_{cb}^{ij} - 4z_{bd}^{kl} t_{kl}^{cd} V_{ac}^{ij} + 2z_{ad}^{kl} t_{kl}^{cd} V_{bc}^{ij} + \cdots \quad \text{(56 terms).} \end{aligned} \tag{71}$$

(Note since $V_{ab}^{ij} = \bar{h}_{ab}^{ij} = g_{ab}^{ij}$, these amplitudes will always be written as V_{ab}^{ij}.) In the first step of expression (70), the expansion from **H** to $\bar{\mathbf{H}}$ initially generates 464 terms, which are then canonically rewritten by `reindex` and combine to the 56 distinct terms in expression (71) above. The `toTransformedHamiltonian` substitution rules used to perform this "reverse-direction" expansion will be considered in the next section. Lastly, permutations on the equivalent $i \leftrightarrow j$ and $a \leftrightarrow b$ external indices are extracted and $\tilde{z}_{cd}^{kl} \equiv 2z_{cd}^{kl} - z_{dc}^{kl}$ is collected, yielding the 12 distinct terms that appear in Table 8,

```
% // extractPermutations
  // collectWiggle[#,{z}]&,
```
(72)

$$\tfrac{1}{2}\big(1 + P_{ij}^{ab}\big)(2 - P_{ij})\big(2z_a^i \bar{h}_b^j + 2\tilde{z}_{ac}^{ik} \bar{h}_{bk}^{jc} - 2\tilde{z}_{ad}^{kl} t_{kl}^{cd} V_{cb}^{ij} + \cdots\big) \quad \text{(12 terms).} \tag{73}$$

In a similar fashion, the homogeneous side of the *one*-body **Z** equation is obtained by instead differentiating with respect to `t[a, i]` in the `derivative` call in expression (68).

The inhomogeneous side of the two-body **Z** equation, formulated in terms of a chain rule, $\sum_\mu (\partial F^{inh}/\partial \bar{h}_\mu)(\partial \bar{h}_\mu/\partial t_{ij}^{ab})$, is obtained in a similarly straightforward manner,

```
functionalEESinglet[]
   /. z[__]->0
   // chainRule[#,t[a,b,i,j]]&                    (74)
```

(the leading minus sign is not included here). In the first step above, the z_μ terms are eliminated from the energy functional to give F^{inh}. In the second step, the `chainRule` function performs a series of direct differentiations in an analogous approach to that described above. Output are the general chain-rule derivative expression $\sum_\mu \bar{D}_\mu(\partial \bar{h}_\mu/\partial t_{ij}^{ab})$ (in Table 8), the EE-STEOM $\bar{D}_\mu$ expressions (in Table 14), and the EE-STEOM explicit derivative contributions (in Table 9). The `chainRule` script thus contains three chief substeps, namely the construction of the general chain-rule expression in terms of dummy $\bar{D}_\mu$ and the actual $\partial \bar{h}_\mu/\partial t_{ij}^{ab}$ expressions, the derivation of the particular $\bar{D}_\mu$ expressions themselves from F^{inh}, and the derivation of the explicit contributions to the derivative. A definitive check of the chain-rule construction is then performed against the full direct t_{ij}^{ab} differentiation result. Although handled automatically, the details of these substeps will now be considered, in particular to show that they are mainly a scripted execution of the direct differentiation technique already described.

First, construction of the general chain-rule derivative expression proceeds by differentiating each of the zero-, one-, and two-body $\bar{\mathbf{H}}$ amplitudes: $\bar{h}_0 \quad \bar{h}_c^k \quad \bar{h}_k^c \quad \bar{h}_l^k \quad \bar{h}_d^c \quad \bar{h}_{k_3k_4}^{k_1k_2} \quad \bar{h}_{ck_3}^{k_1k_2} \quad \bar{h}_{k_2k_3}^{ck_1} \quad V_{cd}^{kl} \quad \bar{h}_{kl}^{cd} \quad \bar{h}_{dl}^{ck} \quad \bar{h}_{dl}^{kc} \quad \bar{h}_{c_2c_3}^{kc_1} \quad \bar{h}_{kc_3}^{c_1c_2} \quad \bar{h}_{c_3c_4}^{c_1c_2}$, with respect to t_{ij}^{ab}: Each $\bar{h}_\mu$ amplitude is expanded to its basic **H** and **T** amplitudes, differentiated directly with respect to t_{ij}^{ab}, and re-expressed back in terms of $\bar{\mathbf{H}}$ amplitudes as factorization. Each $\partial \bar{h}_\mu/\partial t_{ij}^{ab}$ derivative expression is then tensor-multiplied with the corresponding *dummy* $\bar{D}_\mu$ element to construct the general chain-rule expression. For example, the $\bar{D}_{ck_1}^{k_2k_3}(\partial \bar{h}_{k_2k_3}^{ck_1}/\partial t_{ij}^{ab})$ contribution is obtained essentially as

```
dbar[k2,k3,c,k1]*
  (((hbar[c,k1,k2,k3]
     /. toBareHamiltonian)
     // derivative[#,t[a,b,i,j]]&)
     /. toTransformedHamiltonian)
   // extractPermutations                         (75)
```

to yield these chain-rule terms

$$+\tfrac{1}{2}\big(1+P_{ij}^{ab}\big)\big(\bar{D}_{bk}^{ji}\bar{h}_a^k-\bar{D}_{bk}^{li}\bar{h}_{al}^{kj}-\bar{D}_{bk}^{jl}\bar{h}_{al}^{ki}+\bar{D}_{ck}^{ij}\bar{h}_{ba}^{kc}+(2-P_{ij})\big(\bar{D}_{bk}^{jl}\bar{h}_{al}^{ik}\big)\big) \tag{76}$$

appearing in Table 8. The expansion and differentiation (third and fourth lines above) at first generates 26 distinct terms, the re-expression in terms of $\bar{\mathbf{H}}$ (fifth line) reduces this to 12 distinct terms (when reindexed; 40 initially upon expansion), and the extraction of permutations (sixth line) reduces this to the 5 distinct terms of the result.

Second, the `chainRule` script derives the *actual* EE-STEOM $\bar{D}_\mu \equiv \partial F^{inh}/\partial \bar{h}_\mu$ expressions. In order to perform these differentiations with respect to $\bar{h}_\mu$, the input F^{inh} is first expressed completely in terms of the one- and two-body $\bar{\mathbf{H}}$ amplitudes (using `/. toTransformedHamiltonian`). This $\bar{\mathbf{H}}$-only expression is then differentiated directly with

respect to each of the $\bar{h}_\mu$ amplitudes given earlier, yielding the associated $\bar{D}_\mu$ expressions individually. Some factorization is then performed to arrive at the expressions as presented in Table 14.

Third, as a result of the passive expansion of the three-body $\bar{\mathbf{H}}$ amplitudes (see Section 5.2.3), the t_{ij}^{ab} chain-rule derivative additionally includes a small number of explicit contributions, which are collected in Table 9. Although these remaining contributions can trivially be obtained as the difference between the above chain-rule construct and the full $\partial F^{inh}/\partial t_{ij}^{ab}$ direct-differentiation result, they can also be derived from the $\bar{D}_\mu$ expressions that explicitly contain a $\mathbf{T}$ amplitude: Since the input functional is linear in the $\bar{\mathbf{H}}$ amplitudes, it can alternatively be viewed as $F^{inh} = \sum_\mu \bar{D}_\mu \bar{h}_\mu$, and thus if a $\bar{D}_\mu$ expression depends on $\mathbf{T}$, the *product rule* of differentiation defines two parts, a "chain-rule" part and an "explicit" part,

$$\frac{\partial}{\partial t_{ij}^{ab}}(\bar{D}_\mu \bar{h}_\mu) = \underbrace{\bar{D}_\mu \frac{\partial \bar{h}_\mu}{\partial t_{ij}^{ab}}}_{\substack{\text{chain-rule} \\ \text{part}}} + \underbrace{\bar{h}_\mu \frac{\partial \bar{D}_\mu}{\partial t_{ij}^{ab}}}_{\substack{\text{explicit} \\ \text{part}}} . \tag{77}$$

For discussion, see Section 5.2.3. To compute the explicit parts, the `chainRule` function differentiates with respect to t_{ij}^{ab} each such $\bar{D}_\mu$ containing $\mathbf{T}$ and tensor-multiplies the result by the associated $\bar{h}_\mu$ amplitude. For the STEOM methods, only $\bar{D}_{kl}^{cd}$ contains $\mathbf{T}$ amplitudes, and the explicit part is computed automatically as

```
v[k,l,c,d]*
  ((dbar[c,d,k,l]
    /. makeRule[dBarExpressions])
    // derivative[#,t[a,b,i,j]]&)
  // extractPermutations
```
(78)

to yield the EE-STEOM explicit contribution

$$+\tfrac{1}{2}\big(1+P_{ij}^{ab}\big)(2-P_{ij})\big(-2d_{mb}^{ij}V_{ac}^{kl}s_{kl}^{mc}+d_{mb}^{ij}V_{ac}^{kl}s_{lk}^{mc}-2a_{ab}^{ej}V_{cd}^{ik}s_{ek}^{cd}+a_{ab}^{ej}V_{cd}^{ik}s_{ek}^{dc}\big) \tag{79}$$

seen in Table 9. (Above, the `makeRule` function creates substitution rules from the $\bar{D}_\mu$ expressions. On a technical note, the function is fairly elaborate, as it must protect in a general way the dummy summation indices appearing in the $\bar{D}_\mu$ expressions from conflicting with any possible substituted external indices.)

Finally, the above constructions are checked against the straightforward $\partial F^{inh}/\partial t_{ij}^{ab}$ direct-differentiation result. Namely, the full F^{inh} is expanded to basic terms and differentiated directly with respect to t_{ij}^{ab}. This outcome is compared against the chain-rule construction with all the $\bar{D}_\mu$ expressions substituted in (plus the explicit part and with the $\bar{\mathbf{H}}$ and permutations expanded). An exact match ensures that the `chainRule` function has performed properly.

In the same way, the chain-rule inhomogeneous side of the one-body $\mathbf{Z}$ equation is obtained by instead supplying `t[a,i]` as the argument to `chainRule` in expression (74). Likewise in the final D_μ expressions of Table 15, the chain-rule portions,

$\sum_\nu \bar{D}_\nu(\partial \bar{h}_\nu/\partial h_\mu)$, are obtained by now supplying each bare h_μ amplitude as the argument to `chainRule`,

```
functionalEESinglet[]
  /. z[__]->0 // chainRule[#,f[i,a]]&,
functionalEESinglet[]
  /. z[__]->0 // chainRule[#,v[i,j,a,b]]&,
...,
```
(80)

and the reference CCSD portions, $\partial\langle\Phi_0|\hat{Z}\hat{\bar{H}}|\Phi_0\rangle/\partial h_\mu$, are obtained by direct differentiation,

```
Z$equationT[]
  /. toBareHamiltonian // derivative[#,f[i,a]]&,
Z$equationT[]
  /. toBareHamiltonian // derivative[#,v[i,j,a,b]]&,
...,
```
(81)

followed by extraction of permutations and other factorization. Of course for comparison, complete non-chain-rule D_μ expressions could also be computed by differentiating the total functional directly with respect to each bare h_μ amplitude,

```
functionalEESinglet[]
  /. toBareHamiltonian // derivative[#,f[i,a]]&,
functionalEESinglet[]
  /. toBareHamiltonian // derivative[#,v[i,j,a,b]]&,
....
```
(82)

Finally, the $\mathbf{S}^\pm$ derivatives (the $\mathbf{Z}^\pm$ equations) of Tables 11 and 12 are obtained in the same way by fully expanding the functional to the bare Hamiltonian amplitudes, directly differentiating with respect to each of the four types of s_μ amplitudes, and re-expressing the result back in terms of $\bar{\mathbf{H}}$ as factorization. (In actuality, the full expansion to the bare $\mathbf{H}$ is not necessary, since $\bar{\mathbf{H}}$ does not depend on $\mathbf{S}$, and so the functional need only be written exclusively in terms of $\bar{\mathbf{H}}$ amplitudes before differentiation.) In this way, all the derivative expressions needed for the analytical energy gradient are obtained through a systematic, fully algebraic derivation procedure: Starting from the electronic method's input algebraic Lagrange multiplier energy functional, the derivation proceeds by direct differentiation (or scripted direct differentiation for the chain rule) with respect to each non-variational energy parameter or Hamiltonian amplitude.

4.3. Interconversion between H, $\bar{\mathbf{H}}$, and $\mathbf{G_2}$ amplitudes

In the examples of the preceding section, full expansion to the most basic amplitudes was accomplished through the `toBareHamiltonian` expansion rules, and either expansion or factorization was achieved through the `toTransformedHamiltonian` expansion rules. The origin of these interconversion expressions between $\mathbf{H}$, $\bar{\mathbf{H}}$, and $\mathbf{G_2}$ Hamiltonian amplitudes warrants some further consideration. As seen above, the ability to perform such

interconversions is a vital feature for manipulating the algebraic expressions. It allows input in whatever Hamiltonian terms are most convenient and allows one to go back and forth as needed. Before differentiation, for example, all Hamiltonian amplitudes that explicitly depend on the differentiating amplitude must first be expanded to component terms. Relatedly, chain-rule differentiation with $\bar{\mathbf{H}}$ as the intermediate variables requires the expression to first be written in terms of $\bar{\mathbf{H}}$ Hamiltonian amplitudes only. Throughout the equations, the $\bar{\mathbf{H}}$ amplitudes in particular serve as useful intermediates in the compact factorization of the derivative expressions (see Section 4.4).

In the following discussion, only the one- and two-body amplitudes are considered. In *SMART*, the explicit formulas are available for the expansion of every $\bar{\mathbf{H}}$ amplitude in terms of its component $\mathbf{H}$ (and $\mathbf{T}$) amplitudes

$$\bar{h}_\mu = h_\mu + \underset{\sim}{\phi}_\mu(\mathbf{H}, \mathbf{T}) \tag{83}$$

and every $\mathbf{G_2}$ amplitude in terms of its component $\bar{\mathbf{H}}$ (and $\mathbf{S_2}$) amplitudes

$$g_\mu = \bar{h}_\mu + \underset{\sim}{\theta}_\mu(\bar{\mathbf{H}}, \mathbf{S_2}). \tag{84}$$

The $\bar{h}_\mu$ and g_μ formulas are defined by the $\hat{\bar{H}}$ and $\hat{G}_2$ similarity transformations, expressions (2) and (11), and these similarity transformations have been evaluated diagrammatically to yield the explicit algebraic spatial-orbital formulas given, for instance, in references [157] and [3], respectively. For completeness, these "forward-direction" $\bar{h}_\mu$ and g_μ expansion formulas are reproduced here in Tables 5, 6, and 7.

The derivation of the "reverse-direction" expansions, that is, formulas for converting each *untransformed* Hamiltonian amplitude to its "expansion" in terms of the *transformed* amplitudes, is less obvious. To be clear, these formulas refer to the inverses of expressions (83) and (84), namely expansions of every $\mathbf{H}$ amplitude in terms of $\bar{\mathbf{H}}$ amplitudes

$$h_\mu = \bar{h}_\mu - \underset{\sim}{\Phi}_\mu(\bar{\mathbf{H}}, \mathbf{T}) \tag{85}$$

and every $\bar{\mathbf{H}}$ amplitude in terms of $\mathbf{G_2}$ amplitudes

$$\bar{h}_\mu = g_\mu - \underset{\sim}{\Theta}_\mu(\mathbf{G_2}, \mathbf{S_2}). \tag{86}$$

These reverse formulas are in principle defined by the inverse similarity transformations, where the $\hat{\bar{H}}$ and $\hat{G}_2$ expressions (2) and (11) are multiplied from the right and left by the appropriate inverse operators (although the same difficulty in principle is caused by the unknown $\{e^{\hat{S}}\}^{-1}$). In practice, however, the reverse expressions are instead obtained by backward substitution of the forward expressions among themselves. For a complete discussion of such backward substitutions, see reference [25]. To understand the process, first note that $\hat{T}$ and $\hat{S}_2$ are net-excitation operators, and thus, when contracted with a Hamiltonian amplitude, always increase its net-excitation level (*i.e.* increase the net number of q-creation operators and/or decrease the net number of q-annihilation operators). In the forward equations (83) and (84), therefore, a given $\bar{h}_\mu$ or g_μ amplitude can only depend on the matching uncontracted amplitude or on contracted Hamiltonian amplitudes of *lower* net-excitation levels. By ordering the forward equations from least to greatest net-excitation level, each equation then only depends on those that precede it, and backward substitution to convert all the untransformed Hamiltonian amplitudes to the transformed amplitudes proceeds in one cascading step. The forward $\bar{\mathbf{H}}$ and $\mathbf{G_2}$ equations of Tables 6 and 7 are sorted in order of increasing net-excitation level to make clearer this relationship structure.

However, as a result of this inherent structure, brute-force backward substitution of the forward equations in *any* order until the result no longer changes also terminates, although then the number of steps is unknown. While such a clumsy substitution is impractical by hand, it can easily be carried out by computer.

With these explicit forward and reverse formulas, conversion of an expression to be written completely in terms of only one- and two-body **H**, $\bar{\mathbf{H}}$, or $\mathbf{G_2}$ Hamiltonian amplitudes is accomplished by simple global substitution. For example, the `toBareHamiltonian` rules seen in the previous section expand every $\bar{h}_\nu$ or g_γ amplitude by its unique formula in terms of **H** only; the substitution rules are given by the forward equations (83) or (84), respectively (with (83) also substituted into the (84) expressions). Oppositely, to convert an expression to be written in terms of $\bar{\mathbf{H}}$ Hamiltonian amplitudes only, the `toTransformed-Hamiltonian` rules replace every g_γ or (bare) h_ν amplitude by its unique formula in terms of $\bar{\mathbf{H}}$ only, according to expressions (84) or (85), respectively. (Although not needed in this work, `toDoubleTransformedHamiltonian` rules can also be constructed to express all Hamiltonian amplitudes in terms of only $\mathbf{G_2}$, using equations (86) and equations (86) substituted into (85).)

4.4. Factorization approach

Although the detailed algebraic gradient expressions are derived here by computer, their subsequent implementation (into the program code of the ACES II electronic structure suite) is still performed here by hand. The aim of the factorization of the algebraic expressions, therefore, is to create a uniform computational framework for calculating the gradient, requiring the least amount of new programming code per electronic method. To this end, the $\bar{\mathbf{H}}$ amplitudes in particular play a central role, as they are common to all CCSD/PT-based methods. They serve as the linking variables in the chain-rule differentiations, leading to (essentially) method-independent **Z** Lagrange multiplier equations and method-independent **D** conversion expressions, both in terms of the same $\bar{\mathbf{D}}$. Furthermore, the PT-based (ST)EOM gradients also use these same $\bar{\mathbf{D}}$, as the perturbative simplifications to $\bar{\mathbf{H}}$ are isolated outside of $\bar{\mathbf{D}}$. Additionally, employing the $\bar{\mathbf{H}}$ expressions as intermediate quantities leads to compact factorizations in the derivative expressions: In both the homogeneous and inhomogeneous sides of the **Z** equations (Table 8), the $\bar{\mathbf{H}}$ amplitudes effectively condense the expanded $\partial\bar{h}_\mu/\partial t_\nu$ derivative expressions. See, for instance, examples (71) and (76) previously. The basis of this simplification of the **T** derivatives will be examined in Section 5.2.1. Likewise, the $\mathbf{S}^{\pm}$ derivatives (the $\mathbf{Z}^{\pm}$ equations, Tables 11 and 12) find compact expression in terms of $\bar{\mathbf{H}}$. This central role of the $\bar{\mathbf{H}}$ amplitudes, especially the $\bar{\mathbf{D}}$ chain rule, applies systematically to all future CCSD/PT-based electronic methods.

In order to standardize the formulations and to reuse computer code, the factorizations employed in this work are thus motivated firstly by consistency of expression and only secondly by computational efficiency. While the systematics of the $\bar{\mathbf{H}}$ chain-rule derivatives lead to a largely efficient computational structure, the expensive $\bar{D}_{ab}^{cd}$ terms are formulated in the same manner as the inexpensive $\bar{D}_{ij}^{kl}$ terms, for example. Such expensive terms might be computed more efficiently by refining the factorization. The present factorization is generally sufficient, and the expressions are mostly implemented as presented in the tables. To improve the efficiency of some of the most expensive terms, a small number of

refactorizations and file management tweaks are implemented, and these are described in Section 5.6. Although the details are specific to the present ACES II implementation, the issues discussed are quite general.

In addition to the *overall* focus of the factorization/organization of the algebraic expressions, there is a low-level aspect to the factorization as well. In the end, the algebraic expressions are implemented in binary tensor multiplications, *e.g.* $y_{ab}^{ij} \equiv \tilde{z}_{ad}^{kl} t_{kl}^{cd} V_{cb}^{ij} \rightarrow x_a^c = \tilde{z}_{ad}^{kl} t_{kl}^{cd}$; $y_{ab}^{ij} = x_a^c V_{cb}^{ij}$ (and *not* $x_{klb}^{idj} = t_{kl}^{cd} V_{cb}^{ij}$; $y_{ab}^{ij} = \tilde{z}_{ad}^{kl} x_{klb}^{idj}$ or $x_{adcb}^{klij} = \tilde{z}_{ad}^{kl} V_{cb}^{ij}$; $y_{ab}^{ij} = x_{adcb}^{klij} t_{kl}^{cd}$). The goal of the low-level factorization is to minimize the number and expense of these final multiplications. As seen in the examples of Section 4.2 above, the `reindex`, `extractPermutations`, and `collectWiggle` functions serve to compact the algebraic expressions. Other detailed functions are included to aid the *SMART* user in finding and substituting reusable intermediate quantities, such as the u_μ, q_ν, and M_γ intermediates scattered throughout the tables. Functions are available, for instance, to recursively factor out amplitudes with the highest number of external indices or amplitudes of a particular operator type. The `reindex` function can take optional arguments to tailor the assignment of the summation indices in the output expressions. Ultimately, though, while the detailed expressions themselves are derived here by computer, this factorization process is driven largely by the user. And the final implementation is still performed here by hand.

With very recent advances, however, such as the APG [132,133], first generation TCE [134–136], optimizing TCE [137–141], or string-based [128–131] methods described in the Introduction, even the factorization and implementation of the derived expressions can be made automated. General automated factorization schemes might never even construct the $\bar{\mathbf{H}}$ intermediates but instead could factor the primitive, fully-expanded, derivative expressions directly, devising their own organization and reusable intermediate quantities. Such methods could heuristically take into account the characteristics of the computer hardware and software and the chemical system under consideration and could likely yield more efficient, though less transparent, factorizations. Moreover, the factorized expressions could be implemented automatically in error-free computer code, and the individualized implementation need not be constrained by considerations of the code's reusability for different electronic methods. Despite the complexity, great strides have been made in this young field of fully automated derivation and implementation, and further rapid progress is surely forthcoming.

5. THE (ST)EOM-CCSD/PT DETAILED ALGEBRAIC GRADIENT EQUATIONS

In this section, the specific spatial-orbital equations that must be solved for the closed-shell-reference EE-, IP-, and EA-EOM-CCSD/PT and EE-, DIP-, and DEA-STEOM-CCSD/PT analytical first derivatives are presented in full detail. All the *abstract operator* gradient expressions of the theory Sections 3.2 and 3.3 are instead derived here in *explicit algebraic* terms, in an automated straight-algebraic treatment using *SMART*. The *SMART* package is discussed in the previous Section 4. This Section 5 provides an essentially self-contained exposition of the steps involved in the derivation of the detailed (ST)EOM-CCSD/PT gradient equations as well as the steps involved in an actual gradient calculation. The discussion

explains in-depth features that arise in the working equations, many of which would be challenging to organize if derived by hand. Also examined are items relevant to implementing the detailed gradient expressions in an efficient computer code. Note that like Section 4, the index labels in this section and in the tables refer to *spatial* molecular orbitals; for additional comments on the notation, see the start of Section 4.

5.1. The EOM-CCSD/PT and STEOM-CCSD/PT Lagrange multiplier energy functionals

In Tables 3 and 4 (Section 5.8), respectively, the Lagrange multiplier energy functionals that define the EE-, IP-, and EA-EOM-CCSD/PT and the EE-, DIP-, and DEA-STEOM-CCSD/PT methods are presented in explicit algebraic terms. As discussed, the functionals are constructed from the energy expression for an electronic state in the particular method together with the supplementary equations that determine the energy parameters, each set of supplementary constraints tensor-multiplied by associated Lagrange multipliers. The explicit algebraic functionals serve as the input to the *SMART* package, and all subsequent derivative expressions are generated through automated symbolic manipulations.

We now consider some features of the detailed algebraic functionals. In the energy terms, the exact form of the spatial-orbital **L** and **R** amplitudes is not unique, and a spin-adapted form (*e.g.* $\tilde{l}^{ij}_{ab} \equiv 2l^{ij}_{ab} - l^{ij}_{ba}$) is chosen to make the algebraic expressions consistent with those obtained diagrammatically. This flexibility will be true of all the spatial-orbital amplitudes, and the convenient spin-adapted form will always be chosen. Obviously, the detailed gradient equations will depend on the particular choice, but in the end, the numerical value of the gradient (*i.e.* the final GHF effective density **D**) is unique. Note that the particular choice for the spatial-orbital **L** and **R** parameterization determines the specific explicit form of the EOM and STEOM eigenvector equations (equations (30)–(31) and (49)–(50), respectively), and the spin-adapted **L** and **R** are consistent with the EOM- and STEOM-CCSD/PT eigenvector equations as implemented in the ACES II program.

Moving on, the next term in the functionals, $\lambda(1-\langle\Phi_0|\hat{L}\hat{R}|\Phi_0\rangle)$, enforces normalization of the eigenvectors (see equation (29)). This term depends only on the **L** and **R** amplitudes and λ, and it therefore only contributes to the derivatives with respect to these parameters, the normalized EOM and STEOM eigenvector equations. The normalization term does not contribute to any other derivatives and will be omitted from the algebraic functionals.

The next term in the functionals, $\langle\Phi_0|\hat{Z}\hat{\bar{H}}|\Phi_0\rangle$, is associated with the constraint that the underlying CCSD or PT equations for **T** must be satisfied (equations (4) or (16), respectively). This term is the same for all the CCSD-based (ST)EOM methods, as well as for other methods based on a CCSD reference treatment. Its components are greatly simplified for the PT-based methods, due to the elimination of $\bar{h}^{a(1)}_{i}$ and the simplification of the $\bar{h}^{ab(1)}_{ij}$ expression. The explicit algebraic formulas (*e.g.* reference [157]) for these pure-excitation $\bar{\mathbf{H}}$ amplitudes are presented in Table 5. Again, there is a flexibility in choosing the specific spatial-orbital parameterization of the **Z** amplitudes, and the spin-adapted form is chosen. Alternatively, a plainer form could be used, such as

$$\langle\Phi_0|\hat{Z}\hat{\bar{H}}|\Phi_0\rangle = z^{i}_{a}\bar{h}^{a}_{i} + z^{ij}_{ab}\bar{h}^{ab}_{ij}, \tag{87}$$

which would simply lead to different details in the final gradient expressions. A different definition of the spatial-orbital parameterization would automatically be compensated for in the solution of the modified $\mathbf{Z}$ Lagrange multiplier equations.

In addition to the CCSD/PT $\hat{Z}$ Lagrange multiplier term, the STEOM functional contains two additional terms, $\sum_m \langle \Phi_m | \hat{Z}^- [\hat{G}, \hat{m}] | \Phi_0 \rangle$ and $\sum_e \langle \Phi^e | \hat{Z}^+ [\hat{G}, \hat{e}^\dagger] | \Phi_0 \rangle$, associated with the supplementary equations (9) and (10) that determine the $\mathbf{S}^-$ and $\mathbf{S}^+$ parameters, respectively. The spatial-orbital $\mathbf{Z}^-$ Lagrange multiplier amplitudes (d_μ) and $\mathbf{Z}^+$ Lagrange multiplier amplitudes (a_μ) are chosen, as always, to be spin-adapted. The explicit formulas for the full $\mathbf{G}$ (g_μ) amplitudes that determine $\mathbf{S}^\pm$ are reproduced from reference [3] in Table 5, and the explicit formulas for the $\mathbf{G_2}$ (g_μ) amplitudes are reproduced in Table 7; the few typographical errors appearing in reference [3] have been corrected here. The needed spatial-orbital $\bar{\mathbf{H}}$ expressions, adapted from reference [157], are presented in expanded form in Table 6.

5.1.1. Simplifications for the PT-based expressions

The only difference between the energy functionals for the PT-based and CCSD-based (ST)EOM methods is the simplification of the underlying $\bar{\mathbf{H}}$ formulas of Tables 5 and 6. The PT-based $\bar{\mathbf{H}}$ expressions are contained as a subset of the terms in the full CCSD-based $\bar{\mathbf{H}}$ expressions; therefore, the PT-based *functionals* are contained as a subset of the terms in the expanded CCSD-based functionals. The PT-based simplifications to $\bar{\mathbf{H}}$ are described in Section 2.2 and when applied to the CCSD-based functionals, result in the following prescription: $\mathbf{T_1} = \mathbf{0}$, $\mathbf{Z_1} = \mathbf{0}$, and in $\mathbf{Z_2}$ terms $\mathbf{V} = \mathbf{0}$ except V_{ij}^{ab}. This prescription is a convenient summary for extracting the detailed expressions for the PT-based functionals from the fully expanded CCSD-based algebraic expressions.

To elaborate, the first-order $\bar{h}_i^{a(1)} = 0$ automatically for HF orbitals. Thus, the $\mathbf{T_1}$ are not used in the $\hat{\bar{H}}$ similarity transformation, and all terms involving a one-body t_i^a amplitude are eliminated everywhere in the detailed CCSD-based algebraic expressions ($\mathbf{T_1} = \mathbf{0}$). Also, all terms in the functional that originate from the one-body $\bar{h}_i^a$ equation always multiply a one-body z_a^i amplitude and are thus eliminated from the expanded functionals by removing all terms containing $\mathbf{Z_1}$ ($\mathbf{Z_1} = \mathbf{0}$). The explicit first-order $\bar{h}_{ij}^{ab(1)}$ equation, defined abstractly in expression (16), is related to the full CCSD $\bar{h}_{ij}^{ab}$ expression by the above elimination of all $\mathbf{T_1}$ terms, as well as all terms involving a $\mathbf{V}$ amplitude besides V_{ij}^{ab}; since contributions originating from $\bar{h}_{ij}^{ab}$ always multiply a two-body z_{ab}^{ij} amplitude, then all terms containing both $\mathbf{Z_2}$ and a $\mathbf{V}$ amplitude besides V_{ij}^{ab} are not present in the expanded PT-based functionals.

The *derivative expressions* in the PT-based (ST)EOM methods can be obtained either by

1. differentiating the PT-based functionals directly, or
2. by applying the above prescription to the detailed CCSD-based derivative expressions.

An additional set of eliminations arises in the derivatives due to the last condition above: in two-body $\mathbf{D}$ expressions, $\mathbf{Z_2} = \mathbf{0}$ except in D_{ab}^{ij} (discussed below in Section 5.7). This list of simplifications—$\mathbf{T_1} = \mathbf{0}$, $\mathbf{Z_1} = \mathbf{0}$, in $\mathbf{Z_2}$ terms $\mathbf{V} = \mathbf{0}$ except V_{ij}^{ab}, and in two-body $\mathbf{D}$ expressions $\mathbf{Z_2} = \mathbf{0}$ except in D_{ab}^{ij}—can be viewed as a prescription for identifying the (ST)EOM-PT subset of terms that are contained in the full (ST)EOM-CCSD algebraic expressions, and for the remainder of this paper, these explicit simplifications will be referred

to as the PT-based "prescription". These simplifications lead to elimination of the $\mathbf{T_1}$ and $\mathbf{Z_1}$ equations and (using that the Fock matrix is diagonal for canonical HF orbitals) reduction of the $\mathbf{T_2}$ and $\mathbf{Z_2}$ equations to simple division by an energy denominator. Besides this procedural difference, and the straightforward exclusion of unneeded terms summarized by the above prescription, all other parts of the PT-based gradient calculation then proceed identically to that of the CCSD-based methods.

5.2. The (ST)EOM-CCSD/PT Z Lagrange multiplier equations

To emphasize the common features of the EOM-CCSD/PT and STEOM-CCSD/PT gradients, we will first consider the equations that determine the **Z** Lagrange multipliers associated with the non-variational **T** parameters of the underlying CCSD or PT reference treatment. The equations for **Z** are determined by setting to vanish the derivatives of the functional with respect to the associated **T** parameters (see equations (42) or (62)). For all electronic methods based on a CCSD or PT reference treatment, the algebraic spatial-orbital equations for the **Z** Lagrange multipliers are presented in Table 8 (Section 5.8). The homogeneous sides of the **Z** equations originate from the common $\bar{h}_i^a$-and-$\bar{h}_{ij}^{ab}$ or $\bar{h}_{ij}^{ab(1)}$ contributions to the functionals and are thus identical for all CCSD-based or PT-based electronic methods, respectively. The inhomogeneous sides, while containing all of the electronic method dependence, are cast into a method-independent form through a chain rule in the common $\bar{\mathbf{H}}$ amplitudes. The (ST)EOM-variant dependence is then contained completely and compactly in the intermediate density matrix $\bar{\mathbf{D}}$ (and the associated explicit three-body terms). Although discussed next, note that for the STEOM methods, the **Z** equations are solved *after* the $\mathbf{Z}^{\pm}$ equations (due to the presence of $\mathbf{Z}^{\pm}$ in $\bar{\mathbf{D}}$).

5.2.1. Homogeneous sides of the **Z** *equations*

The expressions on the CCSD-based homogeneous left sides in Table 8 are equivalent in form to the $\boldsymbol{\Lambda}$ terms of ground-state CCSD gradient theory, originally derived through the Z-vector method and diagrammatic expansion [109]. In the present work, these homogeneous-side derivative expressions are generated directly by symbolic differentiation of the algebraic Lagrange multiplier energy functionals, through operations that are typical of the *SMART* package (see Section 4.2): Beginning with the simple algebraic form of $\langle \Phi_0 | \hat{Z} \hat{\bar{H}} | \Phi_0 \rangle$ in Table 3/Table 4, the transformed Hamiltonian $\bar{\mathbf{H}}$ amplitudes are first expanded to basic terms, the bare Hamiltonian **H** and **T** amplitudes, to allow differentiation. Direct differentiation is then performed with respect to the appropriate **T** amplitude. The **H** amplitudes are then converted back to $\bar{\mathbf{H}}$ amplitudes to simplify the expressions. The canonical reindexing procedure ensures that only unique terms remain. Permutations are extracted on equivalent external indices, and some additional factorization is performed. For the PT-based methods, the one-body **Z** equation is not present, and the homogeneous side of the two-body equation condenses to a simple energy factor.

As mentioned above, after performing the **T** derivatives on the fully expanded expressions, the conversion from the basic **H** amplitudes *back* to the transformed $\bar{\mathbf{H}}$ amplitudes accounts for a great deal of factorization. Although many terms are initially introduced in the "expansion" of each **H** amplitude to the transformed $\bar{\mathbf{H}}$ amplitudes (using the inverted **H**-to-$\bar{\mathbf{H}}$ expressions (85)), most terms cancel against other expanded terms, leaving

a much-compacted $\bar{\mathbf{H}}$-only expression. Since the derivative of an exponential is again an exponential, it might be expected that the $\mathbf{T}$ derivatives of the $\bar{\mathbf{H}}$ amplitudes (expanded first to basic terms) can regenerate the similarity transformation. More formally, as considered for example in reference [157], the $\mathbf{T}$ derivatives can be written in terms of a commutator involving $\hat{\bar{H}}$,

$$\begin{aligned}\tfrac{\partial}{\partial t_\nu}\langle\Phi_0|\hat{X}\hat{\bar{H}}\hat{Y}|\Phi_0\rangle &= \tfrac{\partial}{\partial t_\nu}\langle\Phi_0|\hat{X}e^{-\hat{T}}\hat{H}e^{\hat{T}}\hat{Y}|\Phi_0\rangle \\ &= \langle\Phi_0|\hat{X}\big(\tfrac{\partial}{\partial t_\nu}e^{-\hat{T}}\big)\hat{H}e^{\hat{T}}\hat{Y}|\Phi_0\rangle + \langle\Phi_0|\hat{X}e^{-\hat{T}}\hat{H}\big(\tfrac{\partial}{\partial t_\nu}e^{\hat{T}}\big)\hat{Y}|\Phi_0\rangle \\ &= \langle\Phi_0|\hat{X}\big(-\hat{\Omega}_\nu e^{-\hat{T}}\big)\hat{H}e^{\hat{T}}\hat{Y}|\Phi_0\rangle + \langle\Phi_0|\hat{X}e^{-\hat{T}}\hat{H}\big(e^{\hat{T}}\hat{\Omega}_\nu\big)\hat{Y}|\Phi_0\rangle \\ &= \langle\Phi_0|\hat{X}[\hat{\bar{H}},\hat{\Omega}_\nu]\hat{Y}|\Phi_0\rangle, \end{aligned} \tag{88}$$

and thus the $\mathbf{T}$ derivatives can be written precisely *and compactly* back in terms of $\bar{\mathbf{H}}$ amplitudes. In expression (88), $\hat{\Omega}_\nu$ is the (pure-excitation) elementary-operator component associated with coefficient t_ν in $\hat{T}$, and $\hat{X}$ and $\hat{Y}$ are arbitrary operators that are independent of $\mathbf{T}$. Note that the above regeneration of the similarity transformation relies on the fact that the pure-excitation operators $\hat{\Omega}_\nu$ and $\hat{T}$ commute (which is not true for the derivatives involving $\hat{S}$, considered later).

Careful examination of the derivative expressions in Table 8, however, reveals the presence of "leftover" $\mathbf{T}$ amplitudes, which seems to contradict the above discussion since they are all expected to be absorbed back into the $\bar{\mathbf{H}}$ amplitudes. These two-body $\mathbf{T}$ amplitudes *could* in fact combine with the two-body $\bar{\mathbf{H}}$ amplitudes to which they are contracted to form three-body $\bar{\mathbf{H}}$ amplitudes. But as noted earlier, all amplitudes are left written here in terms of only one- and two-body components, and these three-body $\bar{\mathbf{H}}$ amplitudes remain automatically in an expanded form. Some more-subtle consequences of this passive expansion of the three-body $\bar{\mathbf{H}}$ amplitudes, but which nevertheless are handled automatically here, are considered in Section 5.2.3.

5.2.2. Inhomogeneous sides of the $\mathbf{Z}$ *equations*

Whereas the homogeneous left sides of the $\mathbf{Z}$ equations depend only on the CCSD/PT reference treatment (*i.e.* $\bar{\mathbf{H}}$) automatically, the inhomogeneous right sides can also be constructed as such through a chain rule in the $\bar{\mathbf{H}}$ amplitudes (expression (43)). All of the post-CCSD/PT (ST)EOM-variant dependence is then isolated in the intermediate density matrix $\bar{\mathbf{D}}$. The chain-rule expressions presented in Table 8 were generated by automated construction from the derivatives of the CCSD $\bar{\mathbf{H}}$ amplitudes (see Section 4.2): Each one- and two-body $\bar{h}_\mu$ amplitude was fully expanded in terms of its component $\mathbf{H}$ and $\mathbf{T}$ amplitudes, differentiated with respect to t_ν, re-expressed back in terms of $\bar{\mathbf{H}}$ amplitudes, and tensor-multiplied with the associated dummy $\bar{D}_\mu$ element. Permutations on external indices were then extracted, and some factorization was performed. The chain-rule constructs can be checked by substitution of the $\bar{\mathbf{D}}$ elements for each method and comparison to the $\mathbf{T}$ derivatives of the functional performed directly (along with the addition of the explicit three-body terms discussed in the next section).

Two simple terms on the inhomogeneous sides whose origin may not be obvious are the isolated Hamiltonian terms $2\bar{h}^i_a$ and $(2 - P_{ij})V^{ij}_{ab}$ that are not multiplied by a $\bar{\mathbf{D}}$ element.

These are the result of chain-rule differentiation with respect to $\bar{h}_0$,

$$\frac{\partial F^{inh}}{\partial \bar{h}_0} \cdot \frac{\partial \bar{h}_0}{\partial t_\nu} \rightarrow \begin{cases} \dfrac{\partial F^{inh}}{\partial \bar{h}_0} \equiv \bar{D}_0 = 1, \\ \dfrac{\partial \bar{h}_0}{\partial t_i^a} = 2\bar{h}_a^i \quad \text{and} \quad \dfrac{\partial \bar{h}_0}{\partial t_{ij}^{ab}} = (2 - P_{ij}) V_{ab}^{ij}, \end{cases} \tag{89}$$

and are the same for all methods (with the exception that the t_i^a derivative is not present for the PT-based methods).

5.2.3. Three-body contributions to the **Z** *equations and* $\bar{\mathbf{D}}$

We now examine the formal modifications that arise from a more practical approach to three-body terms. In principle, the three-body $\bar{\mathbf{H}}$ and $\bar{\mathbf{D}}$ amplitudes could be formulated in the same straightforward manner as the one- and two-body amplitudes. In an actual gradient calculation, however, three-body (six-index) matrices are expensive to store and manipulate, and these handful of contributions are computed more efficiently in terms of their lower-body components. Since all the basic operators employed in this work are at most two-body, all algebraic expressions can therefore be written in terms of zero-, one-, and two-body amplitudes *only*. The three-body amplitudes are simply left expanded in their (up to two-body) component terms. This passive expansion of the three-body $\bar{\mathbf{H}}$ and $\bar{\mathbf{D}}$ amplitudes leads to two departures from the formal chain-rule organization. Although explained in detail here, we emphasize that the resulting modifications are all handled automatically (and correctly!) by the mathematics in the automated algebraic treatment. For the most part, in fact, the *SMART* package takes no special action regarding the expanded three-body terms and treats them as it would any other tensor product. An in-depth understanding of the formal reorganization is not crucial, and the uninterested reader can skip to the next section.

The most noticeable consequence of leaving all expressions written in terms of only up to two-body amplitudes is that the t_{ij}^{ab} chain-rule derivative of Table 8 requires some remaining three-body contributions to be added in explicitly, and the expressions are collected in Table 9 (Section 5.8). These leftover method-dependent three-body contributions can be obtained trivially as the difference between the t_{ij}^{ab} direct-differentiation result and the expansion of the one- and two-body $\bar{\mathbf{D}}$ elements for each variant into the t_{ij}^{ab} chain-rule construct. As mentioned in the *SMART* examples (Section 4.2), however, these additional contributions can also be derived directly, by differentiating the $\bar{\mathbf{D}}$ expressions that contain **T** amplitudes. The appearance of **T** amplitudes in $\bar{\mathbf{D}}$ is a second, more-subtle, consequence of treating everything in terms of only up to two-body amplitudes.

According to the definition of $\bar{\mathbf{D}}$ in expression (44), *i.e.* $\bar{D}_\mu \equiv \partial F^{inh}/\partial \bar{h}_\mu$ (where μ includes three-body indices), one would expect $\bar{\mathbf{D}}$ not to contain any **T** amplitudes. Prior to the above differentiation, F^{inh} must be written exclusively in terms of $\bar{\mathbf{H}}$ amplitudes, and these $\bar{\mathbf{H}}$ should absorb all the **T** amplitudes, as $\bar{\mathbf{H}}$ is their only possible source. However, the three-body $\bar{\mathbf{H}}$ amplitudes are left written in terms of their lower-body (actually two-body) $\bar{h}_\nu$ and t_γ components. In differentiating the functional with respect to these specific two-body $\bar{h}_\nu$ amplitudes, the t_γ amplitudes will remain and thus will appear explicitly in the resulting associated two-body $\bar{D}_\nu$ expressions. These modified $\bar{D}_\nu$ no longer strictly correspond to the *formal* interpretation of expression (44), since they now additionally

contain the contributions that belong to the missing three-body $\bar{\mathbf{D}}$. But these $\bar{D}_\nu$ still satisfy the *algebraic* definition $\partial F^{inh}/\partial \bar{h}_\mu$, where μ now runs over only up to two-body indices.

In the formal chain-rule expression (43), repeated here for convenience,

$$\frac{\partial F^{inh}}{\partial t_\nu} = \sum_\mu \bar{D}_\mu \frac{\partial \bar{h}_\mu}{\partial t_\nu}, \tag{90}$$

the compound index μ runs over all the $\bar{\mathbf{H}}$ amplitudes, including the three-body terms, and *only* $\bar{\mathbf{H}}$ *is assumed to be an explicit function of* $\mathbf{T}$. But since certain $\bar{\mathbf{D}}$ elements are now also explicit functions of $\mathbf{T}$, this formal chain-rule derivative must be generalized to include the product rule of differentiation:

$$\frac{\partial F^{inh}}{\partial t_\nu} = \sum_\mu \bar{D}_\mu \frac{\partial \bar{h}_\mu}{\partial t_\nu} + \sum_\mu \bar{h}_\mu \frac{\partial \bar{D}_\mu}{\partial t_\nu}. \tag{91}$$

If μ includes the three-body indices, then no $\mathbf{T}$ appear in $\bar{\mathbf{D}}$, and the second term above drops out, leaving only the original chain-rule term. If μ includes only up to *two*-body indices, then the contributions arising from the expanded three-body $\bar{\mathbf{H}}$ amplitudes are instead distributed between the two types of terms in the product rule (91). In the first term, the chain-rule term, certain two-body $\bar{\mathbf{D}}$ elements pick up the contributions that formally belong to the absent three-body $\bar{\mathbf{D}}$; these modifications appear as terms that contain a $\mathbf{T}$ amplitude explicitly. Since certain $\bar{\mathbf{D}}$ explicitly now depend on $\mathbf{T}$, the second term in expression (91) generates some additional three-body contributions, which must be added to the chain-rule term. These "explicit" contributions are method-dependent, since they arise from derivatives of the method-dependent $\bar{\mathbf{D}}$. The explicit contributions are a rigorous mathematical consequence of the modified $\bar{\mathbf{D}}$ and the product rule of differentiation.

This abstract discussion is perhaps better understood through example. In the EE-EOM-CCSD/PT method, one of the three-body $\bar{\mathbf{H}}$ contributions appearing the input energy functional looks like

$$\sim \bar{h}^{lc}_{db} t^{ab}_{ij} \in \bar{h}^{acl}_{ijd}, \tag{92}$$

where the $\sim$ represents the factors and permutations (*cf.* Table 3) that have been omitted for clarity. If three-body $\bar{\mathbf{H}}$ amplitudes were written directly, the chain-rule construct in the two-body $\mathbf{Z}$ equation would simply contain the (expensive) expression

$$\bar{D}^{ijd}_{acl} \frac{\partial \bar{h}^{acl}_{ijd}}{\partial t^{ab}_{ij}}. \tag{93}$$

By leaving this three-body $\bar{\mathbf{H}}$ amplitude written in terms of its lower-body components, as above, the product rule of differentiation generates

$$\begin{aligned} \bar{D}^{ijd}_{acl} \frac{\partial \bar{h}^{acl}_{ijd}}{\partial t^{ab}_{ij}} \ni\ & \bar{D}^{ijd}_{acl} \frac{\partial (\sim t^{ab}_{ij} \bar{h}^{lc}_{db})}{\partial t^{ab}_{ij}} \\ &= \underbrace{(\sim \bar{D}^{ijd}_{acl} t^{ab}_{ij}) \left(\frac{\partial \bar{h}^{lc}_{db}}{\partial t^{ab}_{ij}} \right)}_{\substack{\text{contribution} \\ \text{to } \bar{D}^{db}_{lc} \\ \text{chain rule}}} + \underbrace{(\sim \bar{D}^{ijd}_{acl} \bar{h}^{lc}_{db}) \left(\frac{\partial t^{ab}_{ij}}{\partial t^{ab}_{ij}} \right)}_{\substack{\text{explicit} \\ \text{contribution} \\ \sim \bar{D}^{ijd}_{acl} \bar{h}^{lc}_{db}}}. \end{aligned} \tag{94}$$

(For simplicity, a somewhat imprecise notation has been chosen, where i, j, a, b appear both as dummy summation indices and as external indices on the differentiating t_{ij}^{ab}.)

The first term in the product rule (94) is part of the $\bar{h}_{db}^{lc}$ chain rule and thus modifies the associated *two*-body $\bar{D}_{lc}^{db}$ expression to additionally contain a *three*-body contribution $\sim\bar{D}_{acl}^{ijd}t_{ij}^{ab}$ (the **T** term in $\bar{D}_{ia}^{bc}$ in Table 10). This "modified" two-body $\bar{\mathbf{D}}$ element nevertheless retains its simple algebraic definition, $\bar{D}_{lc}^{db} \equiv \partial F^{inh}/\partial\bar{h}_{db}^{lc}$, and this uptake of the three-body contribution happens automatically, by treating all expressions in terms of up to two-body $\bar{\mathbf{H}}$ amplitudes only.

The second term in the product rule (94) contributes to the t_{ij}^{ab} derivative explicitly (and yields the first of the explicit EE-EOM three-body contributions in Table 9). To make the connection with how the explicit contributions are calculated by the `chainRule` function in expression (77) of the *SMART* examples, consider the following. Since the formal three-body $\bar{D}_{acl}^{ijd}$ is independent of **T**, it can be brought inside the derivative in the explicit contribution,

$$\left(\sim\bar{D}_{acl}^{ijd}\bar{h}_{db}^{lc}\right)\left(\frac{\partial t_{ij}^{ab}}{\partial t_{ij}^{ab}}\right) = \bar{h}_{db}^{lc}\frac{\partial(\sim\bar{D}_{acl}^{ijd}t_{ij}^{ab})}{\partial t_{ij}^{ab}} = \bar{h}_{db}^{lc}\frac{\partial\bar{D}_{lc}^{db}}{\partial t_{ij}^{ab}}; \tag{95}$$

the $\sim\bar{D}_{acl}^{ijd}t_{ij}^{ab}$ under the derivative in the middle portion above is precisely the modification to $\bar{D}_{lc}^{db}$ seen in the chain-rule term in expression (94). In this way, the explicit contributions are obtained from the derivatives of the modified $\bar{\mathbf{D}}$ expressions that now contain **T** amplitudes.

These modified two-body $\bar{\mathbf{D}}$ expressions properly carry the three-body contributions throughout the rest of the gradient calculation. For instance, the modified $\bar{D}_{lc}^{db}$ participates in the *one*-body t_i^a chain-rule derivative; even though there is no *explicit* method-dependent three-body contribution as there is in the two-body t_{ij}^{ab} chain rule, there is an *implicit* three-body contribution hidden in the modified $\bar{\mathbf{D}}$. Likewise, the three-body contributions in $\bar{\mathbf{D}}$ carry through to the full effective density matrix **D** and thus to the gradient. For example, the modification of $\bar{D}_{lc}^{db}$ is transparent to the conversion to the full **D**, as it simply amounts to a slightly different partitioning in the final **D** expressions:

$$\begin{aligned}
D_\mu &= \left(\bar{D}_{lc}^{db}\right)_{\text{formal}}\frac{\partial\bar{h}_{db}^{lc}}{\partial h_\mu} + \bar{D}_{acl}^{ijd}\frac{\partial\bar{h}_{ijd}^{acl}}{\partial h_\mu} + \cdots \\
&= \left(\bar{D}_{lc}^{db}\right)_{\text{formal}}\frac{\partial\bar{h}_{db}^{lc}}{\partial h_\mu} + \bar{D}_{acl}^{ijd}\frac{\partial(\sim\bar{h}_{db}^{lc}t_{ij}^{ab})}{\partial h_\mu} + \cdots \\
&= \left(\left(\bar{D}_{lc}^{db}\right)_{\text{formal}} + \sim\bar{D}_{acl}^{ijd}t_{ij}^{ab}\right)\frac{\partial\bar{h}_{db}^{lc}}{\partial h_\mu} + \cdots \\
&= \left(\bar{D}_{lc}^{db}\right)_{\text{modified}}\frac{\partial\bar{h}_{db}^{lc}}{\partial h_\mu} + \cdots .
\end{aligned} \tag{96}$$

This last illustration underscores the fact that there are multiple ways to formulate the detailed gradient expressions, as long as they lead to numerically identical GHF effective density matrix elements in the end.

The above discussion examines the various formal modifications that arise in leaving the three-body $\bar{\mathbf{H}}$ amplitudes expanded in their component terms. These subtleties might be

difficult to organize by hand, but here, they are all treated *automatically* by the mathematics of dealing with the algebraic expressions directly.

5.3. The EOM-CCSD/PT intermediate density matrix $\bar{\mathbf{D}}$

The zero-, one-, and two-body intermediate density matrix elements $\bar{\mathbf{D}}$ for the EE-, IP-, and EA-EOM-CCSD/PT variants are presented in Table 10 (Section 5.8). These $\bar{D}_\mu \equiv \partial F^{inh}/\partial \bar{h}_\mu$ were obtained in *SMART* by expressing the inhomogeneous (non-$\mathbf{Z}$) part of each functional in terms of only (zero-, one-, and two-body) transformed Hamiltonian $\bar{\mathbf{H}}$ amplitudes and differentiating directly with respect to each class of $\bar{\mathbf{H}}$ amplitude. The $\mathbf{T}$ amplitudes that appear in $\bar{D}^{bc}_{ai}$, $\bar{D}^{ka}_{ij}$, and $\bar{D}^{ab}_{ij}$ arise from leaving the three-body $\bar{\mathbf{H}}$ terms expanded in their lower-body components, as discussed in the preceding section.

These $\bar{\mathbf{D}}$ (along with the explicit three-body contributions of Table 9) completely determine the analytical gradient for each method. The $\bar{\mathbf{D}}$ appear in both the chain-rule $\mathbf{Z}$ Lagrange multiplier equations of Table 8 and the chain-rule conversion to the full effective density matrix $\mathbf{D}$ in Table 15/Table 16 later. We contrast the current formulation with that originally derived by Stanton and Gauss [37–42], where the $\mathbf{Z}$ equations and effective density $\mathbf{D}$ expressions are treated independently.

5.3.1. Inclusion of pure-excitation terms in the EOM-CCSD functional

In Sections 2.2 and 3.2, we considered why and how the pure-excitation amplitudes should be excluded from the (non-$\mathbf{Z}$ part of the) energy functionals for the *PT-based* methods. Additionally, we reasoned that inclusion/exclusion of the pure-excitation amplitudes can have no *numerical* effect on the gradient for the *CCSD-based* methods. In this section, we explicitly demonstrate this feature for the EOM-CCSD analytical gradients. The inclusion of $\bar{h}^a_i$ terms in the functionals will lead to final $\mathbf{D}$ effective density matrix elements that are numerically identical but that are partitioned differently due to an equal and opposite modification of $\bar{D}^i_a$ and $2z^i_a$. The detailed discussions that comprise this section can be skipped by the non-specialized reader, if desired.

As considered previously, the commutator formulation is employed in the energy functionals to exclude the pure-excitation terms from the algebraic expressions, yielding a consistent formulation for both the CCSD-based and PT-based (ST)EOM variants. We have, however, the freedom to define the energy functional in different ways, as long as they lead to numerically identical final effective density matrix elements $\mathbf{D}$. If the CCSD-based EOM energy expression is instead written as the biorthogonal expectation value (rather than the commutator form), the following one-body pure-excitation terms are additionally present in the algebraic expansion:

$$\langle \Phi_0|\hat{L}\hat{\bar{H}}\hat{R}|\Phi_0\rangle = \bar{h}_0 + \langle \Phi_0|\hat{L}[\hat{\bar{H}},\hat{R}]|\Phi_0\rangle + \begin{cases} \tilde{l}^{ij}_{ab}(\bar{h}^a_i r^b_j + \bar{h}^b_j r^a_i) & \text{EE-EOM-CCSD,} \\ -\tilde{l}^{ji}_{\ a}(\bar{h}^a_i r_j) & \text{IP-EOM-CCSD,} \\ \tilde{l}_{ba}^{\ i}(\bar{h}^a_i r^b) & \text{EA-EOM-CCSD.} \end{cases} \tag{97}$$

The $\bar{\mathbf{H}}$ chain-rule formulation of the gradient isolates all of the method dependence (besides the CC/PT truncation) in the intermediate density matrix $\bar{\mathbf{D}}$, and thus the effect of

including/excluding these $\bar{h}_i^a$ terms is isolated completely in the associated $\bar{D}_a^i$. With the commutator formulation, no $\bar{h}_i^a$ terms are present (in F^{inh}), and thus $\bar{D}_a^i = 0$ for all methods (see Tables 10 and 14). The inclusion of the pure-excitation $\bar{h}_i^a$ terms according to expressions (97) yields the following non-zero $\bar{D}_a^i$:

$$\begin{aligned} \bar{D}_a^i &= 2\tilde{l}_{ab}^{ij} r_j^b \quad \text{EE-EOM-CCSD,} \\ \bar{D}_a^i &= -\tilde{l}^{ji}{}_a r_j \quad \text{IP-EOM-CCSD,} \\ \bar{D}_a^i &= \tilde{l}_{ba}{}^i r^b \quad \text{EA-EOM-CCSD.} \end{aligned} \tag{98}$$

However, these $\bar{D}_a^i$ will in fact have no effect on the final **D**, as the change will automatically be compensated for by a numerical change in the associated z_a^i Lagrange multipliers.

On the homogeneous left sides of the **Z** Lagrange multiplier equations, $\partial\langle\Phi_0|\hat{Z}\hat{\bar{H}}|\Phi_0\rangle/\partial t_v$, the **Z** amplitudes multiply the derivatives of the pure-excitation coefficients, *e.g.* $2z_a^i(\partial\bar{h}_i^a/\partial t_v)$. On the inhomogeneous right sides, $-\sum_\mu \bar{D}_\mu(\partial\bar{h}_\mu/\partial t_v)$, the pure-excitation $\bar{\mathbf{D}}$ elements multiply *these same derivatives*, *e.g.* $-\bar{D}_a^i(\partial\bar{h}_i^a/\partial t_v)$. These expressions can be combined on the homogeneous side, and thus including pure-excitation components leads to a simple offset of the **Z** Lagrange multipliers, $(\underset{\sim}{z}_\mu)^{\text{pure-excitation}}_{\text{excluded}} = (z_\mu + \bar{D}_\mu)^{\text{pure-excitation}}_{\text{included}}$. More concretely, in the explicit **Z** equations of Table 8, the first three terms on each inhomogeneous side involve $\bar{D}_a^i$ and can be combined with the matching first three terms on each homogeneous side, which involve $2z_a^i$. The remaining inhomogeneous sides are now identical to the case when $\bar{D}_a^i = 0$, and thus a non-zero $\bar{D}_a^i$ simply amounts to an offset to $2z_a^i$, $(2\underset{\sim}{z}_a^i + \cancel{\underset{\sim}{z}}_a)^{\text{pure-excitation}}_{\text{excluded}} = (2z_a^i + \bar{D}_a^i)^{\text{pure-excitation}}_{\text{included}}$. This offset is then returned in the conversion to the final **D**: Everywhere in Table 15, $\bar{D}_a^i$ appears together with $2z_a^i$ (in particular $D_a^i = \bar{D}_a^i + 2z_a^i$), and thus, regardless of a non-zero $\bar{D}_a^i$, the final **D** are always numerically identical.

For the PT-based methods, on the other hand, while the inhomogeneous sides would involve the same ("full"-order) pure-excitation expressions $-\bar{D}_\mu(\partial\bar{h}_\mu/\partial t_v)$, the homogeneous sides involve only the *first-order* pure-excitation expressions $z_\mu(\partial\bar{h}_\mu^{(1)}/\partial t_v)$. Thus the modification to the **Z** Lagrange multipliers would be non-trivial and would not be corrected properly in the conversion to the final **D**. In particular, the one-body z_a^i terms are not even present here for the PT-based methods and thus are not available to correct the inclusion of a non-zero $\bar{D}_a^i$. For the PT-based methods then, inclusion/exclusion of the pure-excitation terms leads to different results, and only the exclusion is consistent with the numerical energy-only gradients, where the pure-excitation terms are assumed fully vanishing and are thus ignored.

Finally, let us note that, in order to facilitate the above discussion of non-zero $\bar{D}_a^i$, the $\bar{D}_a^i$ terms were included in the chain-rule constructs of Table 8, even though they vanish for all the commutator-based functionals employed here. The *two-body* pure-excitation $\bar{D}_{ab}^{ij}$ terms, on the other hand, have *not* been included in the expressions, as two-body $\bar{h}_{ij}^{ab}$ amplitudes cannot contribute here due to the limited determinantal subspaces and the exclusion of the reference determinant from the diagonalizations. Thus $\bar{D}_{ab}^{ij} = 0$ always here, regardless of whether or not the commutator form is employed in the energy functionals, and such terms are thus omitted from the chain rules. Note that the omitted $\bar{D}_{ab}^{ij}(\partial\bar{h}_{ij}^{ab}/\partial t_v)$ terms can easily be reconstructed, if desired, from the CCSD-based $\mathbf{Z_2}$ terms on the homogeneous sides, since these also multiply $\partial\bar{h}_{ij}^{ab}/\partial t_v$.

5.4. The STEOM-CCSD/PT $\mathbf{Z}^-$ and $\mathbf{Z}^+$ Lagrange multiplier equations

We now shift focus toward obtaining the STEOM-CCSD/PT $\bar{\mathbf{D}}$. By construction, solution of the CCSD/PT $\mathbf{T}$, STEOM $\mathbf{S}^-$ and $\mathbf{S}^+$, and STEOM eigenvector equations (right and left) ensures that the functional is automatically stationary with respect to variations in the $\mathbf{Z}$, $\mathbf{Z}^-$, $\mathbf{Z}^+$, $\mathbf{L}$, $\mathbf{R}$, and λ parameters. Satisfaction of the remaining stationarities with respect to $\mathbf{S}^-$, $\mathbf{S}^+$, and $\mathbf{T}$ determines the associated Lagrange multipliers $\mathbf{Z}^-$, $\mathbf{Z}^+$, and $\mathbf{Z}$, respectively. Solution for the $\mathbf{Z}^-$ and $\mathbf{Z}^+$ Lagrange multipliers is required to calculate the STEOM $\bar{\mathbf{D}}$, whereas the subsequent solution for $\mathbf{Z}$, as well as the remainder of the gradient calculation, then proceeds identically to that of EOM-CCSD/PT.

The equations that determine the $\mathbf{Z}^-$ of EE- and DIP-STEOM-CCSD/PT, equations (60), are presented in explicit algebraic form in Table 11 (Section 5.8). The equations that determine the $\mathbf{Z}^+$ of EE- and DEA-STEOM-CCSD/PT, equations (61), are presented in Table 12. These $\mathbf{S}$-derivative expressions were obtained in *SMART* by expanding the $\mathbf{G}$ and $\mathbf{G_2}$ amplitudes in the functionals to their $\bar{\mathbf{H}}$ and $\mathbf{S}$ components, differentiating directly with respect to the four classes of $\mathbf{S}$ amplitudes, canonically reindexing, extracting permutations, and collecting intermediates. Note that it is not advantageous here to express these $\mathbf{S}$ derivatives back in terms of the original $\mathbf{G_2}$ amplitudes. This is in contrast to the $\mathbf{T}$ derivatives (equations for $\mathbf{Z}$), where re-expressing the expanded derivative expressions back in terms of the original $\bar{\mathbf{H}}$ amplitudes leads to very compact factorization (see Section 5.2.1). In essence, the regeneration analogous to expression (88) of the $\hat{G}_2$ similarity transformation does not occur due to the non-commuting nature of $\hat{S}$. There is, however, one (full) $\mathbf{G}$ amplitude that arises in each of the homogeneous-side expressions, which plays a special role in the decoupling of the $\mathbf{Z}^{\pm}$ equations, to be discussed in the next section.

The inhomogeneous sides of the $\mathbf{Z}^{\pm}$ equations are factored in terms of intermediates $\mathbf{M}$, which are collected in Table 13. These $\mathbf{M}$ intermediates involve only the bivariational $\mathbf{L}$ and $\mathbf{R}$ amplitudes from the energy expressions and could perhaps have been defined more formally as $\partial E/\partial \mathbf{G_2}$ (where $E \equiv \bar{h}_0 + \langle \Phi_0 | \hat{L}[\hat{G}_2, \hat{R}] | \Phi_0 \rangle$); the inhomogeneous-side $\mathbf{S}$ derivatives could then have been constructed as explicit chain rules in the $\mathbf{G_2}$ amplitudes (in analogy to the $\bar{\mathbf{H}}$ chain rules of the $\mathbf{Z}$ equations). Mainly for historical reasons, however, the $\mathbf{M}$ elements were implemented with positive unit factors as defined in the upper portion of the table; the numerical factors and signs relating the $\partial E/\partial \mathbf{G_2}$ and the $\mathbf{M}$ elements are presented in the lower portion of the table. Although somewhat analogous to the chain-rule $\bar{\mathbf{D}}$, the chain-rule-like $\mathbf{M}$ elements are substantially less important, since the types of $\mathbf{G_2}$ amplitudes that participate in the energy diagonalizations are quite limited and hardly shared by the STEOM variants, whereas nearly the whole gamut of $\bar{\mathbf{H}}$ amplitudes is employed by all the methods. Also, the fact that this potential analogy was initially overlooked emphasizes the fully algebraic nature of the derivation process here, where such formal considerations are only of modest importance.

Lastly, we note a special symmetry associated with the spatial-orbital $\mathbf{L}$ and $\mathbf{R}$ amplitudes for DIP- and DEA-STEOM that originates from the antisymmetric spin-orbital symmetry, namely that both pairs of indices can be interchanged simultaneously, *e.g.* $l^{ik}r_{jl} = l^{ki}r_{lj}$. Thus, the two-body M_{jl}^{ik} and M_{ac}^{bd} possess the standard pair-interchange symmetry in the same way as all other two-body amplitudes considered here.

5.4.1. *Decoupling of the $\mathbf{Z}^{\pm}$ equations in the active external index*

Rather than solving the equations of Table 11 for all $\mathbf{Z}^{-}$ simultaneously and the equations of Table 12 for all $\mathbf{Z}^{+}$ simultaneously, these equations can first be decoupled in the active external index [10], which greatly improves efficiency and numerical convergence. In the homogeneous-side expressions of Table 11, the active external index m always appears on a $\mathbf{Z}^{-}$ Lagrange multiplier amplitude d_m^{ν}, with the exception of a single term $d_n^{\mu}\mathfrak{g}_m^n$; likewise, in Table 12, the active external index e always appears on a $\mathbf{Z}^{+}$ amplitude a_{ν}^{e}, with the exception of a single term $a_{\mu}^{f}\mathfrak{g}_f^e$. Since the size of the active space is typically on the order of only 10–50 orbitals, the small matrices given by $\mathfrak{g}_m^n$ or $\mathfrak{g}_f^e$ can be diagonalized directly, yielding [3,65] respectively the IP- or EA-EOM-CCSD/PT eigenvalues $\boldsymbol{\xi}$ and the matrices of right-hand eigenvectors $\mathbf{U}$ and left-hand eigenvectors $\mathbf{U}^{-1}$. The $\mathbf{Z}^{-}$ equations can be tensor-multiplied with $\mathbf{U}$ on the right, producing a modified set of linear equations in a new variable $(\mathbf{X}^{-} \equiv \mathbf{Z}^{-}\mathbf{U})_m^{\nu}$ that is decoupled in the active index m. Upon solution, the desired Lagrange multipliers are recovered through the inverse operation $\mathbf{Z}^{-} = (\mathbf{X}^{-})\mathbf{U}^{-1}$. Conversely, the $\mathbf{Z}^{+}$ equations decouple in the active external index e by tensor-multiplying with $\mathbf{U}^{-1}$ on the left, leading to new linear equations in $(\mathbf{X}^{+} \equiv \mathbf{U}^{-1}\mathbf{Z}^{+})_{\nu}^{e}$ and recovery of the original Lagrange multipliers through $\mathbf{Z}^{+} = \mathbf{U}\mathbf{X}^{+}$.

Explicitly, to construct the decoupled $\mathbf{Z}^{-}$ equations, first rename the external index m in Table 11 to a dummy label, say m_1, multiply with the eigenvector elements $u_m^{m_1}$, and sum over m_1. (To avoid any confusion, note that m_1 simply represents another label for active occupied indices, not a particular m orbital.) The already decoupled $\mathbf{Z}^{-}$ amplitudes become $d_m^{\nu} \rightarrow \sum_{m_1} d_{m_1}^{\nu} u_m^{m_1} \equiv x_m^{\nu}$ (in effect just changing names), whereas the once problematic terms become

$$\sum_n d_n^{\mu}\mathfrak{g}_m^n \rightarrow \sum_{n,m_1} d_n^{\mu}\mathfrak{g}_{m_1}^n u_m^{m_1} = \sum_n d_n^{\mu} u_m^n \xi_m \equiv x_m^{\mu}\xi_m, \tag{99}$$

which is completely decoupled in all external indices m and μ. (Although the index m appears twice in the last term of expression (99), no summation is implied.) The inhomogeneous right sides of Table 11 are also tensor-multiplied with $u_m^{m_1}$ in the same way. Analogously, after tensor-multiplying the $\mathbf{Z}^{+}$ equations of Table 12 with $\mathbf{U}^{-1}$ on the left, the modified homogeneous sides then contain $a_{\nu}^{e} \rightarrow \sum_{e_1} (u^{-1})_{e_1}^{e} a_{\nu}^{e_1} \equiv x_{\nu}^{e}$ and

$$\sum_f \mathfrak{g}_f^e a_{\mu}^f \rightarrow \sum_{f,e_1} \big(u^{-1}\big)_{e_1}^{e} \mathfrak{g}_f^{e_1} a_{\mu}^f = \sum_f \xi_e \big(u^{-1}\big)_f^{e} a_{\mu}^f \equiv \xi_e x_{\mu}^{e} \tag{100}$$

(no summation on e), and the inhomogeneous sides are tensor-multiplied with $(u^{-1})_{e_1}^{e}$ in the same way. With this decoupling, the set of $\mathbf{Z}^{-}$ equations can be solved independently for each active external index m, and the set of $\mathbf{Z}^{+}$ equations can be solved independently for each active external index e.

Although now independent in the active external index, it is in practice more efficient to solve all of the decoupled set of linear equations for the auxiliary $\mathbf{X}^{-}$ or $\mathbf{X}^{+}$ together, using a block direct linear equation solver. In this way, the individual tensor multiplications are performed for the entire block of m or e expansion vectors at a time, thereby accessing the $\bar{\mathbf{H}}$ amplitudes only once per multiplication type and reducing the disk access cost. The full set of expansion vectors is used to approximate the solution for each of the individual decoupled equations. Thus, we borrow expansion vectors optimized from adjacent equations,

and this leads to rapid convergence. The total number of expansion vectors (and hence multiplications by $\bar{\mathbf{H}}$) for the overall set of equations is much reduced compared to solving for each linear equation independently. To summarize, using our block direct linear equation solver has two advantages: efficient multiplication of a number of vectors simultaneously and borrowing expansion vectors from adjacent equations to accelerate convergence. There are no significant drawbacks to the block direct strategy, apart from somewhat increased storage requirements, since a larger set of expansion vectors must be kept (up to about 60 in practice).

5.5. The STEOM-CCSD/PT intermediate density matrix $\bar{\mathbf{D}}$

With the solution for the numerical values of the $\mathbf{Z}^{\pm}$ Lagrange multipliers, the STEOM $\bar{\mathbf{D}}$ can now be calculated. The one- and two-body intermediate density matrix elements $\bar{\mathbf{D}}$ for the EE-, DIP-, and DEA-STEOM-CCSD/PT variants are presented in Table 14 (Section 5.8). These $\bar{\mathbf{D}}$ were obtained in *SMART* by expressing the inhomogeneous (non-$\mathbf{Z}$) part of each STEOM functional in terms of only the one- and two-body $\bar{\mathbf{H}}$ amplitudes and differentiating directly with respect to each class of $\bar{\mathbf{H}}$ amplitude. Since the $\mathbf{Z}^{-}$ term in the energy functionals is identical for EE- and DIP-STEOM, the response terms involving d_{μ} in Table 14 are also identical; likewise, the $\mathbf{Z}^{+}$ response terms (involving a_{μ}) are identical in the EE- and DEA-STEOM $\bar{\mathbf{D}}$.

With the construction of the STEOM-CCSD/PT $\bar{\mathbf{D}}$, the remainder of the gradient calculation then proceeds identically to that of EOM-CCSD/PT. The $\bar{\mathbf{D}}$ (and associated explicit three-body terms) contain all of the (ST)EOM-variant dependence and completely define the gradient for each method. Only the shared expressions related to the underlying CCSD/PT reference treatment remain: The $\bar{\mathbf{D}}$ are first applied in the (ST)EOM-variant-independent equations of Table 8 (together with the handful of explicit three-body contributions of Table 9) to determine the $\mathbf{Z}$ Lagrange multipliers associated with the underlying CCSD/PT $\mathbf{T}$ parameters. With the solution for $\mathbf{Z}$, the intermediate density matrix elements $\bar{\mathbf{D}}$ are then converted to the full GHF effective density matrix $\mathbf{D}$ to obtain the analytical gradient (see Section 5.7 below).

5.6. Efficiency tweaks in implementation

In this section, we examine some steps taken to increase the efficiency of the implemented gradient expressions above. While the details may be specific to the present ACES II implementation, the general issues apply to nearly any implementation of tensor algebraic expressions. Broadly speaking, the main considerations are minimization of disk storage, memory usage, and operation count. Whereas some of the adjustments are simple file management issues, others involve fine-tuning the factorization to avoid treating large matrices. All efficiency modifications were tested against the straightforward implementation.

As a rule, the modifications focus on the matrices with three or four virtual indices, which are expensive to store, manipulate, and multiply. Whenever practical, such matrices are made to overwrite other like-sized quantities, even at the cost of having to recompute some expressions. During the solution of the $\mathbf{Z}$ Lagrange multiplier equations, which tends to have large hard-disk storage requirements, the $\bar{D}^{ci}_{ab}$, $\bar{D}^{bc}_{ai}$, $\bar{h}^{ab}_{ci}$, $\bar{h}^{ai}_{bc}$, and V^{ai}_{bc} matrices are

treated carefully to minimize their respective ov^3 storage. The details are cumbersome, but in the end, a storage savings of $2ov^3$ is achieved: ov^3 from storing only one of $\bar{h}_{bc}^{ai}$ or V_{bc}^{ai} and another ov^3 from overwriting $\bar{h}_{ci}^{ab}$ by $\bar{D}_{ab}^{ci}$ (with the additional cost of computing $\bar{h}_{bc}^{ai}$ and $\bar{D}_{ab}^{ci}$ twice).

In a more straightforward modification, the expensive v^4 storage of the $\bar{D}_{ab}^{cd}$ matrix is delayed until after the disk-intensive solution of the **Z** equations. Despite the systematics of the chain-rule formulation, the two terms involving $\bar{D}_{ab}^{cd}$ in Table 8 can be calculated more efficiently by expansion and refactorization. The refactorization reduces both the disk access and the number of multiplications since all four virtual indices no longer need to be treated simultaneously. We should also note that further efficiency improvements can in principle be obtained by *never* constructing the $\bar{D}_{ab}^{cd}$ and D_{ab}^{cd} in the MO basis but instead calculating the final AO-based GHF density directly.

Finally, notwithstanding the parallel with the EE- and DIP-STEOM formulations, the $M_{ab}^{cd} \equiv l_{ab}r^{cd}$ in the DEA-STEOM method is a poor choice for an intermediate quantity, with its four virtual indices. Instead, all terms involving M_{ab}^{cd} and M_{ab}^{ed} (with one index explicitly active) are more efficiently calculated in a refactorized form. Many terms, however, only require the M_{ab}^{ef} subset of elements, and this v^2e^2-sized matrix is constructed and used normally.

In addition to the storage and operation-count savings, expansion of M_{ab}^{cd} provides another, subtle benefit. Because some choice must always be made regarding the indexing of multi-dimensional matrices in a one-dimensional computer memory space, certain tensor multiplications will involve time- and memory-intensive rearrangements (or cumbersome memory addressing). For example, one or both matrices in a binary tensor multiplication may require rearrangement to conform to the details of the computational routine that actually performs the multiplication. Or the *result* of the multiplication may be generated in a form that requires a permutation to store properly. Expanding the M_{ab}^{cd} intermediates provides additional flexibility in the tensor multiplications to avoid such expensive rearrangements. In fact, expansion of certain M_{aj}^{bi} in EE-STEOM, while not important for storage reasons, also reduces some expensive rearrangements, either in a three-virtual matrix that it multiplies or in a three-virtual result of a multiplication. Although the affected terms depend on the particular indexing method in ACES II, *any* indexing choice can require some expensive permutations in the implemented tensor multiplications. Moreover, the necessity of these rearrangements is not apparent in the derivation/factorization of the algebraic expressions but only manifests itself in the actual final implementation. (Such issues underscore the complexity of the general factorization problem and the skillful comprehensiveness required of its automation.)

We end this section by reemphasizing that all of the above modifications are optional and are only included to squeeze more performance out of the implementation.

5.7. The conversion of $\bar{\mathbf{D}}$ to the effective density matrix D

With the solution for the **Z** Lagrange multipliers associated with the underlying CCSD/PT **T** amplitudes, the intermediate density matrix elements $\bar{\mathbf{D}}$ can finally be converted to the full effective density matrix elements **D**. The conversion depends only on the $\bar{\mathbf{H}}$ amplitudes and is performed through the method-independent expression (45) presented in explicit al-

gebraic form for CCSD-based methods in Table 15 (Section 5.8). The chain-rule portion, $\sum_\nu \bar{D}_\nu(\partial\bar{h}_\nu/\partial h_\mu)$, was constructed by the same automated routine used to construct the **Z** chain-rule expressions, $\sum_\nu \bar{D}_\nu(\partial\bar{h}_\nu/\partial t_\mu)$, but with the expanded $\bar{\mathbf{H}}$ amplitudes differentiated with respect to **H** now rather than **T**. The chain-rule construction can again be checked by expansion of all $\bar{\mathbf{D}}$ for each method and comparison to the direct **H** derivatives of the functionals. The remaining $\partial\langle\Phi_0|\hat{Z}\hat{\bar{H}}|\Phi_0\rangle/\partial h_\mu$ portion is obtained normally by expansion of the $\bar{\mathbf{H}}$ amplitudes to component terms, direct differentiation with respect to all classes of **H** amplitudes, extraction of permutations, and factorization.

For the PT-based methods, the simplified $\bar{\mathbf{H}}$ and simplified $\langle\Phi_0|\hat{Z}\hat{\bar{H}}^{(1)}_{\mathrm{MP}}|\Phi_0\rangle$ cause most of the terms to drop out of the **D** expressions of Table 15. For clarity, the terms that remain for the PT-based **D** are presented separately as Table 16. These PT-based **D** expressions can be obtained by performing the same derivation as above, but using the simplified PT-based $\bar{\mathbf{H}}$ and $\bar{h}^{ab(1)}_{ij}$ expressions. The PT-based subset of the full CCSD-based expressions of Table 15 can also/instead be identified by the PT-based prescription summarized in Section 5.1.1: All one-body $\mathbf{T_1}$ and $\mathbf{Z_1}$ terms are not present (this also reduces c^{ab}_{ij} to t^{ab}_{ij}). Since V^{ab}_{ij} is the only two-body Hamiltonian amplitude that contributes to the PT-based $\mathbf{Z_2}$ expression, the only two-body **D** where $\mathbf{Z_2}$ should appear is the associated D^{ij}_{ab}; all $\mathbf{Z_2}$ terms thus drop out from the other two-body **D** expressions. Finally, since the PT-based functionals exclude the pure-excitation $\bar{h}^a_i$ amplitudes by construction, $\bar{D}^i_a$ is always zero and is eliminated everywhere.

Note that the **Z** contributions to **D** in Table 15 are equivalent in form to the reduced density matrix of ground-state CCSD gradient theory [109,118], with **Z** replacing **Λ**. This should be expected, as the **Z** Lagrange multipliers account for the response of the CCSD **T** parameters of the underlying reference treatment. (The *intermediate* density matrix $\bar{\mathbf{D}}$, on the other hand, contains all of the *post*-CCSD information, which for ground-state CCSD gradient theory there is none.) Next, we note three stand-alone terms that multiply neither a $\bar{\mathbf{D}}$ nor **Z** element (1, t^a_i, and c^{ab}_{ij} appearing in D_0, D^a_i, and D^{ab}_{ij}, respectively); these originate from the derivatives of the CCSD energy $\bar{h}_0$ and actually multiply $\bar{D}_0 = 1$ implicitly.

The $\bar{\mathbf{D}}$-to-**D** conversion expressions of Table 15 are factorized to facilitate reuse of intermediate subexpressions. Since certain intermediates build on other intermediates, the expressions must be evaluated in a somewhat careful order (though largely as written) to maximize efficiency. To minimize unnecessary storage allocation, each D_μ overwrites its corresponding $\bar{D}_\mu$, *i.e.* each contribution to D_μ is added directly into the associated stored $\bar{D}_\mu$, being careful to first evaluate the terms involving the unmodified $\bar{\mathbf{D}}$ or the partially calculated **D** elements. Additionally, note that the bare Hamiltonian **H** amplitudes are Hermitian (or rather real-symmetric), as are their perturbation derivatives $\partial\mathbf{H}/\partial\chi$; since these Hermitian $\partial\mathbf{H}/\partial\chi$ are contracted with **D** in the final GHF gradient expression, then **D** elements that are related by transposition (such as D^{bc}_{ai} and D^{ai}_{bc}) can be added together to avoid storing them separately. These combined density matrix elements are then Hermitian by construction. (The individual **D** of Table 15/Table 16 are not Hermitian by nature of the non-Hermiticity of $\bar{\mathbf{H}}$.) At last, with the construction of the bare-Hamiltonian effective density matrix **D**, the calculation of the gradient with respect to an arbitrary perturbation, according to the standard GHF relation discussed in the next section, then proceeds in the same manner as a ground-state CC/MBPT analytical gradient.

All explicit algebraic expressions needed to obtain the (ST)EOM-CCSD/PT intermediate density matrix elements $\bar{\mathbf{D}}$ and needed to convert $\bar{\mathbf{D}}$ to the full effective density matrix

D were implemented manually in the ACES II package. The implementation was checked thoroughly against numerical gradients, as well as at various intermediate steps in the code, for a large number of test cases.

5.7.1. Expression of the energy derivative in terms of elementary Hamiltonian derivative integrals

As outlined at the end of Section 3.1, the final MO-based effective density matrix **D** is backtransformed to the AO basis and is traced directly with the Hamiltonian-integral derivatives in their native AO form [100,101], as is normally done for computational efficiency. This approach both avoids the perturbation-dependent transformation of the AO-based Hamiltonian-integral derivatives to the MO basis as well as circumvents the need to store these derivatives, as they can be multiplied with the appropriate AO-based effective density matrix element immediately upon computation and added to the gradient. To convert the MO-based GHF gradient expression into an efficient AO-based expression, the derivative of the reference-determinant energy $\partial h_0/\partial\chi$ and the Fock-matrix derivatives $\partial f_q^p/\partial\chi$ are expanded in terms of the fundamental Hamiltonian integrals and the reference (usually Hartree–Fock) density matrix. The reference and the correlated contributions are then combined, leading to the definition of the *total* effective density matrix, according to the general procedure discussed below.

The effective density matrix elements derived in this work are defined as $D_\mu \equiv \partial F/\partial h_\mu$, where the h_μ refer to the h_0, f_q^p, and V_{rs}^{pq} amplitudes of the normal-ordered (with respect to the reference determinant) Hamiltonian, expression (1), and the analytical energy gradient is given by the GHF relation, expression (24):

$$\frac{\partial F}{\partial\chi} = \frac{\partial h_0}{\partial\chi} + D_p^q \frac{\partial f_q^p}{\partial\chi} + D_{pq}^{rs} \frac{\partial V_{rs}^{pq}}{\partial\chi}, \tag{101}$$

where $D_0 = 1$ and the indices here refer to unrestricted spatial molecular orbitals. We wish to rewrite this expression in terms of the elementary Hamiltonian integrals. The one-body elementary Hamiltonian integrals contain only the kinetic energy and nuclear-electron attraction terms and are denoted here as $\hbar_q^p$. The two-body elementary Hamiltonian integrals V_{rs}^{pq} are the same as used previously. Equivalently, these fundamental Hamiltonian integrals are the amplitudes of the basic second-quantized Hamiltonian normal-ordered with respect to the *true vacuum* (as opposed to the reference determinant). In terms of these fundamental integrals, the gradient becomes by definition

$$\frac{\partial F}{\partial\chi} = D(\text{total})_p^q \frac{\partial \hbar_q^p}{\partial\chi} + D(\text{total})_{pq}^{rs} \frac{\partial V_{rs}^{pq}}{\partial\chi}. \tag{102}$$

The reference-determinant contribution, contained in the reference energy h_0 and the Fock matrix elements f_q^p, has been moved into the total effective density matrix elements $D(\text{total})_\mu$. This $D(\text{total})_\mu$, after inclusion of the orbital response contribution (discussed below), then goes on to the AO backtransformation to be multiplied with the AO Hamiltonian-integral derivatives in the final gradient calculation.

Conversion of the D_μ of expression (101) to the $D(\text{total})_\mu$ of expression (102) can proceed by returning to the energy functional. Since the functional is linear in the Hamiltonian amplitudes and since the D_μ are independent of the perturbation, the derivative in expression (101) can be "undone", and the functional can alternatively be written as

$$F = h_0 + f_q^p D_p^q + V_{rs}^{pq} D_{pq}^{rs}. \tag{103}$$

The Fock matrix elements are expanded in terms of their fundamental components as

$$f_q^p = \hbar_q^p + 2V_{qi}^{pi} - V_{iq}^{pi} = \hbar_q^p + 2V_{qs}^{pr} D(0)_r^s - V_{sq}^{pr} D(0)_r^s, \tag{104}$$

and the reference-determinant energy is expanded as

$$\begin{aligned} h_0 &= 2\hbar_i^i + 2V_{ij}^{ij} - V_{ji}^{ij} \\ &= 2\hbar_q^p D(0)_p^q + V_{rs}^{pq}\left(2D(0)_p^r D(0)_q^s - D(0)_p^s D(0)_q^r\right), \end{aligned} \tag{105}$$

where $D(0)_p^q$ refers to the reference-determinant density matrix (typically the Hartree–Fock density [116]). The energy functional then becomes

$$F = \hbar_q^p\left(2D(0)_p^q + D_p^q\right) + V_{rs}^{pq}\begin{pmatrix} 2D(0)_p^r D(0)_q^s - D(0)_p^s D(0)_q^r \\ + 2D(0)_q^s D_p^r - D(0)_q^r D_p^s + D_{pq}^{rs} \end{pmatrix}. \tag{106}$$

Extracting the exchange permutation and using the pair-interchange symmetry of the spatial-orbital $V_{rs}^{pq} = V_{sr}^{qp}$, this expression can be written in a symmetrical form, defining $D(\text{total})_\mu$:

$$D(\text{total})_p^q = D_p^q + 2D(0)_p^q \tag{107}$$

and

$$D(\text{total})_{pq}^{rs} = D_{pq}^{rs} + (2 - P_{rs})\left(D(0)_p^r D(0)_q^s + \frac{1}{2}D(0)_q^s D_p^r + \frac{1}{2}D(0)_p^r D_q^s\right). \tag{108}$$

The energy functional

$$F = \hbar_q^p D(\text{total})_p^q + V_{rs}^{pq} D(\text{total})_{pq}^{rs} \tag{109}$$

is now given in terms of the elementary MO $\hbar_q^p$ and V_{rs}^{pq} integrals, and its gradient is given by expression (102).

At last, with this construction of the MO total effective density matrix elements $D(\text{total})_\mu$, the efficiently calculated gradient expression is obtained by transformation of the fundamental MO-based GHF expression (102) to the AO basis. Note that the MO-based $\partial\hbar_q^p/\partial\chi$ and $\partial V_{rs}^{pq}/\partial\chi$ contain both the derivatives of the AO Hamiltonian integrals as well as the response of the MO coefficients. As mentioned previously, this latter so-called coupled-perturbed Hartree–Fock response [163] is perturbation/degree-of-freedom dependent but can instead be eliminated by a Z-vector or Lagrange multiplier construction; for details of this general procedure, see, for example, references [101,108–110] or references [118,120], respectively. In the process, an additional one-body density-matrix-like term (sometimes called the energy-weighted density matrix) is generated that is contracted with the derivatives of the AO overlap integrals. The $D(\text{total})_\mu$ above is straightforwardly converted to the AO basis, the remaining MO-coefficient response is included, and the final AO-based total effective density matrix is traced with the efficiently calculated AO Hamiltonian-integral derivatives. The modules available in ACES II, for instance, to perform these calculations [110] are directly applicable here. In this way, the analytical energy gradient has been constructed to avoid all rate-limiting perturbation-dependent steps and is obtained from the AO elementary Hamiltonian-integral derivatives, the AO-overlap derivatives and associated energy-weighted density, and the AO total effective density matrix only.

5.8. Tables of equations

Table 2. *Computational steps in a STEOM-CCSD/PT analytical gradient calculation, with scaling and storage*. See Section 3.3.1. The energy and gradient calculations proceed sequentially according to the steps listed in the first column. The 'scaling' column presents for each step, the operation scaling order and the types of amplitudes that participate in the most expensive tensor multiplications. The 'storage' column presents the largest separately/newly stored result of each step and its size-scaling. The o refer to the number of occupied molecular orbitals, the v to virtual, the m to active occupied, the e to active virtual; (AO) indicates the entire atomic orbital space; the I indicates the step is iterative; the N indicates the number of STEOM eigenvectors computed; $(\text{hom.})_\nu^\mu$ or $(\text{inh.})_\nu^\mu$ respectively indicate the calculated value of the homogeneous or inhomogeneous side of an equation; χ indicates the number of perturbations.

Step		Cost-determining amplitude	Scaling	Cost-determining amplitude	Storage
SCF calculation $\Rightarrow$ **H** (AO basis) & MO coefficients			$(\text{AO})^4$		$(\text{AO})^4$
AO-to-MO transformation $\Rightarrow$ **H**		V_{cd}^{ab}	$(\text{AO})^4 v$	V_{cd}^{ab}	v^4
DIP-STEOM-PT		V_{bc}^{ia}	$(\text{AO})^4 o$	V_{bc}^{ia}	ov^3
CCSD equations $\Rightarrow$ **T** or		V_{cd}^{ab} in $\bar{h}_{ij}^{ab}$	o^2v^4I	t_{ij}^{ab}	o^2v^2
PT equation $\Rightarrow$ **T**		$\binom{\varepsilon_a+\varepsilon_b}{-\varepsilon_i-\varepsilon_j}$	o^2v^2	t_{ij}^{ab}	o^2v^2
construct $\bar{\mathbf{H}}$		in $\bar{h}_{cd}^{ab}$, $\bar{h}_{ic}^{ab}$	o^2v^4	$\bar{h}_{ic}^{ab}$	ov^3
DIP-STEOM-PT		in $\bar{h}_{bj}^{ia}$, $\bar{h}_{bj}^{ai}$, $\bar{h}_{kj}^{ai}$	o^3v^3	$\bar{h}_{bj}^{ia}$, $\bar{h}_{bj}^{ai}$	o^2v^2
active IP-EOM-CCSD/PT eigenvectors $\Rightarrow$ $\mathbf{S}^-$ EE & DIP		$\bar{h}_{bj}^{ia}$, $\bar{h}_{bj}^{ai}$	o^3v^2mI	s_{ij}^{mb}	o^2vm
active EA-EOM-CCSD/PT eigenvectors $\Rightarrow$ $\mathbf{S}^+$ EE & DEA		$\bar{h}_{cd}^{ab}$	ov^4eI	s_{ej}^{ab}	ov^2e
construct $\mathbf{G_2}$	EE	$\bar{h}_{bc}^{ia}$ in g_{bj}^{ia}, g_{bj}^{ai}	o^2v^3e	g_{bj}^{ia}, g_{bj}^{ai}	o^2v^2
	DIP	V_{ab}^{ij} in g_{kl}^{ij}	o^3v^2m	g_{kl}^{ij}	o^4
	DEA	$\bar{h}_{bc}^{ia}$ in g_{cd}^{ab}	ov^4e	g_{cd}^{ab}	v^4
diagonalize $\mathbf{G_2} \Rightarrow$ **R**, **L**, λ	EE	g_{bj}^{ia}, g_{bj}^{ai}	o^2v^2IN	r_i^a, l_a^i	ovN
	DIP	g_{kl}^{ij}	o^4IN	r_{ij}, l^{ij}	o^2N
	DEA	g_{cd}^{ab}	v^4IN	r^{ab}, l_{ab}	v^2N

Table 2. (*Continued*)

Step		Cost-determining amplitude	Scaling	Cost-determining amplitude	Storage
$\mathbf{Z}^-$ Lagrange multiplier equations				d^{ij}_{mb}	o^2vm
decoupling (diagonalize g^n_m)		$u^n_m, \left(u^{-1}\right)^n_m$	m^3	$u^n_m, \left(u^{-1}\right)^n_m$	m^2
homogeneous side		$\bar{h}^{ia}_{bj}, \bar{h}^{ai}_{bj}$	o^3v^2mI	$(\text{hom.})^{ij}_{mb}$	o^2vm
inhomogeneous side	EE	$\bar{h}^{ia}_{bc}$	ov^3m	$(\text{inh.})^{ij}_{mb}$	o^2vm
	DIP	V^{ij}_{ab}	o^2v^2m	$(\text{inh.})^{ij}_{mb}$	o^2vm
decoupling (recover d^μ_m)		x^{ij}_{mb}	o^2vm^2	–	–
$\mathbf{Z}^+$ Lagrange multiplier equations				a^{ej}_{ab}	ov^2e
decoupling (diagonalize g^e_f)		$\left(u^{-1}\right)^e_f, u^e_f$	e^3	$\left(u^{-1}\right)^e_f, u^e_f$	e^2
homogeneous side		$\bar{h}^{ab}_{cd}$	ov^4eI	$(\text{hom.})^{ej}_{ab}$	ov^2e
inhomogeneous side	EE	$\bar{h}^{ia}_{bc}$	o^2v^3e	$(\text{inh.})^{ej}_{ab}$	ov^2e
	DEA	$\bar{h}^{ia}_{bc}$	ov^3e	$(\text{inh.})^{ej}_{ab}$	ov^2e
decoupling (recover a^e_μ)		x^{ej}_{ab}	ov^2e^2	–	–
construct $\bar{\mathbf{D}}$	EE	in $\bar{D}^{cd}_{ab}$	ov^4e	$\bar{D}^{cd}_{ab}$	v^4
	DIP	in $\bar{D}^{jb}_{ai}, \bar{D}^{bj}_{ai}, \bar{D}^{ab}_{ij}$	o^3v^2m	$\bar{D}^{jb}_{ai}, \bar{D}^{bj}_{ai}, \bar{D}^{ab}_{ij}$	o^2v^2
	DEA	in $\bar{D}^{cd}_{ab}$	ov^4e	$\bar{D}^{cd}_{ab}$	v^4
$\mathbf{Z}$ Lagrange multiplier equations				z^{ij}_{ab}	o^2v^2
homogeneous side	CCSD	$\bar{h}^{ab}_{cd}$	o^2v^4I	$(\text{hom.})^{ij}_{ab}$	o^2v^2
	PT	$\binom{\varepsilon_a+\varepsilon_b}{-\varepsilon_i-\varepsilon_j}$	o^2v^2	–	–
inhomogeneous side	EE	$\bar{D}^{ic}_{ab}$	o^2v^4	$(\text{inh.})^{ij}_{ab}$	o^2v^2
	DIP	$\bar{D}^{jb}_{ai}, \bar{D}^{bj}_{ai}, \bar{D}^{kj}_{ai}$	o^3v^3	$(\text{inh.})^{ij}_{ab}$	o^2v^2
	DEA	$\bar{D}^{ic}_{ab}$	o^2v^4	$(\text{inh.})^{ij}_{ab}$	o^2v^2
convert $\bar{\mathbf{D}}$ to $\mathbf{D}$	EE	in $D^{cd}_{ab}, D^{bc}_{ia}, D^{ab}_{ij}$	o^2v^4	–	–
	DEA	in $D^{cd}_{ab}, D^{bc}_{ia}, D^{ab}_{ij}$	o^2v^4	D^{ak}_{ji}	o^3v
DIP-STEOM-CCSD		in D^{cd}_{ab}	o^2v^4	D^{cd}_{ab}	v^4
DIP-STEOM-PT		in D^{bc}_{ia}, D^{ab}_{ij}	o^3v^3	D^{bc}_{ia}	ov^3

Table 2. (*Continued*)

Step	Cost-determining amplitude	Scaling	Cost-determining amplitude	Storage
convert **D** to AO basis	D_{ab}^{cd}	$(\mathrm{AO})^4 v$		$(\mathrm{AO})^4$
DIP-STEOM-PT	D_{ia}^{bc}	$(\mathrm{AO})^4 o$		$(\mathrm{AO})^4$
compute $\partial \mathbf{H}/\partial \chi$ in AO basis		$(\mathrm{AO})^4 \chi$	on-the-fly	
MO coefficient response		$(\mathrm{AO})^5$		$(\mathrm{AO})^2$
compute gradient by GHF relation		$(\mathrm{AO})^4 \chi$		χ

Table 3. *The EE-, IP-, and EA-EOM-CCSD/PT Lagrange multiplier energy functionals.* See Sections 3.2 and 5.1. The energy functional completely defines the electronic structure method and is constructed from the energy expression for an individual electronic state, together with the supplementary equations that determine the energy parameters, each set of supplementary constraints tensor-multiplied by unknown Lagrange multipliers. The equations that determine the Lagrange multipliers are systematically obtained by defining the energy *functional* to be stationary with respect to all the non-variational *energy* parameters. The analytical gradient can then be calculated by the generalized Hellmann–Feynman (GHF) relation, expression (101), in terms of an effective density matrix that, through the Lagrange multipliers, accounts for all the parameter response but is perturbation-independent. These algebraic functionals serve as the input to the *SMART* (Symbolic Manipulation and Regrouping of Tensors) package for automated symbolic differentiation. The PT-based functionals are contained as a subset of the CCSD-based expressions, given by the simplification of the $\bar{h}_\mu$ formulas in Tables 5 and 6. (The simplifications to the fully expanded functionals are summarized by the prescription $\mathbf{T_1} = \mathbf{0}$, $\mathbf{Z_1} = \mathbf{0}$, and in $\mathbf{Z_2}$ terms $\mathbf{V} = \mathbf{0}$ except V_{ij}^{ab}; see Section 5.1.1.) In all the tables, the amplitudes are based on normal-ordering with respect to the closed-shell reference determinant $|\Phi_0\rangle$, and the indices refer to spatial molecular orbitals.

EOM-CC/PT functional	$F \equiv \bar{h}_0 + \langle\Phi_0\vert\hat{L}[\hat{\bar{H}}, \hat{R}]\vert\Phi_0\rangle + \lambda\big(1 - \langle\Phi_0\vert\hat{L}\hat{R}\vert\Phi_0\rangle\big) + \langle\Phi_0\vert\hat{Z}\hat{\bar{H}}\vert\Phi_0\rangle$
EE-EOM-CCSD/PT	$\langle\Phi_0\vert\hat{L}[\hat{\bar{H}}, \hat{R}]\vert\Phi_0\rangle = 2l_a^i(\bar{H}R)_i^a + \tilde{l}_{ab}^{ij}(\bar{H}R)_{ij}^{ab}$ $(\bar{H}R)_i^a = -\bar{h}_i^k r_k^a + \bar{h}_c^a r_i^c + \bar{h}_c^k \tilde{r}_{ik}^{ac} + \big(2\bar{h}_{ci}^{ka} - \bar{h}_{ci}^{ak}\big) r_k^c - \bar{h}_{ci}^{kl}\tilde{r}_{lk}^{ac} + \bar{h}_{dc}^{ka}\tilde{r}_{ik}^{cd}$ $(\bar{H}R)_{ij}^{ab} = \big(1 + P_{ij}^{ab}\big)\begin{pmatrix} -\bar{h}_j^k r_{ik}^{ab} + \bar{h}_c^a r_{ij}^{cb} - \bar{h}_{ji}^{bk} r_k^a + \bar{h}_{jc}^{ba} r_i^c + \frac{1}{2}\bar{h}_{ij}^{kl} r_{kl}^{ab} \\ + \frac{1}{2}\bar{h}_{cd}^{ab} r_{ij}^{cd} - \bar{h}_{ci}^{bk} r_{jk}^{ca} - \bar{h}_{cj}^{bk} r_{ik}^{ac} \\ + \bar{h}_{cj}^{kb}\tilde{r}_{ik}^{ac} + \big(2\bar{h}_{dc}^{ka} - \bar{h}_{cd}^{ka}\big) r_k^d t_{ij}^{cb} \\ - \big(2\bar{h}_{ci}^{kl} - \bar{h}_{ci}^{lk}\big) r_k^c t_{jl}^{ba} - V_{cd}^{kl}\big(\tilde{r}_{kl}^{ad} t_{ij}^{cb} + \tilde{r}_{il}^{cd} t_{kj}^{ab}\big) \end{pmatrix}$ $\tilde{l}_{ab}^{ij} \equiv 2l_{ab}^{ij} - l_{ba}^{ij}$ $\tilde{r}_{ij}^{ab} \equiv 2r_{ij}^{ab} - r_{ij}^{ba}$
IP-EOM-CCSD/PT	$\langle\Phi_0\vert\hat{L}[\hat{\bar{H}}, \hat{R}]\vert\Phi_0\rangle = -l^i(\bar{H}R)_i - \tilde{l}^{ij}{}_b(\bar{H}R)_{ij}{}^b$ $(\bar{H}R)_i = -\bar{h}_i^k r_k + \bar{h}_c^k \tilde{r}_{ik}{}^c - \bar{h}_{ci}^{kl}\tilde{r}_{lk}{}^c$ $(\bar{H}R)_{ij}^b = \begin{pmatrix} -\bar{h}_j^k r_{ik}{}^b - \bar{h}_i^k r_{kj}{}^b + \bar{h}_c^b r_{ij}{}^c - \bar{h}_{ji}^{bk} r_k + \bar{h}_{ij}^{kl} r_{kl}{}^b \\ - \bar{h}_{ci}^{bk} r_{kj}{}^c - \bar{h}_{cj}^{bk} r_{ik}{}^c + \bar{h}_{cj}^{kb}\tilde{r}_{ik}{}^c - V_{cd}^{kl}\tilde{r}_{kl}{}^d t_{ij}^{cb} \end{pmatrix}$ $\tilde{l}^{ij}{}_b \equiv 2l^{ij}{}_b - l^{ji}{}_b$ $\tilde{r}_{ij}{}^b \equiv 2r_{ij}{}^b - r_{ji}{}^b$

Table 3. (*Continued*)

EOM-CC/PT functional	$F \equiv \bar{h}_0 + \langle \Phi_0 \vert \hat{L}[\hat{\bar{H}}, \hat{R}] \vert \Phi_0 \rangle + \lambda\big(1 - \langle \Phi_0 \vert \hat{L}\hat{R} \vert \Phi_0 \rangle\big) + \langle \Phi_0 \vert \hat{Z}\hat{\bar{H}} \vert \Phi_0 \rangle$
EA-EOM-CCSD/PT	$\langle \Phi_0 \vert \hat{L}[\hat{\bar{H}}, \hat{R}] \vert \Phi_0 \rangle = l_a (\bar{H}R)^a + \tilde{l}_{ab}^{\ j} (\bar{H}R)^{ab}_{\ j}$ $(\bar{H}R)^a = \bar{h}^a_c r^c + \bar{h}^k_c \tilde{r}^{ac}_{\ k} + \bar{h}^{ka}_{cd} \tilde{r}^{dc}_{\ k}$ $(\bar{H}R)^{ab}_{\ j} = \begin{pmatrix} -\bar{h}^k_j r^{ab}_{\ k} + \bar{h}^b_c r^{ac}_{\ j} + \bar{h}^a_c r^{cb}_{\ j} + \bar{h}^{ba}_{jc} r^c + \bar{h}^{ab}_{cd} r^{cd}_{\ j} \\ - \bar{h}^{ak}_{cj} r^{cb}_{\ k} - \bar{h}^{bk}_{cj} r^{ac}_{\ k} + \bar{h}^{kb}_{cj} \tilde{r}^{ac}_{\ k} - V^{kl}_{cd} \tilde{r}^{cd}_{\ l} t^{ba}_{jk} \end{pmatrix}$ $\tilde{l}_{ab}^{\ j} \equiv 2 l_{ab}^{\ j} - l_{ba}^{\ j}$ $\tilde{r}^{ab}_{\ j} \equiv 2 r^{ab}_{\ j} - r^{ba}_{\ j}$
CCSD-based PT-based	$\langle \Phi_0 \vert \hat{Z}\hat{\bar{H}} \vert \Phi_0 \rangle = 2 z^i_a \bar{h}^a_i + \tilde{z}^{ij}_{ab} \bar{h}^{ab}_{ij}$ $\langle \Phi_0 \vert \hat{Z}\hat{\bar{H}} \vert \Phi_0 \rangle = \langle \Phi_0 \vert \hat{Z}\hat{\bar{H}}^{(1)}_{\mathrm{MP}} \vert \Phi_0 \rangle = \tilde{z}^{ij}_{ab} \bar{h}^{ab(1)}_{ij}$ $\tilde{z}^{ij}_{ab} \equiv 2 z^{ij}_{ab} - z^{ij}_{ba}$

Table 4. *The EE-, DIP-, and DEA-STEOM-CCSD/PT Lagrange multiplier energy functionals*. See Sections 3.3 and 5.1. In addition to the CCSD/PT $\mathbf{Z}$ term associated with reference-state $\mathbf{T}$ amplitudes, the STEOM functional contains two additional Lagrange multiplier ($\mathbf{Z}^{\pm}$) terms associated with the equations that define the $\mathbf{S}^{\pm}$ amplitudes. The algebraic functionals serve as the input to the *SMART* package for subsequent automated symbolic differentiation and manipulation. The $\bar{h}_\mu$, g_μ, and $\mathfrak{g}_\mu$ amplitudes are defined in Tables 5, 6, and 7. The PT-based functionals are contained as a subset of the CCSD-based expressions, given by the simplification of the $\bar{h}_\mu$ formulas in Tables 5 and 6 (and summarized by the prescription $\mathbf{T_1} = \mathbf{0}$, $\mathbf{Z_1} = \mathbf{0}$, and in $\mathbf{Z_2}$ terms $\mathbf{V} = \mathbf{0}$ except V_{ij}^{ab}; see Section 5.1.1). For EE-STEOM, $(\ )_{\text{only}}^{\text{singlet}}$ denotes terms that are present for singlet but not for triplet states. For DIP- or DEA-STEOM, the $\hat{Z}^+$ or $\hat{Z}^-$ term, respectively, is not included.

STEOM-CCSD/PT functional	$F \equiv \bar{h}_0 + \langle \Phi_0 \vert \hat{L}[\hat{G}_2, \hat{R}] \vert \Phi_0 \rangle + \lambda\big(1 - \langle \Phi_0 \vert \hat{L}\hat{R} \vert \Phi_0 \rangle\big) + \langle \Phi_0 \vert \hat{Z}\hat{\bar{H}} \vert \Phi_0 \rangle$ $+ \sum_m \langle \Phi_m \vert \hat{Z}^-[\hat{G}, \hat{m}] \vert \Phi_0 \rangle + \sum_e \langle \Phi^e \vert \hat{Z}^+[\hat{G}, \hat{e}^\dagger] \vert \Phi_0 \rangle$
EE-STEOM-CCSD/PT	$\langle \Phi_0 \vert \hat{L}[\hat{G}_2, \hat{R}] \vert \Phi_0 \rangle = 2 l_a^i (G_2 R)_i^a$ $(G_2 R)_i^a = \big(2 g_{ci}^{ka}\big)_{\text{only}}^{\text{singlet}} - g_{ci}^{ak}\big) r_k^c + g_c^a r_i^c - g_i^k r_k^a$
DIP-STEOM-CCSD/PT	$\langle \Phi_0 \vert \hat{L}[\hat{G}_2, \hat{R}] \vert \Phi_0 \rangle = l^{ij} (G_2 R)_{ij}$ $(G_2 R)_{ij} = g_{ij}^{kl} r_{kl} - g_i^k r_{kj} - g_j^l r_{il}$
DEA-STEOM-CCSD/PT	$\langle \Phi_0 \vert \hat{L}[\hat{G}_2, \hat{R}] \vert \Phi_0 \rangle = l_{ab} (G_2 R)^{ab}$ $(G_2 R)^{ab} = g_{cd}^{ab} r^{cd} + g_c^a r^{cb} + g_d^b r^{ad}$
EE- & DIP-STEOM-CCSD/PT	$\sum_m \langle \Phi_m \vert \hat{Z}^-[\hat{G}, \hat{m}] \vert \Phi_0 \rangle = 2 d_m^{i'} \mathfrak{g}_{i'}^m + \tilde{d}_{mb}^{ij} \mathfrak{g}_{ij}^{mb}$ $\tilde{d}_{mb}^{ij} \equiv 2 d_{mb}^{ij} - d_{mb}^{ji}$
EE- & DEA-STEOM-CCSD/PT	$\sum_e \langle \Phi^e \vert \hat{Z}^+[\hat{G}, \hat{e}^\dagger] \vert \Phi_0 \rangle = 2 a_{a'}^e \mathfrak{g}_e^{a'} + \tilde{a}_{ab}^{ej} \mathfrak{g}_{ej}^{ab}$ $\tilde{a}_{ab}^{ej} \equiv 2 a_{ab}^{ej} - a_{ba}^{ej}$
CCSD-based	$\langle \Phi_0 \vert \hat{Z}\hat{\bar{H}} \vert \Phi_0 \rangle = 2 z_a^i \bar{h}_i^a + \tilde{z}_{ab}^{ij} \bar{h}_{ij}^{ab}$
PT-based	$\langle \Phi_0 \vert \hat{Z}\hat{\bar{H}} \vert \Phi_0 \rangle = \big\langle \Phi_0 \big\vert \hat{Z}\hat{\bar{H}}_{\text{MP}}^{(1)} \big\vert \Phi_0 \big\rangle = \tilde{z}_{ab}^{ij} \bar{h}_{ij}^{ab(1)}$ $\tilde{z}_{ab}^{ij} \equiv 2 z_{ab}^{ij} - z_{ba}^{ij}$

Table 5. *The pure-excitation elementary operator coefficients of $\hat{\bar{H}}$ that define the CCSD or PT* **T** *amplitudes and the net-excitation elementary operator coefficients of $\hat{G}$ that define the STEOM-CCSD/PT* $\mathbf{S}^{\pm}$ *amplitudes*. See Sections 2.1 and 5.1. These spatial-orbital expressions are adapted respectively from reference [157] and with corrections from reference [3]. These elementary operator coefficients that are made to vanish are the supplementary equations that define the non-variational **T** and $\mathbf{S}^{\pm}$ parameters in the energy expressions, and thus these equations appear in the energy functionals multiplied by associated Lagrange multipliers. For the PT-based methods, the $\bar{h}_i^{a(1)}$ and $\bar{h}_{ij}^{ab(1)}$ expressions that define the first-order Møller–Plesset $\mathbf{T}^{(1)}$ amplitudes are the first-order terms of the CCSD equations (see Section 2.2). Amplitudes of the full $\hat{G}$ are denoted typographically as g_μ, whereas amplitudes of $\hat{G}_2$ are denoted as g_μ (see Section 2.1). As discussed here and in reference [3], the equations that define $\mathbf{S}^{\pm}$ are closely related to the IP- and EA-EOM-CCSD/PT eigenvector equations. For a computationally efficient factorization of the $\bar{h}_i^a$ and $\bar{h}_{ij}^{ab}$ expressions, see for example reference [44].

$\hat{\bar{H}}$ CCSD-based

$$\begin{aligned}
\bar{h}_i^a &= f_i^a - f_i^k t_k^a + f_c^a t_i^c - f_c^k \big(t_i^c t_k^a - 2t_{ik}^{ac} + t_{ik}^{ca}\big) + \big(2V_{ci}^{ka} - V_{ci}^{ak}\big) t_k^c \\
&\quad - \big(2V_{ci}^{kl} - V_{ci}^{lk}\big)\big(t_l^a t_k^c + t_{lk}^{ac}\big) + \big(2V_{cd}^{ka} - V_{dc}^{ka}\big)\big(t_i^d t_k^c + t_{ik}^{dc}\big) \\
&\quad - \big(2V_{cd}^{kl} - V_{cd}^{lk}\big)\big(t_l^a t_{ik}^{dc} + t_i^c \big(t_k^a t_l^d + t_{kl}^{ad}\big) - t_l^d \big(2t_{ik}^{ac} - t_{ik}^{ca}\big)\big) \\
&\equiv 0 \quad \forall\, i, a
\end{aligned}$$

$$\begin{aligned}
\bar{h}_{ij}^{ab} &= V_{ij}^{ab} + V_{ij}^{kl}\big(t_k^a t_l^b + t_{kl}^{ab}\big) + V_{cd}^{ab}\big(t_i^c t_j^d + t_{ij}^{cd}\big) \\
&\quad + V_{cd}^{kl}\big(t_{ik}^{ca} t_{jl}^{db} + t_{ik}^{db} t_{jl}^{ca} + \big(t_i^c t_j^d + t_{ij}^{cd}\big)\big(t_k^a t_l^b + t_{kl}^{ab}\big)\big) \\
&\quad + 2\big(2V_{cd}^{kl} - V_{cd}^{lk}\big) t_{ik}^{ac} t_{jl}^{bd} \\
&\quad + \big(1 + P_{ij}^{ab}\big) \left(\begin{array}{l}
-f_j^k t_{ik}^{ab} + f_c^b t_{ij}^{ac} - f_c^k \big(t_k^b t_{ij}^{ac} + t_j^c t_{ik}^{ab}\big) \\
\quad - V_{ij}^{ak} t_k^b + V_{ic}^{ab} t_j^c - V_{ci}^{bk}\big(t_j^c t_k^a + t_{jk}^{ca}\big) \\
\quad - V_{ci}^{ka}\big(t_j^c t_k^b + t_{jk}^{cb}\big) + \big(2V_{ci}^{ka} - V_{ci}^{ak}\big) t_{jk}^{bc} \\
\quad + V_{ci}^{kl}\big(t_l^a t_{jk}^{cb} + t_k^b t_{jl}^{ca} + t_j^c \big(t_l^a t_k^b + t_{lk}^{ab}\big)\big) \\
\quad - \big(2V_{ci}^{kl} - V_{ci}^{lk}\big)\big(t_l^a t_{jk}^{bc} + t_k^c t_{jl}^{ba}\big) \\
\quad - V_{cd}^{ka}\big(t_i^d t_{jk}^{cb} + t_j^c t_{ik}^{db} + t_k^b \big(t_i^d t_j^c + t_{ij}^{dc}\big)\big) \\
\quad + \big(2V_{cd}^{ka} - V_{dc}^{ka}\big)\big(t_i^d t_{jk}^{bc} + t_k^c t_{ij}^{db}\big) \\
\quad + V_{cd}^{kl}\big(t_j^d t_{ik}^{ca} + t_i^c t_{jk}^{da}\big) t_l^b \\
\quad - \big(2V_{cd}^{kl} - V_{cd}^{lk}\big) \left(\begin{array}{l}
t_{ij}^{ac}\big(t_k^b t_l^d + t_{kl}^{bd}\big) + t_{ik}^{ab}\big(t_j^c t_l^d + t_{jl}^{cd}\big) \\
\quad + t_{ik}^{ac}\big(t_j^d t_l^b + t_{jl}^{db}\big)
\end{array} \right)
\end{array} \right) \\
&\equiv 0 \quad \forall\, i, j, a, b
\end{aligned}$$

$\hat{\bar{H}}_{\mathrm{MP}}^{(1)}$ PT-based

$$\hat{\bar{H}}_{\mathrm{MP}}^{(1)} = \big[\hat{H}^{(0)}, \hat{T}_2^{(1)}\big] + \hat{V}$$

$$\bar{h}_i^{a(1)} = 0 \rightarrow t_i^a = 0 \quad \forall\, i, a$$

$$\bar{h}_{ij}^{ab(1)} = V_{ij}^{ab} + \big(1 + P_{ij}^{ab}\big)\big(f_c^b t_{ij}^{ac} - f_j^k t_{ik}^{ab}\big) \equiv 0 \quad \forall\, i, j, a, b$$

Table 5. (*Continued*)

$\hat{G}$	$\mathrm{g}^{m}_{i'} = g^{m}_{i'} - \bar{h}^{k'}_{i'} s^{m}_{k'} + \mathrm{g}^{m}_{n} s^{n}_{i'} \equiv 0 \quad \forall\, i', m$
	$\mathrm{g}^{m}_{n} = g^{m}_{n} - \bar{h}^{k'}_{n} s^{m}_{k'}$
	$\mathrm{g}^{mb}_{ij} = g^{bm}_{ji} - \bar{h}^{bk'}_{ji} s^{m}_{k'} - \bar{h}^{k'}_{n} s^{m}_{k'} s^{nb}_{ij} \equiv 0 \quad \forall\, m, b, i, j$
	$\mathrm{g}^{a'}_{e} = g^{a'}_{e} + \bar{h}^{a'}_{c'} s^{c'}_{e} - \mathrm{g}^{f}_{e} s^{a'}_{f} \equiv 0 \quad \forall\, a', e$
	$\mathrm{g}^{f}_{e} = g^{f}_{e} + \bar{h}^{f}_{c'} s^{c'}_{e}$
	$\mathrm{g}^{ab}_{ej} = g^{ba}_{je} + \bar{h}^{ba}_{jc'} s^{c'}_{e} - \bar{h}^{f}_{c'} s^{c'}_{e} s^{ab}_{fj} \equiv 0 \quad \forall\, e, j, a, b$

Table 6. *The CCSD zero-, one-, and two-body amplitudes of* $\hat{\bar{H}}$. See Sections 2.1, 4.3, and 5.1. These spatial-orbital expressions are adapted from reference [157]. The simplified PT-based expressions are obtained by setting $\mathbf{T_1} = \mathbf{0}$ (see Section 2.2). The pure-excitation $\bar{\mathbf{H}}$ expressions that define the $\mathbf{T}$ amplitudes are presented separately in Table 5. The factorization is motivated by typographical compactness rather than computational efficiency. (The expressions are ordered according to increasing net-excitation level to facilitate backward substitution; see Section 4.3.)

$$\hat{\bar{H}} \equiv e^{-\hat{T}} \hat{H} e^{\hat{T}}$$

$$\bar{h}^{ij}_{ab} = V^{ij}_{ab}$$

$$\bar{h}^{i}_{a} = f^{i}_{a} + \big(2V^{ik}_{ac} - V^{ik}_{ca}\big) t^{c}_{k}$$

$$\bar{h}^{ji}_{ak} = V^{ji}_{ak} + V^{ij}_{ca} t^{c}_{k}$$

$$\bar{h}^{ia}_{bc} = V^{ia}_{bc} - V^{ik}_{bc} t^{a}_{k}$$

$$\bar{h}_{0} = h_{0} + 2 f^{k}_{c} t^{c}_{k} + \big(2V^{kl}_{cd} - V^{kl}_{dc}\big)\big(t^{c}_{k} t^{d}_{l} + t^{cd}_{kl}\big)$$

$$\bar{h}^{i}_{j} = f^{i}_{j} + f^{i}_{c} t^{c}_{j} + \big(2V^{ki}_{cj} - V^{ik}_{cj}\big) t^{c}_{k} + \big(2V^{ik}_{cd} - V^{ik}_{dc}\big)\big(t^{c}_{j} t^{d}_{k} + t^{cd}_{jk}\big)$$

$$\bar{h}^{a}_{b} = f^{a}_{b} - f^{k}_{b} t^{a}_{k} + \big(2V^{ka}_{cb} - V^{ka}_{bc}\big) t^{c}_{k} - \big(2V^{kl}_{bc} - V^{lk}_{bc}\big)\big(t^{a}_{k} t^{c}_{l} + t^{ac}_{kl}\big)$$

$$\bar{h}^{ai}_{bj} = V^{ai}_{bj} - V^{ki}_{bj} t^{a}_{k} + V^{ia}_{cb} t^{c}_{j} - V^{ik}_{cb}\big(t^{c}_{j} t^{a}_{k} + t^{ca}_{jk}\big)$$

$$\bar{h}^{ia}_{bj} = V^{ia}_{bj} - V^{ik}_{bj} t^{a}_{k} + V^{ia}_{bc} t^{c}_{j} - V^{ik}_{bc}\big(t^{c}_{j} t^{a}_{k} + t^{ca}_{jk}\big) + \big(2V^{ik}_{bc} - V^{ik}_{cb}\big) t^{ac}_{jk}$$

$$\bar{h}^{ij}_{kl} = V^{ij}_{kl} + V^{ij}_{cd}\big(t^{c}_{k} t^{d}_{l} + t^{cd}_{kl}\big) + \big(1 + P^{kl}_{ij}\big)\big(V^{ij}_{cl} t^{c}_{k}\big)$$

$$\bar{h}^{ab}_{cd} = V^{ab}_{cd} + V^{kl}_{cd}\big(t^{a}_{k} t^{b}_{l} + t^{ab}_{kl}\big) - \big(1 + P^{cd}_{ab}\big)\big(V^{kb}_{cd} t^{a}_{k}\big)$$

$$\begin{aligned}\bar{h}^{ai}_{kj} = {} & V^{ai}_{kj} + f^{i}_{c} t^{ca}_{jk} + V^{ai}_{cj} t^{c}_{k} + V^{ia}_{ck} t^{c}_{j} - V^{il}_{jk} t^{a}_{l} - V^{il}_{ck}\big(t^{c}_{j} t^{a}_{l} + t^{ca}_{jl}\big) - V^{li}_{cj}\big(t^{c}_{k} t^{a}_{l} + t^{ca}_{kl}\big) \\ & + V^{ia}_{cd}\big(t^{c}_{j} t^{d}_{k} + t^{cd}_{jk}\big) + \big(2V^{li}_{cj} - V^{il}_{cj}\big) t^{ac}_{kl} + \big(2V^{il}_{cd} - V^{il}_{dc}\big)\big(t^{d}_{l} t^{ca}_{jk} + t^{c}_{j} t^{ad}_{kl}\big) \\ & - V^{il}_{cd}\big(t^{d}_{k} t^{ca}_{jl} + t^{c}_{j} t^{da}_{kl} + t^{a}_{l}\big(t^{c}_{j} t^{d}_{k} + t^{cd}_{jk}\big)\big)\end{aligned}$$

$$\begin{aligned}\bar{h}^{ab}_{ic} = {} & V^{ab}_{ic} - f^{k}_{c} t^{ab}_{ik} - V^{bk}_{ci} t^{a}_{k} - V^{ka}_{ci} t^{b}_{k} + V^{ab}_{dc} t^{d}_{i} - V^{ka}_{cd}\big(t^{d}_{i} t^{b}_{k} + t^{db}_{ik}\big) - V^{kb}_{dc}\big(t^{d}_{i} t^{a}_{k} + t^{da}_{ik}\big) \\ & + V^{kl}_{ci}\big(t^{a}_{l} t^{b}_{k} + t^{ab}_{lk}\big) + \big(2V^{kb}_{dc} - V^{kb}_{cd}\big) t^{ad}_{ik} - \big(2V^{kl}_{cd} - V^{lk}_{cd}\big)\big(t^{d}_{l} t^{ab}_{ik} + t^{b}_{k} t^{ad}_{il}\big) \\ & + V^{kl}_{cd}\big(t^{a}_{l} t^{db}_{ik} + t^{b}_{k} t^{da}_{il} + t^{d}_{i}\big(t^{a}_{l} t^{b}_{k} + t^{ab}_{lk}\big)\big)\end{aligned}$$

Table 7. *The STEOM-CCSD/PT zero-, one-, and two-body amplitudes of* $\hat{G}_2$. See Sections 2.1, 4.3, and 5.1. These spatial-orbital expressions are adapted from reference [3], with corrections. The $\mathbf{S}^{\pm}$ amplitudes are determined by the net-excitation full **G** expressions in Table 5. The $\bar{\mathbf{H}}$ amplitudes are defined in Table 6. (These $\mathbf{G_2}$ expressions are ordered according to increasing net-excitation level to facilitate backward substitution; see Section 4.3.)

$$\hat{G}_2 \equiv \left\{e^{\hat{S}_2}\right\}^{-1} \hat{\bar{H}} \left\{e^{\hat{S}_2}\right\}$$

$$g_{ab}^{ij} = V_{ab}^{ij}$$

$$g_a^i = \bar{h}_a^i - \delta_{im} V_{ac}^{kl} \tilde{s}_{kl}^{mc} + \delta_{ae} V_{cd}^{ik} \tilde{s}_{ek}^{cd}$$

$$g_{ak}^{ji} = \bar{h}_{ak}^{ji} - \delta_{jm} V_{ca}^{il} s_{lk}^{mc} + \delta_{im}\left(V_{ac}^{jl} \tilde{s}_{kl}^{mc} - V_{ca}^{jl} s_{kl}^{mc}\right) + \delta_{ae} V_{cd}^{ij} s_{ek}^{dc}$$

$$g_{bc}^{ia} = \bar{h}_{bc}^{ia} - \delta_{be} V_{dc}^{ik} s_{ek}^{da} + \delta_{ce}\left(V_{bd}^{ik} \tilde{s}_{ek}^{ad} - V_{db}^{ik} s_{ek}^{ad}\right) + \delta_{im} V_{bc}^{lk} s_{lk}^{ma}$$

$$g_0 = \bar{h}_0$$

$$g_j^i = \bar{h}_j^i + \delta_{im}\left(\bar{h}_c^k \tilde{s}_{jk}^{mc} - \bar{h}_{cj}^{kl} \tilde{s}_{lk}^{mc}\right)$$

$$g_b^a = \bar{h}_b^a + \delta_{be}\left(\bar{h}_c^k \tilde{s}_{ek}^{ac} + \bar{h}_{cd}^{ka} \tilde{s}_{ek}^{dc}\right)$$

$$\begin{aligned} g_{bj}^{ai} = {} & \bar{h}_{bj}^{ai} + \delta_{be}\left(\bar{h}_c^i s_{ej}^{ac} + \bar{h}_{cj}^{ki} \tilde{s}_{ek}^{ac} - \bar{h}_{cj}^{ik} s_{ek}^{ac} + \bar{h}_{cd}^{ia} s_{ej}^{dc}\right) \\ & + \delta_{im}\left(-\bar{h}_b^k s_{jk}^{ma} + \bar{h}_{cb}^{ka} \tilde{s}_{jk}^{mc} - \bar{h}_{bc}^{ka} s_{jk}^{mc} + \bar{h}_{bj}^{kl} s_{lk}^{ma}\right) \\ & + \delta_{be}\delta_{im}\begin{pmatrix} -V_{cd}^{lk} \tilde{s}_{lk}^{md} s_{ej}^{ac} - V_{cd}^{kl} \tilde{s}_{el}^{cd} s_{jk}^{ma} + \left(V_{cd}^{kl} \tilde{s}_{jk}^{mc} - V_{cd}^{lk} s_{jk}^{mc}\right) \tilde{s}_{el}^{ad} \\ + V_{cd}^{lk} s_{kj}^{mc} s_{el}^{ad} + V_{cd}^{lk} s_{ej}^{dc} s_{lk}^{ma} \end{pmatrix} \end{aligned}$$

$$\begin{aligned} g_{bj}^{ia} = {} & \bar{h}_{bj}^{ia} + \delta_{be}\left(\bar{h}_c^i s_{ej}^{ca} - \bar{h}_{cj}^{ik} s_{ek}^{ca} + \bar{h}_{cd}^{ia} s_{ej}^{cd}\right) + \delta_{im}\left(-\bar{h}_b^k s_{kj}^{ma} - \bar{h}_{bc}^{ka} s_{kj}^{mc} + \bar{h}_{bj}^{kl} s_{kl}^{ma}\right) \\ & + \delta_{be}\delta_{im}\left(-V_{cd}^{lk} \tilde{s}_{lk}^{md} s_{ej}^{ca} - V_{cd}^{kl} \tilde{s}_{el}^{cd} s_{kj}^{ma} + V_{cd}^{lk} s_{kj}^{mc} s_{el}^{da} + V_{cd}^{lk} s_{ej}^{dc} s_{kl}^{ma}\right) \end{aligned}$$

$$\begin{aligned} g_{kl}^{ij} = {} & \bar{h}_{kl}^{ij} + \delta_{im}\delta_{jn}\left(V_{cd}^{k_2k_1} s_{k_2l}^{nd} s_{kk_1}^{mc} + V_{cd}^{k_2k_1} s_{k_1k}^{nc} s_{k_2l}^{md} + \left(V_{cd}^{k_1k_2} \tilde{s}_{lk_2}^{nd} - V_{cd}^{k_2k_1} s_{lk_2}^{nd}\right) \tilde{s}_{kk_1}^{mc}\right) \\ & + \left(1 + P_{ij}^{kl}\right)\left(\delta_{im}\left(\bar{h}_c^j s_{kl}^{mc} + \bar{h}_{cl}^{k_1j} \tilde{s}_{kk_1}^{mc} - \bar{h}_{cl}^{jk_1} s_{kk_1}^{mc} - \bar{h}_{ck}^{jk_1} s_{k_1l}^{mc}\right) - \delta_{im}\delta_{jn} V_{cd}^{k_2k_1} \tilde{s}_{k_2k_1}^{nd} s_{kl}^{mc}\right) \end{aligned}$$

$$\begin{aligned} g_{cd}^{ab} = {} & \bar{h}_{cd}^{ab} + \delta_{ce}\delta_{df}\left(V_{c_1c_2}^{lk} s_{fl}^{c_2b} s_{ek}^{ac_1} + V_{c_1c_2}^{lk} s_{fk}^{c_1a} s_{el}^{c_2b} + \left(V_{c_1c_2}^{kl} \tilde{s}_{fl}^{bc_2} - V_{c_1c_2}^{lk} s_{fl}^{bc_2}\right) \tilde{s}_{ek}^{ac_1}\right) \\ & + \left(1 + P_{ab}^{cd}\right)\begin{pmatrix} \delta_{ce}\left(-\bar{h}_d^k s_{ek}^{ab} + \bar{h}_{c_1d}^{kb} \tilde{s}_{ek}^{ac_1} - \bar{h}_{dc_1}^{kb} s_{ek}^{ac_1} - \bar{h}_{dc_1}^{ka} s_{ek}^{c_1b}\right) \\ - \delta_{ce}\delta_{df} V_{c_1c_2}^{kl} \tilde{s}_{fl}^{c_1c_2} s_{ek}^{ab} \end{pmatrix} \end{aligned}$$

$$\begin{aligned} g_{ji}^{bm} = {} & \bar{h}_{ji}^{bm} - \bar{h}_i^k s_{kj}^{mb} - \bar{h}_j^k s_{ik}^{mb} + \bar{h}_c^b s_{ij}^{mc} + \bar{h}_{ij}^{kl} s_{kl}^{mb} + \bar{h}_{cj}^{kb} \tilde{s}_{ik}^{mc} - \bar{h}_{cj}^{bk} s_{ik}^{mc} - \bar{h}_{ci}^{bk} s_{kj}^{mc} \\ & - V_{cd}^{kl} \tilde{s}_{kl}^{md} t_{ij}^{cb} + g_n^m s_{ij}^{nb} \end{aligned}$$

$$\begin{aligned} g_{je}^{ba} = {} & \bar{h}_{je}^{ba} + \bar{h}_c^a s_{ej}^{cb} + \bar{h}_c^b s_{ej}^{ac} - \bar{h}_j^k s_{ek}^{ab} + \bar{h}_{cd}^{ab} s_{ej}^{cd} + \bar{h}_{cj}^{kb} \tilde{s}_{ek}^{ac} - \bar{h}_{cj}^{bk} s_{ek}^{ac} - \bar{h}_{cj}^{ak} s_{ek}^{cb} \\ & - V_{cd}^{kl} \tilde{s}_{el}^{cd} t_{jk}^{ba} - g_e^f s_{fj}^{ab} \end{aligned}$$

$$\tilde{s}_{ij}^{mb} \equiv 2s_{ij}^{mb} - s_{ji}^{mb}$$

$$\tilde{s}_{ej}^{ab} \equiv 2s_{ej}^{ab} - s_{ej}^{ba}$$

Table 8. *The CCSD-based and PT-based* **Z** *Lagrange multiplier equations*. See Sections 3.2, 3.3, and 5.2. The **Z** Lagrange multipliers account for the response of the non-variational **T** parameters of the underlying CCSD/PT reference treatment. These equations—as well as all other derivative expressions presented in the remaining tables—were derived directly from the input algebraic functionals by automated symbolic manipulations in the *SMART* package. The **Z** equations are constructed to be essentially identical for all CCSD-based or PT-based methods through chain-rule derivatives in the common $\bar{\mathbf{H}}$ amplitudes. Nearly all of the (ST)EOM-variant dependence beyond the CCSD/PT reference treatment is isolated in the intermediate density matrix $\bar{\mathbf{D}}$; the explicit three-body contributions to the t_{ij}^{ab} chain rule are collected in Table 9. Since canonical Hartree–Fock orbitals are employed in the PT-based methods here, there is no PT-based one-body **Z** equation, as $\bar{h}_i^{a(1)} = 0$ (and $t_i^{a(1)} = 0$) always, and the homogeneous side of the PT-based $\mathbf{Z_2}$ equation is trivial, due to the simplified $\bar{h}_{ij}^{ab(1)}$ and diagonal $f_q^p = \varepsilon_p \delta_{pq}$, where the ε_p are the orbital energies. Like the $\mathbf{T}_2^{(1)}$ equation, solution for the associated $\mathbf{Z_2}$ Lagrange multipliers in the PT-based methods requires only simple division by an energy denominator.

Z equations $\quad \dfrac{\partial}{\partial t_\nu}\langle \Phi_0|\hat{Z}\hat{\bar{H}}|\Phi_0\rangle = -\left(\dfrac{\partial F^{inh}}{\partial t_\nu} = \sum_\mu \bar{D}_\mu \dfrac{\partial \bar{h}_\mu}{\partial t_\nu} + \sum_\mu \bar{h}_\mu \dfrac{\partial \bar{D}_\mu}{\partial t_\nu}\right) \quad \forall\ \nu$

Homogeneous left sides

CCSD-based

$$\frac{\partial}{\partial t_i^a}\langle \Phi_0|\hat{Z}\hat{\bar{H}}|\Phi_0\rangle = 2\begin{pmatrix} -z_a^k \bar{h}_k^i + z_c^i \bar{h}_a^c + z_c^k\big(2\bar{h}_{ak}^{ic} - \bar{h}_{ak}^{ci}\big) + \tilde{z}_{cd}^{ik}\bar{h}_{ka}^{dc} - \tilde{z}_{ac}^{lk}\bar{h}_{kl}^{ci} \\ + \tilde{z}_{bd}^{kl}t_{kl}^{cd}\big(2\bar{h}_{ac}^{ib} - \bar{h}_{ca}^{ib}\big) - \tilde{z}_{cd}^{kl}t_{jl}^{cd}\big(2\bar{h}_{ak}^{ij} - \bar{h}_{ak}^{ji}\big) \end{pmatrix}$$

$$\frac{\partial}{\partial t_{ij}^{ab}}\langle \Phi_0|\hat{Z}\hat{\bar{H}}|\Phi_0\rangle = \tfrac{1}{2}\big(1 + P_{ij}^{ab}\big)(2 - P_{ij})\begin{pmatrix} 2z_b^j\bar{h}_a^i - 2z_b^k\bar{h}_{ak}^{ij} + 2z_c^j\bar{h}_{ab}^{ic} \\ + 2z_{ac}^{ij}\bar{h}_b^c - 2z_{ab}^{ik}\bar{h}_k^j + z_{cd}^{ij}\bar{h}_{ab}^{cd} + z_{ab}^{kl}\bar{h}_{kl}^{ij} \\ + 2\tilde{z}_{ac}^{ik}\bar{h}_{bk}^{jc} - 2z_{ac}^{ik}\bar{h}_{bk}^{cj} - 2z_{ca}^{jk}\bar{h}_{bk}^{ci} \\ - 2\tilde{z}_{cd}^{jl}t_{kl}^{cd}V_{ab}^{ik} - 2\tilde{z}_{ad}^{kl}t_{kl}^{cd}V_{cb}^{ij} \end{pmatrix}$$

PT-based $\quad \dfrac{\partial}{\partial t_{ij}^{ab}}\big\langle \Phi_0\big|\hat{Z}_2\big(\big[\hat{H}^{(0)}, \hat{T}_2^{(1)}\big] + \hat{V}\big)\big|\Phi_0\big\rangle = \tilde{z}_{ab}^{ij}(\varepsilon_a + \varepsilon_b - \varepsilon_i - \varepsilon_j)$

Inhomogeneous right sides (*without leading minus sign*)

CCSD-based

$$\begin{aligned} \frac{\partial F^{inh}}{\partial t_i^a} = {} & -\bar{D}_a^k\bar{h}_k^i + \bar{D}_c^i\bar{h}_a^c + \bar{D}_c^k\big(2\bar{h}_{ak}^{ic} - \bar{h}_{ak}^{ci}\big) + 2\bar{h}_a^i + \bar{D}_k^i\bar{h}_a^k - \bar{D}_a^c\bar{h}_c^i \\ & + \bar{D}_k^c\big(2V_{ac}^{ik} - V_{ca}^{ik}\big) + \bar{D}_k^l\big(2\bar{h}_{al}^{ik} - \bar{h}_{al}^{ki}\big) + \bar{D}_c^d\big(2\bar{h}_{ad}^{ic} - \bar{h}_{da}^{ic}\big) \\ & + \bar{D}_{kl}^{ci}V_{ac}^{lk} - \bar{D}_{ka}^{cd}V_{dc}^{ik} - \bar{D}_{aj}^{kl}\bar{h}_{kl}^{ij} + \bar{D}_{cd}^{ib}\bar{h}_{ab}^{cd} + 2\bar{D}_{kl}^{ij}\bar{h}_{aj}^{kl} - 2\bar{D}_{ab}^{cd}\bar{h}_{cd}^{ib} \\ & - \bar{D}_{ak}^{lc}\bar{h}_{cl}^{ki} - \bar{D}_{ak}^{cl}\bar{h}_{cl}^{ik} + \bar{D}_{dk}^{ic}\bar{h}_{ca}^{kd} + \bar{D}_{dk}^{ci}\bar{h}_{ac}^{kd} + \bar{D}_{cl}^{ki}\bar{h}_{ak}^{lc} + \bar{D}_{cl}^{ik}\bar{h}_{ak}^{cl} \\ & - \bar{D}_{ca}^{kd}\bar{h}_{dk}^{ic} - \bar{D}_{ac}^{kd}\bar{h}_{dk}^{ci} + \big(-\bar{D}_{db}^{lc}t_{kl}^{bd} + \bar{D}_{dk}^{lj}t_{jl}^{cd}\big)\big(2V_{ac}^{ik} - V_{ca}^{ik}\big) \end{aligned}$$

Table 8. (*Continued*)

Z equations	$\frac{\partial}{\partial t_\nu}\langle\Phi_0\vert\hat{Z}\hat{\bar{H}}\vert\Phi_0\rangle = -\left(\frac{\partial F^{inh}}{\partial t_\nu} = \sum_\mu \bar{D}_\mu \frac{\partial \bar{h}_\mu}{\partial t_\nu} + \sum_\mu \bar{h}_\mu \frac{\partial \bar{D}_\mu}{\partial t_\nu}\right) \quad \forall\ \nu$
CCSD/PT-based	$\frac{\partial F^{inh}}{\partial t_{ij}^{ab}} = \frac{1}{2}(1+P_{ij}^{ab})(2-P_{ij}) \begin{pmatrix} \bar{D}_b^j \bar{h}_a^i - \bar{D}_b^k \bar{h}_{ak}^{ij} + \bar{D}_c^j \bar{h}_{ab}^{ic} \\ + V_{ab}^{ij} + \bar{D}_k^j V_{ab}^{ik} - \bar{D}_b^c V_{ac}^{ij} \\ + \bar{D}_{bk}^{jc} V_{ac}^{ik} + \bar{D}_{bk}^{jl} \bar{h}_{al}^{ik} + \bar{D}_{bc}^{jd} \bar{h}_{ad}^{ic} \end{pmatrix}$
	$+ \frac{1}{2}(1+P_{ij}^{ab}) \begin{pmatrix} \bar{D}_{ak}^{ij} \bar{h}_b^k - \bar{D}_{ab}^{ic} \bar{h}_c^j + \bar{D}_{kl}^{ij} V_{ab}^{kl} + \bar{D}_{ab}^{cd} V_{cd}^{ij} \\ - \bar{D}_{bk}^{jc} V_{ca}^{ik} - \bar{D}_{bk}^{ci} V_{ca}^{jk} - \bar{D}_{bk}^{jl} \bar{h}_{al}^{ki} - \bar{D}_{bk}^{li} \bar{h}_{al}^{kj} \\ - \bar{D}_{bc}^{jd} \bar{h}_{da}^{ic} - \bar{D}_{cb}^{id} \bar{h}_{da}^{jc} + \bar{D}_{ab}^{kc} \bar{h}_{ck}^{ji} + \bar{D}_{ck}^{ji} \bar{h}_{ab}^{kc} \end{pmatrix}$
	$+ \sum_\mu \bar{h}_\mu \frac{\partial \bar{D}_\mu}{\partial t_{ij}^{ab}}$ (see Table 9)

Table 9. *The explicit three-body contributions to the t_{ij}^{ab} chain-rule derivative in Table 8.* For computational storage reasons, we choose to formulate all expressions in terms of only zero-, one-, and two-body amplitudes. As a result of the expanded three-body $\bar{\mathbf{H}}$ amplitudes, certain two-body $\bar{\mathbf{D}}$ elements (those associated with the two-body Hamiltonian amplitudes in this table) are modified to additionally contain the contributions that formally belong in the absent three-body $\bar{\mathbf{D}}$; these three-body contributions appear as the **T** terms in $\bar{D}_{ji}^{ak}$, $\bar{D}_{ia}^{bc}$, and $\bar{D}_{ij}^{ab}$ in Table 10 and in $\bar{D}_{ij}^{ab}$ in Table 14. The product rule of differentiation on these $\bar{\mathbf{D}}$ that explicitly contain **T** then generates the following additional contributions to the chain-rule terms of Table 8. For discussion, see Section 5.2.3. These formally cumbersome modifications are all handled automatically here through the direct algebraic treatment. The $u1_a^m$ and $u2_e^i$ intermediates are defined in Tables 11 and 12, respectively, and the minus sign that precedes the inhomogeneous right side of the **Z** equation has not been included here.

Explicit three-body contributions	$\sum_\mu \bar{h}_\mu \frac{\partial \bar{D}_\mu}{\partial t_{ij}^{ab}}$
EE-EOM-CCSD/PT	$+\frac{1}{2}(1+P_{ij}^{ab}) \begin{pmatrix} 2(2\bar{h}_{db}^{lc} - \bar{h}_{bd}^{lc}) r_l^d \tilde{l}_{ac}^{ij} - 2(2\bar{h}_{dk}^{lj} - \bar{h}_{dk}^{jl}) r_l^d \tilde{l}_{ab}^{ik} \\ - 2(2V_{bd}^{kl} - V_{bd}^{lk}) r_{kl}^{cd} \tilde{l}_{ac}^{ij} \\ - 2(2V_{cd}^{jl} - V_{dc}^{jl}) r_{kl}^{cd} \tilde{l}_{ab}^{ik} \end{pmatrix}$
IP-EOM-CCSD/PT	$+\frac{1}{2}(1+P_{ij}^{ab})\left((2V_{bd}^{kl} - V_{bd}^{lk}) r_{kl}^{\ d} \tilde{l}_{\ a}^{ji}\right)$
EA-EOM-CCSD/PT	$+\frac{1}{2}(1+P_{ij}^{ab})\left(-(2V_{cd}^{jl} - V_{dc}^{jl}) r_{\ l}^{cd} \tilde{l}_{\ ba}^{i}\right)$
EE- and DIP-STEOM-CCSD/PT	$+\frac{1}{2}(1+P_{ij}^{ab})\left(-\tilde{d}_{mb}^{ij} V_{ad}^{kl} \tilde{s}_{kl}^{md}\right) = +\frac{1}{2}(1+P_{ij}^{ab})\left(\tilde{d}_{mb}^{ij} u1_a^m\right)$
EE- and DEA-STEOM-CCSD/PT	$+\frac{1}{2}(1+P_{ij}^{ab})\left(-\tilde{a}_{ab}^{ej} V_{cd}^{il} \tilde{s}_{el}^{cd}\right) = +\frac{1}{2}(1+P_{ij}^{ab})\left(-\tilde{a}_{ab}^{ej} u2_e^i\right)$

Table 10. *The zero-, one-, and two-body intermediate density matrix elements* $\bar{\mathbf{D}}$ *for EE-, IP-, and EA-EOM-CCSD/PT gradients*. See Sections 3.2 and 5.3. These $\bar{D}_\mu \equiv \partial F^{inh}/\partial \bar{h}_\mu$ (along with the associated three-body contributions to the t_{ij}^{ab} chain rule, Table 9) completely define the analytical gradient for each method. Note that upper and lower indices on $\bar{D}_\mu$ are exchanged relative to the differentiating $\bar{h}_\mu$, and F^{inh} is the EOM functional (Table 3) without the CCSD/PT $\hat{Z}$ term. The $\bar{\mathbf{D}}$ determine the analytical gradient through the essentially method-independent chain-rule **Z** Lagrange multiplier equations of Table 8 and through the method-independent chain-rule conversion to the GHF effective density matrix **D** in Table 15/Table 16. In contrast to the full effective density matrix **D**, which contains *all* of the method's GHF response, the intermediate density matrix $\bar{\mathbf{D}}$ contains just the *post-CCSD/PT* response information that is unique to each method.

$\bar{D}_\mu$	EE-EOM-CCSD/PT	IP-EOM-CCSD/PT	EA-EOM-CCSD/PT
$\bar{D}_a^i$	0	0	0
$\bar{D}_{ab}^{ij}$	0	0	0
$\bar{D}_i^a$	$2l_c^k \tilde{r}_{ik}^{ac}$	$-l^k \tilde{r}_{ki}^{\ a}$	$l_c \tilde{r}_i^{ca}$
$\bar{D}_{ij}^{ab}$	$-\big(1+P_{ij}^{ab}\big)\big(\tilde{l}_{cd}^{kl} t_{kl}^{bd} \tilde{r}_{ij}^{ac} + \tilde{l}_{cd}^{kl} t_{jl}^{cd} \tilde{r}_{ik}^{ab}\big)$	$\frac{1}{2}\big(1+P_{ij}^{ab}\big)\tilde{l}_{\ d}^{kl} t_{kl}^{bd} \tilde{r}_{ji}^{\ a}$	$-\frac{1}{2}\big(1+P_{ij}^{ab}\big)\tilde{l}_{cd}^{\ l} t_{jl}^{cd} \tilde{r}_{\ i}^{ba}$
$\bar{D}_i^j$	$-2l_c^j r_i^c - 2l_{cd}^{jk} \tilde{r}_{ik}^{cd}$	$l^j r_i + l^{jk}_{\ \ c} \tilde{r}_{ik}^{\ c} + l^{kj}_{\ \ c} \tilde{r}_{ki}^{\ c}$	$-l_{cd}^{\ j} \tilde{r}_{\ i}^{cd}$
$\bar{D}_a^b$	$2l_a^k r_k^b + 2l_{ac}^{kl} \tilde{r}_{kl}^{bc}$	$-l_{\ a}^{lk} \tilde{r}_{lk}^{\ b}$	$l_a r^b + l_{ca}^{\ \ k} \tilde{r}_{\ k}^{cb} + l_{ac}^{\ \ k} \tilde{r}_{\ k}^{bc}$
$\bar{D}_{ji}^{ak}$	$-2l_c^k \tilde{r}_{ij}^{ca} - 2(2-P_{ij}) \tilde{l}_{cd}^{kl} t_{il}^{cd} r_j^a$	$l^k \tilde{r}_{ij}^{\ a}$	0
$\bar{D}_{ia}^{bc}$	$2l_a^k \tilde{r}_{ik}^{bc} + 2(2-P_{bc}) \tilde{l}_{ad}^{kl} t_{kl}^{cd} r_i^b$	0	$l_a \tilde{r}_i^{cb}$
$\bar{D}_{ij}^{kl}$	$l_{cd}^{kl} \tilde{r}_{ij}^{cd}$	$-\frac{1}{2}\big(1+P_{ij}^{kl}\big) l^{kl}_{\ \ c} \tilde{r}_{ij}^{\ c}$	0
$\bar{D}_{ab}^{cd}$	$\tilde{l}_{ab}^{kl} r_{kl}^{cd}$	0	$\frac{1}{2}\big(1+P_{ab}^{cd}\big) \tilde{l}_{ab}^{\ \ k} r_{\ k}^{cd}$
$\bar{D}_{ai}^{bj}$	$-2l_a^j r_i^b - 2l_{ca}^{jk} \tilde{r}_{ik}^{cb} - 2l_{ac}^{jk} \tilde{r}_{ik}^{bc}$	$l^{jk}_{\ \ a} \tilde{r}_{ik}^{\ b} + l^{kj}_{\ \ a} \tilde{r}_{ki}^{\ b}$	$-l_{ac}^{\ \ j} \tilde{r}_{\ i}^{bc} - l_{ca}^{\ \ j} \tilde{r}_{\ i}^{cb}$
$\bar{D}_{ai}^{jb}$	$4l_a^j r_i^b + 2\tilde{l}_{ac}^{jk} \tilde{r}_{ik}^{bc}$	$-\tilde{l}^{kj}_{\ \ a} \tilde{r}_{ki}^{\ b}$	$\tilde{l}_{ca}^{\ \ j} \tilde{r}_{\ i}^{cb}$
$\bar{D}_{ai}^{kj}$	$-2\tilde{l}_{ca}^{jk} r_i^c$	$\tilde{l}^{jk}_{\ \ a} r_i$	0
$\bar{D}_{ab}^{ic}$	$2\tilde{l}_{ab}^{ik} r_k^c$	0	$\tilde{l}_{ba}^{\ \ i} r^c$
$\bar{D}_0$	1	1	1

Table 11. *The STEOM-CCSD/PT* $\mathbf{Z}^-$ *Lagrange multiplier equations*. See Sections 3.3 and 5.4. The $\mathbf{Z}^-$ Lagrange multipliers account for the response of the non-variational $\mathbf{S}^-$ parameters. The energy functional is made variational with respect to $\mathbf{S}^-$, and the resulting equations determine the associated $\mathbf{Z}^-$ Lagrange multipliers. The $\mathbf{Z}^-$ amplitudes are denoted as d_μ. The u_ν intermediates are the same as in reference [3] (repeated here for convenience), and the $\mathbf{M}$ intermediates are defined in Table 13. These equations can be decoupled in the active external index m by diagonalizing the $\mathfrak{g}^n_m$ matrix, improving efficiency and numerical convergence (see Section 5.4.1).

$\mathbf{Z}^-$ equations	$\frac{\partial}{\partial s^m_\mu}\big(\sum_n \langle\Phi_n\vert\hat{Z}^-[\hat{G},\hat{n}]\vert\Phi_0\rangle\big) = -\frac{\partial}{\partial s^m_\mu}\langle\Phi_0\vert\hat{L}[\hat{G}_2,\hat{R}]\vert\Phi_0\rangle \quad \forall\, m,\mu$
Homogeneous left sides	
EE- & DIP-STEOM–CCSD/PT	$\frac{\partial}{\partial s^m_{i'}}\big(\sum_n \langle\Phi_n\vert\hat{Z}^-[\hat{G},\hat{n}]\vert\Phi_0\rangle\big) = -2d^{k'}_m \bar{h}^{i'}_{k'} - q^n_m \bar{h}^{i'}_n - \tilde{d}^{lk}_{mc}\bar{h}^{ci'}_{kl} + 2d^{i'}_n \mathfrak{g}^n_m$
	$\frac{\partial}{\partial s^{mb}_{ij}}\big(\sum_n \langle\Phi_n\vert\hat{Z}^-[\hat{G},\hat{n}]\vert\Phi_0\rangle\big)$
	$= (2-P_{ij})\begin{pmatrix} \big(2d^{k'}_m\delta_{ik'} + q^n_m\delta_{in}\big)\bar{h}^j_b - 2d^{k'}_m\bar{h}^{ji}_{bk'} - q^n_m\bar{h}^{ji}_{bn} \\ + d^{ij}_{mc}\bar{h}^c_b - d^{kj}_{mb}\bar{h}^i_k - d^{ik}_{mb}\bar{h}^j_k + d^{kl}_{mb}\bar{h}^{ij}_{kl} + \tilde{d}^{ik}_{mc}\bar{h}^{jc}_{bk} \\ - d^{ik}_{mc}\bar{h}^{cj}_{bk} - d^{kj}_{mc}\bar{h}^{ci}_{bk} - \tilde{d}^{kl}_{md}t^{cd}_{kl}V^{ij}_{cb} + d^{ij}_{nb}\mathfrak{g}^n_m \end{pmatrix}$
Inhomogeneous right sides (*without leading minus sign*)	
EE- & DIP-STEOM-CCSD/PT	$\frac{\partial}{\partial s^m_{i'}}\langle\Phi_0\vert\hat{L}[\hat{G}_2,\hat{R}]\vert\Phi_0\rangle = 0$
EE-STEOM-CCSD/PT	$\frac{\partial}{\partial s^{mb}_{ij}}\langle\Phi_0\vert\hat{L}[\hat{G}_2,\hat{R}]\vert\Phi_0\rangle$
	$= 2(2-P_{ij})\begin{pmatrix} -M^i_m\bar{h}^j_b + M^k_m\bar{h}^{ji}_{bk} - M^{ci}_{dm}\bar{h}^{jd}_{bc} - M^{ei}_{cm}u1^{jc}_{be} \\ - M^{ek}_{cm}\big((2s^{dc}_{ek})^{\text{singlet}}_{\text{only}} - s^{cd}_{ek}\big)V^{ij}_{db} \end{pmatrix}$
	$+ 2\big((2)^{\text{singlet}}_{\text{only}} - P_{ij}\big)\begin{pmatrix} -M^{cj}_{bm}\bar{h}^i_c + M^{ck}_{bm}\bar{h}^{ij}_{ck} - M^{dj}_{cm}\bar{h}^{ic}_{db} \\ - M^{ej}_{bm}u2^i_e - M^{ej}_{cm}u2^{ic}_{eb} + M^{ek}_{bm}u3^{ij}_{ek} \end{pmatrix}$
DIP-STEOM-CCSD/PT	$\frac{\partial}{\partial s^{mb}_{ij}}\langle\Phi_0\vert\hat{L}[\hat{G}_2,\hat{R}]\vert\Phi_0\rangle$
	$= 2(2-P_{ij})\begin{pmatrix} -M^i_m\bar{h}^j_b + M^k_m\bar{h}^{ji}_{bk} + M^{ik}_{ml}\bar{h}^{jl}_{bk} \\ + M^{ik}_{mn}u1^{jn}_{bk} - M^{kl}_{mn}s^{nc}_{lk}V^{ij}_{cb} \end{pmatrix}$
	$+ 2\begin{pmatrix} M^{ij}_{mk}\bar{h}^k_b - M^{ik}_{ml}\bar{h}^{lj}_{bk} - M^{jl}_{km}\bar{h}^{ki}_{bl} \\ + M^{ij}_{mn}u1^n_b - M^{ik}_{mn}u2^{nj}_{bk} - M^{jk}_{nm}u2^{ni}_{bk} \end{pmatrix}$

$q^n_m \equiv 2d^{k'}_m s^n_{k'} + \tilde{d}^{lk}_{mc}s^{nc}_{lk}$; $\quad u3^{kl}_{ei} \equiv V^{kl}_{ab}s^{ab}_{ei}$; $\quad u1^{km}_{ci} \equiv V^{kj}_{ca}\tilde{s}^{ma}_{ij} - V^{kj}_{ac}s^{ma}_{ij}$;

$u1^m_a \equiv -V^{ij}_{ab}\tilde{s}^{mb}_{ij}$; $\quad u2^{mk}_{ci} \equiv -V^{kj}_{ac}s^{ma}_{ji}$; $\quad$ for $u2^i_e$, $u1^{ka}_{ce}$, $u2^{ka}_{ec}$ see Table 12.

Table 12. *The STEOM-CCSD/PT* $\mathbf{Z}^+$ *Lagrange multiplier equations*. See Sections 3.3 and 5.4. The $\mathbf{Z}^+$ Lagrange multipliers account for the response of the non-variational $\mathbf{S}^+$ parameters. The energy functional is made variational with respect to $\mathbf{S}^+$, and the resulting equations determine the associated $\mathbf{Z}^+$ Lagrange multipliers. The $\mathbf{Z}^+$ amplitudes are denoted as a_μ. The u_v intermediates are the same as in reference [3] (repeated here for convenience), and the $\mathbf{M}$ intermediates are defined in Table 13. These equations can be decoupled in the active external index e by diagonalizing the g^e_f matrix, improving efficiency and numerical convergence (see Section 5.4.1).

$\mathbf{Z}^+$ equations	$\frac{\partial}{\partial s^\mu_e}\big(\sum_f \langle \Phi^f \vert \hat{Z}^+[\hat{G},\, \hat{f}^\dagger] \vert \Phi_0\rangle\big) = -\frac{\partial}{\partial s^\mu_e}\langle \Phi_0 \vert \hat{L}[\hat{G}_2,\, \hat{R}] \vert \Phi_0\rangle \quad \forall\, e, \mu$

Homogeneous left sides

EE- & DEA-STEOM-CCSD/PT

$$\frac{\partial}{\partial s^{a'}_e}\big(\sum_f \langle \Phi^f \vert \hat{Z}^+[\hat{G},\, \hat{f}^\dagger] \vert \Phi_0\rangle\big) = 2a^e_{c'}\bar{h}^{c'}_{a'} - q^e_f \bar{h}^f_{a'} + \tilde{a}^{ek}_{dc}\bar{h}^{cd}_{ka'} - 2a^f_{a'}\mathsf{g}^e_f$$

EE-STEOM-CCSD/PT

$$\frac{\partial}{\partial s^{ab}_{ej}}\big(\sum_f \langle \Phi^f \vert \hat{Z}^+[\hat{G},\, \hat{f}^\dagger] \vert \Phi_0\rangle\big) = (2 - P_{ab})\begin{pmatrix} \big(2a^e_{c'}\delta_{ac'} - q^e_f\delta_{af}\big)\bar{h}^j_b + 2a^e_{c'}\bar{h}^{jc'}_{ba} - q^e_f\bar{h}^{jf}_{ba} \\ \quad - a^{ek}_{ab}\bar{h}^j_k + a^{ej}_{cb}\bar{h}^c_a + a^{ej}_{ac}\bar{h}^c_b + a^{ej}_{cd}\bar{h}^{cd}_{ab} + \tilde{a}^{ek}_{ac}\bar{h}^{jc}_{bk} \\ \quad - a^{ek}_{ac}\bar{h}^{cj}_{bk} - a^{ek}_{cb}\bar{h}^{cj}_{ak} - \tilde{a}^{el}_{cd}t^{cd}_{kl}V^{jk}_{ba} - a^{fj}_{ab}\mathsf{g}^e_f \end{pmatrix}$$

Inhomogeneous right sides (*without leading minus sign*)

EE- & DEA-STEOM-CCSD/PT

$$\frac{\partial}{\partial s^{a'}_e}\langle \Phi_0 \vert \hat{L}[\hat{G}_2,\, \hat{R}] \vert \Phi_0\rangle = 0$$

EE-STEOM-CCSD/PT

$$\frac{\partial}{\partial s^{ab}_{ej}}\langle \Phi_0 \vert \hat{L}[\hat{G}_2,\, \hat{R}] \vert \Phi_0\rangle = 2(2 - P_{ab})\begin{pmatrix} M^e_a\bar{h}^j_b + M^e_c\bar{h}^{jc}_{ba} - M^{el}_{ak}\bar{h}^{jk}_{bl} - M^{ek}_{am}u1^{jm}_{bk} \\ \quad - M^{ek}_{cm}\big((2s^{mc}_{lk})^{\text{singlet}}_{\text{only}} - s^{mc}_{kl}\big)V^{jl}_{ba} \end{pmatrix}$$
$$+ 2\big((2)^{\text{singlet}}_{\text{only}} - P_{ab}\big)\begin{pmatrix} M^{ej}_{bk}\bar{h}^k_a + M^{ej}_{ck}\bar{h}^{kc}_{ab} - M^{el}_{bk}\bar{h}^{kj}_{al} \\ \quad + M^{ej}_{bm}u1^m_a - M^{ek}_{bm}u2^{mj}_{ak} + M^{ej}_{cm}u3^{mc}_{ab} \end{pmatrix}$$

DEA-STEOM-CCSD/PT

$$\frac{\partial}{\partial s^{ab}_{ej}}\langle \Phi_0 \vert \hat{L}[\hat{G}_2,\, \hat{R}] \vert \Phi_0\rangle = 2(2 - P_{ab})\begin{pmatrix} M^e_a\bar{h}^j_b + M^e_c\bar{h}^{jc}_{ba} + M^{ed}_{ac}\bar{h}^{jc}_{bd} \\ \quad + M^{ef}_{ac}u1^{jc}_{bf} - M^{ef}_{cd}s^{dc}_{fk}V^{jk}_{ba} \end{pmatrix}$$
$$+ 2\begin{pmatrix} -M^{ec}_{ab}\bar{h}^j_c - M^{ed}_{ac}\bar{h}^{jc}_{db} - M^{de}_{bc}\bar{h}^{jc}_{da} \\ \quad - M^{ef}_{ab}u2^j_f - M^{ef}_{ac}u2^{jc}_{fb} - M^{fe}_{bc}u2^{jc}_{fa} \end{pmatrix}$$

$q^e_f \equiv 2a^e_{c'}s^{c'}_f + \tilde{a}^{ek}_{dc}s^{dc}_{fk}$; $\quad u3^{ma}_{cd} \equiv V^{ij}_{cd}s^{ma}_{ij}$; $\quad u1^{ka}_{ce} \equiv V^{ki}_{cb}\tilde{s}^{ab}_{ei} - V^{ki}_{bc}s^{ab}_{ei}$;

$u2^i_e \equiv V^{ij}_{ab}\tilde{s}^{ab}_{ej}$; $\quad u2^{ka}_{ec} \equiv -V^{ki}_{bc}s^{ba}_{ei}$; $\quad$ for $u1^m_a$, $u1^{km}_{ci}$, $u2^{mk}_{ci}$ see Table 11.

Table 13. *The STEOM-CCSD/PT intermediates* **M**. For historical reasons, the **M** intermediates were implemented with positive unit factors, as defined in the upper portion of the table. The factors and signs relating the **M** expressions to the more-formal chain-rule $\partial E/\partial \mathbf{G_2}$ derivatives (see Section 5.4) are given in the lower portion. Note that the DIP $M_{jl}^{ik} = M_{lj}^{ki}$ and DEA $M_{ac}^{bd} = M_{ca}^{db}$ possess the standard pair-interchange symmetry due to the underlying symmetry of the **L** and **R** amplitudes.

EE-STEOM-CCSD/PT	DIP-STEOM-CCSD/PT	DEA-STEOM-CCSD/PT
$M_j^i \equiv l_a^i r_j^a$	$M_j^i \equiv l^{ik} r_{jk}$	$M_a^b \equiv l_{ac} r^{bc}$
$M_a^b \equiv l_a^i r_i^b$	$M_{jl}^{ik} \equiv l^{ik} r_{jl}$	$M_{ac}^{bd} \equiv l_{ac} r^{bd}$
$M_{aj}^{bi} \equiv l_a^i r_j^b$		
$\partial E/\partial g_i^j = -2M_j^i$	$\partial E/\partial g_i^j = -2M_j^i$	$\partial E/\partial g_b^a = 2M_a^b$
$\partial E/\partial g_b^a = 2M_a^b$	$\partial E/\partial g_{ik}^{jl} = M_{jl}^{ik}$	$\partial E/\partial g_{bd}^{ac} = M_{ac}^{bd}$
$\partial E/\partial g_{bi}^{aj} = -2M_{aj}^{bi}$		

Table 14. *The zero-, one-, and two-body intermediate density matrix elements* $\bar{\mathbf{D}}$ *for EE-, DIP-, and DEA-STEOM-CCSD/PT gradients*. See Sections 3.3 and 5.5. In contrast to the full effective density matrix **D**, which contains all of the method's GHF response, the intermediate density matrix $\bar{\mathbf{D}}$ isolates just the post-CCSD/PT gradient information that is unique to each electronic method. The $\bar{\mathbf{D}}$ contains both the contributions from the (bi-) variational parameters and the response contributions from all the non-variational parameters through their associated Lagrange multipliers—with the exception of the common **Z** Lagrange multiplier terms associated with the underlying reference CCSD/PT **T** amplitudes shared by all the methods. These $\bar{D}_\mu \equiv \partial F^{inh}/\partial \bar{h}_\mu$ (along with the associated three-body contributions of Table 9) determine the analytical gradient by the chain-rule **Z** Lagrange multiplier equations in Table 8 and by their subsequent chain-rule conversion to the GHF effective density matrix **D** in Table 15/Table 16. Note that upper and lower indices on $\bar{D}_\mu$ are exchanged relative to the differentiating $\bar{h}_\mu$, and F^{inh} is the STEOM functional (Table 4) without the CCSD/PT $\hat{Z}$ term. The q^n_m and q^e_f intermediates are defined in Tables 11 and 12, respectively.

$\bar{D}_\mu$	EE-STEOM-CCSD/PT	DIP-STEOM-CCSD/PT	DEA-STEOM-CCSD/PT
$\bar{D}^i_a$	0	0	0
$\bar{D}^{ij}_{ab}$	0	0	0
$\bar{D}^a_i$	$2d^{k'}_m \tilde{s}^{ma}_{k'i} + q^n_m \tilde{s}^{ma}_{ni} - 2M^k_m \tilde{s}^{ma}_{ki}$ $+ 2a^e_{c'} \tilde{s}^{c'a}_{ei} - q^e_f \tilde{s}^{fa}_{ei} + 2M^e_c \tilde{s}^{ca}_{ei}$ $- 2M^{ak}_{cm}\left(\left(2s^{mc}_{ik}\right)^{\text{singlet}}_{\text{only}} - s^{mc}_{ki}\right)$ $+ 2M^{ek}_{ci}\left(\left(2s^{ac}_{ek}\right)^{\text{singlet}}_{\text{only}} - s^{ca}_{ek}\right)$	$2d^{k'}_m \tilde{s}^{ma}_{k'i} + q^n_m \tilde{s}^{ma}_{ni}$ $- 2M^k_m \tilde{s}^{ma}_{ki} + 2M^{kl}_{im} s^{ma}_{lk}$	$2a^e_{c'} \tilde{s}^{c'a}_{ei} - q^e_f \tilde{s}^{fa}_{ei}$ $+ 2M^e_c \tilde{s}^{ca}_{ei} - 2M^{ae}_{cd} s^{dc}_{ei}$

Table 14. (*Continued*)

$\bar{D}_\mu$	EE-STEOM-CCSD/PT	DIP-STEOM-CCSD/PT	DEA-STEOM-CCSD/PT
$\bar{D}_{ij}^{ab}$	$\frac{1}{2}\left(1+P_{ij}^{ab}\right)(2-P_{ij})$ $\cdot\begin{pmatrix} -\tilde{d}_{mc}^{kl}t_{kl}^{ac}s_{ij}^{mb}-\tilde{a}_{cd}^{ek}t_{ik}^{cd}s_{ej}^{ab} \\ -2M_{cm}^{ek}\tilde{s}_{ei}^{ca}s_{kj}^{mb}+2M_{cm}^{ek}s_{ei}^{ca}s_{jk}^{mb} \\ -2M_{cm}^{ek}\left((2s_{ik}^{mc})_{\text{only}}^{\text{singlet}}-s_{ki}^{mc}\right)s_{ej}^{ab} \\ -2M_{cm}^{ek}\left((2s_{ek}^{ac})_{\text{only}}^{\text{singlet}}-s_{ek}^{ca}\right)s_{ij}^{mb} \end{pmatrix}$ $+\frac{1}{2}\left(1+P_{ij}^{ab}\right)\left((2)_{\text{only}}^{\text{singlet}}-P_{ij}\right)$ $\cdot\left(2M_{cm}^{ek}s_{ij}^{mc}s_{ek}^{ab}+2M_{cm}^{ek}s_{ei}^{bc}s_{jk}^{ma}\right)$	$\frac{1}{2}\left(1+P_{ij}^{ab}\right)(2-P_{ij})$ $\cdot\begin{pmatrix} -\tilde{d}_{mc}^{kl}t_{kl}^{ac}s_{ij}^{mb} \\ +2M_{mn}^{kl}s_{ki}^{ma}\left(s_{lj}^{nb}-s_{jl}^{nb}\right) \\ -2M_{mn}^{kl}s_{lk}^{na}s_{ij}^{mb} \end{pmatrix}$ $+M_{mn}^{kl}s_{ik}^{ma}s_{jl}^{nb}+M_{mn}^{kl}s_{ik}^{nb}s_{jl}^{ma}$	$\frac{1}{2}\left(1+P_{ij}^{ab}\right)(2-P_{ij})$ $\cdot\begin{pmatrix} -\tilde{a}_{cd}^{ek}t_{ik}^{cd}s_{ej}^{ab} \\ +2M_{cd}^{ef}s_{ei}^{ca}\left(s_{fj}^{db}-s_{fj}^{bd}\right) \\ -2M_{cd}^{ef}s_{fi}^{dc}s_{ej}^{ab} \end{pmatrix}$ $+M_{cd}^{ef}s_{ei}^{ac}s_{fj}^{bd}+M_{cd}^{ef}s_{ei}^{bd}s_{fj}^{ac}$
$\bar{D}_i^j$	$\left(2d_m^{j'}\delta_{jj'}+q_m^n\delta_{jn}\right)\delta_{im}$ $-\left(2d_m^{j'}\delta_{jj'}+q_m^n\delta_{jn}\right)s_{i'}^m\delta_{ii'}$ $-d_{mc}^{kj}\tilde{s}_{ki}^{mc}-d_{mc}^{jk}\tilde{s}_{ik}^{mc}-a_{dc}^{ej}\tilde{s}_{ei}^{dc}-2M_i^j$	$\left(2d_m^{j'}\delta_{jj'}+q_m^n\delta_{jn}\right)\delta_{im}$ $-\left(2d_m^{j'}\delta_{jj'}+q_m^n\delta_{jn}\right)s_{i'}^m\delta_{ii'}$ $-d_{mc}^{kj}\tilde{s}_{ki}^{mc}-d_{mc}^{jk}\tilde{s}_{ik}^{mc}-2M_i^j$	$-a_{dc}^{ej}\tilde{s}_{ei}^{dc}$
$\bar{D}_a^b$	$\left(2a_{a'}^e\delta_{aa'}-q_f^e\delta_{af}\right)\delta_{be}$ $+\left(2a_{a'}^e\delta_{aa'}-q_f^e\delta_{af}\right)s_e^{b'}\delta_{bb'}$ $+a_{ca}^{ek}\tilde{s}_{ek}^{cb}+a_{ac}^{ek}\tilde{s}_{ek}^{bc}+d_{ma}^{lk}\tilde{s}_{lk}^{mb}+2M_a^b$	$d_{ma}^{lk}\tilde{s}_{lk}^{mb}$	$\left(2a_{a'}^e\delta_{aa'}-q_f^e\delta_{af}\right)\delta_{be}$ $+\left(2a_{a'}^e\delta_{aa'}-q_f^e\delta_{af}\right)s_e^{b'}\delta_{bb'}$ $+a_{ca}^{ek}\tilde{s}_{ek}^{cb}+a_{ac}^{ek}\tilde{s}_{ek}^{bc}+2M_a^b$

Table 14. (*Continued*)

$\bar{D}_\mu$	EE-STEOM-CCSD/PT	DIP-STEOM-CCSD/PT	DEA-STEOM-CCSD/PT
$\bar{D}_{ji}^{ak}$	$-\big(2d_m^{k'}\delta_{kk'} + q_m^n\delta_{kn} - 2M_m^k\big)\tilde{s}_{ij}^{ma} - 2M_{ci}^{ek}\tilde{s}_{ej}^{ca}$ $+ 2M_{cm}^{ak}\big(\big(2s_{ji}^{mc}\big)_{\text{only}}^{\text{singlet}} - s_{ij}^{mc}\big)$ $- 2M_{cj}^{ek}\big(\big(2s_{ei}^{ac}\big)_{\text{only}}^{\text{singlet}} - s_{ei}^{ca}\big)$	$-\big(2d_m^{k'}\delta_{kk'} + q_m^n\delta_{kn} - 2M_m^k\big)\tilde{s}_{ij}^{ma}$ $- 2M_{jm}^{kl}s_{li}^{ma} - 2M_{jm}^{lk}s_{il}^{ma}$ $+ 2M_{im}^{kl}\tilde{s}_{lj}^{ma}$	0
$\bar{D}_{ia}^{bc}$	$\big(2a_{a'}^{e}\delta_{aa'} - q_f^e\delta_{af} + 2M_a^e\big)\tilde{s}_{ei}^{cb} - 2M_{am}^{ck}\tilde{s}_{ki}^{mb}$ $+ 2M_{ai}^{ek}\big(\big(2s_{ek}^{bc}\big)_{\text{only}}^{\text{singlet}} - s_{ek}^{cb}\big)$ $- 2M_{am}^{bk}\big(\big(2s_{ik}^{mc}\big)_{\text{only}}^{\text{singlet}} - s_{ki}^{mc}\big)$	0	$\big(2a_{a'}^{e}\delta_{aa'} - q_f^e\delta_{af} + 2M_a^e\big)\tilde{s}_{ei}^{cb}$ $- 2M_{ad}^{be}s_{ei}^{dc} - 2M_{ad}^{eb}s_{ei}^{cd}$ $+ 2M_{ad}^{ce}\tilde{s}_{ei}^{db}$
$\bar{D}_{ij}^{kl}$	$\frac{1}{2}\big(1 + P_{ij}^{kl}\big)\big(d_{mc}^{kl}\tilde{s}_{ij}^{mc}\big)$	$\frac{1}{2}\big(1 + P_{ij}^{kl}\big)\big(d_{mc}^{kl}\tilde{s}_{ij}^{mc}\big) + M_{ij}^{kl}$	0
$\bar{D}_{ab}^{cd}$	$\frac{1}{2}\big(1 + P_{ab}^{cd}\big)\big(a_{ab}^{ek}\tilde{s}_{ek}^{cd}\big)$	0	$\frac{1}{2}\big(1 + P_{ab}^{cd}\big)\big(a_{ab}^{ek}\tilde{s}_{ek}^{cd}\big) + M_{ab}^{cd}$
$\bar{D}_{ai}^{bj}$	$-d_{ma}^{kj}\tilde{s}_{ki}^{mb} - d_{ma}^{jk}\tilde{s}_{ik}^{mb}$ $- a_{ca}^{ej}\tilde{s}_{ei}^{cb} - a_{ac}^{ej}\tilde{s}_{ei}^{bc} - 2M_{ai}^{bj}$	$-d_{ma}^{kj}\tilde{s}_{ki}^{mb} - d_{ma}^{jk}\tilde{s}_{ik}^{mb}$	$-a_{ca}^{ej}\tilde{s}_{ei}^{cb} - a_{ac}^{ej}\tilde{s}_{ei}^{bc}$
$\bar{D}_{ai}^{jb}$	$\tilde{d}_{ma}^{kj}\tilde{s}_{ki}^{mb} + \tilde{a}_{ca}^{ej}\tilde{s}_{ei}^{cb} + \big(4M_{ai}^{bj}\big)_{\text{only}}^{\text{singlet}}$	$\tilde{d}_{ma}^{kj}\tilde{s}_{ki}^{mb}$	$\tilde{a}_{ca}^{ej}\tilde{s}_{ei}^{cb}$
$\bar{D}_{ai}^{kj}$	$\tilde{d}_{ma}^{jk}\delta_{im} - \tilde{d}_{ma}^{jk}s_{i'}^{m}\delta_{ii'}$	$\tilde{d}_{ma}^{jk}\delta_{im} - \tilde{d}_{ma}^{jk}s_{i'}^{m}\delta_{ii'}$	0
$\bar{D}_{ab}^{ic}$	$\tilde{a}_{ba}^{ei}\delta_{ce} + \tilde{a}_{ba}^{ei}s_{e}^{c'}\delta_{cc'}$	0	$\tilde{a}_{ba}^{ei}\delta_{ce} + \tilde{a}_{ba}^{ei}s_{e}^{c'}\delta_{cc'}$
$\bar{D}_0$	1	1	1

Table 15. *The conversion of the intermediate density matrix elements* $\bar{\mathbf{D}}$ *to the GHF effective density matrix elements* $\mathbf{D}$ *for CCSD-based methods*. See Sections 3.2, 3.3, and 5.7. These expressions are based solely on the definition of the $\bar{\mathbf{H}}$ amplitudes and are thus identical for all (ST)EOM-CCSD methods. The much-simplified expressions that remain for the PT-based methods are presented separately as Table 16. The effective density matrix $\mathbf{D}$ contains the all wavefunction response, but in a perturbation-independent formulation, and determines the analytical gradient according to the GHF relation $\partial E/\partial\chi = \sum_\mu D_\mu(\partial h_\mu/\partial\chi)$, expression (101). In these $D_\mu \equiv \partial F/\partial h_\mu$, the h_μ refer to the MO-based h_0, f_q^p, and V_{rs}^{pq} amplitudes of the Hamiltonian normal-ordered with respect to the reference determinant. The contributions to the analytical gradient from the reference determinant and the MO coefficient response are contained in the standard $\partial h_\mu/\partial\chi$ treatment, in which the GHF relation is converted to the AO basis for efficient evaluation (see Section 5.7.1). Below, $c_{ij}^{ab} \equiv t_{ij}^{ab} + t_i^a t_j^b$.

$$D_\mu = \sum_\nu \bar{D}_\nu \frac{\partial \bar{h}_\nu}{\partial h_\mu} + \frac{\partial}{\partial h_\mu}\langle \Phi_0|\hat{Z}\hat{\bar{H}}|\Phi_0\rangle$$

$$D_a^i = \bar{D}_a^i + 2z_a^i$$

$$D_{ab}^{ij} = \tilde{z}_{ab}^{ij}$$

$$\begin{aligned} D_i^a = {} & \bar{D}_i^a + \big(\bar{D}_c^k + 2z_c^k\big)\big(2t_{ik}^{ac} - t_{ik}^{ca}\big) + \bar{D}_{ci}^{kl} t_{lk}^{ac} - \bar{D}_{dc}^{ka} t_{ik}^{cd} \\ & + \big(\bar{D}_i^k - 2\tilde{z}_{cd}^{kl} t_{il}^{cd} - \big(\bar{D}_c^k + 2z_c^k\big)t_i^c\big)t_k^a - \big(\bar{D}_c^a + 2\tilde{z}_{cd}^{kl} t_{kl}^{ad}\big)t_i^c + 2t_i^a \end{aligned}$$

$$\begin{aligned} D_{ij}^{ab} = {} & \tfrac{1}{2}\big(1 + P_{ij}^{ab}\big)(2 - P_{ij}) \\ & \cdot \begin{pmatrix} z_{cd}^{kl} t_{jk}^{da} t_{il}^{cb} - \big(-z_{cd}^{kl} t_{jl}^{db} t_i^c - 2z_{cd}^{kl} t_{il}^{cb} t_j^d\big)t_k^a + z_{cd}^{kl} c_{ij}^{cd} c_{kl}^{ab} \\ \quad + \big(2\tilde{z}_{cd}^{kl} t_{ik}^{ac}\big)t_{jl}^{bd} - \big(2\tilde{z}_{cd}^{kl} t_{ik}^{ac} - z_{cd}^{kl} t_{ik}^{ca}\big)c_{jl}^{db} \\ \quad + \big(\bar{D}_i^k - 2\tilde{z}_{cd}^{kl} t_{il}^{cd} - \big(\bar{D}_c^k + 2z_c^k\big)t_i^c\big)t_{jk}^{ba} \\ \quad - \big(\bar{D}_c^a + 2\tilde{z}_{cd}^{kl} t_{kl}^{ad} + \big(\bar{D}_c^k + 2z_c^k\big)t_k^a\big)t_{ij}^{cb} \\ \quad + \begin{pmatrix} \bar{D}_i^a + \big(\bar{D}_c^k + 2z_c^k\big)\big(2t_{ik}^{ac} - t_{ik}^{ca}\big) + \bar{D}_{ci}^{kl} t_{lk}^{ac} - \bar{D}_{dc}^{ka} t_{ik}^{cd} \\ \quad + \big(\bar{D}_i^k - 2\tilde{z}_{cd}^{kl} t_{il}^{cd} - \big(\bar{D}_c^k + 2z_c^k\big)t_i^c\big)t_k^a - \big(\bar{D}_c^a + 2\tilde{z}_{cd}^{kl} t_{kl}^{ad}\big)t_i^c \end{pmatrix} t_j^b \\ \quad + \big(\bar{D}_{cj}^{kb} + \bar{D}_{cj}^{kl} t_l^b - \bar{D}_{cd}^{kb} t_j^d\big)t_{ik}^{ac} + c_{ij}^{ab} \end{pmatrix} \\ & + \tfrac{1}{2}\big(1 + P_{ij}^{ab}\big) \begin{pmatrix} \bar{D}_{ij}^{ab} + \bar{D}_{ij}^{kl} c_{kl}^{ab} + \bar{D}_{cd}^{ab} c_{ij}^{cd} + \big(\bar{D}_{ji}^{bk} - \bar{D}_{cj}^{kl} c_{il}^{cb} + \bar{D}_{cd}^{kb} c_{ij}^{cd}\big)t_k^a \\ \quad - \bar{D}_{cj}^{kl} t_i^c t_{kl}^{ab} + \bar{D}_{cd}^{kb} t_i^c t_{jk}^{da} - \big(\bar{D}_{cj}^{kl} t_l^b - \bar{D}_{cd}^{kb} t_j^d\big)t_{ik}^{ca} \\ \quad - \bar{D}_{cj}^{kb} c_{ik}^{ca} - \bar{D}_{cj}^{ak} c_{ik}^{cb} - \bar{D}_{jc}^{ba} t_i^c \end{pmatrix} \end{aligned}$$

$$D_i^j = \bar{D}_i^j - 2\tilde{z}_{cd}^{jk} t_{ik}^{cd} - \big(\bar{D}_c^j + 2z_c^j\big)t_i^c$$

$$D_a^b = \bar{D}_a^b + 2\tilde{z}_{ac}^{kl} t_{kl}^{bc} + \big(\bar{D}_a^k + 2z_a^k\big)t_k^b$$

Table 15. (*Continued*)

$D_\mu = \sum_\nu \bar{D}_\nu \frac{\partial \bar{h}_\nu}{\partial h_\mu} + \frac{\partial}{\partial h_\mu} \langle \Phi_0 \vert \hat{Z} \hat{\bar{H}} \vert \Phi_0 \rangle$
$D^{ak}_{ji} = \bar{D}^{ak}_{ji} - \bar{D}^{lk}_{ci} c^{ca}_{jl} - \bar{D}^{kl}_{cj} c^{ca}_{il} + \bar{D}^{ka}_{cd} c^{cd}_{ij} - \bar{D}^{ak}_{ci} t^c_j - \bar{D}^{ka}_{cj} t^c_i + 2\big(\bar{D}^{kl}_{ij} + \tilde{z}^{kl}_{cd} c^{cd}_{ij}\big) t^a_l$ $+ (2 - P_{ij}) \begin{pmatrix} \big(\bar{D}^k_i - 2\tilde{z}^{kl}_{cd} t^{cd}_{il} - \big(\bar{D}^k_c + 2z^k_c\big) t^c_i\big) t^a_j - \big(\bar{D}^k_c + 2z^k_c\big) t^{ca}_{ij} \\ + \bar{D}^{lk}_{ci} t^{ac}_{jl} + \big(-2\tilde{z}^{kl}_{cd} t^{ad}_{jl} + 2z^{kl}_{cd} t^{da}_{jl}\big) t^c_i + \big(2z^{kl}_{cd} t^{ca}_{il}\big) t^d_j \end{pmatrix}$
$D^{bc}_{ia} = \bar{D}^{bc}_{ia} - \bar{D}^{kc}_{da} c^{db}_{ik} - \bar{D}^{kb}_{ad} c^{dc}_{ik} + \bar{D}^{kl}_{ai} c^{bc}_{lk} + \bar{D}^{ck}_{ai} t^b_k + \bar{D}^{kb}_{ai} t^c_k - 2\big(\bar{D}^{cb}_{ad} + \tilde{z}^{kl}_{ad} c^{bc}_{lk}\big) t^d_i$ $+ (2 - P_{bc}) \begin{pmatrix} \big(\bar{D}^c_a + 2\tilde{z}^{kl}_{ad} t^{cd}_{kl} + \big(\bar{D}^k_a + 2z^k_a\big) t^c_k\big) t^b_i + \big(\bar{D}^k_a + 2z^k_a\big) t^{bc}_{ik} \\ + \bar{D}^{kc}_{da} t^{bd}_{ik} - \big(-2\tilde{z}^{kl}_{ad} t^{bd}_{il} + 2z^{kl}_{ad} t^{db}_{il}\big) t^c_k - \big(2z^{kl}_{ad} t^{dc}_{ik}\big) t^b_l \end{pmatrix}$
$D^{kl}_{ij} = \bar{D}^{kl}_{ij} + \tilde{z}^{kl}_{cd} c^{cd}_{ij} + \frac{1}{2}\big(1 + P^{kl}_{ij}\big)\big(-\bar{D}^{kl}_{cj} t^c_i\big)$
$D^{cd}_{ab} = \bar{D}^{cd}_{ab} + \tilde{z}^{kl}_{ab} c^{cd}_{kl} + \frac{1}{2}\big(1 + P^{cd}_{ab}\big)\big(\bar{D}^{kd}_{ab} t^c_k\big)$
$D^{bj}_{ai} = \bar{D}^{bj}_{ai} + \bar{D}^{kj}_{ai} t^b_k - \bar{D}^{jb}_{ca} t^c_i - 2\tilde{z}^{jk}_{ca} c^{cb}_{ik} - \big(\big(\bar{D}^j_a + 2z^j_a\big) t^b_i + 2\tilde{z}^{jk}_{ac} t^{bc}_{ik}\big)$
$D^{jb}_{ai} = \bar{D}^{jb}_{ai} + \bar{D}^{jk}_{ai} t^b_k - \bar{D}^{jb}_{ac} t^c_i - 2\tilde{z}^{jk}_{ac} c^{cb}_{ik} + 2\big(\big(\bar{D}^j_a + 2z^j_a\big) t^b_i + 2\tilde{z}^{jk}_{ac} t^{bc}_{ik}\big)$
$D^{kj}_{ai} = \bar{D}^{kj}_{ai} - 2\tilde{z}^{jk}_{ca} t^c_i$
$D^{ic}_{ab} = \bar{D}^{ic}_{ab} + 2\tilde{z}^{ik}_{ab} t^c_k$
$D_0 = \bar{D}_0 = 1$

Table 16. *The conversion of the intermediate density matrix elements* $\bar{\mathbf{D}}$ *to the GHF effective density matrix elements* $\mathbf{D}$ *for PT-based methods*. See Sections 3.2, 3.3, and 5.7. These expressions are based solely on the definition of the $\bar{\mathbf{H}}$ amplitudes and are thus identical for all (ST)EOM-PT methods. The simplification of the PT-based $\bar{\mathbf{H}}$ expressions leads to the following eliminations from the CCSD-based $\bar{\mathbf{D}}$-to-$\mathbf{D}$ expressions of Table 15 (see Section 5.7): all one-body $\mathbf{T_1}$ and $\mathbf{Z_1}$ terms are not present, all $\mathbf{Z_2}$ terms in the two-body $\mathbf{D}$ except in D_{ab}^{ij} are not present, and all $\bar{D}_a^i = 0$. The perturbation-independent effective density matrix $\mathbf{D}$ contains all the wavefunction response and determines the analytical gradient according to the GHF relation, $\partial E/\partial\chi = \sum_\mu D_\mu(\partial h_\mu/\partial\chi)$, expression (101).

$D_\mu = \sum_\nu \bar{D}_\nu \dfrac{\partial \bar{h}_\nu}{\partial h_\mu} + \dfrac{\partial}{\partial h_\mu}\langle\Phi_0\vert\hat{Z}_2\big(\big[\hat{H}^{(0)}, \hat{T}_2^{(1)}\big] + \hat{V}\big)\vert\Phi_0\rangle$
$D_a^i = \bar{D}_a^i = 0$
$D_{ab}^{ij} = \tilde{z}_{ab}^{ij}$
$D_i^a = \bar{D}_i^a + \bar{D}_{ci}^{kl} t_{lk}^{ac} - \bar{D}_{dc}^{ka} t_{ik}^{cd}$
$D_{ij}^{ab} = \frac{1}{2}\big(1 + P_{ij}^{ab}\big)(2 - P_{ij})\big(\bar{D}_i^k t_{jk}^{ba} - \bar{D}_c^a t_{ij}^{cb} + \bar{D}_{cj}^{kb} t_{ik}^{ac} + t_{ij}^{ab}\big)$ $+ \frac{1}{2}\big(1 + P_{ij}^{ab}\big)\big(\bar{D}_{ij}^{ab} + \bar{D}_{ij}^{kl} t_{kl}^{ab} + \bar{D}_{cd}^{ab} t_{ij}^{cd} - \bar{D}_{cj}^{kb} t_{ik}^{ca} - \bar{D}_{cj}^{ak} t_{ik}^{cb}\big)$
$D_i^j = \bar{D}_i^j - 2\tilde{z}_{cd}^{jk} t_{ik}^{cd}$
$D_a^b = \bar{D}_a^b + 2\tilde{z}_{ac}^{kl} t_{kl}^{bc}$
$D_{ji}^{ak} = \bar{D}_{ji}^{ak} - \bar{D}_{ci}^{lk} t_{jl}^{ca} - \bar{D}_{cj}^{kl} t_{il}^{ca} + \bar{D}_{cd}^{ka} t_{ij}^{cd} + (2 - P_{ij})\big(\bar{D}_{ci}^{lk} t_{jl}^{ac}\big)$
$D_{ia}^{bc} = \bar{D}_{ia}^{bc} - \bar{D}_{da}^{kc} t_{ik}^{db} - \bar{D}_{ad}^{kb} t_{ik}^{dc} + \bar{D}_{ai}^{kl} t_{lk}^{bc} + (2 - P_{bc})\big(\bar{D}_{da}^{kc} t_{ik}^{bd}\big)$
$D_{ij}^{kl} = \bar{D}_{ij}^{kl};$ $\quad D_{ab}^{cd} = \bar{D}_{ab}^{cd};$ $\quad D_{ai}^{bj} = \bar{D}_{ai}^{bj};$ $\quad D_{ai}^{jb} = \bar{D}_{ai}^{jb};$
$D_{ai}^{kj} = \bar{D}_{ai}^{kj};$ $\quad D_{ab}^{ic} = \bar{D}_{ab}^{ic};$ $\quad D_0 = \bar{D}_0 = 1$

6. SUMMARY

For characterizing the manifold of singly excited states in closed-shell species and many classes of open-shell systems, the highly accurate and computationally efficient EE-, DIP-, and DEA-STEOM-CCSD/PT methods are well suited; in this work, we derived for these methods the explicit algebraic spatial-orbital equations for the analytical first derivatives of their electronic energies. The analytical gradient expressions were formulated through Lagrange's method of undetermined multipliers, establishing a systematic derivation procedure in which an energy functional for each method is differentiated individually with respect to each of its parameters. Rather than algebraic or diagrammatic expansion of cumbersome *abstract derivative* expressions, differentiations were performed directly here on the *algebraic energy* expressions themselves, using our newly developed *SMART* package of automated symbolic algebra routines. The Lagrange multiplier formulation and *SMART* manipulation toolkit provide a uniform framework in which to derive the detailed algebraic gradient equations in a standardized, direct, and automated manner.

As a stepping stone towards implementing analytical STEOM-CCSD/PT gradients, the explicit algebraic expressions for closed-shell-reference EE-, IP-, and EA-EOM-CCSD/PT analytical gradients were also derived. The derivative equations for these dozen considered methods were all expressed compactly here in an $\bar{\mathbf{H}}$ chain-rule formulation, isolating the unique post-CCSD/PT information of each electronic method in an intermediate density matrix $\bar{\mathbf{D}}$. The existing EOM-CCSD/PT gradient code in our local ACES II program suite was revised to the present chain-rule/intermediate-density formulation, and the additional Lagrange multiplier equations needed to construct the STEOM-CCSD/PT $\bar{\mathbf{D}}$ were then implemented. Although the computational cost of a STEOM-CCSD/PT analytical first derivative is no better than that of EOM-CCSD/PT, the main advantages of the STEOM methods reside in the types of multi-reference states that can be treated accurately and in the efficiency with which a large number of states can be calculated. This efficiency also makes practical a state-tracking algorithm based on the overlap with the set of nearby states in the next step of an optimization.

In the Lagrange multiplier procedure for deriving the analytical gradient expressions, an energy functional is first constructed from the defining equations of the electronic structure method; in addition to the energy expression for an individual electronic state, all the supplementary constraint equations that determine the non-variational energy parameters are incorporated systematically, with each set of supplementary equations multiplied by (so-far) undetermined Lagrange multipliers. The equations that determine the Lagrange multipliers are then obtained by defining the functional to be stationary with respect to the associated non-variational energy parameters. With the solution of these Lagrange multiplier equations, the energy functional becomes fully variational with respect to all of its parameters, and the generalized Hellmann–Feynman theorem applies. The first derivative of the energy can then be written as the trace of the perturbation derivative of the Hamiltonian with an effective, relaxed, density matrix $\mathbf{D}$. The effective density matrix is calculated only *once* for the state and applies to *all* perturbations and degrees of freedom. The response of the non-variational energy parameters is included, not by expensive calculation of their perturbation derivatives, but by solution of the *perturbation-independent* equations for their associated Lagrange multipliers.

The computational cost of a STEOM-CCSD/PT analytical gradient is thereby made not to scale deleteriously with the number of degrees of freedom, and the cost is comparable to

that of the single-point energy calculation. Chain-rule differentiations through the common transformed Hamiltonian $\bar{\mathbf{H}}$ amplitudes exploit the parts of the gradient that are the same for all CCSD/PT-based methods, and the unified modular structure allows reuse of many sections of implemented computer code. In particular, (nearly) all of the (ST)EOM-variant dependence is isolated in the intermediate density matrix $\bar{\mathbf{D}}$, and the remainder of the gradient calculation then proceeds essentially identically to that of a ground-state CC/MBPT gradient.

The detailed algebraic equations for the Lagrange multipliers and for the effective and intermediate density matrices were derived from the input algebraic energy functionals through a straight symbolic algebraic treatment using *SMART*. The *SMART* package was developed in the *Mathematica* programming language, and key features and examples were considered here. More discussion of its central canonical-ordering function and its function for extracting external-index permutational symmetry can be found in reference [166]. The availability of such an automated manipulation program greatly facilitates the derivation process, eliminating the need to treat the detailed algebraic derivative expressions or the associated diagrams (and even the *abstract* derivative expressions themselves) tediously by hand. The general *SMART* toolkit can be applied to manipulate a variety of tensor algebraic expressions directly. Besides the gradient work described here, the package was also employed in exploring the cumulant expansion of the Contracted Schrödinger Equation [167] and in other unpublished work.

With an efficient implementation of the analytical first derivative, the STEOM-CCSD/PT methods should begin to find wider application in the characterization of excited-state surfaces and the prediction of electronic spectra for a variety of difficult systems. The first extended example of analytical STEOM gradients has already been presented [15] in the application of DIP-STEOM-CCSD to the photoelectron spectrum (the cation states) of the somewhat notorious symmetry-breaking NO_3 radical. The analytical gradient for the DEA-STEOM-CCSD method has also recently been applied in the difficult $(NO)_2$ dimer system [17].

ACKNOWLEDGEMENTS

The authors would like to gratefully acknowledge Steven R. Gwaltney, who, together with M.N., first encoded in ACES II the preliminary EOM-CCSD intermediate density matrix $\bar{\mathbf{D}}$ formulation and $\bar{\mathbf{D}}$ to $\mathbf{D}$ conversion expressions as a first step towards STEOM gradients. M.W. gratefully acknowledges support from the National Science Foundation Graduate Research Fellowship Program. This work was supported partly by a Discovery Grant from the Natural Sciences and Engineering Research Council of Canada (NSERC).

REFERENCES

[1] M. Nooijen, R.J. Bartlett, *J. Chem. Phys.* **106** (1997) 6441.
[2] M. Nooijen, R.J. Bartlett, *J. Chem. Phys.* **106** (1997) 6449.
[3] M. Nooijen, R.J. Bartlett, *J. Chem. Phys.* **107** (1997) 6812.
[4] A.A. Korkin, M. Nooijen, R.J. Bartlett, K.O. Christe, *J. Phys. Chem. A* **102** (1998) 1837.
[5] S.R. Gwaltney, R.J. Bartlett, *J. Chem. Phys.* **108** (1998) 6790.
[6] M. Nooijen, *Spectrochim. Acta A: Molec. Biomolec. Spectr.* **55** (1999) 539.

[7] A.B.J. Parusel, G. Kohler, M. Nooijen, *J. Phys. Chem. A* **103** (1999) 4056.
[8] D.S. Peterka, M. Ahmed, A.G. Suits, K.J. Wilson, A. Korkin, M. Nooijen, R.J. Bartlett, *J. Chem. Phys.* **110** (1999) 6095.
[9] D.S. Peterka, M. Ahmed, A.G. Suits, K.J. Wilson, A. Korkin, M. Nooijen, R.J. Bartlett, *J. Chem. Phys.* **111** (1999) 5279.
[10] S.R. Gwaltney, R.J. Bartlett, M. Nooijen, *J. Chem. Phys.* **111** (1999) 58.
[11] M. Nooijen, *J. Chem. Phys.* **111** (1999) 10815.
[12] M. Nooijen, V. Lotrich, *J. Chem. Phys.* **113** (2000) 494.
[13] M. Nooijen, *J. Phys. Chem. A* **104** (2000) 4553.
[14] S. Fau, R.J. Bartlett, *J. Phys. Chem. A* **105** (2001) 4096.
[15] M. Wladyslawski, M. Nooijen, in: *Low-Lying Potential Energy Surfaces*, in: *ACS Symposium Series*, vol. 828, Amer. Chemical Soc., Washington, 2002, pp. 65–92.
[16] A. Beste, R.J. Bartlett, *Chem. Phys. Lett.* **366** (2002) 100.
[17] M. Tobita, S.A. Perera, M. Musiał, R.J. Bartlett, M. Nooijen, J.S. Lee, *J. Chem. Phys.* **119** (2003) 10713.
[18] M. Nooijen, *Int. J. Quantum Chem.* **95** (2003) 768.
[19] J. Neugebauer, E.J. Baerends, M. Nooijen, *J. Chem. Phys.* **121** (2004) 6155.
[20] A. Hazra, H.H. Chang, M. Nooijen, *J. Chem. Phys.* **121** (2004) 2125.
[21] L.Z. Stolarczyk, H.J. Monkhorst, *Phys. Rev. A* **32** (1985) 725.
[22] L.Z. Stolarczyk, H.J. Monkhorst, *Phys. Rev. A* **32** (1985) 743.
[23] L.Z. Stolarczyk, H.J. Monkhorst, *Phys. Rev. A* **37** (1988) 1908.
[24] L.Z. Stolarczyk, H.J. Monkhorst, *Phys. Rev. A* **37** (1988) 1926.
[25] M. Nooijen, *J. Chem. Phys.* **104** (1996) 2638.
[26] I. Lindgren, *Int. J. Quantum Chem. Symp.* **12** (1978) 33.
[27] I. Lindgren, J. Morrison, *Atomic Many-Body Theory*, Springer, Berlin, 1982.
[28] M.A. Haque, D. Mukherjee, *J. Chem. Phys.* **80** (1984) 5058.
[29] D. Mukherjee, S. Pal, *Adv. Quantum Chem.* **20** (1989) 291.
[30] J.P. Malrieu, P. Durand, J.P. Daudey, *J. Phys. A: Math. Gen.* **18** (1985) 809.
[31] L. Meissner, M. Nooijen, *J. Chem. Phys.* **102** (1995) 9604.
[32] H. Sekino, R.J. Bartlett, *Int. J. Quantum Chem. Symp.* **18** (1984) 255.
[33] J. Geertsen, M. Rittby, R.J. Bartlett, *Chem. Phys. Lett.* **164** (1989) 57.
[34] J.F. Stanton, R.J. Bartlett, *J. Chem. Phys.* **98** (1993) 7029.
[35] D.C. Comeau, R.J. Bartlett, *Chem. Phys. Lett.* **207** (1993) 414.
[36] M. Nooijen, R.J. Bartlett, *J. Chem. Phys.* **102** (1995) 3629.
[37] J.F. Stanton, *J. Chem. Phys.* **99** (1993) 8840.
[38] J.F. Stanton, J. Gauss, *J. Chem. Phys.* **100** (1994) 4695.
[39] J.F. Stanton, J. Gauss, *J. Chem. Phys.* **101** (1994) 8938.
[40] J.F. Stanton, J. Gauss, *Theor. Chim. Acta* **91** (1995) 267.
[41] J.F. Stanton, *J. Chem. Phys.* **101** (1994) 8928.
[42] J.F. Stanton, J. Gauss, *J. Chem. Phys.* **103** (1995) 1064.
[43] G.D. Purvis, R.J. Bartlett, *J. Chem. Phys.* **76** (1982) 1910.
[44] G.E. Scuseria, A.C. Scheiner, T.J. Lee, J.E. Rice, H.F. Schaefer, *J. Chem. Phys.* **86** (1987) 2881.
[45] R.J. Bartlett, in: D.R. Yarkony (Ed.), *Modern Electronic Structure Theory, Part II*, in: *Advanced Series in Physical Chemistry*, vol. 2, World Scientific, Singapore, 1995, pp. 1047–1131.
[46] T.D. Crawford, H.F. Schaefer, *Rev. Comp. Chem.* **14** (2000) 33.
[47] H.J. Monkhorst, *Int. J. Quantum Chem. Symp.* **11** (1977) 421.
[48] D. Mukherjee, P.K. Mukherjee, *Chem. Phys.* **39** (1979) 325.
[49] H. Koch, P. Jørgensen, *J. Chem. Phys.* **93** (1990) 3333.
[50] H. Koch, H.J.Aa. Jensen, P. Jørgensen, T. Helgaker, *J. Chem. Phys.* **93** (1990) 3345.
[51] M. Nooijen, J.G. Snijders, *Int. J. Quantum Chem. Symp.* **26** (1992) 55.
[52] M. Nooijen, J.G. Snijders, *Int. J. Quantum Chem.* **48** (1993) 15.
[53] M. Nooijen, J.G. Snijders, *J. Chem. Phys.* **102** (1995) 1681.
[54] H. Nakatsuji, *Acta Chimica Hungarica: Models in Chemistry* **129** (1992) 719.
[55] M. Ehara, M. Ishida, K. Toyota, H. Nakatsuji, in: K.D. Sen (Ed.), *Reviews of Modern Quantum Chemistry*, World Scientific, Singapore, 2002, pp. 293–319.
[56] T. Nakajima, H. Nakatsuji, *Chem. Phys.* **242** (1999) 177.
[57] M. Ishida, K. Toyota, M. Ehara, M.J. Frisch, H. Nakatsuji, *J. Chem. Phys.* **120** (2004) 2593.

[58] J.A. Pople, M. Head-Gordon, K. Raghavachari, *J. Chem. Phys.* **87** (1987) 5968.
[59] R.J. Rico, T.J. Lee, M. Head-Gordon, *Chem. Phys. Lett.* **218** (1994) 139.
[60] M. Head-Gordon, R.J. Rico, M. Oumi, T.J. Lee, *Chem. Phys. Lett.* **219** (1994) 21.
[61] M. Head-Gordon, M. Oumi, D. Maurice, *Mol. Phys.* **96** (1999) 593.
[62] J.F. Stanton, J. Gauss, N. Ishikawa, M. Head-Gordon, *J. Chem. Phys.* **103** (1995) 4160.
[63] S. Hirata, M. Nooijen, R.J. Bartlett, *Chem. Phys. Lett.* **326** (2000) 255.
[64] S. Hirata, M. Nooijen, R.J. Bartlett, *Chem. Phys. Lett.* **328** (2000) 459.
[65] L. Meissner, R.J. Bartlett, *J. Chem. Phys.* **102** (1995) 7490.
[66] M. Nooijen, K.R. Shamasundar, D. Mukherjee, *Mol. Phys.* **103** (2005) 2277.
[67] J.F. Stanton, *J. Chem. Phys.* **115** (2001) 10382.
[68] A. Ye, Z. Shuai, J.L. Brédas, *Phys. Rev. B* **6504** (2002), art. no. 045208.
[69] S.A. Perera, R.J. Bartlett, *Magn. Reson. Chem.* **39** (2001) S183.
[70] A.I. Krylov, *Chem. Phys. Lett.* **338** (2001) 375.
[71] S.V. Levchenko, A.I. Krylov, *J. Chem. Phys.* **120** (2004) 175.
[72] A.D. Yau, S.A. Perera, R.J. Bartlett, *Mol. Phys.* **100** (2002) 835.
[73] K.W. Sattelmeyer, H.F. Schaefer, *J. Chem. Phys.* **117** (2002) 7914.
[74] M. Nooijen, R.J. Bartlett, *J. Chem. Phys.* **102** (1995) 6735.
[75] K.K. Baeck, R.J. Bartlett, *J. Chem. Phys.* **109** (1998) 1334.
[76] J.D. Watts, R.J. Bartlett, *J. Chem. Phys.* **101** (1994) 3073.
[77] J.D. Watts, S.R. Gwaltney, R.J. Bartlett, *J. Chem. Phys.* **105** (1996) 6979.
[78] O. Christiansen, H. Koch, P. Jørgensen, *J. Chem. Phys.* **103** (1995) 7429.
[79] O. Christiansen, H. Koch, P. Jørgensen, J. Olsen, *Chem. Phys. Lett.* **256** (1996) 185.
[80] J.D. Watts, R.J. Bartlett, *Chem. Phys. Lett.* **258** (1996) 581.
[81] K. Kowalski, P. Piecuch, *J. Chem. Phys.* **115** (2001) 643.
[82] S.A. Kucharski, M. Włoch, M. Musiał, R.J. Bartlett, *J. Chem. Phys.* **115** (2001) 8263.
[83] M. Musiał, S.A. Kucharski, R.J. Bartlett, *J. Chem. Phys.* **118** (2003) 1128.
[84] J.F. Stanton, J. Gauss, J.D. Watts, M. Nooijen, N. Oliphant, S.A. Perera, P.G. Szalay, W.J. Lauderdale, S.A. Kucharski, S.R. Gwaltney, S. Beck, A. Balková, D.E. Bernholdt, K.K. Baeck, P. Rozyczko, H. Sekino, C. Huber, R.J. Bartlett, ACES II is a program product of the Quantum Theory Project, University of Florida, Integral packages included are VMOL (J. Almlöf, P.R. Taylor); VPROPS (P.R. Taylor); ABACUS (T. Helgaker, H.J.Aa. Jensen, P. Jørgensen, J. Olsen, P.R. Taylor).
[85] P. Pulay, *Mol. Phys.* **17** (1969) 197.
[86] M.A. Robb, M. Garavelli, M. Olivucci, F. Bernardi, *Rev. Comp. Chem.* **15** (2000) 87.
[87] D.G. Truhlar, in: D. Heidrich (Ed.), *The Reaction Path in Chemistry: Current Approaches and Perspectives*, in: *Understanding Chemical Reactivity*, vol. 16, Kluwer Academic, Dordrecht, The Netherlands, 1995, pp. 229–255.
[88] M.D. Hack, A.M. Wensmann, D.G. Truhlar, M. Ben-Nun, T.J. Martinez, *J. Chem. Phys.* **115** (2001) 1172.
[89] M. Ben-Nun, T.J. Martinez, *Adv. Chem. Phys.* **121** (2002) 439.
[90] P.-O. Löwdin, *Adv. Chem. Phys.* **2** (1959) 207.
[91] R.J. Bartlett, S.A. Kucharski, J. Noga, J.D. Watts, G.W. Trucks, in: U. Kaldor (Ed.), *Many-Body Methods in Quantum Chemistry*, in: *Lecture Notes in Chemistry*, vol. 52, Springer, Berlin, 1989, pp. 125–149.
[92] P.G. Szalay, M. Nooijen, R.J. Bartlett, *J. Chem. Phys.* **103** (1995) 281.
[93] H. Hellmann, *Einführung in die Quantenchemie*, Deuticke, Leipzig, 1937, *Introduction to Quantum Chemistry*, in German.
[94] R.P. Feynman, *Phys. Rev.* **56** (1939) 340.
[95] V.I. Pupyshev, *Russ. J. Phys. Chem.* **74** (2000) S267.
[96] M. Ernzerhof, C.M. Marian, S.D. Peyerimhoff, *Int. J. Quantum Chem.* **43** (1992) 659.
[97] J. Noga, M. Urban, *Theor. Chim. Acta* **73** (1988) 291.
[98] M. Urban, G.H.F. Diercksen, A.J. Sadlej, J. Noga, *Theor. Chim. Acta* **77** (1990) 29.
[99] M. Medved, M. Urban, J. Noga, *Theor. Chem. Acc.* **98** (1997) 75.
[100] J.E. Rice, R.D. Amos, *Chem. Phys. Lett.* **122** (1985) 585.
[101] J.E. Rice, R.D. Amos, N.C. Handy, T.J. Lee, H.F. Schaefer, *J. Chem. Phys.* **85** (1986) 963.
[102] R. Shepard, *Int. J. Quantum Chem.* **31** (1987) 33.
[103] R.J. Bartlett, in: P. Jørgensen, J. Simons (Eds.), *Geometrical Derivatives of Energy Surfaces and Molecular Properties*, in: *NATO ASI Series C: Mathematical and Physical Sciences*, vol. 166, Reidel, Dordrecht, The Netherlands, 1986, pp. 35–61.

[104] G. Fitzgerald, R.J. Harrison, R.J. Bartlett, *J. Chem. Phys.* **85** (1986) 5143.
[105] A. Dalgarno, A.L. Stewart, *Proc. R. Soc. London Ser. A* **247** (1958) 245.
[106] N.C. Handy, H.F. Schaefer, *J. Chem. Phys.* **81** (1984) 5031.
[107] L. Adamowicz, W.D. Laidig, R.J. Bartlett, *Int. J. Quantum Chem. Symp.* **18** (1984) 245.
[108] A.C. Scheiner, G.E. Scuseria, J.E. Rice, T.J. Lee, H.F. Schaefer, *J. Chem. Phys.* **87** (1987) 5361.
[109] E.A. Salter, G.W. Trucks, R.J. Bartlett, *J. Chem. Phys.* **90** (1989) 1752.
[110] J. Gauss, J.F. Stanton, R.J. Bartlett, *J. Chem. Phys.* **95** (1991) 2623.
[111] P.G. Szalay, *Int. J. Quantum Chem.* **55** (1995) 151.
[112] P. Pulay, *J. Chem. Phys.* **78** (1983) 5043.
[113] T. Helgaker, P. Jørgensen, *Theor. Chim. Acta* **75** (1989) 111.
[114] P. Jørgensen, T. Helgaker, *J. Chem. Phys.* **89** (1988) 1560.
[115] T. Helgaker, P. Jørgensen, in: S. Wilson, G.H.F. Diercksen (Eds.), *Methods in Computational Molecular Physics*, in: *NATO ASI Series B: Physics*, vol. 293, Plenum, New York, 1992, p. 353.
[116] A. Szabo, N.S. Ostlund, *Modern Quantum Chemistry: Introduction to Advanced Electronic Structure Theory*, McGraw-Hill, Mineola, NY, 1989.
[117] T. Helgaker, P. Jørgensen, *Adv. Quantum Chem.* **19** (1988) 183.
[118] H. Koch, H.J.Aa. Jensen, P. Jørgensen, T. Helgaker, G.E. Scuseria, H.F. Schaefer, *J. Chem. Phys.* **92** (1990) 4924.
[119] J. Gauss, J.F. Stanton, *J. Chem. Phys.* **116** (2002) 1773.
[120] K. Hald, A. Halkier, P. Jørgensen, S. Coriani, C. Hättig, T. Helgaker, *J. Chem. Phys.* **118** (2003) 2985.
[121] S.R. Gwaltney, R.J. Bartlett, *J. Chem. Phys.* **110** (1999) 62.
[122] P. Jørgensen, J. Simons, *Second Quantization-Based Methods in Quantum Chemistry*, Academic Press, New York, 1981.
[123] T. Helgaker, P. Jørgensen, J. Olsen, *Modern Electronic-Structure Theory*, Wiley, New York, 2000.
[124] J. Paldus, J. Čížek, *Adv. Quantum Chem.* **9** (1975) 105.
[125] S.A. Kucharski, R.J. Bartlett, *Adv. Quantum Chem.* **18** (1986) 281.
[126] F.E. Harris, H.J. Monkhorst, D.L. Freeman, *Algebraic and Diagrammatic Methods in Many-Fermion Theory*, Oxford Univ. Press, New York, 1992.
[127] Wolfram Research Inc., *Mathematica, Version 3.0*, Wolfram Research Inc., Champaign, IL, 1996.
[128] M. Kállay, P.R. Surján, *J. Chem. Phys.* **115** (2001) 2945.
[129] M. Kállay, P.G. Szalay, P.R. Surján, *J. Chem. Phys.* **117** (2002) 980.
[130] M. Kállay, J. Gauss, P.G. Szalay, *J. Chem. Phys.* **119** (2003) 2991.
[131] M. Kállay, J. Gauss, *J. Chem. Phys.* **120** (2004) 6841.
[132] M. Nooijen, V. Lotrich, *J. Mol. Struct. (Theochem)* **547** (2001) 253.
[133] M. Nooijen, *Int. J. Mol. Sci.* **3** (2002) 656.
[134] S. Hirata, *J. Phys. Chem. A* **107** (2003) 9887.
[135] S. Hirata, *J. Chem. Phys.* **121** (2004) 51.
[136] S. Hirata, P.D. Fan, A.A. Auer, M. Nooijen, P. Piecuch, *J. Chem. Phys.* **121** (2004) 12197.
[137] G. Baumgartner, D.E. Bernholdt, D. Cociorva, R. Harrison, S. Hirata, C.C. Lam, M. Nooijen, R. Pitzer, J. Ramanujam, P. Sadayappan, in: *Proceedings of Supercomputing 2002*, Baltimore, MD, 2002.
[138] G. Baumgartner, D.E. Bernholdt, D. Cociorva, R. Harrison, C.C. Lam, M. Nooijen, J. Ramanujam, P. Sadayappan, in: *Proceedings of the Workshop on Performance Optimization for High-Level Languages and Libraries* (*POHLL-02*), New York, NY, 2002.
[139] D. Cociorva, J. Wilkins, G. Baumgartner, P. Sadayappan, J. Ramanujam, M. Nooijen, D. Bernholdt, R. Harrison, in: *High Performance Computing—HiPC 2001*, 8th International Conference, Hyderabad, India, December 17–20, 2001, Proceedings, in: *Lecture Notes in Computer Science*, vol. 2228, Springer, Heidelberg, 2001, pp. 237–248.
[140] D. Cociorva, G. Baumgartner, C.C. Lam, P. Sadayappan, J. Ramanujam, M. Nooijen, D.E. Bernholdt, R. Harrison, *ACM Sigplan Not.* **37** (2002) 177.
[141] A.A. Auer, G. Baumgartner, D.E. Bernholdt, A. Bibireata, V. Choppella, D. Cociorva, X.Y. Gao, R. Harrison, S. Krishnamoorthy, S. Krishnan, C.C. Lam, Q.D. Lu, M. Nooijen, R. Pitzer, J. Ramanujam, P. Sadayappan, A. Sibiryakov, *Mol. Phys.*, in press.
[142] T. Yanai, M. Kamiya, Y. Kawashima, T. Nakajima, H. Nakano, Y. Nakao, H. Sekino, J. Paulovic, T. Tsuneda, S. Yanagisawa, K. Hirao, UTChem 2004, Department of Applied Chemistry, School of Engineering, University of Tokyo, Tokyo, Japan, 2004.

[143] T. Yanai, H. Nakano, T. Nakajima, T. Tsuneda, S. Hirata, Y. Kawashima, Y. Nakao, M. Kamiya, H. Sekino, K. Hirao, in: P.M.A. Sloot, D. Abramson, A.V. Bogdanov, J.J. Dongarra, A.Y. Zomaya, Y.E. Gorbachev (Eds.), *Computational Science—ICCS 2003*, Pt IV, Proceedings, in: *Lecture Notes in Computer Science*, vol. 2660, Springer-Verlag, Berlin, 2003, pp. 84–95.
[144] T.P. Straatsma, E. Aprà, T.L. Windus, E.J. Bylaska, W. de Jong, S. Hirata, M. Valiev, M.T. Hackler, L. Pollack, R.J. Harrison, M. Dupuis, D.M.A. Smith, J. Nieplocha, V. Tipparaju, M. Krishnan, A.A. Auer, E. Brown, G. Cisneros, G.I. Fann, H. Fruchtl, J. Garza, K. Hirao, R. Kendall, J. Nichols, K. Tsemekhman, K. Wolinski, J. Anchell, D. Bernholdt, P. Borowski, T. Clark, D. Clerc, H. Dachsel, M. Deegan, K. Dyall, D. Elwood, E. Glendening, M. Gutowski, A. Hess, J. Jaffe, B. Johnson, J. Ju, R. Kobayashi, R. Kutteh, Z. Lin, R. Littlefield, X. Long, B. Meng, T. Nakajima, S. Niu, M. Rosing, G. Sandrone, M. Stave, H. Taylor, G. Thomas, J. van Lenthe, A. Wong, Z. Zhang, NWChem, A Computational Chemistry Package for Parallel Computers, Version 4.6, Pacific Northwest National Laboratory, Richland, WA 99352-0999, USA, 2004.
[145] R.A. Kendall, E. Aprà, D.E. Bernholdt, E.J. Bylaska, M. Dupuis, G.I. Fann, R.J. Harrison, J.L. Ju, J.A. Nichols, J. Nieplocha, T.P. Straatsma, T.L. Windus, A.T. Wong, *Comput. Phys. Commun.* **128** (2000) 260.
[146] S. Pal, *Phys. Rev. A* **39** (1989) 39.
[147] S. Pal, *Int. J. Quantum Chem.* **41** (1992) 443.
[148] D. Ajitha, S. Pal, *Phys. Rev. A* **56** (1997) 2658.
[149] D. Ajitha, N. Vaval, S. Pal, *J. Chem. Phys.* **110** (1999) 2316.
[150] S. Pal, D. Ajitha, *Indian J. Chem. Sect A: Inorg. Phys. Theor. Anal. Chem.* **39** (2000) 60.
[151] D. Ajitha, S. Pal, *Chem. Phys. Lett.* **309** (1999) 457.
[152] D. Ajitha, S. Pal, *J. Chem. Phys.* **114** (2001) 3380.
[153] D. Ajitha, S. Pal, *J. Chem. Phys.* **111** (1999) 3832.
[154] D. Ajitha, S. Pal, *J. Chem. Phys.* **111** (1999) 9892.
[155] K.R. Shamasundar, S. Asokan, S. Pal, *J. Chem. Phys.* **120** (2004) 6381.
[156] C. Møller, M.S. Plesset, *Phys. Rev.* **46** (1934) 618.
[157] M. Nooijen, J.G. Snijders, *Int. J. Quantum Chem.* **47** (1993) 3.
[158] E. Merzbacher, *Quantum Mechanics*, second ed., Wiley, New York, 1970.
[159] G.C. Wick, *Phys. Rev.* **80** (1950) 268.
[160] D. Sinha, S.K. Mukhopadhyay, R. Chaudhuri, D. Mukherjee, *Chem. Phys. Lett.* **154** (1989) 544.
[161] D. Mukhopadhyay, S. Mukhopadhyay, R. Chaudhuri, D. Mukherjee, *Theor. Chim. Acta* **80** (1991) 441.
[162] M. Nooijen, R.J. Bartlett, *J. Chem. Phys.* **104** (1996) 2652.
[163] J. Gerratt, I.M. Mills, *J. Chem. Phys.* **49** (1968) 1719.
[164] K.K. Baeck, J.D. Watts, R.J. Bartlett, *J. Chem. Phys.* **107** (1997) 3853.
[165] K.K. Baeck, S.I. Jeon, *Bull. Korean Chem. Soc.* **21** (2000) 720.
[166] M. Wladyslawski, Ph.D. Thesis, Princeton University, Department of Chemistry, 2006 expected.
[167] M. Nooijen, M. Wladyslawski, A. Hazra, *J. Chem. Phys.* **118** (2003) 4832.

This page intentionally left blank

Autoionizing States of Atoms Calculated Using Generalized Sturmians

James Avery and John Avery

Departments of Computer Science and Chemistry, University of Copenhagen, Denmark

Abstract

The generalized Sturmian method is applied to autoionizing states of atoms and ions. If the Goscinskian basis sets allow for a sufficient amount of angular correlation, the calculated energies of doubly-excited (autoionizing) states are found to agree well with the few available experimental energies. A large-Z approximation is discussed, and simple formulas are derived which are valid not only for autoionizing states, but for all states of an isoelectronic atomic series. Diagonalization of a small block of the interelectron repulsion matrix yields roots that can be used for a wide range of Z values.

Contents

1. THE GENERALIZED STURMIAN METHOD FOR SOLVING MANY-PARTICLE SCHRÖDINGER EQUATIONS

If atomic units are used, the non-relativistic many-particle Schrödinger equation can be written in the form

$$\left[-\frac{1}{2}\sum_{j=1}^{N}\frac{1}{m_j}\nabla_j^2 + V(\mathbf{x}) - E_\kappa\right]\Psi_\kappa(\mathbf{x}) = 0. \tag{1}$$

In equation (1), $\mathbf{x}$ is the $3N$-dimensional vector

$$\mathbf{x} \equiv \{\mathbf{x}_1, \mathbf{x}_2, \ldots, \mathbf{x}_N\}, \tag{2}$$

where $\mathbf{x}_j = \{x_j, y_j, z_j\}$ is the 3-dimensional Cartesian coordinate vector of the jth particle. The term $V(\mathbf{x})$ is a potential representing interparticle interactions and externally applied fields. It is usual to solve the many-particle Schrödinger equation by representing the solution $\Psi_\kappa(\mathbf{x})$ as a superposition of basis functions:

$$\Psi_\kappa(\mathbf{x}) = \sum_\nu \Phi_\nu(\mathbf{x}) B_{\nu,\kappa}. \tag{3}$$

ADVANCES IN QUANTUM CHEMISTRY, VOLUME 49
ISSN: 0065-3276 DOI: 10.1016/S0065-3276(05)49002-4

In the generalized Sturmian method, the basis functions $\Phi_\nu(\mathbf{x})$ are chosen to be solutions of an approximate Schrödinger equation of the form

$$\left[-\frac{1}{2}\sum_{j=1}^{N}\frac{1}{m_j}\nabla_j^2+\beta_\nu V_0(\mathbf{x})-E_\kappa\right]\Phi_\nu(\mathbf{x})=0, \tag{4}$$

where $\beta_\nu V_0(\mathbf{x})$ is a weighted zeroth-order potential. The constant weighting factors β_ν are especially chosen in such a way that all of the functions Φ_ν are isoenergetic, all corresponding to the energy E_κ, which is the energy of the state Ψ_κ that they are used to represent. The advantage of such an isoenergetic basis set is that in the asymptotic limit where both V and V_0 become small, all of the basis functions obey the same Schrödinger equation as Ψ_κ, because when $V \approx 0$ and $V_0 \approx 0$, equations (1) and (4) become

$$\left[-\frac{1}{2}\sum_{j=1}^{N}\frac{1}{m_j}\nabla_j^2-E_\kappa\right]\Phi_\nu(\mathbf{x})\approx 0 \tag{5}$$

and

$$\left[-\frac{1}{2}\sum_{j=1}^{N}\frac{1}{m_j}\nabla_j^2-E_\kappa\right]\Psi_\kappa(\mathbf{x})\approx 0. \tag{6}$$

Thus all the basis functions Φ_ν have the correct asymptotic behaviour and all have turning points at positions such that they can contribute usefully to the synthesis of Ψ_κ. By contrast, the functions in conventional basis sets usually correspond to a variety of energies, and many have inappropriate turning points.

2. THE HISTORY OF GENERALIZED STURMIANS

One of the first quantum mechanical problems to be solved exactly was the non-relativistic Schrödinger equation of a hydrogenlike atom. It occurred to early workers in the field that hydrogenlike orbitals might be used as building blocks to construct solutions for more complicated problems. However, it quickly became apparent that sets of hydrogenlike orbitals were unsuitable for this purpose because they lack completeness unless continuum states are included, and inclusion of the continuum makes calculations much more difficult.

The way out of this difficulty was discovered by Shull and Löwdin [1], who introduced basis functions which were formally identical to hydrogenlike orbitals but with Z/n replaced by a constant k, the constant being the same for all the functions in the basis set. These authors were able to show basis sets of this type are complete without the inclusion of the continuum, and that they obey potential-weighted orthonormality relations. Basis sets of the Shull–Löwdin type were named *Sturmians* by Rotenberg [2,3], who wished to emphasize their connection with Sturm–Liouville functional theory.

The momentum-space properties of Sturmians and generalized Sturmians have been extensively studied by Shibuya, Wulfman, Judd, Aquilanti, Koga and others [6–19], building on the early work of V. Fock [4,5]. These authors were able to derive many extremely elegant and useful relationships between Sturmian basis sets and hyperspherical harmonics. Weniger [20] has also pointed out relationships of Sturmians to Sobolev basis sets.

In 1968, Osvaldo Goscinski of Uppsala University completed an important study generalizing the concept of Sturmian basis sets [21]. He considered solutions of a general Schrödinger equation of the form shown in equation (4), with a weighted potential $\beta_\nu V_0(\mathbf{x})$, the weighting factors β_ν being chosen in such a way as to make the set of solutions isoenergetic. Goscinski called this the *conjugate eigenvalue problem*, i.e. instead of a set of energies, the conjugate eigenvalues in equation (4) are the set of weighting factors β_ν. With $N = 1$, $V_0 = -Z/r$, $E_k = -k^2/2$, and $\beta_\nu = nk/Z$, the solutions to equation (4) are the widely-used Coulomb Sturmian functions of Shull and Löwdin. However, the concept discussed by Goscinski is much more general. He was able to show that when $\beta_\nu \neq \beta_{\nu'}$, $\Phi_{\nu'}$ and Φ_ν obey a potential-weighted orthonormality relation. For the familiar one-particle Coulomb Sturmians, this orthonormality relation has the form

$$\int dx\, \Phi^*_{\nu'}(\mathbf{x}) V_0(\mathbf{x}) \Phi_\nu(\mathbf{x}) = \delta_{\nu',\nu} \frac{2E_\kappa}{\beta_\nu}. \tag{7}$$

It is convenient to normalize generalized Sturmian basis sets in such a way that (7) holds in all cases.

Generalized Sturmians can be applied to a wide variety of problems in atomic and molecular quantum theory [22–43].

3. ATOMIC CALCULATIONS

Atomic calculations using generalized Sturmians are particularly simple because if the zeroth-order potential in equation (4) is chosen to be the nuclear attraction potential

$$V_0(\mathbf{x}) = -\sum_{j=1}^{N} \frac{Z}{r_j}, \tag{8}$$

then an exact solution is given by the Slater determinant [21]

$$\Phi_\nu(\mathbf{x}) = |\chi_{n,l,m,m_s} \chi_{n',l',m',m'_s} \chi_{n'',l'',m'',m''_s} \cdots|. \tag{9}$$

In (9), χ_{n,l,m,m_s} is a hydrogenlike spin-orbital with an effective charge

$$Q_\nu = \beta_\nu Z = \left(\frac{-2E_\kappa}{\frac{1}{n^2} + \frac{1}{n'^2} + \cdots} \right)^{1/2}. \tag{10}$$

The effective charge Q_ν is used for all the spin-orbitals in the configuration $\Phi_\nu(\mathbf{x})$, and each configuration has its own effective charge. To see that (9) will then be an exact solution to (4), we note that the one-electron hydrogenlike spin-orbitals obey

$$\left[-\frac{1}{2}\nabla_j^2 + \frac{Q_\nu^2}{2n^2} - \frac{Q_\nu}{r_j} \right] \chi_{n,l,m,m_s}(\mathbf{x}_j) = 0. \tag{11}$$

Thus applying the kinetic energy operator to Φ_ν gives

$$\begin{aligned} \left[-\frac{1}{2}\sum_{j=1}^{N} \nabla_j^2 \right] \Phi_\nu(\mathbf{x}) &= \left[-\frac{Q_\nu^2}{2} \left(\frac{1}{n^2} + \frac{1}{n'^2} + \cdots \right) + \frac{Q_\nu}{r_1} + \frac{Q_\nu}{r_2} + \cdots \right] \Phi_\nu(\mathbf{x}) \\ &= \left[E_\kappa - \beta_\nu V_0(\mathbf{x}) \right] \Phi_\nu(\mathbf{x}) \end{aligned} \tag{12}$$

and thus we see that (4) is satisfied.

It is convenient to introduce the notation

$$p_\kappa \equiv \sqrt{-2E_\kappa} \tag{13}$$

and

$$\mathcal{R}_\nu \equiv \sqrt{\frac{1}{n^2} + \frac{1}{n'^2} + \cdots}. \tag{14}$$

With these definitions, equation (10) can be written in the form

$$Q_\nu = \beta_\nu Z = \frac{p_\kappa}{\mathcal{R}_\nu} \tag{15}$$

while from (13) we have

$$E_\kappa = -\frac{p_\kappa^2}{2}. \tag{16}$$

For atomic calculations in the non-relativistic limit, in the absence of external fields, neglecting spin-orbit coupling and neglecting motion of the nucleus, the potential in equation (1) is given by

$$V(\mathbf{x}) = V_0(\mathbf{x}) + V'(\mathbf{x}) = -\sum_{j=1}^{N} \frac{Z}{r_j} + \sum_{i>i}^{N} \sum_{i=1}^{N} \frac{1}{r_{ij}}. \tag{17}$$

We now introduce the definitions

$$T^0_{\nu',\nu} \equiv -\frac{1}{p_\kappa} \int dx\, \Phi^*_{\nu'}(\mathbf{x}) V_0(\mathbf{x}) \Phi_\nu(\mathbf{x}) \tag{18}$$

and

$$T'_{\nu',\nu} \equiv -\frac{1}{p_\kappa} \int dx\, \Phi^*_{\nu'}(\mathbf{x}) V'(\mathbf{x}) \Phi_\nu(\mathbf{x}). \tag{19}$$

From the potential-weighted orthonormality relations (7) it follows that

$$T^0_{\nu',\nu} = \delta_{\nu'\nu} Z \mathcal{R}_\nu. \tag{20}$$

Thus we see that the nuclear attraction matrix $T^0_{\nu',\nu}$ is independent of p_κ and hence also independent of the energy E_κ. Similarly it can be shown [34] that the interelectron repulsion matrix $T'_{\nu',\nu}$, defined by (19), is also independent of p_κ and E_κ. Two remarks need to be made concerning equations (7), (9) and (20): Firstly, the configurations defined by (9) are already properly normalized [34]. No special normalization needs to be made. Secondly, in atomic calculations (7) holds even when $\nu' \neq \nu$ does not imply $\beta_{\nu'} = \beta_\nu$.

The evaluation of the interelectron repulsion matrix $T'_{\nu',\nu}$ is made somewhat more difficult by the fact that each configuration has its own effective charge Q_ν. For this reason, radial orthonormality cannot be assumed between the hydrogenlike spin-orbitals χ_{n,l,m,m_s} belonging to different configurations, and generalized Slater–Condon rules must be used, as has been discussed by us in previous papers [37–39].

We are now in a position to derive the generalized Sturmian secular equations. Substituting (3) into (1), we have

$$\sum_\nu \left[-\frac{1}{2} \sum_{j=1}^{N} \nabla_j^2 + V(\mathbf{x}) - E_\kappa \right] \Phi_\nu(\mathbf{x}) B_{\nu,\kappa} = 0. \tag{21}$$

We next make use of the fact that all of the Goscinskian configurations Φ_ν in our basis set obey equation (4). Thus (21) can be rewritten in the form

$$\sum_\nu \big[V(\mathbf{x}) - \beta_\nu V_0(\mathbf{x})\big]\Phi_\nu(\mathbf{x})B_{\nu,\kappa} = 0. \tag{22}$$

(Notice that the kinetic energy term has now disappeared!) The next step is to multiply (22) from the left by a conjugate configuration from our basis set and to integrate over all space and spin coordinates:

$$\sum_\nu \int dx\, \Phi^*_{\nu'}(\mathbf{x})\big[V(\mathbf{x}) - \beta_\nu V_0(\mathbf{x})\big]\Phi_\nu(\mathbf{x})B_{\nu,\kappa} = 0. \tag{23}$$

If we now make use of equations (16)–(20) and divide by p_κ, we obtain the set of generalized Sturmian secular equations

$$\sum_\nu [\delta_{\nu',\nu} Z\mathcal{R}_\nu + T'_{\nu',\nu} - p_\kappa \delta_{\nu',\nu}]B_{\nu,\kappa} = 0. \tag{24}$$

The secular equations shown in (24) differ greatly from the conventional set of equations that would be used to diagonalize the Hamiltonian of a system, and they have several remarkable features:

1. The kinetic energy term has vanished.
2. The matrix representing the nuclear attraction potential is diagonal.
3. The eigenvalues are not energies but values of the scaling parameter p_κ, which is proportional to the square root of the binding energy.
4. The basis set is not completely determined before the secular equations have been solved. Only the form of the basis set is known, but not the scaling parameter. By solving (24), one obtains simultaneously a spectrum of energies, an optimal basis set for each energy, and the wave functions of all the states.

The parameter p_κ, defined by equation (13), plays the role of a scaling parameter for the basis set because the effective nuclear charges $Q_\nu = p_\kappa/\mathcal{R}_\nu$ are proportional to p_κ. Everywhere that r_j appears in radial parts of the spin-orbitals χ_{n,l,m,m_s}, the radius is multiplied by p_κ. For example, the Slater exponents that appear in the spin-orbitals have the form $\exp[-p_\kappa r_j/(n\mathcal{R}_\nu)]$. The orbitals corresponding to small values of p_κ are diffuse, while those corresponding to large values are localized in the vicinity of the nucleus. Since small values of p_κ are associated with small values of the binding energy $|E_\kappa|$, the highly excited states of the atom are represented with the help of a diffuse basis set, while the ground state and less highly excited states are represented using more localized basis sets. Qualitatively, we can see that this is what we want. It turns out that quantitatively the scaling parameters that result from the solution of the generalized Sturmian secular equations (24) are almost exactly the ones needed to produce optimal basis sets, i.e. the scaling factors are, to a very close approximation, the ones that would be found by variational optimization of the basis. In the generalized Sturmian method, the time-consuming optimization of a basis set for each state is performed automatically for all states when the secular equations (24) are solved. This feature of the method makes it very suitable for the rapid calculation of large numbers of excited states of few-electron atoms.

4. SYMMETRY-ADAPTED BASIS FUNCTIONS FOR THE 2-ELECTRON ISOELECTRONIC SERIES

In studies of singly-excited states of the 2-electron isoelectronic series, we introduced angular correlation in the hope of improving the accuracy of our results. The accuracy of the ground state and of the lower singly-excited states was slightly improved by the inclusion of angular correlation [42]. However, looking closely at our results, we realized that basis sets allowing for large amounts of angular correlation dramatically improved the accuracy of the doubly-excited (autoionizing) states. Comparing our results with the few available experimental energies for autoionizing states [44–47], we found very good agreement, provided that our basis sets allowed for angular correlation up to $l_{\max} = 4$ or $l_{\max} = 5$. Our calculated energies for some ^{3}S autoionizing states of the 2-electron isoelectronic series are shown in Tables 1–4 and Figs. 1–3.

In order to include angular correlation efficiently, we made use of symmetry-adapted basis functions of the Russell–Saunders type, i.e. eigenfunctions of the total orbital angular momentum operator L^2 and its z-component L_z, and of the total spin operator S^2 and its z-component S_z. These symmetry-adapted basis functions η_j were constructed as sums of primitive configurations of the type shown in equation (9), the coefficients in the sum being products of two Clebsch–Gordan coefficients, one for orbital angular momentum and the other for spin:

$$\eta_j(\mathbf{x}) = \sum_{\nu} \Phi_\nu(\mathbf{x}) C_{\nu,j}, \tag{25}$$

where

$$C_{\nu,j} \equiv \begin{pmatrix} l & l' & L \\ m & m' & M \end{pmatrix} \begin{pmatrix} \frac{1}{2} & \frac{1}{2} & S \\ m_s & m'_s & M_S \end{pmatrix} \tag{26}$$

and where ν stands for the set of indices

$$\nu \equiv \{n, l, m, m_s; n', l', m', m'_s\} \tag{27}$$

while

$$j \equiv \{n, l; n', l'; L, M; S, M_S\}. \tag{28}$$

For the 2-electron case, the primitive configurations have the form

$$\Phi_\nu(\mathbf{x}) \equiv |\chi_{n,l,m,m_s} \chi_{n',l',m',m'_s}|. \tag{29}$$

Because of the unitarity of the Clebsch–Gordan coefficients we have

$$C^\dagger C = I. \tag{30}$$

If we use a tilde to denote matrices based on the symmetry-adapted functions η_j, we have for the transformed nuclear attraction matrix:

$$\tilde{T}^0 = C^\dagger T^0 C. \tag{31}$$

Making use of (20) and (30), we obtain

$$\tilde{T}^0_{j',j} = \delta_{j',j} Z \mathcal{R}_j. \tag{32}$$

Table 1. Doubly-excited (autoionizing) ^{3}S states of the 2-electron isoelectronic series with $n = 2$ and $n' = 3, 4, 5$. See also Fig. 1

	2s3s ^{3}S	2p3p ^{3}S	2s4s ^{3}S	2p4p ^{3}S	2s5s ^{3}S	2p5p ^{3}S
C^{4+}	−6.1198	−5.9299	−5.3750	−5.2906	−5.0469	−5.0028
expt.	−6.1221	−5.9299				
N^{5+}	−8.4020	−8.1756	−7.3629	−7.2614	−6.9017	−6.8484
expt.	−8.4058	−8.1768				
O^{6+}	−11.0452	−10.7824	−9.6633	−9.5447	−9.0464	−8.9839
expt.	−11.0545	−10.7869				
F^{7+}	−14.0496	−13.7504	−12.2762	−12.1405	−11.4812	−11.4095
expt.	−14.0616	−13.7556				
Ne^{8+}	−17.4151	−17.0795	−15.2017	−15.0488	−14.2059	−14.1251
expt.	−17.4350	−17.0905				
Na^{9+}	−21.1417	−20.7697	−18.4396	−18.2696	−17.2207	−17.1307
expt.	−21.1749	−20.7888				
Mg^{10+}	−25.2295	−24.8210	−21.9900	−21.8030	−20.5255	−20.4264
expt.	−25.2767	−24.8504				
Al^{11+}	−29.6783	−29.2334	−25.8529	−25.6488	−24.1203	−24.0121
expt.	−29.7450	−29.2761				
Si^{12+}	−34.4883	−34.0069	−30.0284	−29.8072	−28.0050	−27.8877
expt.	−34.5809	−34.0654				
P^{13+}	−39.6593	−39.1416	−34.5163	−34.2780	−32.1798	−32.0534
expt.	−39.7833	−39.2138				
S^{14+}	−45.1915	−44.6373	−39.3167	−39.0614	−36.6446	−36.5091
expt.	−45.3567	−44.7298				
Cl^{15+}	−51.0848	−50.4942	−44.4296	−44.1573	−41.3994	−41.2548
expt.	−51.2969	−50.6131				
Ar^{16+}	−57.3392	−56.7122	−49.8551	−49.5656	−46.4442	−46.2905
expt.	−46.3829	−45.6295				
K^{17+}	−63.9547	−63.2913	−55.5930	−55.2865	−51.7790	−51.6162
expt.	−64.2961	−63.4726				
Ca^{18+}	−70.9313	−70.2315	−61.6434	−61.3199	−57.4038	−57.2320
expt.	−71.3560	−70.4479				
Sc^{19+}	−78.2690	−77.5329	−68.0064	−67.6657	−63.3186	−63.1377
expt.	−78.7497	−77.7470				
Ti^{20+}	−85.9678	−85.1953	−74.6818	−74.3241	−69.5234	−69.3334
expt.		−85.4971				

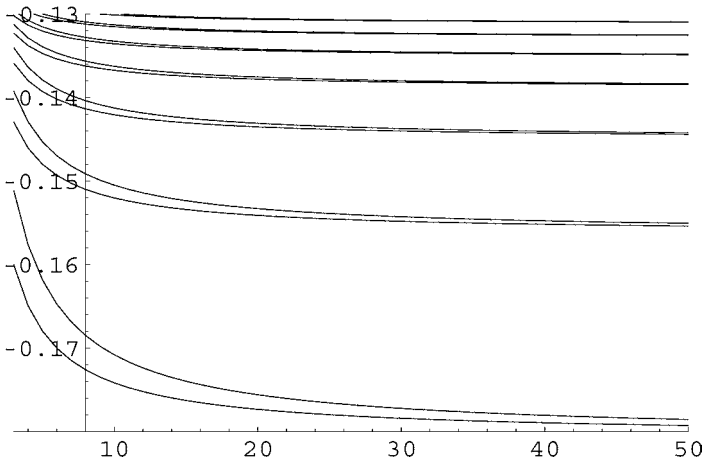

Fig. 1. E_κ/Z^2 in Hartrees as a function of Z for the first series of doubly-excited ^{3}S states of the 2-electron isoelectronic series (Table 1). For this series, $n = 2$, while $n' = 3, 4, 5, 6, \ldots$. In the large-Z limit, E_κ/Z^2 approaches the Z-independent value, $-\mathcal{R}_\nu^2/2$.

Thus the nuclear attraction matrix is still diagonal in the symmetry-adapted representation. The symmetry-adapted interelectron repulsion matrix

$$\tilde{T}' = C^\dagger T' C \tag{33}$$

is block-diagonal, the blocks being labeled by particular values of the quantum numbers L, M, S, and M_S. The secular equation for diagonalizing one of the blocks

$$\sum_{j \subset L,M,S,M_S} [\delta_{j',j} Z\mathcal{R}_j + \tilde{T}'_{j',j} - p_\kappa \delta_{j',j}]\tilde{B}_{j,\kappa} = 0 \tag{34}$$

has a lower dimension than the unsymmetrized secular equation (24), and thus the diagonalization can be quickly performed for many values of Z. Furthermore, by using symmetry-adapted basis functions one can identify the states

$$\Psi_\kappa(\mathbf{x}) = \sum_j \eta_j(\mathbf{x})\tilde{B}_{j,\kappa} \tag{35}$$

more easily, since values of L, M, S, and M_S characterize each of the particular blocks being diagonalized.

As mentioned above, Tables 1–4 and Figs. 1–3 show doubly-excited (autoionizing) ^{3}S states of the 2-electron isoelectronic series, calculated using a symmetry-adapted basis set which allowed for angular correlation up to $l_{\max} = 5$. There were 145 functions η_j in this basis. Having constructed the transformed interelectron repulsion matrix $\tilde{T}'_{j',j}$, and the transformed nuclear attraction matrix $\mathcal{R}_j\delta_{j',j}$, we were able to use the same matrices to obtain all of the states shown in these tables and figures (as well as the singly excited ^{3}S states, which are not shown) by solving equation (34) for various values of Z.

Table 2. Autoionizing ^{3}S states of heliumlike atoms with $n = 3$ and $n' = 4, 5$. See Fig. 2

	3s4s ^{3}S	3p4p ^{3}S	3d4d ^{3}S	3s5s ^{3}S	3p5p ^{3}S	3d5d ^{3}S
C^{4+}	−2.9372	−2.8729	−2.7660	−2.5788	−2.5402	−2.4867
N^{5+}	−4.0338	−3.9576	−3.8293	−3.5368	−3.4908	−3.4260
O^{6+}	−5.3040	−5.2159	−5.0662	−4.6459	−4.5924	−4.5164
F^{7+}	−6.7477	−6.6478	−6.4768	−5.9061	−5.8452	−5.7579
Ne^{8+}	−8.3651	−8.2534	−8.0609	−7.3175	−7.2491	−7.1505
Na^{9+}	−10.1561	−10.0325	−9.8187	−8.8799	−8.8041	−8.6942
Mg^{10+}	−12.1207	−11.9852	−11.7501	−10.5934	−10.5101	−10.3890
Al^{11+}	−14.2590	−14.1116	−13.8551	−12.4581	−12.3673	−12.2349
Si^{12+}	−16.5708	−16.4116	−16.1337	−14.4739	−14.3757	−14.2319
P^{13+}	−19.0562	−18.8851	−18.5860	−16.6408	−16.5351	−16.3801
S^{14+}	−21.7153	−21.5323	−21.2118	−18.9588	−18.8456	−18.6793
Cl^{15+}	−24.5480	−24.3531	−24.0113	−21.4279	−21.3073	−21.1297
Ar^{16+}	−27.5542	−27.3475	−26.9844	−24.0481	−23.9200	−23.7312
K^{17+}	−30.7341	−30.5155	−30.1310	−26.8194	−26.6839	−26.4838
Ca^{18+}	−34.0876	−33.8572	−33.4513	−29.7419	−29.5989	−29.3875
Sc^{19+}	−37.6147	−37.3724	−36.9452	−32.8154	−32.6650	−32.4423
Ti^{20+}	−41.3154	−41.0612	−40.6128	−36.0401	−35.8822	−35.6482
V^{21+}	−45.1898	−44.9237	−44.4539	−39.4159	−39.2505	−39.0053
Cr^{22+}	−49.2377	−48.9598	−48.4686	−42.9428	−42.7699	−42.5134
Mn^{23+}	−53.4593	−53.1695	−52.6570	−46.6208	−46.4404	−46.1727
Fe^{24+}	−57.8544	−57.5527	−57.0189	−50.4499	−50.2621	−49.9831
Co^{25+}	−62.4232	−62.1096	−61.5545	−54.4301	−54.2348	−53.9446
Ni^{26+}	−67.1656	−66.8402	−66.2637	−58.5614	−58.3587	−58.0572
Cu^{27+}	−72.0816	−71.7443	−71.1465	−62.8439	−62.6337	−62.3209
Zn^{28+}	−77.1712	−76.8220	−76.2029	−67.2774	−67.0598	−66.7357

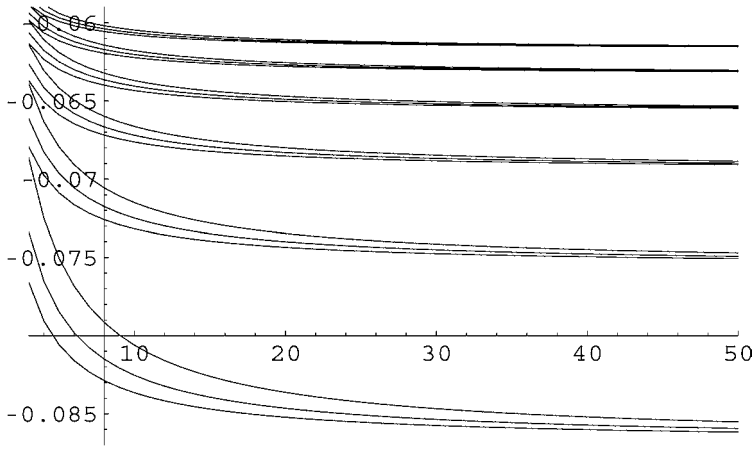

Fig. 2. E_κ/Z^2 as a function of Z for the second series of doubly-excited ^{3}S states of heliumlike atoms and ions (Table 2). For this series, $n = 3$, while $n' = 4, 5, 6, 7, \ldots$.

Table 3. The third series of heliumlike autoionizing states. Here $n = 4$, while $n' = 5, 6$. These states correspond to the lowest curves in Fig. 3

	$4s5s\ ^3S$	$4p5p\ ^3S$	$4d5d\ ^3S$	$4f5f\ ^3S$	$4s6s\ ^3S$	$4p6p\ ^3S$
C^{4+}	−1.7339	−1.7058	−1.6637	−1.5960	−1.5350	−1.5153
N^{5+}	−2.3813	−2.3482	−2.2980	−2.2163	−2.1064	−2.0830
O^{6+}	−3.1312	−3.0930	−3.0349	−2.9391	−2.7682	−2.7410
F^{7+}	−3.9836	−3.9404	−3.8743	−3.7644	−3.5202	−3.4893
Ne^{8+}	−4.9386	−4.8902	−4.8161	−4.6922	−4.3625	−4.3279
Na^{9+}	−5.9960	−5.9426	−5.8605	−5.7226	−5.2950	−5.2568
Mg^{10+}	−7.1559	−7.0974	−7.0073	−6.8554	−6.3179	−6.2759
Al^{11+}	−8.4183	−8.3548	−8.2566	−8.0907	−7.4310	−7.3853
Si^{12+}	−9.7832	−9.7146	−9.6085	−9.4286	−8.6344	−8.5850
P^{13+}	−11.2507	−11.1770	−11.0628	−10.8689	−9.9281	−9.8750
S^{14+}	−12.8206	−12.7418	−12.6197	−12.4118	−11.3120	−11.2552
Cl^{15+}	−14.4930	−14.4092	−14.2790	−14.0571	−12.7863	−12.7258
Ar^{16+}	−16.2679	−16.1790	−16.0408	−15.8050	−14.3508	−14.2866
K^{17+}	−18.1453	−18.0513	−17.9051	−17.6554	−16.0056	−15.9377
Ca^{18+}	−20.1252	−20.0262	−19.8720	−19.6082	−17.7506	−17.6790
Sc^{19+}	−22.2077	−22.1035	−21.9413	−21.6636	−19.5860	−19.5107
Ti^{20+}	−24.3926	−24.2834	−24.1131	−23.8214	−21.5116	−21.4326
V^{21+}	−26.6800	−26.5657	−26.3875	−26.0818	−23.5275	−23.4448
Cr^{22+}	−29.0699	−28.9506	−28.7643	−28.4447	−25.6337	−25.5472
Mn^{23+}	−31.5623	−31.4379	−31.2436	−30.9100	−27.8301	−27.7400
Fe^{24+}	−34.1573	−34.0278	−33.8254	−33.4779	−30.1169	−30.0230
Co^{25+}	−36.8547	−36.7201	−36.5098	−36.1483	−32.4939	−32.3963
Ni^{26+}	−39.6546	−39.5149	−39.2966	−38.9211	−34.9612	−34.8599
Cu^{27+}	−42.5570	−42.4123	−42.1859	−41.7965	−37.5187	−37.4137
Zn^{28+}	−45.5619	−45.4121	−45.1777	−44.7744	−40.1666	−40.0579

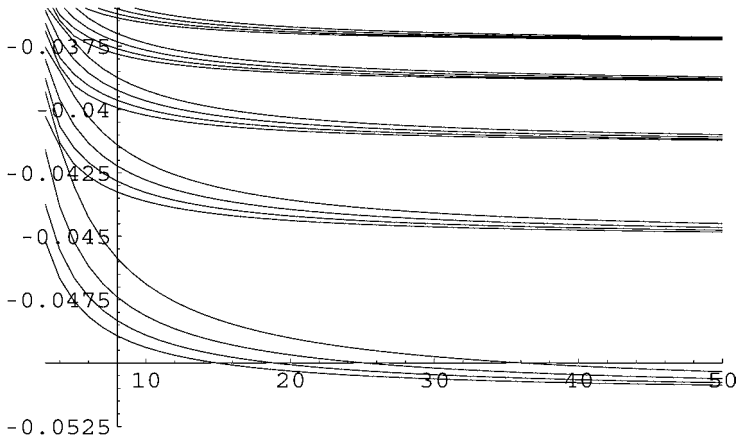

Fig. 3. This figure is similar to Figs. 1 and 2, but it shows the third series of autoionizing ^3S states (Table 3). For this series $n = 4$, while $n' = 5, 6, 7, 8, \ldots$.

Table 4. The fourth series of heliumlike ^{3}S autoionizing states

	5s6s ^{3}S	5p6p ^{3}S	5d6d ^{3}S	5f6f ^{3}S	5g6g ^{3}S	5s7s ^{3}S
C^{4+}	−1.1467	−1.1322	−1.1116	−1.0806	−1.0341	−1.0252
N^{5+}	−1.5749	−1.5577	−1.5334	−1.4967	−1.4401	−1.4073
O^{6+}	−2.0708	−2.0511	−2.0230	−1.9806	−1.9138	−1.8498
F^{7+}	−2.6345	−2.6122	−2.5803	−2.5322	−2.4554	−2.3527
Ne^{8+}	−3.2660	−3.2411	−3.2055	−3.1517	−3.0648	−2.9160
Na^{9+}	−3.9653	−3.9378	−3.8984	−3.8389	−3.7420	−3.5397
Mg^{10+}	−4.7323	−4.7022	−4.6591	−4.5939	−4.4870	−4.2238
Al^{11+}	−5.5672	−5.5344	−5.4875	−5.4166	−5.2998	−4.9684
Si^{12+}	−6.4698	−6.4344	−6.3838	−6.3071	−6.1804	−5.7733
P^{13+}	−7.4402	−7.4022	−7.3478	−7.2655	−7.1288	−6.6387
S^{14+}	−8.4783	−8.4378	−8.3796	−8.2916	−8.1450	−7.5644
Cl^{15+}	−9.5842	−9.5411	−9.4792	−9.3854	−9.2289	−8.5506
Ar^{16+}	−10.7580	−10.7122	−10.6465	−10.5471	−10.3807	−9.5972
K^{17+}	−11.9995	−11.9511	−11.8817	−11.7765	−11.6002	−10.7042
Ca^{18+}	−13.3087	−13.2578	−13.1846	−13.0737	−12.8875	−11.8715
Sc^{19+}	−14.6858	−14.6323	−14.5553	−14.4387	−14.2426	−13.0993
Ti^{20+}	−16.1306	−16.0745	−15.9937	−15.8715	−15.6654	−14.3876
V^{21+}	−17.6432	−17.5845	−17.5000	−17.3720	−17.1561	−15.7362
Cr^{22+}	−19.2236	−19.1623	−19.0740	−18.9403	−18.7145	−17.1452
Mn^{23+}	−20.8717	−20.8078	−20.7158	−20.5764	−20.3407	−18.6146
Fe^{24+}	−22.5877	−22.5212	−22.4254	−22.2803	−22.0347	−20.1445
Co^{25+}	−24.3714	−24.3023	−24.2027	−24.0519	−23.7965	−21.7347
Ni^{26+}	−26.2229	−26.1512	−26.0479	−25.8914	−25.6260	−23.3854
Cu^{27+}	−28.1421	−28.0678	−27.9608	−27.7986	−27.5233	−25.0965
Zn^{28+}	−30.1292	−30.0523	−29.9415	−29.7735	−29.4884	−26.8679

5. THE LARGE-Z APPROXIMATION

It is interesting to ask what happens to the solutions of (24) and (34) when the nuclear charge Z becomes very large: As Z becomes large, interelectron repulsion becomes progressively less important in relation to nuclear attraction. In the extreme high-Z limit interelectron repulsion can be entirely neglected, (24) is already diagonal, and the energies are given by

$$E_\kappa \to -\frac{1}{2}(Z\mathcal{R}_\nu)^2 = -\frac{Z^2}{2n^2} - \frac{Z^2}{2n'^2} - \frac{Z^2}{2n''^2} - \cdots, \tag{36}$$

i.e. they are the energies of N entirely independent electrons in the attractive potential of the nucleus. If all of the n's are unequal, the degeneracy in the extreme high-Z limit is $2n^2 \times 2n'^2 \times 2n''^2 \times \cdots$, since this is the number of configurations corresponding to the same value of $\mathcal{R}_\nu$. If two or more of the n's are equal, the degeneracy will be less than this, since some states are forbidden by the Pauli principle. As one moves back from the extreme high-Z limit towards lower values of Z, the degeneracy is partially removed by interelectron repulsion. If Z is very large but finite, interelectron repulsion hybridizes the

degenerate set of states corresponding to a particular value of $\mathcal{R}_\nu$. One can find the coefficients for this hybridization by diagonalizing the block of the interelectron repulsion matrix $T'_{\nu',\nu}$ corresponding to this particular degenerate value of the nuclear attraction matrix, i.e. by solving

$$\sum_{\nu \subset n,n',\ldots} [T'_{\nu',\nu} - \lambda_\kappa \delta_{\nu',\nu}] B_{\nu,\kappa} = 0 \tag{37}$$

since the eigenvectors of a matrix are unaffected by the addition to it of any multiple of the unit matrix. The eigenvalues all are shifted by a constant amount. Thus for large but finite values of Z we have from (37), (24) and (16),

$$E_\kappa \approx -\frac{1}{2}(Z\mathcal{R}_\nu + \lambda_\kappa)^2, \tag{38}$$

where λ_κ is a root of equation (37). The large-Z approximation consists in the limitation of the basis set to the set of configurations corresponding to a particular value of $\mathcal{R}_\nu$. The root λ_κ is an exact root of (37) with this limited basis set, and, with the same limitation, $Z\mathcal{R}_\nu + \lambda_\kappa$ is an exact root of (24). Because of the minus sign in the definition of $T'_{\nu',\nu}$, its roots λ_κ are always negative. Thus, as we would expect, the effect of interelectron repulsion is to decrease the binding energy. To make this point more apparent, we can write

$$E_\kappa \approx -\frac{1}{2}\big(Z\mathcal{R}_\nu - |\lambda_\kappa|\big)^2. \tag{39}$$

One can also find the large-Z limit by diagonalizing blocks of the symmetry-transformed interelectron repulsion matrix $\tilde{T}'_{j',j}$, using a basis consisting only of those symmetry-adapted functions η_j which correspond to a particular value of $\mathcal{R}_j$. These blocks will of course be much smaller than the ones appearing in equation (37). The advantage in using equation (37) is that one obtains simultaneously all of the roots of an $\mathcal{R}_\nu$-block, regardless of their symmetry. Such a calculation is extremely rapid because an $\mathcal{R}_\nu$-block of $T'_{\nu',\nu}$ is very sparse.

The remarks in this section hold not only for autoionizing states but for any state whatever of an isoelectronic atomic series in the high-Z domain.

6. RANGE OF VALIDITY OF THE LARGE-Z APPROXIMATION

In Table 5, the $|\lambda_\kappa|$ values corresponding to ^{3}S terms are the ones which are needed to construct approximate curves representing E_κ/Z^2 as a function of Z for comparison with the curves shown in Fig. 1. For example, the approximate curve corresponding to the lowest curve in Fig. 1 is given by

$$E_\kappa \approx -\frac{1}{2}\left(Z\sqrt{\frac{1}{2^2}+\frac{1}{3^2}} - 0.108252\right)^2 \tag{40}$$

while the second lowest approximate curve is given by

$$E_\kappa \approx -\frac{1}{2}\left(Z\sqrt{\frac{1}{2^2}+\frac{1}{3^2}} - 0.168814\right)^2 \tag{41}$$

Table 5. Eigenvalues of the 2-electron interelectron repulsion matrix $T'_{\nu',\nu}$ for $S = 1$, $M_S = 1$, $n = 2$ and $n' = 3, 4, 5$

$n' = 3$ $\lvert\lambda_\kappa\rvert$	term	$n' = 4$ $\lvert\lambda_\kappa\rvert$	term	$n' = 5$ $\lvert\lambda_\kappa\rvert$	term
0.108252	^{3}S	0.077484	^{3}S	0.056075	^{3}S
0.134734	^{3}P	0.087582	^{3}P	0.065019	^{3}P
0.135408	^{3}D	0.090845	^{3}D	0.061128	^{3}P
0.138421	^{3}P	0.093401	^{3}P	0.063370	^{3}D
0.155155	^{3}F	0.099235	^{3}F	0.067758	^{3}F
0.160439	^{3}P	0.099991	^{3}P	0.067934	^{3}P
0.165613	^{3}D	0.104253	^{3}D	0.070494	^{3}D
0.168814	^{3}S	0.106271	^{3}D	0.071269	^{3}D
0.173917	^{3}D	0.107976	^{3}S	0.072413	^{3}F
0.186893	^{3}P	0.108188	^{3}F	0.072857	^{3}S
		0.111210	^{3}G	0.073295	^{3}G
		0.111264	^{3}F	0.073588	^{3}G
		0.113313	^{3}P	0.073920	^{3}F
		0.114381	^{3}D	0.074306	^{3}G
				0.074578	^{3}H
				0.074963	^{3}F
				0.075173	^{3}P
				0.075545	^{3}D

and the third lowest by

$$E_\kappa \approx -\frac{1}{2}\left(Z\sqrt{\frac{1}{2^2}+\frac{1}{4^2}} - 0.077484\right)^2 \tag{42}$$

and so on. These curves are shown by solid lines in Fig. 4, while the dots represent points calculated with the full basis set. From Fig. 4 it can be seen that the lowest curve is approximately valid even for very low values of Z, while the higher curves begin to lose accuracy when Z is between 10 and 20, although they retain rough validity for lower Z values. This behaviour can be understood by remembering that for the higher curves, the $\mathcal{R}_\nu$ values of neighbouring blocks become closer together, and therefore interelectron repulsion is better able to introduce hybridization between neighbouring $\mathcal{R}_\nu$-blocks. Such inter-block hybridization is neglected in the large-Z approximation, which limits the basis set to a particular $\mathcal{R}_\nu$-block.

We said in the previous section that all of the remarks contained in the section hold for any state whatever of an atomic isoelectronic series in the large-Z domain. To illustrate this point, we have constructed the roots of the carbonlike 6-electron block with

$$\mathcal{R}_\nu = \sqrt{\frac{2}{1^2}+\frac{4}{2^2}} = \sqrt{3}, \tag{43}$$

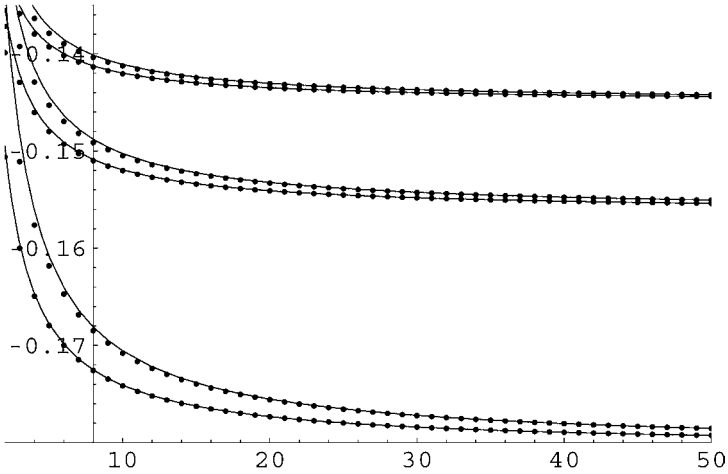

Fig. 4. The large-Z approximation for E_κ/Z^2 as a function of Z (smooth curves) is compared in this figure with values calculated using the full basis set (dots). The curves in the figure, starting from the bottom, correspond to 2s3s ^{3}S states, equation (40), 2p3p ^{3}S states, equation (41), and so on. See also Table 1 and Fig. 1.

Table 6. Eigenvalues of $T'_{\nu',\nu}$ for the carbonlike $\mathcal{R}_\nu = \sqrt{3}$ block

$\lvert\lambda_\kappa\rvert$	term	degen.	configuration
1.88151	^{3}P	9	$0.994467(1s)^2(2s)^2(2p)^2+0.105047(1s)^2(2p)^4$
1.89369	^{1}D	5	$0.994467(1s)^2(2s)^2(2p)^2-0.105047(1s)^2(2p)^4$
1.90681	^{1}S	1	$0.979686(1s)^2(2s)^2(2p)^2+0.200537(1s)^2(2p)^4$
1.91623	^{5}S	5	$(1s)^2(2s)(2p)^3$
1.95141	^{3}D	15	$(1s)^2(2s)(2p)^3$
1.96359	^{3}P	9	$(1s)^2(2s)(2p)^3$
1.98389	^{3}S	3	$(1s)^2(2s)(2p)^3$
1.98524	^{1}D	5	$(1s)^2(2s)(2p)^3$
1.99742	^{1}P	3	$(1s)^2(2s)(2p)^3$
2.04342	^{3}P	9	$0.105047(1s)^2(2s)^2(2p)^2-0.994467(1s)^2(2p)^4$
2.05560	^{1}D	5	$0.105047(1s)^2(2s)^2(2p)^2+0.994467(1s)^2(2p)^4$
2.07900	^{1}S	1	$0.200537(1s)^2(2s)^2(2p)^2-0.979686(1s)^2(2p)^4$

i.e. the block with 2 electrons in the $n = 1$ shell and 4 electrons in the $n = 2$ shell. Table 6 shows the roots of the interelectron repulsion matrix $T'_{\nu',\nu}$ for this block together with the terms, degeneracies and electron configurations to which they correspond.

Table 7 shows a comparison between the energies E_κ generated from

$$E_\kappa \approx -\frac{1}{2}\left(Z\sqrt{\frac{2}{1^2}+\frac{4}{2^2}}-|\lambda_\kappa|\right)^2 \tag{44}$$

using the $|\lambda_\kappa|$ values in Table 6 and experimental energies taken from reference [44]. As can be seen from the table, the number of accurate significant figures improves with in-

Table 7. The approximate validity of the large-Z approximation is illustrated here for the carbonlike 6-electron isoelectronic series. The roots of the 112222 block, Table 6, were substituted into equation (44) to generate the calculated energies in Hartrees. The experimental energies were taken from the NIST tables [44]

	^{3}P	^{1}D	^{1}S	^{5}S	^{3}D	^{3}P
C	−36.217	−36.113	−36.002	−35.922	−35.624	−35.522
expt.	−37.856	−37.809	−37.757	−37.702	−37.564	−37.513
N^+	−52.458	−52.333	−52.199	−52.103	−51.744	−51.621
expt.	−54.078	−54.008	−53.929	−53.865	−53.658	−53.580
O^{2+}	−71.699	−71.553	−71.396	−71.284	−70.864	−70.720
expt.	−73.317	−73.225	−73.121	−73.043	−72.771	−72.669
F^{3+}	−93.940	−93.773	−93.594	−93.465	−92.985	−92.819
expt.	−95.576	−95.461	−95.332	−95.238	−94.902	−94.778
Ne^{4+}	−119.181	−118.993	−118.791	−118.646	−118.105	−117.917
expt.	−120.852	−120.714	−120.561	−120.449	−120.051	−119.903
Na^{5+}	−147.422	−147.213	−146.988	−146.827	−146.225	−146.016
expt.	−149.151	−148.989	−148.812	−148.680	−148.221	−148.051
Mg^{6+}	−178.664	−178.433	−178.186	−178.008	−177.345	−177.115
expt.	−180.469	−180.283	−180.081	−179.931	−179.408	−179.217
Al^{7+}	−212.905	−212.653	−212.383	−212.189	−211.465	−211.214
expt.	−214.823	−214.610	−214.384	−214.213	−213.628	−213.414
Si^{8+}	−250.146	−249.873	−249.580	−249.370	−248.585	−248.313
expt.	−252.209	−251.968	−251.718	−251.522	−250.878	−250.642
P^{9+}	−290.387	−290.094	−289.778	−289.551	−288.705	−288.412
expt.	−292.636	−292.364	−292.089	−291.871	−291.163	−290.905
S^{10+}	−333.628	−333.314	−332.975	−332.732	−331.825	−331.511
expt.	−336.105	−335.799	−335.499	−335.257	−334.487	−334.205
Cl^{11+}	−379.869	−379.534	−379.172	−378.913	−377.945	−377.610
expt.	−382.631	−382.287	−381.962	−381.692	−380.862	−380.556
Ar^{12+}	−429.110	−428.754	−428.370	−428.094	−427.065	−426.709
expt.	−421.019	−420.631	−420.280		−419.093	−418.762
K^{13+}	−481.351	−480.974	−480.567	−480.275	−479.185	−478.808
expt.	−484.878	−484.441	−484.063	−483.736	−482.788	−482.429
Ca^{14+}	−536.593	−536.194	−535.764	−535.456	−534.305	−533.907
expt.	−540.654	−540.159	−539.753	−539.397	−538.391	−538.003
Sc^{15+}	−594.834	−594.414	−593.961	−593.637	−592.425	−592.006
expt.	−599.318	−598.756	−598.322	−597.945	−596.874	−596.454

creasing Z, but even at low values of Z the approximation of equation (44) has some qualitative validity. For example, the ground states of C, N^+, O^{2+}, etc. are predicted to be ^3P states, as is confirmed by experiment, and the order of the higher states shown in Table 7 is correct. We hope to discuss the large-Z approximation in more detail in a future paper.

The programs used in this article will be made available on the following website: http://www.ccs.ki.ku.dk/~john/.

REFERENCES

[1] H. Shull, P.O. Löwdin, *J. Chem. Phys.* **30** (1959) 617.
[2] M. Rotenberg, *Ann. Phys. (New York)* **19** (1962) 62.
[3] M. Rotenberg, *Adv. At. Mol. Phys.* **6** (1970) 233–268.
[4] V.A. Fock, *Z. Phys.* **98** (1935) 145.
[5] V.A. Fock, *Kgl. Norske Videnskab. Forh.* **31** (1958) 138.
[6] T. Shibuya, C.E. Wulfman, *Proc. Roy. Soc. A* **286** (1965) 376.
[7] B.I. Dunlap, *Chem. Phys. Lett.* **30** (1975) 39.
[8] B.R. Judd, *Angular Momentum Theory for Diatomic Molecules*, Academic Press, New York, 1975.
[9] T. Koga, T. Matsuhashi, *J. Chem. Phys.* **89** (1988) 983.
[10] J. Avery, *Hyperspherical Harmonics; Applications in Quantum Theory*, Kluwer Academic, Dordrecht, 1989.
[11] V. Aquilanti, S. Cavalli, D. De Fazio, G. Grossi, Hyperangular momentum: Applications to atomic and molecular science, in: C.A. Tsipis, V.S. Popov, D.R. Herschbach, J.S. Avery (Eds.), *New Methods in Quantum Theory*, Kluwer Academic, Dordrecht, 1996.
[12] V. Aquilanti, S. Cavalli, C. Coletti, G. Grossi, *Chem. Phys.* **209** (1996) 405.
[13] V. Aquilanti, S. Cavalli, C. Coletti, *Chem. Phys.* **214** (1997) 1.
[14] V. Aquilanti, S. Cavalli, C. Coletti, *Phys. Rev. Lett.* **80** (1998) 3209.
[15] V. Aquilanti, S. Cavalli, C. Coletti, D. Di Domenico, G. Grossi, *Int. Rev. Phys. Chem.* **20** (2001) 673.
[16] V. Aquilanti, A. Caligiana, *Chem. Phys. Lett.* **366** (2002) 157.
[17] V. Aquilanti, A. Caligiana, S. Cavalli, *Int. J. Quantum Chem.* **92** (2003) 99.
[18] V. Aquilanti, A. Caligiana, S. Cavalli, C. Coletti, *Int. J. Quantum Chem.* **92** (2003) 212.
[19] V. Aquilanti, A. Caligiana, in: E.J. Brändas, E.S. Kryachko (Eds.), *Fundamental World of Quantum Chemistry: A Tribute to the Memory of P.O. Löwdin, vol. I*, Kluwer Academic, Dordrecht, 2003, p. 297.
[20] E.J. Weniger, *J. Math. Phys.* **26** (1985) 276.
[21] O. Goscinski, *Adv. Quantum Chem.* **41** (2003) 51–85; Preliminary Research Report No. 217, Quantum Chemistry Group, Uppsala University, 1968.
[22] J. Avery, D.R. Herschbach, *Int. J. Quantum Chem.* **41** (1992) 673.
[23] V. Aquilanti, J. Avery, *Chem. Phys. Lett.* **267** (1997) 1.
[24] J. Avery, *J. Math. Chem.* **21** (1997) 285.
[25] J. Avery, F. Antonsen, *J. Math. Chem.* **24** (1998) 175.
[26] J. Avery, *J. Math. Chem.* **24** (1998) 169.
[27] J. Avery, *J. Mol. Struct.* **458** (1999) 1.
[28] J. Avery, *Adv. Quantum Chem.* **31** (1999) 201.
[29] J. Avery, *J. Mol. Struct. (Theochem)* **458** (1999) 1.
[30] J. Avery, R. Shim, *Int. J. Quantum Chem.* **83** (2000) 1.
[31] J. Avery, *J. Math. Chem.* **4** (2000) 279.
[32] J. Avery, R. Shim, *Int. J. Quantum Chem.* **79** (2000) 1.
[33] J. Avery, S. Sauer, *Many-Electron Sturmians Applied to Molecules*, in: A. Hernández-Laguna, J. Maruani, R. McWeeny, S. Wilson (Eds.) *Quantum Systems in Chemistry and Physics*, vol. 1, Kluwer Academic, 2000.
[34] J. Avery, *Hyperspherical Harmonics and Generalized Sturmians*, Kluwer Academic, Dordrecht, 2000.
[35] V. Aquilanti, J. Avery, *Adv. Quantum Chem.* **39** (2001) 71.
[36] J. Avery, R. Shim, *Int. J. Quantum Chem.* **83** (2001) 1.
[37] J. Avery, J. Avery, *J. Math. Chem.* **33** (2003) 145–162.
[38] J. Avery, J. Avery, *Adv. Quantum Chem.* **43** (2003) 185–206.
[39] J. Avery, J. Avery, O. Goscinski, *Adv. Quantum Chem.* **43** (2003) 207–216.

[40] A. Caligiana, Sturmian orbitals in quantum chemistry, Ph.D. thesis, University of Perugia, Italy, October, 2003.
[41] J. Avery, J. Avery, V. Aquilanti, A. Caligiana, *Adv. Quantum Chem.*, 2004, in press.
[42] J. Avery, J. Avery, *J. Phys. Chem.*, 2004, in press.
[43] V. Aquilanti, A. Caligiana, *J. Mol. Structure (Theochem)*, 2004, in press.
[44] NIST Atomic Spectra Database, National Institute of Standards and Technology (NIST), http://physics.nist.gov/asd.
[45] Atomic and Molecular Databases: Data for Autoionizing States, National Institute for Fusion Science (NIFS), http://dprose.nifs.ac.jp/DB/Auto/.
[46] L.A. Vainshtein, V.I. Safronova, *Wavelengths and Transition Probabilities of Satellites to Resonance Lines of H- and He-like Ions*, in: *Atomic Data and Nucl. Data Tables*, vol. 21, 1978, p. 49.
[47] L.A. Vainshtein, V.I. Safronova, *Dielectronic Satellite Spectra for Highly Charged H-like Ions and He-like Ions with* $Z = 6$-33, in: *Atomic Data and Nucl. Data Tables*, vol. 25, 1980, p. 311.

This page intentionally left blank

Mathematical Elements of Quantum Electronic Density Functions

Ramon Carbó-Dorca

Department of Inorganic and Physical Chemistry, Ghent University, Krijgslaan 281, B-9000 Gent, Belgium
and
Institut de Química Computacional, Universitat de Girona, Girona 17071, Catalonia, Spain

This contribution is dedicated to the memory of Professor Odd Gropen, University of Tromsø, Norway

Abstract

This chapter is a discussion on the electronic density functions formal structure and mathematical properties. A primary objective of this study is focused on the easy description of the quantum object concept, in connection with the quantum similarity measures framework. Several mathematical tools are discussed concerning the development of this task, among others: inward matrix products, extended Hilbert and Sobolev spaces, convex sets, vector semispaces, generating rules, diagonal representations, etc.

Contents

ADVANCES IN QUANTUM CHEMISTRY, VOLUME 49
ISSN: 0065-3276 DOI: 10.1016/S0065-3276(05)49003-6

1. INTRODUCTION

Early studies related to *electronic density function* (eDF) structure by Löwdin [1] and McWeeny [2–4], as well as the later contributions of several authors found in the literature within the following time period [5–8], and culminating in the *holographic density theorem* of Mezey [9], form the inspirational background of the present work.

Numerous papers issued from this laboratory recently have been devoted to the development of a specific framework able to be applied to the DF studies. Also included are many related theoretical branches and mathematical practical aspects, in an effort to construct the basis of a well-defined reference foundation of *quantum similarity* (QS) [10–22]. Central to such a mathematical evolution is the presence of DF's theoretical structure and computational algorithms, which has dominated as a leitmotiv many of the internal aspects of the published work. The obvious reason can be found in the fact that probability DF's are the basic material on which *QS measures* (QSM) are essentially built. The importance of DF within any quantum mechanical theoretical structure is, undoubtedly, a consequence of the crucial role DF plays in its basic composition [23,24], and this leading presence has been consequently transmitted into the general QS framework.

Within all these mentioned developments and characteristics, many aspects and properties of the DF are dispersed between varied, already published, material by this laboratory [25–28]. The present chapter aims to gather together all this information, while treating the most interesting aspects of DF general construction, structure and properties in more depth. Such an aim corresponds, finally, to the need of having a really well-established background, where the notion of *quantum object* (QO) [29–33] obtains a solid reference and can be unambiguously defined. Once the QO nature has been established, the definition of QSM becomes a straightforward task. At the same time, the various possible DF forms and their main characteristics will permit us to follow the path, where at the end can be found how to describe the approximate DF, essentially within the so-called

atomic shell approximation (ASA). The ASA DF can be helpful in simplifying some calculations, related to the superposition problem associated with the realm of *molecular QSM* (MQSM) [34] and for other purposes.

This prospect will be perhaps incomplete without mentioning the large amount of mathematical techniques, definitions and procedures related to the DF structure, which have been aggregated into the general framework, while QS theory has been developed. For instance: Tagged sets, convex conditions, generating rules, extended Hilbert spaces, vector semispaces, diagonal representations, inward matrix products, discrete molecular representations, quantum object sets and ensembles, quantum similarity matrices, quantum similarity indices, stochastic transformations, fundamental *quantum QSAR* (QQSAR) equations [35,36] and so on, are at this moment inseparable elements of the theory revolving around the DF conceptual background axis.

Owing to these previous considerations, the present chapter will be organized in the following way:

(A) Basic definitions will be given in order to provide the reader with a specific working language.
(B) The general properties and the generating rules for DF will be discussed.
(C) The inward matrix product will be introduced in order to discuss the intrinsic features of the DF structure and find the way to generally construct them.
(D) The DF discrete form generation and properties will be given and commented upon.
(E) Several examples of approximate DF forms as well as the possible method to construct them will be provided.
(F) Extended Hilbert spaces will be introduced as a manner to obtain a new extended DF family.
(G) Some problems related with the density and shape functions as elements of vector semispaces are finally discussed.

2. INITIAL DEFINITIONS

Numerous introductory definitions will be used to structure the main features of the DF theoretical background. They will try to put in a sound logical basis all the initial knowledge, which can be attached to the DF formalism. In addition, several applications could be obtained with a few fundamental items and the theory can be connected in this fashion to the general definition of QSM.

In order to achieve this preliminary objective, first the algorithm serving to establish the basis of the quantum mechanical background will be described.

ALGORITHM 1 (*Classical Quantum Mechanics*). For a given microscopic system:

(1) Construct the associated Hamilton operator: $\mathbf{H}$.
(2) Compute the state energy-wave function pairs, $\{E; \mathbf{\Psi}\}$ by solving Schrödinger equation: $\mathbf{H\Psi} = E\mathbf{\Psi}$.
(3) Evaluate the state DF's, $\rho = |\mathbf{\Psi}|^2$.

The third point of the previous algorithm can be studied and further developed using the following set of definitions.

2.1. Definitions related to the construction of DF

DEFINITION 1 (*Vector Semispace*). A *Vector Semispace* (VSS) over the *positive definite* (PD) real field $\mathbf{R}^+$, is a *Vector Space* (VS) with the vector addition part provided by a structure of Abelian *semigroup*.

By an additive semigroup [37] an additive group without the presence of reciprocal elements is understood. Thus, all VSS elements can be seen as directed towards the region of the positive axis associated with *all* involved coordinates. It will also be accepted that *null elements* can be chosen to be included in the scalar field as well as in the VSS structure. *Strict VSS* (SVSS) can be the name of all those VSS, which lack null elements. A VSS can be symbolized by means of the VS usual symbol, followed by the PD real field identification: $\mathbf{R}^+$ between parenthesis, for instance: $\boldsymbol{V}(\mathbf{R}^+)$. Examples of VSS or SVSS in theoretical chemistry are easy to furnish, because many aspects of chemical parameters are associated with an ordered PD set of scalars. An obvious molecular SVSS subset is constituted by the ordered set of the *interatomic distances*, $\mathbf{D} = \{d_{ij}\}$, associated with the possible conformations of a given molecular structure made of N atoms. Indeed, the upper triangle of the distance matrix for a given conformation, ordered as an $N(N-1)/2$-dimensional vector, e.g., $(d_{12}, d_{13}, d_{23}, \ldots, d_{N-1N})$, corresponds to an SVSS element. Another example, belonging to a ∞-dimensional space, is constituted by a set of DF possessing an equal number of variables. Any DF, defined according the third step of Algorithm 1, is a PD function for all variable values. PD linear combinations of DF are still PD. This property will appear several times within this chapter.

The construction of DF, can be organized by means of simple rules, which can be easily extended to finite-dimensional VSS.

DEFINITION 2 (*Continuous generating rule*). A *generating rule* can be easily written, summarizing the third step of the quantum mechanical Algorithm 1:

$$\boldsymbol{R}(\Psi \to \rho) = \left\{\forall \Psi \in \boldsymbol{H}(\mathbf{C}) \to \exists \rho = \Psi^* \Psi = |\Psi|^2 \in \boldsymbol{H}\left(\mathbf{R}^+\right)\right\}. \tag{1}$$

In equation (1) are given explicitly the wave function Hilbert VS [6,38], $\boldsymbol{H}(\mathbf{C})$, and the DF VSS, $\boldsymbol{H}(\mathbf{R}^+)$.

The next definition becomes a trivial useful symbol, which will be frequently employed in this chapter.

DEFINITION 3 (*Element sum of an* $(m \times n)$ *matrix* $\mathbf{A}$). For an $(m \times n)$ matrix $\mathbf{A} = \{a_{ij}\}$ designated by the symbol $\langle \mathbf{A} \rangle$ it is meant:

$$\langle \mathbf{A} \rangle = \sum_{i=1}^{m} \sum_{j=1}^{n} a_{ij}.$$

The same summation device, as given in Definition 3, is also a *Fortran 95* compiler intrinsic feature [39]. Moreover, this symbol acts as a linear functional over matrix spaces. It can be considered to apply also over the elements of a set where an additive operation is defined, so one can apply it over a given set $\mathbf{S} = \{s_i\}$, then:

$$\langle \mathbf{S} \rangle = \langle \{s_i\} \rangle = \sum_i s_i.$$

The sum symbol can even be extended and employed over function spaces, where the symbol can be exchanged by an integral. That is, it can be written:

$$\langle \rho(\mathbf{r}) \rangle = \int \rho(\mathbf{r})\, d\mathbf{r}.$$

The matrix elements summation symbol acting on arbitrary vectors or matrices, has been defined and employed some years ago [40] to ease the mathematical notation, as well as in order to define a mathematical symbol set, able to have an immediate translation into a high level programming language like Fortran 95; see, for example, [39].[1]

The summation symbol can also be associated with a linear operator, transforming vector semispace elements into scalars.

Also, *nested summation symbols* (NSS) [40] can be substituted by the sum symbol, like:

$$\langle \mathbf{Z} \rangle = \sum(\mathbf{i}) z(\mathbf{i}),$$

whereby: $\mathbf{i} = (i_1, i_2, \ldots, i_n)$ is symbolized by a set of n indices, which vary according to the NSS:

$$\sum(\mathbf{i}) = \sum_{i_1} \sum_{i_2} \cdots \sum_{i_n},$$

and thus:

$$\sum(\mathbf{i}) z(\mathbf{i}) \equiv \sum_{i_1} \sum_{i_2} \cdots \sum_{i_n} z_{i_1 i_2 \ldots i_n}.$$

From here, a particular N-dimensional form of the ∞-dimensional generating rule given in Definition 2 is readily constructed, allowing the connection of finite-dimensional VS with the infinite-dimensional ones with respect to the DF construction.

Given $\mathbf{W} = \{w_i\} \subset \mathbf{R}^+$ as representing any PD real numerical set, it can be supposedly generated using a complex coefficient set: $\mathbf{X} = \{x_i\} \subset \mathbf{C}$. This can be stated in this way, as the set of coefficients $\mathbf{W}$ can be obtained as the modules of the elements of $\mathbf{X}$: $w_i = |x_i|^2$, $\forall i$. Supposing we define a normalized column vector made with the elements of $\mathbf{X}$: $\mathbf{x} = \{x_i\}$, then the norm $\langle \mathbf{x} | \mathbf{x} \rangle = \mathbf{x}^+ \mathbf{x} = 1$ also corresponds to the last normalization condition in equation (4) below, related to a functional VSS.

For this purpose, the following *discrete generating rule* can be described, after collecting the elements of the set $\mathbf{W}$ into a column vector $\mathbf{w}$:

DEFINITION 4 (*Discrete generating rule*).

$$\boldsymbol{R}(\mathbf{x} \to \mathbf{w}) = \Big\{ \forall \mathbf{x} \in \boldsymbol{V}_N(\mathbf{C}) \to \exists \mathbf{w} = \left\{ w_i = x_i^* x_i = |x_i|^2 \right\} \in \boldsymbol{V}_N\left(\mathbf{R}^+\right) \\ \wedge\, \mathbf{x}^+ \mathbf{x} = \sum\nolimits_i x_i^* x_i = \sum\nolimits_i |x_i|^2 = 1 \to \langle \mathbf{w} \rangle = \sum\nolimits_i w_i = 1 \Big\}. \qquad (2)$$

It is time now to describe a typical first order DF form as a first step model to study other DF structures and extensions.

[1] In Fortran 90 and 95 compilers, an intrinsic function is present, which can be employed to sum up all the elements of a matrix. Such a compiler facility is called within the code by the function symbol written as: SUM([*Argument*]), with [*Argument*] being any previously defined as integer, real or complex *array* name.

DEFINITION 5 (*First order MO electronic DF*). The first-order eDF form, as expressed within MO theory, can be defined by means of the linear combination:

$$\rho(\mathbf{r}) = \sum_i w_i \left|\varphi_i(\mathbf{r})\right|^2. \tag{3}$$

Where the coefficient set $\mathbf{W} = \{w_i\} \subset \mathbf{R}^+$ corresponds to the real PD occupation indices of the MO set, $\{\varphi_i(\mathbf{r})\}$. This MO eDF, for example, within the LCAO approach, can also be written in a general way, as a double sum of products of function pairs, coupled with a set of the so-called charge and bond order matrix coefficients; see, for instance, [41,43]. However, a simple matrix diagonalization, followed by a unitary MO basis set transformation, can revert any DF to the formal expression in equation (3), [6,44–46]. Using an AO basis set $\boldsymbol{\chi} = \{\chi_\mu(\mathbf{r})\}$ to construct the MO within the so-called LCAO MO technique, we get:

$$\varphi_i(\mathbf{r}) = \sum_\mu c_{\mu i}\, \chi_\mu(\mathbf{r}),$$

then one can write:

$$\begin{aligned}\rho(\mathbf{r}) &= \sum_\mu \sum_\nu D_{\mu\nu}\chi_\mu(\mathbf{r})\chi_\nu^*(\mathbf{r}) = \sum_\mu \sum_\nu \left(\sum_i w_i c_{\mu i} c_{\nu i}^*\right)\chi_\mu(\mathbf{r})\chi_\nu^*(\mathbf{r}) \\ &= \sum_i w_i \left(\sum_\mu c_{\mu i}\chi_\mu(\mathbf{r})\right)\left(\sum_\nu c_{\nu i}\chi_\nu(\mathbf{r})\right)^* = \sum_i w_i \left|\varphi_i(\mathbf{r})\right|^2.\end{aligned}$$

Moreover, an MO unit norm convention could be also adopted:

$$\forall i, \quad \int |\varphi_i|^2\, d\mathbf{r} = 1 \quad \Rightarrow \quad \int \rho(\mathbf{r})\, d\mathbf{r} = \sum_i w_i \int |\varphi_i|^2\, d\mathbf{r} = \sum_i w_i = 1, \tag{4}$$

and these results present the PD occupation coefficient set $\mathbf{W} = \{w_i\}$ as a discrete probability distribution. When this kind of properties holds for a known set of functions, then they can be used to construct new functions possessing the same properties. This will be discussed below and later on in more detail in Sections 2.3.2 and 5.1.

From these considerations, the concept of convexity and the definition of convex set, as will be studied below, become necessary elements of the theory.

DEFINITION 6 (*Convex conditions*). By the term *convex conditions* over an N-dimensional vector $\mathbf{w}$ it is formally understood:

$$\boldsymbol{K}_N(\mathbf{w}) \equiv \left\{\mathbf{w} \in \boldsymbol{V}_N\left(\mathbf{R}^+\right) \wedge \langle \mathbf{w}\rangle = \sum_i w_i = 1\right\}. \tag{5}$$

The set of the vector elements, $\mathbf{w}$: $\mathbf{W} = \{w_i\}$, can be used instead in the convex conditions symbol, that is:

$$\boldsymbol{K}_N\left(\{w_i\}\right) \equiv \left\{\forall i\colon\ w_i \in \mathbf{R}^+ \wedge \langle \mathbf{W}\rangle = \sum_i w_i = 1\right\}. \tag{6}$$

Equations (5) and (6) can be considered the discrete counterparts of some *continuous* convex conditions, defining a convex DF:

$$\boldsymbol{K}_{\infty}(\rho) \equiv \left\{ \rho \in \boldsymbol{H}\left(\mathbf{R}^{+}\right) \wedge \langle \rho \rangle = \int \rho(\mathbf{r})\, d\mathbf{r} = 1 \right\}.$$

Convex sets (see, for example, [47,48]) play a leading role in optimization problems. They have been recently introduced to deal with some chemical problems [15a] related to shape analysis.

Elementary Jacobi rotations (EJR) [49] can be applied over a generating vector to obtain optimal coefficients, while preserving convex conditions [51], see also Section 5.2.

Convexity can be used for the construction of a new DF from a set of well-defined DFs. Suppose a set of convex DF associated with an arbitrary but homogeneous set of variables $\mathbf{R}$ is known, that is: $\mathsf{P} = \{\rho_I(\mathbf{R})\} \wedge \forall I\colon\ \boldsymbol{K}_{\infty}(\rho_I)$. Suppose a convex set of coefficients $\mathbf{W} = \{w_I\}$ is known, thus $\boldsymbol{K}(\mathbf{W})$ holds, and then the function

$$\rho(\mathbf{R}) = \sum_I w_I \rho_I(\mathbf{R})$$

is such that $\boldsymbol{K}_{\infty}(\rho)$ holds. This is an obvious consequence of the VSS linearity.

2.2. Definitions leading to quantum similarity measures

While the previous definitions are associated with the idea of DF and the related sets sharing its main properties, the set of definitions provided in this section have been used up to now in order to construct a pathway to the definition of QSM. They start with the concepts of Tagged Set and Tagged Ensembles.

DEFINITION 7 (*Tagged sets*). Let us suppose that a given set, the *Object Set*: $\boldsymbol{S}$, and another set, made of some chosen mathematical elements, which will be hereafter called tags, form a *Tag Set*: $\boldsymbol{T}$. A *Tagged Set*: $\boldsymbol{Z}$, can be constructed by means of the ordered product: $\boldsymbol{Z} = \boldsymbol{S} \times \boldsymbol{T}$, that is:

$$\boldsymbol{Z} = \left\{ \forall z \in \boldsymbol{Z} \mid \exists \sigma \in \boldsymbol{S} \wedge \exists \tau \in \boldsymbol{T} \rightarrow z = (\sigma, \tau) \right\}.$$

For example, a given molecular set taken *a priori* as an object set can be easily transformed into a tagged set, just considering as appropriate tags N-dimensional vectors with their elements associated with an ordered set of properties, attached in turn to any chosen molecule of the object set. The tags can be freely selected with respect to their information content. For instance, they can be made of physicochemical properties such as: boiling and melting points, molecular weight, density, solubility in several solvents, etc. However, the adopted vector tags must be *homogeneous* in the sense that they must contain the *same* kind of information, ordered in the *same* way, for every member of the tagged set. Also, the construction of *Boolean* tagged sets has been studied in previous papers [51–55]. Encompassing *fuzzy sets* as a particular case [59], the Boolean tagged sets constitute a very general example of how tagged sets can be built up. Boolean tagged sets are constructed using bit strings in the Tag Set part, thus they can be considered as a reduction of the information, gathered about the Object Set part, of a great class of Tagged Sets into a binary

tag form. This kind of transformation can be easily accomplished within molecular Tagged Sets, as described above.

Sets made of Tagged Sets are also worthy of being described and studied. The following definition uses the freedom of choice on the nature of the Object Set to allow the formation of larger structures.

DEFINITION 7′ (*Tagged Ensemble*). A Tagged Ensemble is a Tagged Set whose Object Set elements are Tagged Sets.

For example, *quantitative structure-properties relationships* (QSPR) studies could be described as the way where a connection has to be found between tagged objects belonging to a known tagged set and new tags, formed for instance by property values ordered as vectors, defining a Tagged Ensemble. This superstructure may be also considered a way to augment the information associated with a given object set. In order to describe another example, suppose a set of molecular structures, attached to a property vector. As each molecular structure can be associated in turn with a set of nuclear configurations, then to each molecule there can be associated a set of conformations connected, in turn, by means of the Born–Oppenheimer approximation, with a set of energy-DF pairs. Each set of conformers as objects with the pairs of energy-DF acting as tags can be easily considered as forming a tagged set. The former molecular property vector acts as a new tag attachable to each molecular conformer tagged set, the whole structure being a tagged ensemble.

DEFINITION 8 (*Quantum Object*). A *Quantum Object* can be defined as an element of a particular Tagged Set structure: Quantum Systems in well-defined states are taken as the Object Set part and the corresponding quantum DF, associated with the state of the object set elements constituting the Tag Set part.

A collection of Quantum Objects can be consequently called a *Quantum Object Set* (QOS), which becomes a particular kind of tagged set. For example, a set of molecules in well-defined nuclear conformations acting as objects can be transformed into quantum objects by constructing a tag set made by their first order ground state DF, computed for a fixed nuclear conformation. A set of ground state conformers of a given molecular structure or a set of excited states can be considered a QOS, provided that each conformer or each excited state respectively has a known homogeneous DF as a tag. *Homogeneity* in QOS definition and structure has to correspond to the necessary condition consisting in that all the DF tags, intervening in the QOS construction, shall be of the same order, being, thus, functions with the same amount of variables.

These previous definitions lead to the possibility of easily describing in a completely general way a QSM structure.

DEFINITION 9 (*General QSM*). A *General* QSM, $\gamma(\mathbf{\Omega})$, can be considered a PD multiple scalar product defined by a contracted ν-direct product of a QOS, $\boldsymbol{T}$:

$$\gamma(\mathbf{\Omega}) : \bigotimes_{K=1}^{\nu} \boldsymbol{T} \to \mathbf{R}^{+}.$$

This allows us to mix ν DF: $\{\rho_I(\mathbf{r}),\ I = 1, \nu\}$ of the QOS $\boldsymbol{\Gamma}$ with Ω PD operators, collected into a set, $\boldsymbol{\Omega} = \{\Omega_K(\mathbf{r}),\ K = 1, \Omega\}$, belonging to the same VSS, for example:

$$\gamma(\boldsymbol{\Omega}) = \int \left[\prod_{K=1}^{\Omega} \Omega_K(\mathbf{r})\right]\left[\prod_{I=1}^{\nu} \rho_I(\mathbf{r})\right] d\mathbf{r}, \tag{7}$$

where the coordinate vector, $\mathbf{r}$, shall be taken here as a general position vector.

Equation (7) can be interpreted as a quite free system to define generalized expectation values. A general picture of QSM was already given in references [51,60–62]. Section 4.1 will describe particular practical QSM forms and Section 6.1 below will study in detail the connection between QSM and expectation values.

2.3. Definitions related to the algebra of diagonal vector spaces and their applications

Diagonal vector spaces (DVS) are not only related to the construction of general DF but also with the *inward matrix product* (IMP), which will be discussed next in Section 3.1. For this reason DVS will be studied first. Another motivation to proceed in this way is historical, because DVS were used first [54] in connection with the study of DF, before the introduction of IMP for the same purpose.

Compared with Dirac's bra-ket formalism, DVS, except for the possibility to have their elements conjugated, lack the dual space distinction that bra-ket or row-column vectors have. A possible way to overcome this situation is to construct bra-ket diagonal matrices with the aid of a set of auxiliary matrices adopting the appropriate dimension. The following definition will be hereafter useful.

DEFINITION 10 (*Unity matrices*). A unity matrix, $\mathbf{1}$, is an $(n \times m)$ matrix whose elements are entirely made of the scalar multiplicative unit element: $[\mathbf{1}]_{ij} = 1, \forall i, j$. Unity row or column n-dimensional vectors may be also expressed by the symbols $\langle \mathbf{1}|$ and $|\mathbf{1}\rangle$, respectively.

Then, multiplying a given diagonal matrix by a unity matrix on the right or the left, respectively, can generate a bra-ket structure in diagonal spaces. To see this, it is only necessary to observe, for example, that if the diagonal matrix $\mathbf{D} = \mathrm{Diag}(d_i)$ is defined, then the matrix product $\mathbf{1D}$ generates the matrix $\{d_i|\mathbf{1}\rangle\}$, while the product in the alternative order is $\mathbf{D1} \equiv \{d_i\langle \mathbf{1}|\}$.

A tensorial product of two diagonal matrices can be obtained using the unity matrix of the appropriate dimension: $\mathbf{D} \otimes \mathbf{D} = \mathbf{D1D} = \{d_i d_j\}$.

The product of diagonal matrices can be a good vehicle to construct DF with the appropriate properties as discussed in the previous section. In the following section, the technique of constructing DF within the structure of diagonal vector spaces will be outlined as a first step to construct general DF structures based on IMP, which will be given later on.

2.3.1. The structure of the generating N-dimensional VS

The discrete generating rule as described in Definition 4 is a shorthand notation for some non-linear transformation involving the generating VS, $\boldsymbol{V}_N(\mathbf{C})$, and the Final VSS con-

taining the coefficient vectors, $\boldsymbol{U}_N(\mathbf{R}^+)$. The lack of a simple natural operation, producing the desired results, implicitly stated within the generating rule in the discrete case, can be circumvented using the following scheme.

Assume such an isomorphic pair of N-dimensional VS, which will be named $\boldsymbol{G}_N(\mathbf{C})$ and $\boldsymbol{F}_N(\mathbf{R}^+)$. Both can be good substitutes for the original $\boldsymbol{V}_N(\mathbf{C})$ and $\boldsymbol{U}_N(\mathbf{R}^+)$ VS described above, respectively. A sound isomorphism of column or row VS is constituted by DVS, whose elements possess the structure of diagonal matrices. Let us consider that the isomorphic $\boldsymbol{G}_N(\mathbf{C})$ and $\boldsymbol{F}_N(\mathbf{R}^+)$ VS are made of diagonal matrices. The choice has not been arbitrary, because matrix multiplication is closed in DVS, that is: matrix products of diagonal matrices yield diagonal matrices as a result. Moreover, diagonal matrix products are commutative. Considering only the diagonal part of the matrix elements, and discarding the off-diagonal elements, the DVS possess the same dimension as their isomorphic column–row vector counterparts. Then, it is easy to see that using this simple isomorphic device, both the continuous and discrete generating rules, as shown in Definitions 2 and 4, acquire the same formal structure. Indeed, the discrete rule in equation (2) will be rewritten within any DVS framework, as:

$$\begin{aligned}\boldsymbol{R}_N(\mathbf{D} \to \Delta) \equiv \Big\{ &\exists \mathbf{D} \in \boldsymbol{G}_N(\mathbf{C}) \wedge \langle \mathbf{D}^+\mathbf{D} \rangle = \sum_i |d_i|^2 = 1 \quad \Rightarrow \\ &\Delta = \mathbf{D}^+\mathbf{D} = \mathrm{Diag}\big(|d_i|^2\big) \wedge \langle \Delta \rangle = 1 \to \boldsymbol{K}_N(\Delta) \Big\}. \end{aligned} \tag{8}$$

The summation symbol, which is used in this case as in Definition 3 over the diagonal matrix $\mathbf{D}$:

$$\langle \mathbf{D} \rangle = \sum_i d_i,$$

can be made equivalent to the trace of the corresponding diagonal matrix. The convex condition, as set in Definition 6, has to be slightly modified to take into account the new DVS element structure:

$$\boldsymbol{K}_N(\Delta) = \left\{ \Delta = \mathrm{Diag}(\pi_i) \in \boldsymbol{F}_N\big(\mathbf{R}^+\big) \wedge \langle \Delta \rangle = \sum_i \pi_i = 1 \right\}. \tag{9}$$

Thus, working with DVS instead of conventional VS and VSS, the coefficients in discrete DF description possess the same structural properties as the DF themselves. The generating DVS elements, $\mathbf{D} \in \boldsymbol{G}_N(\mathbf{C})$, act in the same manner as the QO wave functions. And the resultant coefficient diagonal matrix, $\Delta \in \boldsymbol{F}_N(\mathbf{R}^+)$, satisfying the convex conditions $\boldsymbol{K}_N(\Delta)$, can be written as a squared module of the former diagonal matrix. This can be done using a discrete form of the generating rule, $\boldsymbol{R}_N(\mathbf{D} \to \Delta)$, similar to the wave function-DF generating rule:

$$\begin{aligned}\boldsymbol{R}_\infty(\Psi \to \rho) &\equiv \boldsymbol{R}_N(\mathbf{D} \to \Delta) \\ &= \big\{ \forall \mathbf{D} \in \boldsymbol{G}_N(\mathbf{C}) \to \\ &\quad \exists \Delta = \mathbf{D}^+\mathbf{D} = \mathbf{D}\mathbf{D}^+ = |\mathbf{D}|^2 = \mathrm{Diag}\big(|d_i|^2\big) \in \boldsymbol{F}_N\big(\mathbf{R}^+\big) \big\}. \end{aligned}$$

The $\boldsymbol{G}_N(\mathbf{C})$ DVS may be considered normed spaces, with one of the possible norms defined as the trace of the squared matrix module, which acts in this way as a sort of Euclidean norm. As a consequence, the DVSS: $\boldsymbol{F}_N(\mathbf{R}^+)$ elements are constructed in such a way that

their trace is always normalizable, and thus an easily made unit. That is, if: $\langle |\mathbf{D}|^2 \rangle \in \mathbf{R}^+$, then: $\Delta = |\mathbf{D}|^2$, can be straightforwardly transformed into Δ_N as to fulfil: $\langle \Delta_N \rangle = 1$.

A Diagonal Tagged Set, $\boldsymbol{D}_N$, can be derived in the usual way by using a given Object Set part, $\boldsymbol{S}$, and a DVSS convex subset, $\boldsymbol{K}$, as the Tag Set part, that is:

$$\boldsymbol{D}_N = \boldsymbol{S} \times \left\{ \boldsymbol{K} \subset \boldsymbol{F}_N\left(\mathbf{R}^+\right) \right\}.$$

The question, now, may *not* need to be: why do the N-dimensional DVS fulfil in a *natural way* the same conditions as the ∞-dimensional function VS? It could be much better stated as: which kind of consequences will produce this DVS characteristic feature in the development of a discrete quantum chemical framework? The next section will try to illustrate some of the possible features of this DVS structure.

2.3.2. Expression of the DF and other problems

It can be shown that the best discrete representation of the DF, when formally expressed as in equation (3), is described as a diagonal matrix instead of a vector as is customary. Then, the *scalar-like* expression of this DF type must be redefined in terms of the operations presented in the discussion of the preceding section.

In order to obtain a coherent image of all the possible redefinitions, which can be found as a consequence of the adoption of the DVS representation, it will be worthwhile to make some preliminary considerations, as follows:

The DF generating rule formal structure is better represented from the point of view of diagonal matrices instead of column–row vectors.

Thus, both the generating and coefficient vectors are transformed into elements of some DVS. The DF form presented in Definition 5, besides the coefficient vector, are associated with a PD function set, which is in turn connected to the squared module of another function set, further belonging to another structure, which can be named as a Generating Functional VS. This situation can be managed in the same way as in the preceding discussion on DVS.

Suppose now that a function basis set is known: $\Phi = \{\varphi_i\}$. Nothing opposes the situation in which the set Φ can always, without loss of generality, be arranged into a diagonal matrix structure, and considered constructed as $\Phi = \mathrm{Diag}(\varphi_1, \varphi_2, \ldots, \varphi_N) \in \boldsymbol{F}(\mathbf{C})$.

Then, it is obvious that when the following diagonal matrix product is made:

$$\mathsf{P} = \Phi^* \Phi = \mathrm{Diag}\left(|\varphi_1|^2, |\varphi_2|^2, \ldots, |\varphi_N|^2\right) \in \boldsymbol{P}\left(\mathbf{R}^+\right),$$

it will always produce a new diagonal matrix, whose elements belong to a special Functional VSS made of PD functions, that is: made of function squared modules. Thus, taking into account the definition of the diagonal product of the initial basis set, one can consider that the result above produces an entirely new PD basis set: $\boldsymbol{P} = \{|\varphi_i|^2\}$.

Also, having defined the generating and coefficient VS, one can construct the following hybrid diagonal matrix:

$$\begin{aligned} &\forall \mathbf{D} = \mathrm{Diag}(d_i) \in \boldsymbol{G}(\mathbf{C}) \wedge \forall \Phi = \mathrm{Diag}(\varphi_i) \in \boldsymbol{F}(\mathbf{C}) \quad \Rightarrow \\ &\quad \Psi = D\Phi = \mathrm{Diag}(d_i \varphi_i) \in \boldsymbol{P}(\mathbf{C}) \subseteq \boldsymbol{G}(\mathbf{C}) \times \boldsymbol{F}(\mathbf{C}). \end{aligned} \tag{10}$$

Once we have constructed this kind of mixed structures, then the DF can be simply built up by computing traces of squared modules of the diagonal structures, Ψ, as defined in

equation (10) above. That is:

$$\rho = \langle \Psi^* \Psi \rangle = \sum_i |d_i \varphi_i|^2 = \sum_i |d_i|^2 |\varphi_i|^2 = \sum_i \Omega_i \rho_i . \tag{11}$$

The formalism appears now clear on how we should construct the necessary generating elements and the road is open to obtain, in a very natural way, the DF structure. The most interesting aspect of the whole procedure, perhaps, will consist in finding out how closely the deducible formal rules, based on discrete DVS, are equivalent to the formalism based on continuous Quantum Mechanics.

In fact, it only remains to express the formal problem, on how an expectation value $\langle \Omega \rangle$ of some observable, associated with an operator Ω, can be computed within the DVS formalism. A possible way could be written using the diagonal matrix algebra properties as:

$$\begin{aligned} \langle \Omega \rangle &= \int \Omega \rho \, dV = \int \Omega \langle \Psi^* \Psi \rangle \, dV = \sum_i |d_i|^2 \int \Omega |\varphi_i|^2 \, dV \\ &= \sum_i \Omega_i \int \Omega \rho_i \, dV \equiv \sum_i \Omega_i \int \varphi_i^* \Omega \varphi_i \, dV = \int \langle \Psi^* \Omega \Psi \rangle \, dV . \end{aligned} \tag{12}$$

The last linear combination of integrals is suited to differential operators, and can be naturally obtained when considering the operator Ω as a scalar matrix: $\Omega \mathbf{I}$. In Section 6 below, the structure of equalities like (12) will be studied in more detail and extended.

3. INWARD MATRIX PRODUCT: DEFINITIONS, PROPERTIES AND EXAMPLES

Fortran 95 contains as a built in feature [39] the Hadamard, Schur or, perhaps a better terminology, the *inward matrix product* (IMP). Such a matrix product is defined between two matrix structures, belonging to the same matrix space. As IMP has been previously used in several papers, related with quantum chemical applications [56,63,69], it will be presented here as a first step to describe its connection with DF structure and generalization. IMP is related to the DVS product structure, and as such can be seen as some sort of generalization of the diagonal matrices product to the general matrix VS. Curiously enough, IMP is scarcely referenced in the current literature, mainly in footnotes in a few books [57].

IMP can be widely used in quantum mechanics for various purposes. In this section, some pages are devoted to this, just to show the simplicity of the concepts that can be built up around it and the interesting problems where IMP can be employed.

3.1. Inward matrix product[2]

IMP can be defined in a simpler way than the classical matrix product, as the associated structure mimics the matrix addition. The next definition tries to provide a general form of this matrix operation.

[2] From now on either the term matrix or hypermatrix will be used in reference to IMP. Such product can be applied either to matrices or hypermatrices, without changing anything but the structure of the involved mathematical objects.

DEFINITION 11 (*Inward matrix product (IMP)*). Consider any arbitrary hypermatrix space over a field: $\boldsymbol{M}_{(\times\mathbf{n})}(\mathbf{R})$. Let $\mathbf{A}, \mathbf{B} \in \boldsymbol{M}_{(\times\mathbf{n})}$. An IMP involving the hypermatrix pair is a closed operation, resulting in a new hypermatrix $\mathbf{P} \in \boldsymbol{M}_{(\times\mathbf{n})}$, and symbolized by: $\mathbf{P} = \mathbf{A} * \mathbf{B}$, whose elements are defined by the algorithm:

$$\forall(\mathbf{i}):\ p(\mathbf{i}) = a(\mathbf{i})b(\mathbf{i}).$$

Above, the elements of the involved hypermatrices are identified by means of an index vector $(\mathbf{i}) \equiv (i_1; i_2; \ldots; i_p)$. Thus, one can consider that the hypermatrix space dimension is given by $(\times\mathbf{n}) \equiv (n_1 \times n_2 \times \cdots \times n_p)$. The notation follows a previous one, employed when dealing with NSS structures [40].

3.1.1. IMP general features

Having presented the simple definition of IMP, some of the most interesting properties and applications will be provided. IMP acts over hypermatrix spaces almost as if hypermatrices were treated as a product of scalars; this attractive feature can be employed in quantum chemistry computational problems (see, for example, [56,63,68,69]) as well as in the development of new theoretical structures, which can present the peculiarity of being easily transferable to a high level programming language like Fortran 95.

3.1.1.1. IMP properties. The following properties can be attached to the IMP, defined over the elements of an arbitrary hypermatrix space $\boldsymbol{M}_{(\times\mathbf{n})}$, provided that it is defined over a field, which is the usual case. IMP, when defined over vectors defined in turn over a field, is distributive with respect to the matrix sum, as well as associative, and commutative [56].

The interest in defining such a matrix product stems from the possibility to attach to it the most usual features of a multiplication composition rule. The following properties can be attached to the IMP:

Let $\mathbf{A}, \mathbf{B}, \mathbf{C}, \ldots, \in \boldsymbol{M}_{(\times\mathbf{n})}$. IMP defined over them are:

(1) Distributive with respect matrix sum:

$$\mathbf{A} * (\mathbf{B} + \mathbf{C}) = \mathbf{A} * \mathbf{B} + \mathbf{A} * \mathbf{C}.$$

(2) Associative:

$$\mathbf{A} * \mathbf{B} * \mathbf{C} = \mathbf{A} * (\mathbf{B} * \mathbf{C}) = (\mathbf{A} * \mathbf{B}) * \mathbf{C}.$$

(3) Commutative:

$$\mathbf{A} * \mathbf{B} = \mathbf{B} * \mathbf{A}.$$

From the inspection of these properties, it is easy to see that IMP acts over matrix spaces in the same way as the matrix product in DVS.

3.1.1.2. IMP unit element and inverse. Also, an Inward Unit Element exists, which can be called the *unity* matrix, $\mathbf{1} \in \boldsymbol{M}_{(\times\mathbf{n})}$, as given in Definition 10, such that:

$$\mathbf{1} * \mathbf{A} = \mathbf{A} * \mathbf{1} = \mathbf{A}.$$

Using the real multiplication unit it can be defined as:

$$\mathbf{1} = \big\{1(\mathbf{i}) = 1,\ \forall(\mathbf{i})\big\}.$$

The existence of an IMP Inverse is subject to the following important limitations imposed by the following definition:

DEFINITION 12 (*Inwardly invertible matrices*). If $\mathbf{A} = \{a(\mathbf{i})\} \wedge \forall(\mathbf{i})$: $a(\mathbf{i}) \neq 0$; then $\mathbf{A}$ can be called *inwardly invertible or regular*. A new matrix defines the IMP inverse of a matrix $\mathbf{A}$: $\mathbf{A}^{[-1]} = \{a^{[-1]}(\mathbf{i})\}$, with elements, which are computed as follows: $\forall(\mathbf{i})$: $a^{[-1]}(\mathbf{i}) = (a(\mathbf{i}))^{-1}$. This definition produces the sequence of equalities: $\mathbf{A} * \mathbf{A}^{[-1]} = \mathbf{A}^{[-1]} * \mathbf{A} = \mathbf{1}$.

These IMP properties are sufficient to define a commutative algebra over any matrix vector space. One can refer to this kind of algebra as *Hadamard or Schur algebra*.

3.1.1.3. IMP powers and functions. IMP powers of a given hypermatrix $\mathbf{A}$ are readily defined as $\mathbf{A}^{[p]} = \{a(\mathbf{i}, \mathbf{j})^p\}$. The square bracket enveloping the exponent is used here to distinguish an IMP power from the one defined involving classical products. For example, whenever $\mathbf{Z} = \mathbf{A} * \mathbf{A}$, then the matrix, $\mathbf{A}$, can be also considered as the IMP square root of $\mathbf{Z}: \mathbf{A} = \mathbf{Z}^{[1/2]} \rightarrow \forall \mathbf{i}, \mathbf{j}$: $a(\mathbf{i}, \mathbf{j}) = \sqrt{z(\mathbf{i}, \mathbf{j})}$.

IMP functions of a given hypermatrix are also easy to define: $\phi[\mathbf{Z}] = \{\phi(z(\mathbf{i}, \mathbf{j}))\}$. As noted in a previous paper [56], and put in evidence, when remembering the discussion on DVS performed in Section 2.3 above; IMP algebra is tightly related to diagonal matrix computational algorithms and the above definitions are the consequence of another shared isomorphic characteristic between DVS and VS associated with an IMP.

3.2. IMP applications

Having described the main features of the IMP and in order that the reader can grasp the interest of such a simple computational structure, two application examples will now be presented and, afterwards, a mathematical development involving the sign part of matrices discussed. This last development connects IMP with tagged set structures.

3.2.1. IMP and Taylor series expansions of multivariate functions

A Taylor series of a multivariate function, $f(\mathbf{x})$, in the neighborhood of a point $\mathbf{x}_0$ could be expressed in a simple form using the IMP of two tensors, as:

$$f(\mathbf{x}) = \sum_{p=0}^{\infty} \left\langle \partial_p \left[f(\mathbf{x}_0) \right] * \otimes_p [\mathbf{x} - \mathbf{x}_0] \right\rangle.$$

Where the symbol $\partial_p[f(\mathbf{x}_0)]$ collects all the pth order partial derivatives of the function evaluated at $\mathbf{x} = \mathbf{x}_0$; and $\otimes_p[\mathbf{x} - \mathbf{x}_0]$ collects the elements of the pth order tensorial product of the vector difference argument. It must be noted that the following conventions must be supposed to hold: $\partial_0[f(\mathbf{x}_0)] = f(\mathbf{x}_0)$ and $\otimes_0[\mathbf{x} - \mathbf{x}_0] = 1$.

This IMP application constitutes a very good example of the vast possibilities presented by the IMP.

3.2.2. Scalar product of two hypermatrices

The IMP involving two hypermatrices can be trivially related to scalar products. If such a scalar product is defined, using a NSS [40], as:

$$\langle \mathbf{A}|\mathbf{B}\rangle = \sum(\mathbf{i})a(\mathbf{i})b(\mathbf{i}),$$

then, we also employ the auxiliary definition $\langle \mathbf{A}\rangle = \sum(\mathbf{i})a(\mathbf{i})$, as provided in Definition 3, to symbolize the sum of all elements of a given hypermatrix. Then, the following equality might be immediately written:

$$\langle \mathbf{A}|\mathbf{B}\rangle = \langle \mathbf{A} * \mathbf{B}\rangle.$$

As an application example of this definition, a special property of quadratic forms can be studied. A quadratic form involving the hypermatrix $\mathbf{A}$ and the hypervector $\mathbf{x}$ may be written accordingly:

$$q(\mathbf{x}) = \mathbf{x}^T\mathbf{A}\mathbf{x} = \sum(\mathbf{i})\sum(\mathbf{j})a(\mathbf{i},\mathbf{j})x(\mathbf{i})x(\mathbf{j}).$$

It is well known that if $\mathbf{A}$ is positive definite, then $\forall \mathbf{x} \neq \mathbf{0} \rightarrow q(\mathbf{x}) > 0$. The quadratic form above can be also written constructing a tensorial product of the variable vector employing the algorithm: $\mathbf{T} = \mathbf{x} \otimes \mathbf{x} = \{t(\mathbf{i},\mathbf{j}) = x(\mathbf{i})x(\mathbf{j})\}$. Then, the following IMP construction of the quadratic form will also be possible:

$$q(\mathbf{x}) = \langle \mathbf{A} * \mathbf{T}\rangle = \sum(\mathbf{i})\sum(\mathbf{j})a(\mathbf{i},\mathbf{j})t(\mathbf{i},\mathbf{j}). \tag{13}$$

The above expression can be analyzed by means of an interesting structure, which can be associated with any matrix: the *matrix signature*. Some details will be given below.

3.2.3. Sign separation in hypermatrix spaces and IMP

In the following description, hypermatrix spaces are used in order to provide the reader with a general situation; of course, when substituting the term hypermatrix by matrix everything continues to hold in the same way, except dimensions. Considering this, suppose any hypermatrix space defined over the real field: $\boldsymbol{M}_{(\times\mathbf{n})}(\mathbf{R})$. A separation between the numeric absolute values of the hypermatrix elements and their signs can be made using two sets: a hypercube made of Boolean strings as elements, $\boldsymbol{H}_{(\times\mathbf{n})}(\mathbf{B})$, with $\mathbf{B} = \{0, 1\}$ acting as the sign symbols $\{-1, +1\}$, respectively, and a VSS, $\boldsymbol{M}_{(\times\mathbf{n})}(\mathbf{R}^+)$. The signs are collected in an array with the same shape as the elements of the parent hypermatrix space, constituting the elements of the hypercube $\boldsymbol{H}_{(\times\mathbf{n})}$, of cardinality $2^{(\times\mathbf{n})}$. Finally, the part made by the positive numeric hypermatrix elements will be associated with the VSS structure $\boldsymbol{M}_{(\times\mathbf{n})}(\mathbf{R}^+)$. Thus, employing the above commented partition, any real hypermatrix can be written by means of some IMP like:

$$\forall \mathbf{A} \in \boldsymbol{M}_{(\times\mathbf{n})}(\mathbf{R}):\ \mathbf{A} = {}_A\mathbf{s} * {}_+\mathbf{A},$$
$$\text{where } {}_A\mathbf{s} \in \boldsymbol{H}_{(\times\mathbf{n})}(\mathbf{B}) \wedge {}_+\mathbf{A} \in \boldsymbol{M}_{(\times\mathbf{n})}\left(\mathbf{R}^+\right).$$

Then, in this case, the IMP involving two hypermatrices can be defined, for example, as:

$$\forall \mathbf{A}, \mathbf{B} \in \boldsymbol{M}_{(\times\mathbf{n})}(\mathbf{R}):\ \mathbf{A} * \mathbf{B} = ({}_A\mathbf{s} * {}_+\mathbf{A}) * ({}_B\mathbf{s} * {}_+\mathbf{B}) = ({}_A\mathbf{s} * {}_B\mathbf{s}) * ({}_+\mathbf{A} * {}_+\mathbf{B}).$$

3.2.4. Sign separation in hypermatrix spaces and Boolean tagged sets: Hypermatrix signature

This last trivial relationship is not the unique IMP-based manipulation one can perform on hypermatrix spaces. For instance, the same discussed relationship may be used to transform hypermatrix spaces into Boolean tagged sets. In the present section, this possibility will now be discussed.

In order to demonstrate that any hypermatrix space can be transformed into a Boolean tagged set, first assume the following partition of the real field, $\mathbf{R}$, into two sets: $\mathbf{R} = \mathbf{R}^+ \cup \mathbf{R}^- \wedge \mathbf{R}^+ \cap \mathbf{R}^- = \{0\}$. An isomorphic Boolean tagged set, $\mathbf{S}$, to the real line, $\mathbf{R}$, can be defined in the following way:

$$\forall r \in \mathbf{S}\colon\ r = (\sigma; \rho) \wedge \sigma \in \mathbf{B} = \{0, 1\}; \quad \rho \in \mathbf{R}^+ \rightarrow \mathbf{S} = \mathbf{B} \times \mathbf{R}^+.$$

Thus, the Boolean tag, σ, acts as the sign of the strictly positive real object, ρ. Then, the Boolean tagged set, $\mathbf{S}$, can be decomposed into a pair of disjoint sets, in a similar way but not exactly equivalent as before:

$$\mathbf{S} = \mathbf{S}^+ \cup \mathbf{S}^- \wedge \mathbf{S}^+ \cap \mathbf{S}^- = \emptyset.^{3}$$

This second relationship is due to the fact that provided it is assumed in this Boolean tagged set context that $0 \in \mathbf{R}^+$ holds, two kinds of neutral elements can be defined: $(0; 0) \in \mathbf{S}^- \wedge (1; 0) \in \mathbf{S}^+$. Moreover, both Boolean tagged sets, $\mathbf{S}^+$ and $\mathbf{S}^-$, are isomorphic. Remembering Definition 7, it is a straightforward matter to construct now Boolean tagged sets from hypermatrix objects, whose elements are defined over $\mathbf{R}$.

To exemplify this last statement, suppose as before any hypermatrix vector space: $\boldsymbol{M}_{(\times\mathbf{n})}(\mathbf{R})$. A Boolean tagged set can be made using $T = \boldsymbol{H}_{(\times\mathbf{n})}(\mathbf{B}) \times \boldsymbol{M}_{(\times\mathbf{n})}(\mathbf{R}^+)$, where the Boolean tags are chosen, in the same way as in Section 3.2.3 above, as elements of some hypercube $\boldsymbol{H}_{(\times\mathbf{n})}$, of cardinality $2^{(\times\mathbf{n})}$, arranged in the same shape as in the associated hypermatrix space.

Therefore, any Boolean tagged set hypermatrix element could be connected to the structure:

$$\forall \mathbf{A} \in T\colon\ \mathbf{A} = ({}_{A}\mathbf{s};\ {}_{+}\mathbf{A}), \quad \text{where: } {}_{A}\mathbf{s} \in \boldsymbol{H}_{(\times\mathbf{n})}(\mathbf{B}) \wedge {}_{+}\mathbf{A} \in \boldsymbol{M}_{(\times\mathbf{n})}\left(\mathbf{R}^+\right).$$

The Boolean tags, in this case, represent the collection of the hypermatrix signs arranged in the same order, shape and dimension as they appear in the parent hypermatrix. One can refer to the tag part of this kind of Boolean tagged set as the *attached hypermatrix object signature*, or simply by the hypermatrix signature. When necessary, a specific hypermatrix signature can be symbolized by ${}_{A}\mathbf{s} = \text{Sign}(\mathbf{A})$. Any signature attached to a given hypermatrix space, due to the usual properties of Boolean algebras [58], can have a dual or antisymmetric one, that is: $\forall\, {}_{A}\mathbf{s} \in \boldsymbol{H}_{(\times\mathbf{n})} \rightarrow \exists(0 \cdot {}_{A}\mathbf{s}) \in \boldsymbol{H}_{(\times\mathbf{n})}$, where all the signs of the initial signature become changed. For example, to the unity signature there corresponds the null signature: $\mathbf{1} \rightarrow \mathbf{0} = (0 \cdot \mathbf{1})$. In a logical context, one can use the expression: $\forall\, {}_{A}\mathbf{s} \rightarrow \exists\neg\, {}_{A}\mathbf{s}$.

[3] The set $\mathbf{S}$ possesses a natural product definition: $(\sigma_a; \rho_a) \circ (\sigma_b; \rho_b) = (\sigma_a \circ \sigma_b; \rho_a \circ \rho_b)$, which has attached the same properties as in $\mathbf{R}$. However, addition does not have so clear and immediate attributes, due to the sign separation from the number body. A special algorithm shall be prepared for classical sum definition, involving the notion of order in $\mathbf{R}^+$.

In case a unity signature has to be associated with a given hypermatrix, $\mathbf{A}$ say, or $\mathrm{Sign}(\mathbf{A}) = \mathbf{1}$, this is equivalent to considering all the hypermatrix elements positive: $\forall \mathbf{i}, \mathbf{j}\colon a(\mathbf{i}, \mathbf{j}) \in \mathbf{R}^+$. See Definition 10 for more details on the unity hypermatrix.

With respect to the previous discussion on hypermatrix signatures, the following definition will be interesting.

DEFINITION 13 (*Strictly positive matrices*). Any matrix $\mathbf{A} = \{a_{ij}\}$ with elements belonging to $\mathbf{R}^+$, that is $\forall i, j\colon a_{ij} \in \mathbf{R}^+$, can be called *strictly positive* and noted as $\mathbf{A} * > 0$ and consequently $\mathrm{Sign}(\mathbf{A}) = \mathbf{1}$.

Signatures are sufficient to classify the entire hypermatrix set in $2^{(\times \mathbf{n})}$ isomorphic classes. In addition, any hypermatrix class obtained in this way can be made isomorphic to the VSS: $\boldsymbol{M}_{(\times \mathbf{n})}(\mathbf{R}^+)$, that is to the class of the strictly positive matrices. Alternatively, owing to the possible translation of Boolean strings into integers, the Boolean signature tags, conveniently transformed, might also be used to order a given hypermatrix subset. With all this in mind, then it is easy to define a relevant product within the hypermatrix Boolean tag set. Using the IMP definition on both the Boolean tags and objects, in such a way that:

$$\forall \mathbf{A}, \mathbf{B} \in T\colon\ \mathbf{A} * \mathbf{B} = ({}_A\mathbf{s} * {}_B\mathbf{s};\ {}_+\mathbf{A} * {}_+\mathbf{B}) \in T.$$

The same can be done with respect to the addition. Adopting a Boolean algebra structure on the Boolean tag elements [51,58], then the whole construct results in such a hypermatrix Boolean tagged set possessing a structure of Hadamard Algebra, see Section 3.1.1.2.

Consequently, it can be concluded that IMP, associated with the Boolean tagged sets of hypermatrix spaces, provides not only a trivial connection to fuzzy set theory [51,53,59], but opens the way to exotic hypermatrix manipulation possibilities. An additional feature, as commented before, consists in that all operations, discussed here or later imagined, could be directly connected to the usual electronic computational structure and programmed at once in a compact way.

3.2.5. Quadratic form signature and strictly positive matrices

Taking into account the matrix signature just defined, and returning to the quadratic form described in equation (13) whenever

$$\mathrm{Sign}(\mathbf{A}) = \mathrm{Sign}(\mathbf{T}) \rightarrow \mathrm{Sign}(\mathbf{A} * \mathbf{T}) = \mathbf{1}$$

holds, then, in this particular circumstance it is always assured that: $q(\mathbf{x}) > 0$ holds. It can be concluded in quadratic form evaluation, when a variable hypervector, $\mathbf{x}$, is chosen such that the following signature relationship holds:

$$\mathrm{Sign}(\mathbf{x}) \otimes \mathrm{Sign}(\mathbf{x}) = \mathrm{Sign}(\mathbf{A}),$$

that this will provide a positive value of the quadratic form.

When a unity signature is present in the hypermatrix $\mathbf{A} * > 0$, the quadratic form positive values, $q(\mathbf{x}) > 0$, will be always assured, when signature $\mathbf{1}$ is chosen in the variable hypervector, that is: $\mathbf{x} * > 0$. This corresponds that within VSS, quadratic forms are PD.

3.3. Normed vector semispaces: Minkowski norm

After this previous discussion intended to make evident the basic nature of vector semispaces, it is time to start a discussion on the natural semispace metric features.

3.3.1. Minkowski norm

A natural norm can be easily adopted in semispaces, and it seems that the most immediate rule at hand for such a task becomes a *Minkowski norm*. Indeed, as vector semispace elements are positive definite, a sum of their components within matrix semispaces, or the integral of the function, when dealing with infinite-dimensional probability density semispaces, will produce a positive real number in any case.

As an example of such a Minkowski norm definition, let us choose a matrix semispace of dimension $(m \times n)$, $\boldsymbol{M}_{(m\times n)}(\mathbf{R}^+)$, supposing in addition that the basic construction algorithm holds:

$$\forall \mathbf{A} \in \boldsymbol{M}_{(m\times n)}\left(\mathbf{R}^+\right) \rightarrow \mathbf{A} = \{a_{ij}\} \wedge \forall i, j\colon a_{ij} \in \mathbf{R}^+.$$

3.3.2. Matrix summation symbols on matrices

Then, a Minkowski norm in such a semispace can be simply symbolized by $\langle \mathbf{A} \rangle$ and computed by means of the algorithm associated with Definition 3:

$$\langle \mathbf{A} \rangle = \sum_i \sum_j a_{ij} \in \mathbf{R}^+.$$

Also, as commented before in Section 2.1, as another example of a Minkowski norm, it is worthwhile to consider the domain of Hilbert semispaces, $\boldsymbol{H}(\mathbf{R}^+)$, where quantum density functions, $\rho(\mathbf{r})$, can be considered as their elements, that is: $\rho(\mathbf{r}) \in \boldsymbol{H}(\mathbf{R}^+)$. There, in the present context, the Minkowski norm is immediately defined as the integral over the appropriate domain of a given function:

$$\left\langle \rho(\mathbf{r}) \right\rangle = \int_D \rho(\mathbf{r})\, d\mathbf{r} \in \mathbf{R}^+.$$

The real positive definite result is a consequence of the real positive definite nature over the domain D, associated by construction to quantum density functions in particular. The same definition can be applied to any set of continuous statistical probability density functions.

3.4. Shell structure in vector semispaces

Vector semispaces possess a characteristic structure, which can be easily exploited in manipulations and property seeking among its member elements. This section is devoted to find out the most relevant outcomes.

3.4.1. α-shells

An interesting albeit immediate application of Minkowski norms can be employed to classify vector semispaces in terms of shells. An *α-shell*, $S(\alpha)$, is defined as a closed subset of a vector semispace, whose elements possess the same Minkowski norm α, that is:

$$S(\alpha) \subset \boldsymbol{V}\left(\mathbf{R}^+\right) \rightarrow \forall \mathbf{x} \in S(\alpha)\colon\ \langle \mathbf{x} \rangle = \alpha.$$

From all the possible shells the *unit shell*, $S(1)$, is the most representative of these elements belonging to a vector semispace, as it is straightforward to demonstrate that from the elements of the unit shell any α-shell element can be constructed, or:

$$\forall \mathbf{a} \in S(\alpha) \rightarrow \exists \mathbf{x} \in S(1)\colon\ \mathbf{a} = \alpha \mathbf{x},$$

and conversely:

$$\forall \mathbf{x} \in S(1) \rightarrow \exists \mathbf{a} \in S(\alpha)\colon\ \mathbf{x} = \alpha^{-1} \mathbf{a}.$$

3.4.2. Homotheties and convex sets

Thus, any α-shell belonging to a given vector semispace is nothing else but a *homothety* of the unit shell. Therefore, and because of the possible primordial role that semispaces can take in order to construct vector spaces, as discussed above, it can be immediately deduced that the unit shell, being the core to construct any other shell in semispaces, can also be considered the ultimate core to generate any vector space.

Moreover, the α-shells in vector semispaces are *convex sets*; see, for example, [96,97]. In order to see this property fulfilled for any arbitrary α-shell, it is worthwhile to define a *convex condition symbol* over a set of appropriate scalars. By the symbol, $K(\{w_I\})$, associated with a known set of scalars $\{w_I\}$, according to Definition 6, we can now understand the pair of features:

$$K\left(\{w_I\}\right) = \left[\forall I\colon\ w_I \in \mathbf{R}^+ \wedge \sum_I w_I = 1\right].$$

Thus, knowing an arbitrary set of vectors belonging to a given α-shell: $\{\mathbf{x}_I\} \in S(\alpha)$ and a convex condition symbol over a known scalar set, $K(\{w_I\})$, then the convex linear combination

$$\mathbf{z} = \sum_I w_I \mathbf{x}_I$$

belongs to the same α-shell as the generating vectors:

$$\langle \mathbf{z} \rangle = \sum_I w_I \langle \mathbf{x}_I \rangle = \alpha \sum_I w_I = \alpha \rightarrow \mathbf{z} \in S(\alpha).$$

3.4.3. Semispace partition and equivalence classes

This last property indicates that any vector semispace can be considered as the union of all of its shells:

$$\boldsymbol{V}_N\left(\mathbf{R}^+\right) = \bigcup_{\forall \alpha \in \mathbf{R}^+} S(\alpha).$$

Still more interesting is the property by which semispace shells are disjoint sets, that is:

$$\forall S(\alpha), S(\beta) \subset \boldsymbol{V}_N\left(\mathbf{R}^+\right)\colon\ S(\alpha) \cap S(\beta) = \emptyset.$$

This allows saying semispaces are *partitioned* by the α-shell structure. In consequence, the α-shells themselves can be considered *equivalence classes* of the semispace [97].

3.4.4. Shell direct sums

A *shell sum* corresponds to another shell, with their elements possessing a Minkowski norm, which is the sum of those associated with the involved shell norm values, that is:

$$S(\alpha) + S(\beta) = \Sigma \to \Sigma \equiv S(\alpha + \beta).$$

To prove this, we simply need to define the shell sum in the usual way:

$$\Sigma = \left\{s \mid s = a + b\colon\ a \in S(\alpha) \wedge b \in S(\beta)\right\},$$

then the elements of the shell sum possess the property:

$$s \in \Sigma \to s = a + b \to \langle s\rangle = \langle a + b\rangle = \langle a\rangle + \langle b\rangle = \alpha + \beta$$
$$\Rightarrow \quad \Sigma = S(\alpha + \beta).$$

Moreover, the shells being disjoint sets as commented above, the shell sum can be written as the *direct sum* of two or more shells, that is:

$$S(\alpha) \oplus S(\beta) = S(\alpha + \beta).$$

3.5. Scalar products in vector semispaces

In the same fashion as Minkowski norms were adopted as a natural way to choose a norm in semispaces, it seems that a natural way to define *scalar products* in vector semispaces could exist as well.

3.5.1. Minkowski scalar products

Such a choice has to be coherently structured in a manner allowing us to match the previously chosen Minkowski norms. This prospect could be initiated by means of the following symbol:

$$\forall \mathbf{x}, \mathbf{y} \in \boldsymbol{V}\left(\mathbf{R}^+\right)\colon\ \langle \mathbf{xy}\rangle \in \mathbf{R}^+,$$

which will be attached to the following algorithm:

$$\langle \mathbf{xy}\rangle = \sum_i (x_i\, y_i)^{1/2}.$$

To stress the parent norm structure, the same symbol as in the Minkowski norm has been assumed, however two or, as it will be studied later on, more vectors are written within the symbol without separation signs added. This scalar product symbol has also been chosen in this way in order to distinguish it from other possibilities already discussed [96,98] and, of course, from the well-known *Euclidean scalar product*.

In this manner, it can immediately be seen that the property below holds, connecting the scalar product, as defined in the algorithm above, with the previously described Minkowski norm:

$$\langle \mathbf{xx} \rangle = \sum_i \left(x_i^2\right)^{1/2} = \sum_i x_i = \langle \mathbf{x} \rangle.$$

Such a coherency characteristic found in this simple manner, tells us it is already time that such a scalar product can be named as the *root*, for short, or *Minkowski scalar product*.

3.5.1.1. Inward matrix product structure and Minkowski scalar product of two vectors. The definition provided above of the root scalar product can be also interpreted in terms of an IMP, only one must take into account the definition of inward product:

$$\mathbf{x} * \mathbf{y} = \{x_i y_i\},$$

which shall be associated with the inward square root form:

$$\mathbf{x}^{[1/2]} = \left\{x_i^{1/2}\right\}.$$

It is obvious that one can then write the equality:

$$\langle \mathbf{xy} \rangle = \left\langle \mathbf{x}^{[1/2]} * \mathbf{y}^{[1/2]} \right\rangle,$$

where the second bracket has to be taken as a matrix summation symbol.

3.5.2. Minkowski scalar product main properties

Due to the nature of vector semispaces, it is interesting to simplify the root scalar product, taking into account the shell structure of the involved vectors:

$$\mathbf{x}^{(\alpha)} \in S(\alpha) \wedge \mathbf{y}^{(\beta)} \in S(\beta) \rightarrow \left\langle \mathbf{x}^{(\alpha)} \mathbf{y}^{(\beta)} \right\rangle = (\alpha\beta)^{1/2} \left\langle \mathbf{x}^{(1)} \mathbf{y}^{(1)} \right\rangle,$$

where superscripts have been used to stress the association of each vector to a given shell. Thus, this result implies that any root scalar product within a vector semispace can be related to the root scalar product of the unit shell associated homothetic vectors, appropriately scaled by the geometric mean of the Minkowski norms of both vectors.

This kind of root scalar product produces a symmetric metric with positive definite elements on it, as the following property:

$$\langle \mathbf{xy} \rangle = \langle \mathbf{yx} \rangle \wedge \langle \mathbf{xy} \rangle \in \mathbf{R}^+$$

holds for any couple of vectors, according to the root scalar product above defined. However, there is no assurance that, in any case, the metric is positive definite, adopting for the metric matrix the usual sense for this property, associated with *Euclidean vector spaces*. In order to discuss this issue, even if it has to be from a simple point of view, the main arguments shall be postponed until some other properties of root scalar product have been studied.

The rest of the main properties of root scalar products have to be observed now, as it is not so obvious whether they are fulfilled in the same way as scalar products in Euclidean spaces. For example, multiplication by a scalar of one of the involved vectors in the root scalar product appears to possess similar properties as the usual Euclidean scalar product:

$$\lambda \in \mathbf{R}^+ \colon \left\langle (\lambda \mathbf{x}) \mathbf{y} \right\rangle = \lambda^{1/2} \langle \mathbf{xy} \rangle.$$

The next property to be handled is related to root scalar product and addition. The adequate handling of this part is most interesting in order to make root products as similar as possible to the Euclidean counterpart.

3.5.3. Distributive law and root scalar products involving linear combinations

A distributive law with respect to vector addition has to be sought through the definition of inward matrix product subjacent structure of root scalar products. The algorithm definition of root scalar product must be adapted to vector sum, and the straightforward way to define the interaction of sum and product is:

$$\big\langle(\mathbf{x}+\mathbf{y})\mathbf{z}\big\rangle = \sum_i \big(x_i^{1/2} + y_i^{1/2}\big) z_i^{1/2} = \langle \mathbf{xz}\rangle + \langle \mathbf{yz}\rangle.$$

At the same time, in order to obtain a coherent reduction to the Minkowski norm, the product of two vector sums has to be structured in the form of a *Hadamard product*, that is, just dropping the cross terms while keeping the diagonal ones:

$$\big\langle(\mathbf{x}+\mathbf{y})(\mathbf{t}+\mathbf{u})\big\rangle = \langle \mathbf{xt}\rangle + \langle \mathbf{yu}\rangle.$$

With these definitions the Minkowski norm of a sum is preserved as can be easily deduced:

$$\big\langle(\mathbf{x}+\mathbf{y})(\mathbf{x}+\mathbf{y})\big\rangle = \langle \mathbf{xx}\rangle + \langle \mathbf{yy}\rangle = \langle \mathbf{x}\rangle + \langle \mathbf{y}\rangle = \langle \mathbf{x}+\mathbf{y}\rangle,$$

and the product of two linear combinations, *restricted* to possess an equal number of terms, can be handled in the following way, using again the Hadamard diagonal formalism:

$$\mathbf{x} = \sum_i^P \alpha_i \mathbf{a}_i \wedge \mathbf{y} = \sum_i^P \beta_i \mathbf{b}_i:$$

$$\langle \mathbf{xy}\rangle = \sum_i^P (\alpha_i \beta_i)^{1/2} \langle \mathbf{a}_i \mathbf{b}_i\rangle = \sum_i^P \left[(\alpha_i \beta_i)^{1/2} \sum_k (a_{ki} b_{ki})^{1/2} \right].$$

A final remark should be given, before we proceed with the study of the possibilities of root scalar products in semispaces. One must insist that Hadamard products were originally defined within infinite sums pairs of elements [99]. When described, as in the present case, within sums possessing a finite number of terms, then the sum upper limit shall be the same in both factors. Otherwise the product is not feasible.

3.6. Angles subtended by two vectors

Root scalar products and Minkowski norms can be joined together in order to construct, as in the classical Euclidean way, the cosine of the angle subtended by two semispace vectors. To grasp such a goal, we only need the following practical definition, based on Minkowski norms and root scalar products as defined beforehand:

$$\forall \mathbf{x}, \mathbf{y} \in \boldsymbol{V}\big(\mathbf{R}^+\big) \wedge \mathbf{x} \in S(\alpha),\ \mathbf{y} \in S(\beta):$$

$$\cos(\phi) = \frac{\langle \mathbf{xy}\rangle}{(\langle \mathbf{x}\rangle \langle \mathbf{y}\rangle)^{1/2}} = (\alpha\beta)^{-1/2} \langle \mathbf{xy}\rangle = \big\langle \mathbf{x}^{(1)} \mathbf{y}^{(1)} \big\rangle.$$

Such a classical definition demonstrates again the coherent result that, under the present semispace description, the angle subtended by a pair of semispace vectors, even if they belong to different shells, can be established within the unit shell by the root scalar product of the unit shell vectors. In order to stress the different nature of the cosine defined here from the usual Euclidean algorithm, the present cosine computation will be named the *root or Minkowski cosine*.

3.7. Minkowski metric properties

Minkowski products possess a set of interesting properties, which will be discussed in the following sections.

3.7.1. Minkowski product fundamental property involving unit shell vectors

There is still a point to be demonstrated, which can be postulated in the following way:

$$\forall \mathbf{x}, \mathbf{y} \in S(1) \rightarrow \langle \mathbf{xy} \rangle \leqslant 1.$$

A straightforward demonstration of the previous inequality can be put in the following terms. Given two arbitrary vectors of the unit shell, $\mathbf{x}, \mathbf{y} \in S(1)$, then one can suppose that both unit shell elements are constructed by means of the rules[4] $\mathbf{x} = \{u_I^2\}$ and $\mathbf{y} = \{v_I^2\}$, just to fulfil: $\langle \mathbf{x} \rangle = \langle \mathbf{y} \rangle = 1$. Using generating symbols we can simply write $R(\mathbf{u} \rightarrow \mathbf{x}) \wedge R(\mathbf{v} \rightarrow \mathbf{y})$, and the unit shell association of both generated vectors can be symbolized by the convex conditions: $K(\mathbf{x}) \wedge K(\mathbf{y})$.

The sets $\{u_I\}$ and $\{v_I\}$ can always be found, the vector components in semispaces being real positive definite scalars. This also becomes the same as considering that the generating vectors, $\mathbf{u} = \{u_I\}$ and $\mathbf{v} = \{v_I\}$, are normalized in the Euclidean space sense:

$$\mathbf{u}^T \mathbf{u} = \mathbf{v}^T \mathbf{v} = 1.$$

This can be always stated because, for example:

$$\mathbf{u}^T \mathbf{u} = \sum_I u_I^2 = \sum_I x_I = \langle \mathbf{x} \rangle = 1,$$

can be directly written and an equivalent relationship holds relating the components of the other chosen vectors $\mathbf{y}$ and $\mathbf{v}$.

From here, recalling the well-known *Schwartz inequality* in Euclidean spaces [100]:

$$\left(\mathbf{u}^T \mathbf{v}\right)^2 \leqslant \left(\mathbf{u}^T \mathbf{u}\right)\left(\mathbf{v}^T \mathbf{v}\right),$$

which, in this particular case where the involved vectors are normalized, permits us to finally write:

$$\mathbf{u}^T \mathbf{v} \leqslant 1.$$

[4] Such a procedure has been formally described [96,101,102] with the use of a *generating symbol*: $R(\mathbf{u} \rightarrow \mathbf{x}) = \{\mathbf{x} = \mathbf{u} * \mathbf{u}\}$, where the inward matrix product is explicitly written. This kind of symbolic form can be easily extended in order to connect Hilbert spaces and semispaces, one just has to remember the construction of density functions with squared modules of wave functions.

As a consequence, the scalar product used here can be written as:

$$\langle \mathbf{xy} \rangle = \sum_I (x_I y_I)^{1/2} = \sum_I u_I v_I = \mathbf{u}^T \mathbf{v} \leqslant 1.$$

Thus, the root scalar product obtained with a pair of arbitrary vectors of the unit shell is always less or equal to one, and consequently behaves as a cosine, inducing the same behaviour into the previously defined root cosine.

3.7.2. A property of the elements of the unit shell vectors

It is interesting to know a general form of this cosine definition based on root scalar products, when one of the vectors involved in the root scalar product is the unity vector, $\mathbf{1} = \{1_I = 1\}$, already described. Such a vector in any N-dimensional semispace, in order that it is forced to belong to the unit shell, has to be written with a normalization factor N^{-1}. Then, choosing any unit shell semispace vector, defined for instance as:

$$\mathbf{z} = \{\theta_I\} \in S(1) \rightarrow \langle \mathbf{z} \rangle = \sum_I \theta_I = 1,$$

it produces the following root cosine, when confronted with the unity vector:

$$\cos(\phi) = \left\langle \mathbf{z}\left(N^{-1}\mathbf{1}\right) \right\rangle = N^{-1/2} \sum_I \theta_I^{1/2}.$$

According to the previous discussion this particular root cosine expression, as obtained above, has to be less than or equal to one. From here, one can deduce that the unit shell vector components in any N-dimensional semispace will fulfil in any case the relationship:

$$\sum_I \theta_I^{1/2} \leqslant N^{1/2}.$$

The unity vector used twice within this argument will allow the equality to hold.

3.7.3. Positive definite structure of Minkowski metric matrices involving two unit shell vectors

The property $\langle \mathbf{xy} \rangle \leqslant 1$, associated with unit shell vectors and demonstrated above, can be used to build up a particular proof of the positive definiteness of metric matrices involving two vectors of $S(1)$. Assume two linearly independent unit shell vectors: $\mathbf{x}, \mathbf{y} \in \mathbf{S}(1)$. The root metric matrix associated with both vectors can be written as:

$$\begin{pmatrix} 1 & \langle \mathbf{xy} \rangle \\ \langle \mathbf{xy} \rangle & 1 \end{pmatrix} = \begin{pmatrix} 1 & p \\ p & 1 \end{pmatrix}.$$

The characteristic polynomial, and its roots, of such a metric matrix is simply:

$$\mathrm{Det} \begin{bmatrix} 1-\lambda & p \\ p & 1-\lambda \end{bmatrix} = (1-\lambda)^2 - p^2 = 0 \quad \Rightarrow \quad \lambda = 1 \pm p.$$

This proves that being the root scalar product: $p < 1$, because the vectors have been chosen linearly independent, then, the two possible eigenvalues will bear the property: $\lambda > 0$. Thus, the root metric matrix associated with a couple of linearly independent unit shell vectors is positive definite.

3.7.4. Linear independence of unit shell vectors

Here a remark must be proposed, concerning the unit shell elements and, by extension, implying the elements of any shell. By construction, the vector pairs of a given shell are linearly independent. This can be proved by using the fact that Minkowski norms of all shell components are equal. Then, there is no scalar $\lambda \neq 1$ for which two vectors, say $\mathbf{x}, \mathbf{y} \in S(1)$, fulfil $\mathbf{x} = \lambda \mathbf{y}$. This is so, because $\langle \mathbf{x} \rangle = \langle \lambda \mathbf{y} \rangle = \lambda \langle \mathbf{y} \rangle \to 1 = \lambda$.

3.8. Positive definite nature of root metric matrices

In order to get a hint about the positive definiteness of root metric matrices of arbitrary dimension, one can also employ the argument consisting in the following reasoning. Suppose a set of M linearly independent vectors belonging to some vector space is known:

$$Z = \{\mathbf{z}_1, \mathbf{z}_2, \ldots, \mathbf{z}_M\} \subset \boldsymbol{V}(\mathbf{R}),$$

such that their inward product generates another set:

$$X = \{\mathbf{x}_1, \mathbf{x}_2, \ldots, \mathbf{x}_M\} \to \forall I\colon \mathbf{x}_I = \mathbf{z}_I * \mathbf{z}_I = \mathbf{z}_I^{[2]}.$$

Euclidean normalization of the set Z is equivalent to Minkowski normalization of the set X, as can be easily proved:

$$\forall I\colon 1 = \langle \mathbf{z}_I | \mathbf{z}_I \rangle = \sum_P z_{PI}^2 = \sum_P x_{PI} = \langle \mathbf{x}_I \rangle \to \mathbf{x}_I \in S(1),$$

so, using this construction, the set $X \subseteq S(1)$. As the set Z has been chosen linearly independent, then the Gram matrix of the set Z: $\mathbf{G} = \{g_{IJ} = \langle \mathbf{z}_I | \mathbf{z}_J \rangle\}$, is positive definite: $\mathbf{G} > 0$. However, the matrix constructed with the root scalar products of the parent set X, can be manipulated in such a way that:

$$\begin{aligned}
\mathbf{R} &= \left\{ r_{IJ} = \langle \mathbf{x}_I \mathbf{x}_J \rangle \right\} \to \forall I, J\colon r_{IJ} = \langle \mathbf{x}_I \mathbf{x}_J \rangle = \sum_P (x_{PI} x_{PJ})^{1/2} \\
&= \sum_P \left(z_{PI}^2 z_{PJ}^2 \right)^{1/2} = \sum_P z_{PI} z_{PJ} = \langle \mathbf{z}_I | \mathbf{z}_J \rangle = g_{IJ} \\
&\Rightarrow \quad \mathbf{R} = \mathbf{G} \wedge \mathbf{R} > 0.
\end{aligned}$$

Then, as a unit shell subset X can always be supposed to be generated by a set like the set Z, one arrives at the conclusion that a root metric matrix over a set of unit shell elements will be positive definite, or at least that, when the generating vectors are not linearly independent, it will be non-negative definite.

3.9. Root distances in vector semispaces

From the previous definition of the root scalar product, it is almost compulsory that an associated *root or Minkowski distance* definition be also proposed. This can be done again by inspection of the classical Euclidean definition, while substituting the usual distance elements by the appropriate Minkowski ones. After scaling by two, the following rule can

be used, despite the need of using a difference in a strictly positive definite set:

$$d(\mathbf{x},\mathbf{y}) = \frac{1}{2}\big(\langle\mathbf{x}\rangle + \langle\mathbf{y}\rangle\big) - \langle\mathbf{xy}\rangle.$$

Now supposing that $\mathbf{x} \in S(\alpha) \wedge \mathbf{y} \in S(\beta)$, the algorithm, which takes into account the shell structure in semispaces, is easily deduced:

$$d(\mathbf{x},\mathbf{y}) = \frac{1}{2}(\alpha+\beta) - (\alpha\beta)^{1/2}\big\langle\mathbf{x}^{(1)}\mathbf{y}^{(1)}\big\rangle,$$

and, using the definition of the root cosine of the angle subtended by both vectors, the root distance can be also written as:

$$d(\mathbf{x},\mathbf{y}) = \frac{1}{2}(\alpha+\beta) - (\alpha\beta)^{1/2}\cos(\phi).$$

This proves that, under the proposed definition, root distances in vector semispaces can be computed over the unit shell with the *arithmetic mean shell* value as origin and the *geometrical mean shell* value as scale factor.

3.9.1. Root distance properties

Also, the root distance symmetry obviously holds, that is:

$$d\big(\mathbf{x}^{(\alpha)},\mathbf{y}^{(\beta)}\big) = d\big(\mathbf{y}^{(\alpha)},\mathbf{x}^{(\beta)}\big).$$

The following property must also be noted now, when both vectors are equal:

$$d(\mathbf{x},\mathbf{x}) = \alpha\big(1 - \big\langle\mathbf{x}^{(1)}\mathbf{x}^{(1)}\big\rangle\big) = \alpha\big(1 - \big\langle\mathbf{x}^{(1)}\big\rangle\big) = \alpha 0 = 0.$$

The interesting result must be also noted which appears when two homothetic vectors, related to the same unit shell vector, are studied:

$$d\big(\mathbf{x}^{(\alpha)},\mathbf{x}^{(\beta)}\big) = \frac{1}{2}(\alpha+\beta) - (\alpha\beta)^{1/2}\big\langle\mathbf{x}^{(1)}\mathbf{x}^{(1)}\big\rangle = \frac{1}{2}(\alpha+\beta) - (\alpha\beta)^{1/2}.$$

This result may be taken as a constant, connecting any α-shell with another β-shell. One can, then, speak of a *shell root distance* when referring to this quantity. As arithmetic means are always greater than or equal to geometric means, then this statistical property assures the positive definite nature of shell root distances.

The same root distance positive definiteness property holds as well in the general algorithm involving any pair of vectors, as the root scalar product or the equivalent root cosine within the unit shell are less than one. Then one can write, in general, that the positive definiteness of root distances is fulfilled:

$$d\big(\mathbf{x}^{(\alpha)},\mathbf{y}^{(\beta)}\big) \in \mathbf{R}^{+}.$$

There is no proof by which the *triangle inequality* [100] generally holds within the root distance description. We can easily find a counterexample, involving for instance the shell root distances of three different collinear homothetic vectors, proving that the root distances in this case *do not* fulfil the triangle inequality. Thus, perhaps one can speak of an *ultrametric* definition in the present root distance case and in further generalizations, employing this word to represent the distance axioms when void of the triangle inequality.

3.10. Generalized root scalar products and distances

It is interesting to study, besides the highlights and limitations of both semispaces and their natural root operations, if such algorithmic definitions can be associated with more than a vector couple. Such an aim is unusual in Euclidean spaces, although some attempts have been made recently [96,98] within other ideas, just to provide a prospect of open computational horizons in the field of QS descriptors.

As has been previously described, various QS measures involving the density tags of several quantum objects can be computed [98,101,102]. One of such possible definitions is the so-called *triple density QS measures*, where three quantum object density functions are involved in the measure computation. Such measures involving multiple quantum object tags are not unique, due to possible alternative definitions of the density functions [1–3]. Because of this lack of uniqueness, several possible forms have been put forward (see, for example, [96,98]) although the most straightforwardly defined triple density measure, associated with the integral of a triple product of first order density functions, is the one which has been employed several times [103,104].

3.10.1. Generalized root scalar products involving several vectors

Now, the structure of the root scalar product is such that it can be also naturally generalized into a form involving an arbitrary number of vectors. In order to obtain a general algorithm for a root scalar product, assume a set of vectors of some semispace, $X = \{\mathbf{x}_I\}(I = 1, P) \subset V(\mathbf{R}^+)$, defined in such a way as allowing each of them to belong to an arbitrary shell, that is: $\forall I\colon\ \mathbf{x}_I \in S(\alpha_I) \subset V(\mathbf{R}^+)$. A *root scalar product of order* P can be defined over the set X by means of the algorithm:

$$\langle \mathbf{x}_1 \mathbf{x}_2 \dots \mathbf{x}_P \rangle = \sum_I (x_{I1} x_{I2} \dots x_{IP})^{1/P} = \sum_I \left(\prod_{J=1}^{P} x_{IJ} \right)^{1/P}.$$

Taking into account the above definition, the already discussed root scalar product corresponds to a second order algorithm. In any case and up to any order, the root scalar product reverts to the Minkowski norm when the involved vectors are the same. Also, it is trivial to see that the root scalar product bears permutational symmetry, and thus is independent of the order of the factors.

Besides, the following property is also trivially demonstrated:

$$\begin{aligned} \langle \mathbf{x}_1 \mathbf{x}_2 \dots \mathbf{x}_P \rangle &= (\alpha_1 \alpha_2 \dots \alpha_P)^{1/P} \sum_I \left(x_{I1}^{(1)} x_{I2}^{(1)} \dots x_{IP}^{(1)} \right)^{1/P} \\ &= (\alpha_1 \alpha_2 \dots \alpha_P)^{1/P} \langle \mathbf{x}_1^{(1)} \mathbf{x}_2^{(1)} \dots \mathbf{x}_P^{(1)} \rangle, \end{aligned}$$

which shows that the root scalar product can be referred to the homothetic unit shell vectors, while scaled by the geometric mean of their shell values.

3.10.2. Generalized root distances involving several vectors

It is straightforward to construct a generalized root distance. Owing to the previous discussion and the second order formalism discussed above, we can write the *root distance of*

order P as:

$$d(\mathbf{x}_1\mathbf{x}_2\ldots\mathbf{x}_P)=\frac{1}{P}\left(\sum_I^P\alpha_I\right)-(\alpha_1\alpha_2\ldots\alpha_P)^{1/P}\langle\mathbf{x}_1^{(1)}\mathbf{x}_2^{(1)}\ldots\mathbf{x}_P^{(1)}\rangle.$$

Thus, we produce a computational structure with the same properties as the second order root distance previously discussed.

3.10.3. Proving the fundamental property of generalized scalar products involving unit shell elements

Moreover, if the following conjecture can be admitted to hold for any number of semispace unit shell vectors:

$$\langle\mathbf{x}_1^{(1)}\mathbf{x}_2^{(1)}\ldots\mathbf{x}_P^{(1)}\rangle\leqslant 1,$$

then, not only will this ensure the positive definiteness associated with the root distances of any order, but it also will permit us to define a kind of generalized root cosines of the *pseudo-angle* subtended by P semispace vectors. To illustrate this affirmation one could write, mimicking the second order result:

$$\cos(\Phi_P)=\langle\mathbf{x}_1^{(1)}\mathbf{x}_2^{(1)}\ldots\mathbf{x}_P^{(1)}\rangle.$$

In order to demonstrate the above stated conjecture, consisting in the root scalar product of an arbitrary number of unit shell vectors being less than or equal to one, assume a set of unit shell vectors with the superscript dropped to simplify notation: $X=\{\mathbf{x}_I\}\subset S(1)$. Then, the following equalities will be associated with the elements of the set X: $\forall\mathbf{x}_I\in X$: $\langle\mathbf{x}_I\rangle=1$. Keeping this in mind, one can recall the definition of the root product involving the elements of X, supposedly associated with a cardinality P:

$$\begin{aligned}\langle\mathbf{x}_1\mathbf{x}_2\ldots\mathbf{x}_P\rangle&=\sum_j(x_{j1}x_{j2}\ldots x_{jP})^{1/P}<\sum_j\left[\frac{1}{P}(x_{j1}+x_{j2}+\cdots+x_{jP})\right]\\&=\frac{1}{P}\left[\sum_I\sum_j x_{jI}\right]=\frac{1}{P}\sum_I\langle\mathbf{x}_I\rangle=\frac{1}{P}P=1.\end{aligned}$$

Then, in this way the less than sign part of the conjecture is simply proved. We just needed the already employed argument, consisting the well-known property of making geometric means less than arithmetic means, and this property, holding for each term in the sum, produces the global result. Such a property involving the arithmetic–geometric means has an exception when all the terms are the same. In this situation equality will hold between both means, even if this is not the most interesting case. It is obvious that under this circumstance the property:

$$\forall\mathbf{x}\in S(1)\text{: }\langle\mathbf{x}\mathbf{x}\ldots\mathbf{x}\rangle=\sum_j(x_jx_j\ldots x_j)^{1/P}=\sum_j\left(x_j^P\right)^{1/P}=\sum_j x_j=\langle\mathbf{x}\rangle=1$$

will be found. Then, it has been proved that in any situation the root scalar product, involving an arbitrary number of unit shell vectors, will always be less than or equal to one.

3.11. Inward matrix structure of generalized root scalar products

It has been proved that the cornerstone of semispace metric can be associated with the root scalar product of an arbitrary number of vectors, belonging to arbitrary shells, which can always be associated with the product of the homothetic unit shell parent vectors. This is so because it has been proved that, when all vectors in the root scalar product are the same, then the Minkowski norm is recuperated as a result. So, the scalar product is involved in the same manner in order to describe root cosines of the subtended pseudo-angle and root distances as well. Keeping these considerations in mind, then it is straightforward to write in the same way as it was set for the second order root scalar product:

$$X = \{\mathbf{x}_I\}(I = 1, P) \subset V\left(\mathbf{R}^+\right) \rightarrow$$
$$\langle \mathbf{x}_1 \mathbf{x}_2 \dots \mathbf{x}_P \rangle = \sum_I (x_{I1} x_{I2} \dots x_{IP})^{1/P} \equiv \left\langle [\mathbf{x}_1 * \mathbf{x}_2 * \dots * \mathbf{x}_P]^{[1/P]} \right\rangle.$$

Here the last expression present within the matrix elements sum corresponds to the inward matrix power of the inward matrix product involving the vectors of the set X, and is defined accordingly as:

$$[\mathbf{x}_1 * \mathbf{x}_2 * \dots * \mathbf{x}_P]^{[1/P]} = \left\{(x_{I1} x_{I2} \dots x_{IP})^{1/P}\right\}.$$

4. DISCRETE DF FORMS AND RELATED QUESTIONS

The following section sets the mathematical structure to show that any discrete DF has to be accepted as the usual, practical, computational tool, related with the quantum mechanical use of the DF as a source of QO information. Discrete DF's appear when practical numerical uses of the quantum theory are sought. In this case, finite-dimensional subspaces of the functional infinite-dimensional space have to be used to construct practical DF structures, and then discrete DF forms can be defined and evaluated. Section 2.3.2 gives a previous simplified account of this occurrence. A possible way to obtain such discrete DF forms can be based on the definition of QSM within the elements of a QO set. The development given below will provide details of this question.

4.1. Quantum similarity measures involving two QO

The first precise definition of QSM was proposed several years ago [10]. Actually, any QSM can be made by an application of the direct product of two, or more, QO tags, belonging to some QOS, into the set of the positive definite real numbers, $\mathbf{R}^+$ [29].

To start developing the necessary basic concepts, Definition 9 presents a general basis of QSM. On the other hand, in the simplest way and from a practical point of view, a QSM is defined involving only two QO, $\{\Omega_A; \Omega_B\}$, and then using their tags in terms of quantum mechanical DF: $\{\rho_A; \rho_B\}$. Finally, a way is structured to connect the involved DF by means of a chosen positive definite operator, Ω, through the volume integral:

$$z_{AB}(\Omega) = \iint \rho_A(\mathbf{r}_1) \Omega(\mathbf{r}_1; \mathbf{r}_2) \rho_B(\mathbf{r}_2)\, d\mathbf{r}_1\, d\mathbf{r}_2. \tag{14}$$

Equation (14) has been used as the computational starting point to practically implement QSM calculations. Several QSM variant forms have been defined. For instance, substituting the positive definite operator, Ω, in equation (14), by the Dirac's delta function, $\delta(\mathbf{r}_1 - \mathbf{r}_2)$, an *overlap-like* QSM is obtained:

$$z_{AB} = \int \rho_A(\mathbf{r})\rho_B(\mathbf{r})\, d\mathbf{r}. \tag{15}$$

Similarly, when a Coulomb operator is employed in equation (14), $\Omega(\mathbf{r}_1;\mathbf{r}_2) = |\mathbf{r}_1 - \mathbf{r}_2|^{-1}$, a *Coulomb-like* QSM appears to be connected with the integral form:

$$z_{AB}\left(\mathbf{r}^{-1}\right) = \iint \rho_A(\mathbf{r}_1)|\mathbf{r}_1 - \mathbf{r}_2|^{-1}\rho_B(\mathbf{r}_2)\, d\mathbf{r}_1\, d\mathbf{r}_2. \tag{16}$$

A QSM z_{AA}, involving only a unique QO tag, is usually called a *Quantum Self-Similarity Measure* (QSSM) and can be written as:

$$z_{AA}(\Omega) = \iint \rho_A(\mathbf{r}_1)\Omega(\mathbf{r}_1;\mathbf{r}_2)\rho_A(\mathbf{r}_2)\, d\mathbf{r}_1\, d\mathbf{r}_2. \tag{17}$$

Other operators can be employed instead of the previously described ones, even another QO DF tag can be used for this purpose, producing *triple density* QSM's [60].

In any case and whatever choice is made, QSM defined in these particular ways can be interpreted as generalized volumes and they can be easily connected with quantum mechanical expectation values [23,24], see Section 6 below. Other alternative QSM definitions are possible, and throughout its historical development, quantum similarity has become an extremely flexible and general theoretical tool [29–33,35,36,61,98].

4.2. Similarity matrices and discrete QOS

Similarity matrices (SM) are obtained when a QOS is studied and some kind of QSM is computed among the involved QO. After construction of an SM, then the corresponding elements can be used as a new set of tags to describe in a discrete environment the QOS anew. A simple definition gives the basic ideas, which can be used for this purpose.

DEFINITION 14 (*Similarity matrix*). Given a well-designed QOS, constructed according to Definition 8, the collection of QSM involving all the QO pairs can be ordered in the form of a symmetric matrix: $\mathbf{Z} = \{z_{ij}\}$. Such an ordered array is called a *Similarity matrix* (SM).

Any SM can be partitioned in terms of its columns (or rows),[5] that is:

$$\mathbf{Z} = (\mathbf{z}_1, \mathbf{z}_2, \ldots, \mathbf{z}_N) = \{\mathbf{z}_I\}, \tag{18}$$

where every column corresponds to a precise QO, belonging to the studied QOS [52,53,63].

Thus, if Ω_A is a given QO and ρ_A is associated with its DF tag, then the corresponding column of the SM, $\mathbf{z}_A$, is in correspondence to the Ω_A QO DF tag, and can be consequently

[5] The usual convention consists into performing a column matrix partition. However, later on, a row transformation will be also used. Whenever appears important to describe which one of the two possible vector forms is adopted, then bra-ket formalism will be used to note the difference between row and column vectors.

considered as a discrete QO representation. This situation may be written symbolically as: $\Omega_A \leftrightarrow \rho_A \leftrightarrow \mathbf{z}_A$; or, in a better way as: $(\Omega_A; \rho_A) \leftrightarrow (\Omega_A; \mathbf{z}_A)$, taking into account the QO structure, made by the ordered pairs like (quantum system; DF). In this manner, the QSM collection of any chosen Ith QO with respect to all the elements of the QOS, defines a discrete set of N-dimensional tags: $\{\mathbf{z}_I\}$, N being the cardinality of the QOS, which can substitute the former DF tags.

DEFINITION 15 (*Discrete QOS*). A *discrete QOS* (DQOS), of the same cardinality as an original QOS, can be constructed in this way: the Tagged Set objects are the same quantum systems of the QOS as before, but the columns or rows of the SM, substitute the former DF Tag Set elements.

From this last definition, the next one is easy to formulate:

DEFINITION 16 (*QO point cloud*). The set of DQOS discrete tags naturally define a polyhedron in N-dimensional space. The DQOS Tag Set, for obvious reasons, can be called a *QO point cloud* [29–33].

This ends the simple conceptual framework where discrete QOS can be made. In the next sections several developments will be presented. One of the most appealing is the description of stochastic matrix structures, which can be made from plain SM, just by using an elementary transformation.

4.3. Stochastic transformations of QSM

The computation of SM over a QOS providing a new DQOS structure, as discussed above, produces a set of N-dimensional tags, which can be associated with the original infinite-dimensional DF tags in several modes.

Despite the strict positive definiteness of the SM column (or row) set elements, $\{\mathbf{z}_I\}$, which appear as a consequence of the QSM definition presented in equation (14), the connection between the N-dimensional tags and the DF is not immediately evident. However, it can be deduced after taking into account the nature of the involved DF tags [4,5], which can be considered in turn either as PD functions or projection operators. The present section will present an SM transformation, producing a new collection of N-dimensional tags, which are provided with such a structure that they can be considered to form a discrete probability distribution. This possibility shall be expected as a plausible outcome of QSM theory, due to the quantum mechanical origin of all the QO tags employed so far.

N-dimensional quantum SM columns (or rows), $\{\mathbf{z}_I\}$, or, simply, their elements, are made, by construction, of strictly positive definite real, in computational practice rational, numbers. This characteristic property can be summarized again, saying that the set of the SM columns or rows, the molecular point cloud, belongs to a VSS: $\{\mathbf{z}_I\} \subset \boldsymbol{V}_N(\mathbf{R}^+)$, that is: the SM is a strictly positive matrix: $\mathbf{Z}* > 0$.

It must be noted, for example, that the QO point cloud, defined by the DQOS tag set elements and commented on a few lines ago in the previous section as in Definition 16, provides a characteristic set of points: the QO point cloud. They belong to some N-dimensional VSS, because due to the nature of the QSM definition strictly positive numbers constitute all their components.

The VSS structure in general and, in particular, the construction of SM precludes that, in any case, the sum of every SM row (or column) elements is a positive real number, for example: $\langle \mathbf{z}_I \rangle = \sum_J z_{IJ} \in \mathbf{R}^+$. These sums can be used as row (or column) scale factors in order to trivially obtain a new row (or column) set belonging to the same VSS, i.e. $\mathbf{s}_I = \langle \mathbf{z}_I \rangle^{-1} \mathbf{z}_I$, but possessing the imposed form of a discrete probability distribution. That is, the following equalities can be easily written:

$$\langle \mathbf{s}_I \rangle = \left\langle \langle \mathbf{z}_I \rangle^{-1} \mathbf{z}_I \right\rangle = \langle \mathbf{z}_I \rangle^{-1} \langle \mathbf{z}_I \rangle = 1.$$

So the following definition is easily made:

DEFINITION 17 (*Stochastic similarity matrix*). The set of the N SM based rows (or columns): $\mathbf{S} = \{\mathbf{s}_I = \langle \mathbf{z}_I \rangle^{-1} \mathbf{z}_I\}$, ordered forming a square $(N \times N)$ matrix $\mathbf{S}$, produce a non-symmetric *stochastic similarity matrix* [63] as a result.

A trivial, compact way to produce the *row* stochastic matrix is to first construct the diagonal matrix, $\mathbf{D}$, whose elements are made by the sums of row (or column) SM elements:

$$\mathbf{D} = \mathrm{Diag}\big(\langle \mathbf{z}_1 \rangle, \langle \mathbf{z}_2 \rangle, \ldots, \langle \mathbf{z}_N \rangle\big), \tag{19}$$

and then produce the matrix product: $\mathbf{S} = \mathbf{D}^{-1}\mathbf{Z}$. In the same manner, a *column* stochastic matrix can be defined straightforwardly by computing the transpose of the previous definition: $\mathbf{S}^T = \mathbf{Z}\mathbf{D}^{-1}$, where one must take into account the symmetrical structure of the original SM.

The row $\{\langle \mathbf{s}_I |\}$ or column $\{|\mathbf{s}_I \rangle\}$ stochastic sets, being associable to a collection of discrete probability distributions, may be even better connected to the DF tag set: $\{\rho_I\}$ of the original QOS, than simply the rows or columns of the attached SM.

DEFINITION 18 (*Discrete stochastic QOS*). When combined with the microscopic systems belonging to the object set: $\{\Omega_I\}$, of the original QOS, the row: $\{\langle \mathbf{s}_I |\}$ or column: $\{|\mathbf{s}_I \rangle\}$ stochastic vectors can be used in either of both forms as forming a tag set to create an attached tagged set, which can be called a *Discrete stochastic QOS* (DSQOS).

For instance, taking into account the same considerations as those used before, see Section 4.2, when previously discussing the nature of the SM rows, the connection between the original QOS elements with the stochastic matrix rows: $(\Omega_I; \rho_I) \leftrightarrow (\Omega_I; \langle \mathbf{s}_I |), \forall I$, defines the elements of a DSQOS.

Such newly formed tagged sets, in the same fashion as the formerly constructed QOS, possess tag parts which can supposedly bear a probability distribution, contrary to the DQOS defined through the columns or rows of the associated plain SM.

4.4. Matrix representation of density functions

In this section, first order density matrices are viewed as Hermitian operators and thus their matrix representation is sought. Then, once the molecular density function matrix representation (DMR) is computed, for every molecular structure in a well defined state, such a matrix can be seen as a discrete representation of the corresponding state density function. Such a representation may be used afterwards to compare quantum objects. In a

molecular collection a set of DMR acts as quantum object tags, so in this way molecules and DMR attain the structure of a tagged set. Comparison of the DMR tags can lead to quantum object similarity measures, where if the objects are molecules the superposition could be avoided. This possibility demands the definition of some sort of metric between the elements of matrix spaces of different dimension.

4.4.1. Diagonal elements of the density matrix

Suppose the diagonal elements of the first order density matrix are defined within the LCAO MO theory as:

$$\rho(\mathbf{r}) = \sum_{\alpha}\sum_{\beta} D_{\alpha\beta}|\alpha\rangle\langle\beta| = \sum_{\alpha}\sum_{\beta} D_{\alpha\beta}\chi_{\alpha}(\mathbf{r})\chi^{*}_{\beta}(\mathbf{r}), \tag{20}$$

where $\{|\alpha\rangle\} = \{\chi_{\alpha}(\mathbf{r})\}$ is the set of monoelectronic basis set functions.

4.4.1.1. Matrix representation. As the first order density function (20) can be viewed at the same time as an operator, its matrix representation could be written as:

$$\mathbf{P} = \left\{P_{\mu\nu} = \int \chi^{*}_{\mu}(\mathbf{r})\rho(\mathbf{r})\chi_{\nu}(\mathbf{r})\,d\mathbf{r}\right\}. \tag{21}$$

A simple form of equation (21) can be immediately deduced because the density operator matrix elements can be expressed, after using definition (20) in equation (21):

$$P_{\mu\nu} = \int \chi^{*}_{\mu}(\mathbf{r})\rho(\mathbf{r})\chi_{\nu}(\mathbf{r})\,d\mathbf{r} = \sum_{\alpha}\sum_{\beta} D_{\alpha\beta}\int \chi^{*}_{\mu}(\mathbf{r})\chi_{\alpha}(\mathbf{r})\chi^{*}_{\beta}(\mathbf{r})\chi_{\nu}(\mathbf{r})\,d\mathbf{r}. \tag{22}$$

However, the fourfold overlap integral:

$$\int \chi^{*}_{\mu}(\mathbf{r})\chi_{\alpha}(\mathbf{r})\chi^{*}_{\beta}(\mathbf{r})\chi_{\nu}(\mathbf{r})\,d\mathbf{r} = (\mu\alpha\beta\nu) \tag{23}$$

becomes nothing else than the well-known overlap self-similarity basic building blocks.

In this manner, the matrix elements of equation (21), can be written:

$$P_{\mu\nu} = \sum_{\alpha}\sum_{\beta} D_{\alpha\beta}(\mu\alpha\beta\nu). \tag{24}$$

4.4.1.2. Mulliken approximation. The Mulliken approach can be used in the definition (24) to obtain the elements of equation (24) in simpler integral forms, that is:

$$(\mu\alpha\beta\nu) = \frac{1}{4}S_{\mu\alpha}S_{\beta\nu}\big[(\alpha\alpha\beta\beta) + (\alpha\alpha\nu\nu) + (\mu\mu\beta\beta) + (\mu\mu\nu\nu)\big],$$

where the integrals $(\alpha\alpha\beta\beta)$ and so on, are nothing else but the overlap integrals of the basis functions squared modules:

$$(\alpha\alpha\beta\beta) = \int \big|\chi_{\alpha}(\mathbf{r})\big|^{2}\big|\chi_{\beta}(\mathbf{r})\big|^{2}\,d\mathbf{r}.$$

4.4.1.3. ASA approximation. This last result suggests that, instead of the Mulliken approach, one can also substitute the AO basis set by an Atomic Shell Approximation (ASA) expression [50], see Sections 5.1 and 5.2 below for more details. In this case, the first order density function becomes:

$$\rho(\mathbf{r}) \approx \sum_A Q_A \rho_A(\mathbf{r} - \mathbf{r}_A),$$

where $\{Q_A\}$ are atomic density condensed charges and $\{\rho_A(\mathbf{r} - \mathbf{r}_A)\}$ atomic density functions centered at the points $\{\mathbf{r}_A\}$, which can be associated with linear combinations of fitted s-type functions as usually used in ASA theory. The DMR can be reduced in this case to a vector with the dimension equal to the number of atoms in a given molecule, using:

$$\mathbf{p} = \{p_I\}$$

and defining the vector elements as:

$$\begin{aligned} p_I &= \int \rho(\mathbf{r})\rho_I(\mathbf{r} - \mathbf{r}_I)\, d\mathbf{r} \\ &= \sum_A Q_A \int \rho_A(\mathbf{r} - \mathbf{r}_A)\rho_I(\mathbf{r} - \mathbf{r}_I)\, d\mathbf{r} = \sum_A Q_A \langle \rho_A \rho_I \rangle. \end{aligned} \tag{25}$$

So, under the ASA theory the integrals required are to be computed over s-type orbitals only:

$$\langle \rho_A \rho_I \rangle = \sum_{a \in A} w_a^A \sum_{i \in I} w_i^I \int \left| s_a^A(\mathbf{r} - \mathbf{r}_A) \right|^2 \left| s_i^I(\mathbf{r} - \mathbf{r}_I) \right|^2 d\mathbf{r}.$$

This can be written in terms of a matrix containing the overlap integrals:

$$\mathbf{S}^{AI} = \left\{ S_{ai}^{AI} = \int \left| s_a^A(\mathbf{r} - \mathbf{r}_A) \right|^2 \left| s_i^I(\mathbf{r} - \mathbf{r}_I) \right|^2 d\mathbf{r} \right\}$$

and, furthermore:

$$\langle \rho_A \rho_I \rangle = \left\langle \mathbf{w}^A \middle| \mathbf{S}^{AI} \middle| \mathbf{w}^I \right\rangle.$$

The set of vectors $\mathbf{p}$, defined in this way, are elements of a vector semispace as their elements will always be positive definite real numbers.

4.4.1.4. Atomic DMR. The ASA idea can be combined with *ab initio* density matrices, simply taking into account that the density function can be rewritten as a sum of atomic contributions:

$$\rho(\mathbf{r}) = \sum_A \rho_A(\mathbf{r}) \rightarrow \rho_A(\mathbf{r}) = \sum_{\alpha \in A} \sum_\beta D_{\alpha\beta} \chi_\alpha(\mathbf{r}) \chi_\beta^*(\mathbf{r}); \tag{26}$$

then, it is straightforward to construct a vector $\mathbf{p}$ like in equation (25), using the atomic density definitions as constructed in equation (26) as basis functions for the DMR. Subsequently, we obtain for each component:

$$p_I = \int \rho(\mathbf{r})\rho_I(\mathbf{r})\, d\mathbf{r} = \sum_A \int \rho_A(\mathbf{r})\rho_I(\mathbf{r})\, d\mathbf{r} = \sum_A \langle \rho_A \rho_I \rangle \tag{27}$$

so each element is reduced to an easily defined sum of terms:

$$\langle \rho_A \rho_I \rangle = \sum_{\alpha \in A} \sum_{\beta} D_{\alpha\beta} \sum_{\kappa \in I} \sum_{\lambda} D_{\kappa\lambda} \int \chi_\alpha(\mathbf{r}) \chi_\beta^*(\mathbf{r}) \chi_\kappa(\mathbf{r}) \chi_\lambda^*(\mathbf{r})\, d\mathbf{r}$$
$$= \sum_{\alpha \in A} \sum_{\beta} D_{\alpha\beta} \sum_{\kappa \in I} \sum_{\lambda} D_{\kappa\lambda} (\beta\alpha\lambda\kappa)$$

using the fourfold overlap integral definition as previously described in equation (23).

An alternative possibility is to construct a matrix representation, like:

$$p_{IJ} = \langle \rho_I \rho_J \rangle,$$

but this choice will not possess the mathematical background which can be attached to the vector definition (27). However it can obviously be considered the metric of the atomic density set: $\{\rho_I\}$, within a given molecule.

4.4.2. Off-diagonal elements of the first order density matrix

Alternatively, one can employ the corresponding off-diagonal element of the density matrix in expression (21), then:

$$\mathbf{P} = \left\{ P_{\mu\nu} = \iint \chi_\mu^*(\mathbf{r}_1) \rho(\mathbf{r}_1; \mathbf{r}_2) \chi_\nu(\mathbf{r}_2)\, d\mathbf{r}_1\, d\mathbf{r}_2 \right\}$$

in this context one will have:

$$P_{\mu\nu} = \iint \chi_\mu^*(\mathbf{r}_1) \rho(\mathbf{r}_1; \mathbf{r}_2) \chi_\nu(\mathbf{r}_2)\, d\mathbf{r}_1\, d\mathbf{r}_2$$
$$= \sum_{\alpha} \sum_{\beta} D_{\alpha\beta} \iint \chi_\mu^*(\mathbf{r}_1) \chi_\alpha(\mathbf{r}_1) \chi_\beta^*(\mathbf{r}_2) \chi_\nu(\mathbf{r}_2)\, d\mathbf{r}_1\, d\mathbf{r}_2$$
$$= \sum_{\alpha} \sum_{\beta} D_{\alpha\beta} \int \chi_\mu^*(\mathbf{r}_1) \chi_\alpha(\mathbf{r}_1)\, d\mathbf{r}_1 \int \chi_\beta^*(\mathbf{r}_2) \chi_\nu(\mathbf{r}_2)\, d\mathbf{r}_2$$
$$= \sum_{\alpha} \sum_{\beta} D_{\alpha\beta} S_{\mu\alpha} S_{\beta\nu} = [\mathbf{SDS}]_{\mu\nu}.$$

So, the DMR becomes the symmetric product:

$$\mathbf{P} = \mathbf{SDS}.$$

In this case the DMR can be written as a new charge and bond order matrix. Defining a new set of vectors:

$$\mathbf{f}_i = \mathbf{S}\mathbf{c}_i, \tag{28}$$

then

$$\mathbf{P} = \sum_i \Omega_i \mathbf{f}_i \mathbf{f}_i^+.$$

This construction has the disadvantage of being constituted by sums of tensorial column vector products. They are Hermitian but positive semi-definite.

The matrix whose columns are the transformed vectors (28):

$$\mathbf{F} = (\mathbf{f}_1; \mathbf{f}_2; \ldots; \mathbf{f}_n)$$

has the following property:

$$\mathbf{F} = \mathbf{SC} \rightarrow \mathbf{F}^+\mathbf{F} = \mathbf{C}^+\mathbf{S}^2\mathbf{C} \wedge \mathbf{F}\mathbf{F}^+ = \mathbf{SCC}^+\mathbf{S},$$

but as the original MO coefficient matrix is orthogonal with respect to the AO metric:

$$\mathbf{C}^+\mathbf{SC} = \mathbf{I} \rightarrow \mathbf{S}^{-1} = \mathbf{C}\mathbf{C}^+,$$

one arrives at the conclusion that:

$$\mathbf{F}\mathbf{F}^+ = \mathbf{S}$$

and at the same time that:

$$\mathbf{C}\mathbf{F}^+\mathbf{F}\mathbf{C}^+ = \mathbf{I} \wedge \mathbf{C}^+\mathbf{F}\mathbf{F}^+\mathbf{C} = \mathbf{I}.$$

Also, it can be said that:

$$\mathbf{C}^+\mathbf{F} = \mathbf{C}^+\mathbf{SC} = \mathbf{I} \wedge \mathbf{F}^+\mathbf{C} = \mathbf{C}^+\mathbf{SC} = \mathbf{I},$$
$$\mathbf{F}\mathbf{C}^+ = \mathbf{SCC}^+ = \mathbf{I} \wedge \mathbf{C}\mathbf{F}^+ = \mathbf{C}\mathbf{C}^+\mathbf{S} = \mathbf{I}.$$

So one can write easily that:

$$\mathbf{C}^+ = \mathbf{F}^{-1} \wedge \mathbf{C} = \left(\mathbf{F}^+\right)^{-1} \leftrightarrow \left(\mathbf{C}^+\right)^{-1} = \mathbf{F} \wedge \mathbf{C}^{-1} = \mathbf{F}^+.$$

Thus, the transformed columns of matrix **C** constituting the columns of matrix **F** can be considered the system MO eigenvectors in a dual reciprocal space.

4.4.3. The practical use of the DMR

Given an arbitrary number of molecular structures: How can the associated DMR be used in order to compare them, in the way the continuous function counterparts are employed in molecular similarity? Such a question appears to be an obvious proposal of paramount importance. In any case, vector or matrix representations of different molecular structures will be of different dimension. The situation is well studied when dealing with vectors belonging to the same space, but it is not so obviously defined when two objects of different dimension have to be compared. Thus, the problem inside the initial question has to be reformulated as: How can two DMR matrices of different dimension be compared? Then, it is easy to pose the required question in a general, mathematical way as: How can one compare elements of two or more matrix spaces of different dimension? Formally the question can be stated with:

$$\forall x \in V_M \wedge \forall y \in V_N \rightarrow \exists (x : y) \in \mathbf{R}^+? \tag{29}$$

where the symbol $(x : y)$ is employed in equation (29) to denote any kind of comparison involving the vectors x and y. Suppose that $M > N$, then it is perhaps possible to define a linear operator **P**, such that:

$$\mathbf{P} : V_M \rightarrow V_N.$$

Admitting that the lower dimension vector space will contain the images of the vectors of the higher-dimensional space upon application of the linear operator:

$$\mathbf{P}(x) = x_{(N)} \in V_N,$$

then, it is always possible to compare two elements belonging to the same space, and one can envisage next the choice of the algorithm leading to the comparison:

$$\big(\mathbf{P}(x) : y\big) = (x_{(N)} : y).$$

The problem now stated is how the linear operator $\mathbf{P}$ could be defined. An immediate possibility to solve it consists of the construction of an overlap matrix relating the ASA s-type functions of both molecules, say:

$$\mathbf{S}^{AB} = \left\{S^{AB}_{a,\alpha;b,\beta}\right\}$$

referring to molecule A with atomic centers a and functions α centered in atom a. Where there are M atoms in molecule A and N atoms in molecule B, then the overlap matrix: $\mathbf{S}^{AB}$, will certainly transform vectors from one space into another. When knowing two DMR vectors $\{\mathbf{p}_A; \mathbf{p}_B\}$, associated with a pair of molecules A and B, respectively, one can write:

$$(\mathbf{p}_A : \mathbf{p}_B) = \mathbf{p}_A^T \mathbf{S}^{AB} \mathbf{p}_B. \tag{30}$$

However, the structure of this comparison type will depend on the relative positions of the atoms of both molecules, because the matrix $\mathbf{S}^{AB}$ elements depend on the relative molecular positions. This fact is the point which one is trying to avoid; otherwise the comparison (30) will possess the same intermolecular relative position dependence as in the superposition optimization encountered in the evaluation of quantum similarity measures.

Now the crucial question can be formulated as: Can we define at all a possible matrix structure, which provides an equivalent result as the matrix $\mathbf{S}^{AB}$, without depending on atomic positions? If such a projector or linear transformation can be described, the problem will be solved.

4.4.3.1. Redundant solutions. A simple solution could consist of substituting the overlap matrix by some standard constant matrix, like the unity matrix: $\mathbf{1} = \{1_{ij} = 1\}$, however, the construction of a few examples shows how the resultant comparisons can become quite redundant.

Another highly redundant solution may be associated with a tensorial product of the vectors to be compared. An hybrid scalar product can be composed by the tensorial products:

$$\mathbf{T}_{AB} = \mathbf{p}_A \otimes \mathbf{p}_B \wedge \mathbf{T}_{BA} = \mathbf{p}_B \otimes \mathbf{p}_A, \tag{31}$$

followed by a complete summation of the resultant matrix elements:

$$\tau_{AB} = \langle \mathbf{T}_{AB} \rangle = \langle \mathbf{p}_A \otimes \mathbf{p}_B \rangle \wedge \tau_{BA} = \langle \mathbf{T}_{BA} \rangle = \langle \mathbf{p}_B \otimes \mathbf{p}_A \rangle.$$

The couple of scalars could be employed afterwards as generalized scalar products, but one must note that, for instance:

$$\tau_{AB} = \langle \mathbf{p}_A \otimes \mathbf{p}_B \rangle = \sum_i \sum_j p_{A,i} p_{B,j} = \left(\sum_i p_{A,i}\right)\left(\sum_j p_{B,j}\right) = \langle \mathbf{p}_A \rangle \langle \mathbf{p}_B \rangle, \tag{32}$$

then, it is obvious that the following equality will hold:

$$\tau_{AB} = \tau_{BA}.$$

Although the crossed products of the matrices (31) may lead to better comparison structures, it is also easy to show that:

$$\mathbf{R}_{AA} = \mathbf{T}_{AB}\mathbf{T}_{BA} = \langle \mathbf{p}_B * \mathbf{p}_B \rangle (\mathbf{p}_A \otimes \mathbf{p}_A) \wedge$$
$$\mathbf{R}_{BB} = \mathbf{T}_{BA}\mathbf{T}_{AB} = \langle \mathbf{p}_A * \mathbf{p}_A \rangle (\mathbf{p}_B \otimes \mathbf{p}_B)$$

so the resultant matrices are still more simple than the preceding ones. Furthermore:

$$\langle \mathbf{R}_{AA} \rangle = \langle \mathbf{p}_B * \mathbf{p}_B \rangle \tau_{AA} \wedge \langle \mathbf{R}_{BB} \rangle = \langle \mathbf{p}_A * \mathbf{p}_A \rangle \tau_{BB}.$$

The use of the preceding matrices and of the sums of their elements will lead to highly redundant comparison measures. For instance, in case one tries to define a squared distance as:

$$d_{AB}^2 = \big\langle (\mathbf{p}_A - \mathbf{p}_B) \otimes (\mathbf{p}_A - \mathbf{p}_B) \big\rangle = \tau_{AA} + \tau_{BB} - 2\tau_{AB}$$

however, taking into account the definition (32), one can also write:

$$d_{AB}^2 = \langle \mathbf{p}_A \rangle^2 + \langle \mathbf{p}_B \rangle^2 - 2\langle \mathbf{p}_A \rangle \langle \mathbf{p}_B \rangle = \langle \mathbf{p}_A \rangle^2 - \langle \mathbf{p}_B \rangle^2 = \tau_{AA} - \tau_{BB}.$$

4.4.3.2. Averaged submatrices. A completely different approach solves the problem provisionally, but further research should refine the procedure or lead to other more sophisticated and accurate algorithms. As a starting point suppose two column vectors $\{\mathbf{p}_A; \mathbf{p}_B\}$ possessing dimensions: $M > N$, respectively. They can be reduced to the same dimension, 2 say, with the following algorithm:

$$\mathbf{r}_A^{(2)} = \begin{pmatrix} r_{A,1} \\ r_{A,2} \end{pmatrix} = R_2^M(\mathbf{p}_A) = W \sum_{i=1}^{M-1} \sum_{j=i+1}^{M} \begin{pmatrix} p_{A,i} \\ p_{A,j} \end{pmatrix} = W \sum_{i=1}^{M-1} \begin{pmatrix} (M-i)\, p_{A,i} \\ \sum_{j=i+1}^{M} p_{A,j} \end{pmatrix} \quad (33)$$

with the averaging weight W defined as:

$$W = 2\big(M(M-1)\big)^{-1}. \quad (34)$$

The same procedure can be used over the vector $\mathbf{p}_B$, leading to a two-dimensional vector $\mathbf{r}_B^{(2)} = R_2^N(\mathbf{p}_B)$. Now, for example, one can write the comparison in a cosine-like fashion:

$$(\mathbf{p}_A : \mathbf{p}_B)_C^{(2)} = \big\langle \mathbf{r}_A^{(2)} * \mathbf{r}_B^{(2)} \big\rangle \Big(\big\langle \mathbf{r}_A^{(2)} * \mathbf{r}_A^{(2)} \big\rangle \big\langle \mathbf{r}_B^{(2)} * \mathbf{r}_B^{(2)} \big\rangle \Big)^{-1/2} \quad (35)$$

or alternatively in an Euclidean distance form:

$$(\mathbf{p}_A : \mathbf{p}_B)_D^{(2)} = \Big(\big\langle \mathbf{r}_A^{(2)} * \mathbf{r}_A^{(2)} \big\rangle + \big\langle \mathbf{r}_B^{(2)} * \mathbf{r}_B^{(2)} \big\rangle - 2\big\langle \mathbf{r}_A^{(2)} * \mathbf{r}_B^{(2)} \big\rangle \Big)^{-1/2}. \quad (36)$$

The average represented by equation (33) corresponds to a linear operator transforming some M-dimensional vector space into a bi-dimensional one. It is easily found that if $\{\mathbf{p}, \mathbf{q}\}$ are M-dimensional column vectors and $\{\alpha, \beta\}$ two arbitrary scalars, then:

$$R_2^M(\alpha\mathbf{p} + \beta\mathbf{q}) = \alpha R_2^M(\mathbf{p}) + \beta R_2^M(\mathbf{q}).$$

Similar definitions to the bi-dimensional ones in equations (33)–(36), can be easily generalized to three or higher-dimensional transformations.

To obtain such a general dimension reduction formalism, one has just to take the $\binom{M}{N}$ combinations of M indices taken N by N without repetition, then construct an N-dimensional sub-vector containing the corresponding index combination of the initial vector elements, summing up all the resulting sub-vectors, averaging finally the result with the inverse number of combinations. Using a nested summation symbol, see Section 2.1, one can write:

$$\mathbf{r}^{(N)} = R_N^M(\mathbf{p}) = \binom{M}{N}^{-1} \sum_N (\mathbf{i}) F(\mathbf{i}) \begin{pmatrix} p_{i_1} \\ p_{i_2} \\ \cdots \\ p_{i_N} \end{pmatrix}, \tag{37}$$

where $\sum_N(\mathbf{i})$ is a nested summation symbol [40] formed by N sums. $F(\mathbf{i})$ is a filter leaving overall the generated possible index vectors: $\mathbf{i} = (i_1, i_2, \ldots, i_N)$, only those corresponding to the needed combinations; that is, one can write: $F(\mathbf{i}) = \delta(i_1 < i_2 < \cdots < i_N)$, where a logical Kronecker's delta[6] [40] is employed within the filter definition. The reduced vectors of type $\mathbf{r}^{(N)}$, can be then compared with any N-dimensional vector.

However, the resulting comparisons:

$$(\mathbf{p}_A : \mathbf{p}_B)_C^{(N)} \wedge (\mathbf{p}_A : \mathbf{p}_B)_D^{(N)} \tag{38}$$

will possess a quite annoying drawback: As the involved vectors are dependent on the ordering of the atoms in the respective molecules, then the measures (38) will not be invariant upon molecular atomic indices reordering. And this will not be overridden by the dimension reduction; the non-invariance could even be enhanced by the use of a linear operator (33).

A possibility to take into account is that the optimal match between both vectors will be obtained when the following conditions are met:

$$\max_{\mathbf{i}}(\mathbf{p}_A : \mathbf{p}_B)_C^{(N)} \wedge \min_{\mathbf{i}}(\mathbf{p}_A : \mathbf{p}_B)_D^{(N)}, \tag{39}$$

where the vector $\mathbf{i}$ indicates any permutation of the dimension of both involved vectors. From this point of view the search for the best matching appears as a discrete counterpart of the molecular superposition problem encountered when computing quantum similarity measures. The amount of work involved would not be as overwhelming as the molecular superposition problem. Forcibly, in some cases, redundant solutions may be met, but then it will be a matter of choice to accept one or another atomic ordering.

4.4.3.3. Optimization algorithm. Certainly, a brute force algorithm in order to choose the proper atomic ordering should test all the possible $N!$ index permutations, making it almost impossible to apply the algorithm to molecules with reduced vectors still possessing a dimension larger than 10 to 12, depending on the available processor speed. A massive parallel computer allows us to arrive at higher dimensions, but in a good guess a computation of no more than a dimension around 20 could be reached, unless a special computer is designed to cope with this numerical explosion. Even so, the impractical growing rate of the permutation number seems hopeless. However the problem can be stated, as equation (39)

[6] A logical Kronecker delta $\delta(L)$ is a generalization of the Kronecker symbol δ_{ij}, where L is a logical expression, then when: $L = \text{True} \rightarrow \delta(L) = 1 \wedge L = \text{False} \rightarrow \delta(L) = 0$; one can consequently write: $\delta_{ij} \equiv \delta(i = j)$.

shows, as a mini-max one, thus this may make the development of game-like algorithms to solve the discrete superposition problem easier. As the vector norms remain invariant upon index permutation, the problem remains one of obtaining a maximal scalar product; that is, the optimal problem can be limited to solve the optimal problem for n-dimensional reduced vectors:

$$\max_{\mathbf{i}} \left\langle R_n^M(\mathbf{p}_A) * R_n^N(\mathbf{p}_B) \right\rangle,$$

in complete parallel with quantum similarity measure optimization. Of course, lower-dimensional reduced vector problems will be easily handled with a total permutation superposition. These results connect without doubt quantum similarity with discrete density matrix representations, but also the optimal discrete reduced vector products connect the theoretical discrete similarities with the procedures described several years ago by Avnir and coworkers [42].

4.4.3.4. Simpler representation. In case the reader wants an easer framework, then the one provided by the density function itself may be sufficient as a starting point for molecular description. Indeed, it has been described that easily constructed, appropriate projection operators can project the density function into atomic or fragment parts, which in turn sum up into the initial density. Taking the expression (20), and defining the atomic projector:[7]

$$P_I = \sum_{\mu \in I} \sum_{\nu} S_{\mu\nu}^{-1} |\mu\rangle\langle\nu|,$$

then it is easy to see that the partial density associated with the considered Ith atom can be obtained as:

$$\begin{aligned} P_I\big(\rho(\mathbf{r})\big) &= \sum_{\alpha} \sum_{\beta} D_{\alpha\beta} \sum_{\mu \in I} \sum_{\nu} S_{\mu\nu}^{-1} |\mu\rangle\langle\nu|\alpha\rangle\langle\beta| \\ &= \sum_{\alpha} \sum_{\beta} D_{\alpha\beta} \sum_{\mu \in I} \sum_{\nu} \delta_{\mu\alpha} |\mu\rangle\langle\beta| = \sum_{\mu \in I} \sum_{\beta} D_{\mu\beta} |\mu\rangle\langle\beta| = \rho_I(\mathbf{r}) \end{aligned}$$

and in summing up the atomic projectors of a molecule M the unit operator is found:

$$\sum_{I \in M} P_I = \mathbf{I},$$

then it is obvious that:

$$\sum_{I} \rho_I(\mathbf{r}) = \rho(\mathbf{r}).$$

Thus, one can construct a vector, which contains as elements atomic densities, so:

$$|\rho\rangle = \begin{pmatrix} \rho_1 \\ \rho_2 \\ \cdots \\ \rho_{N_A} \end{pmatrix} = \{\rho_I\} \rightarrow \big\langle |\rho\rangle \big\rangle = \rho. \tag{40}$$

[7] Such a projector definition has been recently employed to set the quantum mechanical basis of atomic charges and bond indices [110,111].

Integrating the vector (40), we obtain a charge vector attached to condensed density into atomic fragments:

$$\mathbf{Q} = \int_D |\rho\rangle \, d\mathbf{r} = \begin{pmatrix} \int_D \rho_1 \, d\mathbf{r} \\ \int_D \rho_2 \, d\mathbf{r} \\ \cdots \\ \int_D \rho_{N_A} \, d\mathbf{r} \end{pmatrix} = \begin{pmatrix} Q_1 \\ Q_2 \\ \cdots \\ Q_{N_A} \end{pmatrix} = \{Q_I\} \rightarrow \langle \mathbf{Q} \rangle = \sum_I Q_I = N,$$

N being the number of electrons in molecule M, as the elements of the vector $\mathbf{Q}$ are nothing but Mulliken's gross atomic populations. Thus pairs of atomic charge vectors, attached to molecular pairs, can be employed for the same comparison purpose as before. Of course, to the same extent atomic projectors can be added to define some molecular fragment, like:

$$P_F = \sum_{I \in F \subset M} P_I.$$

The molecular vector $\mathbf{Q}$ can be made of fragments instead of atoms, and compared with other vectors constructed in a similar way.

In an approximate way, one can consider that: $\forall I \in M$: $Q_I = Z_I$ and proceed accordingly in a kind of non-polarized molecular atoms way.

5. APPROXIMATE, GENERALIZED AND AVERAGE DENSITY FUNCTIONS

DF can possess various structures, mainly related to the form they bear with respect to an appropriate DF basis set. In this section some analysis of such a property and related items will be done in reference to eDF.

It is well known [1–7] how eDF can be variable reduced. Integrating the raw eDF definition over the entire system particle coordinates, except r of them, produces an rth order eDF. The procedure may be schematized within the third step of Algorithm 1 or as depicted in the generating rule of Definition 2. This kind of coordinate or, which is the same, random variable reduction, has been studied in many ways [1–7] and will not be repeated here.

In the practical implementation of QSM, a simplified manner to construct the first-order eDF form [8] has been proposed and is named the Atomic Shell Approximation (ASA) eDF. A procedure has been recently described [50] with the necessary conditions to obtain positive definite ASA eDF, and possessing appropriate probability distribution properties.

5.1. Convex conditions and ASA fitting

Definition 5 in Section 2.1 succinctly presents the structural details of first order eDF, and connects their form with the ASA eDF. The ASA eDF coefficients vector, $\mathbf{w} = \{w_i\}$, must be optimized in order to obtain an approximate function that is completely adapted to *ab initio* eDF. In order that these last conditions hold, the $\mathbf{w}$ vector component values are restricted to lie within the boundaries of some VSS: $\boldsymbol{V}_N(\mathbf{R}^+)$, see Definition 1, and its element sum, $\langle \mathbf{w} \rangle$, see Definition 3, shall be unity. As commented previously, this feature

can be cast into a unique symbol, which can be referred to as *convex conditions*: $\boldsymbol{K}_N(\mathbf{w})$, applying over the N-dimensional vector $\mathbf{w}$. Details can be found within the corresponding Definition 6.

As commented in Definition 5, the DF form shown in equation (3) can be used to build up new DF elements, while preserving $\boldsymbol{K}_\infty(\rho)$ as set in Definition 6. If $\mathbf{w}$ is taken as a vector, assuming that $\boldsymbol{P} = \{\rho_i(\mathbf{r})\} \subset \boldsymbol{H}(\mathbf{R}^+)$ is used as a given set of homogeneous order DF, and that convex conditions $\boldsymbol{K}_N(\mathbf{w})$ hold, then the linear combination:

$$\rho(\mathbf{r}) = \sum_i w_i \rho_i(\mathbf{r}) \in \boldsymbol{H}\left(\mathbf{R}^+\right) \rightarrow \boldsymbol{K}_\infty(\rho) \tag{41}$$

can be used to produce a new DF with the same order and characteristic properties as the ones associated with the elements of the set $\boldsymbol{P}$. It can be said that convex conditions over vector coefficients, affecting DF superpositions, are the way to allow the construction of new DF of the same nature. Quite a considerable proportion of chemical computations, performed over large molecular systems, are based on such a principle. A recent paper [50e] and its sequel [50f] provide a complete up-to-date study of ASA eDF fitting and some detailed analysis will be given below in Section 5.2.

On the other hand, the DF themselves may in general be considered as elements of a VSS or, alternatively, as members of a PD Operator Set, which can be collected in turn into another isomorphic VSS, whose elements may be PD Operators.

The most important thing to be noted in the context of PD Operator VSS, as well as in the isomorphic VSS companions, is the *closed nature* of such VSS, when appropriate PD coefficient sets are known. That is, PD linear combinations of PD Operators remain PD Operators. Discrete matrix representations of such PD Operators are PD too, and PD linear combinations of PD matrices will remain PD in the same way. Identical properties can be described using convex conditions symbols, if $\{\boldsymbol{K}_\infty(\rho_i);\ \forall i\}$ and $\boldsymbol{K}_n(\mathbf{w})$ hold, then equation (41) is a convex function fulfilling $\boldsymbol{K}_\infty(\rho)$.

A connection between these considerations on PD operators and functions and Diagonal Matrix VS can now be easily made as previously discussed in Section 2.3.

5.2. ASA and CASA

Although a set of recent papers [50] gives the complete details of ASA fitting, recent algorithm developments and new atomic fitting tables will be of help to the readers interested in applications of the ASA DF [50f].

Essentially, the ASA fitting algorithm can be divided into three well-defined parts:

(a) generation of ASA exponents using *even-tempered* geometric sequences [64];
(b) coefficient optimization using an *elementary Jacobi rotation* (EJR) technique [49,50e, 50f];
(c) DF basis set exponent optimization using a Newton method [65].

In the present study only point (b) will be discussed, being the most relevant to DF analysis. Several basis sets collections, already obtained in this way, can be downloaded from a www site [66].

Optimal sets of ASA coefficients and exponents are obtained by minimizing the function:

$$\varepsilon^{(2)} = \int \left|\rho(\mathbf{r}) - \rho^{\mathrm{ASA}}(\mathbf{r})\right| d\mathbf{r} \tag{42}$$

which corresponds to the common definition of the quadratic error integral function between *ab initio* DF, $\rho(\mathbf{r})$, and ASA DF, $\rho^{\mathrm{ASA}}(\mathbf{r})$, eDF, subject to the convex conditions $\boldsymbol{K}_{\infty}(\rho^{\mathrm{ASA}})$ as described in Definition 6.

On the other hand, equation (42) possesses the structure of an overlap QSSM, involving the difference of the implied DF: $\Delta(\mathbf{r}) = \rho(\mathbf{r}) - \rho^{\mathrm{ASA}}(\mathbf{r})$; see equation (15) to grasp this fact. Thus, although the usual practice shows the quadratic error integral with the simple overlap QSSM structure, there is nothing to prevent us defining a general quadratic error form, weighted by a chosen PD operator $\Omega(\mathbf{r}_1; \mathbf{r}_2)$, as in a general formulation of a QSSM associated with equation (17), that is:

$$\varepsilon^{(2)}(\Omega) = \iint \Delta(\mathbf{r}_1)\Omega(\mathbf{r}_1; \mathbf{r}_2)\Delta(\mathbf{r}_2)\, d\mathbf{r}_1\, d\mathbf{r}_2.$$

Substituting the ASA DF defined in equation (41) into the integral (42) and using matrix notation, the function $\varepsilon^{(2)}$ can now be written as:

$$\varepsilon^{(2)} = \theta + \mathbf{w}^T Z \mathbf{w} - 2\mathbf{a}^T \mathbf{w}, \tag{43}$$

where:

$$\theta = \iint \rho(\mathbf{r}_1)\Omega(\mathbf{r}_1; \mathbf{r}_2)\rho(\mathbf{r}_2)\, d\mathbf{r}_1\, d\mathbf{r}_2$$

can be interpreted as an *ab initio* QSSM over the original DF to be fitted. The elements of the matrix $\mathbf{Z} = \{Z_{ij}\}$ as well as those of vector $\mathbf{a} = \{a_i\}$ are given, respectively, by the integrals:

$$Z_{ij} = \iint \left|\varphi_i(\mathbf{r}_1)\right|^2 \Omega(\mathbf{r}_1; \mathbf{r}_2) \left|\varphi_j(\mathbf{r}_2)\right|^2 d\mathbf{r}_1\, d\mathbf{r}_2$$

and

$$a_i = \iint \left|\varphi_i(\mathbf{r}_1)\right|^2 \Omega(\mathbf{r}_1; \mathbf{r}_2)\rho(\mathbf{r}_2)\, d\mathbf{r}_1\, d\mathbf{r}_2.$$

The first set of integrals can be interpreted as QSM involving the basis set functions, transformed into DF, and the second set can be associated with a QSM between the basis set functions transformed into DF and the exact DF.

The ASA functions not only can be applied to QS measures calculation—see reference [122] for a recent example on antimalarial QSAR—but appear to be interesting for initial HF procedures in molecular structures with heavy elements [123], among other applications [124–126].

5.2.1. ASA coefficient optimization using elementary Jacobi rotations

The set of positive coefficients collected as a vector: $\mathbf{w} = \{w_i\}$, in equation (41) can be defined as the square modules of some auxiliary vector components: $\mathbf{x} = \{x_i\}$, which could be called the *generating vector*:

$$w_i = |x_i|^2, \quad \forall i, \tag{44}$$

that is: $\boldsymbol{R}_N(\mathbf{x} \rightarrow \mathbf{w})$, and in this way the convex condition $\boldsymbol{K}_N(\mathbf{w})$ could be easily fulfilled. Moreover, because the matrix $\mathbf{Z}$ is PD, a unitary matrix $\mathbf{U}$ can be found such as:

$$\mathbf{U}^{+}\mathbf{Z}\mathbf{U} = \mathbf{D},$$

where $\mathbf{D}$ is a diagonal matrix with positive real elements, that is: $\mathbf{D}* > 0$. The first step in the procedure consists in diagonalizing the matrix $\mathbf{Z}$, in order to obtain their eigenvalues and eigenvectors. Then, the initial coefficients $\{w_i\}$ can be made equal to the squares of the most suitable normalized eigenvector of the matrix $\mathbf{Z}$, acting as generating vector, and consequently the required convex constraints are automatically fulfilled. Starting from this generating vector, and applying orthogonal EJR, the constraints will hold along the optimization process.

ASA coefficients are obtained by an optimization procedure, which minimizes the quadratic error integral between the exact and the ASA DF's. Substituting every ASA coefficient w_i by $|x_i|^2$, and only considering the case of *real* generating vector coefficients, the quadratic error integral function can be rewritten as:

$$\varepsilon^{(2)} = \theta + \sum_{i,j \in a} x_i^2 x_j^2 Z_{ij} - 2\sum_{i \in a} x_i^2 a_i, \tag{45}$$

where θ the exact self-similarity measure, $\{Z_{ij}\}$ the QSM between the basis DF and $\{a_i\}$ the QSM between the exact DF and the DF basis set, have been already defined.

EJR are easily constructed norm-conserving tools to obtain unitary or orthogonal transformations usable over vectors or matrices. The origin of such transformation matrices can be found in the paper of Jacobi [49], dating to the past century. Being orthogonal, EJR may also be viewed as rotation matrices over real (or complex) valued N-dimensional spaces. Applied to a given N-dimensional vector, an EJR, which will be written here as $J_{pq}(\alpha)$, will transform the vector components p and q only, keeping the rest of them invariant. The EJR transformation on the generating vector chosen components is defined by the equations:

$$\begin{aligned} x_p^r &\leftarrow c x_p - s x_q, \\ x_q^r &\leftarrow s x_p + c x_q, \end{aligned} \tag{46}$$

where c and s are the cosine and sine of the EJR angle α, acting over the components: $\{x_p; x_q\}$ and transforming them into the new rotated values: $\{x_p^r; x_q^r\}$. The norm of the transformed vector remains invariant with respect to the initial one, as orthogonal vector transformations possess this property.

Over the generating vector coefficients in equation (45) it is easy to apply the EJR represented by equation (46), and then, the variation of $\varepsilon^{(2)}$ with respect to the active pair of elements$\{x_p; x_q\}$ may be easily expressed. To compute $\delta\varepsilon^{(2)}$ it is necessary to evaluate the *second* and *fourth order* variation of the transformed elements: $\{x_p^r; x_q^r\}$. Substituting such variations into the corresponding equation and collecting terms, one finally arrives at a quartic polynomial on the rotation sine:

$$\delta\varepsilon^{(2)} = E_{04}s^4 + E_{13}cs^3 + E_{02}s^2 + E_{11}cs, \tag{47}$$

where the parameters $\{E_{IJ}\}$, appearing in equation (47), are described as follows:

$$E_{04} = \Theta\left[\left(x_p^2 - x_q^2\right)^2 - 4x_p^2 x_q^2\right],$$

$$E_{13} = 4\Theta\left(x_p^2 - x_q^2\right)x_p x_q,$$
$$E_{02} = 4\Theta x_p^2 x_q^2 - 2\left(x_p^2 - x_q^2\right)G,$$
$$E_{11} = -4x_p x_q G,$$

using the following auxiliary terms:

$$\Theta = Z_{pp} + Z_{qq} - 2Z_{pq}$$

and

$$G = \sum_{i \neq p,q} x_i^2 (Z_{pi} - Z_{qi}) + x_p^2 Z_{pp} - x_q^2 Z_{qq} - \left(x_p^2 - x_q^2\right)Z_{pq} - a_p + a_q.$$

The optimal sine can be chosen with the null gradient condition $\frac{d\delta\varepsilon^{(2)}}{ds} = 0$, taking into account that $\frac{s}{c} = t$ and that $\frac{dc}{ds} = -t$, then:

$$\frac{d\delta\varepsilon^{(2)}}{ds} = -c\left(T_1 t^2 - 2T_2 t - T_3\right) = 0 \tag{48}$$

holds with the auxiliary definitions:

$$T_1 = E_{13}s^2 + E_{11},$$
$$T_2 = 2E_{04}s^2 + E_{02},$$
$$T_3 = 3E_{13}s^2 + E_{11}.$$

The best Jacobi rotation angle is found by solving the quadratic polynomial equation in the EJR tangent $\{t\}$, appearing in expression (48). The optimization is conducted through an iterative procedure, until the global variation of Jacobi rotation angles or the quadratic error integral function become negligible, see reference [50e] for more details. A simplified algorithm can also be used, the interested reader should consult reference [50f], for a complete account.

5.2.2. Alternative approximate expression of density functions: Complete ASA (CASA)

Although losing the elegant simplicity of the ASA approach, there appears to be an alternative, very natural way to express the first order DF, using the same *generating vector* concept as before, within the ASA approach, as discussed above.

Assume a spherical basis set made as is usual in ASA environment of nS-type functions $\{S_i\}$. Then, the first order DF may be approximated by a function like:

$$\rho_a^{\mathrm{CASA}}(\mathbf{r}) = \sum_{i,j \in a} x_i x_j S_i(\mathbf{r}) S_j(\mathbf{r}), \tag{49}$$

where $\{x_i\}$ are the elements of the generating vector $\mathbf{x}$. This approach will be called from now on the *Complete Atomic Shell Approximation* (CASA). The quadratic error function can be written in a similar manner as using an ASA DF expression:

$$\varepsilon^{(2)} = z_{aa} + \sum_{i,j,k,l \in a} x_i x_j x_k x_l z_{ijkl} - 2\sum_{i,j \in a} x_i x_j B_{ij}, \tag{50}$$

where the hypermatrix elements: $\{z_{ijkl}\}$ are overlap-like similarity integrals involving four different S-type spherical basis functions:

$$z_{ijkl} = \int S_i(\mathbf{r}_1) S_j(\mathbf{r}_1) \Omega(\mathbf{r}_1; \mathbf{r}_2) S_k(\mathbf{r}_2) S_l(\mathbf{r}_2)\, d\mathbf{r}_1\, d\mathbf{r}_2$$

while the matrix $\mathbf{B} = \{B_{ij}\}$ corresponds to an integral between a pair of S-type functions and two AO's:

$$B_{ij} = \sum_{\mu,\nu} D_{\mu\nu} \int S_i(\mathbf{r}_1) S_j(\mathbf{r}_1) \Omega(\mathbf{r}_1; \mathbf{r}_2) \chi_\mu^*(\mathbf{r}_2) \chi_\nu(\mathbf{r}_2)\, d\mathbf{r}_1\, d\mathbf{r}_2.$$

EJR can be used in the same way as in the ASA approach in order to optimize the new CASA quadratic error expression; although with adapted different variation terms for the generating vector coefficients. Nevertheless, the structure of the CASA DF permits an alternative proposal, which leads to an elegant matrix formalism, identical to the mono-configurational SCF computational structure [41,67].

Here the new approximate expression of the density function leads to the normalization condition, which must fulfill the CASA generating vector coefficients:

$$\int \rho_a^{\text{CASA}}(\mathbf{r})\, d\mathbf{r} = \sum_{i,j \in a} x_i x_j \int S_i(\mathbf{r}) S_j(\mathbf{r})\, d\mathbf{r} = \sum_{i,j \in a} x_i x_j S_{ij} = 1. \tag{51}$$

That is, in matrix form: $\mathbf{x}^T \mathbf{S} \mathbf{x} = 1$, whenever the matrix: $\mathbf{S} = \{S_{ij}\}$ collects the metric matrix elements of the S-type basis function set.

Thus, the problem is reduced to minimizing equation (50), submitted to the constraint (51). A Lagrange multiplier technique can produce a more elegant result here than EJR. The Euler equations of the constrained optimization problem are written easily in terms of a generalized secular equation [67]:

$$\mathbf{G}\mathbf{x} = \gamma \mathbf{S}\mathbf{x}, \tag{52}$$

where γ is half of the necessary Lagrange multiplier, while the matrix structure, $\mathbf{G}$, depends on the generating vector coefficients and the involved integrals already defined:

$$G_{ij} = -B_{ij} + \sum_{k,l \in a} x_k x_l z_{ijkl}, \quad \forall i, j.$$

The CASA generating vector coefficients computational procedure should be made iterative, and during the process, the eigenvalue γ has to be chosen as the one with minimal module. This has to be done in this way, because eigenvalues in equation (52) can be shown to be the same as the scalar product between the CASA DF and the difference between this approximate DF and the exact one.

5.2.3. Bader's analysis of ASA DF

It is well known that ASA DF, as discussed before, provides a reliable and sufficiently accurate formulation to be used for quantum similarity measures calculations and in order to obtain iso-density surfaces for large molecular structures.

5.2.3.1. ASA atomic and molecular density functions definition. ASA density functions are constructed by means of simple rules, taking as basic building blocks 1s GTO functions. That is, suppose that the following symbol:

$$|\alpha; \mathbf{A}\rangle = N(\alpha) \exp\left(-\alpha |\mathbf{r} - \mathbf{A}|^2\right) \tag{53}$$

is used to denote such a GTO, centred at some point in space with coordinates $\mathbf{A}$, α being a scaling parameter and finally $N(\alpha)$ representing a normalization factor such that:

$$\langle \mathbf{A}; \alpha | \alpha; \mathbf{A}\rangle = \left|N(\alpha)\right|^2 \int_D \exp\left(-2\alpha |\mathbf{r} - \mathbf{A}|^2\right) d\mathbf{r} = 1. \tag{54}$$

An atomic ASA density can thus be built up by means of the convex linear combination:

$$\rho(\mathbf{r}; \mathbf{A}) = \sum_I^N \Omega_I \left||\alpha_I; \mathbf{A}\rangle\right|^2 = \sum_I^N \Omega_I |\alpha_I; \mathbf{A}\rangle\langle \mathbf{A}; \alpha_I|, \tag{55}$$

by *convex linear combination* it is meant that the convexity property, represented by the *convexity symbol*,

$$K_N\left(\{\Omega_I\}\right) = \left(\{\Omega_I\} \;\middle|\; \forall I\colon\ \Omega_I \in \mathbf{R}^+ \wedge \sum_{I=1}^N \Omega_I = 1\right),$$

holds for the coefficient set $\{\Omega_I\}$.

A molecular ASA DF, as mentioned before, can be obtained by means of the convex linear combination:

$$\rho_M(\mathbf{r}) = \sum_{A \in M} w_A \rho(\mathbf{r}; \mathbf{A}) \tag{56}$$

with the convex property $K(\{w_A\})$ being considered active for the molecular coefficients.

In this way, the molecular ASA density function (56) is chosen as a *shape function*, that is, will be normalized in the sense:

$$\int_D \rho_M(\mathbf{r})\, d\mathbf{r} = 1.$$

The alternative normalization to the number of electrons, N_e, can be obtained simply by using in equation (56) the coefficient set:

$$Z_A = N_e w_A$$

instead of the convex set $\{w_A\}$.

5.2.3.2. Gradient and Hessian of a molecular ASA density function.

(A) *Gradient.* The gradient of an ASA molecular density function can be written as:

$$\frac{\partial}{\partial \mathbf{r}}\left[\rho_M(\mathbf{r})\right] = \sum_{A \in M} w_A \frac{\partial}{\partial \mathbf{r}}\left[\rho_A(\mathbf{r}; \mathbf{A})\right],$$

so, in this way, one arrives finally at a convex linear combination of 1s GTO functions, as:

$$\frac{\partial}{\partial \mathbf{r}}\big[\rho(\mathbf{r};\mathbf{A})\big] = \sum_{I}^{N} \Omega_I \frac{\partial}{\partial \mathbf{r}}\big[\big|\langle \alpha_I;\mathbf{A}\rangle\big|^2\big] = 2\sum_{I}^{N} \Omega_I \frac{\partial}{\partial \mathbf{r}}\big[\langle \alpha_I;\mathbf{A}\rangle\big].$$

Thus, because the 1s GTO gradient can be easily written as a vector with the form:

$$\frac{\partial}{\partial \mathbf{r}}\big[\langle \alpha;\mathbf{A}\rangle\big] = N(\alpha)\frac{\partial}{\partial \mathbf{r}}\big[\exp\big(-\alpha|\mathbf{r}-\mathbf{A}|^2\big)\big] = -2\alpha(\mathbf{r}-\mathbf{A})\langle \alpha;\mathbf{A}\rangle.$$

Then, the gradient of the molecular ASA density function can be written:

$$\frac{\partial}{\partial \mathbf{r}}\big[\rho_M(\mathbf{r})\big] = -2\sum_{A\in M} w_A(\mathbf{r}-\mathbf{A})\Bigg(\sum_{I\in A} \Omega_I^A \alpha_I^A \big|\alpha_I^A;\mathbf{A}\big\rangle\Bigg). \tag{57}$$

(B) *Hessian.* The *Hessian* of an ASA density function is easily constructed too, taking into account that it can be formally written by means of the tensor product of a gradient vector symbol: $\frac{\partial}{\partial \mathbf{r}} \otimes \frac{\partial}{\partial \mathbf{r}}$. So, the second partial derivatives matrix of a 1s GTO function can be written using:

$$\begin{aligned}\frac{\partial}{\partial \mathbf{r}} \otimes \frac{\partial}{\partial \mathbf{r}}\big[\langle \alpha;\mathbf{A}\rangle\big] &= N(\alpha)\frac{\partial}{\partial \mathbf{r}} \otimes \frac{\partial}{\partial \mathbf{r}}\big[\exp\big(-\alpha|\mathbf{r}-\mathbf{A}|^2\big)\big] \\ &= (-2\alpha)\frac{\partial}{\partial \mathbf{r}} \otimes \big[(\mathbf{r}-\mathbf{A})\langle \alpha;\mathbf{A}\rangle\big]\end{aligned}$$

and one can finally write:

$$\begin{aligned}\frac{\partial}{\partial \mathbf{r}} \otimes \frac{\partial}{\partial \mathbf{r}}\big[\langle \alpha;\mathbf{A}\rangle\big] &= \frac{\partial}{\partial \mathbf{r}} \otimes \big[(\mathbf{r}-\mathbf{A})\langle \alpha;\mathbf{A}\rangle\big] \\ &= \big(-2\alpha\langle \alpha;\mathbf{A}\rangle\big)\big(\mathbf{I}_3 - 2\alpha\big[(\mathbf{r}-\mathbf{A})\otimes(\mathbf{r}-\mathbf{A})\big]\big),\end{aligned}$$

where $\mathbf{I}_3$ corresponds to the (3×3) identity matrix.

Thus, the Hessian matrix of an ASA density function may be written in a similar way as the gradient expression (57):

$$\begin{aligned}&\frac{\partial}{\partial \mathbf{r}} \otimes \frac{\partial}{\partial \mathbf{r}}\big[\rho_M(\mathbf{r})\big] \\ &\quad = -2\sum_{A\in M} w_A\Bigg(\sum_{I\in A} \Omega_I^A \alpha_I^A\big(\mathbf{I} - 2\alpha_I^A\big[(\mathbf{r}-\mathbf{A})\otimes(\mathbf{r}-\mathbf{A})\big]\big)\big|\alpha_I^A;\mathbf{A}\big\rangle\Bigg).\end{aligned} \tag{58}$$

(C) *Further gradient and Hessian forms.* Equations (57) and (58), can be easily transformed using simple definitions. Suppose that a new set of functions can be defined using:

$$|\mathbf{r};\mathbf{A}|p\rangle = \sum_{I}^{N} \Omega_I(-2\alpha_I)^p|\alpha_I;\mathbf{A}\rangle,$$

the gradient can be rewritten as:

$$\frac{\partial}{\partial \mathbf{r}}\big[\rho_M(\mathbf{r})\big] = \sum_{A\in M} w_A(\mathbf{r}-\mathbf{A})|\mathbf{r};\mathbf{A}|1\rangle \tag{59}$$

and, in this manner, the Hessian can be rewritten in a simplified form as well:

$$\frac{\partial}{\partial \mathbf{r}} \otimes \frac{\partial}{\partial \mathbf{r}}\big[\rho_M(\mathbf{r})\big] = \sum_{A \in M} w_A\big(|\mathbf{r};\mathbf{A}|1\rangle \mathbf{I}_3 + |\mathbf{r};\mathbf{A}|2\rangle\big[(\mathbf{r}-\mathbf{A}) \otimes (\mathbf{r}-\mathbf{A})\big]\big).$$

5.2.3.3. Bader analysis on ASA density functions. Although there is now a wide discussion about certain mathematical aspects in the literature [68], by knowing the gradient and Hessian of density functions a so-called Bader analysis can be easily performed [8]. According to Bader, the null gradient density function surfaces are interesting elements to be connected with chemical information about bonds and so on.

Null gradient ASA conditions are quite easy to obtain from equation (59), as one can see that some gradient terms will be null just in the sites where the atomic ASA functions have been centred. Moreover, equation (59), after equalizing it to zero, can be arranged in such a way that the following expression can be written:

$$\mathbf{r} = \left(\sum_{A \in M} w_A |\mathbf{r};\mathbf{A}|1\rangle\right)^{-1} \left(\sum_{A \in M} w_A \mathbf{A} |\mathbf{r};\mathbf{A}|1\rangle\right), \tag{60}$$

thus one can try to find out iteratively which values of the position vector, surrounding the associated molecular structure, produce a null gradient result.

In any case, the situation may be obtained, where for a sufficiently far from the molecule position vector, the exponentials could be considered small enough to become equal to a similar number: ε. Then:

$$|\mathbf{r};\mathbf{A}|1\rangle = -2\varepsilon \sum_{I}^{N} \Omega_I \alpha_I = -2\varepsilon \langle \Omega * \alpha \rangle_A,$$

and, in this manner it can be written:

$$\mathbf{r}_0 = \sum_{A \in M} \gamma_A \mathbf{A}, \tag{61}$$

where the coefficient set $\{\gamma_A\}$ is immediately defined by means of:

$$\gamma_A = \left(\sum_{A \in M} w_A \langle \Omega * \alpha \rangle_A\right)^{-1} \big(w_A \langle \Omega * \alpha \rangle_A\big).$$

However, as the sum of the coefficients $\{\gamma_A\}$ is the unit, that is:

$$\sum_A \gamma_A = 1$$

as well as being positive definite, the set is convex: $K(\{\gamma_A\})$ holds. So, the value of the electron position at this point, $\mathbf{r}_0$, given by equation (61), can be seen as an average of the atomic centres with weights provided by the coefficients $\{\gamma_A\}$. This means that the values of the null gradient condition are to be found inside the polyhedron defined by the atomic centres.

This result provides a solution, contradicting the assumption that these points are far away in space. It can be concluded that there are no such kind of null gradient surfaces far away from the molecular centre of mass.

5.3. Generalized density functions

In order to describe a general DF form, the definition and properties of IMP are needed, as found in Section 3 above.

These IMP features and definitions permit us to express DF's in a compact and extremely general form [68,69]. The previous discussion may be employed, first constructing a matrix $\mathbf{W}$ as bearing a convex coefficient hypermatrix of arbitrary dimensions: $\mathrm{Dim}(\mathbf{W}) = \{\delta\}$, that is the convex condition $\boldsymbol{K}_{\{\delta\}}(\mathbf{W})$ holds. In general, this can be obtained by choosing a complex matrix $\mathbf{X}$ with adequate dimension, $\mathrm{Dim}(\mathbf{X}) = \{\delta\}$, such that the inward product is: $\mathbf{W} = \mathbf{X}^* * \mathbf{X}$.

Then, symbolically it is assured that the generating rule also holds, as follows:

$$\boldsymbol{R}(\mathbf{X} \to \mathbf{W}) = \left\{\forall \Omega \in \mathbf{W} \to \exists \chi \in \mathbf{X}\colon\ \Omega = \chi^* \chi = |\chi|^2 \in \mathbf{R}^+\right\}.$$

This special choice can be also described by imposing convex conditions on $\mathbf{W}$, that is:

$$\boldsymbol{K}_{\{\delta\}}(\mathbf{W}) = \left\{\forall \Omega \in \mathbf{W} \to \Omega \in \mathbf{R}^+ \wedge \langle \mathbf{W} \rangle = 1\right\}.$$

In the previous definitions and in what follows next, hypermatrix elements are written without subindices. This is permitted because in IMP definitions the involved hypermatrix elements have to bear the *same* subindex set.

Let us define now a hypermatrix $\mathbf{P}$, possessing such a dimension that: $\mathrm{Dim}(\mathbf{P}) = \mathrm{Dim}(\mathbf{W}) = \{\delta\}$. Moreover, the chosen matrix $\mathbf{P}$ contains, as elements, normalized positive definite multivariate functions of a position vector $\mathbf{R}$ of arbitrary dimension. That is, it can be formally written: $\int \mathbf{P}(\mathbf{R})\, d\mathbf{R} = \mathbf{1}$, $\mathbf{1}$ being the unity matrix, as appears in Definition 10, such that $\mathrm{Dim}(\mathbf{1}) = \{\delta\}$. More specifically, one can compactly write the convenient structure of $\mathbf{P}$, using the following construction rules, which can be summarized by a unique hypermatrix convex condition:

$$\boldsymbol{K}_{\{\delta\}}(\mathbf{P}) = \left\{\forall \mathbf{p}(\mathbf{R}) \in \mathbf{P} \to \forall \mathbf{R}\colon\ \mathbf{p}(\mathbf{R}) \in \mathbf{R}^+ \wedge \int \mathbf{p}(\mathbf{R})\, d\mathbf{R} = 1\right\}.$$

This convex structure can be accomplished by constructing an IMP like $\mathbf{P} = \boldsymbol{\Psi}^* * \boldsymbol{\Psi}$, being $\mathrm{Dim}(\boldsymbol{\Psi}) = \{\delta\}$, so that a generating rule may be issued in such terms that:

$$\boldsymbol{R}(\boldsymbol{\Psi} \to \mathbf{P}) = \left\{\forall \mathbf{p} \in \mathbf{P} \to \exists \varphi \in \boldsymbol{\Psi}\colon\ \mathbf{p} = |\varphi|^2\right\}.$$

Keeping this in mind, a normalized density function of the position variables vector $\mathbf{R}$ can be also expressed as an IMP, like:

$$\rho(\mathbf{R}) = \langle \mathbf{W} * \mathbf{P} \rangle \Rightarrow \int \rho(\mathbf{R})\, d\mathbf{R} = 1,$$

where the matrix elements sum has been used as previously commented in Definition 3.

5.4. Average density functions

Several examples of average DF can be imagined from the DF properties described in preceding sections. Some particular cases have been chosen in order to describe representative problems in the field of QSM evaluation for molecular sets, possessing some kind of degrees of freedom not yet taken into account in the usual computations performed to date.

A recent paper by Mezey [70] describes several aspects of the theoretical basis of the DF distribution problem when numerous conformational coordinates are active, although it must be said that the paper studies some formal aspects, which are not taken into account here.

Two sections will present, first, the problems posed by conformational Boltzmann averages within a discrete as well as in a continuous framework. Next, a DF chiral average will be analyzed in order to take into account possible similarity comparisons in molecular structures within the presence of R-S isomers. Finally, a general algorithm to perform any kind of DF average will be presented.

5.4.1. Discrete conformational Boltzmann averages

One of the most obvious problems in quantum chemistry, when studying a molecular structure possessing a flexible atomic backbone, is how to use the conformational surface in order to take into account, simultaneously and as much as possible, the information associated with the presence of conformers. This is most necessary, for example, in QQSAR studies based on molecular QSM, where by employing a unique conformation the associated molecular discrete description could deviate from the optimal values.

The problem posed when comparing two molecules with a chosen number of internal degrees of freedom, besides presenting great difficulties, is a challenging one. Here, we present a possible solution, which will be based on the theoretical description previously given. Essentially, the discussion accompanying equation (41) and the generalized DF form of the preceding paragraph can be taken into account to seek a solution to the problem.

From the point of view of the clamped nuclei approach, for every Kth conformer of a given molecular structure, M, there can be associated a set of fixed atomic coordinates: $\mathbf{R}_K^M = \{\mathbf{r}_{IK}^M\}$, $I = 1, N$, where N is the number of atoms in the molecule M. For each molecular state, every conformer K can be associated with a particular pair of energy and DF: $\{E_K^M; \rho_K^M(\mathbf{r}; \mathbf{R}_K^M)\}$, as already discussed in Section 2.2.

A unique DF, representative of the average molecular conformations, can be easily built up, by means of the definition of the energy differences: $\{\Delta E_K^M = E_K^M - E_0^M\}$, being $E_0^M = \min_K(E_K^M)$. With the set of conformational energy differences a convex vector can be built up, simply using a Boltzmann distribution, with a partition function immediately defined with the conformational energy information as:

$$\mathbf{z}_M = \left\{z_K^M = \exp\left(-\Delta E_K^M / kT\right)\right\} \in \boldsymbol{V}_\nu\left(\mathbf{R}^+\right) \wedge \theta_M = \langle \mathbf{z}_M \rangle \rightarrow$$
$$\mathbf{w}_M = \theta_M^{-1}\mathbf{z}_M \wedge \boldsymbol{K}_\nu(\mathbf{w}_M). \tag{62}$$

The Boltzmann partition function vector $\mathbf{w}_M = \{w_K^M\}$ can be used as a set of weights over the conformation DF set in order to obtain a unique average DF:

$$\rho_M(\mathbf{r}) = \sum_{K=1}^{\nu} w_K^M \rho_K^M\left(\mathbf{r}; \mathbf{R}_K^M\right). \tag{63}$$

In this way a unique similarity measure, involving two molecular structures $\{A, B\}$ say, but possessing several conformers: $\{\nu_A, \nu_B\}$ in number, can be obtained as:

$$z_{AB}(\Omega) = \sum_K^{\nu_A} \sum_L^{\nu_B} w_K^A w_L^B \left\langle \rho_K^A \middle| \Omega \middle| \rho_L^B \right\rangle. \tag{64}$$

Expression (64) amounts to the same as considering each conformer like a distinct molecular species, because of the Born–Oppenheimer approximation. Gathering all QSM pairs between conformers into a unique $(\nu_A \times \nu_B)$ SM: $\mathbf{Z}^{AB} = \{z_{KL}^{AB} = \langle \rho_K^A | \Omega | \rho_L^B \rangle\}$, then the conformationally averaged QSM (64) can be conveniently expressed in terms of a bilinear functional. Using the Boltzmann weight vectors $\{\mathbf{w}_A; \mathbf{w}_B\}$ for each conformer molecular set, hence:

$$z_{AB}(\Omega) = \mathbf{w}_A^T \mathbf{Z}^{AB} \mathbf{w}_B.$$

5.4.2. Continuous conformational Boltzmann averages

Where the conformational surface can be associated with a continuous set of variables $\{\mathbf{t}\}$, then instead of discrete energy-DF pairs, two functions of $\{\mathbf{t}\}$ can be associated with each state, and symbolized by: $\{E_M(\mathbf{t}), \rho_M(\mathbf{r}, \mathbf{t})\}$. From the energy set a convex partition function may be obtained, using:

$$E_M^0(\mathbf{t}) = \min_{\mathbf{t}} \{E_M(\mathbf{t})\} \wedge \Delta E_M(\mathbf{t}) = E_M(\mathbf{t}) - E_M^0(\mathbf{t})$$

thus, a partition function is easily constructed:

$$z_M(\mathbf{t}) = \exp\left(-\Delta E_M(\mathbf{t})/kT\right)$$

and then a continuous Boltzmann weight function can be defined as:

$$w_M(\mathbf{t}) = \theta_M^{-1} z_M(\mathbf{t}) \wedge \theta_M = \int z_M(\mathbf{t})\, d\mathbf{t} \to \boldsymbol{K}_\infty(w_M),$$

so, an average DF can be readily computed by means of the integral:

$$\rho_M(\mathbf{r}) = \int w_M(\mathbf{t}) \rho_M(\mathbf{r}, \mathbf{t})\, d\mathbf{t}. \tag{65}$$

Equation (65) appears to be the continuous equivalent of expression (63).

Finally, the QSM between two continuous averaged DF can be also expressed in a compact integral form:

$$\begin{aligned} z_{AB}(\Omega) &= \iint \rho_A(\mathbf{r}_1) \Omega(\mathbf{r}_1, \mathbf{r}_2) \rho_B(\mathbf{r}_2)\, d\mathbf{r}_1\, d\mathbf{r}_2 \\ &= \iint \left(\int w_A(\mathbf{t}_1) \rho_A(\mathbf{r}_1, \mathbf{t}_1)\, d\mathbf{t}_1 \right) \Omega(\mathbf{r}_1, \mathbf{r}_2) \\ &\quad \times \left(\int w_B(\mathbf{t}_2) \rho_B(\mathbf{r}_2, \mathbf{t}_2)\, d\mathbf{t}_2 \right) d\mathbf{r}_1\, d\mathbf{r}_2 \\ &= \iint w_A(\mathbf{t}_1) w_B(\mathbf{t}_2) \left(\iint \rho_A(\mathbf{r}_1, \mathbf{t}_1) \Omega(\mathbf{r}_1, \mathbf{r}_2) \rho_B(\mathbf{r}_2, \mathbf{t}_2)\, d\mathbf{r}_1\, d\mathbf{r}_2 \right) d\mathbf{t}_1\, d\mathbf{t}_2 \\ &= \iint w_A(\mathbf{t}_1) w_B(\mathbf{t}_2) \Theta_{AB}(\mathbf{t}_1, \mathbf{t}_2)\, d\mathbf{t}_1\, d\mathbf{t}_2 \end{aligned}$$

which is the continuous equivalent part of equation (64).

5.4.3. Chiral R-S averages

When R-S chiral structures are to be studied and included in similarity studies, a Boltzmann average computation is not possible, for the simple reason that in the absence of a chiral field the Schrödinger equation will yield the same energy value for both R-S enantiomeric forms. However, this is not the same when similarity integrals are concerned, see [71] for a recent application.

To understand the problem, let us suppose that the DF of the enantiomers are written as the pair: $\{\rho_R; \rho_S\}$. The QSSM will yield the same values, that is:

$$z_{RR} = z_{SS} = \alpha;$$

however, the cross-QSM between the enantiomers will be symmetric:

$$z_{RS} = z_{SR} = \beta,$$

but different from the common R-S QSSM. Both values will be related as:

$$\alpha > \beta.$$

Therefore, the symmetric (2×2) similarity matrix involving the chiral DF will present two definite positive eigenvalues in the form:

$$\theta_{\pm} = \alpha \pm \beta,$$

to which corresponds the following eigenvector pair:

$$\mathbf{u}_{\pm} = \frac{1}{\sqrt{2}}(1; \pm 1)^T. \tag{66}$$

The corresponding orthogonal (2×2) matrix, which has the eigenvector couple, as described above, as columns, can be considered as a possible transformation of the (2×2) SM so as to make it diagonal. The maximal eigenvalue, θ_+, corresponds to a maximal QSSM of the R-S pair, which results in a value like:

$$z_{\max} = z_{RR} + z_{RS} = z_{SS} + z_{RS}.$$

This is the same as is used for the chiral system, a corrected DF average expressed as an arithmetic mean mixture of both enantiomers:

$$\rho^{av} = \frac{1}{2}(\rho_R + \rho_S).$$

Thus, the difficult case, from the point of view of classical QSAR treatment, associated with the descriptors of molecular chiral structures, can be solved in this simple, but logical, way. An SM element between two chiral systems of this sort is computed straightforwardly as:

$$z_{AB}^{av} = \langle \rho_A^{av} | \Omega | \rho_B^{av} \rangle = \frac{1}{4}\left(z_{AB}^{RR} + z_{AB}^{RS} + z_{AB}^{SR} + z_{AB}^{SS}\right).$$

The integrals involving R-R and S-S pairs will be equivalent, and the central terms involving the R-S and S-R DF may differ slightly due to the need to search for a superposition of both structures to achieve a maximal QSM. However, due to the average even these slight differences could be smoothed. Then, the averaged QSM will become equivalent to the one

involving a unique chiral system, with the crossed term transformed into a possible arithmetic average. Finally, the form which SM element values take when a chiral structure is compared with some achiral one should be noted. Then, for example, it can be written:

$$z_{AB}^{av} = \langle \rho_A^{av} | \Omega | \rho_B \rangle = \frac{1}{2}\left(z_{AB}^{R} + z_{AB}^{S}\right).$$

The most general case, where several chiral centers are present, generating an indefinite amount of chiral pair structures, cannot be studied in this simple way but demands a deeper analysis. The section below presents a possible solution of the average problem, which can be widely used in all the discussed cases and in other situations involving the same QO but diverse independent DF.

5.4.4. General average DF

The R-S case analyzed above is nothing more than a very particular case of a possible general situation, which was studied several years ago [25] in another context and in a quite schematic way, in reference to SCF Theory.

In order to see how an average DF can be obtained from QSM analysis, suppose that for a given QO—A, say—there are N known sub-structural features, which can produce a homogeneous set of DF: $\mathsf{P}_A = \{\rho_I^A(\mathbf{R});\ (I = 1, N)\}$, reflecting in turn the differences between the isomers, conformers, states or whatever source of diversity can be taken into account over the original QO A. In order to have a generic name for these difference characteristics one can choose the description: *QO distinct features* (*QODF*). Thus, QODF split a given QO into several QO's and can be considered, according to Definition 7′, as a source to build of Tagged Ensembles.

As discussed above, an SM attached to the QO A can be built-up from a chosen PD weight operator, Ω, and the DF set P_A. At this stage one can easily see that the QO A sub-structural QODF can be considered as a QOS itself, where the distinct QO A DF's, act as tags. Such a QOS can be named as a QOS *generated by the QO A*. The attached SM, whose columns can be used to build an attached DQOS to QO A up, may be identified as:

$$\mathbf{Z}_{AA} = \left\{z_{IJ}^{AA} = \langle \rho_I^A | \Omega | \rho_J^A \rangle\right\}.$$

The SM $\mathbf{Z}_{AA}$, itself can be used in turn as a source of averaging coefficients in a straightforward manner. Suppose the eigensystem of the SM $\mathbf{Z}_{AA}$ has been computed and can be expressed by the symbol: $Eigensys[\mathbf{Z}_{AA}] = [\{\theta_I^A; \mathbf{c}_I^A\};\ (I = 1, N)]$. This means, then, that the following secular equation is fulfilled:

$$\forall I:\ \mathbf{Z}_{AA}\mathbf{c}_I^A = \theta_I^A \mathbf{c}_I^A.$$

In addition, the following relevant properties also hold:

$$\forall I:\ \left(\mathbf{c}_I^A\right)^T \mathbf{Z}_{AA}\mathbf{c}_I^A = \theta_I^A \wedge \left(\mathbf{c}_I^A\right)^T \mathbf{c}_I^A = 1. \tag{67}$$

These eigensystem properties allow us to consider at least two possible forms of weighting coefficient averages.

5.4.4.1. Frobenius average DF. Because any SM has the feature $\mathbf{Z}_{AA}* > 0$, see Definition 13, of being strictly positive, then the Frobenius theorem [72] can be invoked to confirm that if the spectrum of $\mathbf{Z}_{AA}$ is ordered in such a way that $\theta_1^A > \theta_2^A > \cdots > \theta_N^A$,

then consequently $\mathbf{c}_1^A * > 0$. Thus, a convex transformation can be easily imagined, producing a new vector:

$$\mathbf{w}_A = \langle \mathbf{c}_1^A \rangle^{-1} \mathbf{c}_1^A = \{ w_I^A = \langle \mathbf{c}_1^A \rangle^{-1} c_{I1}^A \} \to \boldsymbol{K}_N(\mathbf{w}_A).$$

Afterwards, the convex vector $\mathbf{w}_A$ can be used to obtain an averaged DF, which can be considered as a unique tag for the QO A, including contributions over all the tag set P_A, as:

$$\rho_A = \sum_I w_I^A \rho_I^A, \tag{68}$$

with the important additional structure such that $\boldsymbol{K}_\infty(\rho_A)$ holds. So an average QSSM can be easily written for the QO A:

$$\begin{aligned} z_{AA}^{av} &= \langle \rho_A | \Omega | \rho_A \rangle = \mathbf{w}_A^T \mathbf{Z}_{AA} \mathbf{w}_A = \sum_I \sum_J w_I^A w_J^A z_{IJ}^{AA} \\ &= \langle \mathbf{c}_1^A \rangle^{-2} (\mathbf{c}_1^A)^T \mathbf{Z}_{AA} \mathbf{c}_1^A = \langle \mathbf{c}_1^A \rangle^{-2} \theta_1^A. \end{aligned}$$

Invoking the same arguments and using the appropriate QODF for another QO B, an average SM element can be described in the same fashion:

$$\begin{aligned} z_{AB}^{av} &= \langle \rho_A | \Omega | \rho_B \rangle = \mathbf{w}_A^T \mathbf{Z}_{AB} \mathbf{w}_B = \sum_I \sum_J w_I^A w_J^B z_{IJ}^{AB} \\ &= \left(\langle \mathbf{c}_1^A | \langle \mathbf{c}_1^B \rangle \right)^{-1} (\mathbf{c}_1^A)^T \mathbf{Z}_{AB} \mathbf{c}_1^B. \end{aligned} \tag{69}$$

Such an average procedure leading to a specific DF, which can be called, for obvious reasons, a *Frobenius average DF*, has the disadvantage of providing, as Boltzmann averages, a unique possible DF choice. In the next section a more flexible approach will be analyzed.

5.4.4.2. IMP average DF. IMP properties can be invoked once the $\mathbf{Z}_{AA}$ eigensystem is known. The set $\{\mathbf{c}_I^A;\ (I = 1, N)\}$ of $\mathbf{Z}_{AA}$ eigenvectors are a natural source of normalized vectors, which can be used as generating vectors for another set of convex vectors weights, that is:

$$\forall I\colon \boldsymbol{R}_N(\mathbf{c}_I^A \to \mathbf{w}_I^A) \Rightarrow \boldsymbol{K}_N(\mathbf{w}_I^A),$$

or, alternatively, using the properties in equation (67) plus the IMP definition a set of average convex weights can be easily defined as:

$$\forall I\colon \mathbf{w}_I^A = \mathbf{c}_I^A * \mathbf{c}_I^A \to \boldsymbol{K}_N(\mathbf{w}_I^A).$$

The possible average DF, which can be constructed in this framework, can be written in the form:

$$\rho_{A;I}^{av} = \sum_J w_{JI}^A \rho_J^A.$$

In this case the averaged QSSM will be written as:

$$\begin{aligned} z_{AA;I}^{av} &= \langle \rho_{A;I}^{av} | \Omega | \rho_{A;I}^{av} \rangle = (\mathbf{w}_I^A)^T \mathbf{Z}_{AA} \mathbf{w}_I^A = \sum_J \sum_K w_{JI}^A w_{KI}^A z_{JK}^{AA} \\ &= \sum_J \sum_K (c_{JI}^A)^2 (c_{KI}^A)^2 z_{JK}^{AA}. \end{aligned}$$

So, adopting the *principle of the maximal QSSM value*, the final average QSSM associated with the QO A, may be easily chosen with the algorithm:

$$z_{AA}^{av} = \max_{I}\left(z_{AA;I}^{av}\right).$$

QSM between two different QO can be obtained in a similar way as in equation (69), just substituting the involved average DF by the corresponding ones obtained in this approach. The IMP convex averaging in front of the former Frobenius average has the freedom of N possible choices.

5.4.4.3. Concluding remarks. Consequently, one can say that general algorithms to construct DF and QSM averages over QOS, where specific QODF are well defined, can be easily applied to any QOS tagged ensemble to reduce it to a simpler QOS. Those described *geometry based average algorithms* can be used, of course, instead of the Boltzmann average procedures, even in the conformer average case.

6. EXTENDED HILBERT SPACES, SOBOLEV SPACES AND DENSITY FUNCTIONS

Following the previous discussion, we now develop some ideas about the connection between DF as a product of the squared wave function module and the distribution-like function, arising from the squared module associated with the gradient of the wave function itself, which has been formerly considered as a distribution [73,74] in the literature.

This study, connecting wave functions and their attached gradients, may have interesting consequences when writing expectation values in the fashion QSM needs to attain a coherent theoretical background. Several arguments permit us to discover the role performed by the practical formalism attached to *extended Hilbert spaces* (EHS), where wave functions and their gradients are taken simultaneously into account. In EHS one can connect expectation values to a unique statistical formalism. Mainly, this theoretical structure is related to the approximate way the Schrödinger equation has to be studied, when a molecular solution is looked for.

There is another interesting question, not yet discussed in the quantum mechanical literature as it deserves, and which will be studied as far as possible here. It could be attached to the interpretation of the differential operators role, as momentum representatives within the framework of classical quantum mechanics, when the position space point of view is chosen.

In order to achieve these objectives, we first discuss several novel aspects of the expectation value concept.

6.1. Expectation values

When studying a quantum mechanical system, the expectation value of some observable Ω, in a well-defined QO system state, can be written by means of the integral:

$$\langle \Omega \rangle = \int W(\mathbf{r})\rho(\mathbf{r})\, d\mathbf{r}, \tag{70}$$

where $W(\mathbf{r})$ is an associated Hermitian operator to be determined for a given QOS, and $\rho(\mathbf{r})$ the system state density function.

On the other hand, the expression (70), from a QQSAR point of view, can be interpreted as a scalar product [36a], that is:

$$\langle \Omega \rangle = \langle W|\rho \rangle. \tag{71}$$

Taking into account the unknown nature of the QQSAR operator $W(\mathbf{r})$, one can consider that it can be decomposed as a product of the operator leading to the expectation value $W_\Omega(\mathbf{r})$, still unknown and to be determined, by a known PD weight operator, $\Omega(\mathbf{r}, \mathbf{r}_0)$. Thus, the expectation value as presented in expression (70) can be written now as:

$$\langle \Omega \rangle = \langle W_\Omega|\Omega|\rho \rangle. \tag{72}$$

This is the same as transforming equation (70) into the equivalent, more general integral:

$$\langle \Omega \rangle = \iint W_\Omega(\mathbf{r})\Omega(\mathbf{r}, \mathbf{r}_0)\rho(\mathbf{r}_0)\, d\mathbf{r}\, d\mathbf{r}_0. \tag{73}$$

It is easy to see that the PD weight operator $\Omega(\mathbf{r}, \mathbf{r}_0)$ can particularly be chosen as the Dirac's delta function, $\delta(\mathbf{r}-\mathbf{r}_0)$, and, thus, in doing so, equation (70) is recovered. In order to distinguish the expectation value general definition, as presented in equation (73) from the usual choice in equation (70), where the weight can be considered a unit operator, the general integral (73) can be named as a *weighted expectation value* integral expression. It is interesting to note that expression (73) has a formal structure highly resembling the two-system QSM integral as given in equation (14).

6.2. Problem setup

After structuring the statistical representation of the expectation value integrals, a more in-depth study shows that there appears to be present a formal quantum mechanical puzzle when one tries to connect a second order differential operator, representing a QO kinetic energy (KE), using the expression of an expectation value in the statistical formalism, represented by equation (70). KE expectation values, as usually presented in the literature, do not fulfil the general statistical formalism represented by equations (71)–(73). On the contrary, as they are described, they possess a kind of expression according to the following well-known equation:

$$\langle \Omega \rangle = \langle \Psi|\Omega|\Psi \rangle = \iint \Psi^*(\mathbf{r}_1)\Omega(\mathbf{r}_1; \mathbf{r}_2)\Psi(\mathbf{r}_2)\, d\mathbf{r}_1\, d\mathbf{r}_2, \tag{74}$$

as can be found in any treatise; see, for instance, the Bohm [24], Messiah [75] or Shankar [76] discussions. However, the KE expectation value adequately transformed and, avoiding some scalar factors, looks like a norm. This can be easily seen when writing the following equalities:

$$2\langle K \rangle = -\int \Psi^* \nabla^2 \Psi\, d\mathbf{r} = \int (\nabla\Psi)^*(\nabla\Psi)\, d\mathbf{r}, \tag{75}$$

where the change of sign can be attributed to Green's first identity [77]. A similar procedure has been also used in the evaluation of KE integral representation over atomic

basis sets [78]. Equation (75) has been customarily employed since the first description of DFT [73] and is used as a working tool in this context hereafter [74]. Concerning the absence of a scalar imaginary unit factor accompanying the *nabla* operator in expression (75) and in the following equations, it is apparently not imperative for the purpose of the present discussion to use this imaginary scalar factor. Moreover, equation (75) indicates that KE will necessarily become a PD quantity, being the result of a norm-like expression.

Available textbooks do not explain this situation; see for a recent example reference [79]. However, the current literature presents it as a *de facto* characteristic feature of quantum mechanics. The usual trend is to classify this oddity within the fuzziness of quantum mechanical postulates.[8] Other authors introduce KE expectation values throughout mathematical manipulations that are not exempt of difficulty [24].

6.3. Extended Hilbert spaces

In order to summarize the whole picture concerning expectation values, it can be said that quantum mechanics allows generic expectation values as computational forms, like the integral (70). When using this formal structure and the particular examples, where the involved Hermitian operator is expressed by functions of the position coordinates, the integral values represent an expectation value, exactly in the same way as in theoretical statistics. However, when gradient operators appear in the computational scenario, the expectation value integral has to be modified, adopting a form as the one shown in equation (74). This kind of integral expression transforms into equation (70) only in the case where the operator, Ω, does not depend on the momentum as a variable. Equation (70) loses sense, for instance, when the kinetic energy Laplacian operator is to be computed, and integral (74) necessarily emerges. On the contrary, when the involved operator is a function of the position only, then both integrals are equivalent. Thus, one could take the decision to accept the form given in the integral (74) as the adequate quantum mechanical expression of the expectation values that should be always adopted. However, when doing so, the presence of the DF role is paradoxically lost.

The question may be formulated whether it is possible to find a coherent computational way to obtain a statistically meaningful expression for expectation values in any observable operator case. This is irrespective of the system's observables being made either of momentum or position functions. Moreover, if it is possible to find such a general way, in the expectation value general expression, the DF must be explicitly present and featuring the customary role of probability distributions as in theoretical statistics.

A possible way to solve the problem will be shortly described in terms of the points discussed up to now, a detailed account will be presented elsewhere [89]. Suppose that the original Hilbert space, $\boldsymbol{H}(\mathbf{C})$, where wave functions belong, is extended into another one, $\boldsymbol{H}^{(\nabla)}(\mathbf{C})$, which contains *both wave functions and their first derivatives*, the quantum mechanical momentum representation accompanying the wave function is:

$$\forall \Psi \in \boldsymbol{H}(\mathbf{C}) \quad \Rightarrow \quad \Psi \in \boldsymbol{H}^{(\nabla)}(\mathbf{C}) \wedge \exists \nabla(\Psi) \in \boldsymbol{H}^{(\nabla)}(\mathbf{C}).$$

[8] Proposed since the formulation of quantum theory, the quantum mechanical postulates in the literature are characterized by quite a large set of variants. This can be evidenced by perusal of several reference texts [75, 76,79–86]. One can find there, from no postulate description at all [87], up to quite long lists of them [85]. The suggestion can even be found that quantum mechanical postulates should be substituted by adequate definitions instead [88].

Such a possible feature can be found, as an example, within a typical set of solutions of the Schrödinger equation. The harmonic oscillator provides an obvious particular case of such an EH space. It is well known that harmonic oscillator solutions constitute the set of Hermite polynomials, weighted by a Gaussian function [80]. These polynomials can be considered to be related to the GTO basis functions most widely used in contemporary Quantum Chemistry. First derivatives of Hermite polynomials are always well defined, producing another polynomial of the same kind.

Following this line of thought, besides the properties customarily attached to wave functions [75], a need for an additional condition can be stressed. It might consist in that the same properties of wave functions must be fulfilled by their first derivatives. This has not to be taken as an oddity, but it has been clearly noted in the quantum mechanical analysis of wave functions. See, for instance, the work of Messiah [75] or Bohm [24] and the Hilbert space properties provided by Löwdin [6], where it is said that the norms of both wave function and its gradient must be finite. In these studies, it was repeated many times that both wave functions and their first derivatives must possess the same mathematical characteristics.

6.4. Considerations on EHS functions

Then, considering the attached VSS, $\boldsymbol{H}(\mathbf{R}^+)$, where the DF belong, one can also accept that:

$$\forall \rho = |\Psi|^2 \in \boldsymbol{H}\left(\mathbf{R}^+\right) \quad \Rightarrow \quad \exists \kappa = |\nabla \Psi|^2 \in \boldsymbol{H}\left(\mathbf{R}^+\right)$$

to every DF, ρ, there exists in this way a momentum DF. Perhaps, in order to distinguish one DF from another, a better description would be to call this kind, κ, of first derivative distribution: *kinetic energy DF* (KE DF), in the same way as March [74] refers to it. The KE DF belongs to a specific Hilbert VSS, and when integrated provides the expectation value of the associated QO KE. The following sequence, developing details appearing in equation (75), will shed light on the proposed question:

$$\begin{aligned} 2\langle K \rangle &= \int \kappa \, dV = \int |\nabla \Psi|^2 \, dV = \int (\nabla \Psi)^* \cdot (\nabla \Psi) \, dV \\ &= -\int \Psi^* |\nabla|^2 \Psi \, dV = -\left\langle |\nabla|^2 \right\rangle \equiv -\int \Psi^* \Delta \Psi \, dV = -\langle \Delta \rangle, \end{aligned} \tag{76}$$

where the negative sign appears as a consequence of Green's first identity [77], as has been commented upon when equation (75) was discussed. KE DF can be considered normalized, in the same way as eDF can be normalized too. In this case the norm of KE DF is twice the system's KE.

It can be concluded that KE can be considered as related to the norm of the QO wave functions gradient. As a consequence it could be interesting to obtain KE DF, κ, maps or images in the same way as they are customarily obtained for the eDF, ρ [8,15a]. Complementary information to eDF will surely be obtained from these representations. Similar shapes of both functions at large distances from the molecular nuclei can be expected, but having very different behaviour near the nuclei.

A related discussion can be found in Bohm's treatise [24], when diverse possible time-dependent DF forms in a relativistic framework are presented. For non-stationary relativistic states, a function made of a combination of eDF and KE DF is proposed and rejected

afterwards by this author, due to the variant character of such a function. However, for stationary states and in a non-relativistic, classical quantum mechanical environment such a proposal may become interesting and could be related to Bader's analysis [8]. The term KE DF, as it was commented before, can be considered here and is borrowed from March volume on DFT [74]. In this study, KE DF is widely used in connection with the DFT of exchange and potential contributions.

As pointed out in Section 2.3 above and later on, being both DF, ρ and κ, elements of a VSS, then there is nothing to oppose performing a convex linear combination as:

$$\lambda(\mathbf{r}) = \alpha\rho(\mathbf{r}) + (1-\alpha)\kappa(\mathbf{r}), \tag{77}$$

where the scalar coefficient $\alpha \in [0, 1]$, acts as a weight balancing both density distributions. The combined DF still will bear a structure of probability distribution whenever the KE DF is adequately normalized. The KE DF normalization factor can be trivially deduced from equation (76) to be: $(2\langle K\rangle)^{-1}$, but in the present study, the same can be achieved whenever the ASA approach is used with every term present in the linear combination normalized.

This new function will propose a way to describe, within the framework of the uncertainty principle, a joint particle-momentum distribution. Equation (77), if interpreted from the underlying statistical point of view, can be associated with the joint probability of observing the electronic density *or* the kinetic energy density, weighted by the convex scalars α and $(1-\alpha)$. This choice has been used to study a pretended MO paradox [90].

6.5. Generating rules in EH spaces

It now seems plausible to summarize the features of this discussion. To obtain a coherent picture, with KE occupying an important place, among other quantum mechanical structures, then the EH VS, $\boldsymbol{H}^{(\nabla)}(\mathbf{C})$, could be defined as not only containing raw wave functions but their first derivatives too. This allows us to construct the associated DF VSS, $\boldsymbol{H}^{(\nabla)}(\mathbf{R}^{+})$, as containing not only DF but also KE DF. The elements of this peculiar EH VS, where both wave functions and their gradients are contained, can be ordered in the form of column vectors, like:

$$|\Phi\rangle = |\Psi; \nabla\Psi\rangle \in \boldsymbol{H}^{(\nabla)}(\mathbf{C}), \tag{78}$$

and this form could be attached to some scalar-to-vector transformation using a vector operator, involving the gradient, such as:

$$|1; \nabla\rangle[\Psi] = |\Psi; \nabla\Psi\rangle = |\Phi\rangle. \tag{79}$$

In the case of one particle QO, the necessary quadrivector structure, which must adopt the extended wave functions, acquires a qualitative similarity to relativistic spinors [91]. In order to obtain mathematical coherence, even in non-relativistic Quantum Mechanics, it seems that it can be easily employed a vector-like wave function representation, originating from the presence of momentum and thus of KE differential operators. An idea of Levy-Leblond [92], recently quoted by Karwowski [93] can be related to this feature.

An appropriate *generating rule* defined within the extended wave function domain, can now be written as:

$$\boldsymbol{R}\big(|\Phi\rangle \to |\rho;\kappa\rangle\big) = \big\{\forall|\Phi\rangle = |\Psi;\nabla\Psi\rangle \in \boldsymbol{H}^{(\nabla)}(\mathbf{C}) \to \exists\rho = \Psi^*\Psi = |\Psi|^2 \wedge \exists\kappa = (\nabla\Psi)^*(\nabla\Psi) = |\nabla\Psi|^2 \quad \Rightarrow |\rho;\kappa\rangle \in \boldsymbol{H}^{(\nabla)}\big(\mathbf{R}^+\big)\big\}. \tag{80}$$

6.5.1. Diagonal representations in EHS

The structure of EHS elements can be also cast into a diagonal form. To present this possibility, the structure of equation (79) wave function should be visualized in another formal context, where the same potential operations can be performed.

Assume that the extended wave functions can be written as:

$$|\Phi\rangle = |\Psi;\nabla\Psi\rangle \equiv \mathrm{Diag}(\Psi;\nabla\Psi).$$

Then, the generating rule (80) can be applied in the same manner, but with the additional easiness that the product of diagonal matrices can be used. Then, the extended DF can be obtained by means of the simple operation:

$$\begin{aligned}\mathrm{Diag}(\rho;\kappa) &= \big|\mathrm{Diag}(\Psi;\nabla\Psi)\big|^2 = \mathrm{Diag}(\Psi;\nabla\Psi)^*\,\mathrm{Diag}(\Psi;\nabla\Psi)\\ &= \mathrm{Diag}\big(|\Psi|^2;|\nabla\Psi|^2\big).\end{aligned}$$

Finally, it should be noted that IMP can be also employed with similar results, taking into account the close connection between the diagonal matrix product and IMP.

6.6. Extended wave function projectors

The projectors, associated with the extended quantum mechanical wave functions $|\Phi\rangle$, as defined in equation (79), will possess a matrix structure, which can be written as:

$$|\Phi\rangle\langle\Phi| = \begin{pmatrix} |\Psi|^2 & \Psi^*(\nabla\Psi) \\ (\nabla\Psi)^*\Psi & (\nabla\Psi)^* \otimes (\nabla\Psi) \end{pmatrix} = P. \tag{81}$$

Then, using the symmetrization $Q = \frac{1}{2}(P^+ + P)$, the new projector could be rewritten as the matrix:

$$Q = \begin{pmatrix} \rho & |\mathbf{j}\rangle \\ \langle\mathbf{j}| & \mathbf{K} \end{pmatrix},$$

where $\mathbf{K}$ bears a certain resemblance to the Hessian matrix of the eDF. Then, defining the composite density:

$$\kappa = \mathrm{Tr}(\mathbf{K}): \quad \mathrm{Tr}(Q) = \mathrm{Tr}(P) = \rho + \kappa,$$

and the off-diagonal elements can be related to the current density (see, for example, [75]) except for an imaginary constant factor:

$$|\mathbf{j}\rangle = \frac{1}{2}\big(\Psi^*(\nabla\Psi) + (\nabla\Psi)^*\Psi\big).$$

6.7. Sobolev spaces

The resultant structure of the extended Hilbert space norms can be associated with the usual form of a Sobolev space [94]. In Sobolev spaces [95], the norm of any of their elements, Ψ say, is defined within a general formulation as:

$$\|\Psi\|_n^m = \sum_{p=0}^{m} \left\| \nabla^p \Psi \right\|_n, \tag{82}$$

where the first term on the sum in equation (82) has to be considered as a way to write the bulk wave function:

$$\nabla^0 \Psi \equiv \Psi. \tag{83}$$

It is obvious that the extended Hilbert space functions from the point of view of the above-defined norms can be considered a Sobolev space with the norm defined as:

$$\langle \Phi | \Phi \rangle \equiv \|\Psi\|_2^1. \tag{84}$$

6.7.1. Generalized Sobolev spaces

A trivial generalization of Sobolev spaces can be readily described, taking as a starting point the extended Hilbert spaces as defined above. Suppose that the Sobolev definition (82) can be generalized in such a way that it can be written, among other possibilities, as:

$$\|\Psi\|_n^{r;s} = \sum_{p=1}^{r} \left\| |\Psi|^p \right\|_n + \sum_{q=1}^{s} \left\| \nabla^q \Psi \right\|_n. \tag{85}$$

In a symmetrical way with the first term in equation (85), the following norm can be also defined:

$$\|\Psi\|_n^{r;s;t} = \sum_{p=1}^{r} \left\| |\Psi|^p \right\|_n + \sum_{k=1}^{t} \sum_{q=1}^{s} \left\| \left| \nabla^q \Psi \right|^k \right\|_n, \tag{86}$$

so, in fact equation (86) transforms into (85), when $t = 1$, in the same way as equation (85) transforms into the original Sobolev definition (82) when $r = 1$.

Taking this into account and the conventional meaning of the zeroth order gradient symbol, as already described in equation (83), one can first try to reach an extended Hilbert space whose functions can be associated with a generalized Sobolev space (85) with the following norm structure:

$$\langle \Phi | \Phi \rangle \equiv \|\Psi\|_2^{2;1} = \|\Psi\|_2 + \left\| |\Psi|^2 \right\|_2 + \|\nabla \Psi\|_2.$$

So, we may write anew the vector form of the extended wave functions as a three-dimensional column matrix:

$$|\Phi\rangle = \begin{pmatrix} \Psi \\ |\Psi|^2 \\ \nabla \Psi \end{pmatrix} = \begin{pmatrix} \Psi \\ \rho \\ \nabla \Psi \end{pmatrix} \tag{87}$$

taking into account that the density function ρ in the expression (87) is the squared module of the initial wave function form. The explicit extended function norm will be written now as:

$$\langle \Phi | \Phi \rangle = 1 + \langle \rho | \rho \rangle + 2\langle K \rangle. \tag{88}$$

The Hilbert norm of the total density form appears in equation (88) as another term in the extended Hilbert space norm. The new positive definite term corresponds to an integral with the form:

$$\langle \rho | \rho \rangle = \int \rho^2 \, d\mathbf{r} = \left\langle |\Psi|^2 \middle| |\Psi|^2 \right\rangle = \int |\Psi|^4 \, d\mathbf{r}. \tag{89}$$

This kind of integrals is well known in the field of quantum similarity and corresponds to a quantum self-similarity overlap-like measure [96] involving the Nth order density matrices.

6.8. Non-linear Schrödinger equation generated throughout extended Hilbert space wave functions

An application of the extended Hilbert spaces over the non-linear structure of Schrödinger equation will be sketched in this section.

6.8.1. Classical Schrödinger energy expression from extended wave functions

The extended wave function form (78) and any of the following definitions can be used with the appropriately modified Hamilton operator in order to obtain the system's energy expectation value [89]. For an application to a generalized form of Hohenberg–Kohn theorem [73]; see, for example, [99]. In order to arrive at this expression the Hamilton operator could be written as a diagonal matrix with the form:

$$\boldsymbol{H} = \begin{pmatrix} \boldsymbol{V} & 0 \\ 0 & \frac{1}{2} I \end{pmatrix} = \mathrm{Diag}\left(\boldsymbol{V}; \frac{1}{2} I \right) \tag{90}$$

where $\boldsymbol{V}$ is the potential operator and I an appropriate dimension unit operator. Taking into account the definition (90) and the extended wave function structure in equation (78), as well as the following discussion, the energy expression is obtained in a quantum mechanical expectation value form:

$$\begin{aligned} E = \langle \Phi | \boldsymbol{H} | \Phi \rangle &= \langle \Psi | \boldsymbol{V} | \Psi \rangle + \frac{1}{2} \langle \nabla \Psi | \nabla \Psi \rangle = \langle \boldsymbol{V} \rangle + \langle K \rangle \\ &= \int \boldsymbol{V} \rho \, d\mathbf{r} + \frac{1}{2} \int |\nabla \Psi|^2 \, d\mathbf{r} \end{aligned} \tag{91}$$

but it is readily expressible within a statistical density probability function integral structure. This is obvious for the potential part and elementary to see that for kinetic energy the same holds, as the square module of the wave function gradient can be considered too as a kinetic energy density function, using the simple definition:

$$\kappa(\mathbf{r}) = \left| \nabla \Psi(\mathbf{r}) \right|^2. \tag{92}$$

This last equality also permits us to construct a total or extended density function starting in the usual way to construct density functions from general well-behaved functions:

$$\tau(\mathbf{r}) = |\Phi|^2 = |\Psi|^2 + |\nabla\Psi|^2 = \rho(\mathbf{r}) + \kappa(\mathbf{r}).$$

6.8.2. Energy expression from generalized extended wave functions

If one takes into account the alternative extended wave function (87), then the appropriate Hamiltonian to be used here, in order to write an energy-like expectation value, has to be constructed in a similar way as the diagonal operator (90), just taking into account the extra functional term in the wave function (87):

$$\boldsymbol{H}_\alpha = \begin{pmatrix} \boldsymbol{V} & 0 & 0 \\ 0 & \alpha & 0 \\ 0 & 0 & \frac{1}{2}I \end{pmatrix} = \mathrm{Diag}\left(\boldsymbol{V}; \alpha; \frac{1}{2}I\right), \tag{93}$$

where only a scalar value: $\alpha \in \mathbf{R}$, is added [105]. As in the Hamiltonian expectation value expression (91), the operator (93) with the wave function (87) will produce the energy-like form:

$$\begin{aligned} E_\alpha &= \langle\Phi|\boldsymbol{H}_\alpha|\Phi\rangle = \langle\boldsymbol{V}\rangle + \alpha\langle\Psi|\rho|\Psi\rangle + \langle K\rangle = \langle\Psi|\boldsymbol{H}|\Psi\rangle + \alpha\langle\Psi|\rho|\Psi\rangle \\ &= E + \alpha\langle\rho|\rho\rangle \end{aligned} \tag{94}$$

in the resultant ending expression, E is the expectation value as discussed in equation (91), while the last term corresponds to the overlap-like self-similarity over the Nth order density function as commented in equation (89).

This result will be obvious if it could not be associated with the Hamiltonian operator of the so-called non-linear Schrödinger equation. See for an excellent review on this subject the book of Fraga et al. [106]. In such an equation, to the usual Hamilton operator of the linear Schrödinger equation is added the density function multiplied by a real scalar factor. Thus, in the same manner as equation (91) corresponds to the energy expectation value of the linear Schrödinger equation, to equation (94) one can attach the form of the energy expectation value associated with a stationary non-linear Schrödinger equation.

In this formalism, the unique difference between both linear and non-linear equations corresponds to the presence of the overlap-like self-similarity term and so, variation of expression (94) will coincide with expression (91), but the integral $\langle\rho|\rho\rangle$ shall be taken into account. A self-similarity term can be interpreted in several ways [89,96], however in the present case it could be seen as the expectation value of the density function itself, which can be considered as a distribution and as a projection operator as well, then:

$$\langle\rho|\rho\rangle = \langle\rho\rangle.$$

6.9. Extended non-linear Schrödinger equation

When observing the structure of the non-linear form of both the Hamilton operator and the extended wave function, one can easily propose a symmetrical extended Schrödinger equation with respect to the wave function and their gradient powers. This will correspond not only to the presence of a second-order wave function term, a density function term appearing in the system Hamiltonian, but owing to the kinetic energy interpretation as

given in equation (92), one can construct a similar term with respect to the kinetic energy to be used in the extended wave function. This can be obtained throughout an extended Sobolev space as defined in equation (86), with a norm particularly defined for this case as:

$$\langle \Phi | \Phi \rangle \equiv \| \Psi \|_2^{2;1;2} = \| \Psi \|_2 + \left\| |\Psi|^2 \right\|_2 + \| \nabla \Psi \|_2 + \left\| |\nabla \Psi|^2 \right\|_2$$

which will correspond to a possible four-dimensional extended wave function, that could be expressed in turn as:

$$|\Phi\rangle = \begin{pmatrix} \Psi \\ |\Psi|^2 \\ \nabla \Psi \\ |\nabla \Psi|^2 \end{pmatrix} \equiv \begin{pmatrix} \Psi \\ \rho \\ \nabla \Psi \\ \kappa \end{pmatrix}, \tag{95}$$

where κ is the kinetic energy density, as defined in equation (92), and in this manner the corresponding diagonal Hamilton operator could be written just as the non-linear Hamiltonian discussed so far, and described in equation (93) with an extra term:

$$\boldsymbol{H}_{\alpha;\beta} = \begin{pmatrix} \boldsymbol{V} & 0 & 0 & 0 \\ 0 & \alpha & 0 & 0 \\ 0 & 0 & \frac{1}{2} I & 0 \\ 0 & 0 & 0 & \beta \end{pmatrix} = \mathrm{Diag}\left(\boldsymbol{V}; \alpha; \frac{1}{2} I; \beta \right), \tag{96}$$

where the parameter $\beta \in \mathbf{R}$, can be used in the same manner as the former non-linear term α was defined. Alternatively, there are also other possibilities, which can be associated with the parameter β.

The first one corresponds to considering the geometrical nature of the kinetic energy density. In some discussion about the extended wave function (78) and the corresponding total density function [89,96] and earlier in this chapter the construction of a convex mixture of the space and kinetic energy densities was proposed. In this proposal, if the parameter: $\Omega \in [0, 1]$ is defined, then a composite density can be obtained with the simple form:

$$\gamma(\mathbf{r}) = \Omega \rho(\mathbf{r}) + (1 - \Omega) \kappa(\mathbf{r}).$$

Some visual examples of this density convex mixture can be obtained from reference [89]. Thus, from this point of view the non-linear parameters can be taken as convex coefficients and chosen in the Hamiltonian (96) accordingly, for example using: $\alpha \in [0, 1] \wedge \beta = 1 - \alpha$.

A physical interpretation of both the non-linear parameter β and the possibly connected extended energy term is somehow related to the variation of mass with velocity in the Breit Hamiltonian [91a,107,108]. Indeed, if the associated energy in the present extended wave function (95) and Hamiltonian (96) is obtained in the same way as in the other previously studied cases, the following expression appears:

$$E_{\alpha;\beta} = \langle \Phi | \boldsymbol{H}_{\alpha;\beta} | \Phi \rangle = E_\alpha + \beta \left\langle |\nabla \Psi|^2 \middle| |\nabla \Psi|^2 \right\rangle = E_\alpha + \beta \langle \kappa | \kappa \rangle,$$

so the last term, owing to the similarity with the Breit Hamiltonian interpretation, can be supposedly multiplied by a corresponding constant composed of equivalent units [108]. The resultant integral form of the similar Breit term corresponds to the norm of the kinetic energy density function, or employing quantum similarity terminology, this term is a self-similarity measure involving the kinetic energy density distribution. It is structured in a

similar norm form to the one Bethe and Salpeter [109] recommend computing the variation of mass with velocity integral, as will be discussed below. However, one can insist that the extra term in this extended non-linear Schrödinger equation energy expression can be also described as a kinetic energy distribution self-similarity.

The exact form of the Breit Hamiltonian term, associated with the variation of the mass with velocity, can be obtained by means of a Sobolev space of the kind related to the norms defined in equation (85). Indeed, using the Sobolev norm:

$$\langle \Theta | \Theta \rangle \equiv \|\Psi\|_2^{2;2} = \|\Psi\|_2 + \left\| |\Psi|^2 \right\|_2 + \|\nabla \Psi\|_2 + \|\nabla^2 \Psi\|_2,$$

then, to this extended Sobolev norm one can attach the following extended wave function:

$$|\Theta\rangle = \begin{pmatrix} \Psi \\ |\Psi|^2 \\ \nabla \Psi \\ \nabla^2 \Psi \end{pmatrix} \equiv \begin{pmatrix} \Psi \\ \rho \\ \nabla \Psi \\ \Delta \Psi \end{pmatrix},$$

which can be used with the same Hamilton operator (96) as in the previous case, yielding the energy form:

$$E_{\alpha;\beta}^{(\Theta)} = \langle \Theta | \boldsymbol{H}_{\alpha;\beta} | \Theta \rangle = E_\alpha + \beta \langle \Delta \Psi | \Delta \Psi \rangle,$$

which has the Breit correction in the appropriate form recommended by Bethe and Salpeter [108]. Therefore, in this situation, the corresponding parameter β has the true meaning of the mass variation with velocity Breit Hamiltonian constant.

6.10. General non-linear terms in Schrödinger equation

The results obtained so far show without doubt that not only first order terms on the density function can play a role in the definition of non-linear Schrödinger equations but that there are no obstacles to considering more general non-linear structures. In order to provide an example of this possibility for both electronic and kinetic density functions, a schematic discussion will be developed.

Supposing that the density functions: $\{\rho; \kappa\}$ are known, then the following Hamiltonian operator can be used within the extended wave function form provided with equation (78):

$$\boldsymbol{H} = \mathrm{Diag}\left(\boldsymbol{V} + a\big(\exp(\alpha\rho) - 1\big); \frac{1}{2} I + b\big(\exp(\beta\kappa) - 1\big) \right),$$

where $\{a; \alpha\}$ and $\{b; \beta\}$ are parameters associated with the non-linear density contributions. The zeroth order Hamiltonian will be the classical one as expressed in equation (90), and the present exponential terms will produce the non-linear contributions in both density classes. It is easy to see, employing a trivial Taylor series expansion on every exponential, that the included pth order Hamiltonian non-linear terms could be written in this case:

$$\boldsymbol{H}_p = \frac{1}{p!} \mathrm{Diag}\big(a(\alpha\rho)^p; b(\beta\kappa)^p\big), \quad \forall p \geqslant 1. \tag{97}$$

The corresponding expectation value can be obtained considering the pth order Hamiltonian term (97) as an isomorphic two-component vector. In this case the following extended density vector can also be defined:

$$|\mathsf{P}\rangle = \begin{pmatrix} \rho \\ \kappa \end{pmatrix},$$

so the pth order contribution to the energy expectation value could be simply written as:

$$\boldsymbol{E}_p = \langle \mathsf{P}|\boldsymbol{H}_p\rangle = \frac{1}{p!}\left(a\alpha^p\langle\rho|\rho^p\rangle + b\beta^p\langle\kappa|\kappa^p\rangle\right) = \frac{1}{p!}\left(a\alpha^p\langle\rho^p\rangle + b\beta^p\langle\kappa^p\rangle\right).$$

A general framework containing non-linear terms in the Schrödinger equation is set in this manner. It must be finally noted that the nature of these pth order correction terms can be associated with $(p+1)$th order self-similarity measures involving the two density classes.

7. DENSITY AND SHAPE FUNCTIONS SEMISPACES

In this last section several problems related to the density functions and to their homothetic parent functions, the so-called shape functions, will be discussed.

7.1. Hilbert semispaces and root products

All the definitions, algorithms and properties of Minkowski operations on vector semispaces can be translated to the spaces of density functions or *Hilbert semispaces*. An example of this possibility has already been described when Minkowski norms were defined in semispaces. Another application has been based on the possibility to use unit shell functions to construct, by means of convex linear combinations, other unit shell density functions. This relates the discussion in this section to the so-called shape function, and a brief analysis of this subject with respect to quantum similarity will be also given.

7.1.1. Atomic shell approximation functions

The already discussed *atomic shell approximation* (ASA) can be considered a practical consequence of the theoretical ideas developed in Section 3, specially starting at the 3.5 paragraph and further. The ASA technique constructs quite accurate approximate atomic density functions by using a convex restricted fitting of a known set, Σ, made of spherical density functions, to atomic *ab initio* densities. This can be summarized by the statement:

$$K\left(\{w_I\}\right) \wedge \Sigma = \left\{s_I(\mathbf{r})\right\} \subseteq S(1) \subseteq \boldsymbol{H}\left(\mathbf{R}^+\right) \rightarrow \rho(\mathbf{r}) = \sum_I w_I s_I(\mathbf{r}) \in S(1).$$

7.1.2. Minkowski scalar products between ASA functions

Minkowski scalar products, as described in Section 3, may be employed within the ASA approximation, but may produce difficult integrals when applied over exact *ab initio* density functions. Coming back to the ASA possibility in order to describe feasible computational structures, the appropriate root product involving a pair of ASA density functions

may be defined as:

$$\langle \rho_A(\mathbf{r})\rho_B(\mathbf{r})\rangle = \int \left(\rho_A(\mathbf{r})\rho_B(\mathbf{r})\right)^{[1/2]} d\mathbf{r} = \int \left(\rho_A(\mathbf{r})^{[1/2]} * \rho_B(\mathbf{r})^{[1/2]}\right) d\mathbf{r},$$

defining the square root of both ASA density functions as an inward power:

$$\rho(\mathbf{r}) = \sum_I w_I s_I(\mathbf{r}) \rightarrow \rho(\mathbf{r})^{[1/2]} = \sum_I w_I^{1/2} s_I^{1/2}(\mathbf{r}),$$

while the inward matrix product, involving both density functions, can be expressed as a *Hadamard product*. Then one can finally write:

$$\langle \rho_A(\mathbf{r})\rho_B(\mathbf{r})\rangle = \sum_I w_{AI}^{1/2} w_{BI}^{1/2} \int s_{AI}^{1/2}(\mathbf{r}) s_{BI}^{1/2}(\mathbf{r})\, d\mathbf{r}.$$

Such an algorithm, although unusual has been described to coherently describe the Minkowski norm, in the same way as the related property is fulfilled in finite-dimensional vector spaces:

$$\langle \rho_A(\mathbf{r})\rho_A(\mathbf{r})\rangle = \langle \rho_A(\mathbf{r})\rangle.$$

From this definition cosines and distances involving two ASA density functions can be straightforwardly computed. In the same way, products of higher order than two can be so easily defined, that there is no need of supplementary description. The limitation here appears to be that both expressions for the ASA densities involved had to possess the same number of terms. The general case will be discussed below.

7.1.3. ASA pseudo-wave functions

The Hadamard square root of an ASA density function can be defined as:

$$\rho(\mathbf{r})^{[1/2]} = \sum_I w_I^{1/2} s_I^{1/2}(\mathbf{r}) = \Psi(\mathbf{r}),$$

and may be employed, in the same way as semispace vectors have been used, that is to construct any vector space element. However in the Hilbert semispace case one is facing continuous vectors, so as the *pseudo-wave function*, $\Psi(\mathbf{r})$, is positive definite everywhere in the associated domain, as is the original ASA density function. The function signature and nullity may be structured as a phase function, so one can construct in general a Hilbert space function as:

$$\Psi(\mathbf{r}) = \Psi(\mathbf{r})e^{i\alpha} \in \boldsymbol{H}(\mathbf{C}).$$

Then, it is quite interesting to note how the phase function acts in this case as a signature-nullity tag of the Hilbert semispace pseudo-wave function. The most similar finite-dimensional tag to the phase functions tags to be used in the pseudo-wave functions may be the ternary tags involving sign and nullity, already discussed above.

7.1.4. Minkowski scalar product between ASA functions belonging to different Hilbert semispaces

In order to find a Minkowski scalar product between two functions belonging to different Hilbert semispaces, for instance:

$$\rho_A \in \boldsymbol{H}_\infty^{(N_A)}\left(\mathbf{R}^+\right) \wedge \rho_B \in \boldsymbol{H}_\infty^{(N_B)}\left(\mathbf{R}^+\right)$$

in this case, one is facing the impossibility of performing an appropriate inward product between both expressions whenever $N_A \neq N_B$. However the inward power of both functions is in any case well defined, as in general it can be written for any function and any Hilbert semispace:

$$\forall \rho = \sum_{I=1}^{N} \Omega_I \sigma_I \in H_{\infty}^{(N)} \rightarrow \rho^{[1/2]} \equiv p = \sum_{I=1}^{N} x_I s_I,$$

where: $x_I = \sqrt{\Omega_I} \wedge s_I = \sqrt{\sigma_I}$.

In this sense, the square root density functions obtained in this manner approach the form of a *pseudo* wave function. It must be taken into account that pseudo wave functions present an undefined signature. See Section 7.2 for a discussion of this feature.

Then, a first approach may be taken employing the Euclidean scalar product of the inward square roots:

$$\langle p_A | p_B \rangle = \sum_{I=1}^{N_A} \sum_{J=1}^{N_B} x_I^A x_J^B \int_D s_I^A(\mathbf{r}) s_J^B(\mathbf{r})\, d\mathbf{r} = \sum_{I=1}^{N_A} \sum_{J=1}^{N_B} x_I^A x_J^B S_{IJ}^{AB} = \langle \mathbf{x}_A | \mathbf{S}_{AB} | \mathbf{x}_B \rangle,$$

constituting an obvious definition, but with the characteristic that the overlap matrix $\mathbf{S}_{AB}$ is in general no longer square but rectangular with $(N_A \times N_B)$ dimension. On the other hand, the Euclidean norm of the involved inward square roots can be written in the same manner, for example:

$$\begin{aligned} \langle p_A | p_A \rangle &= \langle \mathbf{x}_A | \mathbf{S}_{AA} | \mathbf{x}_A \rangle = \langle \mathbf{w}_A \rangle + 2 \sum_{I}^{N_A} \sum_{J>I} x_I^A x_J^A S_{IJ}^{AA} \\ &= \langle \mathbf{w}_A \rangle + \langle \mathbf{x}_A | \mathbf{S}_{AA} - \mathbf{I}_{AA} | \mathbf{x}_A \rangle \end{aligned}$$

with a completely equal expression for the other function, which can be obtained by simply exchanging the index A by B.

One can then define in this case the Minkowski scalar product by means of:

$$\langle \rho_A : \rho_B \rangle \approx \langle p_A | p_B \rangle - \frac{1}{2} \big[\langle \mathbf{x}_A | \mathbf{S}_{AA} - \mathbf{I}_{AA} | \mathbf{x}_A \rangle + \langle \mathbf{x}_B | \mathbf{S}_{BB} - \mathbf{I}_{BB} | \mathbf{x}_B \rangle \big],$$

an equation which, when $\rho_A = \rho_B$, transforms into the appropriate Minkowski norm. The expression above also can be written as:

$$\langle \rho_A : \rho_B \rangle \approx \langle p_A | p_B \rangle - \frac{1}{2} \big[\langle p_A | p_A \rangle + \langle p_B | p_B \rangle \big] + \frac{1}{2} \big[\langle \mathbf{w}_A \rangle + \langle \mathbf{w}_B \rangle \big].$$

However the first term is just half of the negative squared distance between the involved functions square root density functions:

$$\langle \rho_A : \rho_B \rangle \approx \frac{1}{2} \big[\langle \mathbf{w}_A \rangle + \langle \mathbf{w}_B \rangle \big] - \| p_A - p_B \|^2.$$

This may be a good answer for a general Minkowski expression for the scalar product of two different ASA-like densities.

7.2. Density functions and generating wave functions

Eleven years ago Hohenberg, Kohn and Sham (HHS) [112], in the introductory chapter of an issue especially dedicated to Density Functional Theory (DFT): the 1990 volume 21 of Advances in Quantum Chemistry, presented in a masterly way both the historical development of the ideas, which conformed the DFT throughout time, and proposed new thoughts on the future of the theoretical and practical issues of DFT. There, a sentence caught my eye, it was literally written as follows, with straightforward changes of notation to fit the present chapter: ... *through* H, *a knowledge of* $\rho(\mathbf{r})$, *a function of three variables, implicitly defines the entire* $3N$*-dimensional ground state wave function* $\Psi(\mathbf{r}_1, \mathbf{r}_2, \ldots, \mathbf{r}_N)$ *and its energy* E. *For that matter it also defines all excited states* $\Psi_j(\mathbf{r}_1, \mathbf{r}_2, \ldots, \mathbf{r}_N)$ *and energies* E_j... After reading the HHS chapter I was puzzled, as their authors probably were, when disclosing this property of the density function. I tried to find out by myself if there were other possible proofs or additional properties related to this extraordinary result. Not far away in the same paper, HHS disclosed similar situations, apparently produced earlier also in the minds of other researchers... and HHS somehow concluded that it was the *reductio ad absurdum* argument of the, now called, Hohenberg–Kohn theorem (HKT), which could be used in order to overcome the possible scepticism.

In this aspect, this was not the first time that I was interested into the HKT. In fact, along with Sen and Besalú [99] we studied the implications of the original HKT formulation in a paper devoted to celebrate the Kohn and Pople Nobel prize-winning event. There, the main argument, in order to reformulate the HKT, was the possibility to express directly approximate quantum mechanical system energy expectation values, through the knowledge of the system Hamiltonian and the density function, instead of the usual formulation. This statistical way to define quantum mechanical expectation values could be employed in the mentioned work because, reformulating the way wave functions are written, in fact defining the concept of extended wave function as previously described along Section 6, then any expectation value could be written in such a statistical manner. This was not only a completely new formulation: earlier discussions based on the so-called density matrix elements, which can be found, masterly described, in the first edition of McWeeny's book [4], have been developed leading to the same formalism as the one proposed by us employing other arguments. Also, in a parallel way, the work which has been done on the computational problems and correct expression of the approximate density functions, when fitted by linear combinations of s-type Gaussian functions, has produced the so-called atomic shell approximation (ASA), as described earlier in Section 5.

The sentence quoted from the HHS chapter, along with these previous experiences, has inspired the structure of this section. Here, from the necessary properties which density functions must possess, the concept of generating wave function will be presented and its non-unique character will be shown. Afterwards, the concept of extended wave function will provide a simple reformulation of the variational principle, based on the density function statistical expression of energy expectation values.

7.2.1. Structure of density functions

7.2.1.1. Convex conditions. Consider a set of positive definite functions of an, in principle not restricted to three, indefinite number of variables. Let us call $\mathsf{P} = \{\rho_{\mathrm{I}}(\mathbf{r})\}$ such a previously described set. Suppose additionally that concerning the elements of the set P,

the following property holds: $\forall \rho_I(\mathbf{r}) \in \mathsf{P} \rightarrow \int_V \rho_I(\mathbf{r})\, d\mathbf{r} = 1$. Then, P can be considered a subset of some functional Hilbert semispace: $\mathsf{P} \subset V_\infty(\mathbf{R}^+)$. The important property concerning such semispaces can be formulated in the following way: Whenever one tries to construct a function $\rho(\mathbf{r})$, fulfilling the convex conditions:

$$K_\infty\big(\rho(\mathbf{r})\big) = \left[\rho(\mathbf{r}) \in \boldsymbol{V}_\infty\big(\mathbf{R}^+\big) \wedge \int_V \rho(\mathbf{r})\, d\mathbf{r} = \mathbf{1}\right], \tag{98}$$

in the way Definition 6 is set. Then all that is needed is any set P, as defined before, along a vector of real and positive coefficients, whose sum is unity. This is the same as employing a vector, $\mathbf{w}$: $K_N(\mathbf{w})$, whenever the cardinality of the set P: $\#(\mathsf{P}) = N$. This simply can be expressed by means of the alternative N-dimensional definition of the one previously presented for functions:

$$K_N(\mathbf{w}) = \left[\mathbf{w} = \{w_I\} \in \boldsymbol{V}_N\big(\mathbf{R}^+\big) \wedge \langle \mathbf{w} \rangle = \sum_I w_I = 1\right]. \tag{99}$$

Using such a vector, fulfilling the appropriate convex conditions, then it can be written:

$$\rho(\mathbf{r}) = \sum_I w_I \rho_I(\mathbf{r}). \tag{100}$$

It is a trivial matter to show that this expression fulfils the convex conditions presented before, or shortly to say that $K_\infty(\rho(\mathbf{r}))$ holds.

The consequence of these definitions and properties can be expressed as follows: in order to obtain a density function one just needs to know a set of density functions, with all elements possessing homogeneous variables, and a convex vector of the appropriate dimension.

7.2.1.2. Generating wave functions. Moreover, the nature of both the convex vector $\mathbf{w}$ and the set of convex functions P, can be easily found in the usual vector and Hilbert spaces, respectively. Indeed, using the current way to produce density functions within the quantum mechanical structure as shown in the Definition 2, to each density function one can attach a wave function belonging to an appropriate Hilbert space, whose squared module produces the required density function.

This is the same as to say that to the density function set P one can attach another function set: $F = \{\varphi_I(\mathbf{r})\} \subset \boldsymbol{V}_\infty(\mathbf{C})$. Both function sets are related by the simple set of relationships: $\forall \rho_I(\mathbf{r}) \in \mathsf{P} \rightarrow \exists \varphi_I(\mathbf{r}) \in F$: $\rho_I(\mathbf{r}) = |\varphi_I(\mathbf{r})|^2$. Thus the set F can be said to be composed of the generating wave functions of the density function set P. The problem consists at this stage of how to express the generating wave function of a density function described as the linear superposition (100).

For this purpose it is easy to translate in a similar manner the generating function definition into any N-dimensional vector space. That is, the following construction rule can be easily written:

$$\forall \mathbf{w} = \{w_I\} \in \boldsymbol{V}_N\big(\mathbf{R}^+\big) \rightarrow \exists \mathbf{x} = \{x_I\} \in \boldsymbol{V}_N(\mathbf{C})\colon\ w_I = |x_I|^2, \quad \forall I. \tag{101}$$

This can be expressed elegantly, employing the inward matrix product (IMP), as defined in Section 3:

$$\mathbf{w} = \mathbf{x}^* * \mathbf{x} = |\mathbf{x}|^{[2]}. \tag{102}$$

The convex conditions $K_N(\mathbf{w})$, see Definition 6, attributed to the vector $\mathbf{w}$, can be written as a normalization condition imposed on the generating vector $\mathbf{x}$:

$$\langle \mathbf{w} \rangle = 1 \rightarrow \sum_I w_I = \sum_I |x_I|^2 = \mathbf{x}^+ \mathbf{x} = 1,$$

an equivalent condition to the wave function–density function generating relationships.

The generating function for a density function form, like the one presented in equation (100), can be thus represented by the following two vector entities: one constructed by the elements of the density function set P and the other being simply $\mathbf{w}$. The first vector may be considered an element of a Hilbert semispace product:

$$|\mathsf{P}\rangle = \left\{\rho_I(\mathbf{r})\right\} \in \overset{N}{\underset{I=1}{\times}} \boldsymbol{V}_\infty\left(\mathbf{R}^+\right),$$

and a simple IMP operation will then give a new vector:

$$|p\rangle = \mathbf{w} * |\mathsf{P}\rangle = \left\{w_I \rho_I(\mathbf{r})\right\},$$

which produces the density function (100), simply by summing up their elements:

$$\rho(\mathbf{r}) = \left\langle |p\rangle \right\rangle. \tag{103}$$

This result would be useless if it could not be related to the generating function set F. In order to obtain such a relationship, one can define the generating function vector:

$$|F\rangle = \left\{\varphi_I(\mathbf{r})\right\} \in \overset{N}{\underset{I=1}{\times}} \boldsymbol{V}_\infty(\mathbf{C})$$

as well as the hybrid vector obtained through an appropriate IMP by the general coefficient vector $\mathbf{x}$:

$$|f\rangle = \mathbf{x} * |F\rangle. \tag{104}$$

Then, it is straightforward to see that the IMP of the squared module of $|f\rangle$ is nothing else but $|p\rangle$:

$$|p\rangle = |f\rangle * |f\rangle^* = \left[|f\rangle\right]^{[2]},$$

whenever one defines:

$$|f\rangle^* = \left\{x_I^* \varphi_I^*\right\} = \mathbf{x}^* * |F\rangle^*.$$

From these previous definitions equation (103) is simply deduced. Therefore, nothing opposes admitting the superposition of generating functions:

$$\varphi(\mathbf{r}) = \left\langle |f\rangle \right\rangle = \sum_I x_I \varphi_I(\mathbf{r}) \tag{105}$$

as a generating wave function for the composite density function, which can be alternatively written in terms of a Hadamard product, similar in this case to the IMP:

$$\rho(\mathbf{r}) = \left|\varphi(\mathbf{r})\right|^{[2]} \equiv \varphi(\mathbf{r}) * \varphi(\mathbf{r})^*.$$

In this framework it must be noted here that one can even consider the structure of the generating basis set functions and by extension of the generating function (105), as the

IMP square root, in the following way:

$$|f\rangle = \left[|p\rangle\right]^{[1/2]}.$$

Also, a completely equivalent result could have been obtained using the previous isomorphic semispaces and spaces made of diagonal matrices, substituting the IMP by the usual matrix product, and being the operation sum of all matrix elements, $\langle\ \rangle$, substituted by the trace of the matrix.

7.2.1.3. Non-uniqueness of the generating wave functions. Once the previous results, leading to the structure of density functions and generating wave functions, are obtained, there appears in the first place the interesting relationship between density function and generating wave function. From one part, this relationship has to be connected with the original HKS quoted sentence where in fact the findings of this work were included. On the other hand, the nature of such a result can be the starting point for further analysis.

As it seems obvious that knowledge of the density function is related to the knowledge of the generating wave function, it is not so obvious how the vector $\mathbf{w}$ has to be related to the generating vector $\mathbf{x}$, the relationship between the function vectors $|\mathsf{P}\rangle$ and $|F\rangle$ being clearly established. It is easy to see that from equation (102), the elements of vectors $\mathbf{w}$ and $\mathbf{x}$, according to the relationships (101), are related by the equations:

$$w_I = |x_I|^2 = a_I^2 + b_I^2 \wedge a_I = \mathrm{Re}(x_I), \quad b_I = \mathrm{Im}(x_I). \tag{106}$$

However, equation (106) shows that, generally speaking, there are two signs not well defined in every $\mathbf{x}$ element: those related to the real and imaginary parts of the $\{x_I\}$ components. This property does not seem weird in this context, as it is well known that every element of the generating wave function set is also undefined by a phase factor. The undefined signs of every component of $\mathbf{x}$ have the same role as the wave functions' phase factors. Such signs can be chosen arbitrarily and thus can constitute in turn a large set of quite arbitrary vectors, all of them producing the same density coefficient weight vector $\mathbf{w}$. The question of how many vectors $\mathbf{x}$ are, within this sign sense, degenerate to $\mathbf{w}$, can be easily answered.

Any vector $\mathbf{x} \in \boldsymbol{V}_N(\mathbf{C})$, and in a less general manner real defined vectors, can be written separating its components from their signs using IMP. That is:

$$\mathbf{x} = \mathbf{s}_a * \mathbf{a} + i\mathbf{s}_b * \mathbf{b}, \tag{107}$$

where, now within by the vector pair sum (107), it is understood that: $\mathbf{a}; \mathbf{b} \in \boldsymbol{V}_N(\mathbf{R}^+)$ are vectors made of real positive elements, belonging to some appropriate vector semispace. Moreover, the pair of vectors $\mathbf{s}_a; \mathbf{s}_b$ are Boolean-like vectors, whose elements can only possess the sign values $\{-1; +1\}$ or equivalently$\{0; 1\}$. As has been discussed in Section 3, this kind of vectors can be called the signature of the attached vector (or matrix), and this decomposition is such that any vector or matrix can be written in the following manner: as an IMP of the signature vector or matrix by an element of a semispace of the appropriate dimension. Thus, the signature vectors for a real N-dimensional vector space can be constructed in 2^{N-1} ways, and in a complex space in a 2^{2N-1} fashion. This is so, because although there are 2^N possible signatures in the real case or 2^{2N} in the complex situation, it also appears that half of the signatures correspond to the other half multiplied by -1 in a product by a scalar fashion, producing in this manner redundant information in order to construct the generating function vector $|f\rangle$, as can be easily seen from equation (104).

Thus, in general one can expect that a density function like the one constructed according to equation (100), has an attached generating wave function with the form as expressed in equation (105), which is undetermined in the signs of the coefficients, in general in a 2^{2N-1} degenerate way. So, within the present reasoning one can affirm that the knowledge of a density function precludes the knowledge of a generating wave function whose coefficients can be undetermined by a signature vector, possessing in turn a degeneracy which is associated with the dimension of the involved coefficient space. There is a relationship as the one described by HKS, but it is not unique in the simple framework proposed here.

7.2.2. Extended wave functions and the Schrödinger equation

The analysis of the quantum mechanical expectation value expression was important to the development of the connection between quantum similarity measures and QSAR [36]. The continued studies on this subject recently permitted a description of quantum QSAR procedures, demonstrating as a collateral benefit the quantum mechanical origin of the structure-activity relationships.

In order to show that, when solving the Schrödinger equation in an approximate manner, as discussed in depth in Section 6, there was no problem in expressing the wave function by a general extended manner, which formally can be expressed as a diagonal matrix:

$$|\Phi\rangle = \begin{pmatrix} \Psi & 0 \\ 0 & \Omega[\Psi] \end{pmatrix} = \mathrm{Diag}\big(\Psi; \Omega[\Psi]\big), \tag{108}$$

where Ψ is the classical wave function and Ω an appropriate operator. Choosing the operator in equation (108) as the nabla, a diagonal choice of the Hamiltonian operator as:

$$H = \begin{pmatrix} V & 0 \\ 0 & \frac{1}{2}\mathbf{I} \end{pmatrix} = \mathrm{Diag}\left(V; \frac{1}{2}\mathbf{I}\right), \tag{109}$$

where V is the potential, permits us to write the energy expression in the classical way, provided that the original wave function is normalized, that is: $\langle\Psi|\Psi\rangle = 1$, as:

$$E = \mathrm{Tr}\big[\langle\Phi|H|\Phi\rangle\big] = \langle V\rangle + \langle K\rangle, \tag{110}$$

where

$$\langle V\rangle = \langle\Psi|V|\Psi\rangle \wedge \langle K\rangle = \frac{1}{2}\langle\nabla\Psi|\nabla\Psi\rangle.$$

However, as one can write, thinking of the diagonal nature of the involved elements in equation (110) provided by equations (108) and (109):

$$E = \mathrm{Tr}\big[\langle\Phi|H|\Phi\rangle\big] = \mathrm{Tr}\big[\langle H|\tau\rangle\big]. \tag{111}$$

Using the total density function involving both electronic ρ and kinetic energy κ densities:

$$\tau = \mathrm{Diag}\big(|\Psi|^2; |\nabla\Psi|^2\big) = \mathrm{Diag}(\rho; 2\kappa).$$

This is another proof that the quantum mechanical expectation values can be written within the statistical formalism, as in the last equality of equation (111).

7.2.3. Variational principle in density function formalism

The results obtained above permit expression of the approximate energy expectation value, employing density function structures, similar to the one described in equation (100), and formally using the expression:

$$E = \langle H|\rho\rangle = \sum_I \Omega_I \langle H|\rho_I\rangle = \sum_I \Omega_I \varepsilon_I,$$

supposing that the operations described in the previous section hold implicitly. In the usual case where one considers the sequence of expectation values $\{\varepsilon_I\}$ ordered increasingly upwards, then taking into account the convex conditions (99) on the set $\{\Omega_I\}$, one can write:

$$E - \varepsilon_1 = \sum_{I>1} \Omega_I (\varepsilon_I - \varepsilon_1),$$

and from here one can deduce the usual variational result:

$$E - \varepsilon_1 \geqslant 0,$$

as $\Omega_I \in \mathbf{R}^+$ and $\varepsilon_I - \varepsilon_1 \geqslant 0$. A similar formalism structure has been successfully employed to prove the Hohenberg–Kohn theorem [105].

7.3. Density functions difference, Fukui functions and quantum dissimilarity indices

A controversial point associated with DFT applications regards the definition and values of Fukui functions [113,114]. Although the original definition of Fukui [115] implies a density-like set of functions belonging to the unit shell, the DFT environment definition [114] sometimes produces negative results, as recently discussed [116–118].

7.3.1. The zero shell

In order to discuss the issue of Fukui functions, one can analyze the possible extension of vector semispaces, relaxing the possibility of performing differences among the elements of the same shell. This induces the appearance of a *zero shell*. Indeed, assuming that a given semispace λ-shell is known, one can define the following construction:

$$\forall \rho_A, \rho_B \in S(\lambda) \rightarrow d = \rho_A - \rho_B \in \Sigma(0).$$

Here the notation $\Sigma(0)$ is used to distinguish it from the notation $S(\lambda)$ since $\Sigma(0) \subset V(\mathbf{R})$ and $S(\lambda) \subset V(\mathbf{R}^+)$. The meaning of the zero shell becomes clear when the vector sum of the difference is computed:

$$\langle d\rangle = \langle \rho_A - \rho_B\rangle = \langle \rho_A\rangle - \langle \rho_B\rangle = 0.$$

Such a result was already described by Parr and Bartolotti in another context [119] where density functions are the semispace elements studied.

7.3.2. Fukui functions

Suppose now that, within the same spirit of the semispace extension leading to the 0-shell, one analyzes first a reduced density function, $\rho_A^{(N)}$, associated with some N particle quantum system A, then one will have: $\langle \rho_A^{(N)} \rangle = N \rightarrow \rho_A^{(N)} \in S(N)$. In the same manner, consider the homogeneous reduced density function for the same quantum system with an extra electron on it, that is: $\langle \rho_A^{(N+1)} \rangle = N+1 \rightarrow \rho_A^{(N+1)} \in S(N+1)$. The well-defined difference between both densities generates nothing but the vector space unit shell, as:

$$f_A = \rho_A^{(N+1)} - \rho_A^{(N)} : \left\langle \rho_A^{(N+1)} - \rho_A^{(N)} \right\rangle = 1 \rightarrow f_A \in \Sigma(1).$$

In fact, the function f_A is the approximate Fukui function associated with the system A, as according to the usual DFT framework definition [114] one can write:

$$\left(\frac{\partial \rho_A}{\partial N} \right)_V \approx \frac{\rho_A^{(N+1)} - \rho_A^{(N)}}{(N+1) - N} = \rho_A^{(N+1)} - \rho_A^{(N)} = f_A$$

and this result proves that Fukui functions have to belong to the unit shell. This does not imply that they are positive definite functions since they do not belong to the semispace unit shell $S(1)$. They do, however, if a Koopmans approach is taken. If all orbitals are considered frozen, the Fukui function will correspond to the electron density of the first orbital available, which is naturally positive definite and belongs to $S(1)$. Allowing relaxation infers that the shell to which Fukui functions belong may change from $S(1)$ to $\Sigma(1)$.

7.3.3. Vector spaces generated throughout semispace element subtraction

At this stage of the discussion and as a prior step to further analysis it can be briefly studied how the difference of two elements of a vector semispace can generate the elements of the associated vector space. Consider two elements of a vector semispace, belonging to a pair of different shells, as the same shell case has been already discussed:

$$S(\alpha);\ S(\beta) \subset \boldsymbol{V}\left(\mathbf{R}^+\right) \wedge a \in S(\alpha);\ b \in S(\beta),$$

then, a difference between both semispace elements can be written, leading to a real vector sum:

$$d = a - b \rightarrow \langle d \rangle = \langle a \rangle - \langle b \rangle = \alpha - \beta = \delta \in \mathbf{R} \rightarrow d \in \Sigma(\delta) \subset \boldsymbol{V}(\mathbf{R}).$$

This property permits construction of real vector space elements from the corresponding vector semispace shell structure. Realizing that the vector semispace elements can be constructed by homothetic manipulations of the unit shell, then one can consider the unit shell as the generating nuclear structure in vector spaces [120], as discussed in Section 3. Complex vector spaces can be constructed in the same homothetic way.

7.3.4. Quantum dissimilarity indices

Quantum dissimilarity indices were proposed already in 1980 [10] in the form of the Euclidean distance between two homogeneous density functions belonging to distinct systems. This needed difference between density functions can certainly be performed when both densities, even if they are associated with different shells, have the same number of

variables. One can have:

$$\rho_A \in S(\alpha) \wedge \rho_B \in S(\beta) \rightarrow \rho_A - \rho_B \in \Sigma(\alpha - \beta)$$

in the same way as in the previous discussion, providing a function which, generally speaking, belongs to the associated vector space. The difference function can be reversely transformed into a semispace element again by computing the square power of the difference $|\rho_A - \rho_B|^2 \in \boldsymbol{V}(\mathbf{R}_0^+)$. In this way, the squared Euclidean distance between both densities can be written as a Minkowski norm of the squared difference function:

$$D^2(\rho_A; \rho_B) = \langle |\rho_A - \rho_B|^2 \rangle = \langle \rho_A^2 \rangle + \langle \rho_B^2 \rangle - 2\langle \rho_A \rho_B \rangle,$$

where the symbol $\langle \rho_A \rho_B \rangle$ stands for the overlap integral:

$$\langle \rho_A \rho_B \rangle = \int_D \rho_A(\mathbf{r}) \rho_B(\mathbf{r})\, d\mathbf{r},$$

which as a measure appears to be one of the basic tools employed in quantum similarity [10, 36].

The Minkowski norm structure has been used in the expression above in order to stress the direct dependence of higher order norms from the Minkowski norm definition.

7.3.5. Quantum similarity index: Carbó index

An often used similarity index, known as the Carbó index [10] is given by:

$$C(\rho_A; \rho_B) = \langle \rho_A \rho_B \rangle \left(\langle \rho_B^2 \rangle \langle \rho_B^2 \rangle \right)^{-1/2}.$$

The Carbó index can easily be related to a distance measure [35c] and is invariant about the character of the shells, where both density functions have to belong. It is readily seen how this occurs using unit shell homotheties to express the density functions:

$$\text{iff: } \rho_A = \alpha \sigma_A \wedge \rho_B = \beta \sigma_B \rightarrow C(\rho_A; \rho_B) = C(\sigma_A; \sigma_B).$$

This property enhances once more the fundamental role of the unit shell elements in vector semispaces.

7.3.5.1. Convex sets of scalars. A set of scalars $\{w_I\}$ or the elements of a vector $\mathbf{w}$ can be called *convex* and noted, according to Definition 6, as $K(\{w_I\})$ or $K(\mathbf{w})$, whenever they are positive definite real numbers and their sum is one, or alternatively the vector is a semispace element belonging to the unit shell. One can use Definition 6, that is:

$$K\left(\{w_I\}\right) = \left\{ \forall w_I \in \mathbf{R}^+ \wedge \sum_I w_I = 1 \right\}$$

alternatively:

$$K(\mathbf{w}) = \left\{ \mathbf{w} \in V\left(\mathbf{R}^+\right) \wedge \langle \mathbf{w} \rangle = 1 \right\}.$$

7.3.5.2. Convex linear combinations within vector semispace shells. A convex linear combination of elements of a vector semispace belonging to the same shell results in a new element belonging to this shell, meaning that:

$$\{\rho_I\} \subset S(\lambda) \subset \boldsymbol{V}(\mathbf{R}^+) \wedge K(\{w_I\}) \rightarrow \rho = \sum_I w_I \rho_I \in S(\lambda).$$

This is true because:

$$\langle \rho \rangle = \left\langle \sum_I w_I \rho_I \right\rangle = \sum_I w_I \langle \rho_I \rangle = \sum_I w_I \lambda = \lambda \sum_I w_I = \lambda.$$

That is: any vector semispace shell is *closed* upon convex linear combinations of its elements.

It easy to prove that closure under convex linear combinations also holds in shells defined within vector spaces.

The vector semispace properties so far disclosed may be employed to search for any useful connection between vector semispaces and the associated vector spaces. Such a relationship is of capital interest to relate DFT resulting density functions and wave function theoretical structure. Such a possible connection has been preliminarily discussed [121] and summarized in Sections 7.1 and 7.2.

7.4. Norm variation and Fukui functions

Consider a quantum system whose state density function, $\rho_A^{(\alpha)}$ belongs to some vector semispace shell, $S(\alpha)$. Suppose that the same system underwent some change which produces as a result a new density function, $\rho_A^{(\alpha+\delta\alpha)}$, where $\delta\alpha$ is a suitable variation of the vector sum. Then one has the possibility to construct the density difference as a semispace $\delta\alpha$-shell element:

$$\rho_A^{(\alpha+\delta\alpha)} - \rho_A^{(\alpha)} = \rho_A^{(\delta\alpha)} \in S(\delta\alpha),$$

which can be written in terms of an homothety of some appropriate shape function, $\sigma_A^{(1)}$ belonging to the unit shell, or:

$$\rho_A^{(\delta\alpha)} = (\delta\alpha)\sigma_A^{(1)}.$$

It is interesting to note here that one can arrive at an equivalent expression to the one defining a Fukui function, that is:

$$\sigma_A^{(1)} = \frac{\delta\rho_A^{(\delta\alpha)}}{\delta\alpha},$$

which can be related to the discussion about possible non-integer particle time fluctuations, studied by Perdew et al. [127].

7.5. DFT variational theorem over shape functions

The possibility to use the shape function to set up the DFT variational theorem [73,112] has apparently not attracted research attention in the DFT field and related problems. Therefore, to complete this review of the shape functions in relation to the vector semispace

structure, a reformulation of the DFT variational theorem will be given in terms of the unit shell elements.

It has been shown that, owing to the possible definition of extended wave functions, the energy $E^{(N)}$ of an N particle quantum system associated with a Hamiltonian $H^{(N)}$ and described by some state density function $\rho^{(N)}$ can be formally expressed by means of the integral:

$$E^{(N)} = \left\langle H^{(N)} \rho^{(N)} \right\rangle = \int_D H^{(N)}(\mathbf{r}) \rho^{(N)}(\mathbf{r})\, d\mathbf{r}.$$

Using the shape function homothety:

$$\rho^{(N)} = N\sigma^{(1)}$$

and substituting one arrives at the definition of a *single electron energy* form:

$$E^{(N)} = \left\langle H^{(N)} \left(N\sigma^{(1)} \right) \right\rangle = N \left\langle H^{(N)} \sigma^{(1)} \right\rangle = N E^{(1)}.$$

Then, the DFT variational principle, which can be written by means of the expression:

$$\delta \left[E^{(N)} \left(\rho^{(N)}; V \right) - \mu \left(\left\langle \rho^{(N)} \right\rangle - N \right) \right] = 0,$$

where V is the external potential and μ a Lagrange multiplier, can be rewritten in terms of the shape function as:

$$\delta \left[E^{(1)} \left(\sigma^{(1)}; V \right) - \lambda \left(\left\langle \sigma^{(1)} \right\rangle - 1 \right) \right] = 0.$$

Of course, this DFT unit shell variational theorem corresponds to the homothetical counterpart of the original one, associated with the N particle density and has to provide derivation algorithms furnishing comparable results as well.

CONCLUSIONS

It is difficult to enumerate all the implications that can be attached to the analysis performed on the eDF structure from such a wide variety of points of view as presented in this work. The most important conclusion one can draw, perhaps, from the present discussion, is the fact that eDF possess a rich source of problems which can be connected with an imaginative set of algorithms and techniques, encompassing a broad class of mathematical structures and theoretical concepts. Most of these points have been curiously forgotten in the literature.

The leading role eDF has with respect to the QSM and related topics provides the possibility to obtain information, in exchange, about eDF discrete representations.

Therefore, the description of QO in general and in particular of molecular structures appears as a subordinate problem of eDF structure. Extensions and averages of eDF can be related to this framework, and the innermost eDF structure has been shown that can be simply elucidated by means of a blend of classical matrix algebra as well as of new ideas on matrix manipulation. The way is open to interesting research paths and rewarding computational procedures.

A significant sample of possible uses of extended Hilbert spaces and the related generalized Sobolev spaces has been studied. In particular, as a consequence of the broad

application scope connected with both extended Sobolev and Hilbert spaces, the non-linear Schrödinger equation has been analyzed, as a mathematical structure issued of particular extended wave functions.

Two points should finally be noted. First, from the exposed naïve formalism it seems that addition of higher order terms as elements of the extended wave function vector could be propitiated by the structure of the extended Sobolev spaces, posing no other problems than those associated with the increasingly difficult structure of the implied integrals in the corresponding energy expressions. Second, and nonetheless important, this study clearly shows the close connection of the non-linear Schrödinger equation structure with quantum similarity measures.

USED ABBREVIATIONS

AO	*Atomic Orbital*
ASA	*Atomic Shell Approximation*
CASA	*Complete ASA*
DF	*Density Function*
DMR	*Density Matrix Representation*
DQOS	*Discrete Quantum Object Set*
DSQOS	*Discrete Stochastic Quantum Object Set*
DVS	*Diagonal Vector Space*
DVSS	*Diagonal Vector Semispace*
eDF	*Electronic Density Function*
EHS	*Extended Hilbert Space*
EJR	*Elementary Jacobi Rotations*
GTO	*Gaussian Type Orbitals*
IMP	*Inward Matrix Product*
KE	*Kinetic Energy*
LCAO	*Linear Combination of Atomic Orbitals*
MO	*Molecular Orbital*
MQSM	*Molecular Quantum Similarity Measure*
NSS	*Nested Summation Symbol*
PD	*Positive Definite*
QO	*Quantum Object*
QODF	*Quantum Object Distinct Features*
QOS	*Quantum Object Set*
QSAR	*Quantitative Structure-Activity Relationships*
QQSAR	*Quantum QSAR*
QS	*Quantum Similarity*
QSM	*Quantum Similarity Measure*
QSSM	*Quantum Self-Similarity Measure*
SCF	*Self Consistent Field*
SM	*Similarity Matrix*
SVSS	*Strict Vector Semispace*
VS	*Vector Space*
VSS	*Vector Semispace*

ACKNOWLEDGEMENTS

Several fundamental aspects of this work have been discussed many times with quite a great number of people. Among those to whom the author is indebted, there must be quoted Professors: Gropen (University of Tromso), Mezey (Institute of Advanced Studies; Budapest and Memorial University of Saint John's Newfoundland), Ponec (Czech Academy of Sciences, Prague) and Karwowski (University N. Copernicus, Torun). The author also wishes to express his most grateful thanks to Dr. E. Besalú, as well as to Ll. Amat, X. Gironés and D. Robert. Without their enthusiastic dedication, the development of the ideas around the Schrödinger equation and the density function structure might never be able to have taken place. The author also wishes to specially thank Prof. P. Bultinck and the University of Gent for the hospitality during my 2004–2005 stage at the Department of Inorganic and Physical Chemistry. Finally, the author wants to express his acknowledgement to the Ministerio de Ciencia y Tecnología for the grant: BQU2003-07420-C05-01; which has partially sponsored this work and also for a Salvador de Madariaga fellowship reference: PR2004-0547, which has made possible to develop the final form of the work in a stage at the University of Ghent.

REFERENCES

[1] P.O. Löwdin, *Phys. Rev.* **97** (1955) 1474.
[2] R. McWeeny, *Rev. Mod. Phys.* **32** (1960) 335.
[3] R. McWeeny, *Proc. Roy. Soc. A* **253** (1959) 242.
[4] R. McWeeny, *Methods of Molecular Quantum Mechanics*, Academic Press, London, 1992.
[5] E.R. Davidson, *Reduced Density Matrices in Quantum Chemistry*, Academic Press, New York, 1976.
[6] P.O. Löwdin, *Linear Algebra for Quantum Theory*, Wiley–Interscience, New York, 1998.
[7] R. Carbó, E. Besalú, *J. Math. Chem.* **18** (1995) 37.
[8] R.F.W. Bader, *Atoms in Molecules, a Quantum Theory*, Clarendon Press, Oxford, 1990.
[9] See, for example:
(a) P.G. Mezey, *Mol. Phys.* **96** (1999) 169;
(b) P.G. Mezey, *J. Math. Chem.* **23** (1998) 65;
(c) P.G. Mezey, *J. Chem. Inf. Comp. Sci.* **39** (1999) 224;
(d) P.G. Mezey, *J. Comp. Chem.* **19** (1999) 1337.
[10] R. Carbó, M. Arnau, L. Leyda, *Int. J. Quantum Chem.* **17** (1980) 1185.
[11] See, for example:
(a) E.E. Hodgkin, W.G. Richards, *Int. J. Quantum Chem.* **14** (1987) 105;
(b) C. Burt, W.G. Richards, Ph. Huxley, *J. Comp. Chem.* **11** (1990) 1139;
(c) A.C. Good, E.E. Hodgkin, W.G. Richards, *J. Chem. Inf. Comp. Sci.* **32** (1992) 188;
(d) A.C. Good, S.-S. So, W.G. Richards, *J. Math. Chem.* **36** (1993) 433;
(e) A.C. Good, W.G. Richards, *J. Chem. Inf. Comp. Sci.* **33** (1993) 112.
[12] See, for example:
(a) D.L. Cooper, N.L. Allan, *J. Comp. Aid. Mol. Des.* **3** (1989) 253;
(b) D.L. Cooper, N.L. Allan, *J. Am. Chem. Soc.* **114** (1992) 4773;
(c) D.L. Cooper, K.A. Mort, N.L. Allan, D. Kinchington, Ch. McGuidan, *J. Am. Chem. Soc.* **115** (1993) 12615;
(d) N.L. Allan, D.L. Cooper, *Topics in Current Chemistry* **173** (1995) 85.
[13] See, for example:
(a) J. Cioslowski, E.D. Fleishmann, *J. Am. Chem. Soc.* **113** (1991) 64;
(b) J.B. Ortiz, J. Cioslowski, *Chem. Phys. Lett.* **185** (1991) 270;
(c) J. Cioslowski, M. Challacombe, *Int. J. Quantum Chem. S* **25** (1991) 81;
(d) J. Cioslowski, S.T. Mixon, *Can. J. Chem.* **70** (1992) 443;

(e) J. Cioslowski, A. Nanayakkara, *J. Am. Chem. Soc.* **115** (1993) 11213;
(f) J. Cioslowski, B.B. Stefanov, P. Constans, *J. Comp. Chem.* **17** (1996) 1352.
[14] See, for example:
(a) R. Ponec, M. Strnad, *Collect. Czech. Chem. Commun.* **55** (1990) 896;
(b) R. Ponec, M. Strnad, *Collect. Czech. Chem. Commun.* **55** (1990) 2583;
(c) R. Ponec, M. Strnad, *J. Phys. Org. Chem.* **4** (1991) 701;
(d) R. Ponec, M. Strnad, *J. Math. Chem.* **8** (1991) 103;
(e) R. Ponec, M. Strnad, *Int. J. Quantum Chem.* **42** (1992) 501;
(f) R. Ponec, *J. Chem. Inf. Comp. Sci.* **33** (1993) 805;
(g) R. Ponec, *Overlap Determinant Method in the Theory of Pericyclic Reactions*, in: *Lecture Notes in Chemistry*, vol. 65, Springer-Verlag, Berlin, 1995.
[15] See, for example:
(a) P.G. Mezey, *Shape in Chemistry: An Introduction to Molecular Shape and Topology*, VCH, New York, 1993;
(b) P.G. Mezey, in: K. Sen (Ed.), *Molecular Similarity I, Topics in Current Chemistry*, vol. 173, Springer-Verlag, Berlin, 1995, pp. 63–83.
[16] Ch. Lee, Sh. Smithline, *J. Phys. Chem.* **98** (1994) 1135.
[17] C. Amovilli, R. McWeeny, *J. Mol. Struct. (Theochem)* **227** (1991) 1.
[18] A.C. Good, *J. Mol. Graph.* **10** (1992) 144.
[19] R. Benigni, M. Cotta-Ramusino, F. Giorgi, G. Gallo, *J. Med. Chem.* **38** (1995) 629.
[20] J.D. Petke, *J. Comp. Chem.* **14** (1993) 928.
[21] A. Riera, *J. Mol. Struct. (Theochem)* **259** (1992) 83.
[22] For an exhaustive account of the recent work on this subject, see references [35] and [36] below.
[23] J. Von Neumann, *Mathematical Foundations of Quantum Mechanics*, Princeton Univ. Press, Princeton, NJ, 1955.
[24] D. Bohm, *Quantum Theory*, Dover, New York, 1989.
[25] R. Carbó, Ll. Domingo, *Int. J. Quantum Chem.* **23** (1987) 517.
[26] R. Carbó-Dorca, *J. Math. Chem.* **23** (1998) 353.
[27] R. Carbó-Dorca, *J. Math. Chem.* **23** (1998) 365.
[28] R. Carbó-Dorca, in: R. Carbó-Dorca, P.G. Mezey (Eds.), *Advances in Molecular Similarity*, vol. 2, JAI Press, Greenwich, CT, 1998, pp. 43–72.
[29] See, for example:
(a) R. Carbó, B. Calabuig, *Comp. Phys. Commun.* **55** (1989) 117;
(b) R. Carbó, B. Calabuig, *J. Mol. Struct. (Theochem)* **254** (1992) 517;
(c) R. Carbó, B. Calabuig, in: S. Fraga (Ed.), *Computational Chemistry: Structure, Interactions and Reactivity*, Elsevier, Amsterdam, 1992, pp. 300–324, Part A.
[30] R. Carbó, B. Calabuig, L. Vera, E. Besalú, *Adv. Quantum Chem.* **25** (1994) 253.
[31] R. Carbó, B. Calabuig, *Int. J. Quantum Chem.* **42** (1992) 1681.
[32] R. Carbó, E. Besalú, in: R. Carbó (Ed.), *Molecular Similarity and Reactivity: From Quantum Chemistry to Phenomenological Approaches*, Kluwer Academic, Dordrecht, 1995, pp. 3–30.
[33] R. Carbó, B. Calabuig, *J. Chem. Inf. Comp. Sci.* **32** (1992) 600.
[34] P. Constans, L. Amat, R. Carbó-Dorca, *J. Comp. Chem.* **18** (1997) 826.
[35] See, for example:
(a) D. Robert, R. Carbó-Dorca, *J. Math. Chem.* **23** (1998) 327;
(b) D. Robert, R. Carbó-Dorca, *Il Nuovo Cimiento A* **111** (1998) 1311;
(c) X. Fradera, L. Amat, E. Besalú, R. Carbó-Dorca, *Quantum Struct.-Act. Relat.* **16** (1997) 25;
(d) M. Lobato, L. Amat, E. Besalú, R. Carbó-Dorca, *Scientia Gerundensis* **23** (1998) 17;
(e) M. Lobato, L. Amat, E. Besalú, R. Carbó-Dorca, *Quantum Struct.-Act. Relat.* **16** (1997) 465;
(f) D. Robert, R. Carbó-Dorca, *J. Chem. Inf. Comp. Sci.* **38** (1998) 620;
(g) L. Amat, D. Robert, E. Besalú, R. Carbó-Dorca, *J. Chem. Inf. Comp. Sci.* **38** (1998) 624;
(h) R. Ponec, L. Amat, R. Carbó-Dorca, *J. Comp.-Aided Mol. Des.* **13** (1999) 259;
(i) L. Amat, R. Carbó-Dorca, R. Ponec, *J. Comp. Chem.* **19** (1998) 1575;
(j) R. Ponec, L. Amat, R. Carbó-Dorca, *J. Phys. Org. Chem.* **12** (1999) 447;
(k) X. Gironés, L. Amat, R. Carbó-Dorca, *Comp. Aided Mol. Des.* **14** (2000) 477;
(l) A. Gallegos, D. Robert, X. Gironés, R. Carbó-Dorca, *J. Comp.-Aided Mol.* **15** (2001) 67;
(m) L. Amat, E. Besalú, R. Carbó-Dorca, *J. Chem. Inf. Comp. Sci.* **41** (2001) 978;

(n) X. Gironés, R. Carbó-Dorca, *J. Chem. Inf. Comp. Sci.* **42** (2002) 317;
(o) R. Ponec, X. Gironés, R. Carbó-Dorca, *J. Chem. Inf. Comp. Sci.* **42** (2002) 564;
(p) E. Besalú, X. Gironés, L. Amat, R. Carbó-Dorca, *Accounts of Chemical Research* **35** (2002) 289;
(q) X. Gironés, A. Gallegos, R. Carbó-Dorca, *J. Comp.-Aided Mol. Design* **15** (2001) 1053;
(r) X. Gironés, R. Carbó-Dorca, *J. Chem. Inf. Comp. Sci.* **42** (2002) 1185;
(s) A. Gallegos, L. Amat, R. Carbó-Dorca, T.W. Schultz, M. Cronin, *J. Chem. Inf. Comp. Sci.* **43** (2003) 1166;
(t) L. Amat, R. Carbó-Dorca, D.L. Cooper, N.L. Allan, P. Ponec, *Mol. Phys.* **101** (2003) 3159;
(u) X. Gironés, R. Carbó-Dorca, R. Ponec, *J. Chem. Inf. Comp. Sci.* **43** (2003) 2033;
(v) A. Gallegos, R. Carbó-Dorca, R. Ponec, K. Waisser, *Int. J. Pharm.* **269** (2004) 51;
(w) X. Gironés, R. Carbó-Dorca, Molecular similarity and quantitative structure-activity relationships, in: P. Bultinck, H. DeWinter, W. Langenaeker, J.P. Tollenaere (Eds.), *Computational Medicinal Chemistry for Drug Discovery*, Marcel Dekker, New York, 2004, pp. 365–385;
(x) R. Carbó-Dorca, X. Gironés, *Int. J. Quantum Chem.* **101** (2005) 8.

[36] See, for more details:
(a) R. Carbó, E. Besalú, L. Amat, X. Fradera, *J. Math. Chem.* **19** (1996) 47;
(b) D. Robert, R. Carbó-Dorca, *J. Chem. Inf. Comput. Sci.* **38** (1998) 469;
(c) L. Amat, D. Robert, E. Besalú, R. Carbó-Dorca, *J. Chem. Inf. Comput. Sci.* **38** (1998) 624;
(d) D. Robert, R. Carbó-Dorca, *J. Chem. Inf. Comput. Sci.* **38** (1998) 620;
(e) D. Robert, L. Amat, R. Carbó-Dorca, *J. Chem. Inf. Comput. Sci.* **39** (1999) 333;
(f) X. Gironés, L. Amat, R. Carbó-Dorca, *SAR QSAR Environ. Res.* **10** (1999) 545;
(g) R. Carbó, E. Besalú, L. Amat, X. Fradera, *J. Math. Chem.* **18** (1995) 237;
(h) E. Besalú, R. Carbó, J. Mestres, M. Solà, *Molecular Similarity*, in: I.K. Sen (Ed.), *Topics in Current Chemistry*, vol. 173, Springer-Verlag, Berlin, 1995, pp. 31–62;
(i) R. Carbó-Dorca, *Int. J. Quantum Chem.* **79** (2000) 163;
(j) R. Carbó-Dorca, *J. Math. Chem.* **27** (2000) 357;
(k) R. Carbó-Dorca, E. Besalú, *Contributions to Science* **1** (2000) 399;
(l) R. Carbó-Dorca, L. Amat, E. Besalú, X. Gironès, D. Robert, Quantum molecular similarity: Theory and applications to the evaluation of molecular properties, biological activity and toxicity, in: *Mathematical and Computational Chemistry: Fundamentals of Molecular Similarity*, Kluwer Academic/Plenum, 2001, pp. 187–320;
(m) R. Carbó-Dorca, E. Besalú, *Int. J. Quantum Chem.* **88** (2002) 167;
(n) P. Bultinck, R. Carbó-Dorca, *J. Chem. Inf. Comp. Sci.* **43** (2003) 170.

[37] I.M. Vinogradov (Ed.), *Encyclopaedia of Mathematics*, vol. 8, Reidel/Kluwer Academic, Dordrecht, 1987, p. 249.

[38] S.K. Berberian, *Introducción al Espacio de Hilbert*, Editorial Teide, Barcelona, 1970.

[39] See, for example: *LF 95 Language Reference*, Lahey Computer Systems, Incline Village NV (199X). For more details browse at: http://www.lahey.com.

[40] See, for example:
(a) R. Carbó, E. Besalú, *J. Math. Chem.* **13** (1993) 331;
(b) R. Carbó, E. Besalú, *Computers Chem.* **18** (1994) 117;
(c) R. Carbó, E. Besalú, *J. Math. Chem.* **18** (1995) 37;
(d) R. Carbó, E. Besalú, in: Y. Ellinger, M. Defranceschi (Eds.), *Strategies and Applications in Quantum Mechanics*, Kluwer Academic, Dordrecht, 1996, pp. 229–248.

[41] R.G. Parr, *The Quantum Theory of Molecular Electronic Structure*, W.A. Benjamin, New York, 1963.

[42] See, for example: H. Zabrodsky, S. Peleg, D. Avnir, *J. Am. Chem. Soc.* **114** (1992) 7843.

[43] F.L. Pilar, *Elementary Quantum Chemistry*, McGraw–Hill, Princeton, NJ, 1990.

[44] P.W. Atkins, R.S. Friedman, *Molecular Quantum Mechanics*, Oxford Univ. Press, Oxford, 1997.

[45] E.V. Ludeña, in: S. Fraga (Ed.), *Química Teórica, Nuevas Tendencias*, vol. 4, Consejo Superior de Investigaciones Científicas, Madrid, 1987, pp. 117–160.

[46] Shavitt, Methods of electronic structure theory, in: H.F. Schaefer III (Ed.), in: *Modern Theoretical Chemistry*, vol. 3, Plenum, New York, 1977, pp. 189–275.

[47] J. Stoer, Ch. Witzgall, *Convexity and Optimization in Finite Dimensions, Die Grundlehren der matematischen Wissenchaften in Einzeldarstellungen*, vol. 163, Springer-Verlag, Berlin, 1970.

[48] P.M. Gruber, J.M. Wills (Eds.), *Handbook of Convex Geometry*, North-Holland, Amsterdam, 1993.

[49] C.G.J. Jacobi, *J. Reine Angew. Math.* **30** (1846) 51.

[50] See, for example:
(a) J. Mestres, M. Solà, M. Duran, R. Carbó, *J. Comp. Chem.* **15** (1994) 1113;
(b) P. Constans, R. Carbó, *J. Chem. Inf. Comput. Sci.* **35** (1995) 1046;
(c) P. Constans, L. Amat, X. Fradera, R. Carbó-Dorca, in: R. Carbó-Dorca, P.G. Mezey (Eds.), *Advances in Molecular Similarity*, vol. 1, JAI Press, Greenwich, CT, 1996, pp. 187–211;
(d) L. Amat, R. Carbó, P. Constans, *Scientia Gerundensis* **22** (1996) 109;
(e) L. Amat, R. Carbó-Dorca, *J. Comp. Chem.* **18** (1997) 2023;
(f) L. Amat, R. Carbó-Dorca, *J. Comp. Chem.* **20** (1999) 911;
(g) X. Gironés, R. Carbó-Dorca, P.G. Mezey, *J. Mol. Graphics Mod.* **19** (2001) 343;
(h) L. Amat, R. Carbó-Dorca, *Int. J. Quantum Chem.* **87** (2002) 59.
[51] R. Carbó-Dorca, *J. Math. Chem.* **22** (1997) 143.
[52] R. Carbó-Dorca, in: R. Carbó-Dorca, P.G. Mezey (Eds.), *Advances in Molecular Similarity*, vol. 2, JAI Press, Greenwich, 1998, pp. 43–72.
[53] R. Carbó-Dorca, E. Besalú, *J. Mol. Struct. (Theochem)* **451** (1998) 11.
[54] R. Carbó-Dorca, *J. Math. Chem.* **23** (1998) 353.
[55] R. Carbó-Dorca, *J. Math. Chem.* **23** (1998) 365.
[56] K.D. Sen, R. Carbó-Dorca, *J. Mol. Struct. (Theochem)* **501** (2000) 173.
[57] See, for example:
(a) for a definition: C. Roos, T. Terlaky, J.-Ph. Vial, in: *Theory and Algorithms for Linear Optimization*, Wiley, New York, 1997, p. 11;
(b) for the origin: I.M. Vinogradov (Ed.), *Encyclopaedia of Mathematics*, vol. 4, Kluwer Academic, Dordrecht, 1989, p. 351.
[58] J.E. Whitesitt, *Boolean Algebra and Its Applications*, Dover, New York, 1995.
[59] See, for example:
(a) L.A. Zadeh, *Inform. Control* **8** (1965) 338;
(b) E. Trillas, C. Alsina, J.M. Terricabras, *Introducción a la Lógica Difusa*, Ariel Matemática, Barcelona, 1995.
[60] R. Carbó, B. Calabuig, E. Besalú, A. Martínez, *Molecular Engineering* **2** (1992) 43.
[61] R. Carbó-Dorca, L. Amat, E. Besalú, M. Lobato, in: R. Carbó-Dorca, P.G. Mezey (Eds.), *Advances in Molecular Similarity*, vol. 2, JAI Press, Greenwich, 1998, pp. 1–42.
[62] See, for example:
(a) M.A. Johnson, G. Maggiora (Eds.), *Concepts and Applications of Molecular Similarity*, Wiley, New York, 1990;
(b) R. Carbó (Ed.), *Molecular Similarity and Reactivity: From Quantum Chemical to Phenomenological Approaches*, *Understanding Chemical Reactivity*, vol. 14, Kluwer Academic, Dordrecht, 1995;
(c) K. Sen (Ed.), *Molecular Similarity*, *Topics in Current Chemistry*, vols. 173, 174, Springer-Verlag, Berlin, 1995;
(d) P.M. Dean (Ed.), *Molecular Similarity in Drug Design*, Blackie Academic & Professional, London, 1995;
(e) R. Carbó-Dorca, P.G. Mezey (Eds.), *Advances in Molecular Similarity*, vol. 1, JAI Press, Greenwich, 1996;
(f) R. Carbó-Dorca, P.G. Mezey (Eds.), *Advances in Molecular Similarity*, vol. 2, JAI Press, Greenwich, 1998.
[63] R. Carbó-Dorca, *Int. J. Quantum Chem.* **79** (2000) 163.
[64] S. Huzinaga, M. Klobukowski, *J. Mol. Struct. (Theochem)* **167** (1998) 1.
[65] See, for example: D.A. Pierre, *Optimization Theory with Applications*, Wiley, New York, 1969.
[66] ASA coefficients and exponents can be seen and downloaded from the WWW site: http://iqc.udg.es/cat/similarity/ASA/basisset.html.
[67] R. Carbó, J.M. Riera, *A General SCF Theory*, *Lecture Notes in Chemistry*, vol. 5, Springer-Verlag, Berlin, 1978.
[68] P. Cassam-Chenai, *J. Math. Chem.* **31** (2002) 145.
[69] R. Carbó-Dorca, *J. Mol. Struct. (Theochem)* **537** (2001) 41.
[70] P.G. Mezey, *J. Comp. Chem.* **19** (1998) 1337.
[71] P.G. Mezey, R. Ponec, Ll. Amat, R. Carbó-Dorca, *Enantiomer* **4** (1999) 371.
[72] F.R. Gantmacher, *Théorie des Matrices*, Dunod, Paris, 1966.
[73] P. Hohenberg, W. Kohn, *Phys. Rev.* **136** (1964) B864.

[74] N.H. March, *Electron Density Theory of Atoms and Molecules*, Academic Press, London, 1992.
[75] A. Messiah, *Mécanique Quantique*, Dunod, Paris, 1959.
[76] R. Shankar, *Principles of Quantum Mechanics*, Plenum, New York, 1994.
[77] A. Jeffrey, *Handbook of Mathematical Formulas and Integrals*, Academic Press, New York, 1995.
[78] V.R. Saunders, *NATO Advanced Study Institute Series* **15** (1975) 347.
[79] P.W. Atkins, R.S. Friedman, *Molecular Quantum Mechanics*, Oxford Univ. Press, Oxford, 1997.
[80] H. Eyring, J. Walter, G.E. Kimball, *Quantum Chemistry*, Wiley, New York, 1944.
[81] H. Clark, *Quantum Mechanics*, Van Nostrand–Reinhold, New York, 1982.
[82] L. Pauling, E.B. Wilson Jr., *Introduction to Quantum Mechanics*, Dover, New York, 1985.
[83] A.S. Davydov, *Quantum Mechanics*, Pergamon, New York, 1965.
[84] H.A. Bethe, R. Jackiw, *Intermediate Quantum Mechanics*, Benjamin, Menlo Park, 1986.
[85] C. Cohen-Tannoudji, B. Diu, F. Laloë, *Mécanique Quantique*, Hermann, Paris, 1992.
[86] E.E. Dykstra, *Introduction to Quantum Chemistry*, Prentice Hall, Englewood Cliffs, NJ, 1991.
[87] P.A.M. Dirac, *The Principles of Quantum Mechanics*, Clarendon, Oxford, 1958.
[88] J.S. Bell, *Speakable and Unspeakable in Quantum Mechanics*, Cambridge Univ. Press, Cambridge, 1993.
[89] R. Carbó-Dorca, E. Besalú, X. Gironés, Extended density functions, *Adv. Quantum Chem.* **38** (2000) 3.
[90] R. Carbó-Dorca, *J. Math. Chem.* **27** (2000) 35.
[91] See, for example:
(a) R.E. Moss, *Advanced Molecular Quantum Mechanics*, Chapman and Hall, London, 1973;
(b) E. Cartan, *The Theory of Spinors*, Dover, New York, 1966.
[92] J.M. Levy-Leblond, *Commun. Math. Phys.* **6** (1997) 286.
[93] J. Karwowski, G. Pestka, M. Stanke, *Adv. Quantum Chem.* **24** (1998) 1.
[94] I.M. Vinogradov (Ed.), *Encyclopaedia of Mathematics*, vol. 8, Kluwer Academic, Dordrecht, 1992, p. 379.
[95] S.L. Sobolev, *Math. Sb.* **4** (1938) 471.
[96] R. Carbó-Dorca, L. Amat, E. Besalú, X. Gironés, D. Robert, *J. Mol. Struct. (Theochem)* **504** (2000) 181.
[97] I.M. Vinogradov (Ed.), *Encyclopaedia of Mathematics*, vol. 3, Kluwer Academic, Dordrecht, 1989, p. 402.
[98] R. Carbó-Dorca, L. Amat, E. Besalú, X. Gironés, D. Robert, Quantum molecular similarity: Theory and applications to the evaluation of molecular properties, biological activities and toxicity, in: R. Carbó-Dorca, X. Gironés, P.G. Mezey (Eds.), *Math. and Comp. Chem.: Fundamentals of Molecular Similarity*, Kluwer Academic/Plenum, New York, 2001, p. 187, Proceedings of 4th Girona Seminar on Molecular Similarity.
[99] I.M. Vinogradov (Ed.), *Encyclopaedia of Mathematics*, vol. 4, Kluwer Academic, Dordrecht, 1989, p. 351.
[100] See, for example: D.T. Finkbeiner, *Matrices and Linear Transformations*, W.H. Freeman, San Francisco, 1966.
[101] R. Carbó-Dorca, *J. Math. Chem.* **23** (1998) 365.
[102] R. Carbó-Dorca, E. Besalú, Huzinaga symposium, Fukuoka, *J. Molec. Struct. Theochem* **451** (1998) 11.
[103] D. Robert, R. Carbó-Dorca, *J. Chem. Inf. Comp. Sci.* **38** (1998) 620.
[104] R. Carbó, B. Calabuig, E. Besalú, A. Martínez, *Mol. Engineering* **2** (1992) 43.
[105] K.D. Sen, E. Besalú, R. Carbó-Dorca, *J. Math. Chem.* **25** (1999) 213.
[106] S. Fraga, J.M. García de la Vega, E.S. Fraga, *The Schrödinger and Riccati Equations*, *Lecture Notes in Chemistry*, vol. 70, Springer-Verlag, Berlin, 1999.
[107] R. Carbó-Dorca, L. Amat, E. Besalú, X. Gironés, D. Robert, *J. Mol. Struct. (Theochem)* **504** (2000) 1.
[108] G. Breit, *Phys. Rev.* **34** (1929) 553;
G. Breit, *Phys. Rev.* **36** (1930) 383;
G. Breit, *Phys. Rev.* **39** (1932) 616.
[109] H.A. Bethe, E.E. Salpeter, *Quantum Mechanics of One- and Two-Electron Systems*, Springer-Verlag, Berlin, 1957.
[110] R. Carbó-Dorca, P. Bultinck, *J. Math. Chem.* **36** (2004) 201.
[111] R. Carbó-Dorca, P. Bultinck, *J. Math. Chem.* **36** (2004) 231.
[112] P.C. Hohenberg, W. Kohn, L.J. Sham, *Adv. Quantum Chem.* **21** (1990) 7.
[113] P. Geerlings, F. De Proft, W. Langenaeker, *Chem. Rev.* **103** (2003) 1793.
[114] R.G. Parr, W. Yang, *Density Functional Theory of Atoms and Molecules*, Oxford Univ. Press, New York, 1989.
[115] (a) K. Fukui, T. Yonezawa, H. Shingu, *J. Chem. Phys.* **20** (1952) 722;
(b) K. Fukui, T. Yonezawa, C. Nagata, H. Shingu, *J. Chem. Phys.* **22** (1954) 1433.
[116] P.W. Ayers, R.C. Morrison, R.K. Roy, *J. Chem. Phys.* **116** (2002) 8731.
[117] P. Bultinck, R. Carbó-Dorca, W. Langenaeker, *J. Chem. Phys.* **118** (2003) 4349.

[118] P. Bultinck, R. Carbó-Dorca, *J. Math. Chem.* **34** (2003) 67.
[119] R.G. Parr, L.J. Bartolotti, *J. Phys. Chem.* **87** (1983) 2810.
[120] R. Carbó-Dorca, *J. Math. Chem.* **33** (2003) 227.
[121] R. Carbó-Dorca, Density functions and generating wave functions, in: K.D. Sen (Ed.), *Reviews in Modern Quantum Chemistry: A Celebration of the Contributions of R.G. Parr*, World Scientific, Singapore, 2002, p. 401.
[122] X. Gironés, A. Gallegos, R. Carbó-Dorca, *J. Comp. Aided Mol. Des.* **15** (2001) 1053.
[123] Ll. Amat, R. Carbó-Dorca, *Int. J. Quantum Chem.* **87** (2002) 59.
[124] X. Gironés, L. Amat, R. Carbó-Dorca, *J. Mol. Graph. Mod.* **16** (1998) 190.
[125] X. Gironés, R. Carbó-Dorca, P.G. Mezey, *J. Mol. Graph. Mod.* **19** (2001) 343.
[126] X. Gironés, Ll. Amat, R. Carbó-Dorca, *J. Chem. Inf. Comput. Sci.* **42** (2002) 847.
[127] J.P. Perdew, R.G. Parr, M. Levy, J.L. Balduz Jr., *Phys. Rev. Lett.* **49** (1982) 1691.

This page intentionally left blank

Quantum Monte Carlo: Theory and Application to Molecular Systems

Alán Aspuru-Guzik[1,*] and William A. Lester Jr.[1,2]

[1]*Kenneth S. Pitzer Center for Theoretical Chemistry, Department of Chemistry, University of California, Berkeley, CA 94720-1460, USA*
E-mail: alan@aspuru.com
[2]*Chemical Sciences Division, Lawrence Berkeley National Laboratory, Berkeley, CA 94720, USA*
E-mail: walester@lbl.gov

Contents

1. INTRODUCTION

This presentation will describe the quantum Monte Carlo (QMC) method for the determination of the electronic structure of molecules [1–14]. QMC methods have several advantages:

- Computer time scales with system size roughly as N^3, where N is the number of particles of the system. Recent developments have made possible the approach to linear scaling in certain cases [15–18].
- Computer memory requirements are small and grow modestly with system size.
- QMC is intrinsically parallel so that associated computer codes are significantly smaller and more readily adapted to parallel computers than basis set molecular quantum mechanics computer programs.
- Basis set truncation and basis set superposition errors are absent in one of the variants (diffusion MC) of QMC computations.

* Gates Millennium Scholarship Holder.

ADVANCES IN QUANTUM CHEMISTRY, VOLUME 49
ISSN: 0065-3276 DOI: 10.1016/S0065-3276(05)49004-8

- Monte Carlo numerical precision can be arbitrarily increased. QMC calculations have an accuracy dependence of $\sqrt{T}$, where T is the computer time. This enables one to choose an accuracy range and readily estimate the computer time needed for performing a calculation of an observable with an acceptable error bar.

The goal of the QMC method is to solve the Schrödinger equation, which in the time independent form is given by

$$\widehat{H}\Psi_n(\mathbf{R}) = E_n\Psi_n(\mathbf{R}). \tag{1}$$

Here, $\widehat{H}$ is the Hamiltonian operator of the system, with wave function $\Psi_n(\mathbf{R})$ and energy E_n. The index n denotes a particular state, $n = 0, 1, \ldots$. Here $\mathbf{R}$ is a vector that denotes the $3M$ coordinates of the system of M particles (electrons and nuclei), $\mathbf{R} \equiv \{\mathbf{r}_1, \ldots, \mathbf{r}_{3M}\}$. For molecular systems, in the absence of electric or magnetic fields, the Hamiltonian has the form $\widehat{H} \equiv \widehat{T} + \widehat{V}$, where $\widehat{T}$ is the kinetic energy operator, $\widehat{T} \equiv -\frac{1}{2}\nabla^2_{\mathbf{R}}$, and $\widehat{V}(\mathbf{R})$ is the potential energy operator. For atomic and molecular systems $\widehat{V}$ is the Coulomb potential between particles of charge q_i, *i.e.*, $\widehat{V} \equiv \sum_{ij} \frac{q_i q_j}{r_{ij}}$.

The first suggestion of a Monte Carlo solution of the Schrödinger equation dates back to Enrico Fermi [19] who indicated that a solution to the stationary state equation

$$-\frac{1}{2}\nabla^2_{\mathbf{R}}\Psi(\mathbf{R}) = E\Psi(\mathbf{R}) - V(\mathbf{R})\Psi(\mathbf{R}) \tag{2}$$

could be obtained by introducing a wave function of the form $\Psi(\mathbf{R}, \tau) = \Psi(\mathbf{R})e^{-E\tau}$. This yields the equation

$$\frac{\partial\Psi(\mathbf{R}, \tau)}{\partial\tau} = \frac{1}{2}\nabla^2\Psi(\mathbf{R}, \tau) - V(\mathbf{R})\Psi(\mathbf{R}, \tau), \tag{3}$$

where $\tau = it$ is imaginary time. Taking the limit $\tau \to \infty$, in equation (3) recovers equation (2). If the second term on the right-hand side of equation (3) is ignored, the equation is isomorphic with a diffusion equation, which can be simulated by a random walk [20,21], where random walkers diffuse in an $\mathbf{R}$-dimensional space. If the first term is ignored, the equation is a first-order kinetics equation with a position-dependent rate constant, $V(\mathbf{R})$, which can also be interpreted as a stochastic survival probability. A numerical simulation in which random walkers diffuse through $\mathbf{R}$-space, reproduce in regions of low potential, and die in regions of high potential leads to a stationary distribution proportional to $\Psi(\mathbf{R})$, from which expectation values can be obtained.

Since the pioneering work of the late forties to early sixties [19,22,23] the MC and related methods have grown in interest. The QMC methods have an advantage over wave function methods with system size scaling, in the simplicity of algorithms and in trial wave function forms that can be used for importance sampling.

2. NUMERICAL SOLUTION OF THE SCHRÖDINGER EQUATION

Most efforts to solve the Schrödinger equation depend on basis sets. These approaches rely almost exclusively on one or a linear combination of Slater determinants, and include the Hartree–Fock (HF), the density functional theory (DFT), the configuration interaction (CI), and the multi-configuration self-consistent field (MCSCF) methods. There are perturbation approaches, for example, the Møller–Plesset methods (MP(N), N = 2–4), and

coupled cluster (CC) approaches, which are presently popular computational procedures. An exact basis set calculation with a given basis set expansion requires $N!$ computer operations, where N is the number of basis functions. A method that competes in accuracy with QMC, such as coupled cluster with singles, doubles, and perturbative treatment of triple excitations, CCSD(T), scales as N^7.[1]

A term that we will use later is correlation energy (CE). It is defined as the difference between the exact non-relativistic energy and the HF energy in the limit of an infinite basis set [28,29], *i.e.*,

$$E_{\text{corr}} = E_{\text{exact}} - E_{\text{HF}}. \tag{4}$$

The CI, MCSCF, MP(N), and CC methods are all directed at generating energies that approach E_{exact}. Other methods that have been developed include dimensional expansions [30], and the contracted Schrödinger equation [31].

3. TRIAL WAVE FUNCTIONS

In contrast to wave function methods, where the wave function is usually constructed from determinants of orbitals, QMC methods can use arbitrary functional forms for the wave function, as long as it is antisymmetric with respect to particle exchange. Because QMC trial wave functions are not restricted to expansions in one-electron functions, more compact representations are routinely used.

The most commonly used trial wave function is the product of a determinant or linear combination of determinants, *e.g.*, HF, MCSCF, CASSCF, CI, and a correlation function that is symmetric with respect to particle exchange,

$$\Psi_T = \mathcal{D}\mathcal{F}. \tag{5}$$

Here $\mathcal{D}$ denotes the antisymmetric wave function factor and $\mathcal{F}$ is the symmetric factor. We now describe some of the forms used for $\mathcal{D}$ and then we describe forms for $\mathcal{F}$. Such products are also known as the correlated molecular orbital (CMO) wave functions.

With CMO wave functions, the antisymmetric part of the wave function is constructed as a linear combination of determinants of independent particle functions, ϕ_i. The ϕ_i are usually formed as a linear combination of basis functions centered on atomic centers,

$$\phi_i = \sum_j c_{ij}\chi_j.$$

The antisymmetric part of the wavefunction scales computationally as N^3, where N is the number of particles, compared to $N!$ for the fully antisymmetrized form.[2]

The symmetric part of the wave function is usually built as a product of terms explicitly dependent on inter-particle distance, $r_{ij} = |\mathbf{r}_i - \mathbf{r}_j|$. These functions are usually constructed to reproduce the form of the wave function at electron–electron and electron–nucleus cusps. A now familiar form is that proposed by Bijl [32], Dingle [33], and Jastrow [34]

[1] For a more detailed analysis of the scaling of wave-function-based methods see, for example, [25] and [26]. For a general overview of these methods, see Ref. [27].

[2] The evaluation of a determinant of size N requires N^2 computer operations. If the one-electron functions scale with system size as well, the scaling becomes N^3.

and known as the Jastrow *ansatz*:

$$\mathcal{F} \equiv e^{U(r_{ij})} \equiv e^{\sum_{i<j} g_{ij}}, \tag{6}$$

where the correlation function g_{ij} is

$$g_{ij} \equiv \frac{a_{ij} r_{ij}}{1 + b_{ij} r_{ij}} \tag{7}$$

with constants specified to satisfy the cusp conditions

$$a_{ij} \equiv \begin{cases} \frac{1}{4} & \text{if } ij \text{ are like spins,} \\ \frac{1}{2} & \text{if } ij \text{ are unlike spins,} \\ -Z_\alpha & \text{if } ij \text{ are electron/nucleus pairs,} \end{cases} \tag{8}$$

where Z_α is the atomic number of the αth nucleus. Electron correlation for parallel spins is taken into account by the Slater determinant.

This simple Slater–Jastrow *ansatz* has a number of desirable properties. As stated above, scaling with system size for the evaluation of the trial function is N^3, where N is the number of particles in the system. Second, the correct cusp conditions are satisfied at two-body coalescence points and the correlation function g_{ij} correctly approaches a constant at large distance.

The inclusion of 3-body correlation terms has been shown to improve wave function quality [35,36]. The work of Huang *et al.* [37] shows that if the determinant parameters λ_D are optimized along with the correlation function parameters, λ_C, the nodal structure of the wave function does not significantly improve by including 4-body correlation terms. This finding suggests that increasing the number of determinants is more important than adding fourth- and higher-order correlation terms.

4. VARIATIONAL MONTE CARLO

Variational methods involve the calculation of the expectation value of the Hamiltonian operator using a trial wave function Ψ_T. This function is dependent on a set of parameters, Λ, that are varied to minimize the expectation value of the energy, *i.e.*,

$$\langle \widehat{H} \rangle = \frac{\langle \Psi_T | \widehat{H} | \Psi_T \rangle}{\langle \Psi_T | \Psi_T \rangle} \equiv E[\Lambda] \geqslant E_0. \tag{9}$$

Equation (9) can be sampled from a probability distribution proportional to Ψ_T^2, and evaluated from the expression

$$\frac{\int d\mathbf{R} \left[\frac{\widehat{H}\Psi_T(\mathbf{R})}{\Psi_T(\mathbf{R})} \right] \Psi_T^2(\mathbf{R})}{\int d\mathbf{R}\, \Psi_T^2(\mathbf{R})} \equiv \frac{\int d\mathbf{R}\, E_L \Psi_T^2(\mathbf{R})}{\int d\mathbf{R}\, \Psi_T^2(\mathbf{R})} \geqslant E_0, \tag{10}$$

where $E_L \equiv \frac{\widehat{H}\Psi(\mathbf{R})}{\Psi(\mathbf{R})}$ is the local energy. The procedure involves sampling random points in $\mathbf{R}$-space from

$$\mathcal{P}(\mathbf{R}) \equiv \frac{\Psi_T^2(\mathbf{R})}{\int d\mathbf{R}\, \Psi_T^2(\mathbf{R})}. \tag{11}$$

The advantage of using equation (11) as the probability density function is that one need not perform the averaging of the numerator and denominator of equation (10). The calculation of the ratio of two integrals with the MC method is biased by definition: the average of a quotient is not equal to the quotient of the averages, and equation (11) avoids this problem.

In general, sampling is done using the Metropolis method [38], that is well described in Chapter 3 of Ref. [39], and briefly summarized later in this section.

Expectation values can be obtained using the VMC method from the following general expressions [8]:

$$\langle \widehat{O} \rangle \equiv \frac{\int d\mathbf{R}\, \Psi_T(\mathbf{R})^2 \widehat{O}(\mathbf{R})}{\int d\mathbf{R}\, \Psi_T(\mathbf{R})^2} \cong \frac{1}{N} \sum_{i=1}^{N} \widehat{O}(\mathbf{R}_i), \tag{12}$$

$$\langle \widehat{O}_d \rangle \equiv \frac{\int d\mathbf{R} \left[\frac{\widehat{O}_d \Psi_T(\mathbf{R})}{\Psi_T(\mathbf{R})} \right] \Psi_T(\mathbf{R})^2}{\int d\mathbf{R}\, \Psi_T(\mathbf{R})^2} \cong \frac{1}{N} \sum_{i=1}^{N} \frac{\widehat{O}_d \Psi_T(\mathbf{R}_i)}{\Psi_T(\mathbf{R}_i)}. \tag{13}$$

Equation (12) is for a coordinate operator, $\widehat{O}$, and equation (13) is preferred for a differential operator, $\widehat{O}_d$.

The main idea of the Metropolis algorithm is to sample the electron density, $\Psi_T^2(\mathbf{R})$, using fictitious kinetics that in the limit of large simulation time yields the density at equilibrium. A coordinate move is proposed, $\mathbf{R} \rightarrow \mathbf{R}'$, which has the probability of being accepted given by

$$P(\mathbf{R} \rightarrow \mathbf{R}') = \min\left(1, \frac{T(\mathbf{R}' \rightarrow \mathbf{R}) \Psi_T^2(\mathbf{R}')}{T(\mathbf{R} \rightarrow \mathbf{R}') \Psi_T^2(\mathbf{R})}\right), \tag{14}$$

where $T(\mathbf{R} \rightarrow \mathbf{R}')$ denotes the transition probability for a coordinate move from $\mathbf{R}$ to $\mathbf{R}'$. Condition (14) is necessary to satisfy the detailed balance condition

$$T(\mathbf{R}' \rightarrow \mathbf{R}) \Psi_T^2(\mathbf{R}') = T(\mathbf{R} \rightarrow \mathbf{R}') \Psi_T^2(\mathbf{R}) \tag{15}$$

which is needed for $\Psi_T^2(\mathbf{R})$ to be the equilibrium distribution of the sampling process.

Several improvements to the Metropolis method have been pursued both in classical and in quantum simulations. These improvements involve new transition probability functions and other sampling procedures. See, for example, Refs. [8,40–52].

5. DIFFUSION MONTE CARLO

If one transforms the time-dependent Schrödinger equation (equation (2)) to imaginary time τ, *i.e.*,

$$it \rightarrow \tau, \tag{16}$$

then one obtains, after introducing an energy offset E_R as reference energy,

$$\frac{\partial}{\partial \tau} \Psi(\mathbf{R}, \tau) = (\widehat{H} - E_R) \Psi(\mathbf{R}, \tau). \tag{17}$$

For real $\Psi(\mathbf{R}, \tau)$, equation (17) has the advantage of being in $\mathcal{R}^N$, whereas equation (2) has, in general, complex solutions.

Equation (17) can be cast into integral form,

$$\Psi(\mathbf{R}, \tau + \delta\tau) = \lambda_\tau \int G(\mathbf{R}, \mathbf{R}', \delta\tau)\Psi(\mathbf{R}', \tau)\, d\mathbf{R}'. \tag{18}$$

The Green's function, $G(\mathbf{R}', \mathbf{R}, \delta\tau)$, satisfies the same boundary conditions as equation (17):

$$\frac{\partial}{\partial\tau} G(\mathbf{R}, \mathbf{R}', \delta\tau) = (\widehat{H} - E_R) G(\mathbf{R}, \mathbf{R}', \delta\tau) \tag{19}$$

with the initial conditions associated with the propagation of a Dirac delta function, namely,

$$G(\mathbf{R}, \mathbf{R}', 0) = \delta(\mathbf{R} - \mathbf{R}'). \tag{20}$$

The form of the Green's function that satisfies equation (19), subject to equation (20), is

$$G(\mathbf{R}, \mathbf{R}', \delta\tau) = \left\langle \mathbf{R} \middle| e^{-\tau(\widehat{H} - E_R)} \middle| \mathbf{R}' \right\rangle \tag{21}$$

which can be expanded in eigenfunctions, Ψ_α, and eigenvalues E_α of the system, *i.e.*,

$$G(\mathbf{R}, \mathbf{R}', \delta\tau) = \sum_\alpha e^{-\tau(E_\alpha - E_R)} \Psi_\alpha^*(\mathbf{R}')\Psi_\alpha(\mathbf{R}). \tag{22}$$

For an arbitrary initial trial function, $\Psi(\mathbf{R})$, as $\tau \to \infty$, one has

$$\begin{aligned} \lim_{\tau\to\infty} e^{-\tau(\widehat{H} - E_R)}\Psi &= \lim_{\tau\to\infty} \int G(\mathbf{R}', \mathbf{R}, \tau)\Psi(\mathbf{R}')\, d\mathbf{R}' \\ &= \lim_{\tau\to\infty} \langle \Psi | \Psi_0 \rangle e^{-\tau(E_0 - E_R)} \Psi_0, \end{aligned} \tag{23}$$

and only the ground state wave function Ψ_0 is obtained from any initial wave function.

Sampling equation (21) cannot be done exactly, because the argument of the exponential is an operator composed of two non-commuting terms. In practice, approximate forms of the propagator are used.

In the short-time approximation (STA), the propagator $G(\mathbf{R}, \mathbf{R}', \tau)$ is approximated as if the kinetic and potential energy operators commuted, *i.e.*,

$$e^{(T+V)\delta\tau} \approx e^{T\delta\tau} \cdot e^{V\delta\tau} + \mathcal{O}\big((\delta\tau)^2\big) \equiv G_{ST} \equiv G_D \cdot G_B. \tag{24}$$

The Green's function becomes the product of a diffusion factor G_D and a branching factor G_B. Both propagators are known:

$$G_D = (2\pi\tau)^{-3N/2} e^{-\frac{(\mathbf{R}-\mathbf{R}')^2}{2\delta\tau}} \tag{25}$$

and

$$G_B = e^{-\delta\tau(V(\mathbf{R}) - E_R)}. \tag{26}$$

G_D is a fundamental solution of a Fourier equation that describes a diffusion process in wave function space, and G_B is the fundamental solution of a first-order kinetic birth–death process.

The Campbell–Baker–Hausdorff (CBH) [82–85] formula,

$$e^A e^B = e^{A + B + \frac{1}{2}[A,B] + \frac{1}{12}[(A-B),[A,B]] + \cdots} \tag{27}$$

makes possible more accurate decompositions, such as an expansion with a cubic error $\mathcal{O}((\delta\tau)^3)$,

$$e^{\delta\tau(T+V)} = e^{\delta\tau(V/2)} e^{\delta\tau T} e^{\delta\tau(V/2)} + \mathcal{O}\big((\delta\tau)^3\big). \tag{28}$$

There are also more sophisticated second-order [86,87] and fourth-order [88,89] expansions that reduce the error considerably and generate higher accuracy DMC algorithms at the expense of a more complex propagator. On top of improvements in the CBH expansion, there is additional expense to achieve higher accuracy in the treatment of atoms and molecules: the cusp conditions must be satisfied and continuity corrections are required for the drift velocity [90].

The most common implementation uses G_D as a stochastic transition probability $T(\mathbf{R} \rightarrow \mathbf{R}')$, and G_B as a weighting or branching factor, $B(\mathbf{R})$. Sampling equation (25) can be achieved by obtaining random variates from a Gaussian distribution of variance δ_τ.

Direct application of the above algorithm to systems governed by the Coulomb potential leads to large population fluctuations. These arise because the potential $\widehat{V}(\mathbf{R})$ can become unbounded and induce large fluctuations in the random walker population. A remedy, importance sampling [24] was extended to the DMC method by Ceperley and Alder [44].

In importance sampling Monte Carlo, the goal is to reduce fluctuations, by multiplying the probability distribution by a known trial function, $\Psi_T(\mathbf{R})$, that is expected to be a good approximation for the wave function of the system. Rather than $\Psi(\mathbf{R}, \tau)$, one samples the product

$$f(\mathbf{R}, \tau) = \Psi_T(\mathbf{R})\Psi(\mathbf{R}, \tau). \tag{29}$$

Multiplying equation (18) by $\Psi_T(\mathbf{R})$ yields

$$f(\mathbf{R}, \tau + d\tau) = \int K(\mathbf{R}', \mathbf{R}, \delta\tau) f(\mathbf{R}', \tau)\, d\mathbf{R}', \tag{30}$$

where $K(\mathbf{R}, \mathbf{R}', \delta\tau) \equiv e^{-\tau(\widehat{H}-E_R)} \frac{\Psi_T(\mathbf{R})}{\Psi_T(\mathbf{R}')}$. Expanding K in a Taylor series gives

$$K = N e^{-(\mathbf{R}_2 - \mathbf{R}_1 + \frac{1}{2}\nabla \ln \Psi_T(\mathbf{R}_1)\delta\tau)^2/(2\delta\tau)} \times e^{-(\frac{\widehat{H}\Psi_T(\mathbf{R}_1)}{\Psi_T(\mathbf{R}_1)} - E_R)\delta\tau} \equiv K_D \times K_B. \tag{31}$$

Equation (31) is closely associated with the product of the kernel of the Smoluchowski equation, which describes a diffusion process with drift, multiplied by a first-order rate process. Here the rate process is dominated by the local energy, instead of the potential. The random walk is modified by appearance of a drift term, that moves configurations to regions of large values of the wave function.

Importance sampling with appropriate trial functions, such as those used for accurate VMC calculations, can increase the efficiency of the random walk by several orders of magnitude. In the limit of the exact trial function as the importance sampling function, only a single evaluation of the local energy yields the exact answer. Importance sampling has made atomic, molecular and nano-structure calculations feasible. Note that the drift velocity term, $\frac{1}{2}\nabla \ln \Psi_T(\mathbf{R}_1)$, of equation (31) also moves random walkers away from nodal regions to regions of large values of the trial wave function, reducing the number of attempted node crossings by typically several orders of magnitude (author's unpublished observation).

5.1. Fixed-node approximation

In this section, we discuss the implications of the fermion character of $\Psi(\mathbf{R})$. It is an excited state in a manifold containing all the fermionic and bosonic states. A fermion wave function has positive and negative regions that are difficult to sample with the DMC algorithm. For real wave functions, $\Psi(\mathbf{R})$ contains positive and negative regions, $\Psi^{+}(\mathbf{R})$, and $\Psi^{-}(\mathbf{R})$ that, in principle, could be represented as probabilities. The sign of the wave function could be used as an extra weight for the random walk. In practice, doing so leads to a slowly convergent method for estimating the energy [3].

Returning to the importance sampling algorithm, recall that the initial distribution, $|\Psi(\mathbf{R})|^2$, is positive. Nevertheless, the Green's function, $K(\mathbf{R}, \mathbf{R}')$, can become negative if a random walker crosses a node of the trial wave function. Again, the sign of $K(\mathbf{R}, \mathbf{R}')$ could be used as a weight for sampling $|K(\mathbf{R}, \mathbf{R}')|$. The problem is that the statistics of this process lead to exponential growth of the variance of the observable.

The simplest approach to avoid exponential growth is to forbid moves in which the distribution f changes sign, see equation (29). This boundary condition on permitted moves is the defining characteristic of the fixed-node approximation (FNA). The nodes of the sampled wave function are *fixed* to be the nodes of the trial wave function. The FNA is an inherent feature of the DMC method, which is, by far, the most commonly used method for atomic and molecular MC applications [91,92].

The fixed-node energy is an upper bound to the exact energy of the system [3]. In fact, the fixed-node wave function is the best solution for that fixed set of nodes. The DMC method has much higher accuracy than the VMC method. For atomic and molecular systems, it is common to recover 95–100% of the CE, cf. Section 2, whereas the CE recovered with the VMC approach is typically less than 80% of the total.

6. TRIAL WAVE FUNCTION OPTIMIZATION

Trial wave functions $\Psi_T(\mathbf{R}, \Lambda)$ for QMC are dependent on n-variational parameters $\Lambda = \{\lambda_1, \ldots, \lambda_n\}$. Optimization of Λ is a key element for obtaining accurate trial functions. Importance sampling using an optimized trial function increases the efficiency of DMC simulations. There is a direct relationship between trial-function accuracy and the computer time required to calculate accurate expectation values. Some of the parameters λ_i may be fixed by imposing appropriate wave function properties, such as cusp conditions.

It is useful to divide Λ into groups distinguished by whether the parameter affects the nodes of the wave function. The Slater determinant parameters, $\lambda_D^{\uparrow\downarrow}$ and the Slater determinant weights, λ_{k_i} change wave function nodal structure [35,53–58]. The correlation function parameters, λ_C do not change the nodal structure of the overall wave function, and therefore the DMC energy. For some systems, the optimization of λ_C is sufficient for building reliable trial functions for the DMC method, because the correlation function is designed in part to satisfy cusp conditions [59,60].

Several optimization methods have been proposed previously. Some involve the use of analytical derivatives [61–66], others use of a fixed sample for variance minimization [67], and more recently [53,68,69]. Histogram analysis can be useful for the optimization of energy, variance and geometries [70].

The variance functional (*VF*) [53] is given by

$$VF = \frac{\sum_{i=1}^{N}\left[\frac{\hat{H}\Psi(\mathbf{R}_i,\Lambda)}{\Psi(\mathbf{R}_i,\Lambda)} - E_T\right]^2 w_i}{\sum_{i=1}^{N} w_i}, \tag{32}$$

where E_T is a trial energy, w_i is a weighting factor defined by

$$w_i(\Lambda) = \frac{\Psi^2(\mathbf{R}_i, \Lambda)}{\Psi^2(\mathbf{R}_i, \Lambda_0)}, \tag{33}$$

and Λ_0 is an initial set of parameters. The sum in equation (32) is over configurations initially distributed as $\Psi^2(\mathbf{R}, \Lambda_0)$. Numerical optimization methods are used to find the minimum of *VF*.

When a fixed sample is used, the optimization of *VF* can be sensible to outliers. A proposed solution to the outlier problem are robust optimization approaches [71,72].

Optimization of the energy has shown to be advantageous and superior to variance optimization in certain cases [73–76]. Recently, a very promising algorithm for optimization of λ_C and λ_D simultaneously has been proposed [77,78], and successfully applied to the evaluation of excitation energies [79,80]. A powerful and related approach has been proposed independently by Sorella [81].

7. TREATMENT OF HEAVY ELEMENTS

There is a steep computational dependence of QMC methods with atomic number Z. The computational cost of QMC methods has been estimated to scale as $Z^{5.5-6.5}$ [93,94]. This has motivated the replacement of the core electrons by effective core potentials (ECPs). With this modification, scaling with atomic number is improved to $Z^{3.4}$ [94]. Other approaches involve the use of core-valence separation schemes [95] model potentials [96], and effective Hamiltonians [97,98].

8. APPLICATIONS

A range of chemical reactions, atoms, molecules, and solids has been computed using the QMC method. Properties including atomization energies, heats of formation, optical transitions, and relative stabilities have been computed to a high degree of accuracy with this method. The DMC approach typically recovers ≈95% of the correlation energy and does not suffer from the strong basis set dependence of other *ab initio* methods such as HF, DFT, and coupled-cluster CC methods. There are however, systematic errors that can be encountered in QMC calculations: fixed-node error in DMC and localization error with ECPs [94,99,100]. The fixed-node error can be as much as ≈5% of the total correlation energy. The localization error is typically not of significance and is often masked by the fixed-node error.

A sample of recent applications of QMC to molecular systems includes electronic excitations of ethylene [101], porphyrin [102], and small Cu-doped clusters [103]. We summarize findings of these studies.

8.1. Singlet–triplet energy splitting in ethylene

Ethylene is the prototypical π-electron system whose photochemical behavior is of importance in chemistry, biology and technology [104,105]. Several large scale *ab initio* computational investigations of the singlet–triplet transition energy in ethylene have been carried out. The methods used in these studies were: configuration interaction with single excitations (CIS) [106,107], multi-reference CI (MR-CI) [108] and complete active space self-consistent field (CASSCF) [109].

In our study, the electronic structure of the ground and the lowest triplet states of ethylene were examined using the diffusion Monte Carlo (DMC) method. This study is motivated by recent photodissociation studies of C_2H_4S conducted at 193 nm that yielded the triplet-state heat of formation, and the adiabatic energy splitting of the singlet–triplet excitation [110–112]. We reported equilibrium properties of the ground and lowest triplet states of ethylene including adiabatic and vertical energy splittings, heats of formation, and atomization energies. These quantities have been computed by the DMC method using Hartree–Fock (HF), and single-reference functions, the latter with natural orbitals (NOs) obtained from complete active space self-consistent field (CASSCF), and multi-configuration self-consistent field (MCSCF) trial functions. In addition, for comparison, Møller–Plesset second-order perturbation theory (MP2), density functional theory (DFT) in the local density approximation (LDA) and B3LYP generalized gradient approximation (GGA) results, were carried out and reported.

Table 1 shows that DMC splittings lie within 0.1 kcal/mol of each other statistically so that the use of a HF or a CASSCF trial function with a soft ECP yields no numerical difference from the use of the all-electron HF trial function. These adiabatic energy differences together with the results of earlier studies and other *ab initio* approaches determined in this study (LDA, MP2, and B3LYP) are also listed in Table 1. The MR-CI adiabatic energy splitting [108] is found to be in closer accord with the DMC values than the results from the other *ab initio* approaches.

8.2. Electronic excitations of free-base porphyrin

The porphyrin molecule and its derivatives play an essential role in numerous biological processes including photosynthesis and oxygen transport, and in emerging medical technologies—for example, anti-viral therapeutics. A detailed understanding of the excited states of these systems is essential to elucidating key mechanisms such as oxygen binding and transport, and electron transfer as they occur in biological systems. Despite numerous experimental and *ab initio* theoretical studies, the basic photophysics of porphyrins is not completely understood. For example, recent theoretical studies have proposed reinterpretations of the different features of the spectrum of free base porphyrin (FBP, $C_{20}N_4H_{14}$).

The electronic spectrum of FBP is characterized by three regions: the so-called Q band in the visible region which is relatively weak, the intense B band which occurs in the near UV, and the higher UV bands, N, L and M, which are broader and diffuse. Owing to the inherent sensitivity of the excitation spectra of these systems to structural and chemical changes, it is necessary to employ highly accurate methods in order to make reliable theoretical predictions and to have useful comparisons with experiment.

Table 1. C_2H_4 adiabatic and vertical energy differences (kcal/mol)

Method	Adiabatic[a]	Vertical
CIS[b]	46.0	NA[c]
LDA	68.1	112.4
MP2	68.5	104.9
B3LYP	61.5	102.9
MR-CI[d]	64.0	106.0
DMC (*ECP*)[e]		
HF (soft ECP)	66.0(3)	104.2(3)
CASSCF(4,8) soft ECP	66.4(3)	103.5(3)
DMC (*all-electron*)[f]		
HF(cc-pVDZ/no cusp)	61.0(6)	NA[g]
HF(cc-pVDZ/cusp)	66.3(4)	103.8(6)
Experiment		
Photodissociation[h]	58(3)	NA[g]
EELS[i]	NA[g]	97
EIS[j]	NA[g]	108

[a] The use of unscaled frequencies changes the adiabatic energy difference by less than 0.1 kcal/mol.

[b] Reference [106].

[c] Reference [106] does not report the CIS vertical excitation energy.

[d] Reference [108].

[e] Trial wave function constructed with HF orbitals using the Partridge basis set [129] and soft effective core potentials [130].

[f] All-electron trial wave function constructed with HF orbitals. In the second case, the 1s orbitals were corrected near the nuclei to satisfy cusp conditions.

[g] Not available.

[h] Reference [111].

[i] References [131,132].

[j] Reference [133].

In this study, the transition energy between the ground state and lowest excited state of the Q band of FBP was calculated using the DMC method for all electrons of the molecule; ECPs were not introduced. A simple method for constructing excited-state trial wave functions was followed, and its accuracy compared to alternative approaches and to experiment.

For the DMC approach used in this study [3], a variational trial wave function was constructed as a product of a Slater determinant of HF orbitals and a correlation function for both singlet and triplet states. For the triplet excited state, the trial wave function was a restricted-open shell HF (ROHF) determinant. For the singlet excited state, the ROHF triplet wave function was modified by altering the spin occupation of the HOMO, which converted the ROHF triplet state, 1^3B_{3u}, into a singlet with the same spatial sym-

Table 2. Excitation energies (eV) from the ground state to the 1^1B_{2u} and 1^3B_{3u} states of free-base porphyrin. Empty slots indicate the absence of data

Method	Vertical excitation (eV) 1^1B_{2u}	Vertical excitation (eV) 1^1B_{3u}	Adiabatic energy difference (eV) 1^3B_{2u}
CIS[a]	2.66	1.23	
SAC-CI[b]	2.25		
CASPT2[c]	2.26	1.37	
TD-DFT[d]	2.39		
DFT-MRCI[e]	2.38		
MRSDCI[f]	2.40		
STEOM-CCSD(T)[g]	2.40	1.20	
DMC	2.45(8)		1.60(10)[k]
Experiment			
Vapor phase[h]	2.42		
Supersonic jet[i]	2.46		
Frozen solvent[j]			1.58

[a] Reference [106].
[b] Reference [134].
[c] Reference [113].
[d] Reference [135].
[e] Reference [136].
[f] Reference [137].
[g] 1^1B_{2u}: Reference [138], 1^3B_{3u}: Reference [114].
[h] Reference [139].
[i] Reference [140].
[j] Reference [141].
[k] Calculation performed at the minimum geometry of the B3LYP potential energy surface.

metry, namely, 1^1B_{2u}. The proper spin-adapted two-determinant configuration was then constructed.

The ground state singlet to second-excited singlet state excitation energies from several theoretical methods as well as experiment are listed in Table 2. The DMC value agrees with experiment to within statistical error bars (*i.e.*, 0.1 eV). The MRSDCI results are also in good accord with experiment. Merchán *et al.* have suggested, however, that the latter results arise from a fortuitous cancellation of errors due to the choice of active space [113]. Similarly, Nooijen and Bartlett suggest that there is no reason to expect the MRSDCI results to be converged [114]. Excited-state extensions of DFT, such as time-dependent DFT and DFT-MRCI show good agreement with experiment.

Results for the lowest triplet excitation energy are also listed in Table 2. Nooijen and Bartlett suggest that the low-lying triplet states of FBP pose a serious challenge for cor-

related treatments [114]. For this energy difference, the DMC results are found again to agree with the experimental excitation energy to within the error bars.

8.3. Characterization of $CuSi_4$ and $CuSi_6$

Considerable interest in pure silicon and metal-doped silicon clusters exists found in chemistry as well as in molecular and solid state physics. One of the reasons for this attention is that the properties of these cluster systems are notably different from those of the bulk materials [115]. In addition, promising applications of materials with novel properties based on metal-doped-silicon clusters and metal-doped fullerenes are of significant importance for the semiconductor industry. Numerous experimental [116–120] and theoretical [121–127] studies have been devoted to the determination of equilibrium geometries, electronic and bonding structures, as well as structural transitions of different size pure silicon and alkali-metal-doped silicon clusters. It has been shown, notwithstanding the occurrence of carbon and silicon in the same column of the periodic table, that there are big differences in the geometries of the clusters of these elements.

Despite the general interest in metal-doped silicon clusters, the number of studies devoted to this area is limited compared to the analogous metal-doped carbon clusters. The influence of transition metals on the geometry and bonding of doped silicon clusters warrants investigation.

Various theoretical methods applied to pure and metal-doped silicon clusters have revealed equilibrium geometries that are rather similar in selected respects. Recently, Xiao and Hagelberg (XH) [128] carried out a HF and DFT study of pure and Cu-doped Si_4 and Si_6 clusters and found an energy difference of only 0.005 eV among $CuSi_4$ isomers and 0.832 eV for $CuSi_6$ isomers.

The focus here is on three $CuSi_4$ and two $CuSi_6$ clusters previously investigated by XH [128] who optimized the geometry of these systems with the B3LYP DFT method. These geometries were used in the present study and the structures are presented in Figs. 1 and 2. The figures also show the relative energies between the different structures.

Energies, relative, binding, and adsorption, for the three $CuSi_4$ and two $CuSi_6$ clusters were obtained using the *ab initio* CASSCF, B3LYP DFT, and FNDMC methods. The use of the FNDMC method was validated by the significant correlation energy recovered for the present systems. The use of two different, but closely related, basis sets for the B3LYP case provides a useful measure of basis set dependence of these results; see Tables 3 and 4.

One sees that the FNDMC binding energies for all the clusters lie between the B3LYP DFT and HF results. A comparison of the relative values shows that DFT theory overestimates the binding energy, while the HF theory underestimates it. Qualitatively B3LYP DFT binding energies are found to be closer to the FNDMC ones than HF or CASSCF, but they still are outside of the statistical error bars of the FNDMC results. The important feature found in all the calculations is the close value of the binding energy for all the isomers of the particular cluster and the larger binding energy per atom for $CuSi_6$ clusters relative to $CuSi_4$ clusters.

Analysis of Cu atom adsorption energy shows the contradictory behavior of the methods applied relative to FNDMC/ECP. Qualitative agreement is found comparing CASSCF and FNDMC methods. Both approaches give t similar scaling of the adsorption energy for the

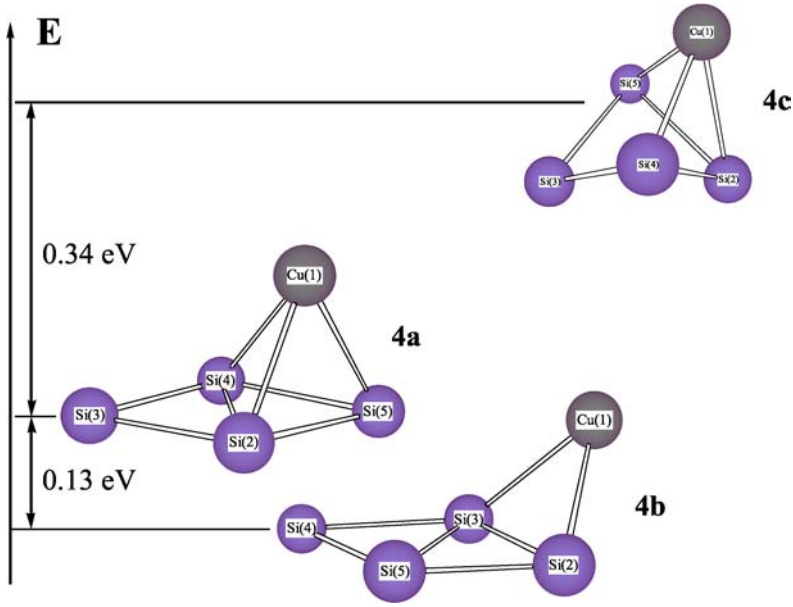

Fig. 1. Schematic structure, atom labeling, and relative energies of $CuSi_4$ isomers. Energy differences were obtained using the fixed-node diffusion Monte Carlo method.

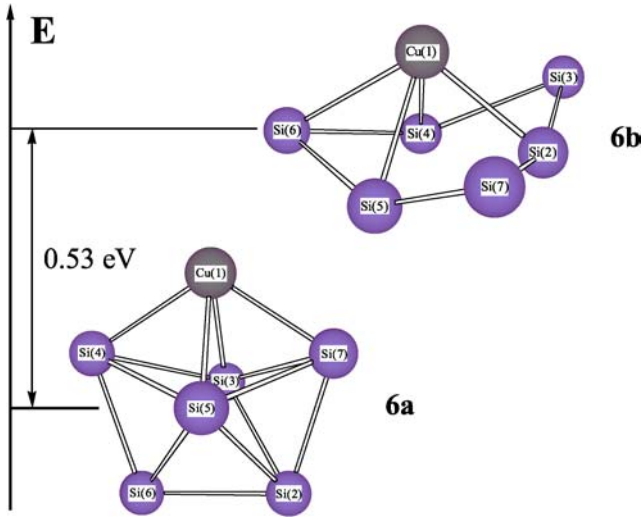

Fig. 2. Schematic structure, atom labeling, and relative energies of $CuSi_6$ isomers. Energy differences were obtained using the fixed-node diffusion Monte Carlo method.

$CuSi_4$ and $CuSi_6$ clusters. We note that XH also found a negative adsorption energy for the 6b isomer of the $CuSi_6$ cluster in the HF method. The Cu atom adsorption by the Si_4 and Si_6 clusters is found to be endothermic.

Table 3. Binding energies (eV/atom) of CuS_4 and $CuSi_6$ clusters

	$CuSi_4$			$CuSi_6$	
	4a	4b	4c	6a	6b
HF/GEN[a]	1.383	1.366	1.314	1.583	1.139
B3LYP/GEN[a]	2.474	2.475	2.455	2.802	2.683
B3LYP/6-311G**	2.590	2.594	2.574	2.906	2.762
CASSCF/6-311G**	0.567	0.553	0.506	0.632	0.608
DMC	1.82(4)	1.85(4)	1.76(5)	2.22(4)	2.15(4)

[a] Reference [128].

Table 4. Adsorption energy (eV/atom) of $CuSi_4$ and $CuSi_6$ clusters

	$CuSi_4$			$CuSi_6$	
	4a	4b	4c	6a	6b
HF/GEN[a]	0.593	0.508	0.251	0.518	−2.589
B3LYP/GEN[a]	1.315	1.320	1.221	1.364	0.533
B3LYP/6-311G**	2.114	2.134	2.037	2.396	1.382
CASSCF/6-311G**	−0.471	−0.544	−0.775	−1.781	−1.945
DMC	−1.31(9)	−1.18(9)	1.65(12)	2.81(13)	−3.34(12)

[a] Reference [128].

ACKNOWLEDGEMENTS

A.A.G. was supported by the Gates Millennium Scholarship Program. Work supported in part by the Director, Office of Science, Office of Basic Energy Sciences, Chemical Sciences Division of the U.S. Department of Energy under Contract No. DE-AC03-76SF0098, and by the National Science Foundation through the CREST Program (HRD-9085465).

REFERENCES

[1] K.E. Schmidt, Variational and Green's function Monte Carlo calculations of few body systems, in: Conference on Models and Methods in Few Body Physics, Lisbon, 1986.
[2] W.A. Lester Jr., B.L. Hammond, *Ann. Rev. Phys. Chem.* **41** (1990) 283.
[3] B.L. Hammond, W.A. Lester Jr., P.J. Reynolds, *Monte Carlo Methods in Ab Initio Quantum Chemistry*, World Scientific, Singapore, 1994.
[4] S.E. Koonin, D.C. Meredith, *Computational Physics, FORTRAN Version*, third ed., Addison–Wesley, 1995.
[5] H. Gould, J. Tobochnik, *An Introduction to Computer Simulation Methods: Applications to Physical Systems*, second ed., Addison–Wesley, 1996.
[6] D.M. Ceperley, L. Mitas, Quantum Monte Carlo methods in chemistry, in: I. Prigogine, S.A. Rice (Eds.), *New Methods in Computational Quantum Mechanics*, in: *Adv. Chem. Phys.*, vol. XCIII, Wiley, 1996.
[7] P.H. Acioli, *J. Mol. Struct. (Theochem)* **394** (1997) 75.
[8] D. Bressanini, P.J. Reynolds, *Adv. Chem. Phys.* **105** (1998) 37.

[9] L. Mitas, Diffusion Monte Carlo, in: M.P. Nightingale, C.J. Umrigar (Eds.) *Quantum Monte Carlo Methods in Physics and Chemistry*, vol. 525, Kluwer Academic, 1998, p. 247.
[10] J.B. Anderson, Quantum Monte Carlo: Atoms, molecules, clusters, liquids and solids, in: K.B. Lipkowitz, D.B. Boyd (Eds.) *Reviews in Computational Chemistry*, vol. 13, Wiley, New York, 1999, p. 133.
[11] J.M. Thijssen, *Computational Physics*, first ed., Cambridge Univ. Press, 1999.
[12] A. Lüchow, J.B. Anderson, *Ann. Rev. Phys. Chem.* **51** (2000) 501.
[13] M. Foulkes, L. Mitas, R. Needs, G. Rajagopal, *Rev. Mod. Phys.* **73** (2001) 33.
[14] A. Aspuru-Guzik, W.A. Lester Jr., Quantum Monte Carlo methods for the solution of the Schrödinger equation for molecular systems, in: C. Le Bris (Ed.), *Computational Chemistry*, first ed., in: *Handbook of Numerical Analysis*, vol. X, Elsevier, Amsterdam, The Netherlands, 2003, p. 485.
[15] A.J. Williamson, R.Q. Hood, J.C. Grossman, *Phys. Rev. Lett.* **87** (2001) 2466406.
[16] S. Manten, A. Lüchow, Improved scaling in diffusion quantum Monte Carlo with localized molecular orbitals, in: S.M. Rothstein, W.A. Lester Jr., S. Takata (Eds.), *Recent Advances in Quantum Monte Carlo Methods, Part II*, World Scientific, Singapore, 2002, p. 30.
[17] D. Alfe, M.J. Gillan, *J. Phys.: Condens. Matter* **16** (2004) 305.
[18] A. Aspuru-Guzik, R. Salomón-Ferrer, B. Austin, W. A. Lester Jr., *J. Comput. Chem.* **26** (2005) 708.
[19] N. Metropolis, S. Ulam, *J. Amer. Statist. Assoc.* **44** (1949) 335.
[20] A. Einstein, *Investigations in the Theory ƒ Brownian Motion*, Metheun, 1926, English translation of Einstein's original paper.
[21] R. Courant, K.O. Friedrichs, H. Lewy, *Math. Ann.* **100** (1928) 32.
[22] M.D. Donsker, M. Kac, *J. Res. Nat. Bur. Standards* **44** (1950) 551.
[23] M.H. Kalos, *Phys. Rev.* **68** (1962).
[24] R.C. Grimm, R.G. Storer, *J. Comp. Phys.* **7** (1971) 134.
[25] M. Head-Gordon, *J. Phys. Chem.* **100** (1996) 13213.
[26] K. Raghavachari, J.B. Anderson, *J. Phys. Chem.* **100** (1996) 12960.
[27] E. Cancès, M. Defranceschi, W. Kutzelnigg, C. Le Bris, Y. Maday, The models of quantum chemistry and their discretizations, in: C. Le Bris (Ed.), *Computational Chemistry*, first ed., in: *Handbook of Numerical Analysis*, vol. X, Elsevier, Amsterdam, The Netherlands, 2003, Chapter 1.
[28] P.-O. Löwdin, *Adv. Chem. Phys.* **2** (1959) 207.
[29] G. Senatore, N.H. March, *Rev. Mod. Phys.* **66** (1994) 445.
[30] D. Watson, M. Dunn, T.C. Germann, D.R. Herschbach, D.Z. Goodson, Dimensional expansions for atomic systems, in: C.A. Tsipis, V.S. Popov, D.R. Herschbach, J. Avery (Eds.), *New Methods in Quantum Theory*, Kluwer Academic, Dordrecht, 1996, p. 83.
[31] D.A. Mazziotti, *Phys. Rev. A* **57** (1998) 4219.
[32] A. Bijl, *Physica* **7** (1940) 869.
[33] R.B. Dingle, *Phil. Mag.* **40** (1949) 573.
[34] R. Jastrow, *Phys. Rev.* **98** (1955) 1479.
[35] K.E. Schmidt, J.W. Moskowitz, *J. Chem. Phys.* **93** (1990).
[36] N.D. Drummond, M.D. Towler, R.J. Needs, *Phys. Rev. B* **70** (2004) 235119.
[37] C. Huang, C.J. Umrigar, M.P. Nightingale, *J. Chem. Phys.* **107** (1997) 3007.
[38] N. Metropolis, A.W. Rosenbluth, M.N. Rosenbluth, N.M. Teller, E. Teller, *J. Chem. Phys.* **21** (1953) 1087.
[39] M.H. Kalos, P.A. Whitlock, *Monte Carlo Methods Volume 1: Basics*, Wiley, New York, 1986.
[40] M.H. Kalos, D. Levesque, L. Verlet, *Phys. Rev. A* **9** (1974) 2178.
[41] D. Ceperley, G.V. Chester, M.H. Kalos, *Phys. Rev. B* **16** (1977) 3081.
[42] M. Rao, B.J. Berne, *J. Chem. Phys.* **71** (1979) 129.
[43] C. Pangali, M. Rao, B.J. Berne, *Mol. Phys.* **37** (1979) 1773.
[44] D.M. Ceperley, B.J. Alder, *Phys. Rev. Lett.* **45** (1980) 566.
[45] J.B. Anderson, *J. Chem. Phys.* **73** (1980) 3897.
[46] M. Dewing, *J. Chem. Phys.* **113** (2000) 5123.
[47] C.J. Umrigar, *Phys. Rev. Lett.* **71** (1993) 408.
[48] P. Belhorec, S.M. Rothstein, J. Vrbik, *J. Chem. Phys.* **98** (1993) 3446.
[49] Z.W. Sun, M.M. Soto, R.N. Barnett, W.A. Lester Jr., *J. Chem. Phys.* **101** (1994) 394.
[50] M. Mella, A. Lüchow, J.B. Anderson, *Chem. Phys. Lett.* **265** (1997) 467.
[51] D. Bressanini, P.J. Reynolds, *J. Chem. Phys.* **111** (1999) 6180.
[52] D. Bressanini, G. Morosi, S. Tarasco, A. Mira, *J. Chem. Phys.* **121** (2004) 3446.
[53] C.J. Umrigar, K.G. Wilson, J.W. Wilkins, *Phys. Rev. Lett.* **60** (1988) 1719.

[54] Z. Sun, R.N. Barnett, W.A. Lester Jr., *Chem. Phys. Lett.* **195** (1992) 365.
[55] C. Filippi, C.J. Umrigar, *J. Chem. Phys.* **105** (1996) 213.
[56] H.-J. Flad, M. Caffarel, A. Savin, Quantum Monte Carlo calculations with multi-reference trial wave functions, in: W.A. Lester Jr. (Ed.), *Recent Advances in Quantum Monte Carlo Methods*, Wold Scientific, 1997, pp. 73–98, Chapter 5.
[57] R.N. Barnett, Z. Sun, W.A. Lester Jr., *Chem. Phys. Lett.* **273** (1997) 321.
[58] R.N. Barnett, Z. Sun, W.A. Lester Jr., *J. Chem. Phys.* **114** (2001) 2013.
[59] T. Kato, *Comm. Pure. Appl. Math.* **10** (1957) 151.
[60] C.R. Meyers, C.J. Umrigar, J.P. Sethna, J.D. Morgan, *Phys. Rev. A* **44** (1991) 5537.
[61] S.-Y. Huang, Z. Sun, W.A. Lester Jr., *J. Chem. Phys.* **92** (1990) 597.
[62] H. Bueckert, S.M. Rothstein, J. Vrbik, *Can. J. Chem.* **70** (1992) 366.
[63] A. Lüchow, J.B. Anderson, *J. Chem. Phys.* **105** (1996) 7573.
[64] H. Huang, Z. Cao, *J. Chem. Phys.* **104** (1996) 1.
[65] H. Huang, Q. Xie, Z. Cao, Z. Li, Z. Yue, L. Ming, *J. Chem. Phys.* **110** (1999) 3703.
[66] X. Lin, H. Zhang, A.M. Rappe, *J. Chem. Phys.* **112** (2000) 2650.
[67] H. Conroy, *J. Chem. Phys.* **41** (1964) 1331.
[68] Z. Sun, S.-Y. Huang, R.N. Barnett, W.A. Lester Jr., *J. Chem. Phys.* **93** (1990) 5.
[69] M.P. Nightingale, C.J. Umrigar, Monte Carlo optimization of trial wave functions in quantum mechanics and statistical mechanics, in: W.A. Lester Jr. (Ed.), *Recent Advances in Quantum Monte Carlo Methods*, World Scientific, 1997, pp. 201–227, Chapter 12.
[70] M. Snajdr, J.R. Dwyer, S.M. Rothstein, *J. Chem. Phys.* **111** (1999) 9971.
[71] A. Aspuru-Guzik, O. Couronne, I. Ovcharenko, W.A. Lester Jr., *Abstr. Pap. Am. Chem. Soc.* **221** (2001) 275.
[72] D. Bressanini, G. Morosi, M. Mella, *J. Chem. Phys.* **116** (2002) 5345.
[73] J. Goodisman, *J. Chem. Phys.* **45** (1966) 3659;
Rothstein, *et al.*, *J. Chem. Phys.* **112** (2000) 4935;
Galvez, *et al.*, *J. Chem. Phys.* **115** (2001) 1166;
Rappe, *et al.*, *J. Chem. Phys.* **118** (2003) 7193.
[74] M. Snajdr, S.M. Rothstein, *J. Chem. Phys.* **112** (2000) 4395.
[75] F.J. Galvez, E. Buendía, A. Sarsa, *J. Chem. Phys.* **115** (2001) 1166.
[76] M. Casalegno, M. Mella, A.M. Rappe, *J. Chem. Phys.* **118** (2003) 7193.
[77] C. Filippi, S. Fahy, *J. Chem. Phys.* **112** (2000) 3523.
[78] F. Schautz, S. Fahy, *J. Chem. Phys.* **116** (2002) 3533.
[79] F. Schautz, C. Filippi, *J. Chem. Phys.* **120** (2004) 10931.
[80] F. Schautz, F. Buda, C. Filippi, *J. Chem. Phys.* **121** (2004) 5836.
[81] S. Sorella, *Phys. Rev. B* **64** (2001) 024512.
[82] J.E. Campbell, *Proc. London Math. Soc. (1)* **28** (1897) 381.
[83] J.E. Campbell, *Proc. London Math. Soc. (1)* **29** (1897) 14.
[84] H.F. Baker, *Proc. London Math. Soc. (2)* **3** (1905) 24.
[85] F. Hausdorff, *Leipz. Ber.* **58** (1906) 19.
[86] J. Vbrik, S.M. Rothstein, *J. Comp. Phys.* **63** (1986) 130.
[87] S.A. Chin, *Phys. Rev. A* **42** (1990) 6991.
[88] S.A. Chin, *Phys. Lett. A* **226** (1997) 344.
[89] H.A. Forbert, S.A. Chin, *Int. J. Mod. Phys. B* **15** (2001) 1752.
[90] C.J. Umrigar, M.P. Nightingale, K.J. Runge, *J. Chem. Phys.* **99** (1993) 2865.
[91] J.B. Anderson, *J. Chem. Phys.* **65** (1976) 4121.
[92] P.J. Reynolds, D.M. Ceperley, B. Alder, W.A. Lester Jr., *J. Chem. Phys.* **77** (1982) 5593.
[93] D.M. Ceperley, *J. Stat. Phys.* **43** (1986) 815.
[94] B.L. Hammond, P.J. Reynolds, W.A. Lester Jr., *J. Chem. Phys.* **87** (1987) 1130.
[95] V.N. Staroverov, P. Langfelder, S.M. Rothstein, *J. Chem. Phys.* **108** (1998) 2873.
[96] T. Yoshida, K. Iguchi, *J. Chem. Phys.* **88** (1988) 1032.
[97] J. Carlson, J. Moskowitz, K. Schmidt, *J. Chem. Phys.* **90** (1989) 1003.
[98] G. Bachelet, D. Ceperley, M. Chiocchetti, *Phys. Rev. Lett.* **62** (1989) 2088.
[99] M.M. Hurley, P.A. Christiansen, *J. Chem. Phys.* **86** (1987) 1069.
[100] L. Mitas, E.L. Shirley, D.M. Ceperley, *J. Chem. Phys.* **95** (1991).
[101] O. El Akramine, A.C. Kollias, W.A. Lester Jr., *J. Chem. Phys.* **119** (2003) 1483.

[102] A. Aspuru-Guzik, O. El Akramine, J.C. Grossman, W.A. Lester Jr., *J. Chem. Phys.* **120** (2004) 3049.
[103] I.V. Ovcharenko, W.A. Lester Jr., C. Xiao, F. Hagelberg, *J. Chem. Phys.* **114** (2001) 9028.
[104] M. Pirrung, *Acc. Chem. Res.* **32** (1999) 711.
[105] T. Younkin, E. Conner, J. Henderson, S. Friedrich, R. Grubbs, D. Bansleben, *Science* **287** (2000) 460.
[106] J. Foresman, M. Head-Gordon, J. Pople, M. Frisch, *J. Phys. Chem.* **96** (1992) 135.
[107] K. Wiberg, C. Hadad, J. Foresman, W. Chupka, *J. Phys. Chem.* **96** (1992) 10756.
[108] B. Gemein, S. Peyerimhoff, *J. Phys. Chem.* **100** (1996) 19257.
[109] L.S. Andres, M. Merchan, I. Nebotgil, R. Lindh, B. Roos, *J. Chem. Phys.* **98** (1993) 3151.
[110] F. Qi, O. Sorkhabi, A. Suits, *J. Chem. Phys.* **112** (2000) 10707.
[111] F. Qi, O. Sorkhabi, A. Suits, S. Chien, W. Li, *J. Am. Chem. Soc.* **123** (2001) 148.
[112] A. Suits, F. Qi, *J. Electron Spectrosc. Relat. Phenom.* **119** (2001) 127.
[113] M. Merchan, E. Orti, B. Roos, *Chem. Phys. Lett.* **226** (1994) 27.
[114] M. Nooijen, R. Bartlett, *J. Chem. Phys.* **106** (1997) 6449.
[115] J.C. Grossman, L. Mitas, *Phys. Rev. Lett.* **74** (1995) 1323.
[116] T. Kendelewicz, P. Soukiassian, R. List, J. Woicik, P. Pianetta, I. Lindau, W. Spicer, *Phys. Rev. B* **37** (1988) 7115.
[117] M. Jarrold, V. Constant, *Phys. Rev. Lett.* **67** (1991) 2994.
[118] K. Rinnen, M. Mandich, *Phys. Rev. Lett.* **69** (1992) 1823.
[119] R. Kishi, S. Iwata, A. Nakajima, K. Kaya, *J. Chem. Phys.* **107** (1997) 3056.
[120] R. Kishi, H. Kawamata, Y. Negishi, S. Iwata, A. Nakajima, K. Kaya, *J. Chem. Phys.* **107** (1997) 10029.
[121] R. Fournier, S. Sinnott, A. DePristo, *J. Chem. Phys.* **97** (1992) 4149.
[122] U. Rothlisberger, W. Andreoni, P. Gianozzi, *J. Chem. Phys.* **96** (1992) 1248.
[123] J. Phillips, *Phys. Rev. B* **47** (1993) 14132.
[124] U. Rothlisberger, W. Andreoni, M. Parrinello, *Phys. Rev. Lett.* **72** (1994) 665.
[125] R. Kishi, A. Nakajima, S. Iwata, K. Kaya, *Chem. Phys. Lett.* **224** (1994) 200.
[126] F. Hagelberg, S. Neeser, N. Sahoo, T. Das, K. Weil, *Phys. Rev. A* **50** (1994) 557.
[127] K. Raghavachari, *J. Chem. Phys.* **84** (1986) 5672.
[128] C. Xiao, F. Hagelberg, *J. Mol. Struct. (Theochem)* **529** (2000) 241.
[129] H. Partridge, *J. Chem. Phys.* **90** (1989) 1043.
[130] I. Ovcharenko, A. Aspuru-Guzik, W.A. Lester Jr., *J. Chem. Phys.* **114** (2001) 7790.
[131] D. Wilden, P. Hicks, J. Comer, *J. Phys. B* **12** (1979) 1579.
[132] D. Love, K. Jordan, *Chem. Phys. Lett.* **235** (1995) 479.
[133] E. Vanveen, *Chem. Phys. Lett.* **41** (1976) 540.
[134] H. Nakatsuji, J. Hasegawa, M. Hada, *J. Chem. Phys.* **104** (1996) 2321.
[135] D. Sundholm, *Phys. Chem. Chem. Phys.* **2** (2000) 2275.
[136] A. Parusel, S. Grimme, *J. Porph. Phthal.* **5** (2001) 225.
[137] Y. Yamamoto, T. Noro, K. Ohno, *Int. J. Quantum. Chem.* **42** (1992) 1563.
[138] S. Gwaltney, R. Bartlett, *J. Chem. Phys.* **108** (1998) 6790.
[139] L. Edwards, D. Dolphin, M. Gouterman, A. Adler, *J. Mol. Spectrosc.* **38** (1971) 16.
[140] U. Even, J. Jortner, *J. Chem. Phys.* **77** (1982) 4391.
[141] M. Gouterman, G. Khalil, *J. Mol. Spectrosc.* **53** (1974) 88.

From Fischer Projections to Quantum Mechanics of Tetrahedral Molecules: New Perspectives in Chirality

Salvatore Capozziello[1] and Alessandra Lattanzi[2]

[1]*Dipartimento di Scienze Fisiche and INFN (sez. di Napoli), Università di Napoli "Federico II", Complesso Universitario di Monte S. Angelo, Via Cinthia, I-80126, Napoli, Italy*
E-mail: capozziello@sa.infn.it
[2]*Dipartimento di Chimica, Università di Salerno, Via S. Allende, I-84081 Baronissi, Salerno, Italy*
E-mail: lattanzi@unisa.it

Abstract

The algebraic structure of central molecular chirality can be achieved starting from the geometrical representation of bonds of tetrahedral molecules, as complex numbers in polar form, and the empirical Fischer projections used in organic chemistry. A general orthogonal $O(4)$ algebra is derived from which we obtain a chirality index χ, related to the classification of a molecule as achiral, diastereoisomer or enantiomer. Consequently, the chiral features of tetrahedral chains can be predicted by means of a molecular Aufbau. Moreover, a consistent Schrödinger equation is developed, whose solutions are the bonds of tetrahedral molecules in complex number representation. Starting from this result, the $O(4)$ algebra can be considered as a "quantum chiral algebra". It is shown that the operators of such an algebra preserve the parity of the whole system.

Contents

1. INTRODUCTION

Understanding the fundamental nature of chirality is an issue involving several disciplines of science like physics, chemistry and mathematics [1]. Chirality is a symmetry emerging in abstract spaces (*e.g.*, the spin configuration space of elementary particles) and in real physical space–time (*e.g.*, the Lorentz group of transformations acting on molecules). In any case, it is a discrete symmetry and, from several viewpoints, scientists are wondering if it is a conserved quantity or if it can be violated [2]. In other words, it is not completely clear, up to now, if objects with different states of chirality are different objects or

ADVANCES IN QUANTUM CHEMISTRY, VOLUME 49
ISSN: 0065-3276 DOI: 10.1016/S0065-3276(05)49005-X

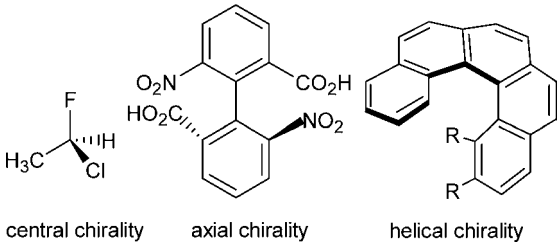

Fig. 1. Different forms of molecular chirality.

are indistinguishable from a physical point of view (*i.e.*, they have exactly the same energy configuration, the same angular momentum, in modulus, and so on). This question involves subatomic particles (*e.g.*, right-handed and left-handed neutrinos) or molecules (*e.g.*, enantiomers), or even huge macrosystems of astrophysical size as spiral galaxies [3].

Another and deeper issue is related to the observational fact that Nature seems to prefer, in most cases, just one modality: left-handed neutrinos [4], L-aminoacids and D-sugars [5], spiral galaxies with trailing arms [6]. In some sense, we observe a sort of chirality selection rule in our Universe, even if the opposite chiral state is mathematically and physically consistent and can be obtained as a reaction product (*e.g.*, racemization processes and asymmetric synthesis [7]) or happens as secondary process (spiral galaxies with leading arms seem to be the results of interactions in clusters of galaxies) [6].

For example, the origin of homochirality for L-aminoacids and D-sugars is still an open problem and several mechanisms have been proposed [8]. Among them, the spontaneous chiral symmetry breaking represents a fascinating theory. Significant enantiomeric excesses and chirally symmetry breaking can be generated by chirally autocatalytic systems. In particular, the chiral asymmetry generated during a stirred crystallization [9] shows that significant chiral autocatalysis can occur in the proximity of a chiral solid surface; this process might be important to be considered to explain the observed enantiomeric excess in L-amino acids in meteorites [10].

The program to understand dynamics of chiral structures ranges from microscopic to astrophysical scales, and it is very likely that the whole observable Universe has its own state of chirality [2a,11].

More specifically, following Lord Kelvin [12], chirality can be defined as: “I call any geometrical figure, or groups of points, chiral, and say it has chirality, if its image in a plane mirror, ideally realized, cannot be brought to coincide with itself”. On the other hand, an achiral molecule can be defined as: “If a structure and its mirror image are superimposable by rotation or any motion other than bond making and breaking, than they are identical”. Chiral molecules having central chirality contain stereogenic centres (Fig. 1) [13]. Given two molecules with identical chemical formulas, if they are not superimposable, they are called *enantiomers*. In general, the term chirality has a broader sense, for example, chirality can be due to a spatial isomerism resulting from the lack of free rotation around single or double bonds (which means that the molecule has a chiral axis) such as in biphenyl [14] compounds (Fig. 1).

Chirality can be even due to a helical shape of the molecule which can be left- or right-handed [15] (Fig. 1).

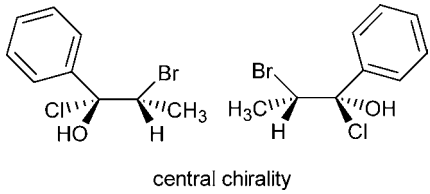

Fig. 2. Example of a couple of diastereoisomers.

When a molecule contains more than one chiral centre, a further definition has to be introduced. In this case, two molecules with identical structural formulas, which are not mirror images of each other and not superimposable, are termed *diastereoisomers* (Fig. 2).

Most properties of molecules are invariant under reflection (scalar properties), when examined in an achiral environment and enantiomers are identical in many respects such as solubility, density, melting point, chromatographic retention times, spectroscopic behaviour. It is only with respect to those properties that change sign, but not magnitude under reflection (pseudoscalar properties), that enantiomers differ, such as optical rotation [16], optical rotatory dispersion (ORD) [17], circular dichroism (CD) [18], vibrational circular dichroism (VCD) [19]. In contrast, diastereoisomers exhibit different chemical and physical properties. It is evident that molecular chirality is fundamentally connected to spatial symmetry operations [20] and has the features of a geometrical property. Interestingly, chirality has been treated as a continuous phenomenon [21] of achiral symmetry breaking and this approach has brought to the description of molecules as “more or less chiral” just as a door which is more or less open.

In the last decades, discrete mathematics and qualitative descriptions of the spatial features of molecules provided a large development of theoretical stereochemistry [22]. Molecular chirality has been studied by algebraic methods based on permutation group theory and group representation theory [23]. Several topological indexes have been proposed to describe 3D molecular structures and shapes [24]. Chirality of molecules has been as well the subject of studies aimed to achieve numerical indexes as a measurement of this property, so, discrete and continuous measurements of chirality have been proposed in order to determine the degree of chirality of a molecule [25]. Such measurements are related to the methods used for the characterization of physical and chemical features of a given compound. Empirical classification of organic molecules is based on the properties of functional groups, such as hydroxy group in alcohols, C–C double and triple bonds, CO group in ketones, aldehydes, etc. In general, organic compounds are collected in homologous series, differing by the number of carbons present in the structure. The most important classification of organic molecules, from this point of view, is the Beilstein system, where each compound finds an indexed place in the Beilstein Handbook of Organic Chemistry [26]. Various parameters as thermodynamic enthalpies of formation have been used as a basis for classification in homologous series [27], and additivity schemes for atoms are introduced in order to predict the enthalpies for compounds of homologous series. Furthermore, quantum mechanical quantities such as molecular total and partial energies have been statistically treated for the same purpose [28].

The above discussion tells us that several approaches can be pursued but, up to now, scientific community is far from a comprehensive and final theory of chirality. A new approach to figure out the problem could be to plan, as in other fields of science, a sort of

"Erlangen program". In fact, according to Felix Klein [29], every geometry and dynamics of objects can be characterized by their own group of transformations, thus we have, in general the following process:

$$\text{Geometry} \quad \Rightarrow \quad \text{Space and Group Transformations} \quad \Rightarrow \quad \text{Dynamics.}$$

Following these steps, we can fully characterize a theory which finally is well established if experimental data fit the solutions of dynamics.

All physical theories agree with this scheme. As examples, we have:

$$\begin{aligned}
&\text{Euclidean Space} \quad \Rightarrow \quad \text{Galilei Group} \quad \Leftrightarrow \quad \text{Classical Mechanics}\\
&\text{Minkowski Space} \quad \Rightarrow \quad \text{Poincaré Group} \quad \Leftrightarrow \quad \text{Special Relativity}\\
&\text{Phase Space} \quad \Rightarrow \quad \text{Canonical Transformations} \quad \Leftrightarrow \quad \text{Hamiltonian Dynamics}\\
&\text{Hilbert Space} \quad \Rightarrow \quad \text{Unitary Transformations} \quad \Leftrightarrow \quad \text{Quantum Mechanics}
\end{aligned}$$

and this approach holds for any self-consistent theory.

Chirality could be dealt, from a theoretical viewpoint, with the same standard by the following steps:

1. given a class of chiral objects identify their configuration space;
2. try to develop the algebra and the group of their configurations and transformations;
3. identify symmetries, conservation laws and then define the dynamical problem;
4. achieve a full theory where objects and their motions are treated at a fundamental level.

Following the above schemes, we should have:

$$\text{Configuration Space} \quad \Rightarrow \quad \text{Chirality Transformations} \quad \Leftrightarrow \quad \text{Chiral Mechanics.}$$

The approach could involve microscopic (*e.g.*, molecules) and macroscopic (*e.g.*, spiral galaxies) objects, so a full theory of chirality should be a quantum one, but it should work out, in the limits of classical mechanics, also with extremely large objects. In other words, a comprehensive theory of chirality should be independent of objects size.

In this article, this program is outlined for tetrahedral molecules, starting from an elementary geometrical representation.

A tetrahedral molecule is a system of four bonds connected at the origin to a central atom (*e.g.*, a carbon atom). These bonds can be represented as complex numbers in polar form. A chiral transformation between a couple of bonds is nothing else but a complex conjugation and then, taking into account all possible transformations, the elements of the group can be derived. It is interesting to observe that the 24 Fischer projections, coinciding with these elements, constitute an $O(4)$ algebra, so that transformations can be read as rotations and inversions in an abstract 4D-space.

Being the bonds non-relativistic quantum objects, they have to satisfy a Schrödinger equation, so $O(4)$, as it will be shown, can be read as a "quantum chiral algebra" by which it is possible to classify chiral transformations and to construct, in principle, any tetrahedral chain knowing their chiral features.

The layout of the paper is the following. Firstly, the geometry of tetrahedral chains, based on a complex numbers representation, is described. This approach allows a first qualitative classification of molecules as achiral, diastereoisomers and enantiomers. Secondly, we discuss the Fischer projections and show that they can be seen as elements of

$O(4)$ algebra. The further step is the extension to a sort of molecular Aufbau for tetrahedral chains. A quantum mechanical approach for tetrahedral molecules is developed by seeking for a consistent Schrödinger equation for bonds. Finally, the quantum chiral algebra is discussed with respect to point transformations and Hund result [30] $[\widehat{P}, \widehat{\mathcal{H}}] = 0$ is recovered, if parity states are nothing else but superpositions of chiral states.

2. GEOMETRICAL APPROACH TO CENTRAL MOLECULAR CHIRALITY BASED ON COMPLEX NUMBERS

The spatial properties of achiral molecules, enantiomers and diastereoisomers can be considered under a geometrical description. Some features exist in order to characterize such classes of molecules by the same parameters.

The approach proposed [31] is based on complex numbers since this is a straightforward way to represent the "length" of the bond with respect to the stereogenic centre and the "angular position" with respect to the other bonds. In general, given a tetrahedral molecule with a stereogenic centre, it can always be projected on a plane containing the stereogenic centre as in Fig. 3. Every bond, in the plane $\{x, y\}$, can be given in polar representation by

$$\Psi_j = \rho_j e^{i\theta_j}, \tag{1}$$

where ρ_j is the "modulus", *i.e.*, the projected length of the bond, θ_j is the "anomaly", *i.e.*, the position of the bond with respect to the x, y axes (and then with respect to the other bonds). The number $i = \sqrt{-1}$ is the imaginary unit. A molecule with one stereogenic centre is then given by the sum vector

$$\mathcal{M} = \sum_{j=1}^{4} \rho_j e^{i\theta_j} \tag{2}$$

in any symmetry plane. If the molecule has n stereogenic centres, we can define n planes of projection (one for each centre). Such planes can be parallel among them, even if this feature is not essential. If a molecule with one centre has four bonds, a molecule with two

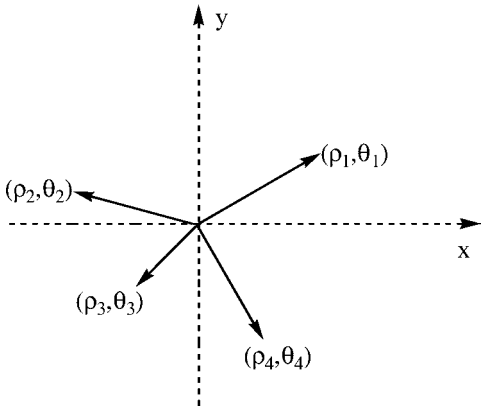

Fig. 3. Projection of a tetrahedral molecule on a plane containing the stereogenic centre.

centres has seven bonds and so on. The general rule is

$$n = \text{centres} \quad \Leftrightarrow \quad 4n - (n-1) = 3n + 1 \text{ bonds} \tag{3}$$

assuming simply connected tetrahedra. If atoms acting as "spacers" are present between chiral centres, the number of bonds changes from $3n + 1$ to $4n$, but the following considerations for consecutive connected tetrahedra remain valid. A molecule with n stereogenic centres is then given by the sum vector

$$\mathcal{M}_n = \sum_{k=1}^{n} \sum_{j=1}^{3n+1} \rho_{jk} e^{i\theta_{jk}}, \tag{4}$$

where k is the "centre-index" and j is the "bond-index". Again, for any k, a projective plane of symmetry is defined. The couple of numbers $\{\rho, \theta\} \equiv \{0, 0\}$ assigns the centre in every plane. In other words, a molecule $\mathcal{M}_n$ is assigned by the two sets of numbers

$$\begin{aligned} &\{\rho_{1k}, \ldots, \rho_{jk}, \ldots, \rho_{(3n+1)k}\}, \\ &\{\theta_{1k}, \ldots, \theta_{jk}, \ldots, \theta_{(3n+1)k}\}. \end{aligned} \tag{5}$$

Having in mind the definition of chirality, the behaviour of the molecule under rotation and superimposition has to be studied in order to check if the structure and its mirror image are superimposable. Chirality emerges when two molecules with identical structural formulas are not superimposable. Considering the geometrical representation reported in Fig. 3, a possible situation is the following: let us take into account a rotation of 180° in the space around a generic axis L passing through the stereogenic centre. Such an axis can coincide, for the sake of simplicity, with one of the bonds. After the rotation, two bonds result superimposable while the other two are inverted. The situation can be illustrated by the projection on the plane $\{x, y\}$ as shown in Fig. 4.

In formulae, for the inverted bonds, we have

$$\left\{\Psi_1 = \rho_1 e^{i\theta_1},\ \Psi_3 = \rho_3 e^{i\theta_3}\right\} \quad \Rightarrow \quad \left\{\overline{\Psi}_1 = \rho_1 e^{i\theta_3},\ \overline{\Psi}_3 = \rho_3 e^{i\theta_1}\right\}. \tag{6}$$

In order to observe the reflection, the four groups must be of different nature. This simple observation shows that the chirality is connected with an inversion of two bonds in the projective symmetry plane. On the contrary, if after the rotation and superimposition

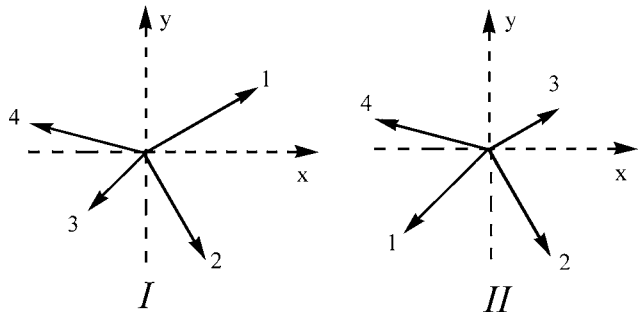

Fig. 4. Picture of the projected situations before and after the rotation of a chiral tetrahedron over its mirror image. Groups 2 and 4 coincide while 3 and 1 are inverted.

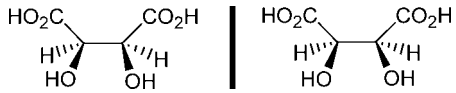

Fig. 5. Mirror structures of *meso*-tartaric acid.

(Fig. 4), molecule I is identical to molecule II, we are in an achiral situation. Such a treatment can be repeated for any projective symmetry plane which can be defined for the n centres. The possible results are that the molecule is fully invariant after rotation(s) and superimposition with respect to its mirror image (achiral); the molecule is partially invariant after rotation(s) and superimposition, *i.e.*, some tetrahedra are superimposable while others are not (diastereoisomers); the molecule presents an inversion for each stereogenic centre (enantiomers).

The following rule can be derived: central chirality is assigned by the number χ given by the couple n, p that is

$$\chi = \{n, p\}, \tag{7}$$

where χ is the chirality index, n is the principal chiral number and p the secondary chiral number, that is n is the number of stereogenic centres, p is the number of permutations (at most one for any centre). The constraint

$$0 \leqslant p \leqslant n \tag{8}$$

has to hold.

This definition of chirality is related to the structure of the molecule and its properties under rotations and superimposition.

The sequence between achiral and chiral molecules is given by

$\chi \equiv \{n, 0\}$ *achiral molecules*,

$\chi \equiv \{n, p < n\}$ *diastereoisomers*,

$\chi \equiv \{n, n\}$ *enantiomers*.

As an example, the chirality of degenerate case, *meso*-tartaric acid (Fig. 5), can be reduced to this rule. In this case, three groups of two tetrahedra are identical and the fourth group is the other stereogenic carbon centre. As it can be seen from the figure, the molecule is fully invariant by superimposition to its mirror image, hence $p = 0$ and the structure is achiral ($\chi \equiv \{2, 0\}$).

3. FISCHER PROJECTIONS FOR TETRAHEDRAL MOLECULES

An extremely useful method to represent tetrahedral molecules was reported in 1891 by Emil Fischer, who proposed the well-known planar projection formulas. When describing a molecule in this representation, some rules have to be followed (Fig. 6): the atoms pointing sideways must project forward in the model, while those pointing up and down in the projection must extend toward the rear. As an example, let us take into account (*S*)-(+)-lactic acid.

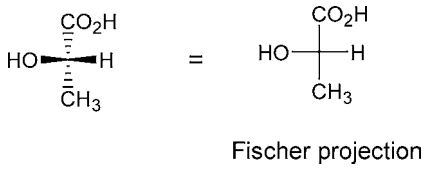

Fig. 6. Fischer projection of (*S*)-(+)-lactic acid.

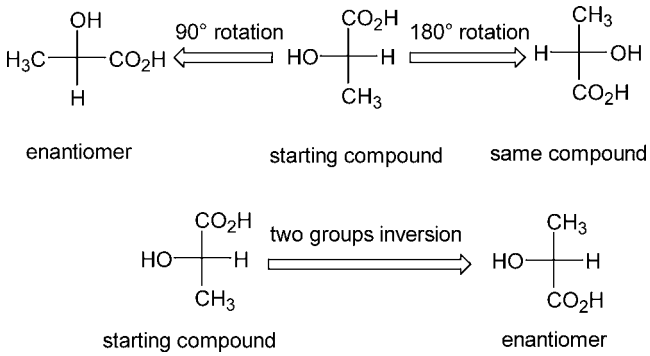

Fig. 7. Fundamental rules to handle Fischer projections.

In order to obtain proper results using Fischer projections, they must be treated differently from models in testing superimposability. Projections may not be rotated of 90°, while a 180° rotation is allowed. The interchange of any two groups results in the conversion of an enantiomer into its mirror image (Fig. 7).

Let us indicate the chemical groups by numbers running from 1 to 4. For the example which we are considering: OH = 1, CO_2H = 2, H = 3, CH_3 = 4, without taking into account the effective priorities of the groups [13]. There are 24 (=4! the number of permutations of 4 ligands among 4 sites) projections.

Twelve of these correspond to the (+) enantiomer and are illustrated in Fig. 8.

The other 12 graphs in Fig. 9 represent the (−) enantiomer.

The permutations shown in Fig. 8 can be obtained, either by permuting groups of three bonds or by turning the projections by 180°. The permutations outlined in Fig. 9 derive by those in Fig. 8 simply by interchanging two groups. With these considerations in mind, it is immediate asking for an algebraic structure which can be built from Fischer projections [32].

4. ALGEBRAIC STRUCTURE OF CENTRAL MOLECULAR CHIRALITY

In order to reduce the Fischer rules to an algebraic structure, we define an operator χ_k acting on a tetrahedral molecule. We shall take into account only one tetrahedron, but the generalization of the following results to simply connected chains of tetrahedra is easily accomplished as we shall see below.

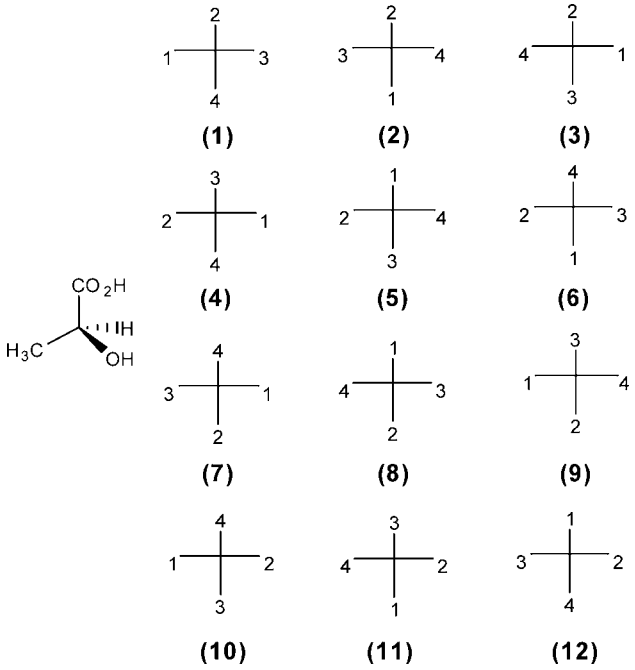

Fig. 8. Twelve Fischer projections of (*S*)-(+)-lactic acid.

A tetrahedral molecule can be assigned by a column vector $\mathcal{M}$, rewriting equation (2) as

$$\mathcal{M} = \begin{pmatrix} \Psi_1 \\ \Psi_2 \\ \Psi_3 \\ \Psi_4 \end{pmatrix}, \tag{9}$$

Ψ_j are defined in equation (1).

The corresponding Fischer projection is

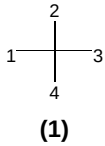

which is the first in Fig. 8. The position of the bonds in the column vector (9) are assigned starting from the left and proceeding clockwise in the Fischer projection.

The matrix representation of the projection **(1)** is assumed as "fundamental", *i.e.*,

$$\boldsymbol{\chi}_1 = \begin{pmatrix} 1 & 0 & 0 & 0 \\ 0 & 1 & 0 & 0 \\ 0 & 0 & 1 & 0 \\ 0 & 0 & 0 & 1 \end{pmatrix} \tag{10}$$

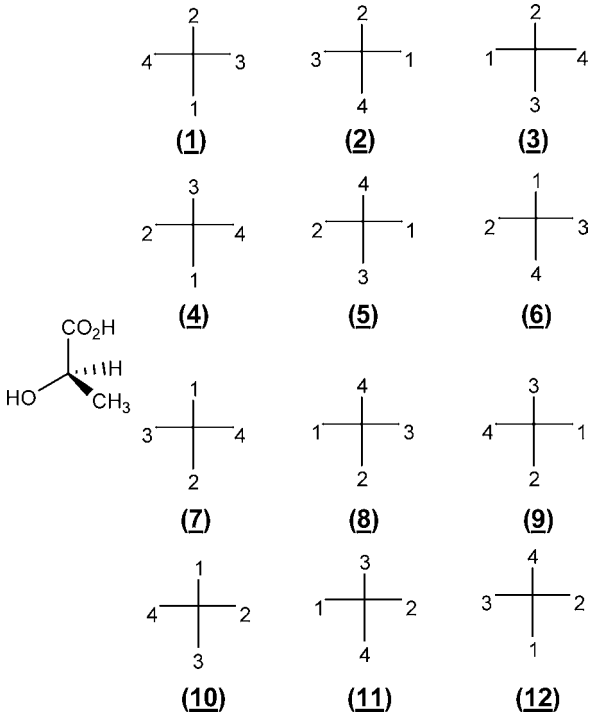

Fig. 9. Twelve Fischer projections of (R)-(−)-lactic acid.

so the action on the column vector $\mathcal{M}$ is

$$\chi_1 \begin{pmatrix} \Psi_1 \\ \Psi_2 \\ \Psi_3 \\ \Psi_4 \end{pmatrix} = \begin{pmatrix} \Psi_1 \\ \Psi_2 \\ \Psi_3 \\ \Psi_4 \end{pmatrix}, \tag{11}$$

χ_1 is nothing else but the identity operator. The configuration **(2)** of Fig. 8 can be achieved as soon as we define an operator χ_2 acting as

$$\chi_2 \begin{pmatrix} \Psi_1 \\ \Psi_2 \\ \Psi_3 \\ \Psi_4 \end{pmatrix} = \begin{pmatrix} \Psi_3 \\ \Psi_2 \\ \Psi_4 \\ \Psi_1 \end{pmatrix} \tag{12}$$

which corresponds to the matrix

$$\chi_2 = \begin{pmatrix} 0 & 0 & 1 & 0 \\ 0 & 1 & 0 & 0 \\ 0 & 0 & 0 & 1 \\ 1 & 0 & 0 & 0 \end{pmatrix}, \tag{13}$$

it is clear that χ_2 is a rotation. On the other hand, the configuration **(1)** of the (−) enantiomer can be obtained starting from the column vector (9), if we define an operator $\overline{\chi}_1$ which acts

as

$$\bar{\chi}_1 \begin{pmatrix} \Psi_1 \\ \Psi_2 \\ \Psi_3 \\ \Psi_4 \end{pmatrix} = \begin{pmatrix} \Psi_4 \\ \Psi_2 \\ \Psi_3 \\ \Psi_1 \end{pmatrix}. \tag{14}$$

Explicitly, we have

$$\bar{\chi}_1 = \begin{pmatrix} 0 & 0 & 0 & 1 \\ 0 & 1 & 0 & 0 \\ 0 & 0 & 1 & 0 \\ 1 & 0 & 0 & 0 \end{pmatrix}. \tag{15}$$

It generates the inversion between the bonds Ψ_1 and Ψ_4.

By this approach, all the 24 projections can be obtained (12 for the (+) enantiomer and 12 for the (−) enantiomer represented in Figs. 8 and 9) by matrix operators acting on the fundamental projection **(1)**. The following tables summarize the situation. The operators χ_k give rise to the representations of the (+) enantiomer, while the operators $\bar{\chi}_k$ give rise to those of the (−) enantiomer. Obviously $k = 1, \ldots, 12$.

Table I, (+) enantiomer:

$$\chi_1 = \begin{pmatrix} 1 & 0 & 0 & 0 \\ 0 & 1 & 0 & 0 \\ 0 & 0 & 1 & 0 \\ 0 & 0 & 0 & 1 \end{pmatrix}, \quad \chi_2 = \begin{pmatrix} 0 & 0 & 1 & 0 \\ 0 & 1 & 0 & 0 \\ 0 & 0 & 0 & 1 \\ 1 & 0 & 0 & 0 \end{pmatrix}, \quad \chi_3 = \begin{pmatrix} 0 & 0 & 0 & 1 \\ 0 & 1 & 0 & 0 \\ 1 & 0 & 0 & 0 \\ 0 & 0 & 1 & 0 \end{pmatrix},$$

$$\chi_4 = \begin{pmatrix} 0 & 1 & 0 & 0 \\ 0 & 0 & 1 & 0 \\ 1 & 0 & 0 & 0 \\ 0 & 0 & 0 & 1 \end{pmatrix}, \quad \chi_5 = \begin{pmatrix} 0 & 1 & 0 & 0 \\ 1 & 0 & 0 & 0 \\ 0 & 0 & 0 & 1 \\ 0 & 0 & 1 & 0 \end{pmatrix}, \quad \chi_6 = \begin{pmatrix} 0 & 1 & 0 & 0 \\ 0 & 0 & 0 & 1 \\ 0 & 0 & 1 & 0 \\ 1 & 0 & 0 & 0 \end{pmatrix},$$

$$\chi_7 = \begin{pmatrix} 0 & 0 & 1 & 0 \\ 0 & 0 & 0 & 1 \\ 1 & 0 & 0 & 0 \\ 0 & 1 & 0 & 0 \end{pmatrix}, \quad \chi_8 = \begin{pmatrix} 0 & 0 & 0 & 1 \\ 1 & 0 & 0 & 0 \\ 0 & 0 & 1 & 0 \\ 0 & 1 & 0 & 0 \end{pmatrix}, \quad \chi_9 = \begin{pmatrix} 1 & 0 & 0 & 0 \\ 0 & 0 & 1 & 0 \\ 0 & 0 & 0 & 1 \\ 0 & 1 & 0 & 0 \end{pmatrix},$$

$$\chi_{10} = \begin{pmatrix} 1 & 0 & 0 & 0 \\ 0 & 0 & 0 & 1 \\ 0 & 1 & 0 & 0 \\ 0 & 0 & 1 & 0 \end{pmatrix}, \quad \chi_{11} = \begin{pmatrix} 0 & 0 & 0 & 1 \\ 0 & 0 & 1 & 0 \\ 0 & 1 & 0 & 0 \\ 1 & 0 & 0 & 0 \end{pmatrix}, \quad \chi_{12} = \begin{pmatrix} 0 & 0 & 1 & 0 \\ 1 & 0 & 0 & 0 \\ 0 & 1 & 0 & 0 \\ 0 & 0 & 0 & 1 \end{pmatrix}.$$

Table II, (−) enantiomer:

$$\bar{\chi}_1 = \begin{pmatrix} 0 & 0 & 0 & 1 \\ 0 & 1 & 0 & 0 \\ 0 & 0 & 1 & 0 \\ 1 & 0 & 0 & 0 \end{pmatrix}, \quad \bar{\chi}_2 = \begin{pmatrix} 0 & 0 & 1 & 0 \\ 0 & 1 & 0 & 0 \\ 1 & 0 & 0 & 0 \\ 0 & 0 & 0 & 1 \end{pmatrix}, \quad \bar{\chi}_3 = \begin{pmatrix} 1 & 0 & 0 & 0 \\ 0 & 1 & 0 & 0 \\ 0 & 0 & 0 & 1 \\ 0 & 0 & 1 & 0 \end{pmatrix},$$

$$\bar{\chi}_4 = \begin{pmatrix} 0 & 1 & 0 & 0 \\ 0 & 0 & 1 & 0 \\ 0 & 0 & 0 & 1 \\ 1 & 0 & 0 & 0 \end{pmatrix}, \quad \bar{\chi}_5 = \begin{pmatrix} 0 & 1 & 0 & 0 \\ 0 & 0 & 0 & 1 \\ 1 & 0 & 0 & 0 \\ 0 & 0 & 1 & 0 \end{pmatrix}, \quad \bar{\chi}_6 = \begin{pmatrix} 0 & 1 & 0 & 0 \\ 1 & 0 & 0 & 0 \\ 0 & 0 & 1 & 0 \\ 0 & 0 & 0 & 1 \end{pmatrix},$$

$$\overline{\chi}_7 = \begin{pmatrix} 0 & 0 & 1 & 0 \\ 1 & 0 & 0 & 0 \\ 0 & 0 & 0 & 1 \\ 0 & 1 & 0 & 0 \end{pmatrix}, \quad \overline{\chi}_8 = \begin{pmatrix} 1 & 0 & 0 & 0 \\ 0 & 0 & 0 & 1 \\ 0 & 0 & 1 & 0 \\ 0 & 1 & 0 & 0 \end{pmatrix}, \quad \overline{\chi}_9 = \begin{pmatrix} 0 & 0 & 0 & 1 \\ 0 & 0 & 1 & 0 \\ 1 & 0 & 0 & 0 \\ 0 & 1 & 0 & 0 \end{pmatrix},$$

$$\overline{\chi}_{10} = \begin{pmatrix} 0 & 0 & 0 & 1 \\ 1 & 0 & 0 & 0 \\ 0 & 1 & 0 & 0 \\ 0 & 0 & 1 & 0 \end{pmatrix}, \quad \overline{\chi}_{11} = \begin{pmatrix} 1 & 0 & 0 & 0 \\ 0 & 0 & 1 & 0 \\ 0 & 1 & 0 & 0 \\ 0 & 0 & 0 & 1 \end{pmatrix}, \quad \overline{\chi}_{12} = \begin{pmatrix} 0 & 0 & 1 & 0 \\ 0 & 0 & 0 & 1 \\ 0 & 1 & 0 & 0 \\ 1 & 0 & 0 & 0 \end{pmatrix}.$$

The matrices in Tables I and II are the elements of a 4-parameter algebra. Those in Table I are a representation of rotations, while those in Table II are inversions. Both sets constitute the group $O(4)$ of 4×4 orthogonal matrices. The matrices in Table I are the remarkable subgroup $SO(4)$ of 4×4 matrices with determinant $+1$. The matrices in Table II have determinant -1, being inversions (or reflections). They do not constitute a group since the product of any two of them has determinant $+1$. This fact means that the product of two inversions generates a rotation (this is obvious by inverting both the couples of bonds in a tetrahedron). In fact, we have

$$\chi_k \chi_l = \chi_m, \quad \overline{\chi}_k \overline{\chi}_l = \chi_m, \quad \overline{\chi}_k \chi_l = \overline{\chi}_m \quad \text{for } k, l, m, = 1, \ldots, 12. \tag{16}$$

For example, straightforward calculations give

$$\chi_8 \chi_9 = \chi_5, \quad \overline{\chi}_5 \overline{\chi}_2 = \chi_9, \quad \overline{\chi}_{10} \chi_{10} = \overline{\chi}_7 \tag{17}$$

and so on. In summary, the product of two rotations is a rotation, the product of two reflections is a rotation, while the product of a reflection and a rotation is again a reflection. In any case, the total algebra is closed [33]. Below the complete set of commutation relations is given.

The 24 matrices in Tables I and II are not all independent. They can be grouped as different representations of the same operators. To this aim, we make use of a fundamental theorem of algebra which states that all matrices, representing the same operator, have the same characteristic polynomial [34]. In other words, the characteristic equation of a matrix is invariant under vector base changes. In $(+)$ enantiomer case, the characteristic eigenvalue equation is

$$\det \| \chi_k - \lambda \mathbf{I} \| = 0, \tag{18}$$

where λ are the eigenvalues and $\mathbf{I}$ is the identity matrix.

The following characteristic polynomials can be derived:

$$(1-\lambda)^4 = 0 \qquad \text{for } \chi_1, \tag{19}$$

$$(1-\lambda)^2\left(1+\lambda+\lambda^2\right) = 0 \qquad \text{for } \chi_2, \chi_3, \chi_4, \chi_6, \chi_8, \chi_9, \chi_{10}, \chi_{12}, \tag{20}$$

$$(1-\lambda)^2(1+\lambda)^2 = 0 \qquad \text{for } \chi_5, \chi_7, \chi_{11}. \tag{21}$$

In the case of $(-)$ enantiomer, we have

$$\det \| \overline{\chi}_k - \lambda \mathbf{I} \| = 0 \tag{22}$$

and the characteristic polynomials are

$$(1-\lambda)^3(1+\lambda)=0 \qquad \text{for } \overline{\chi}_1, \overline{\chi}_2, \overline{\chi}_3, \overline{\chi}_6, \overline{\chi}_8, \overline{\chi}_{11}, \tag{23}$$

$$(1-\lambda)(1+\lambda)\left(\lambda^2+1\right)=0 \quad \text{for } \overline{\chi}_4, \overline{\chi}_5, \overline{\chi}_7, \overline{\chi}_9, \overline{\chi}_{10}, \overline{\chi}_{12}. \tag{24}$$

There are 6 independent eigenvalues:

$$\lambda_{1,2}=\pm 1, \quad \lambda_{3,4}=\pm i, \quad \lambda_{5,6}=\frac{-1\pm i\sqrt{3}}{2}. \tag{25}$$

Inserting them into equations (18) and (22), it is easy to determine the eigenvectors

$$(\boldsymbol{\chi}_k-\lambda\mathbf{I})\mathcal{M}=0, \qquad (\overline{\boldsymbol{\chi}}_k-\lambda\mathbf{I})\mathcal{M}=0 \tag{26}$$

with obvious calculations depending on the choice of $\boldsymbol{\chi}_k$ and $\overline{\boldsymbol{\chi}}_k$. $\mathcal{M}$ is given by equation (9). It is worth noting that the number of independent eigenvalues (and then eigenvectors) is related to the number of independent elements in each member of the group $O(N)$ we are considering. N^2 is the total number of elements, while $\frac{1}{2}N(N+1)$ are the orthogonality conditions, so we have

$$N^2-\frac{1}{2}N(N+1)=\frac{1}{2}N(N-1). \tag{27}$$

For $O(4)$, it is 6, which is the number of independent generators of the group [33], giving the "dimension" of the group. With these considerations in mind, it can be stated that Fischer projections generates the algebraic structure of tetrahedral molecules.

5. GENERALIZATION TO MOLECULES WITH *n* STEREOGENIC CENTRES: A MOLECULAR AUFBAU FOR TETRAHEDRAL CHAINS

The results of the previous section can be extended to more general cases. For a molecule with n stereogenic centres, we can define n planes of projection and the bonds among the centres have to be taken into account.

Equation (4) can be written as

$$\mathcal{M}_n=\sum_{k=1}^{p}\overline{\mathcal{M}}_k+\sum_{k=p+1}^{n}\mathcal{M}_k, \tag{28}$$

where $\overline{\mathcal{M}}_k$ and $\mathcal{M}_k$ are generic tetrahedra on which are acting the operators $\overline{\boldsymbol{\chi}}_1^k$ and $\boldsymbol{\chi}_1^k$ respectively; k is the center index running from 1 to n; 1 is the operator index ranging from 1 to 12.

For any tetrahedron, two possibilities are available:

$$\mathcal{M}_k=\boldsymbol{\chi}_1^k\mathcal{M}_k^{(0)}, \qquad \overline{\mathcal{M}}_k=\overline{\boldsymbol{\chi}}_1^k\mathcal{M}_k^{(0)}, \tag{29}$$

where $\mathcal{M}_k^{(0)}$ is the starting fundamental representation of the k-tetrahedron given by the column vector in equation (9). Explicitly we have

$$\mathcal{M}_k^{(0)}=\begin{pmatrix}\Psi_{1k}\\ \Psi_{2k}\\ \Psi_{3k}\\ \Psi_{4k}\end{pmatrix}. \tag{30}$$

In other words, $\mathcal{M}_k$ and $\overline{\mathcal{M}}_k$ are the result of the application of one of the above matrix operators on the starting column vector $\mathcal{M}_k^{(0)}$.

A particular discussion deserves the index p, which, as previously stated, ranges $0 \leqslant p \leqslant n$. It is the number of permutations, which occur when the operators $\overline{\boldsymbol{\chi}}_l^k$ act on tetrahedra. It corresponds to the number of reflections occurring in an n-centre tetrahedral chain. No inversions, but rotations occur when $\boldsymbol{\chi}_l^k$ operators act on the molecule. Having this rule in mind, it follows that

$$\mathcal{M}_n = \sum_{k=1}^{n} \mathcal{M}_k, \quad p = 0, \tag{31}$$

is an achiral molecule (in this case only $\boldsymbol{\chi}_1^k$ operators act on $\mathcal{M}_k^{(0)}$);

$$\mathcal{M}_n = \sum_{k=1}^{p} \overline{\mathcal{M}}_k + \sum_{k=p+1}^{n} \mathcal{M}_k, \quad 0 < p < n, \tag{32}$$

is a diastereoisomer since $[n - (p + 1)]$ tetrahedra result superimposable after rotations, while p-ones are not superimposable, having, each of them, undergone an inversion of two of their bonds.

Finally, an enantiomer results if

$$\mathcal{M}_n = \sum_{k=1}^{n} \overline{\mathcal{M}}_k, \quad n = p, \tag{33}$$

where every tetrahedron results a mirror image of its starting situation after the application of any of the $\overline{\boldsymbol{\chi}}_1^k$ operators. The chirality selection rule, geometrically deduced (equation (7)), is fully recovered. In other words, this selection rule gives a classification of tetrahedral chains by their chirality structure.

A building-up process (Aufbau-like) is consequently derivable [35]. The building-up process gives rise to a chirality index which assigns the intrinsic chiral structure of the final compound. As we have seen, the chirality index χ allows an immediate chiral characterization of a given tetrahedral chain. Let us take into account a molecule, which is well defined in its chiral feature, in the sense that, considering also its mirror image, it is clear to assess if the molecule is an enantiomer, a diastereoisomer or an achiral molecule. After the addition of a further chiral centre to this structure and its mirror image, the resulting structure will be

$$\chi \equiv \{n + 1, p + \Delta p\}, \tag{34}$$

where $\Delta p = 0, 1$. The chiral properties of the new molecule are assigned by the Δp value according to the following possibilities.

If $\Delta p = 0$, we can have

$$\chi_s \equiv \{n, 0\} \quad \Rightarrow \quad \chi_f \equiv \{n + 1, 0\} \tag{35}$$

in this case, the starting compound is an achiral molecule as well as the final one.

Again, for $\Delta p = 0$, we can have

$$\chi_s \equiv \{n, p\} \quad \Rightarrow \quad \chi_f \equiv \{n + 1, p\} \tag{36}$$

in this case, the starting molecule is a diastereoisomer, being $n > p$, as well as the final structure.

Finally, if

$$\chi_s \equiv \{n, n\} \quad \Rightarrow \quad \chi_f \equiv \{n+1, n\} \tag{37}$$

the starting molecule is an enantiomer, while the final one is a diastereoisomer.

If $\Delta p = 1$, the situations can be

$$\chi_s \equiv \{n, 0\} \quad \Rightarrow \quad \chi_f \equiv \{n+1, 1\} \tag{38}$$

from an achiral molecule, a diastereoisomer is obtained;

$$\chi_s \equiv \{n, p\} \quad \Rightarrow \quad \chi_f \equiv \{n+1, p+1\} \tag{39}$$

from a diastereoisomer, another diastereoisomer is obtained;

$$\chi_s \equiv \{n, n\} \quad \Rightarrow \quad \chi_f \equiv \{n+1, n+1\} \tag{40}$$

from an enantiomer, we get another enantiomer.

Equations (35)–(40) take into account all the possibilities, which can be easily iterated adding up any number of chiral centres to a given chain. In the general case, the *Aufbau rule* is

$$\chi \equiv \{n+n', p+p'\}; \quad \forall n' \geqslant 1, \; p' = \sum_{j=1}^{n'} \Delta p_j, \; \Delta p_j = 0, 1. \tag{41}$$

However, we have to consider that the rule works only for simply connected tetrahedral chains, where the chiral features are well established with respect to the mirror image. In this sense, chirality is not an absolute feature of the molecules [2a,20]. Adding up a chiral centre to a structure gives rise to a new molecule, where $\chi \equiv \{n+1, p+\Delta p\}$. The fact that, in the addition, the variation of p can be $\Delta p = 0, 1$, assigns the chiral feature of the new compound.

An example of the building-up process is reported in Fig. 10. In Fig. 11, a degenerate case [13] is reported, where the two chiral centres are identical, introducing a further degree of symmetry to the final structure. In this case, the situation $\chi_f \equiv \{2, 2\}$ for $\Delta p = 1$ is equivalent to $\chi_f \equiv \{2, 0\}$, since the two molecules are superimposable, hence the structure is achiral.

6. QUANTUM MECHANICAL APPROACH

In order to carry on with our Erlangen-like program, the next step required is dealing with dynamics of tetrahedra starting from the previous geometrical and algebraic considerations.

Being microscopic objects, a quantum mechanical treatment has to be pursued. First of all, we have to probe if the mathematical representation of bond given in equation (1), and then the superpositions (2) and (4), are solutions of a suitable Schrödinger equation. Furthermore, in order to build up a self-consistent quantum mechanics of chiral eigenstates, relations among such eigenstates, energy and parity eigenstates need to be found [20]. The final step is to understand which is the fundamental meaning of chirality transformations.

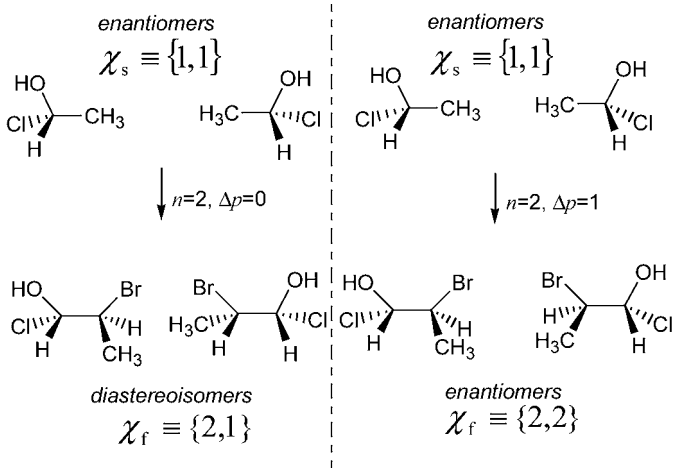

Fig. 10. Aufbau process consisting in adding up a chiral centre to a given chiral tetrahedron. Last consideration indicates that such an Aufbau approach is working only if the chiral centres are different and, in this respect, the procedure is suitable for the description of chiral structures.

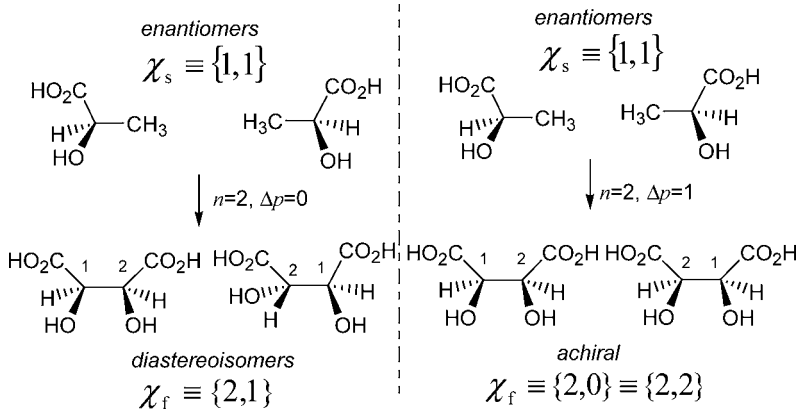

Fig. 11. A degenerate example of Aufbau process consisting in adding up a chiral centre, having identical substituents of the starting chiral tetrahedron.

In order to answer such questions, we have to discuss the possible quantum mechanical interpretation of the above formulae and then the consistency of the problem in the perspective of a full quantum mechanical treatment.

We proceed by an inverse problem approach, considering a Schrödinger equation for the "solution" (1) and the sums of solutions (2) and (4) [36].

The problem is set in the Born–Oppenheimer approximation by which a given stereogenic centre is considered fixed and dynamics of the four bonds is reduced to it.

This position is supported by an appropriate change of coordinates, since the problem can be reduced to a coordinate system fixed in the stereogenic centre.

A time-independent three-dimensional Schrödinger equation is

$$\left\{-\frac{\hbar^2}{2\mu}\nabla^2 + V(x, y, z)\right\}\eta(x, y, z) = E_j\eta(x, y, z), \tag{42}$$

where E_j are the energy eigenvalues, "μ" is a given reduced mass and ∇^2 the Laplace operator. The index j will be defined below. Our tetrahedron can be idealized as a system in a central potential with a spherical symmetry, so that, the potential depends only on the radius r: $V(\vec{r}) \equiv V(r)$. The general solution of the angular part of Schrödinger equation is

$$Y_{l,m}(\vartheta, \varphi) = N_{l,m}P_l^m(\cos\varphi)(\sin\varphi)^{|m|}e^{im\vartheta}, \tag{43}$$

where $P_l^m(\cos\varphi)$ are Legendre polynomials and $N_{l,m}$ is a normalization factor depending on the orbital and azimuthal quantum numbers l and m. Coming back to the former problem, the aim was to see if equation (1) is a solution of Schrödinger equation. Concerning the angular component, it can be interpreted as the azimuthal part of angular momentum.

For the radial component, it can be chosen

$$\rho(r) = \left(\frac{r}{r_0}\right), \tag{44}$$

where r_0 is a normalization length (*e.g.*, $\approx 1.09 \div 1.54$ Å a typical C–X length bond) useful to restore the probabilistic interpretation of our approach. Immediately, the form of the potential $V(r)$ is obtained

$$V(r) = E_j - \frac{\alpha_0}{r^2}, \quad \alpha_0 = \frac{\hbar^2}{2\mu}\big[l(l+1) - 2\big] \tag{45}$$

depending on the eigenvalue E_j, the angular momentum l and the mass μ.

Finally, the solution $\Psi_j = \rho_j e^{i\theta_j}$ with the positions

$$\rho_j(r) = \left(\frac{r_j}{r_0}\right), \qquad \vartheta_j = m_j\vartheta \tag{46}$$

is composed by the radial and azimuthal parts of a complete solution of Schrödinger equation. Clearly, $j = 1, 2, 3, 4$, E_j are the bonds energies and $\mathcal{M} = \sum_{j=1}^{4}\rho_j e^{i\vartheta j}$ is the superposition of four single particular solutions. This result can be extended to equation (4) considering n Schrödinger problems, one for each stereogenic centre [36]. At this point, the role of operators χ_s^k and $\overline{\chi}_s^k$ has to be investigated in order to see if they are quantum operators implementing chiral transformations.

7. QUANTUM CHIRAL ALGEBRA AND PARITY

Previous treatment shows that equation (1) can be considered as a solution of a "reduced" Schrödinger problem, where, due to the separation of variables, the Hamiltonian operator is projected on the $\{r, \vartheta\}$-plane and a part of the general solution $\Phi = \Phi(r, \vartheta, \varphi, t)$ is nothing else but $\Psi(r, \vartheta) = \rho e^{i\vartheta}$. Operators $\widehat{\mathcal{H}}_k(r, \vartheta)$, $\boldsymbol{\chi}_s^k$ and $\overline{\boldsymbol{\chi}}_s^k$, act on the four bonds of the k-stereogenic centre inducing the following transformations:

$$i\hbar\frac{\partial}{\partial t}\mathcal{M}_k = \widehat{\mathcal{H}}_k\mathcal{M}_k = E_{jk}\mathcal{M}_k, \quad \mathcal{M}_k = \boldsymbol{\chi}_s^k\mathcal{M}_k^{(0)}, \tag{47}$$

and

$$i\hbar\frac{\partial}{\partial t}\overline{\mathcal{M}}_k = \widehat{\mathcal{H}}_k\overline{\mathcal{M}}_k = E_{jk}\overline{\mathcal{M}}_k, \quad \overline{\mathcal{M}}_k = \overline{\boldsymbol{\chi}}_s^k\mathcal{M}_k^{(0)}, \tag{48}$$

where E_{jk} are the energy egeinstates of bonds with respect to the k-stereogenic centre.

Rotations $\boldsymbol{\chi}_s^k$ and inversions $\overline{\boldsymbol{\chi}}_s^k$ operate on bonds of the starting fundamental representation $\mathcal{M}_k^{(0)}$ given by equation (30).

It is straightforward to see that $\boldsymbol{\chi}_s^k$ and $\widehat{\mathcal{H}}_k$ commute between them being

$$\left[\widehat{\mathcal{H}}_k, \boldsymbol{\chi}_s^k\right] = 0. \tag{49}$$

Similarly, it can be obtained

$$\left[\widehat{\mathcal{H}}_k, \overline{\boldsymbol{\chi}}_s^k\right] = 0. \tag{50}$$

Furthermore, we have

$$\left[\boldsymbol{\chi}_s^k, \boldsymbol{\chi}_m^k\right] = 0 \qquad \text{for } s, m = 5, 7, 11, \tag{51}$$

$$\left[\overline{\boldsymbol{\chi}}_s^k, \overline{\boldsymbol{\chi}}_m^k\right] = \boldsymbol{\chi}_l^k - \boldsymbol{\chi}_g^k \quad \text{for } l, m, g, s = 1, \ldots, 12, \tag{52}$$

$$\left[\boldsymbol{\chi}_s^k, \boldsymbol{\chi}_m^k\right] = \boldsymbol{\chi}_l^k - \boldsymbol{\chi}_g^k \quad \text{for } l, m, g, s = 1, \ldots, 12 \text{ with } s, m \neq 5, 7, 11, \tag{53}$$

$$\left[\boldsymbol{\chi}_s^k, \overline{\boldsymbol{\chi}}_m^k\right] = \boldsymbol{\chi}_l^k - \boldsymbol{\chi}_g^k \quad \text{for } l, m, g, s = 1, \ldots, 12 \tag{54}$$

and

$$\left[\boldsymbol{\chi}_s^k, \boldsymbol{\chi}_m^g\right] = 0, \quad \left[\overline{\boldsymbol{\chi}}_s^k, \overline{\boldsymbol{\chi}}_m^g\right] = 0, \quad \left[\overline{\boldsymbol{\chi}}_s^k, \boldsymbol{\chi}_m^g\right] = 0 \tag{55}$$

being $k \neq g$.

Relations (49)–(55) constitute a quantum chiral algebra and the eigenstates of $\boldsymbol{\chi}_s^k$ and $\overline{\boldsymbol{\chi}}_s^k$ operators are, in general, solutions of Schrödinger equation. The way in which operators $\widehat{\mathcal{H}}_k$, $\boldsymbol{\chi}_s^k$, $\overline{\boldsymbol{\chi}}_s^k$ work on quantum states of chiral molecules deserves a particular discussion.

Taking into account the fundamental representation (30) of a given k-tetrahedron, the action of the operator $\boldsymbol{\chi}_s^k$ and $\overline{\boldsymbol{\chi}}_s^k$ defines the "chiral state" of the molecule being

$$|\Psi_R\rangle = \mathcal{M}_k = \boldsymbol{\chi}_s^k\mathcal{M}_k^{(0)} \tag{56}$$

and

$$|\Psi_L\rangle = \overline{\mathcal{M}}_k = \overline{\boldsymbol{\chi}}_s^k\mathcal{M}_k^{(0)}, \tag{57}$$

where $|\Psi_R\rangle$ and $|\Psi_L\rangle$ indicate right- and left-handed quantum states of the molecule using the Dirac ket notation. Operators $\boldsymbol{\chi}_s^k$ "rotate" the k-tetrahedron, while $\overline{\boldsymbol{\chi}}_s^k$ "invert" a couple of bonds. Dropping, for simplicity, the indexes, the following relations:

$$\boldsymbol{\chi}|\Psi_R\rangle = |\Psi_R\rangle, \qquad \boldsymbol{\chi}|\Psi_L\rangle = |\Psi_L\rangle, \tag{58}$$

$$\overline{\boldsymbol{\chi}}|\Psi_R\rangle = |\Psi_L\rangle, \qquad \overline{\boldsymbol{\chi}}|\Psi_L\rangle = |\Psi_R\rangle \tag{59}$$

hold. The $\overline{\boldsymbol{\chi}}$ operators interconvert two handed forms and, in some sense, work as an algebraic counterpart of quantum tunneling [2a,37]. Parity eigenstates of a chiral molecule, ignoring parity violation effects [38], are energy eigenstates and can be obtained as superpositions of handed states [39]. It follows that

$$|\Psi_\pm\rangle = \frac{1}{\sqrt{2}}\left(|\Psi_L\rangle \pm |\Psi_R\rangle\right) \tag{60}$$

which are, respectively, even- and odd-parity eigenstates. Chirality operators $\boldsymbol{\chi}$ and $\overline{\boldsymbol{\chi}}$ do not alter the parity of a given enantiomer being

$$\boldsymbol{\chi}|\Psi_{\pm}\rangle = \frac{1}{\sqrt{2}}\big(\boldsymbol{\chi}|\Psi_L\rangle \pm \boldsymbol{\chi}|\Psi_R\rangle\big) = \frac{1}{\sqrt{2}}\big(|\Psi_L\rangle \pm |\Psi_R\rangle\big), \tag{61}$$

$$\overline{\boldsymbol{\chi}}|\Psi_{\pm}\rangle = \frac{1}{\sqrt{2}}\big(\overline{\boldsymbol{\chi}}|\Psi_L\rangle \pm \overline{\boldsymbol{\chi}}|\Psi_R\rangle\big) = \frac{1}{\sqrt{2}}\big(|\Psi_R\rangle \pm |\Psi_L\rangle\big), \tag{62}$$

which means that $\overline{\boldsymbol{\chi}}$-operators allow transitions between $|\Psi_R\rangle$ and $|\Psi_L\rangle$ (as in a quantum tunneling process) and parity is the conserved quantum mechanical quantity [30].

It is worth noting that the total Hamiltonian operator for the degenerate isomers of an optically active molecule always consists of an even and an odd part [40]

$$\widehat{\mathcal{H}}^{\text{tot}} = \widehat{\mathcal{H}}^{\text{even}} + \widehat{\mathcal{H}}^{\text{odd}}. \tag{63}$$

This is the energy operator involved in the Hund result, which is

$$\big[\widehat{P}, \widehat{\mathcal{H}}^{\text{tot}}\big] = 0. \tag{64}$$

On the other hand, the Hamiltonian operators considered above (*i.e.*, $\widehat{\mathcal{H}}_k$) refer to bond-eigenstates of the k-tetrahedron. Due to relations (49) and (50), these eigenstates are "conserved" with respect to the Hamiltonian $\widehat{\mathcal{H}}_k$ and not with respect to the total Hamiltonian $\widehat{\mathcal{H}}^{\text{tot}}$, so the parity and not chirality is the true conserved quantum mechanical quantity.

8. SUMMARY AND CONCLUSIONS

At this point, it is interesting to quote Heisenberg's remark [41] which suggested that elementary particles are much more akin to molecules than to atoms. This statement underlines the importance of fundamental symmetry arguments to pursue analogies between quantum states of chiral molecules and those of elementary particles. Hence, the developments in fundamental physics can give access to concepts which could form the basis of a new quantum chemistry. With this perspective in mind, we have developed a new description of chirality of tetrahedral molecules, which takes into account the geometrical and algebraic structure of such objects with implications for their quantum mechanical properties.

On the basis of empirical Fischer projections, it is possible to derive an algebraic approach to central molecular chirality of tetrahedral molecules. The elements of such an algebra are obtained from the 24 projections which a single chiral tetrahedron can generate in S and R configurations. They constitute a matrix representation of $O(4)$ orthogonal group. Twelve of them are rotations, while the other twelve are inversions. All the projections are algebraically generated starting from a fundamental one, where the positions of chemical groups are established *a priori* in a clockwise sequence $1 \to 2 \to 3 \to 4$. The generalization to chains of tetrahedra is straightforward.

According to this representation, given a molecule with n chiral centres, it is possible to define an index of chirality $\chi \equiv \{n, p\}$, where n is the number of stereogenic centres of the molecule and p the number of permutations observed under rotations and superimposition of the tetrahedral molecule to its mirror image.

Consequently, a "chirality selection rule" comes out which allows the characterization of a molecule as *achiral*, *enantiomer* or *diastereoisomer*. The chirality index, not only assigns

the global chirality of a given tetrahedral chain, but indicates also a way to predict the same property for new compounds, which can be built up. In fact, a sort of molecular Aufbau for tetrahedra has been proposed. It is possible to recognize a set of rules which allows the classification of new compounds, obtained after the addition of another chiral centre, by the determination of the selection rule $\Delta p = 0, 1$ with respect to the added centre.

Such a chiral algebra can be discussed in the framework of quantum mechanics. In fact, it is possible to show that the elements of the $O(4)$ group are operators, which commute with the Hamiltonian of the system, and give rise to Heisenberg relations implying conservations laws. In this sense, this algebra can be defined as a "quantum chiral algebra". Moreover, the operators, acting on the molecular chiral states, preserve the parity of the whole system as stated by Hund [30].

This result is clearly in agreement with the fact that the true stationary states of the systems are the parity ones, while chiral states $|\Psi_R\rangle$ and $|\Psi_L\rangle$ can be interchanged by a quantum tunneling mechanism [37a].

These new perspectives can give rise to a wide debate on the role of group theory in order to seek for the fundamental features of chirality.

REFERENCES

[1] (a) G.R. Gribbin, *The Search for Superstring, Symmetry, and the Theory of Everything*, Little Brown, New York, 1999;
(b) K. Gottfried, V.F. Weisskopf, *Concepts of Particle Physics, vol. 1*, Oxford Univ. Press, New York, 1984;
(c) L.D. Barron, in: B.D. Cline (Ed.), *Physical Origin of Homochirality in Life*, American Institute of Physics, Woodbury, NY, 1996.
[2] (a) M. Quack, *Angew. Chem. Int. Ed.* **41** (2002) 4618;
(b) M. Avalos, R. Babiano, P. Cintas, J.L. Jiménez, J.C. Palacios, *Tetrahedron: Asymmetry* **11** (2000) 2845.
[3] D.K. Kondepudi, D.J. Durand, *Chirality* **13** (2001) 351.
[4] M. Kaku, *Quantum Field Theory*, Oxford Univ. Press, Oxford, 1993.
[5] B.L. Feringa, R.A. van Delden, *Chem. Rev.* **38** (1999) 3418.
[6] B.A. Carroll, D.A. Ostlie, *An Introduction to Modern Astrophysics*, Addison–Wesley, Reading, MA, 1996.
[7] E.N. Jacobsen, A. Pfaltz, H. Yamamoto (Eds.), *Comprehensive Asymmetric Catalysis*, Springer-Verlag, New York, 1999.
[8] (a) W.A. Bonner, *Biosphere* **21** (1991) 59;
(b) W.A. Bonner, *Biosphere* **24** (1994) 63.
[9] D.K. Kondepudi, *Int. J. Quantum Chem.* **98** (2004) 222, and references cited therein.
[10] (a) J.P. Cronin, S. Pizzarello, *Science* **275** (1997) 951;
(b) M.H. Engel, S.A. Macko, *Nature* **389** (1997) 265.
[11] G. Basini, S. Capozziello, G. Longo, *La Riv. del N. Cimento* **25** (2002) 11.
[12] W.T. Kelvin, *Baltimore Lectures on Molecular Dynamics and the Wave Theory of Light*, C.J. Clay, London, 1904, p. 619.
[13] E.L. Eliel, S.H. Wilen, L.N. Mander, *Stereochemistry of Organic Compounds*, Wiley, New York, 1994.
[14] (a) M. Oki, *The Chemistry of Rotational Isomers*, Springer, New York, 1993;
(b) W. Runge, in: S.R. Landor (Ed.), *The Chemistry of the Allenes*, vol. 2, Academic Press, 1982.
[15] (a) W.H. Laarhoven, W.J. Prinsen, *Top. Curr. Chem.* **125** (1984) 63;
(b) F. Vögtle, *Fascinating Molecules in Organic Chemistry*, Wiley, New York, 1992, p. 156.
[16] H. Landolt, *Optical Activity and Chemical Composition*, Whittaker, New York, 1899, English transl.
[17] E. Charney, *The Molecular Basis of Optical Activity. Optical Rotatory Dispersion and Circular Dichroism*, Wiley, New York, 1979.
[18] R. Kuroda, in: N. Berova, K. Nakanishi, R. Woody (Eds.), *Circular Dichroism: Principles and Applications*, Wiley, New York, 2000.
[19] (a) L.A. Nafie, T.A. Keiderling, P.J. Stephens, *J. Am. Chem. Soc.* **98** (1976) 2715;
(b) P.J. Stephens, F.J. Devlin, *Chirality* **12** (2000) 172.

[20] L.D. Barron, *Chem. Soc. Rev.* **15** (1986) 189.
[21] P. Le Guennec, *J. Math. Phys.* **41** (2000) 5954.
[22] V.I. Sokolov, *Introduction to Theoretical Stereochemistry*, Gordon and Breach Science, New York, 1991.
[23] (a) E. Ruch, *Acc. Chem. Res.* **5** (1972) 49;
(b) P.G. Mezey, *New Developments in Molecular Chirality*, Kluwer Academic, Dordrecht, 1991, pp. 131–164.
[24] (a) M. Randic, Topological indices, in: P. von Ragué Schleyer, N.L. Allinger, T. Clark, J. Gasteiger, P.A. Kollman, H.F. Schaefer III, P.R. Schreiner (Eds.), *Encyclopedia of Computational Chemistry*, Wiley, Chichester, 1998, p. 3018;
(b) M. Randic, *J. Chem. Inf. Comput. Sci.* **37** (1997) 672;
(c) G. Gilat, *J. Phys. A: Math. Gen.* **22** (1989) L545;
(d) M. Randic, *J. Chem. Inf. Comput. Sci.* **41** (2001) 607;
(e) P.G. Mezey, *New Developments in Molecular Chirality*, Kluwer Academic, Dordrecht, 1991.
[25] (a) A.B. Buda, T. Heyde, K. Mislow, *Angew. Chem. Int. Ed. Engl.* **31** (1992) 989;
(b) D. Avnir, H.Z. Hel-Or, P.G. Mezey, Symmetry and chirality: Continuous measures, in: P. von Ragué Schleyer, N.L. Allinger, T. Clark, J. Gasteiger, P.A. Kollman, H.F. Schaefer III, P.R. Schreiner (Eds.), *Encyclopedia of Computational Chemistry*, Wiley, Chichester, 1998, p. 2890;
(c) H. Zabrodsky, D. Avnir, *J. Am. Chem. Soc.* **117** (1995) 462.
[26] Beilstein Handbook of Organic Chemistry, Beilstein Institut für Literatur der Organischen Chemie, Frankfurt am Main, 1881–2001.
[27] N. Cohen, S.W. Benson, *Chem. Rev.* **93** (1993) 2419.
[28] (a) D. Šatkovskiene, V. Gineityte, *J. Mol. Struct. (Theochem)* **31** (1994) 1137;
(b) A. Neugebauer, G. Häfelinger, *J. Phys. Org. Chem.* **15** (2002) 677.
[29] F. Klein, *Vorlesungen über die Entwicklung der Mathematik im 19. Jahrhundert*, Springer, Berlin, 1926.
[30] (a) F. Hund, *Z. Phys.* **43** (1927) 788;
(b) F. Hund, *Z. Phys.* **43** (1927) 805.
[31] S. Capozziello, A. Lattanzi, *Chirality* **15** (2003) 227.
[32] S. Capozziello, A. Lattanzi, *Chirality* **15** (2003) 466.
[33] R. Gilmore, *Lie Groups, Lie Algebras, and Some of Their Applications*, Krieger, Malabar, FL, 1994.
[34] S. Lang, *Linear Algebra*, Addison–Wesley, Reading, MA, 1966.
[35] S. Capozziello, A. Lattanzi, *J. Mol. Struct. (Theochem)* **671** (2004) 205.
[36] S. Capozziello, A. Lattanzi, *Chirality* **16** (2004) 162.
[37] (a) R.A. Harris, L. Stodolsky, *Phys. Lett. B* **78** (2–3) (1978) 313;
(b) L.D. Barron, *Molecular Light Scattering and Optical Activity*, Cambridge Univ. Press, 1982;
(c) L.D. Barron, in: W.J. Lough, W.I. Wainer (Eds.), *Chirality in Natural and Applied Science*, Blackwell, Oxford, 2004;
(d) R. Janoschek, *Chirality*, Springer, Berlin, 1991.
[38] (a) S.F. Manson, G.E. Tranter, *Mol. Phys.* **53** (1984) 1091;
(b) M. Quack, *Chem. Phys. Lett.* **132** (1986) 147.
[39] M. Quack, *Angew. Chem. Int. Ed. Engl.* **28** (1989) 571.
[40] R. Wesendrup, J.K. Laerdahl, R.N. Compton, P. Schwerdtfeger, *J. Phys. Chem. A* **107** (2003) 6668.
[41] W. Heisenberg, *Introduction to the Unified Field Theory of Elementary Particles*, Wiley, New York, 1966.

This page intentionally left blank

On the Canonical Formulation of Electrodynamics and Wave Mechanics

David Masiello, Erik Deumens and Yngve Öhrn

Quantum Theory Project, University of Florida, Gainesville, FL 32611-8435, USA

Abstract

Nonperturbative analytical and numerical methods are presented for the solution of the coupled nonlinear Maxwell–Schrödinger system of partial differential equations. These equations have been derived within the Hamiltonian or canonical formalism. The canonical approach to dynamics, which begins with the Maxwell and Schrödinger Lagrangians together with a Lorenz gauge fixing term, yields a set of first order Hamilton equations which form a well-posed initial value problem. That is, their solution is uniquely determined once the initial values for each of the dynamical variables are specified. The equations are closed since the Schrödinger wavefunction is chosen to be the source for the electromagnetic field and the electromagnetic field acts back upon the wavefunction, thus producing new fields. In practice, the Maxwell–Schrödinger Lagrangian is represented in a spatial basis of Gaussian functions. Application of the calculus of variations leads to a set of dynamical equations that, for that choice of basis, represent the coupled first order Maxwell–Schrödinger equations. In the limit of a complete basis these equations are exact and for any finite choice of basis they form an approximate system of dynamical equations that can be integrated in time and made systematically more accurate by enriching the basis. The dynamics of the basis-represented Maxwell–Schrödinger system is numerically investigated for a single spinless hydrogen atom interacting with the electromagnetic field in a cavity.

Contents

ADVANCES IN QUANTUM CHEMISTRY, VOLUME 49
ISSN: 0065-3276 DOI: 10.1016/S0065-3276(05)49006-1

1. INTRODUCTION

Chemistry encompasses a broad range of Nature that varies over orders of magnitude in energy from the ultracold nK Bose–Einstein condensation temperatures [1,2] to the keV collision energies that produce the Earth's aurorae [3–5]. At the most fundamental level, the study of chemistry is the study of electrons and nuclei. The interaction of electrons and nuclei throughout this energy regime is mediated by the photon which is the quantum of the electromagnetic field. The equations which govern the dynamics of electrons, nuclei, and photons are therefore the same equations which govern all of chemistry [6]. They are the Schrödinger equation [7,8]

$$i\dot{\Psi} = H\Psi \tag{1}$$

and Maxwell's equations [9]

$$\nabla \cdot \mathbf{E} = 4\pi\rho, \qquad \nabla \times \mathbf{B} = \frac{4\pi}{c}\mathbf{J} + \frac{\dot{\mathbf{E}}}{c}, \qquad \nabla \cdot \mathbf{B} = 0, \qquad \nabla \times \mathbf{E} + \frac{\dot{\mathbf{B}}}{c} = \mathbf{0}. \tag{2}$$

As they stand these dynamical equations are uncoupled. The solutions of the Schrödinger equation (1) do not *a priori* influence the solutions of the Maxwell equations (2) and vice versa. The development of analytic and numerical methods for the solution of the coupled Maxwell–Schrödinger equations is the main purpose of this paper. Before delving into the details of these methods a physical motivation as well as a historical and mathematical background is provided.

1.1. Physical motivation

Many situations of physical interest are described by the system of Maxwell–Schrödinger equations. Often these situations involve electromagnetic processes that occur on drastically different timescales from that of the matter. An example of such a situation is the

stimulated absorption or emission of electromagnetic radiation by a molecule. The description of this process by (1) and (2) accounts for a theoretical understanding of all of spectroscopy, which has provided an immense body of chemical knowledge.

However, there do exist situations where the dynamics of the electromagnetic field and the matter occur on the same timescale. For example, in solid state physics certain electronic wavepackets exposed to strong magnetic fields in semiconductor quantum wells are predicted to demonstrate rapid decoherence [10]. The dynamics of the incident field, of the electronic wavepacket, and of the phonons emitted are coupled and occur on the femtosecond timescale. In atomic physics, the long timescale for the dynamics of cold and ultracold collisions of atoms in electromagnetic traps has been observed to exceed lifetimes of excited states, which are on the order of 10^{-8} s. Thus, spontaneous emission can occur during the course of collision and this may alter the atomic collision dynamics [11,12]. Cold atom phenomena are being merged with cavity quantum electrodynamics to realize single atom lasers [13–15]. The function of these novel devices is based on strong coupling of the atom to a single mode of the resonant cavity. Lastly, in polymer chemistry, ultrafast light emission has been observed in certain ladder polymer films following ultrafast laser excitation [16]. A fundamental understanding of the waveguiding process that occurs in these polymers is challenging. *It is precisely these situations, where the electromagnetic and matter dynamics occur on the same timescale and are strongly coupled, that are the motivation for this paper*.

1.2. Historical and mathematical background

The history of the Maxwell–Schrödinger equations dates back to the early twentieth century when the founding fathers of quantum mechanics worked out the theoretical details of the interaction of electrodynamics with quantum mechanics [17]. It was realized early on that the electromagnetic coupling to matter was through the potentials Φ and $\mathbf{A}$, and not the fields $\mathbf{E}$ and $\mathbf{B}$ themselves [6,18,19]. The potentials and fields are related by

$$\mathbf{E} = -\nabla\Phi - \dot{\mathbf{A}}/c, \qquad \mathbf{B} = \nabla \times \mathbf{A} \tag{3}$$

which can be confirmed by inspecting the homogeneous Maxwell equations in (2). Unlike in classical theory where the potentials were introduced as a convenient mathematical tool, the quantum theory requires the potentials and not the fields. That is, the potentials are fundamental dynamical variables of the quantum theory but the fields are not. A concrete demonstration of this fact was presented in 1959 by Aharonov and Bohm [20].

1.2.1. Gauge symmetry of electrodynamics

It was well known from the classical theory of electrodynamics [9] that working with the potentials leads to a potential form of Maxwell's equations that is more flexible than that in terms of the fields alone (2). In potential form, Maxwell's equations become

$$\nabla^2\mathbf{A} - \frac{\ddot{\mathbf{A}}}{c^2} - \nabla\left[\nabla\cdot\mathbf{A} + \frac{\dot{\Phi}}{c}\right] = -\frac{4\pi}{c}\mathbf{J}, \tag{4a}$$

$$\nabla^2\Phi + \frac{\nabla\cdot\dot{\mathbf{A}}}{c} = -4\pi\rho. \tag{4b}$$

The homogeneous Maxwell equations are identically satisfied. These potential equations enjoy a symmetry that is not present in the field equations (2). This symmetry is called the *gauge symmetry* and can be generated by the transformation

$$\mathbf{A} \to \mathbf{A}' = \mathbf{A} + \nabla F, \qquad \Phi \to \Phi' = \Phi - \dot{F}/c, \tag{5}$$

where F is a well-behaved but otherwise arbitrary function called the *gauge generator*. Applying this *gauge transformation* to the potentials in (4) leads to exactly the same set of potential equations. In other words, these equations are invariant under arbitrary gauge transformation or are *gauge invariant*. They possess the full gauge symmetry. Notice also that the electric and magnetic fields are gauge invariant. In fact, it turns out that all physical observables are gauge invariant.

That electrodynamics possesses gauge symmetry places it in a league of theories known as gauge theories [21]. These theories include general relativity [22,23] and Yang–Mills theory [24–26]. Gauge theories all suffer from an indeterminateness due to their gauge symmetry. In an effort to deal with this indeterminateness, it is common to first eliminate the symmetry (usually up to the residual symmetry; see Section 2) by *gauge fixing* and then work within that particular gauge. That is, the flexibility implied by the gauge transformation (5) allows for the potentials to satisfy certain constraints. These constraints imply a particular choice of gauge and gauge generator. Gauge fixing is the act of constraining the potentials to satisfy a certain constraint throughout space–time. For example, in electrodynamics the potential equations (4) form an ill-posed initial value problem. However, they can be converted to a well-defined initial value problem by adding an equation of constraint to them. For example, adding the constraint $\dot{\Phi}/c + \nabla \cdot \mathbf{A} = 0$ leads to the well-defined Lorenz gauge equations

$$\nabla^2 \mathbf{A} - \frac{\ddot{\mathbf{A}}}{c^2} = -\frac{4\pi}{c}\mathbf{J}, \qquad \nabla^2 \Phi - \frac{\ddot{\Phi}}{c^2} = -4\pi\rho, \tag{6}$$

while adding $\nabla \cdot \mathbf{A} = 0$ leads to the well-defined Coulomb gauge equations

$$\nabla^2 \mathbf{A} - \frac{\ddot{\mathbf{A}}}{c^2} = -\frac{4\pi}{c}\mathbf{J}_T, \qquad \nabla^2 \Phi = -4\pi\rho, \tag{7}$$

where $\mathbf{J}_T$ is the transverse projection of the current $\mathbf{J}$. There are many other choices of constraint, each leading to a different gauge. It is always possible to find a gauge function that will transform an arbitrary set of potentials to satisfy a particular gauge constraint. The subject of the gauge symmetry of electrodynamics, which is a subtle but fundamental aspect of this paper, is discussed in detail in Section 2. In particular, it will be argued that fixing a particular gauge, which in turn eliminates the gauge from the theory, is not necessarily optimal. Rather, it is stressed that the gauge freedom is a fundamental variable of the theory and has its own dynamics.

1.2.2. Gauge symmetry of electrodynamics and wave mechanics

Since the gauge symmetry of electrodynamics was well known, it was noticed by the founding fathers that if quantum mechanics is to be coupled to electrodynamics, then the Schrödinger equation (1) needs to be gauge invariant as well. The most simple way of achieving this is to require the Hamiltonian appearing in (1) to be of the form

$$H = \frac{[\mathbf{P} - q\mathbf{A}/c]^2}{2m} + V + q\Phi, \tag{8}$$

where $\mathbf{P}$ is the quantum mechanical momentum, V is the potential energy, and m is the mass of the charge q. This is in analogy with the Hamiltonian for a classical charge in the presence of the electromagnetic field [27,28]. The coupling scheme embodied in (8) is known as *minimal coupling*, since it is the simplest gauge invariant coupling imaginable. The gauge symmetry inherent in the combined system of Schrödinger's equation and Maxwell's equations in potential form can be generated by the transformation

$$\begin{aligned} &\mathbf{A} \to \mathbf{A}' = \mathbf{A} + \nabla F, \qquad \Phi \to \Phi' = \Phi - \dot{F}/c, \\ &\Psi \to \Psi' = \exp(iqF/c)\Psi. \end{aligned} \tag{9}$$

The transformation on the wavefunction is called a *local gauge transformation* and differs from the *global gauge transformation* $\exp(i\theta)$, where θ is a constant. These global gauge transformations are irrelevant in quantum mechanics where the wavefunction is indeterminate up to a global phase. Application of the gauge transformation (9) to the Schrödinger equation with Hamiltonian (8) and to Maxwell's equations in potential form leads to exactly the same equations after the transformation. Therefore, like the potential equations (4) by themselves, the system of Maxwell–Schrödinger equations

$$i\dot{\Psi} = \frac{[\mathbf{P} - q\mathbf{A}/c]^2\Psi}{2m} + V\Psi + q\Phi\Psi, \tag{10}$$

$$\nabla^2\mathbf{A} - \frac{\ddot{\mathbf{A}}}{c^2} - \nabla\left[\nabla\cdot\mathbf{A} + \frac{\dot{\Phi}}{c}\right] = -\frac{4\pi}{c}\mathbf{J}, \tag{11a}$$

$$\nabla^2\Phi + \frac{\nabla\cdot\dot{\mathbf{A}}}{c} = -4\pi\rho \tag{11b}$$

is invariant under the gauge transformation (9). There are several other symmetries that are enjoyed by this system of equations. For example, they are invariant under spatial rotations, nonrelativistic (Galilei) boosts, and time reversal. As a result, the Maxwell–Schrödinger equations enjoy charge, momentum, angular momentum, and energy conservation. That each continuous symmetry gives rise to an associated conservation law was proven by Emmy Noether in 1918 (see Goldstein [27], José and Saletan [28], and Abraham and Marsden [29], and the references therein).

It is worthwhile mentioning that the Maxwell–Schrödinger equations are obtainable as the nonrelativistic limit of the Maxwell–Dirac equations

$$i\dot{\Psi}_D = \beta mc^2\Psi_D + c\boldsymbol{\alpha}\cdot[\mathbf{P} - q\mathbf{A}/c]\Psi_D + q\Phi\Psi_D, \tag{12}$$

$$\nabla^2\mathbf{A} - \frac{\ddot{\mathbf{A}}}{c^2} - \nabla\left[\nabla\cdot\mathbf{A} + \frac{\dot{\Phi}}{c}\right] = -\frac{4\pi}{c}\mathbf{J}, \tag{13a}$$

$$\nabla^2\Phi + \frac{\nabla\cdot\dot{\mathbf{A}}}{c} = -4\pi\rho \tag{13b}$$

which are the equations of quantum electrodynamics (QED) [19,24,30]. Here the wavefunction Ψ_D is a 4-component spinor where the first two components represent the electron and the second two components represent the positron, each with spin-$1/2$. The matrices β and $\boldsymbol{\alpha}$ are related to the Pauli spin matrices [7,8] and c is the velocity of light. This system of equations possesses each of the symmetries of the Maxwell–Schrödinger equations and in addition is invariant under relativistic boosts.

1.3. Approaches to the solution of the Maxwell and Schrödinger equations

Solving the Maxwell–Schrödinger equations as a coupled and closed system embodies the theory of radiation reaction [9,26,31], which is a main theme of this paper. However, it should first be pointed out that (1) and (2) are commonly treated separately. In these cases, the effects of one system on the other are handled in one of the following two ways:

- The arrangement of charge and current is specified and acts as a source for the electromagnetic field according to (2).
- The dynamics of the electromagnetic field is specified and modifies the dynamics of the matter according to (1).

It is not surprising that either of these approaches is valid in many physical situations. Most of the theory of electrodynamics, in which the external sources are prescribed, fits into the first case, while all of classical and quantum mechanics in the presence of specified external fields fits into the second.

As a further example of the first case, the dipole power radiated by oscillating dipoles generated by charge transfer processes in the interaction region of p–H collisions can be computed in a straightforward manner [32,33]. It is assumed that the dynamics of the oscillating dipole is known and is used to compute the dipole radiation, but this radiation does not influence the p–H collision. As a result energy, momentum, and angular momentum are not conserved between the proton, hydrogen atom, and electromagnetic field system. As a further example of the second case, the effects of stimulated absorption or emission of electromagnetic radiation by a molecular target can be added to the molecular quantum mechanics as a first order perturbative correction. The electrodynamics is specified and perturbs the molecule but the molecule does not itself influence the electrodynamics. This approach, which is known as Fermi's golden rule (see Merzbacher [7], Craig and Thirunamachandran [34], and Schatz and Ratner [35]) is straightforward and barring certain restrictions can be applied to many physical systems.

The system of Maxwell–Schrödinger equations or its relativistic analog can be closed and is coupled when the Schrödinger wavefunction Ψ, which is the solution of (1), is chosen to be the source for the scalar potential Φ and vector potential $\mathbf{A}$ in (4). In particular, the sources of charge ρ and current $\mathbf{J}$, which produce the electromagnetic potentials according to (4), involve the solutions Ψ of the Schrödinger equation according to

$$\rho = q\Psi^*\Psi, \qquad \mathbf{J} = q\left\{\Psi^*[-i\nabla - q\mathbf{A}/c]\Psi + \Psi[i\nabla - q\mathbf{A}/c]\Psi^*\right\}/2m. \tag{14}$$

On the other hand, the wavefunction Ψ is influenced by the potentials that appear in the Hamiltonian H in (8).

The interpretation of the Schrödinger wavefunction as the source for the electromagnetic field was *Schrödinger's electromagnetic hypothesis*, which dates back to 1926. The discovery of the quantum mechanical continuity equation and its similarity to the classical continuity equation of electrodynamics only reinforced the hypothesis. However, it implied the electron to be smeared out throughout the atom and not located at a discrete point, which may be viewed to be in contradiction to the accepted Born probabilistic or Copenhagen interpretation. Schrödinger's wave mechanics had some success, especially with the interaction of the electromagnetic field with bound states, but failed to properly describe scattering states due to the probabilistic nature of measurement of the wavefunction. In

addition, certain properties of electromagnetic radiation were found to be inconsistent with experiment.

Schrödinger's electromagnetic hypothesis was extended by Fermi in 1927 and later by Jaynes and Cummings in 1963 [36] and Crisp and Jaynes in 1969 [37] to incorporate the nonquantum electromagnetic self-fields into the theory. That is, the classical electromagnetic fields produced by the atom were allowed to act back upon the atom. The solutions of this extended semiclassical theory captured certain aspects of spontaneous emission as well as frequency shifts like the Lamb shift. However, it was quickly noticed that some deviations from QED existed [38]. For example, Fermi's and Jaynes' theories predicted a time-dependent form for spontaneous decay that is not exponential. There are many properties that are correctly predicted by this semiclassical theory and are also in agreement with QED. In the cases where the semiclassical theory disagrees with QED [38], it has always been experimentally verified that QED is correct. Nevertheless, the semiclassical theory does not suffer from the mathematical and logical difficulties that are present in QED. To this end, the semiclassical theory, when it is correct, provides a useful alternative to the quantum field theory. It is generally simpler and its solutions provide a more detailed dynamical description of the interaction of an atom with the electromagnetic field.

Since 1969 many others have followed along the semiclassical path of Crisp and Jaynes. Nesbet [39] computed the gauge invariant energy production rate from a many particle system. Cook [40] used a density operator approach to account for spontaneous emission without leaving the atomic Hilbert space. Barut and Van Huele [41] and Barut and Dowling [42,43] formulated a self-field quantum electrodynamics for Schrödinger, Pauli, Klein–Gordon, and Dirac matter theories. They were able to eliminate all electromagnetic variables in favor of Green's function integrals over the sources and were able to recover the correct exponential spontaneous decay from an excited state. Some pertinent critiques of this work are expressed by Bialynicki-Birula in [44] and by Crisp in [45]. Bosanac [46–48] and Došlić and Bosanac [49] argued that the instantaneous effects of the self interaction are unphysical. As a result, they formulated a theory of radiation reaction based on the retarded effects of the self-fields. Milonni, Ackerhalt, and Galbraith [50] predicted chaotic dynamics in a collection of two-level atoms interacting with a single mode of the classical electromagnetic field. Crisp has contributed some of the finest work in semiclassical theory. He computed the radiation reaction associated with a rotating charge distribution [51], the atomic radiative level shifts resulting from the solution of the semiclassical nonlinear integro-differential equations [52], the interaction of an atomic system with a single mode of the quantized electromagnetic field [53,54], and the extension of the semiclassical theory to include relativistic effects [55].

Besides semiclassical theory, a vast amount of research has been conducted in the quantum theory of electrodynamics and matter. QED [19,24,30,56], which is the fully relativistic and quantum mechanical theory of electrons and photons, has been found to agree with all associated experiments. The coupled equations of QED can be solved nonperturbatively [57,58], but are most often solved by resorting to perturbative methods. As was previously mentioned, there are some drawbacks to these methods that are not present in the semiclassical theory. In addition to pure QED in terms of electrons and photons, there has also been an increasing interest in molecular quantum electrodynamics [34]. Power and Thirunamachandran [59,60], Salam and Thirunamachandran [61], and Salam [62] have used perturbative methods within the minimal-coupling and multipolar formalisms to study the quantized electromagnetic field surrounding a molecule. In particular, they

have clarified the relationship between the two formalisms and in addition have calculated the Poynting vector and spontaneous emission rates for magnetic dipole and electric quadrupole transitions in optically active molecules.

In both the semiclassical and quantum mechanical context the self-energy of the electron has been studied [63–66]. The self-energy arises naturally in the minimal coupling scheme as the $q\Phi$ term in the Hamiltonian (8). More specifically, the electron's self-energy in the nonrelativistic theory is defined as

$$U = \int_V d^3x q\Phi(\mathbf{x},t)\Psi^*(\mathbf{x},t)\Psi(\mathbf{x},t) = \int_V d^3x \int_V d^3x' \frac{\rho(\mathbf{x},t)\rho(\mathbf{x}',t)}{|\mathbf{x}-\mathbf{x}'|}. \tag{15}$$

As a result of the $q\Phi$ term, the Schrödinger equation (10) is nonlinear in Ψ. It resembles the nonlinear Schrödinger equation [67]

$$i\dot{u} = -a\left(d^2u/dx^2\right) + b|u|^2u \tag{16}$$

which arises in the modeling of the dynamics of Bose–Einstein condensates with the Gross–Pitaevskii equation and in the modeling of superconductivity with the Ginzburg–Landau equation.

In the relativistic theory, the electron is forced to lack structure due to relativistic invariance. As a result, the corresponding self-energy is infinite. On the other hand, the electron may have structure in the nonrelativistic theory. Consequently, the self-energy is finite. The self-energy of the electron will be discussed in Section 2 in more detail.

1.4. Canonical formulation of the coupled Maxwell–Schrödinger equations

The work presented in this paper [68,69] continues the semiclassical story originally formulated by Fermi, Crisp, and Jaynes. Unlike other semiclassical and quantum mechanical theories of electrodynamics and matter where the gauge is fixed at the beginning, it will be emphasized that the gauge is a fundamental degree of freedom in the theory and should not be eliminated. As a result, the equations of motion are naturally well balanced and form a well-defined initial value problem when the gauge freedom is retained. This philosophy was pursued early on by Dirac, Fock, and Podolsky [70] (see Schwinger [19]) in the context of the Hamiltonian formulation of QED. However, their approach was quickly forgotten in favor of the more practical Lagrangian based perturbation theory that now dominates the QED community. More recently, Kobe [71] studied the Hamiltonian approach in semiclassical theory.

We believe that the Hamiltonian formulation of dynamics offers a natural and powerful theoretical approach to the interaction of electrodynamics and wave mechanics that has not yet been fully explored. To this end, the Hamiltonian or canonical[1] formulation of the Maxwell–Schrödinger dynamics is constructed in this paper. The associated work involves nonperturbative analytic and numerical methods for the solution of the coupled and closed nonlinear system of Maxwell–Schrödinger equations. The flexibility inherent in these methods captures the nonlinear and nonadiabatic effects of the coupled system and has the potential to describe situations where the atomic and electromagnetic dynamics occur on the same timescale.

[1] *Canonical* means according to the canons, *i.e.*, standard or conventional.

The canonical formulation is set up by applying the time-dependent variational principle [72,73] to the Schrödinger Lagrangian

$$\mathcal{L}_{\text{Sch}} = i\Psi^*\dot{\Psi} - \frac{[i\nabla - q\mathbf{A}/c]\Psi^* \cdot [-i\nabla - q\mathbf{A}/c]\Psi}{2m} - V\Psi^*\Psi - q\Phi\Psi^*\Psi, \tag{17}$$

and Maxwell Lagrangian together with a Lorenz gauge fixing term, *i.e.*,

$$\begin{aligned}\mathcal{L}^L_{\text{Max}} &= \mathcal{L}_{\text{Max}} - \frac{[\dot{\Phi}/c + \nabla \cdot \mathbf{A}]^2}{8\pi} \\ &= \frac{[-\dot{\mathbf{A}}/c - \nabla\Phi]^2 - [\nabla \times \mathbf{A}]^2}{8\pi} - \frac{[\dot{\Phi}/c + \nabla \cdot \mathbf{A}]^2}{8\pi}.\end{aligned} \tag{18}$$

This yields a set of coupled nonlinear first order differential equations in time of the form

$$\boldsymbol{\omega}\dot{\boldsymbol{\eta}} = \partial H/\partial\boldsymbol{\eta}, \tag{19}$$

where $\boldsymbol{\omega}$ is a symplectic form, $\boldsymbol{\eta}$ is a column vector of the dynamical variables, and H is the Maxwell–Schrödinger Hamiltonian (see Section 2). These matrix equations form a well-defined initial value problem. That is, the solution to these equations is uniquely determined and known in principle once the initial values for each of the dynamical variables $\boldsymbol{\eta}$ are specified. These equations are also closed since the Schrödinger wavefunction acts as the source, which is nonlinear (see ρ and $\mathbf{J}$ in (14)), for the electromagnetic potentials and these potentials act back upon the wavefunction. By representing each of the dynamical variables in a basis of Gaussian functions $G_{\mathcal{K}}$, *i.e.*, $\eta(\mathbf{x}, t) = \sum_{\mathcal{K}} G_{\mathcal{K}}(\mathbf{x})\eta_{\mathcal{K}}(t)$, where the time-dependent superposition coefficients $\eta_{\mathcal{K}}(t)$ carry the dynamics, the time-dependent variational principle generates a hierarchy of approximations to the coupled Maxwell–Schrödinger equations. In the limit of a complete basis these equations recover the exact Maxwell–Schrödinger theory, while in any finite basis they form a basis representation that can systematically be made more accurate with a more robust basis.

The associated basis equations have been implemented in a FORTRAN 90 computer program [69] that is flexible enough to handle arbitrarily many Gaussian basis functions, each with adjustable widths and centers. In addition, a numerical convergence accelerator has been developed based on removing the large Coulombic fields surrounding a charge (that can be computed analytically from Gauss's law, *i.e.*, $\nabla \cdot \mathbf{E} = -\nabla^2\Phi = 4\pi\rho$, once the initial conditions are provided) by applying a certain canonical transformation to the dynamical equations. The canonical transformation separates the dynamical radiation from the Coulombic portion of the field. This in turn allows the basis to describe only the dynamics of the radiation fields and not the large Coulombic effects. The canonical transformed equations, which are of the form $\tilde{\boldsymbol{\omega}}\dot{\tilde{\boldsymbol{\eta}}} = \partial\tilde{H}/\partial\tilde{\boldsymbol{\eta}}$, have been added to the existing computer program and the convergence of the solution of the Maxwell–Schrödinger equations is studied.

The canonical approach to dynamics enjoys a deep mathematical foundation and permits a general application of the theory to many physical problems. In particular, the dynamics of the hydrogen atom interacting with its electromagnetic field in a cavity has been investigated. Stationary state solutions of the combined hydrogen atom and electromagnetic field system as well as nonstationary states that produce electromagnetic radiation have been constructed. This radiation carries away energy, momentum, and angular momentum from the hydrogen atom such that the total energy, momentum, angular momentum, and charge of the combined system are conserved. A series of plots are presented to highlight this atom-field dynamics.

1.5. Notation and units

A brief statement should be made about notation. All work will be done in the $(1+3)$-dimensional background of special relativity with diagonal metric tensor $g_{\alpha\beta} = g^{\alpha\beta}$ with elements $g_{00} = g^{00} = 1$ and $g_{11} = g_{22} = g_{33} = -1$. All 3-vectors will be written in bold faced Roman while all 4-vectors will be written in italics. As usual, Greek indices run over 0, 1, 2, 3 or ct, x, y, z and Roman indices run over 1, 2, 3 or x, y, z. The summation convention is employed over repeated indices. For example, the 4-potential $A^\mu = (A^0, A^k) = (\Phi, \mathbf{A})$ and $A_\mu = g_{\mu\nu}A^\nu = (\Phi, -\mathbf{A})$. The D'Alembertian operator $\Box = \nabla^2 - \partial^2/\partial(ct)^2 = -\partial^2$ is used at times in favor of ∂^2. Fourier transforms will be denoted with tildes, *e.g.*, $\tilde{F}$ is the Fourier transform of F. The representation independent Dirac notation $|h\rangle$ will be used in the numerical analysis, but for the most part functions $h(\mathbf{x}) = \langle \mathbf{x}|h\rangle$ or $\tilde{h}(\mathbf{k}) = \langle \mathbf{k}|h\rangle$ will be used. (It will be assumed that all of the functions of physics are infinitely differentiable, continuous, square integrable, and Fourier transformable over either the real or complex field.) Since it is the radiation effects present on the atomic scale that are of interest, it is beneficial to work in natural (Gaussian atomic) units where $\hbar = -|e| = m_e = 1$. In these units the speed of light $c \approx 137$ atomic units of velocity.

2. CANONICAL STRUCTURE

The governing equation of quantum mechanics is the Schrödinger equation [7,8]. In the minimal coupling prescription it is

$$i\dot{\Psi} = \frac{[-i\nabla - q\mathbf{A}/c]^2\Psi}{2m} + V\Psi + q\Phi\Psi. \tag{1}$$

The dynamics of the scalar potential Φ and vector potential $\mathbf{A}$ are not described by this linear equation. Specification of these potentials as well as the initial values for the wavefunction Ψ casts the Schrödinger equation into a well-defined boundary value problem that is also a well-defined initial value problem.

The governing equations of electrodynamics are Maxwell's equations [9]:

$$\nabla\cdot\mathbf{E} = 4\pi\rho, \qquad \nabla\times\mathbf{B} = \frac{4\pi}{c}\mathbf{J} + \frac{\dot{\mathbf{E}}}{c}, \qquad \nabla\cdot\mathbf{B} = 0, \qquad \nabla\times\mathbf{E} + \frac{\dot{\mathbf{B}}}{c} = \mathbf{0}. \tag{2}$$

The dynamics of the charge density ρ and current density $\mathbf{J}$ are not described by these linear equations. Specification of the external sources as well as the initial values for the electric and magnetic fields $\mathbf{E}$ and $\mathbf{B}$ satisfying $\nabla\cdot\mathbf{E} = 4\pi\rho$ and $\nabla\cdot\mathbf{B} = 0$ casts the Maxwell equations into a well-defined boundary value problem that is also a well-defined initial value problem.

Each of these theories are significant in and of themselves. Given a particular arrangement of sources throughout space–time and the initial values for $\mathbf{E}$ and $\mathbf{B}$, the Maxwell equations govern the dynamics of the resulting electromagnetic field. Likewise, given a particular external field throughout space–time and the initial value for Ψ, the Schrödinger equation governs the dynamics of the sources. However, notice that the Maxwell equations do not say anything about the dynamics of the sources and the Schrödinger equation does not say anything about the electrodynamics.

It is possible to couple the linear Maxwell and Schrödinger equations. The resulting nonlinear Maxwell–Schrödinger theory accounts for the dynamics of the charges and the electromagnetic field as well as their mutual interaction. For example, given an initial source and its corresponding Coulomb field, a wavefunction and electromagnetic field are generated. The electromagnetic field has its own dynamics and acts back upon the wavefunction. This in turn causes different fields to be generated. It will be demonstrated that these coupled nonlinear Maxwell–Schrödinger equations can be cast into a well-defined initial value problem and solved in an efficient numerical manner.

2.1. Lagrangian electrodynamics

Consider the Maxwell Lagrangian density

$$\mathcal{L}_{\text{Max}} = \frac{[-\dot{\mathbf{A}}/c - \nabla\Phi]^2 - [\nabla \times \mathbf{A}]^2}{8\pi} - \rho\Phi + \frac{\mathbf{J}\cdot\mathbf{A}}{c} \tag{20}$$

with external sources ρ and $\mathbf{J}$. Variation of this Lagrangian leads to the governing equations of electrodynamics, *i.e.*,

$$\begin{aligned} &\nabla^2\mathbf{A} - \frac{\ddot{\mathbf{A}}}{c^2} - \nabla\left[\nabla\cdot\mathbf{A} + \frac{\dot{\Phi}}{c}\right] = -\frac{4\pi}{c}\mathbf{J}, \\ &\nabla^2\Phi + \frac{\nabla\cdot\dot{\mathbf{A}}}{c} = -4\pi\rho. \end{aligned} \tag{4}$$

These Maxwell equations (in terms of the potentials) do not form a well-defined initial value problem. But, by choosing a particular gauge they can be turned into one. In other words, these equations are ill-posed as they stand. However, they do enjoy both Lorentz and gauge invariance as does the Lagrangian (20).

2.1.1. Choosing a gauge

Working in a particular gauge can be organized into the following hierarchy involving three tiers:

1. At the solution level, a gauge generator F can be chosen so that a gauge transformation of the solutions, *i.e.*, $\Phi \to \Phi' = \Phi - \dot{F}/c$ and $\mathbf{A} \to \mathbf{A}' = \mathbf{A} + \nabla F$, maps them to new solutions that satisfy the gauge condition.
2. At the equation level, the set consisting of (4) together with a gauge constraint has only solutions that satisfy the gauge condition.
3. At the Lagrangian level, a gauge fixing term can be added to (20) so that the resulting Euler–Lagrange equations automatically include the gauge constraint.

2.1.2. The Lorenz and Coulomb gauges

The first two tiers can be elaborated on as follows. With a gauge function F satisfying $\nabla^2 F - \ddot{F}/c^2 = -[\dot{\Phi}/c + \nabla\cdot\mathbf{A}]$ a solution $A^\alpha = (\Phi, \mathbf{A})$ of the potential equations (4) can be mapped to the Lorenz gauge solution A^α_{Lorenz} according to the gauge transformation:

$$\Phi \to \Phi_{\text{Lorenz}} = \Phi - \dot{F}/c, \qquad \mathbf{A} \to \mathbf{A}_{\text{Lorenz}} = \mathbf{A} + \nabla F. \tag{21}$$

Alternatively, adding the gauge constraint $\dot{\Phi}/c + \nabla\cdot\mathbf{A} = 0$ to (4) leads to the Lorenz gauge equations of motion:

$$\nabla^2\mathbf{A} - \frac{\ddot{\mathbf{A}}}{c^2} = -\frac{4\pi}{c}\mathbf{J}, \qquad \nabla^2\Phi - \frac{\ddot{\Phi}}{c^2} = -4\pi\rho. \tag{22}$$

With ρ and $\mathbf{J}$ specified throughout space–time, the Lorenz gauge equations of motion are well defined once the initial values for $\mathbf{A}$, $\dot{\mathbf{A}}$, Φ, and $\dot{\Phi}$ are known. There is some symmetry left in the solutions to these equations. Namely, the residual gauge freedom left in the homogeneous equation $\nabla^2 F - \ddot{F}/c^2 = 0$ allows for gauge transformations on the solutions such that the new solutions do not leave the Lorenz gauge. However, these gauge transformed solutions do correspond to different initial conditions. Note that the Lorenz gauge enjoys relativistic or Lorentz invariance. It will be shown, that the Lorenz gauge is the most appropriate gauge for dynamics.

With another gauge function G satisfying $\nabla^2 G = -\nabla\cdot\mathbf{A}$ a solution $A^\alpha = (\Phi, \mathbf{A})$ of the potential equations (4) can be mapped to the Coulomb gauge solution $A^\alpha_{\text{Coulomb}}$ according to:

$$\Phi \to \Phi_{\text{Coulomb}} = \Phi - \dot{G}/c, \qquad \mathbf{A} \to \mathbf{A}_{\text{Coulomb}} = \mathbf{A} + \nabla G. \tag{23}$$

Alternatively, adding the gauge constraint $\nabla\cdot\mathbf{A} = 0$ to (4) leads to the Coulomb gauge equations of motion:

$$\nabla^2\mathbf{A} - \frac{\ddot{\mathbf{A}}}{c^2} = -\frac{4\pi}{c}\mathbf{J} + \frac{\nabla\dot{\Phi}}{c}, \qquad \nabla^2\Phi = -4\pi\rho. \tag{24}$$

Again with ρ and $\mathbf{J}$ specified throughout space–time, the Coulomb gauge equations of motion are well defined once the initial values for $\mathbf{A}$, $\dot{\mathbf{A}}$, Φ, and $\dot{\Phi}$ are known. As before, there remains a symmetry or residual gauge freedom from the homogeneous equation $\nabla^2 G = 0$. Note that in the Coulomb gauge Gauss' law reduces to $\nabla^2\Phi = -4\pi\rho$. Inverting this equation specifies Φ in terms of ρ. That is $\Phi = (1/\nabla^2)[-4\pi\rho]$. The scalar potential can now be totally removed from the theory by substitution of this Green's function integral. This may be done at the expense of Lorentz invariance. In practice, where the equations are to be expanded in a basis of s-Gaussians, either transverse basis functions would have to be used or the transverse fields would have to be generated from a standard basis. The former case would require a major revision of most existing integral codes, which are in direct space, while the latter would require the instantaneous transverse projection $P_T^{ab} = \delta^{ab} - \partial^a\partial^b/\nabla^2$. This operation, which is over all space, is difficult to describe in terms of a local set of basis functions.

Lastly, for the third tier, consider the Lagrangian density (20) together with a gauge fixing term for the Lorenz gauge, *i.e.*,

$$\begin{aligned}\mathcal{L}^L_{\text{Max}} &= \mathcal{L}_{\text{Max}} - \frac{[\dot{\Phi}/c + \nabla\cdot\mathbf{A}]^2}{8\pi} \\ &= \frac{[-\dot{\mathbf{A}}/c - \nabla\Phi]^2 - [\nabla\times\mathbf{A}]^2}{8\pi} - \rho\Phi + \frac{\mathbf{J}\cdot\mathbf{A}}{c} - \frac{[\dot{\Phi}/c + \nabla\cdot\mathbf{A}]^2}{8\pi}.\end{aligned} \tag{18}$$

The resulting Euler–Lagrange equations obtained from $\mathcal{L}^L_{\text{Max}}$ are identical to the Lorenz gauge wave equations in (22) which are equivalent to the general potential equations (4) together with the constraint $\dot{\Phi}/c + \nabla\cdot\mathbf{A} = 0$.

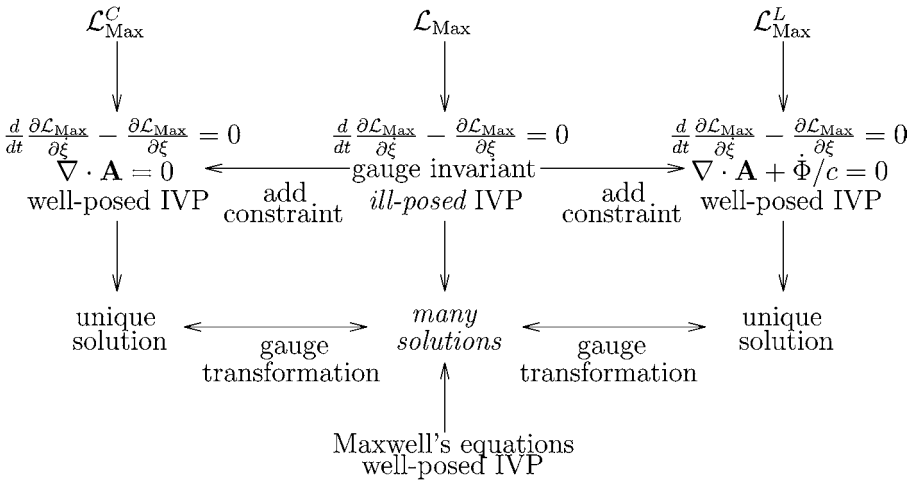

Fig. 1. A limited but relevant portion of the gauge story in the Lagrangian formalism is organized in this picture. The middle column (*i.e.*, the column below $\mathcal{L}_{\rm Max}$) enjoys full gauge freedom. The far left (Coulomb gauge) and far right (Lorenz gauge) columns have limited gauge freedom. That is, there are a limited class of gauge transformations that can be made on the solutions such that they remain in the same gauge. This symmetry is due to the residual gauge freedom. Note that these solutions correspond to different initial conditions within the gauge. Also note that the Euler–Lagrange equations together with a particular gauge constraint are equivalent to the Euler–Lagrange equations derived from that particular gauge fixed Lagrangian.

There are many other known gauges, the choice of which is arbitrary. All choices of gauge lead to the same physically observable electromagnetic fields **E** and **B**. Together with the definitions $\mathbf{E} = -\dot{\mathbf{A}}/c - \nabla\Phi$ and $\mathbf{B} = \nabla \times \mathbf{A}$, the Lorenz and Coulomb gauge equations of motion as well as the general potential equations (4) imply Maxwell's equations (2). A diagram of this gauge story in the Lagrange formulation is presented in Fig. 1.

2.2. Hamiltonian electrodynamics

In the Hamiltonian prescription, the momentum conjugate to **A** with respect to the Maxwell Lagrangian (20) is

$$\mathbf{\Pi} \equiv \frac{\partial \mathcal{L}_{\rm Max}}{\partial \dot{\mathbf{A}}} = \frac{1}{4\pi c}[\dot{\mathbf{A}}/c + \nabla\Phi]. \tag{25}$$

The momentum conjugate to Φ is identically zero, *i.e.*,

$$\Theta \equiv \frac{\partial \mathcal{L}_{\rm Max}}{\partial \dot{\Phi}} = 0. \tag{26}$$

A Hamiltonian density can still be defined as the time-time component of the Maxwell stress-energy tensor $T^{\alpha\beta}_{\rm Max} = \{\partial \mathcal{L}_{\rm Max}/\partial(\partial_\alpha \xi)\}\partial^\beta \xi - g^{\alpha\beta}\mathcal{L}_{\rm Max}$. It is

$$\mathcal{H}_{\text{Max}} \equiv T^{00}_{\text{Max}} = \boldsymbol{\Pi}\cdot\dot{\mathbf{A}} + \Theta\dot{\Phi} - \mathcal{L}_{\text{Max}}$$
$$= \frac{[-4\pi c\boldsymbol{\Pi}]^2 + [\nabla\times\mathbf{A}]^2}{8\pi} - c\nabla\Phi\cdot\boldsymbol{\Pi} + \rho\Phi - \frac{\mathbf{J}\cdot\mathbf{A}}{c} \tag{27}$$

and the resulting equations of motion are:

$$\dot{\mathbf{A}} \equiv \frac{\partial\mathcal{H}_{\text{Max}}}{\partial\boldsymbol{\Pi}} = 4\pi c^2\boldsymbol{\Pi} - c\nabla\Phi, \qquad -\dot{\boldsymbol{\Pi}} \equiv \frac{\partial\mathcal{H}_{\text{Max}}}{\partial\mathbf{A}} = \frac{\nabla\times\nabla\times\mathbf{A}}{4\pi} - \frac{\mathbf{J}}{c} + c\nabla\Theta,$$
$$\dot{\Phi} \equiv \frac{\partial\mathcal{H}_{\text{Max}}}{\partial\Theta} = 0, \qquad -\dot{\Theta} \equiv \frac{\partial\mathcal{H}_{\text{Max}}}{\partial\Phi} = \rho + c\nabla\cdot\boldsymbol{\Pi}. \tag{28}$$

Since the momentum Θ defined in (26) is identically zero, so is its time derivative $\dot{\Theta}$ and gradient $\nabla\Theta$. Notice that these Hamilton equations form a well-posed initial value problem. The machinery inherent in the Hamiltonian formalism automatically adds a momentum and automatically adds the additional equation of constraint $\dot{\Phi} = 0$. It turns out that this extra equation fixes a particular gauge where $\dot{\Phi} = 0$. This gauge can always be fixed by a gauge transformation whose generator satisfies $\ddot{F}/c = \dot{\Phi}$. The residual gauge freedom left in the homogeneous equation $\ddot{F} = 0$ does allow for a gauge transformation on the solutions to (28). These new gauge transformed solutions do not leave the $\dot{\Phi} = 0$ gauge, but do correspond to a different initial value problem within this gauge. In other words, they are solutions to (28) with different initial values. Pay careful attention to the fact that these Hamilton equations of motion form a well-posed initial value problem even though a gauge fixed Lagrangian was not knowingly used. The Hamiltonian formalism automatically added the extra equation $\dot{\Phi} = 0$.

2.2.1. Hamiltonian formulation of the Lorenz gauge

Rather than fixing the Coulomb gauge at the equation level it may be beneficial to work in a more general theory where a gauge is chosen at the Lagrangian level and retains all of the 4-potential, is Lorentz invariant, and does not require any instantaneous or nonlocal operations. To this end, consider the Lorenz gauge Lagrangian density from (18), *i.e.*,

$$\mathcal{L}^L_{\text{Max}} = \frac{[-\dot{\mathbf{A}}/c - \nabla\Phi]^2 - [\nabla\times\mathbf{A}]^2}{8\pi} - \rho\Phi + \frac{\mathbf{J}\cdot\mathbf{A}}{c} - \frac{[\dot{\Phi}/c + \nabla\cdot\mathbf{A}]^2}{8\pi}. \tag{18}$$

It will be shown that the equations of motion derived from $\mathcal{L}^L_{\text{Max}}$ are well defined because of the addition of the last term in this expression. It turns out that this term is known in the literature [24,70] and is a gauge fixing term for the Lorenz gauge. From (18), the momentum conjugate to $\mathbf{A}$ is

$$\boldsymbol{\Pi} \equiv \frac{\partial\mathcal{L}^L_{\text{Max}}}{\partial\dot{\mathbf{A}}} = \frac{1}{4\pi c}[\dot{\mathbf{A}}/c + \nabla\Phi] \tag{29}$$

and the momentum conjugate to Φ is

$$\Theta \equiv \frac{\partial\mathcal{L}^L_{\text{Max}}}{\partial\dot{\Phi}} = -\frac{1}{4\pi c}[\dot{\Phi}/c + \nabla\cdot\mathbf{A}]. \tag{30}$$

With these momenta and coordinates, electrodynamics is given a symplectic structure. The Hamiltonian density is

$$\mathcal{H}^L_{\text{Max}} = \frac{[-4\pi c\mathbf{\Pi}]^2 + [\nabla \times \mathbf{A}]^2 - [4\pi c\Theta]^2}{8\pi} - c\nabla\Phi \cdot \mathbf{\Pi} - c\Theta\nabla \cdot \mathbf{A} + \rho\Phi - \frac{\mathbf{J} \cdot \mathbf{A}}{c} \tag{31}$$

and the resulting equations of motion are:

$$\begin{aligned} \dot{\mathbf{A}} &= 4\pi c^2\mathbf{\Pi} - c\nabla\Phi, & -\dot{\mathbf{\Pi}} &= \frac{\nabla \times \nabla \times \mathbf{A}}{4\pi} - \frac{\mathbf{J}}{c} + c\nabla\Theta, \\ \dot{\Phi} &= -4\pi c^2\Theta - c\nabla \cdot \mathbf{A}, & -\dot{\Theta} &= \rho + c\nabla \cdot \mathbf{\Pi}. \end{aligned} \tag{32}$$

These equations, which are a generalization of (22), together with the initial values for $\mathbf{A}$, $\mathbf{\Pi}$, Φ, and Θ form a well-posed initial value problem. The residual gauge freedom resulting from the homogeneous equation $\Box F = 0$ does allow for a gauge transformation on the solutions to (32). These new gauge transformed solutions do not leave the Lorenz gauge, but do correspond to a different initial value problem within the Lorenz gauge. In other words, they are solutions to (32) with different initial values.

Notice that a relationship exists between the momentum Θ and the gauge function F leading to the Lorenz gauge. That is, from $\Theta = -[\dot{\Phi}/c + \nabla \cdot \mathbf{A}]/4\pi c$ and $\ddot{F}/c^2 - \nabla^2 F = \dot{\Phi}/c + \nabla \cdot \mathbf{A}$ notice that $\Theta \equiv \Box F/4\pi c$. So the D'Alembertian of the gauge function F acts as a generalized coordinate in this phase space. It becomes the momentum conjugate to the scalar potential Φ.

In matrix form, the dynamical equations in (32) are

$$\begin{pmatrix} 0 & 0 & -\mathbf{1} & 0 \\ 0 & 0 & 0 & -1 \\ \mathbf{1} & 0 & 0 & 0 \\ 0 & 1 & 0 & 0 \end{pmatrix} \begin{pmatrix} \dot{\mathbf{A}} \\ \dot{\Phi} \\ \dot{\mathbf{\Pi}} \\ \dot{\Theta} \end{pmatrix} = \begin{pmatrix} \nabla \times \nabla \times \mathbf{A}/4\pi - \mathbf{J}/c + c\nabla\Theta \\ \rho + c\nabla \cdot \mathbf{\Pi} \\ 4\pi c^2\mathbf{\Pi} - c\nabla\Phi \\ -4\pi c^2\Theta - c\nabla \cdot \mathbf{A} \end{pmatrix}, \tag{33}$$

where $\mathbf{1}$ is the 3×3 identity matrix. Notice that (33) is of the Hamiltonian form

$$\boldsymbol{\omega}\dot{\boldsymbol{\eta}} = \partial H/\partial\boldsymbol{\eta}. \tag{34}$$

More specifically $\omega_{ab}\dot{\eta}^b = \partial H/\partial\eta^a$, where η^b is a column matrix of the generalized positions and momenta, *i.e.*,

$$\eta^b(\mathbf{x}, t) = \begin{pmatrix} A^k \\ \Phi \\ \Pi^k \\ \Theta \end{pmatrix}, \tag{35}$$

where $k = 1, 2, 3$. The antisymmetric matrix ω_{ab} is the (canonical) symplectic form associated with the phase space of electrodynamics in the Lorenz gauge. By substitution, these first order Hamiltonian equations of motion can be shown to be equivalent to the second order Lorenz gauge equations $\Box\Phi = -4\pi\rho$ and $\Box\mathbf{A} = -4\pi\mathbf{J}/c$. Together with the definition of the electric and magnetic fields, (32) imply

$$\begin{aligned} \nabla \cdot \mathbf{E} &= 4\pi\rho + 4\pi\dot{\Theta}, & \nabla \times \mathbf{B} &= \frac{4\pi}{c}\mathbf{J} + \frac{\dot{\mathbf{E}}}{c} - 4\pi c\nabla\Theta, \\ \nabla \cdot \mathbf{B} &= 0, & \nabla \times \mathbf{E} + \frac{\dot{\mathbf{B}}}{c} &= \mathbf{0}. \end{aligned} \tag{36}$$

These equations are not equivalent to Maxwell's equations unless $\Theta(\mathbf{x}, t)$ remains constant in space–time throughout the dynamics. In order to analyze this question, the dynamics of the sources must be considered. It should be noticed that the inhomogeneous equations in (36) imply

$$\Box\Theta \equiv \nabla^2\Theta - \frac{\ddot{\Theta}}{c^2} = \frac{1}{c^2}[\dot{\rho} + \nabla \cdot \mathbf{J}]. \tag{37}$$

If the matter theory is such that the equation of continuity $\dot{\rho} = -\nabla \cdot \mathbf{J}$ is satisfied, then $\Box\Theta = 0$. So if $\Theta(t = 0) = \dot{\Theta}(t = 0) = 0$, then $\Theta(t) = 0$ at all times t. In other words, if the sources of charge and current satisfy the equation of continuity, then the dynamical theory arising from the Lagrangian (18) is the Maxwell theory of electrodynamics.

Note that while (28) and (32) do not enjoy the full gauge symmetry as do the general potential equations (4), this does not mean that the observables resulting from (28) or (32) are not gauge invariant. Any observable that is calculated will be invariant to the choice of gauge generator. Moreover, once the solutions to these well-defined equations are constructed, these solutions belong to the many solutions of (4). This family of solutions is the most general solutions of the potential form of Maxwell's equations. In fact, gauge transformations can even be made from one particular gauge to another [74]. A diagram depicting the relevant gauge story in the Hamiltonian formulation is presented in Fig. 2. Notice that there is no Hamiltonian theory that enjoys the full gauge symmetry of (4). The Hamiltonian $\mathcal{H}_{\text{Max}}$ in the far right column is obtained by a Legendre transformation of the gauge invariant Lagrangian $\mathcal{L}_{\text{Max}}$ in (20). However, the Hamiltonian dynamics stemming from the gauge invariant $\mathcal{L}_{\text{Max}}$ is not gauge invariant, but rather occurs in the gauge where $\dot{\Phi} = 0$.

2.2.2. Poisson bracket for electrodynamics

The phase space that carries the associated dynamics is naturally endowed with a Poisson bracket $\{\cdot, \cdot\}$. This may be seen by considering the variation of ξ along the dynamics $\Delta_H \equiv (\partial/\partial\boldsymbol{\eta})\dot{\boldsymbol{\eta}}$. That is

$$\Delta_H(\xi) \equiv (d/dt)\xi = \left(\partial\xi/\partial\eta^b\right)\dot{\eta}^b = \left(\partial\xi/\partial\eta^b\right)\omega^{-1}_{ab}\left(\partial H/\partial\eta^a\right) \equiv \{\xi, H\}, \tag{38}$$

where $\boldsymbol{\eta}$ are the generalized coordinates. In general, the Poisson bracket of the dynamical variable F with the dynamical variable G is

$$\{F, G\} = \begin{pmatrix} \partial F/\partial\mathbf{A} \\ \partial F/\partial\Phi \\ \partial F/\partial\boldsymbol{\Pi} \\ \partial F/\partial\Theta \end{pmatrix}^T \begin{pmatrix} 0 & 0 & -\mathbf{1} & 0 \\ 0 & 0 & 0 & -1 \\ \mathbf{1} & 0 & 0 & 0 \\ 0 & 1 & 0 & 0 \end{pmatrix}^{-1} \begin{pmatrix} \partial G/\partial\mathbf{A} \\ \partial G/\partial\Phi \\ \partial G/\partial\boldsymbol{\Pi} \\ \partial G/\partial\Theta \end{pmatrix}. \tag{39}$$

Since the symplectic form $\boldsymbol{\omega}$ is canonical its inverse is trivial, *i.e.*, $\boldsymbol{\omega}^{-1} = \boldsymbol{\omega}^T = -\boldsymbol{\omega}$. Also notice that $\boldsymbol{\omega}^2 = -\mathbf{1}$, $\boldsymbol{\omega}^T\boldsymbol{\omega} = \mathbf{1}$, and $\det\boldsymbol{\omega} = 1$.

2.3. Hamiltonian electrodynamics and wave mechanics in complex phase space

Consider the matter theory associated with the Schrödinger Lagrangian ($\hbar = 1$)

$$\mathcal{L}_{\text{Sch}} = i\Psi^*\dot{\Psi} - \frac{[i\nabla - q\mathbf{A}/c]\Psi^* \cdot [-i\nabla - q\mathbf{A}/c]\Psi}{2m} - V\Psi^*\Psi - q\Phi\Psi^*\Psi, \tag{17}$$

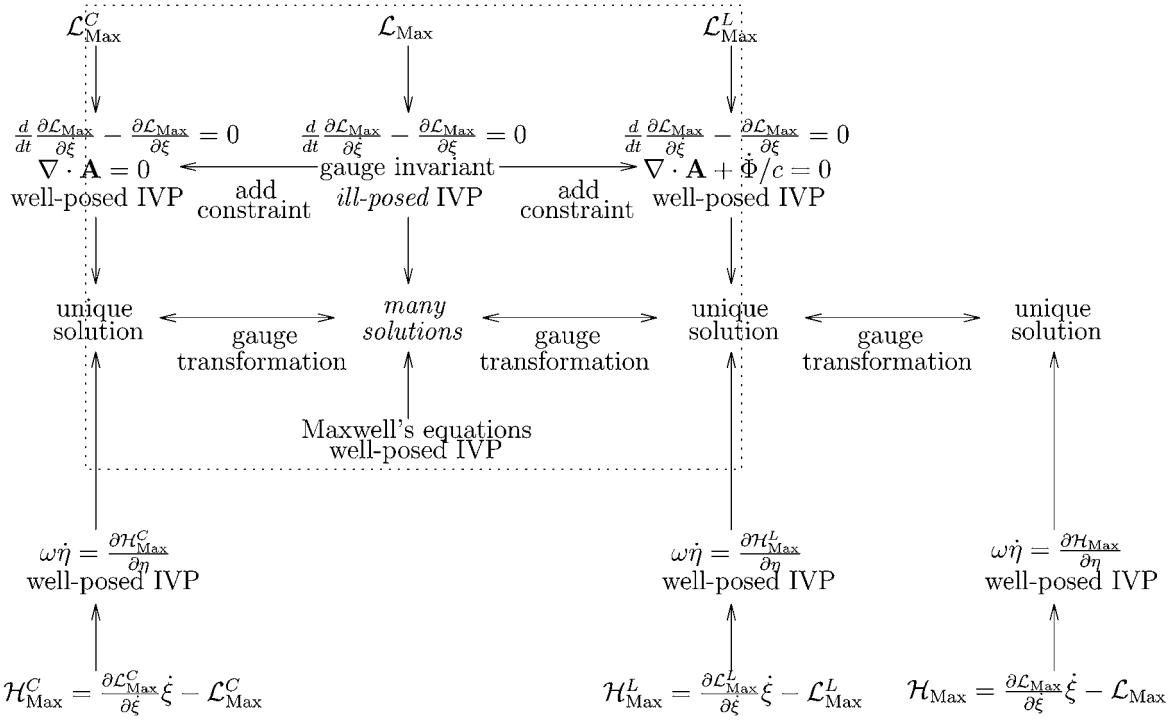

Fig. 2. The Hamiltonian formulation of the gauge story is organized in this picture with respect to the previous Lagrangian formulation. Figure 1 is depicted in the box with dotted borders. It can now be seen how the Coulomb and Lorenz gauges connect in both formalisms.

where Ψ is the wavefunction for a single electron, $V = q\bar{q}/|\mathbf{x}|$ is the static Coulomb potential energy of a proton, and $(\Phi, \mathbf{A})$ are the electron's scalar and vector potentials. Notice that this Lagrangian is already written in phase space. The momentum conjugate to the wavefunction Ψ is $i\Psi^*$. Together with the previous Maxwell Lagrangian, the coupled nonlinear dynamical theory arising from the Lagrangians

$$\mathcal{L}_{\text{Max}} = \frac{1}{2}[\mathbf{\Pi}\cdot\dot{\mathbf{A}} - \dot{\mathbf{\Pi}}\cdot\mathbf{A}] - \left\{\frac{[-4\pi c\mathbf{\Pi}]^2 + [\nabla\times\mathbf{A}]^2}{8\pi} - c\nabla\Phi\cdot\mathbf{\Pi}\right\}, \tag{40}$$

$$\mathcal{L}_{\text{Sch}} = \frac{i}{2}[\Psi^*\dot{\Psi} - \dot{\Psi}^*\Psi] - \left\{\frac{[i\nabla - q\mathbf{A}/c]\Psi^*\cdot[-i\nabla - q\mathbf{A}/c]\Psi}{2m} + V\Psi^*\Psi + q\Phi\Psi^*\Psi\right\}, \tag{41}$$

$$\mathcal{L}_{\text{gauge}} = \frac{1}{2}[\Theta\dot{\Phi} - \dot{\Theta}\Phi] - \left\{-2\pi c^2\Theta^2 - c\Theta\nabla\cdot\mathbf{A}\right\} \tag{42}$$

yields the following equations of motion:

$$\begin{aligned}
&\dot{\mathbf{A}} = 4\pi c^2\mathbf{\Pi} - c\nabla\Phi, && -\dot{\mathbf{\Pi}} = \frac{\nabla\times\nabla\times\mathbf{A}}{4\pi} - \frac{\mathbf{J}}{c} + c\nabla\Theta,\\
&\dot{\Phi} = -4\pi c^2\Theta - c\nabla\cdot\mathbf{A}, && -\dot{\Theta} = \rho + c\nabla\cdot\mathbf{\Pi},\\
&i\dot{\Psi} = \frac{[-i\nabla - q\mathbf{A}/c]^2\Psi}{2m} + V\Psi + q\Phi\Psi,\\
&-i\dot{\Psi}^* = \frac{[i\nabla - q\mathbf{A}/c]^2\Psi^*}{2m} + V\Psi^* + q\Phi\Psi^*.
\end{aligned} \tag{43}$$

Surface terms of the form $(d/dt)\{pq/2\}$ have been added in the above Lagrangians in order to symmetrize them, *i.e.*, $L = p\dot{q} - H - (d/dt)\{pq/2\}$ becomes $L = [p\dot{q} - \dot{p}q]/2 - H$. This can always be done since the action $I = \int L\,dt = \int[L + (d/dt)g]\,dt$ is invariant to the addition of a pure surface term to the Lagrangian. Note that the Schrödinger wavefunctions Ψ and Ψ^* are complex-valued while the remaining electromagnetic variables are all real-valued. These dynamical equations may be put into matrix form as

$$\begin{pmatrix} i & 0 & 0 & 0 & 0 & 0\\ 0 & -i & 0 & 0 & 0 & 0\\ 0 & 0 & 0 & 0 & -\mathbf{1} & 0\\ 0 & 0 & 0 & 0 & 0 & -1\\ 0 & 0 & \mathbf{1} & 0 & 0 & 0\\ 0 & 0 & 0 & 1 & 0 & 0 \end{pmatrix} \begin{pmatrix} \dot{\Psi}\\ \dot{\Psi}^*\\ \dot{\mathbf{A}}\\ \dot{\Phi}\\ \dot{\mathbf{\Pi}}\\ \dot{\Theta} \end{pmatrix} = \begin{pmatrix} [-i\nabla - q\mathbf{A}/c]^2\Psi/2m + V\Psi + q\Phi\Psi\\ [i\nabla - q\mathbf{A}/c]^2\Psi^*/2m + V\Psi^* + q\Phi\Psi^*\\ \nabla\times\nabla\times\mathbf{A}/4\pi - \mathbf{J}/c + c\nabla\Theta\\ \rho + c\nabla\cdot\mathbf{\Pi}\\ 4\pi c^2\mathbf{\Pi} - c\nabla\Phi\\ -4\pi c^2\Theta - c\nabla\cdot\mathbf{A} \end{pmatrix}, \tag{44}$$

where the symplectic form is canonical. The electromagnetic sector of it is identical to (33). These dynamical equations define the coupled Maxwell–Schrödinger theory. This theory is well defined and closed. In other words, the dynamics of the charges, currents, and fields are all specified as well as their mutual interaction. Given initial values for Ψ, Ψ^*, $\mathbf{A}$, $\mathbf{\Pi}$, Φ, and Θ determines their coupled dynamics throughout space–time.

With the dynamics of the charges defined, the problem in (36) can now be addressed. The Schrödinger equation in (43) implies the continuity equation

$$(d/dt)q\Psi^*\Psi = -\nabla\cdot q\big\{\Psi^*[-i\nabla - q\mathbf{A}/c]\Psi + \Psi[i\nabla - q\mathbf{A}/c]\Psi^*\big\}/2m \tag{45}$$

which may be written more compactly as $\dot\rho = -\nabla\cdot\mathbf{J}$. From the definition of the momentum Θ in (30) and the wave equations $\Box\Phi = -4\pi\rho$ and $\Box\mathbf{A} = -4\pi\mathbf{J}/c$, notice that

$$\begin{aligned}\Box\Theta &= \frac{-1}{4\pi c}\big[(d/dt)\Box\Phi/c + \nabla\cdot\Box\mathbf{A}\big]\\ &= \frac{1}{4\pi c}\big[(d/dt)4\pi\rho/c + \nabla\cdot 4\pi\mathbf{J}/c\big] = \frac{1}{c^2}[\dot\rho + \nabla\cdot\mathbf{J}] = 0\end{aligned} \tag{46}$$

by appealing to (45). So if $\Theta(t=0) = \dot\Theta(t=0) = 0$, then the electrodynamics stays in the Lorenz gauge for all time since the only solution of $\Box\Theta = 0$ with $\Theta(t=0) = \dot\Theta(t=0) = 0$ is $\Theta(t) = 0$.

It is worth mentioning that if $\dot\Theta(t=0) = 0$ for all time, then the electron–electron self interaction makes no contribution to the Schrödinger energy. This is true since the self interaction term $q\Phi\Psi^*\Psi$ in the above Schrödinger Lagrangian cancels exactly with $-c\nabla\Phi\cdot\mathbf{\Pi}$ in the Maxwell Lagrangian. The cancellation requires a partial integration of $-c\nabla\Phi\cdot\mathbf{\Pi}$ to $c\Phi\nabla\cdot\mathbf{\Pi}$ followed by a substitution of $0 = \rho + c\nabla\cdot\mathbf{\Pi}$ from $\dot\Theta(t=0) = 0$ in (43). However, there is still a contribution from the self-energy arising in the Maxwell energy of the Coulombic field.

2.4. Hamiltonian electrodynamics and wave mechanics in real phase space

The dynamical equations (111) are mixed, real and complex. For consistency these equations are put into real form with the Lagrangian densities:

$$\mathcal{L}_{\text{Max}} = \frac{1}{2}[\mathbf{\Pi}\cdot\dot{\mathbf{A}} - \dot{\mathbf{\Pi}}\cdot\mathbf{A}] - \left\{\frac{[-4\pi c\mathbf{\Pi}]^2 + [\nabla\times\mathbf{A}]^2}{8\pi} - c\nabla\Phi\cdot\mathbf{\Pi}\right\}, \tag{47}$$

$$\mathcal{L}_{\text{Sch}} = \frac{1}{2}[P\dot Q - \dot P Q] - \begin{Bmatrix}\{[\nabla Q + q\mathbf{A}P/c]^2 + [-\nabla P + q\mathbf{A}Q/c]^2\}/4m\\ + V[Q^2+P^2]/2 + q\Phi[Q^2+P^2]/2\end{Bmatrix}, \tag{48}$$

$$\mathcal{L}_{\text{gauge}} = \frac{1}{2}[\Theta\dot\Phi - \dot\Theta\Phi] - \big\{-2\pi c^2\Theta^2 - c\Theta\nabla\cdot\mathbf{A}\big\}. \tag{49}$$

The functions P and Q are related to the real and imaginary parts of Ψ and Ψ^* according to $\Psi = [Q + iP]/\sqrt{2}$ and $\Psi^* = [Q - iP]/\sqrt{2}$. The equations of motion that are associated with these Lagrangians are:

$$\begin{aligned}\dot{\mathbf{A}} &= 4\pi c^2\mathbf{\Pi} - c\nabla\Phi, & -\dot{\mathbf{\Pi}} &= \frac{\nabla\times\nabla\times\mathbf{A}}{4\pi} - \frac{\mathbf{J}}{c} + c\nabla\Theta,\\ \dot\Phi &= -4\pi c^2\Theta - c\nabla\cdot\mathbf{A}, & -\dot\Theta &= \rho + c\nabla\cdot\mathbf{\Pi},\end{aligned} \tag{50a}$$

$$\begin{aligned}\dot Q &= \frac{-\nabla^2 P + q\nabla\cdot(\mathbf{A}Q)/c + q\mathbf{A}\cdot\nabla Q/c + q^2\mathbf{A}^2P/c^2}{2m} + VP + q\Phi P,\\ -\dot P &= -\frac{\nabla^2 Q + q\nabla\cdot(\mathbf{A}P)/c + q\nabla P\cdot\mathbf{A}/c - q^2\mathbf{A}^2Q/c^2}{2m} + VQ + q\Phi Q.\end{aligned} \tag{50b}$$

These dynamical equations may be put into matrix form as

$$\begin{pmatrix} 0 & 0 & 0 & -\mathbf{1} & 0 & 0 \\ 0 & 0 & 0 & 0 & -1 & 0 \\ 0 & 0 & 0 & 0 & 0 & -1 \\ \mathbf{1} & 0 & 0 & 0 & 0 & 0 \\ 0 & 1 & 0 & 0 & 0 & 0 \\ 0 & 0 & 1 & 0 & 0 & 0 \end{pmatrix} \begin{pmatrix} \dot{\mathbf{A}} \\ \dot{\Phi} \\ \dot{Q} \\ \dot{\mathbf{\Pi}} \\ \dot{\Theta} \\ \dot{P} \end{pmatrix} = \begin{pmatrix} \nabla \times \nabla \times \mathbf{A}/4\pi - \mathbf{J}/c + c\nabla\Theta \\ \rho + c\nabla \cdot \mathbf{\Pi} \\ -[\nabla^2 Q + q\nabla \cdot (\mathbf{A}P)/c + q\nabla P \cdot \mathbf{A}/c - q^2\mathbf{A}^2 Q/c^2]/2m + VQ + q\Phi Q \\ 4\pi c^2 \mathbf{\Pi} - c\nabla\Phi \\ -4\pi c^2\Theta - c\nabla \cdot \mathbf{A} \\ [-\nabla^2 P + q\nabla \cdot (\mathbf{A}Q)/c + q\mathbf{A} \cdot \nabla Q/c + q^2\mathbf{A}^2 P/c^2]/2m + VP + q\Phi P \end{pmatrix}, \tag{51}$$

where the symplectic form is again canonical. Note that the equation of continuity $\dot{\rho} = -\nabla \cdot \mathbf{J}$ still holds with the real charge and current densities

$$\begin{aligned} \rho &= q\big[Q^2 + P^2\big]/2, \\ \mathbf{J} &= \frac{q}{2m}\{Q\nabla P - P\nabla Q - qQ\mathbf{A}Q/c - qP\mathbf{A}P/c\}. \end{aligned} \tag{52}$$

2.5. The Coulomb reference by canonical transformation

As was mentioned previously the numerical implementation of the theory can be made to converge more quickly if the basis is chosen judiciously. Recall that the electromagnetic field generated by any charge contains a Coulombic contribution. This monopole term accounts for a large portion of the local electromagnetic field surrounding the charge. It would be advantageous not to describe this large contribution in terms of the basis but rather to calculate its dynamics analytically. The remaining smaller portion of the radiative or dynamical electromagnetic field can then be described in terms of the basis.

To this end, notice that the scalar potential $\Phi = \Phi_C + (\Phi - \Phi_C) \equiv \Phi_C + \Phi_D$ may be split into a Coulombic portion satisfying $\nabla^2\Phi_C = -4\pi\rho$ that can be calculated analytically and a remainder Φ_D regardless of the choice of gauge. The Coulombic potential is not itself a dynamical variable but depends on the dynamical variables Q and P. That is $\Phi_C(\mathbf{x}, t) = \int_V d^3x' |\mathbf{x} - \mathbf{x}'|^{-1} q[Q(\mathbf{x}', t)Q(\mathbf{x}', t) + P(\mathbf{x}', t)P(\mathbf{x}', t)]/2$. The dynamical portion Φ_D is a generalized coordinate and is represented in the basis. Similarly, the momentum conjugate to $\mathbf{A}$ may be split into a Coulombic and dynamical piece according to

$$\mathbf{\Pi} \equiv \frac{\partial \mathcal{L}_{\text{Max}}}{\partial \dot{\mathbf{A}}} = \mathbf{\Pi}_C + \mathbf{\Pi}_D = \frac{\nabla\Phi_C}{4\pi c} + \frac{1}{4\pi c}[\dot{\mathbf{A}}/c + \nabla\Phi_D]. \tag{53}$$

Like Φ_D, the dynamical portion $\mathbf{\Pi}_D$ is a generalized coordinate and is represented in the basis.

2.5.1. Symplectic transformation to the Coulomb reference

The transformation to these new coordinates, *i.e.*, Φ_D and $\mathbf{\Pi}_D$, is obtained by the canonical or symplectic transformation

$$\mathbf{T}: \begin{pmatrix} \mathbf{A} \\ \Phi \\ Q \\ \mathbf{\Pi} \\ \Theta \\ P \end{pmatrix} \to \begin{pmatrix} \tilde{\mathbf{A}}(\mathbf{A}) \\ \tilde{\Phi}(\Phi, Q, P) \\ \tilde{Q}(Q) \\ \tilde{\mathbf{\Pi}}(\mathbf{\Pi}, Q, P) \\ \tilde{\Theta}(\Theta) \\ \tilde{P}(P) \end{pmatrix} = \begin{pmatrix} \mathbf{A} \\ \Phi - \Phi_C(Q, P) \\ Q \\ \mathbf{\Pi} - \mathbf{\Pi}_C(Q, P) \\ \Theta \\ P \end{pmatrix}, \tag{54}$$

where $\tilde{\Phi} \equiv \Phi_D$ and $\tilde{\mathbf{\Pi}} \equiv \mathbf{\Pi}_D$. The variables Q, P, $\mathbf{A}$, and Θ are unchanged by $\mathbf{T}$. Since both Φ_C and $\mathbf{\Pi}_C$ are complicated functions of Q and P, the inversion of $\mathbf{T}$ may be quite involved. However, it will be shown that the inverse of $\mathbf{T}$ does exist. In fact both the $\mathbf{T}$ and $\mathbf{T}^{-1}$ are differentiable mappings on symplectic manifolds. Therefore the canonical transformation is a symplectic diffeomorphism or symplectomorphism [29].

The theory of restricted (explicitly time-independent) canonical transformations [27,28] gives the general prescription for the transformation of the old Hamilton equations (51) to the new Hamilton equations in terms of $\mathbf{T}$ (and $\mathbf{T}^T$) only. In symbols, that is

$$\dot{\boldsymbol{\eta}} = \boldsymbol{\omega}^{-1} \frac{\partial H}{\partial \boldsymbol{\eta}} \to \dot{\tilde{\boldsymbol{\eta}}} = \tilde{\boldsymbol{\omega}}^{-1} \frac{\partial \tilde{H}}{\partial \tilde{\boldsymbol{\eta}}}, \tag{55}$$

where the new Hamiltonian $\tilde{H}$ is equivalent to the old Hamiltonian H expressed in terms of the new variables $\tilde{\boldsymbol{\eta}}$. (For simplicity $\tilde{H}$ will be written as H from this point forward.) To this end, consider the time derivative of the new column matrix

$$\dot{\tilde{\eta}}_i = \frac{\partial \tilde{\eta}_i}{\partial \eta_j} \dot{\eta}_j \equiv T_{ij} \dot{\eta}_j \quad \text{or} \quad \dot{\tilde{\boldsymbol{\eta}}} = \mathbf{T} \dot{\boldsymbol{\eta}}. \tag{56}$$

Substituting $\dot{\boldsymbol{\eta}}$ from (55) results in

$$\dot{\tilde{\eta}}_i = T_{ij} \omega^{-1}_{jk} \frac{\partial H}{\partial \eta_k} \quad \text{or} \quad \dot{\tilde{\boldsymbol{\eta}}} = \mathbf{T} \boldsymbol{\omega}^{-1} \frac{\partial H}{\partial \boldsymbol{\eta}}. \tag{57}$$

Lastly the column matrix $\partial H / \partial \boldsymbol{\eta}$ can be written as

$$\frac{\partial H}{\partial \eta_k} = \frac{\partial H}{\partial \tilde{\eta}_l} \frac{\partial \tilde{\eta}_l}{\partial \eta_k} \equiv T^T_{kl} \frac{\partial H}{\partial \tilde{\eta}_l} \quad \text{or} \quad \frac{\partial H}{\partial \boldsymbol{\eta}} = \mathbf{T}^T \frac{\partial H}{\partial \tilde{\boldsymbol{\eta}}} \tag{58}$$

so that the new equations of motion (57) become

$$\dot{\tilde{\eta}}_i = T_{ij} \omega^{-1}_{jk} T^T_{kl} \frac{\partial H}{\partial \tilde{\eta}_l} \quad \text{or} \quad \dot{\tilde{\boldsymbol{\eta}}} = \mathbf{T} \boldsymbol{\omega}^{-1} \mathbf{T}^T \frac{\partial H}{\partial \tilde{\boldsymbol{\eta}}} \equiv \tilde{\boldsymbol{\omega}}^{-1} \frac{\partial H}{\partial \tilde{\boldsymbol{\eta}}}. \tag{59}$$

This canonical transformation on the equations of motion leaves only the computation of $\tilde{\boldsymbol{\omega}}^{-1} \equiv \mathbf{T} \boldsymbol{\omega}^{-1} \mathbf{T}^T$ since the Hamiltonian automatically becomes

$$\mathcal{H} = \frac{[-4\pi c\{\tilde{\mathbf{\Pi}} + \mathbf{\Pi}_C(\tilde{Q}, \tilde{P})\}]^2 + [\nabla \times \tilde{\mathbf{A}}]^2 - [4\pi c \tilde{\Theta}]^2}{8\pi} + q\big[\tilde{\Phi} + \Phi_C(\tilde{Q}, \tilde{P})\big] \frac{\tilde{Q}^2 + \tilde{P}^2}{2}$$

$$
\begin{aligned}
&- c\nabla\big[\tilde{\Phi} + \Phi_C(\tilde{Q}, \tilde{P})\big] \cdot \big[\tilde{\mathbf{\Pi}} + \mathbf{\Pi}_C(\tilde{Q}, \tilde{P})\big] - c\tilde{\Theta}\nabla \cdot \tilde{\mathbf{A}} \\
&+ \frac{[\nabla\tilde{Q} + q\tilde{\mathbf{A}}\tilde{P}/c]^2 + [-\nabla\tilde{P} + q\tilde{\mathbf{A}}\tilde{Q}/c]^2}{4m} + V\frac{\tilde{Q}^2 + \tilde{P}^2}{2}
\end{aligned} \tag{60}
$$

in terms of the new coordinates. However, the inversion of $\boldsymbol{\omega}$ is not simple in practice. It turns out that the equations of motion (55) are most practically written as

$$
\frac{\partial H}{\partial \tilde{\boldsymbol{\eta}}} = \tilde{\boldsymbol{\omega}}\dot{\tilde{\boldsymbol{\eta}}} = \big(\mathbf{T}^{-1}\big)^T \boldsymbol{\omega}\mathbf{T}^{-1}\dot{\tilde{\boldsymbol{\eta}}} \quad \text{not} \quad \dot{\tilde{\boldsymbol{\eta}}} = \tilde{\boldsymbol{\omega}}^{-1}\frac{\partial H}{\partial \tilde{\boldsymbol{\eta}}} = \mathbf{T}\boldsymbol{\omega}^{-1}\mathbf{T}^T\frac{\partial H}{\partial \tilde{\boldsymbol{\eta}}}, \tag{61}
$$

where the inverse transformation $\mathbf{T}^{-1}$ is the transformation of the inverse mapping, *i.e.*, $T^{-1}_{ij} \equiv \partial\eta_i/\partial\tilde{\eta}_j$. It will be shown that $\det\mathbf{T} \neq 0$ so the mapping is well defined. These equations of motion are of the desired form because they involve $\boldsymbol{\omega}$ and not $\boldsymbol{\omega}^{-1}$. That $\boldsymbol{\omega}^{-1}$ is undesirable is seen by going to the basis. In the basis, the canonical symplectic form becomes

$$
\begin{pmatrix} 0 & -1 \\ 1 & 0 \end{pmatrix} \to \begin{pmatrix} 0 & -\frac{\partial^2\langle Q|P\rangle}{\partial q_{\mathcal{K}}\partial p_{\mathcal{J}}} \\ \frac{\partial^2\langle P|Q\rangle}{\partial p_{\mathcal{K}}\partial q_{\mathcal{J}}} & 0 \end{pmatrix} \tag{62}
$$

which is not easily inverted. As a result it is simpler to compute $(\mathbf{T}^{-1})^T\boldsymbol{\omega}\mathbf{T}^{-1}$ than $\mathbf{T}\boldsymbol{\omega}^{-1}\mathbf{T}^T$ even though $\mathbf{T}^{-1}$ is needed in the former case. It will be shown that the explicit evaluation of $\mathbf{T}^{-1}$ is not necessary.

To continue with the transformed equations of motion in (61), which only require $\boldsymbol{\omega}$, the mapping $(\mathbf{T}^{-1})^T : \partial/\partial\boldsymbol{\eta} \to \partial/\partial\tilde{\boldsymbol{\eta}}$ must first be set up. The transposed inverse transformation $(\mathbf{T}^{-1})^T$ is defined on the vector fields themselves according to

$$
\begin{pmatrix} \partial/\partial\tilde{\mathbf{A}} \\ \partial/\partial\tilde{\Phi} \\ \partial/\partial\tilde{Q} \\ \partial/\partial\tilde{\mathbf{\Pi}} \\ \partial/\partial\tilde{\Theta} \\ \partial/\partial\tilde{P} \end{pmatrix}
= \begin{pmatrix}
\partial\mathbf{A}/\partial\tilde{\mathbf{A}} & 0 & 0 & 0 & 0 & 0 \\
0 & \partial\Phi/\partial\tilde{\Phi} & 0 & 0 & 0 & 0 \\
0 & \partial\Phi/\partial\tilde{Q} & \partial Q/\partial\tilde{Q} & \partial\mathbf{\Pi}/\partial\tilde{Q} & 0 & 0 \\
0 & 0 & 0 & \partial\mathbf{\Pi}/\partial\tilde{\mathbf{\Pi}} & 0 & 0 \\
0 & 0 & 0 & 0 & \partial\Theta/\partial\tilde{\Theta} & 0 \\
0 & \partial\Phi/\partial\tilde{P} & 0 & \partial\mathbf{\Pi}/\partial\tilde{P} & 0 & \partial P/\partial\tilde{P}
\end{pmatrix}
\begin{pmatrix} \partial/\partial\mathbf{A} \\ \partial/\partial\Phi \\ \partial/\partial Q \\ \partial/\partial\mathbf{\Pi} \\ \partial/\partial\Theta \\ \partial/\partial P \end{pmatrix}. \tag{63}
$$

Notice that

$$
\begin{aligned}
\det\big(\mathbf{T}^{-1}\big)^T &= \det\mathbf{T}^{-1} = (\det\mathbf{T})^{-1} \equiv \frac{\partial(\mathbf{A}, \Phi, Q, \mathbf{\Pi}, \Theta, P)}{\partial(\tilde{\mathbf{A}}, \tilde{\Phi}, \tilde{Q}, \tilde{\mathbf{\Pi}}, \tilde{\Theta}, \tilde{P})} \\
&= (\partial\tilde{\mathbf{A}}/\partial\mathbf{A})(\partial\tilde{\Phi}/\partial\Phi)(\partial\tilde{Q}/\partial Q)(\partial\tilde{\mathbf{\Pi}}/\partial\mathbf{\Pi})(\partial\tilde{\Theta}/\partial\Theta)(\partial\tilde{P}/\partial P) = 1
\end{aligned} \tag{64}
$$

so that the transformation is canonical and symplectic or area preserving. In other words, the new infinitesimal volume element $d\tilde{\boldsymbol{\eta}}$ is related to the old infinitesimal volume element $d\boldsymbol{\eta}$ by

$$
d\tilde{\boldsymbol{\eta}} = \det\mathbf{T}\, d\boldsymbol{\eta} = d\boldsymbol{\eta} \tag{65}
$$

since the determinant of the Jacobian is unity. Thus, the volume element of phase space is the same before and after the transformation. It is a canonical invariant.

With $(\mathbf{T}^{-1})^T$ the similarity transformation of the canonical symplectic form in (51) becomes

$$\tilde{\boldsymbol{\omega}} \equiv \left(\mathbf{T}^{-1}\right)^T \boldsymbol{\omega} \mathbf{T}^{-1} = \begin{pmatrix} \boldsymbol{\Omega}_M & \boldsymbol{\Omega}^{>} \\ \boldsymbol{\Omega}^{\vee} & \boldsymbol{\Omega}_G \end{pmatrix}, \tag{66}$$

where

$$\boldsymbol{\Omega}^{>} = \begin{pmatrix} \frac{\partial \mathbf{A}}{\partial \tilde{\mathbf{A}}}(-\mathbf{1})\frac{\partial \boldsymbol{\Pi}}{\partial \tilde{\boldsymbol{\Pi}}} & 0 & -\frac{\partial \mathbf{A}}{\partial \tilde{\mathbf{A}}}\frac{\partial \boldsymbol{\Pi}}{\partial \tilde{P}} \\ 0 & \frac{\partial \Phi}{\partial \tilde{\Phi}}(-1)\frac{\partial \Theta}{\partial \tilde{\Theta}} & 0 \\ 0 & -\frac{\partial \Phi}{\partial \tilde{Q}}\frac{\partial \Theta}{\partial \tilde{\Theta}} & \frac{\partial Q}{\partial \tilde{Q}}(-1)\frac{\partial P}{\partial \tilde{P}} \end{pmatrix}, \tag{67}$$

$$\boldsymbol{\Omega}^{\vee} = \begin{pmatrix} \frac{\partial \boldsymbol{\Pi}}{\partial \tilde{\boldsymbol{\Pi}}}(\mathbf{1})\frac{\partial \mathbf{A}}{\partial \tilde{\mathbf{A}}} & 0 & 0 \\ 0 & \frac{\partial \Theta}{\partial \tilde{\Theta}}(1)\frac{\partial \Phi}{\partial \tilde{\Phi}} & \frac{\partial \Theta}{\partial \tilde{\Theta}}\frac{\partial \Phi}{\partial \tilde{Q}} \\ \frac{\partial \boldsymbol{\Pi}}{\partial \tilde{P}}\frac{\partial \mathbf{A}}{\partial \tilde{\mathbf{A}}} & 0 & \frac{\partial P}{\partial \tilde{P}}(1)\frac{\partial Q}{\partial \tilde{Q}} \end{pmatrix}, \tag{68}$$

$$\boldsymbol{\Omega}_M = \begin{pmatrix} 0 & 0 & -\frac{\partial \mathbf{A}}{\partial \tilde{\mathbf{A}}}\frac{\partial \boldsymbol{\Pi}}{\partial \tilde{Q}} \\ 0 & 0 & 0 \\ \frac{\partial \boldsymbol{\Pi}}{\partial \tilde{Q}}\frac{\partial \mathbf{A}}{\partial \tilde{\mathbf{A}}} & 0 & 0 \end{pmatrix}, \tag{69}$$

$$\boldsymbol{\Omega}_G = \begin{pmatrix} 0 & 0 & 0 \\ 0 & 0 & \frac{\partial \Theta}{\partial \tilde{\Theta}}\frac{\partial \Phi}{\partial \tilde{P}} \\ 0 & -\frac{\partial \Phi}{\partial \tilde{P}}\frac{\partial \Theta}{\partial \tilde{\Theta}} & 0 \end{pmatrix}. \tag{70}$$

The factors of 1 and -1 are explicitly written in $\boldsymbol{\Omega}^{>}$ and $\boldsymbol{\Omega}^{\vee}$ to bring out their similarity to the canonical symplectic form in (51). After computing the derivatives in $\tilde{\boldsymbol{\omega}}$ it can be shown that

$$\tilde{\boldsymbol{\omega}} = \begin{pmatrix} 0 & 0 & -\frac{\partial \boldsymbol{\Pi}_C(\tilde{Q},\tilde{P})}{\partial \tilde{Q}} & -\mathbf{1} & 0 & -\frac{\partial \boldsymbol{\Pi}_C(\tilde{Q},\tilde{P})}{\partial \tilde{P}} \\ 0 & 0 & 0 & 0 & -1 & 0 \\ \frac{\partial \boldsymbol{\Pi}_C(\tilde{Q},\tilde{P})}{\partial \tilde{Q}} & 0 & 0 & 0 & -\frac{\partial \Phi_C(\tilde{Q},\tilde{P})}{\partial \tilde{Q}} & -1 \\ \mathbf{1} & 0 & 0 & 0 & 0 & 0 \\ 0 & 1 & \frac{\partial \Phi_C(\tilde{Q},\tilde{P})}{\partial \tilde{Q}} & 0 & 0 & \frac{\partial \Phi_C(\tilde{Q},\tilde{P})}{\partial \tilde{P}} \\ \frac{\partial \boldsymbol{\Pi}_C(\tilde{Q},\tilde{P})}{\partial \tilde{P}} & 0 & 1 & 0 & -\frac{\partial \Phi_C(\tilde{Q},\tilde{P})}{\partial \tilde{P}} & 0 \end{pmatrix} \tag{71}$$

with

$$\Phi_C(\mathbf{x},t) = \frac{q}{2}\int_V \frac{Q(\mathbf{x}',t)^2 + P(\mathbf{x}',t)^2}{|\mathbf{x}-\mathbf{x}'|}\, d^3x' \tag{72}$$

and

$$\boldsymbol{\Pi}_C(\mathbf{x},t) = \frac{q}{8\pi c}\nabla \int_V \frac{Q(\mathbf{x}',t)^2 + P(\mathbf{x}',t)^2}{|\mathbf{x}-\mathbf{x}'|}\, d^3x'. \tag{73}$$

And so the new symplectic form contains extra elements that are not present in the canon-

ical $\boldsymbol{\omega}$. These extra elements add additional time-dependent couplings to the theory. As before, the associated phase space has the Poisson bracket

$$\{F, G\}_{\tilde{\boldsymbol{\eta}}} = (\partial F/\partial\tilde{\boldsymbol{\eta}})^T \tilde{\boldsymbol{\omega}}^{-1} (\partial G/\partial\tilde{\boldsymbol{\eta}}). \tag{74}$$

The transformed equations of motion with symplectic form (71) may be written in full as:

$$\begin{aligned}
&-\frac{\partial \boldsymbol{\Pi}_C}{\partial \tilde{Q}}\dot{\tilde{Q}} - \dot{\tilde{\boldsymbol{\Pi}}} - \frac{\partial \boldsymbol{\Pi}_C}{\partial \tilde{P}}\dot{\tilde{P}} = \frac{\partial H}{\partial \tilde{\mathbf{A}}} \\
&\quad = \frac{\nabla\times\nabla\times\tilde{\mathbf{A}}}{4\pi} + c\nabla\tilde{\Theta} - \frac{q}{2mc}\left\{\tilde{Q}\nabla\tilde{P} - \tilde{P}\nabla\tilde{Q} - \frac{q}{c}\tilde{Q}\tilde{\mathbf{A}}\tilde{Q} - \frac{q}{c}\tilde{P}\tilde{\mathbf{A}}\tilde{P}\right\}, \\
&-\dot{\tilde{\Theta}} = \frac{\partial H}{\partial \tilde{\Phi}} = q\frac{\tilde{Q}^2+\tilde{P}^2}{2} + c\nabla\cdot[\tilde{\boldsymbol{\Pi}} + \boldsymbol{\Pi}_C], \\
&\frac{\partial \boldsymbol{\Pi}_C}{\partial \tilde{Q}}\cdot\dot{\tilde{\mathbf{A}}} - \frac{\partial \Phi_C}{\partial \tilde{Q}}\dot{\tilde{\Theta}} - \dot{\tilde{P}} = \frac{\partial H}{\partial \tilde{Q}} \\
&\quad = \frac{-\nabla^2\tilde{Q} - \frac{q}{c}\nabla\cdot(\tilde{\mathbf{A}}\tilde{P}) - \frac{q}{c}\nabla\tilde{P}\cdot\tilde{\mathbf{A}} + \frac{q^2}{c^2}\tilde{\mathbf{A}}^2\tilde{Q}}{2m} \\
&\qquad + V\tilde{Q} + q[\tilde{\Phi} + \Phi_C]\tilde{Q} + \left\{4\pi c^2[\tilde{\boldsymbol{\Pi}} + \boldsymbol{\Pi}_C] - c\nabla[\tilde{\Phi} + \Phi_C]\right\}\cdot\frac{\partial \boldsymbol{\Pi}_C}{\partial \tilde{Q}} \\
&\qquad + \left\{q\frac{\tilde{Q}^2+\tilde{P}^2}{2} + c\nabla\cdot[\tilde{\boldsymbol{\Pi}} + \boldsymbol{\Pi}_C]\right\}\frac{\partial \Phi_C}{\partial \tilde{Q}}, \\
&\dot{\tilde{\mathbf{A}}} = \frac{\partial H}{\partial \tilde{\boldsymbol{\Pi}}} = 4\pi c^2[\tilde{\boldsymbol{\Pi}} + \boldsymbol{\Pi}_C] - c\nabla[\tilde{\Phi} + \Phi_C], \\
&\dot{\tilde{\Phi}} + \frac{\partial \Phi_C}{\partial \tilde{Q}}\dot{\tilde{Q}} + \frac{\partial \Phi_C}{\partial \tilde{P}}\dot{\tilde{P}} = \frac{\partial H}{\partial \tilde{\Theta}} = -4\pi c^2\tilde{\Theta} - c\nabla\cdot\tilde{\mathbf{A}}, \\
&\frac{\partial \boldsymbol{\Pi}_C}{\partial \tilde{P}}\cdot\dot{\tilde{\mathbf{A}}} + \dot{\tilde{Q}} - \frac{\partial \Phi_C}{\partial \tilde{P}}\dot{\tilde{\Theta}} = \frac{\partial H}{\partial \tilde{P}} \\
&\quad = \frac{-\nabla^2\tilde{P} + \frac{q}{c}\nabla\cdot(\tilde{\mathbf{A}}\tilde{Q}) + \frac{q}{c}\tilde{\mathbf{A}}\cdot\nabla\tilde{Q} + \frac{q^2}{c^2}\tilde{\mathbf{A}}^2\tilde{P}}{2m} \\
&\qquad + V\tilde{P} + q[\tilde{\Phi} + \Phi_C]\tilde{P} + \left\{4\pi c^2[\tilde{\boldsymbol{\Pi}} + \boldsymbol{\Pi}_C] - c\nabla[\tilde{\Phi} + \Phi_C]\right\}\cdot\frac{\partial \boldsymbol{\Pi}_C}{\partial \tilde{P}} \\
&\qquad + \left\{q\frac{\tilde{Q}^2+\tilde{P}^2}{2} + c\nabla\cdot[\tilde{\boldsymbol{\Pi}} + \boldsymbol{\Pi}_C]\right\}\frac{\partial \Phi_C}{\partial \tilde{P}},
\end{aligned} \tag{75}$$

where $\boldsymbol{\Pi}_C \equiv \boldsymbol{\Pi}_C(\tilde{Q}, \tilde{P})$ and $\Phi_C \equiv \Phi_C(\tilde{Q}, \tilde{P})$. The forces appearing on the right-hand side of these equations have become more complicated, especially those in the Schrödinger equations. There are new nonlinear terms. However, it is possible to substitute these equations among themselves in order to simplify them. Notice that parts of the $\partial H/\partial\tilde{\Phi}$ and $\partial H/\partial\tilde{\boldsymbol{\Pi}}$ equations appear in the forces of the Schrödinger equations. Substitution of $\partial H/\partial\tilde{\Phi}$ and $\partial H/\partial\tilde{\boldsymbol{\Pi}}$ into the Schrödinger equations results in the following simplified equations:

$$
\begin{aligned}
&-\frac{\partial \mathbf{\Pi}_C}{\partial \tilde{Q}}\dot{\tilde{Q}} - \dot{\tilde{\mathbf{\Pi}}} - \frac{\partial \mathbf{\Pi}_C}{\partial \tilde{P}}\dot{\tilde{P}} \\
&\quad = \frac{\nabla \times [\nabla \times \tilde{\mathbf{A}}]}{4\pi} + c\nabla\tilde{\Theta} - \frac{q}{2mc}\left\{\tilde{Q}\nabla\tilde{P} - \tilde{P}\nabla\tilde{Q} - \frac{q}{c}\tilde{Q}\tilde{\mathbf{A}}\tilde{Q} - \frac{q}{c}\tilde{P}\tilde{\mathbf{A}}\tilde{P}\right\}, \\
&-\dot{\tilde{\Theta}} = q\frac{\tilde{Q}^2 + \tilde{P}^2}{2} + c\nabla\cdot[\tilde{\mathbf{\Pi}} + \mathbf{\Pi}_C], \\
&-\dot{\tilde{P}} = -\frac{\nabla^2\tilde{Q} + q\nabla\cdot(\tilde{\mathbf{A}}\tilde{P})/c + q\nabla\tilde{P}\cdot\tilde{\mathbf{A}}/c - q^2\tilde{\mathbf{A}}^2\tilde{Q}/c^2}{2m} \\
&\qquad + V\tilde{Q} + q[\tilde{\Phi} + \Phi_C]\tilde{Q}, \\
&\dot{\tilde{\mathbf{A}}} = 4\pi c^2[\tilde{\mathbf{\Pi}} + \mathbf{\Pi}_C] - c\nabla[\tilde{\Phi} + \Phi_C], \\
&\dot{\tilde{\Phi}} + \frac{\partial \Phi_C}{\partial \tilde{Q}}\dot{\tilde{Q}} + \frac{\partial \Phi_C}{\partial \tilde{P}}\dot{\tilde{P}} = -4\pi c^2\tilde{\Theta} - c\nabla\cdot\tilde{\mathbf{A}}, \\
&\dot{\tilde{Q}} = \frac{-\nabla^2\tilde{P} + q\nabla\cdot(\tilde{\mathbf{A}}\tilde{Q})/c + q\tilde{\mathbf{A}}\cdot\nabla\tilde{Q}/c + q^2\tilde{\mathbf{A}}^2\tilde{P}/c^2}{2m} \\
&\qquad + V\tilde{P} + q[\tilde{\Phi} + \Phi_C]\tilde{P}.
\end{aligned}
\tag{76}
$$

The generalized forces appearing on the right-hand side are now very similar to the forces in (50). In fact, the equations of motion 76 can be further simplified to read:

$$
\begin{aligned}
&-\left[\dot{\mathbf{\Pi}} + \dot{\mathbf{\Pi}}_C(Q,P)\right] = \partial H/\partial \mathbf{A}, && \dot{\mathbf{A}} = \partial H/\partial \mathbf{\Pi}, \\
&-\dot{\Theta} = \partial H/\partial \Phi, && \dot{\Phi} + \dot{\Phi}_C(Q,P) = \partial H/\partial \Theta, \\
&-\dot{P} = \partial H/\partial Q, && \dot{Q} = \partial H/\partial P,
\end{aligned}
\tag{77}
$$

where the tildes were omitted to show the resemblance between (77) and (50).

2.5.2. The Coulomb reference by change of variable

It can be shown that the new equations of motion $\tilde{\boldsymbol{\omega}}\dot{\tilde{\boldsymbol{\eta}}} = \partial H/\partial\tilde{\boldsymbol{\eta}}$, which were obtained by a symplectic transformation in phase space, may also be obtained by a change of variable in the Lagrangians (47)–(49). The new Lagrangian density is:

$$
\begin{aligned}
\tilde{\mathcal{L}}_{\text{Max}} &= \frac{1}{2}\left[(\tilde{\mathbf{\Pi}} + \mathbf{\Pi}_C)\cdot\dot{\tilde{\mathbf{A}}} - (\dot{\tilde{\mathbf{\Pi}}} + \dot{\tilde{\mathbf{\Pi}}}_C)\cdot\tilde{\mathbf{A}}\right] \\
&\quad - \begin{Bmatrix} \{[-4\pi c(\tilde{\mathbf{\Pi}} + \mathbf{\Pi}_C)]^2 + [\nabla\times\tilde{\mathbf{A}}]^2\}/8\pi \\ -c\nabla[\tilde{\Phi} + \Phi_C]\cdot[\tilde{\mathbf{\Pi}} + \mathbf{\Pi}_C] \end{Bmatrix},
\end{aligned}
\tag{78}
$$

$$
\tilde{\mathcal{L}}_{\text{Sch}} = \frac{1}{2}[\tilde{P}\dot{\tilde{Q}} - \dot{\tilde{P}}\tilde{Q}] - \begin{Bmatrix} \{[\nabla\tilde{Q} + q\tilde{\mathbf{A}}\tilde{P}/c]^2 + [-\nabla\tilde{P} + q\tilde{\mathbf{A}}\tilde{Q}/c]^2\}/4m \\ +[V + q(\tilde{\Phi} + \Phi_C)]\{\tilde{Q}^2 + \tilde{P}^2\}/2 \end{Bmatrix},
\tag{79}
$$

$$
\tilde{\mathcal{L}}_{\text{gauge}} = \frac{1}{2}\left[\tilde{\Theta}(\dot{\tilde{\Phi}} + \dot{\Phi}_C) - \dot{\tilde{\Theta}}(\tilde{\Phi} + \Phi_C)\right] - \left\{-2\pi c^2\tilde{\Theta}^2 - c\tilde{\Theta}\nabla\cdot\tilde{\mathbf{A}}\right\}.
\tag{80}
$$

That the transformation to the Coulomb reference holds at both Lagrangian and equation of motion level demonstrates the commutativity of the diagram in Fig. 3.

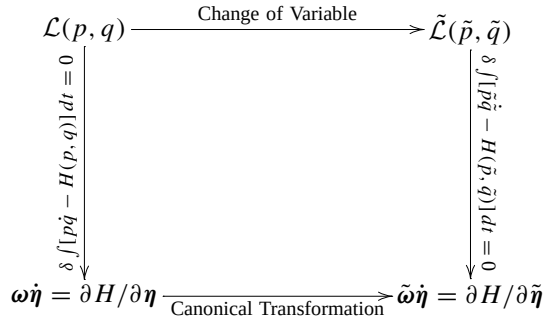

Fig. 3. Commutative diagram representing the change of coordinates (q, p) to $(\tilde{p}, \tilde{q})$ at both the Lagrangian and equation of motion levels.

2.6. Electron spin in the Pauli theory

The electron field used so far in the nonrelativistic Schrödinger theory is a field of spin zero, *i.e.*, a scalar field. It is a simple generalization of the theory to add in the electron's spin. The electron field would then be a two component spinor field, *i.e.*, a spin-1/2 field, and would be of the form

$$\Psi_P(\mathbf{x},t)=\begin{pmatrix}\Psi_\uparrow(\mathbf{x},t)\\ \Psi_\downarrow(\mathbf{x},t)\end{pmatrix}. \tag{81}$$

The first component $\Psi_\uparrow$ is spin up and the second component $\Psi_\downarrow$ is spin down. The dynamics of Ψ_P is governed by the Pauli equation [30]

$$i\dot{\Psi}_P=\frac{[-i\nabla-q\mathbf{A}/c]^2\Psi_P}{2m}+V\Psi_P+q\Phi\Psi_P-\frac{q}{2mc}\boldsymbol{\sigma}\cdot[\nabla\times\mathbf{A}]\Psi_P \tag{82}$$

which is the nonrelativistic limit of the Dirac equation

$$i\dot{\Psi}_D=\beta mc^2\Psi_D+c\boldsymbol{\alpha}\cdot[-i\nabla-q\mathbf{A}/c]\Psi_D+q\Phi\Psi_D \tag{83}$$

in terms of the four component spinor Ψ_D, where the β and $\boldsymbol{\alpha}$ matrices are

$$\beta=\begin{pmatrix}I & 0\\ 0 & -I\end{pmatrix},\qquad \boldsymbol{\alpha}=\begin{pmatrix}0 & \boldsymbol{\sigma}\\ \boldsymbol{\sigma} & 0\end{pmatrix} \tag{84}$$

and

$$\sigma_x=\begin{pmatrix}0 & 1\\ 1 & 0\end{pmatrix},\qquad \sigma_y=\begin{pmatrix}0 & -i\\ i & 0\end{pmatrix},\qquad \sigma_z=\begin{pmatrix}1 & 0\\ 0 & -1\end{pmatrix}. \tag{85}$$

Notice that taking the nonrelativistic limit of the Dirac equation involves the elimination of the two component positron field from Ψ_D. Also note that the current density associated with the Pauli theory [75] is different from that in the Schrödinger theory (see (14)). It is

$$\mathbf{J}_P=q\left\{\Psi_P^\dagger[-i\nabla-q\mathbf{A}/c]\Psi_P+\Psi_P[i\nabla-q\mathbf{A}/c]\Psi_P^\dagger+\nabla\times\left[\Psi_P^\dagger\boldsymbol{\sigma}\Psi_P\right]\right\}/2m, \tag{86}$$

where $\Psi_P^\dagger=(\Psi_\uparrow^*\ \Psi_\downarrow^*)$ is the adjoint of Ψ_P. This can be derived by taking the nonrelativistic limit of the Dirac current density. The last term in (86) is only present in the Pauli current. This term does not effect the continuity equation $\dot{\rho}=-\nabla\cdot\mathbf{J}$ since $\nabla\cdot\nabla\times[\Psi_P^\dagger\boldsymbol{\sigma}\Psi_P]=0$.

2.7. Proton dynamics

In the theory set up so far, the matter dynamics was entirely described by the electronic wavefunction Ψ. The proton had no dynamics whatsoever. Only the electrostatic scalar potential $\Phi_{\bar{q}} = \bar{q}/|\mathbf{x}|$ of the structureless proton of charge $\bar{q}$ entered so as to bind the electron in the hydrogen atom. A first step in the direction of atomic and molecular collisions requires the dynamics of the proton as well (and eventually a few other particles). Suppose the proton is described by its own wavefunction Ω and Lagrangian density

$$\mathcal{L}^{\bar{q}}_{\text{Sch}} = i\Omega^*\dot{\Omega} - \frac{[i\nabla - \bar{q}\mathbf{A}/c]\Omega^* \cdot [-i\nabla - \bar{q}\mathbf{A}/c]\Omega}{2m_{\bar{q}}} - \bar{q}\Phi\Omega^*\Omega, \tag{87}$$

where $(\Phi, \mathbf{A})$ are the scalar and vector potentials arising from the charge and current densities

$$\rho = q\Psi^*\Psi + \bar{q}\Omega^*\Omega, \tag{88}$$

$$\mathbf{J} = q\left\{\Psi^*[-i\nabla - q\mathbf{A}/c]\Psi + \Psi[i\nabla - q\mathbf{A}/c]\Psi^*\right\}/2m_q + \bar{q}\left\{\Omega^*[-i\nabla - \bar{q}\mathbf{A}/c]\Omega + \Omega[i\nabla - \bar{q}\mathbf{A}/c]\Omega^*\right\}/2m_{\bar{q}}. \tag{89}$$

These densities are just the sum of the individual electronic and proton densities. The proton density is not a delta function. Thus, the proton wavefunction is not a delta function either. Rather it is described by a wavepacket and has some structure.

With (87) the total Lagrangian is

$$\mathcal{L}_{\text{Max}} = \frac{1}{2}[\mathbf{\Pi}\cdot\dot{\mathbf{A}} - \dot{\mathbf{\Pi}}\cdot\mathbf{A}] - \left\{\frac{[-4\pi c\mathbf{\Pi}]^2 + [\nabla\times\mathbf{A}]^2}{8\pi} - c\nabla\Phi\cdot\mathbf{\Pi}\right\}, \tag{90}$$

$$\mathcal{L}^{q}_{\text{Sch}} = \frac{i}{2}[\Psi^*\dot{\Psi} - \dot{\Psi}^*\Psi] - \left\{\frac{[i\nabla - q\mathbf{A}/c]\Psi^* \cdot [-i\nabla - q\mathbf{A}/c]\Psi}{2m_q} + q\Phi\Psi^*\Psi\right\}, \tag{91}$$

$$\mathcal{L}^{\bar{q}}_{\text{Sch}} = \frac{i}{2}[\Omega^*\dot{\Omega} - \dot{\Omega}^*\Omega] - \left\{\frac{[i\nabla - \bar{q}\mathbf{A}/c]\Omega^* \cdot [-i\nabla - \bar{q}\mathbf{A}/c]\Omega}{2m_{\bar{q}}} + \bar{q}\Phi\Omega^*\Omega\right\}, \tag{92}$$

$$\mathcal{L}_{\text{gauge}} = \frac{1}{2}[\Theta\dot{\Phi} - \dot{\Theta}\Phi] - \left\{-2\pi c^2\Theta^2 - c\Theta\nabla\cdot\mathbf{A}\right\}. \tag{93}$$

Notice that the electron Lagrangian (91) does not explicitly contain the static proton potential energy $V = q\bar{q}/|\mathbf{x}|$ as did the previous Schrödinger Lagrangian (17). The two matter fields are coupled entirely through electrodynamics. That is, the electron–proton interaction is mediated by the electrodynamics. The Coulombic potential is included implicitly in $q\Phi\Psi^*\Psi$ and $\bar{q}\Phi\Omega^*\Omega$ in the above matter Hamiltonians. In other words, the scalar potential Φ contains (in any gauge) a Coulomb piece of the form

$$\Phi_C(\mathbf{x},t) = \Phi + (\Phi_C - \Phi) = \int_V \frac{\rho(\mathbf{x}',t)}{|\mathbf{x}-\mathbf{x}'|}\,d^3x' = \int_V \frac{q\Psi^*(\mathbf{x}',t)\Psi(\mathbf{x}',t)}{|\mathbf{x}-\mathbf{x}'|}\,d^3x' + \int_V \frac{\bar{q}\Omega^*(\mathbf{x}',t)\Omega(\mathbf{x}',t)}{|\mathbf{x}-\mathbf{x}'|}\,d^3x'. \tag{94}$$

With this potential, the $q\Phi\Psi^*\Psi$ term in the electron Hamiltonian contains the electron–proton attraction as well as electron–electron self interaction. Similarly the $\bar{q}\Phi\Omega^*\Omega$ in the proton Hamiltonian contains the electron–proton attraction and proton–proton self interaction.

The self-energies that are computed from the aforementioned self interactions are finite because Ψ and Ω are square integrable functions. That is

$$E_{\text{int}} = \int_V \rho(\mathbf{x},t)\Phi_C(\mathbf{x},t)\,d^3x = \int_V d^3x \int_V d^3x' \frac{\rho(\mathbf{x},t)\rho(\mathbf{x}',t)}{|\mathbf{x}-\mathbf{x}'|} < \infty \tag{95}$$

for both the cross terms (electron–proton attraction) and the direct terms (electron–electron and proton–proton repulsion). Note that in the relativistic quantum theory the direct terms are infinite and there are infinitely many Coulomb states of the bare problem to sum over [41]. These infinities do not arise in the semiclassical theory presented in this paper. While the self interactions do appear in the above matter Hamiltonians, the resulting self-energies are finite and moreover do not even contribute to the electron or proton portions of the energy. This is due to $-c\nabla\Phi\cdot\mathbf{\Pi}$ in the above Maxwell Hamiltonian. After a partial integration this term becomes $c\Phi\nabla\cdot\mathbf{\Pi}$. Substitution of $-\dot{\Theta} = \rho + c\nabla\cdot\mathbf{\Pi} = 0$ from (50) turns $c\Phi\nabla\cdot\mathbf{\Pi}$ into $-\rho\Phi$, which cancels $+\rho\Phi$ in the electron and proton energies. However, the self interactions do remain in the Coulomb energy $\mathbf{E}^2/8\pi$ of the electromagnetic field. Note that the self interactions do appear in the Hamiltonians and therefore do make a contribution to the overall dynamics.

It should be mentioned that this theory of electron–proton dynamics can be applied to electron–positron dynamics as well. While there is a 2000-fold difference in mass between the proton and the positron, the two theories are otherwise identical. In either case, the theory may be rich enough to capture bound states of hydrogen or positronium.

3. NUMERICAL IMPLEMENTATION

The formal theory of Maxwell–Schrödinger dynamics was constructed in the previous chapter. In particular, the coupled and nonlinear Maxwell and Schrödinger equations

$$i\dot{\Psi} = \frac{[\mathbf{P} - q\mathbf{A}/c]^2\Psi}{2m} + V\Psi + q\Phi\Psi, \tag{96}$$

$$\nabla^2\mathbf{A} - \frac{\ddot{\mathbf{A}}}{c^2} - \nabla\left[\nabla\cdot\mathbf{A} + \frac{\dot{\Phi}}{c}\right] = -\frac{4\pi}{c}\mathbf{J}, \tag{97a}$$

$$\nabla^2\Phi + \frac{\nabla\cdot\dot{\mathbf{A}}}{c} = -4\pi\rho \tag{97b}$$

were recognized to be ill-posed unless an extra equation of constraint is added to them. Using the Hamiltonian approach to dynamics, this extra equation was automatically generated by adding a Lorenz gauge fixing term at the Lagrangian level. It was emphasized in Section 2 that the resulting Hamiltonian system of differential equations, which are of first order in time, form a well-defined initial value problem. That is, the Maxwell–Schrödinger dynamics are known in principle once the initial values are specified for each of the dynamical variables.

The details of converting the formal mathematics of Section 2 to a form that can be practically implemented in a computer are presented in this chapter. The Hamiltonian system of partial differential equations will be reduced to a Hamiltonian system of ordinary differential equations in time by introducing a spatial basis for each of the dynamical variables. The resulting basis equations are coded in a FORTRAN 90 computer program. With this program, various pictures are made to depict the dynamics of the hydrogen atom interacting with the electromagnetic field in a cavity.

3.1. Maxwell–Schrödinger theory in a complex basis

Each of the Maxwell–Schrödinger dynamical variables, which are themselves fields, may be expanded into a complete basis of functions $G_{\mathcal{K}}$ according to

$$\begin{aligned}
\Psi(\mathbf{x},t) &= \sum_{\mathcal{K}} G_{\mathcal{K}}(\mathbf{x})\psi_{\mathcal{K}}(t), & \Psi^*(\mathbf{x},t) &= \sum_{\mathcal{K}} G_{\mathcal{K}}(\mathbf{x})\psi^*_{\mathcal{K}}(t),\\
A_k(\mathbf{x},t) &= \sum_{\mathcal{K}} G_{\mathcal{K}}(\mathbf{x})a_{k\mathcal{K}}(t), & \Pi_k(\mathbf{x},t) &= \sum_{\mathcal{K}} G_{\mathcal{K}}(\mathbf{x})\pi_{k\mathcal{K}}(t),\\
\Phi(\mathbf{x},t) &= \sum_{\mathcal{K}} G_{\mathcal{K}}(\mathbf{x})\phi_{\mathcal{K}}(t), & \Theta(\mathbf{x},t) &= \sum_{\mathcal{K}} G_{\mathcal{K}}(\mathbf{x})\theta_{\mathcal{K}}(t),
\end{aligned} \tag{98}$$

where the index $\mathcal{K}$ runs over the basis and the index k runs over 1, 2, 3 or x, y, z. Any complete set of functions such as the oscillator eigenstates will suffice. In the following work the set of Gaussian functions of the form

$$G_{\mathcal{K}}(\mathbf{x}) = G^*_{\mathcal{K}}(\mathbf{x}) = N_{\mathcal{K}} \exp\bigl(-\ell_{\mathcal{K}}[\mathbf{x}-\mathbf{r}_{\mathcal{K}}]^2\bigr) \tag{99}$$

are used. These functions are centered on $\mathbf{r}_{\mathcal{K}}$, normalized to unity by $N_{\mathcal{K}}$, and are real-valued. Additionally, they span L^2 so that any square integrable function may be represented in this basis. In principle the sums in (98) are to infinity. However, a complete basis cannot be realized in practice. But for all practical purposes the numerical results can be shown to converge to within an arbitrary accuracy in a finite basis. In fact, with a smart choice of basis, the numerical results may converge with just a few terms. Here the basis coefficients, which are complex- and real-valued as well as time-dependent, carry the dynamics.

The basis representation of the previous Lagrangians is

$$L_{\text{Max}} = \sum_{\mathcal{K}\mathcal{M}} \frac{1}{2}\bigl[(\partial/\partial a_{m\mathcal{M}})\dot{a}_{m\mathcal{M}} - (\partial/\partial \pi_{m\mathcal{M}})\dot{\pi}_{m\mathcal{M}}\bigr]S_{\text{Max}} - H_{\text{Max}}, \tag{100}$$

$$L_{\text{Sch}} = \sum_{\mathcal{K}} \frac{i}{2}\bigl[(\partial/\partial \psi_{\mathcal{K}})\dot{\psi}_{\mathcal{K}} - (\partial/\partial \psi^*_{\mathcal{K}})\dot{\psi}^*_{\mathcal{K}}\bigr]S_{\text{Sch}} - H_{\text{Sch}}, \tag{101}$$

$$L_{\text{gauge}} = \sum_{\mathcal{K}\mathcal{M}} \frac{1}{2}\bigl[(\partial/\partial \phi_{\mathcal{K}})\dot{\phi}_{\mathcal{K}} - (\partial/\partial \theta_{\mathcal{K}})\dot{\theta}_{\mathcal{K}}\bigr]S_{\text{gauge}} - H_{\text{gauge}} \tag{102}$$

with integrals

$$S_{\text{Max}} = \int_V \boldsymbol{\Pi}\cdot\mathbf{A}\, d^3x, \qquad S_{\text{Sch}} = \int_V \Psi^*\Psi\, d^3x, \qquad S_{\text{gauge}} = \int_V \Theta\Phi\, d^3x. \tag{103}$$

The calculus of variations leads to the following dynamical equations:

$$\frac{\partial^2 S_{\text{Max}}}{\partial\pi_{m\mathcal{M}}\partial a_{n\mathcal{N}}}\dot{a}_{n\mathcal{N}} = \frac{\partial H}{\partial\pi_{m\mathcal{M}}} \quad \text{or} \quad M_{m\mathcal{M},n\mathcal{N}}\dot{a}_{n\mathcal{N}} = \nabla_{\pi_{m\mathcal{M}}} H, \tag{104}$$

$$\frac{\partial^2 S_{\text{gauge}}}{\partial\theta_{\mathcal{I}}\partial\phi_{\mathcal{L}}}\dot{\phi}_{\mathcal{L}} = \frac{\partial H}{\partial\theta_{\mathcal{I}}} \quad \text{or} \quad N_{\mathcal{I}\mathcal{L}}\dot{\phi}_{\mathcal{L}} = \nabla_{\theta_{\mathcal{I}}} H, \tag{105}$$

$$\frac{\partial^2 i S_{\text{Sch}}}{\partial\psi^*_{\mathcal{I}}\partial\psi_{\mathcal{L}}}\dot{\psi}_{\mathcal{L}} = \frac{\partial H}{\partial\psi^*_{\mathcal{I}}} \quad \text{or} \quad iC_{\mathcal{I}\mathcal{L}}\dot{\psi}_{\mathcal{L}} = \nabla_{\psi^*_{\mathcal{I}}} H, \tag{106}$$

$$-\frac{\partial^2 S_{\text{Max}}}{\partial a_{n\mathcal{N}}\partial\pi_{m\mathcal{M}}}\dot{\pi}_{m\mathcal{M}} = \frac{\partial H}{\partial a_{n\mathcal{N}}} \quad \text{or} \quad -M^T_{n\mathcal{N},m\mathcal{M}}\dot{\pi}_{m\mathcal{M}} = \nabla_{a_{n\mathcal{N}}} H, \tag{107}$$

$$-\frac{\partial^2 S_{\text{gauge}}}{\partial\phi_{\mathcal{J}}\partial\theta_{\mathcal{K}}}\dot{\theta}_{\mathcal{K}} = \frac{\partial H}{\partial\phi_{\mathcal{J}}} \quad \text{or} \quad -N^T_{\mathcal{J}\mathcal{K}}\dot{\theta}_{\mathcal{K}} = \nabla_{\phi_{\mathcal{J}}} H, \tag{108}$$

$$-\frac{\partial^2 i S_{\text{Sch}}}{\partial\psi_{\mathcal{J}}\partial\psi^*_{\mathcal{K}}}\dot{\psi}^*_{\mathcal{K}} = \frac{\partial H}{\partial\psi_{\mathcal{J}}} \quad \text{or} \quad -iC^*_{\mathcal{J}\mathcal{K}}\dot{\psi}^*_{\mathcal{K}} = \nabla_{\psi_{\mathcal{J}}} H, \tag{109}$$

which are of the Hamiltonian form $\omega\dot{\eta} = \partial H/\partial\eta$. The summation convention is used throughout. These equations may be written more compactly as

$$\begin{aligned} M\dot{a} &= \nabla_\pi H, & -M^T\dot{\pi} &= \nabla_a H, \\ N\dot{\phi} &= \nabla_\theta H, & -N^T\dot{\theta} &= \nabla_\phi H, \\ iC\dot{\psi} &= \nabla_{\psi^*} H, & -iC^*\dot{\psi}^* &= \nabla_\psi H \end{aligned} \tag{110}$$

and can be cast into matrix form as

$$\begin{pmatrix} iC & 0 & 0 & 0 & 0 & 0 \\ 0 & -iC^* & 0 & 0 & 0 & 0 \\ 0 & 0 & 0 & 0 & -M^T & 0 \\ 0 & 0 & 0 & 0 & 0 & -N^T \\ 0 & 0 & M & 0 & 0 & 0 \\ 0 & 0 & 0 & N & 0 & 0 \end{pmatrix} \begin{pmatrix} \dot{\psi} \\ \dot{\psi}^* \\ \dot{a} \\ \dot{\phi} \\ \dot{\pi} \\ \dot{\theta} \end{pmatrix} = \begin{pmatrix} \partial H/\partial\psi^* \\ \partial H/\partial\psi \\ \partial H/\partial a \\ \partial H/\partial\phi \\ \partial H/\partial\pi \\ \partial H/\partial\theta \end{pmatrix}, \tag{111}$$

where the matrices M, N, and C and defined in (104)–(109). This symplectic form almost has the canonical structure of (44). In a basis of rank N, the contractions involving a and π run to $3N$ while the contractions involving the remaining dynamical variables run to N. This is because a and π are spatial vectors that have (x, y, z)-components whereas the remaining dynamical variables are scalars.

With the choice of representation in (98) and the choice of basis in (99) all approximations are specified. The equations of motion in (111) are the basis representation of the coupled Maxwell–Schrödinger equations. They are automatically obtained by applying the time-dependent variational principle to the Lagrangians (100)–(102). In the limit of a complete basis these equations are exact.

The complex phase space that carries the associated dynamics is endowed with the Poisson bracket

$$\{F,G\}=\begin{pmatrix}\partial F/\partial\psi^*\\ \partial F/\partial\psi\\ \partial F/\partial a\\ \partial F/\partial\phi\\ \partial F/\partial\pi\\ \partial F/\partial\theta\end{pmatrix}^T\begin{pmatrix}iC&0&0&0&0&0\\0&-iC^*&0&0&0&0\\0&0&0&0&-M^T&0\\0&0&0&0&0&-N^T\\0&0&M&0&0&0\\0&0&0&N&0&0\end{pmatrix}^{-1}\begin{pmatrix}\partial G/\partial\psi^*\\ \partial G/\partial\psi\\ \partial G/\partial a\\ \partial G/\partial\phi\\ \partial G/\partial\pi\\ \partial G/\partial\theta\end{pmatrix}. \tag{112}$$

Even though the symplectic form is not canonical, its inversion is simple. The matrix elements in $\boldsymbol{\omega}$ involve Gaussian overlap integrals like

$$\langle G_{\mathcal{I}}|G_{\mathcal{K}}\rangle=\int_V\langle G_{\mathcal{I}}|\mathbf{x}\rangle\langle\mathbf{x}|G_{\mathcal{K}}\rangle\,d^3x.$$

3.2. Maxwell–Schrödinger theory in a real basis

As was done previously, each dynamical variable may be expanded into a complete basis of functions $G_{\mathcal{K}}$ as

$$\begin{aligned}Q(\mathbf{x},t)&=\sum_{\mathcal{K}}G_{\mathcal{K}}(\mathbf{x})q_{\mathcal{K}}(t), & P(\mathbf{x},t)&=\sum_{\mathcal{K}}G_{\mathcal{K}}(\mathbf{x})p_{\mathcal{K}}(t),\\ A_k(\mathbf{x},t)&=\sum_{\mathcal{K}}G_{\mathcal{K}}(\mathbf{x})a_{k\mathcal{K}}(t), & \Pi_k(\mathbf{x},t)&=\sum_{\mathcal{K}}G_{\mathcal{K}}(\mathbf{x})\pi_{k\mathcal{K}}(t),\\ \Phi(\mathbf{x},t)&=\sum_{\mathcal{K}}G_{\mathcal{K}}(\mathbf{x})\phi_{\mathcal{K}}(t), & \Theta(\mathbf{x},t)&=\sum_{\mathcal{K}}G_{\mathcal{K}}(\mathbf{x})\theta_{\mathcal{K}}(t),\end{aligned} \tag{113}$$

where the index $\mathcal{K}$ runs over the basis and the index k runs over 1, 2, 3 or x, y, z. Unlike in (98), the coefficients in (113) that carry the dynamics are all real-valued. In this basis, the real Lagrangian densities become

$$L_{\text{Max}}=\sum_{\mathcal{K}\mathcal{M}}\frac{1}{2}\big[(\partial/\partial a_{m\mathcal{M}})\dot{a}_{m\mathcal{M}}-(\partial/\partial\pi_{m\mathcal{M}})\dot{\pi}_{m\mathcal{M}}\big]S_{\text{Max}}-H_{\text{Max}}, \tag{114}$$

$$L_{\text{Sch}}=\sum_{\mathcal{K}}\frac{1}{2}\big[(\partial/\partial q_{\mathcal{K}})\dot{q}_{\mathcal{K}}-(\partial/\partial p_{\mathcal{K}})\dot{p}_{\mathcal{K}}\big]S_{\text{Sch}}-H_{\text{Sch}}, \tag{115}$$

$$L_{\text{gauge}}=\sum_{\mathcal{K}\mathcal{M}}\frac{1}{2}\big[(\partial/\partial\phi_{\mathcal{K}})\dot{\phi}_{\mathcal{K}}-(\partial/\partial\theta_{\mathcal{K}})\dot{\theta}_{\mathcal{K}}\big]S_{\text{gauge}}-H_{\text{gauge}} \tag{116}$$

with integrals

$$S_{\text{Max}}=\int_V\boldsymbol{\Pi}\cdot\mathbf{A}\,d^3x,\qquad S_{\text{Sch}}=\int_V PQ\,d^3x,\qquad S_{\text{gauge}}=\int_V\Theta\Phi\,d^3x. \tag{117}$$

Applying the calculus of variations to the above Lagrangians leads to the equations of motion:

$$\frac{\partial^2 S_{\text{Max}}}{\partial\pi_{m\mathcal{M}}\partial a_{n\mathcal{N}}}\dot{a}_{n\mathcal{N}}=\frac{\partial H}{\partial\pi_{m\mathcal{M}}}\quad\text{or}\quad M_{m\mathcal{M},n\mathcal{N}}\dot{a}_{n\mathcal{N}}=\nabla_{\pi_{m\mathcal{M}}}H, \tag{118}$$

$$\frac{\partial^2 S_{\text{gauge}}}{\partial\theta_{\mathcal{I}}\partial\phi_{\mathcal{L}}}\dot{\phi}_{\mathcal{L}} = \frac{\partial H}{\partial\theta_{\mathcal{I}}} \quad \text{or} \quad N_{\mathcal{I}\mathcal{L}}\dot{\phi}_{\mathcal{L}} = \nabla_{\theta_{\mathcal{I}}} H, \tag{119}$$

$$\frac{\partial^2 S_{\text{Sch}}}{\partial p_{\mathcal{I}}\partial q_{\mathcal{L}}}\dot{q}_{\mathcal{L}} = \frac{\partial H}{\partial p_{\mathcal{I}}} \quad \text{or} \quad C_{\mathcal{I}\mathcal{L}}\dot{q}_{\mathcal{L}} = \nabla_{p_{\mathcal{I}}} H, \tag{120}$$

$$-\frac{\partial^2 S_{\text{Max}}}{\partial a_{n\mathcal{N}}\partial\pi_{m\mathcal{M}}}\dot{\pi}_{m\mathcal{M}} = \frac{\partial H}{\partial a_{n\mathcal{N}}} \quad \text{or} \quad -M^T_{n\mathcal{N},m\mathcal{M}}\dot{\pi}_{m\mathcal{M}} = \nabla_{a_{n\mathcal{N}}} H, \tag{121}$$

$$-\frac{\partial^2 S_{\text{gauge}}}{\partial\phi_{\mathcal{J}}\partial\theta_{\mathcal{K}}}\dot{\theta}_{\mathcal{K}} = \frac{\partial H}{\partial\phi_{\mathcal{J}}} \quad \text{or} \quad -N^T_{\mathcal{J}\mathcal{K}}\dot{\theta}_{\mathcal{K}} = \nabla_{\phi_{\mathcal{J}}} H, \tag{122}$$

$$-\frac{\partial^2 S_{\text{Sch}}}{\partial q_{\mathcal{J}}\partial p_{\mathcal{K}}}\dot{p}_{\mathcal{K}} = \frac{\partial H}{\partial q_{\mathcal{J}}} \quad \text{or} \quad -C^T_{\mathcal{J}\mathcal{K}}\dot{p}_{\mathcal{K}} = \nabla_{q_{\mathcal{J}}} H, \tag{123}$$

which are of the Hamiltonian form $\omega\dot{\eta} = \partial H/\partial\eta$. These equations may be written more compactly as

$$\begin{aligned} M\dot{a} &= \nabla_\pi H, \qquad -M^T\dot{\pi} = \nabla_a H, \\ N\dot{\phi} &= \nabla_\theta H, \qquad -N^T\dot{\theta} = \nabla_\phi H, \\ C\dot{q} &= \nabla_p H, \qquad -C^T\dot{p} = \nabla_q H, \end{aligned} \tag{124}$$

and can be cast into matrix form as

$$\begin{pmatrix} 0 & 0 & 0 & -M^T & 0 & 0 \\ 0 & 0 & 0 & 0 & -N^T & 0 \\ 0 & 0 & 0 & 0 & 0 & -C^T \\ M & 0 & 0 & 0 & 0 & 0 \\ 0 & N & 0 & 0 & 0 & 0 \\ 0 & 0 & C & 0 & 0 & 0 \end{pmatrix} \begin{pmatrix} \dot{a} \\ \dot{\phi} \\ \dot{q} \\ \dot{\pi} \\ \dot{\theta} \\ \dot{p} \end{pmatrix} = \begin{pmatrix} \partial H/\partial a \\ \partial H/\partial\phi \\ \partial H/\partial q \\ \partial H/\partial\pi \\ \partial H/\partial\theta \\ \partial H/\partial p \end{pmatrix}, \tag{125}$$

where the matrices M, N, and C and defined in (118)–(123). Again they are the basis representation of the coupled Maxwell–Schrödinger equations of motion.

The real phase space that carries the associated dynamics is endowed with the Poisson bracket

$$\{F, G\} = \begin{pmatrix} \partial F/\partial a \\ \partial F/\partial\phi \\ \partial F/\partial q \\ \partial F/\partial\pi \\ \partial F/\partial\theta \\ \partial F/\partial p \end{pmatrix}^T \begin{pmatrix} 0 & 0 & 0 & -M^T & 0 & 0 \\ 0 & 0 & 0 & 0 & -N^T & 0 \\ 0 & 0 & 0 & 0 & 0 & -C^T \\ M & 0 & 0 & 0 & 0 & 0 \\ 0 & N & 0 & 0 & 0 & 0 \\ 0 & 0 & C & 0 & 0 & 0 \end{pmatrix}^{-1} \begin{pmatrix} \partial G/\partial a \\ \partial G/\partial\phi \\ \partial G/\partial q \\ \partial G/\partial\pi \\ \partial G/\partial\theta \\ \partial G/\partial p \end{pmatrix}. \tag{126}$$

Even though the symplectic form is not canonical, its inversion is simple once again. The matrix elements in $\boldsymbol{\omega}$ involve Gaussian overlap integrals like

$$\langle G_{\mathcal{I}}|G_{\mathcal{K}}\rangle = \int_V \langle G_{\mathcal{I}}|\mathbf{x}\rangle\langle\mathbf{x}|G_{\mathcal{K}}\rangle\, d^3x.$$

3.2.1. Overview of computer program

The equations of motion (125) are coded in FORTRAN 90. The computer program is called Electron Nuclear Radiation Dynamics or ENRD. Each matrix element in the symplectic form and in the forces is performed analytically. The program is flexible enough to handle a rank N basis of s-Gaussians, each with an adjustable width and an arbitrary center. A numerical solution to (125) is determined once the initial value data is specified for η^b. The forces $\partial H/\partial \eta^a$ are constructed from this data. The symplectic form ω_{ab} is then inverted with the LAPACK [76] subroutine DGESVX, which is the expert driver for the $AX = B$ solver DGESV. This establishes a first order system of differential equations of the form $\dot{\eta}^b = \omega_{ab}^{-1}\partial H/\partial \eta^a$ which may be solved, for example, with an Euler stepping method. That is

$$\eta^b(t + \Delta t) = \eta^b(t) + (\Delta t)\dot{\eta}^b(t) = \eta^b(t) + (\Delta t)\big[\omega_{ab}^{-1}\partial H/\partial \eta^a\big](t). \tag{127}$$

In practice, the Euler method is not accurate enough so the more sophisticated RK4 method [77] is implemented in the code. The equations of motion are advanced at a fixed stepsize of 10^{-3} au. For typical basis function widths and centers, the estimated condition number reported by DGESVX is about 30.

Lastly, it should be pointed out that the equations of motion (125) are numerically implemented in terms of the electric field $\mathbf{E} \equiv -4\pi c\mathbf{\Pi}$ rather than the momentum $\mathbf{\Pi}$. It was found that working in terms of this new (scaled) coordinate provides a more balanced set of dynamical equations. Nevertheless, the electromagnetic radiation is still quite small compared to the dynamics of the matter. An overview of the ENRD program is presented in Fig. 4.

3.2.2. Stationary states: s- and p-waves

The ENRD program was first tested with a stationary state of the hydrogen atom. In a basis of six Gaussians an s-wave was constructed as well as the corresponding basis representation of the Coulombic scalar potential and the Coulombic electric field. In fact, any spherically symmetric distribution of charge along with the corresponding Coulomb fields would suffice. This delicate balance of charges and fields proved to be a stationary state of the combined system. No electromagnetic radiation was produced. The total charge $q = \int_V \rho(\mathbf{x})\, d^3x$ remained constant. A p_x-wave and its associated Coulombic fields were also created in the same basis. This again is a stationary state.

3.2.3. Nonstationary state: Mixture of s- and p-waves

After identifying some stationary states, a nonstationary state that is a mixture of s- and p_x-waves was constructed in the same rank six basis. Both the Coulombic scalar potential and the Coulombic electric field that are associated with this charge distribution were created as well. Electromagnetic radiation was produced as the electron oscillated between stationary states. Energy, momentum, and angular momentum were exchanged between the electron and the electromagnetic field. It was shown that the total energy and total Hamiltonian are conserved to four decimal places. The total charge $q = \int_V \rho(\mathbf{x})\, d^3x$ remained constant. The phase space contours for the electromagnetic field, matter field, and gauge field are presented in Figs. 5, 6, and 7, respectively.

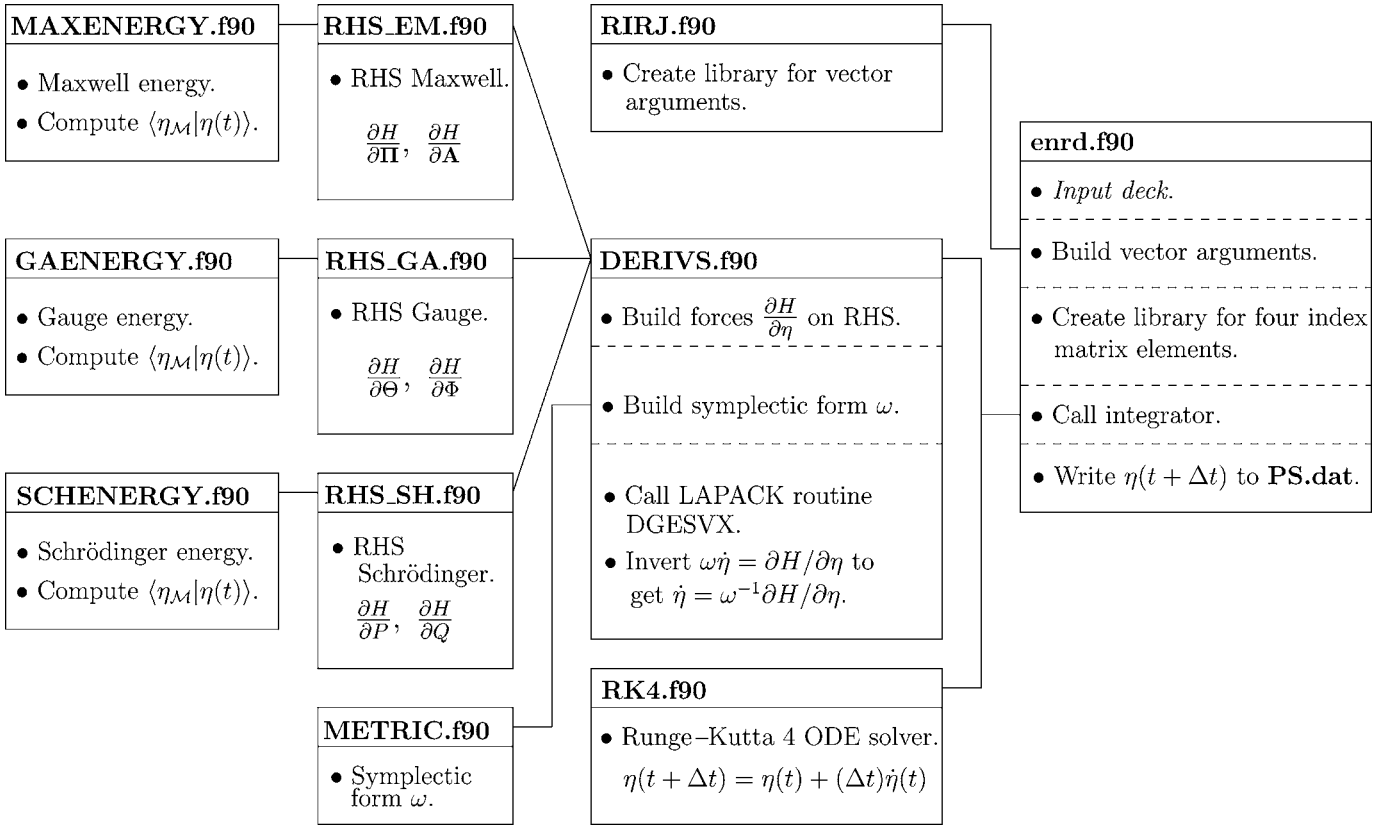

Fig. 4. Schematic overview of ENRD computer program.

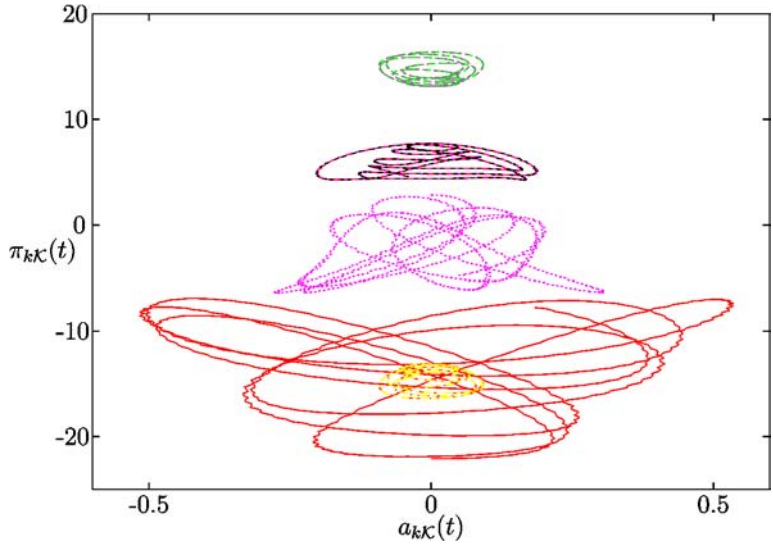

Fig. 5. Phase space contour for the coefficients of the vector potential **A** and its momentum **Π**.

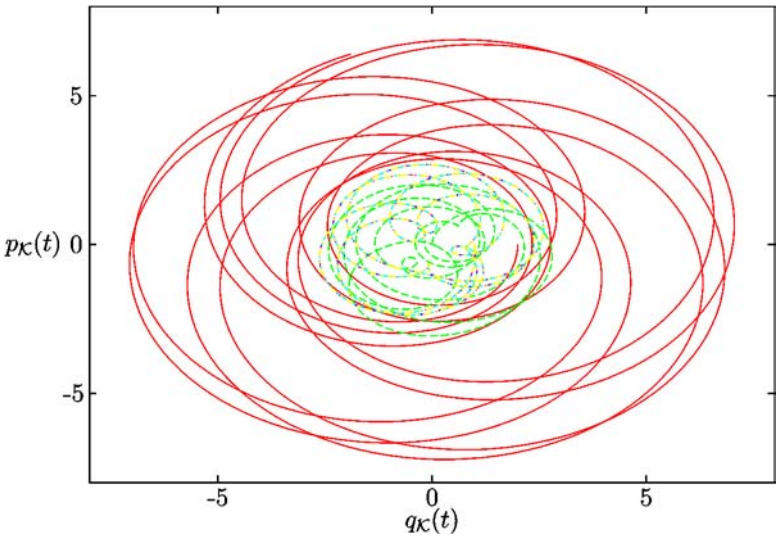

Fig. 6. Phase space contour for the coefficients of the real-valued Schrödinger field Q and its momentum P.

3.2.4. Free electrodynamics

Lastly a free electromagnetic field was constructed. In this case no charge was created. Energy, momentum, and angular momentum were exchanged only between the electromagnetic and gauge degrees of freedom. The total energy remained constant.

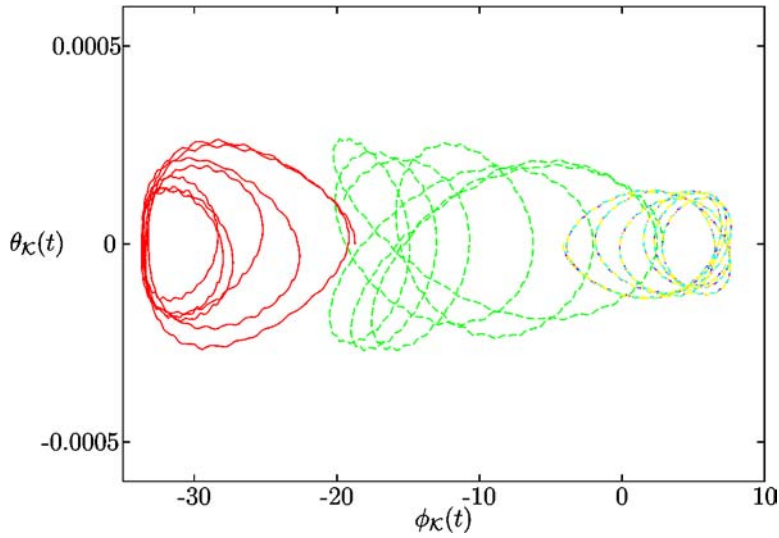

Fig. 7. Phase space contour for the coefficients of the scalar potential Φ and its momentum Θ.

3.2.5. Analysis of solutions in numerical basis

The solutions $\eta(t)$ of the equations of motion (125) are further analyzed by expansion into the basis eigenstates $\eta_{\mathcal{M}}$. The Schrödinger eigenstates are found by diagonalizing the time-independent Schrödinger equation

$$\mathbf{HC} = \mathbf{SC}\boldsymbol{\epsilon}, \tag{128}$$

where **H** is the basis representation of the Hamiltonian $H = -\nabla^2/2m + V$, **C** is the matrix of basis expansion coefficients, **S** is the basis overlap matrix, and $\boldsymbol{\epsilon}$ is the matrix of energy eigenvalues. Similarly, the Maxwell eigenstates are found by diagonalizing the free wave equation $\nabla^2\phi - \ddot{\phi}/c^2 = 0$, where ϕ can be the scalar potential Φ or any component of the vector potential **A**. Fourier inversion of the free wave equation results in $-c^2\nabla^2\tilde{\phi} = \omega^2\tilde{\phi}$, where ω is the frequency. In a basis this equation turns into the matrix equation

$$\mathbf{HC} = \mathbf{SC}\boldsymbol{\omega}^2, \tag{129}$$

where **H** is the basis representation of the Hamiltonian-like quantity $H = -c^2\nabla^2$, **C** is the matrix of basis expansion coefficients, **S** is the basis overlap matrix, and $\boldsymbol{\omega}^2$ is the matrix of frequencies squared. Recall that energy is related to frequency by $E = \hbar\omega$, so that in atomic units energy is equivalent to frequency.

Both of these basis equations (128) and (129) are recognized as belonging to the generalized eigenvalue problem $\mathbf{A}\boldsymbol{\eta} = \mathbf{B}\boldsymbol{\eta}\boldsymbol{\lambda}$, which can be inverted with the LAPACK routine DSYGV. The ENRD program employs DSYGV to solve both (128) and (129) for their corresponding eigenvalues $\lambda_{\mathcal{M}}$ and eigenvectors $\eta_{\mathcal{M}}$.

With the eigenvectors $\eta_{\mathcal{M}}$, the evolving state vector $\eta(t)$ can be expanded according to

$$|\eta(t)\rangle = \sum_{\mathcal{M}} |\eta_{\mathcal{M}}\rangle\langle\eta_{\mathcal{M}}|\eta(t)\rangle, \tag{130}$$

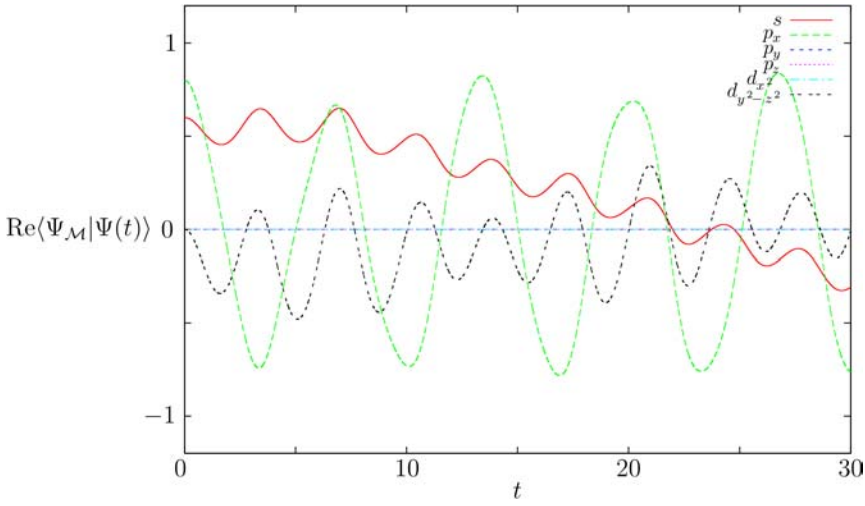

Fig. 8. Real part of the Schrödinger coefficients $C_{\mathcal{M}}(t) \equiv \langle\eta_{\mathcal{M}}|\eta(t)\rangle$, where $\eta(t)$ is a superposition of s- and p_x-waves.

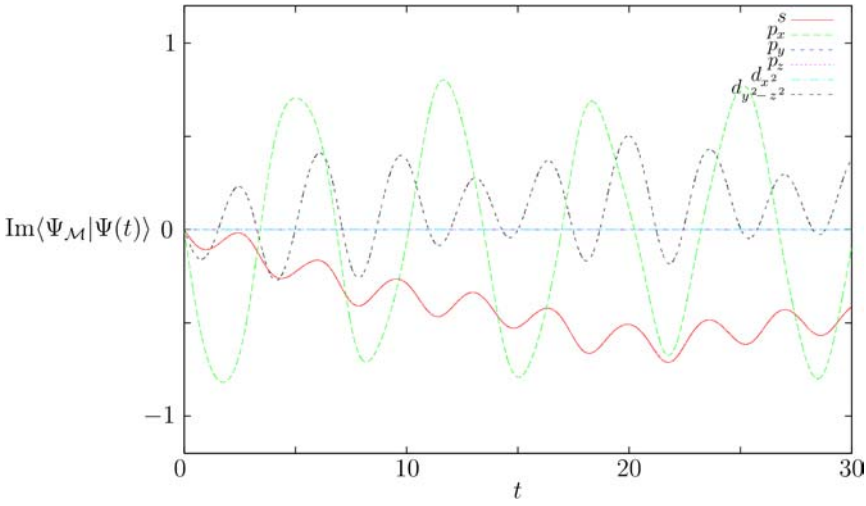

Fig. 9. Imaginary part of the Schrödinger coefficients $C_{\mathcal{M}}(t) \equiv \langle\eta_{\mathcal{M}}|\eta(t)\rangle$, where $\eta(t)$ is a superposition of s- and p_x-waves.

where $C_{\mathcal{M}}(t) \equiv \langle\eta_{\mathcal{M}}|\eta(t)\rangle$ are the basis expansion coefficients. The real and imaginary parts of the Schrödinger coefficients for a superposition of s- and p_x-waves are plotted versus time in Figs. 8 and 9, respectively. The squares of these coefficients are plotted versus time in Figs. 10 and 11. Notice in Figs. 8 and 9 that there are three frequencies involved in the dynamics, which correspond to excitations of the s-, p_x-, and $d_{y^2-z^2}$-waves. Figure 10 suggests that the electron decays from p_x to s in under 10 au of time. However, due to the finite size of the basis, the electron is excited back to the p_x-state as the electromagnetic

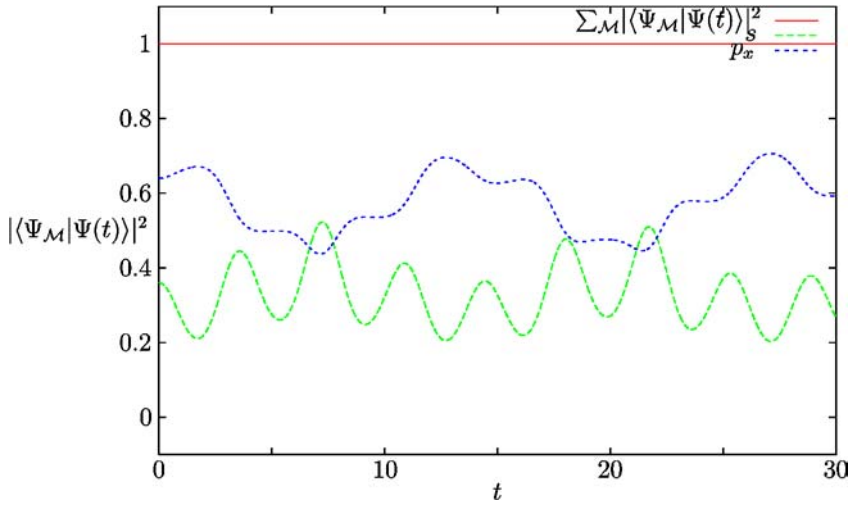

Fig. 10. Probability for the electron to be in a particular basis eigenstate.

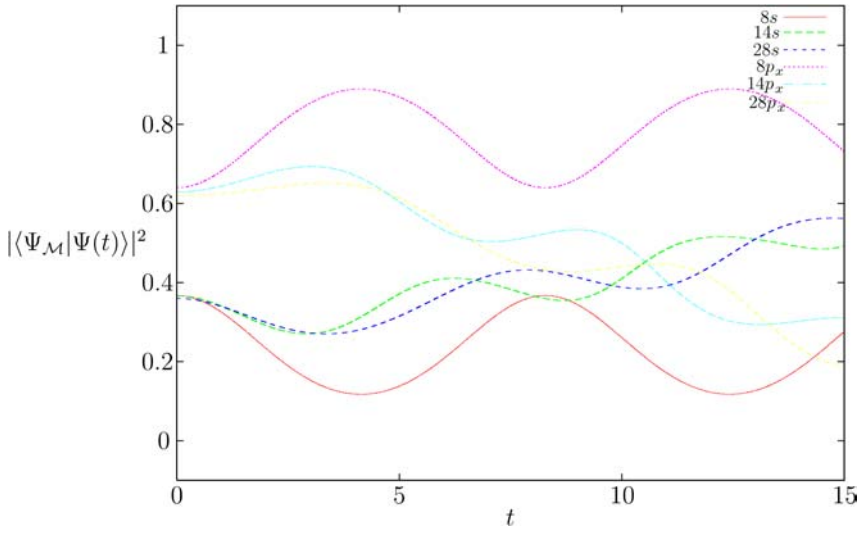

Fig. 11. In the rank 8, 14, and 28 bases, the probability for an atomic electron to be in a particular Schrödinger eigenstate is presented. The lowest s and p_x atomic stationary states are largely responsible for the dynamics. The amplitudes are very small for all other stationary states.

fields reflect off of the artificial basis boundaries. In this sense, the numerical results are more descriptive of an atom in a cavity than an atom in free space. To check the convergence of these results, the Schrödinger probabilities are recomputed in Fig. 11 for three larger bases. Bases of rank 8, 14, and 28 are used, where the dynamics has converged between the numerical and Coulomb bases. The rank 8 basis has Gaussian basis functions

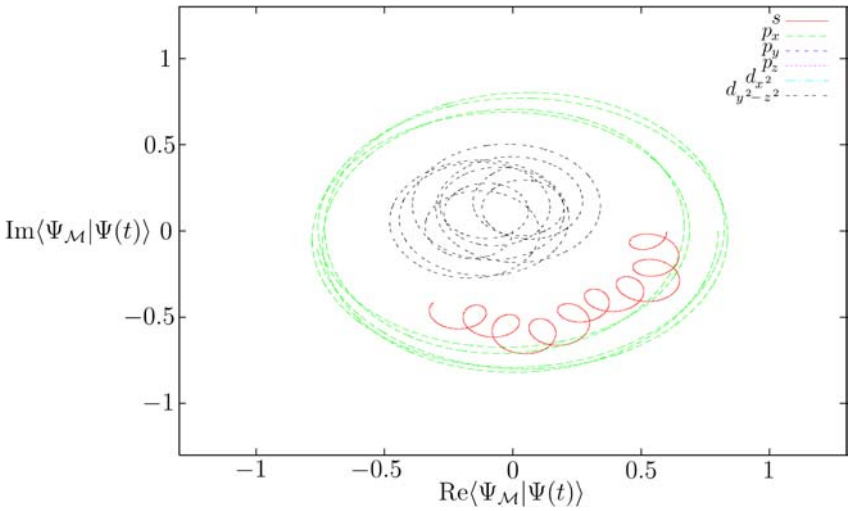

Fig. 12. Phase space of the Schrödinger coefficients $C_{\mathcal{M}}(t) \equiv \langle \eta_{\mathcal{M}} | \eta(t) \rangle$, where $\eta(t)$ is a superposition of s- and p_x-waves.

centered on the corners of a cube with edges of 2 au in length. The rank 14 basis adds two more Gaussians on each coordinate axis to the rank 8 basis. The rank 14 basis, therefore, has 14 basis functions uniformly arranged on the surface of a sphere of radius $\sqrt{3}$ au. The rank 28 basis adds a second sphere of radius $2\sqrt{3}$ au around the inner rank 14 basis. Phase space contours of the Schrödinger coefficients are presented in Fig. 12.

3.3. Symplectic transformation to the Coulomb reference

Recall the basis representation of the Maxwell–Schrödinger equations of motion in (125). They are

$$\begin{pmatrix} 0 & 0 & 0 & -M^T & 0 & 0 \\ 0 & 0 & 0 & 0 & -N^T & 0 \\ 0 & 0 & 0 & 0 & 0 & -C^T \\ M & 0 & 0 & 0 & 0 & 0 \\ 0 & N & 0 & 0 & 0 & 0 \\ 0 & 0 & C & 0 & 0 & 0 \end{pmatrix} \begin{pmatrix} \dot{a} \\ \dot{\phi} \\ \dot{q} \\ \dot{\pi} \\ \dot{\theta} \\ \dot{p} \end{pmatrix} = \begin{pmatrix} \partial H/\partial a \\ \partial H/\partial \phi \\ \partial H/\partial q \\ \partial H/\partial \pi \\ \partial H/\partial \theta \\ \partial H/\partial p \end{pmatrix}, \tag{125}$$

where

$$M_{\mathcal{K}\mathcal{M}} \equiv \frac{\partial^2 \langle \mathbf{\Pi} | \mathbf{A} \rangle}{\partial \boldsymbol{\pi}_{\mathcal{K}} \partial \boldsymbol{a}_{\mathcal{M}}}, \qquad N_{\mathcal{K}\mathcal{M}} \equiv \frac{\partial^2 \langle \Theta | \Phi \rangle}{\partial \theta_{\mathcal{K}} \partial \phi_{\mathcal{M}}}, \qquad C_{\mathcal{K}\mathcal{M}} \equiv \frac{\partial^2 \langle P | Q \rangle}{\partial p_{\mathcal{K}} \partial q_{\mathcal{M}}} \tag{131}$$

and where the integrals $\langle \cdot | \cdot \rangle$ involve only Gaussian functions.

In analogy to the transformation $(\mathbf{T}^{-1})^T$ in (63) that was defined on the vector fields $\partial/\partial \boldsymbol{\eta}$ in function space, a basis representation of $(\mathbf{T}^{-1})^T$ can be made. This basis represen-

tation is defined in terms of the coefficients according to

$$\begin{pmatrix} \partial/\partial\tilde{a} \\ \partial/\partial\tilde{\phi} \\ \partial/\partial\tilde{q} \\ \partial/\partial\tilde{\pi} \\ \partial/\partial\tilde{\theta} \\ \partial/\partial\tilde{p} \end{pmatrix} = \begin{pmatrix} \partial a/\partial\tilde{a} & 0 & 0 & 0 & 0 & 0 \\ 0 & \partial\phi/\partial\tilde{\phi} & 0 & 0 & 0 & 0 \\ 0 & \partial\phi/\partial\tilde{q} & \partial q/\partial\tilde{q} & \partial\pi/\partial\tilde{q} & 0 & 0 \\ 0 & 0 & 0 & \partial\pi/\partial\tilde{\pi} & 0 & 0 \\ 0 & 0 & 0 & 0 & \partial\theta/\partial\tilde{\theta} & 0 \\ 0 & \partial\phi/\partial\tilde{p} & 0 & \partial\pi/\partial\tilde{p} & 0 & \partial p/\partial\tilde{p} \end{pmatrix} \begin{pmatrix} \partial/\partial a \\ \partial/\partial\phi \\ \partial/\partial q \\ \partial/\partial\pi \\ \partial/\partial\theta \\ \partial/\partial p \end{pmatrix} \tag{132}$$

so that the symplectic form in (125) transforms as

$$\begin{pmatrix} 0 & 0 & 0 & -M^T & 0 & 0 \\ 0 & 0 & 0 & 0 & -N^T & 0 \\ 0 & 0 & 0 & 0 & 0 & -C^T \\ M & 0 & 0 & 0 & 0 & 0 \\ 0 & N & 0 & 0 & 0 & 0 \\ 0 & 0 & C & 0 & 0 & 0 \end{pmatrix}$$
$$\to \begin{pmatrix} 0 & 0 & -M_{\tilde{A}\tilde{Q}} & -M_{\tilde{A}\tilde{\Pi}} & 0 & -M_{\tilde{A}\tilde{P}} \\ 0 & 0 & 0 & 0 & -N_{\tilde{\Phi}\tilde{\Theta}} & 0 \\ M_{\tilde{Q}\tilde{A}} & 0 & 0 & 0 & -N_{\tilde{Q}\tilde{\Theta}} & -C_{\tilde{Q}\tilde{P}} \\ M_{\tilde{\Pi}\tilde{A}} & 0 & 0 & 0 & 0 & 0 \\ 0 & N_{\tilde{\Theta}\tilde{\Phi}} & N_{\tilde{\Theta}\tilde{Q}} & 0 & 0 & N_{\tilde{\Theta}\tilde{P}} \\ M_{\tilde{P}\tilde{A}} & 0 & C_{\tilde{P}\tilde{Q}} & 0 & -N_{\tilde{P}\tilde{\Theta}} & 0 \end{pmatrix}, \tag{133}$$

where the new matrix elements are:

$$\begin{aligned} M_{\tilde{X}\tilde{Y}} &\equiv \frac{\partial\pi}{\partial\tilde{X}} M \frac{\partial a}{\partial\tilde{Y}} = \frac{\partial\pi}{\partial\tilde{X}} \frac{\partial^2\langle\tilde{\mathbf{\Pi}} + \mathbf{\Pi}_C|\tilde{\mathbf{A}}\rangle}{\partial\pi\,\partial a} \frac{\partial a}{\partial\tilde{Y}} = \frac{\partial^2\langle\tilde{\mathbf{\Pi}} + \mathbf{\Pi}_C|\tilde{\mathbf{A}}\rangle}{\partial\tilde{X}\partial\tilde{Y}}, \\ N_{\tilde{X}\tilde{Y}} &\equiv \frac{\partial\theta}{\partial\tilde{X}} N \frac{\partial\phi}{\partial\tilde{Y}} = \frac{\partial\theta}{\partial\tilde{X}} \frac{\partial^2\langle\Theta|\tilde{\Phi} + \Phi_C\rangle}{\partial\theta\partial\phi} \frac{\partial\phi}{\partial\tilde{Y}} = \frac{\partial^2\langle\tilde{\Theta}|\tilde{\Phi} + \Phi_C\rangle}{\partial\tilde{X}\partial\tilde{Y}}, \\ C_{\tilde{X}\tilde{Y}} &\equiv \frac{\partial p}{\partial\tilde{X}} C \frac{\partial q}{\partial\tilde{Y}} = \frac{\partial p}{\partial\tilde{X}} \frac{\partial^2\langle P|Q\rangle}{\partial p\partial q} \frac{\partial q}{\partial\tilde{Y}} = \frac{\partial^2\langle\tilde{P}|\tilde{Q}\rangle}{\partial\tilde{X}\partial\tilde{Y}} \end{aligned} \tag{134}$$

for X and Y an arbitrary dynamical variable. The remaining elements are determined by transposition. Again the extra terms in $\tilde{\boldsymbol{\omega}}$ add new time-dependent couplings to the theory. These new terms can all be performed analytically. The resulting equations of motion are

$$\begin{pmatrix} 0 & 0 & -M_{\tilde{A}\tilde{Q}} & -M_{\tilde{A}\tilde{\Pi}} & 0 & -M_{\tilde{A}\tilde{P}} \\ 0 & 0 & 0 & 0 & -N_{\tilde{\Phi}\tilde{\Theta}} & 0 \\ M_{\tilde{Q}\tilde{A}} & 0 & 0 & 0 & -N_{\tilde{Q}\tilde{\Theta}} & -C_{\tilde{Q}\tilde{P}} \\ M_{\tilde{\Pi}\tilde{A}} & 0 & 0 & 0 & 0 & 0 \\ 0 & N_{\tilde{\Theta}\tilde{\Phi}} & N_{\tilde{\Theta}\tilde{Q}} & 0 & 0 & N_{\tilde{\Theta}\tilde{P}} \\ M_{\tilde{P}\tilde{A}} & 0 & C_{\tilde{P}\tilde{Q}} & 0 & -N_{\tilde{P}\tilde{\Theta}} & 0 \end{pmatrix} \begin{pmatrix} \dot{\tilde{a}} \\ \dot{\tilde{\phi}} \\ \dot{\tilde{q}} \\ \dot{\tilde{\pi}} \\ \dot{\tilde{\theta}} \\ \dot{\tilde{p}} \end{pmatrix} = \begin{pmatrix} \partial H/\partial\tilde{a} \\ \partial H/\partial\tilde{\phi} \\ \partial H/\partial\tilde{q} \\ \partial H/\partial\tilde{\pi} \\ \partial H/\partial\tilde{\theta} \\ \partial H/\partial\tilde{p} \end{pmatrix}. \tag{135}$$

3.3.1. *Numerical implementation*

Recall that the forces appearing in the canonical transformed equations (76) could be simplified by substituting these equations among themselves. As a result,

$$\tilde{\boldsymbol{\omega}} \rightarrow \begin{pmatrix} 0 & 0 & -M_{\tilde{A}\tilde{Q}} & -M_{\tilde{A}\tilde{\Pi}} & 0 & -M_{\tilde{A}\tilde{P}} \\ 0 & 0 & 0 & 0 & -N_{\tilde{\Phi}\tilde{\Theta}} & 0 \\ 0 & 0 & 0 & 0 & 0 & -C_{\tilde{Q}\tilde{P}} \\ M_{\tilde{\Pi}\tilde{A}} & 0 & 0 & 0 & 0 & 0 \\ 0 & N_{\tilde{\Theta}\tilde{\Phi}} & N_{\tilde{\Theta}\tilde{Q}} & 0 & 0 & N_{\tilde{\Theta}\tilde{P}} \\ 0 & 0 & C_{\tilde{P}\tilde{Q}} & 0 & 0 & 0 \end{pmatrix}. \tag{136}$$

Note that (136) is not a symplectic form. After making this substitution, the Hamiltonian structure is lost. However, the numerical implementation is greatly facilitated with the simplified equations (76) instead of those in (75). Since the ENRD program does not rely on a symplectic integrator scheme to advance the dynamics, the symplectic structure is not numerically important anyway.

The equations of motion (76) has been added to the ENRD code. The Coulomb reference can be conveniently turned on or off (resulting in (51)) with an optional flag. As before, the program is flexible enough to handle a rank N basis of s-Gaussians, each with an adjustable width and an arbitrary center. A solution to (76) may be obtained once the initial value data is specified for $\tilde{\eta}^b$. The forces $\partial H/\partial\tilde{\eta}^a$ are constructed from this data. The new terms appearing on left-hand side of (76) are coded analytically. Notice that these terms make up the elements of a matrix that is not a symplectic form. Nevertheless, the resulting matrix equations are integrated with the same RK4 stepping method and the DGESVX subroutine of LAPACK. For typical basis function widths and centers, the condition number reported by DGESVX is on the order of 10^3.

3.3.2. *Stationary states: s- and p-waves*

The ENRD program with the Coulomb reference was first tested with a stationary state of the hydrogen atom. In a basis of six Gaussians an s-wave was constructed. The corresponding basis representation of the Coulombic scalar potential and the Coulombic electric field were not needed. All Coulombic properties are treated analytically once the Coulomb reference is chosen. Again, it was found that any spherically symmetric distribution of charge will suffice to produce an s-wave that is a stationary state of the combined system. No electromagnetic radiation was produced. The total charge $q = \int_V \rho(\mathbf{x})\, d^3x$ remained constant. A p_x-wave was also created in the same basis. This again was a stationary state of the combined system.

3.3.3. *Nonstationary state: Mixture of s- and p-waves*

After identifying some stationary states, a nonstationary state that is a mixture of s- and p_x-waves was constructed in the same rank six basis. Both the Coulombic scalar potential and the Coulombic electric field that are associated with this charge distribution were done analytically by the canonical transformation to the Coulomb reference. Electromagnetic radiation was produced as the electron oscillated between stationary states. Energy, momentum, and angular momentum were exchanged between the electron and the electromagnetic field. It was shown that the total energy and total Hamiltonian are conserved to two decimal places. The total charge $q = \int_V \rho(\mathbf{x})\, d^3x$ remained constant.

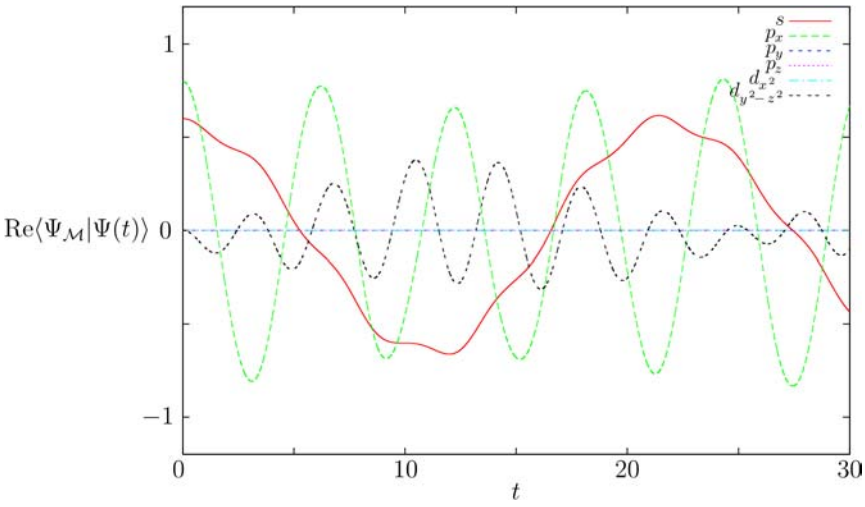

Fig. 13. Real part of the Schrödinger coefficients $C_{\mathcal{M}}(t) \equiv \langle\eta_{\mathcal{M}}|\eta(t)\rangle$, where $\eta(t)$ is a superposition of s- and p_x-waves.

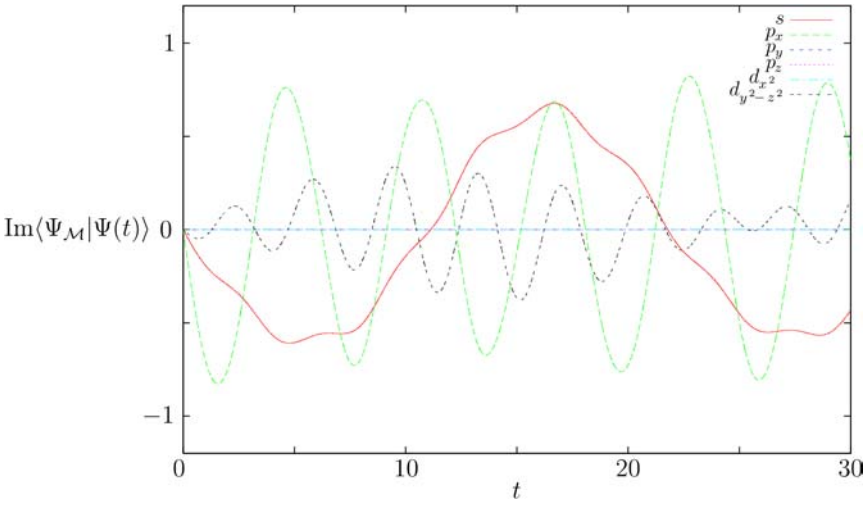

Fig. 14. Imaginary part of the Schrödinger coefficients $C_{\mathcal{M}}(t) \equiv \langle\eta_{\mathcal{M}}|\eta(t)\rangle$, where $\eta(t)$ is a superposition of s- and p_x-waves.

3.3.4. Free electrodynamics

Lastly a free electromagnetic field was constructed. In this case no charge was created. Energy, momentum, and angular momentum were exchanged only between the electromagnetic and gauge degrees of freedom. The total energy remained constant.

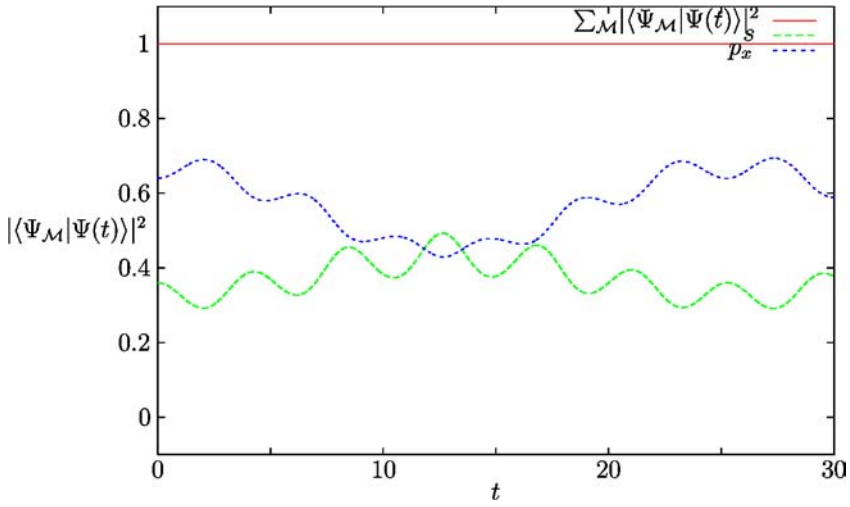

Fig. 15. Probability for the electron to be in a particular basis eigenstate.

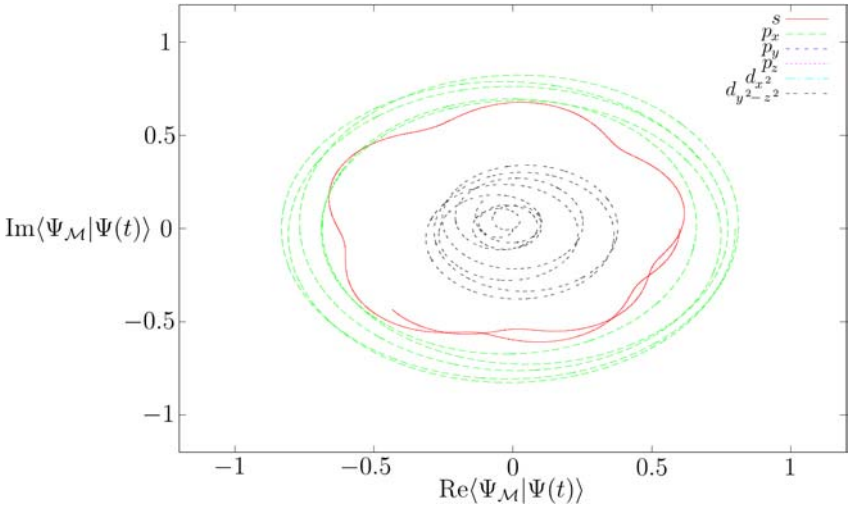

Fig. 16. Phase space of the Schrödinger coefficients $C_{\mathcal{M}}(t) \equiv \langle\eta_{\mathcal{M}}|\eta(t)\rangle$, where $\eta(t)$ is a superposition of s- and p_x-waves.

3.3.5. Analysis of solutions in Coulomb basis

As done previously, the evolving state vector $\tilde{\eta}(t)$ in the Coulomb basis is expanded in terms of the stationary eigenbasis $\tilde{\eta}_{\mathcal{M}} \equiv \eta_{\mathcal{M}}$ according to

$$|\tilde{\eta}(t)\rangle = \sum_{\mathcal{M}} |\tilde{\eta}_{\mathcal{M}}\rangle\langle\tilde{\eta}_{\mathcal{M}}|\tilde{\eta}(t)\rangle. \tag{130}$$

As before, the real and imaginary parts of the Schrödinger coefficients for a superposition of s- and p_x-waves are plotted versus time in Figs. 13 and 14, respectively. The squares of

these coefficients are plotted versus time in Fig. 15. Notice in Figs. 13 and 14 that there are again three frequencies involved in the dynamics, which correspond to excitations of the s-, p_x-, and $d_{y^2-z^2}$-waves. Figure 15 suggests that the electron decays from p_x to s in under 15 au of time. However, due to the same aforementioned basis effects, the electron oscillates between the s- and p_x-states. Lastly, the phase space contour of the Schrödinger coefficients are presented in Fig. 16.

3.4. Asymptotic radiation

It has been demonstrated that the dynamics of the hydrogen atom's electron in the presence of the electromagnetic field was quasiperiodic. This unphysical behavior is due to the fact the electromagnetic radiation produced by the electron cannot escape to infinity and carry away energy, momentum, and angular momentum. Rather, the radiation reflects off of the artificial boundaries of the finite spatial basis and reexcites the electron.

The asymptotic problem, be it electromagnetic radiation or free (ionized) electrons, has posed a difficult numerical challenge. Free electromagnetic radiation in vacuum does not spread in time, since there is no dispersion, but does travel at the speed of light $c \approx 137$ au. However, the velocity of the sources of charge and current, *e.g.*, the electron in the hydrogen atom, is on the order of 1 au. This drastically different velocity scale makes a numerical description of the time-dependent theory in direct space quite demanding.

On the other hand, the description of the free nonrelativistic electron is made difficult by a combination of its large velocity v ($v < c$), the spreading of its wavepacket, and the rapid oscillation of its phase. Even in vacuum, the Schrödinger equation is dispersive so that the electronic wavepacket width grows proportionally with time and its phase grows quadratically with the distance from the center of the wavepacket. Several techniques have been developed to partially treat these problems. In 1947, Wigner and Eisenbud [78] developed the R-matrix method, which provides a technique for matching the solutions on some surface separating the inner bound state region and outer scattering state region. More recently, masking functions, repetitive projection and complex rotation methods, and Siegert pseudostates are common theoretical tools. These techniques are discussed by Yoshida, Watanabe, Reinhold, and Burgdörfer in [79] and by Tolstikhin, Ostrovsky, and Nakamura in [80]. A scaling transformation method that eliminates the rapid phase variation and wavepacket expansion and requires no matching at infinity has been presented by Sidky and Esry in [81]. Lastly, McCurdy and collaborators [82–84] have effectively implemented an exterior complex scaling method [85] in the time-independent formulation of scattering theory. The exterior complex scaling method maps all coordinates beyond a certain radius to a contour that is rotated by some fixed angle into the complex plane. This technique damps all purely outgoing scattered waves to zero exponentially which permits a numerical treatment on a finite domain or grid.

A formulation of the asymptotic numerical problem that falls more in line with the canonical treatment presented in this paper would begin at the Lagrangian level with a Lagrangian of the form

$$\mathcal{L} = \mathcal{L}_{\text{ENRD}} + \mathcal{L}_{\text{coupling}} + \mathcal{L}_{\text{free}}. \tag{137}$$

The ENRD Lagrangian $\mathcal{L}_{\text{ENRD}}$ would be the Maxwell and Schrödinger Lagrangians in (17) and (18). The dynamics of this system would be described by two different types of basis

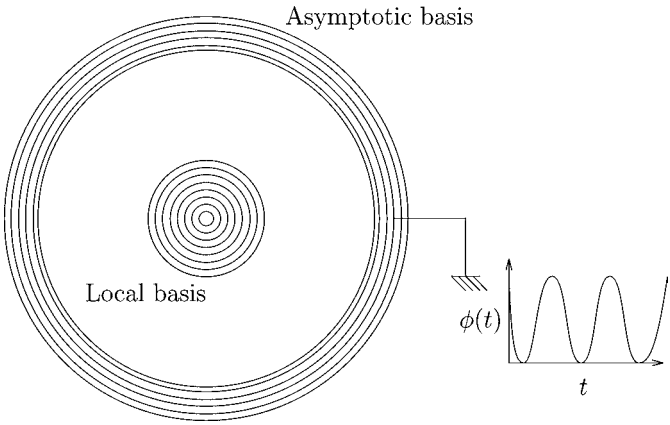

Fig. 17. Schematic picture of the local and asymptotic basis proposed for the description of electromagnetic radiation and electron ionization. The amplitude from the asymptotic basis is dumped into the free field ϕ, which acts as a storage tank for energy and probability.

functions. As pictured in Fig. 17, the atomic or molecular system would have a local basis representation in terms of real Gaussian basis functions of the form

$$G_{\mathcal{K}}(\mathbf{x}) = G^*_{\mathcal{K}}(\mathbf{x}) = N_{\mathcal{K}} \exp\bigl(-\ell_{\mathcal{K}}[\mathbf{x} - \mathbf{r}_{\mathcal{K}}]^2\bigr). \tag{99}$$

Further away, a set of complex basis functions of the form

$$\mathcal{G}_k(\mathbf{x}) = \sum_{lm} C_{lm} Y_{lm}(\hat{\mathbf{x}}) \frac{e^{ikr}}{r} \exp\bigl(-ar^2\bigr) \tag{138}$$

would be used, where the wavevector magnitude $k = \omega/c$ could be chosen to lie in some range $k_{\min} \leqslant k \leqslant k_{\max}$ and most likely only a few l would be necessary. These complex basis functions will require the calculation of new matrix elements. The free Lagrangian $\mathcal{L}_{\text{free}}$ would be the free particle Lagrangian $i\psi^*\dot{\psi} - \{i\nabla\psi^* \cdot -i\nabla\psi\}/2m$ or the free field Lagrangian $\partial_\alpha\phi^*\partial^\alpha\phi$. The solutions of the free equations of motion derived from these free Lagrangians are known analytically and are of the form $\exp(i[\mathbf{k}\cdot\mathbf{x} - \omega t])$. The coupling Lagrangian should be a Lorentz scalar that is made up of a certain combination or product of dynamical variables of $\mathcal{L}_{\text{ENRD}}$ and of $\mathcal{L}_{\text{free}}$. If amplitude is put into the coefficients of the asymptotic basis functions $\mathcal{G}_k$, then the amplitude will transfer to the free solutions ψ or ϕ. This amplitude will provide an initial condition for the free fields, thereby defining ψ or ϕ throughout space–time. The free fields will store the energy and probability (and momentum and angular momentum) radiated at infinity, which is needed to maintain the various conservation laws.

3.5. Proton dynamics in a real basis

The previous complex Schrödinger Lagrangians may be written in real form by taking the electronic wavefunction $\Psi = [Q + iP]/\sqrt{2}$ and the protonic wavefunction $\Omega = [U + iW]/\sqrt{2}$. In terms of these real dynamical variables the Hamiltonian density becomes

$$\mathcal{H} = \frac{[-4\pi c\mathbf{\Pi}]^2 + [\nabla \times \mathbf{A}]^2 - [4\pi c\Theta]^2}{8\pi} - c\nabla\Phi \cdot \mathbf{\Pi} - c\Theta\nabla \cdot \mathbf{A}$$
$$+ \frac{[\nabla Q + q\mathbf{A}P/c]^2 + [-\nabla P + q\mathbf{A}Q/c]^2}{4m_q} + q\Phi\frac{Q^2+P^2}{2}$$
$$+ \frac{[\nabla U + \bar{q}\mathbf{A}W/c]^2 + [-\nabla W + \bar{q}\mathbf{A}U/c]^2}{4m_{\bar{q}}} + \bar{q}\Phi\frac{U^2+W^2}{2}. \tag{139}$$

As in (98), each of the dynamical variables may be expanded into a basis. In particular, the real and imaginary components of Ψ and Ω are expanded as

$$Q(\mathbf{x},t) = \sum_{\mathcal{K}} G_{\mathcal{K}}(\mathbf{x})q_{\mathcal{K}}(t), \qquad U(\mathbf{x},t) = \sum_{\mathcal{K}} G_{\mathcal{K}}(\mathbf{x})u_{\mathcal{K}}(t),$$
$$P(\mathbf{x},t) = \sum_{\mathcal{K}} G_{\mathcal{K}}(\mathbf{x})p_{\mathcal{K}}(t), \qquad W(\mathbf{x},t) = \sum_{\mathcal{K}} G_{\mathcal{K}}(\mathbf{x})w_{\mathcal{K}}(t). \tag{140}$$

The basis functions $G_{\mathcal{K}}$ are chosen to be simple s-Gaussians. The Hamilton equations of motion associated with these real dynamical variables are

$$\begin{pmatrix} 0 & 0 & 0 & -M^T & 0 & 0 & 0 \\ 0 & 0 & 0 & 0 & -N^T & 0 & 0 \\ 0 & 0 & 0 & 0 & 0 & -C^T & 0 \\ 0 & 0 & 0 & 0 & 0 & 0 & -K^T \\ M & 0 & 0 & 0 & 0 & 0 & 0 \\ 0 & N & 0 & 0 & 0 & 0 & 0 \\ 0 & 0 & C & 0 & 0 & 0 & 0 \\ 0 & 0 & 0 & K & 0 & 0 & 0 \end{pmatrix} \begin{pmatrix} \dot{a} \\ \dot{\phi} \\ \dot{q} \\ \dot{u} \\ \dot{\pi} \\ \dot{\theta} \\ \dot{p} \\ \dot{w} \end{pmatrix} = \begin{pmatrix} \partial H/\partial a \\ \partial H/\partial \phi \\ \partial H/\partial q \\ \partial H/\partial u \\ \partial H/\partial \pi \\ \partial H/\partial \theta \\ \partial H/\partial p \\ \partial H/\partial w \end{pmatrix}, \tag{125}$$

where

$$M_{\mathcal{K}\mathcal{M}} \equiv \frac{\partial^2\langle \mathbf{\Pi}|\mathbf{A}\rangle}{\partial \boldsymbol{\pi}_{\mathcal{K}}\partial \boldsymbol{a}_{\mathcal{M}}}, \qquad N_{\mathcal{K}\mathcal{M}} \equiv \frac{\partial^2\langle \Theta|\Phi\rangle}{\partial\theta_{\mathcal{K}}\partial\phi_{\mathcal{M}}},$$
$$C_{\mathcal{K}\mathcal{M}} \equiv \frac{\partial^2\langle P|Q\rangle}{\partial p_{\mathcal{K}}\partial q_{\mathcal{M}}}, \qquad K_{\mathcal{K}\mathcal{M}} \equiv \frac{\partial^2\langle W|U\rangle}{\partial w_{\mathcal{K}}\partial u_{\mathcal{M}}} \tag{141}$$

and where the integrals $\langle\cdot|\cdot\rangle$ involve only Gaussian functions.

4. CONCLUSION

Nonperturbative analytical and numerical methods for the solution of the nonlinear Maxwell–Schrödinger equations have been presented including the complete coupling of both systems. The theory begins by applying the calculus of variations to the Maxwell and Schrödinger Lagrangians together with a gauge fixing term for the Lorenz gauge. Within the Hamiltonian or canonical prescription, this yields a set of first order differential equations in time of the form

$$\omega_{ab}\dot{\eta}^b = \partial H/\partial\eta^a. \tag{142}$$

These Maxwell–Schrödinger equations are closed when the Schrödinger wavefunction is chosen as a source for the electromagnetic field and the electromagnetic field acts back

upon the wavefunction. Moreover, this system of equations forms a well-defined initial value problem. That is, the entire dynamics is known in principle once the initial values for each of the dynamical variables η are specified. The resulting dynamics enjoys conservation of energy, momentum, angular momentum, and charge between the matter and the electromagnetic field.

In practice, the Maxwell–Schrödinger equations are represented in a finite basis of Gaussian functions $G_{\mathcal{K}}(\mathbf{x})$ and solved numerically. That is, each dynamical variable is expanded in this basis according to

$$\eta(\mathbf{x}, t) = \sum_{\mathcal{K}} G_{\mathcal{K}}(\mathbf{x}) \eta_{\mathcal{K}}(t), \tag{143}$$

where the time-dependent coefficients $\eta_{\mathcal{K}}(t)$ carry the dynamics. As a result, a hierarchy of approximate equations of motion are generated that basis-represent the exact Maxwell–Schrödinger equations and can be made systematically more and more accurate by enriching the basis. In the limit of a complete basis, these approximate equations would be exact since the Gaussian functions span L^2.

The basis representation of the Maxwell–Schrödinger equations of motion has been numerically implemented in a FORTRAN 90 computer program. This program allows for an arbitrary rank basis of s-Gaussians of varying widths and centers. It has been used to explore the dynamics of the hydrogen atom interacting with the electromagnetic field. In particular, stationary states of the combined atom-field system have been constructed as well as nonstationary states that radiate. This radiation carries away energy, momentum, and angular momentum from the hydrogen atom. A series of plots are presented to document the radiative decay of hydrogen's electron from a superposition of s and p_x states to the s ground state.

In order to improve numerical convergence, a canonical transformation was performed on the Maxwell–Schrödinger equations to isolate the Coulombic or electrostatic contribution to the scalar potential Φ_C and electric field $\mathbf{E}_C$. This portion of the fields can be performed analytically once the source ρ is specified by solving the Poisson equation $\nabla^2 \Phi_C = -4\pi\rho$ and then calculating $\mathbf{E}_C = -\nabla\Phi_C$. By removing the burden of describing both the Coulombic and radiative contributions to the electrodynamics, the efforts of the basis are focused entirely on the description of the radiation. The canonical transformed equations of motion have been represented in a Gaussian basis as done previously and have been added to the existing FORTRAN 90 computer program. With an optional flag the Coulomb reference can be used. Otherwise the raw numerical basis is used by default. As before, a series of plots are presented to document the dynamics of the hydrogen atom interacting with the electromagnetic field. The results in both cases are analyzed.

The work presented in this paper is particularly applicable to physical situations where the dynamics of the sources of charge and current occurs on the same timescale as the dynamics of the electromagnetic field. In these situations, adiabatic and perturbative approaches may be insufficient to describe the strongly coupled matter–field dynamics. Possible applications of the Maxwell–Schrödinger theory lie in photon–electron–phonon dynamics in semiconductor quantum wells [10], spontaneous emission in cold atom collisions [11,12], atom–photon interaction in single atom laser cavities [14,15], and photon–exciton dynamics in fluorescent polymers [16].

REFERENCES

[1] M.H. Anderson, J.R. Ensher, M.R. Matthews, C.E. Wieman, E.A. Cornell, *Science* **269** (1995) 198.
[2] K.B. Davis, *et al.*, *Phys. Rev. Lett.* **75** (1995) 3969.
[3] A. Keiling, J.R. Wygant, C.A. Cattell, F.S. Mozer, C.T. Russell, *Science* **299** (2003) 383.
[4] G.T. Marklund, *et al.*, *Nature* **414** (2001) 724.
[5] P.T. Newell, *Nature* **414** (2001) 700.
[6] P.A.M. Dirac, *The Principles of Quantum Mechanics*, fourth ed., Oxford Univ. Press, Oxford, 1958.
[7] E. Merzbacher, *Quantum Mechanics*, third ed., Wiley, New York, 1998.
[8] A. Messiah, *Quantum Mechanics*, first ed., Wiley, Amsterdam, 1961.
[9] J.D. Jackson, *Classical Electrodynamics*, third ed., Wiley, New York, 1999.
[10] K. El Sayed, J.A. Kenrow, C.J. Stanton, *Phys. Rev. B* **57** (1998) 12369.
[11] C. Orzel, S.D. Bergeson, S. Kulin, S.L. Rolston, *Phys. Rev. Lett.* **80** (1998) 5093.
[12] S.D. Gensemer, P.L. Gould, *Phys. Rev. Lett.* **80** (1998) 936.
[13] Y. Mu, C.M. Savage, *Phys. Rev. A* **46** (1992) 5944.
[14] J. McKeever, A. Boca, A.D. Boozer, J.R. Buck, H.J. Kimble, *Nature* **425** (2003) 268.
[15] H. Carmichael, L.A. Orozco, *Nature* **425** (2003) 246.
[16] M. Nisoli, S. Stagira, M. Zavelani-Rossi, S. DeSilvestri, P. Mataloni, C. Zenz, *Phys. Rev. B* **59** (1999) 11328.
[17] W. Heitler, *The Quantum Theory of Radiation*, vol. 3, Oxford Univ. Press, Oxford, 1954.
[18] E. Fermi, *Rev. Modern Phys.* **4** (1932) 87.
[19] J. Schwinger, *Selected Papers on Quantum Electrodynamics*, Dover Publications, New York, 1958.
[20] Y. Aharonov, D. Bohm, *Phys. Rev.* **115** (1959) 485.
[21] M. Guidry, *Gauge Field Theories*, Wiley, New York, 1980.
[22] C.W. Misner, K.S. Thorne, J.A. Wheeler, *Gravitation*, W.H. Freeman & Company, San Francisco, 1973.
[23] H.C. Ohanian, R. Ruffini, *Gravitation and Spacetime*, second ed., W.W. Norton & Company, New York, 1976.
[24] M.E. Peskin, D.V. Schroeder, *An Introduction to Quantum Field Theory*, Perseus Books, Cambridge, 1995.
[25] D. Griffiths, *Introduction to Elementary Particles*, Wiley, New York, 1987.
[26] A.O. Barut, *Electrodynamics and Classical Theory of Fields and Particles*, Dover, New York, 1964.
[27] H. Goldstein, *Classical Mechanics*, second ed., Addison–Wesley, Reading, MA, 1980.
[28] J.V. José, E.J. Saletan, *Classical Dynamics: A Contemporary Approach*, Cambridge Univ. Press, Cambridge, 1998.
[29] R. Abraham, J.E. Marsden, *Foundations of Mechanics*, second ed., Benjamin/Cummings, Reading, MA, 1978.
[30] C. Cohen-Tannoudji, J. Dupont-Roc, G. Grynberg, *Photons and Atoms*, Wiley, New York, 1989.
[31] H.A. Lorentz, *Theory of Electrons*, second ed., Dover, New York, 1952.
[32] H.F.M. DaCosta, D.A. Micha, K. Runge, *Phys. Rev. A* **56** (1997) 3334.
[33] H.F.M. DaCosta, D.A. Micha, K. Runge, *J. Chem. Phys.* **107** (1997) 9018.
[34] D.P. Craig, T. Thirunamachandran, *Molecular Quantum Electrodynamics*, Dover, New York, 1984.
[35] G.C. Schatz, M.A. Ratner, *Quantum Mechanics in Chemistry*, Prentice Hall, Englewood Cliffs, NJ, 1993.
[36] E.T. Jaynes, F.W. Cummings, *Proc. IEEE* **51** (1963) 89.
[37] M.D. Crisp, E.T. Jaynes, *Phys. Rev.* **179** (1969) 1253.
[38] R.K. Nesbet, *Phys. Rev. Lett.* **27** (1971) 553.
[39] R.K. Nesbet, *Phys. Rev. A* **4** (1971) 259.
[40] R.J. Cook, *Phys. Rev. A* **27** (1983) 2265.
[41] A.O. Barut, J.F. Van Huele, *Phys. Rev. A* **32** (1985) 3187.
[42] A.O. Barut, J.P. Dowling, *Phys. Rev. A* **41** (1990) 2284.
[43] A.O. Barut, J.P. Dowling, *Phys. Rev. A* **43** (1991) 4060.
[44] I. Bialynicki-Birula, *Phys. Rev. A* **34** (1986) 3500.
[45] M.D. Crisp, *Phys. Rev. A* **43** (1991) 4058.
[46] S.D. Bosanac, *J. Phys. A* **27** (1994) 1723.
[47] S.D. Bosanac, *Phys. Rev. A* **50** (1994) 2899.
[48] S.D. Bosanac, *J. Phys. A* **34** (2001) 473.
[49] N. Došlić, S.D. Bosanac, *Phys. Rev. A* **51** (1995) 3485.
[50] P.W. Milonni, J.R. Ackerhalt, H.W. Galbraith, *Phys. Rev. Lett.* **50** (1983) 966.
[51] M.D. Crisp, *Phys. Rev. A* **39** (1989) 6224.

[52] M.D. Crisp, *Phys. Rev. A* **42** (1990) 3703.
[53] M.D. Crisp, *Phys. Rev. A* **44** (1991) 563.
[54] M.D. Crisp, *Phys. Rev. A* **46** (1992) 4138.
[55] M.D. Crisp, *Phys. Rev. A* **54** (1996) 87.
[56] R.P. Feynman, *Phys. Rev.* **76** (1949) 769.
[57] J.R. Ackerhalt, P.L. Knight, J.H. Eberly, *Phys. Rev. Lett.* **30** (1973) 456.
[58] J.V. Shebalin, *Phys. Lett. A* **226** (1997) 1.
[59] E.A. Power, T. Thirunamachandran, *Phys. Rev. A* **28** (1983) 2649.
[60] E.A. Power, T. Thirunamachandran, *Phys. Rev. A* **28** (1983) 2663.
[61] A. Salam, T. Thirunamachandran, *Phys. Rev. A* **50** (1994) 4755.
[62] A. Salam, *Phys. Rev. A* **56** (1997) 2579.
[63] E.J. Moniz, D.H. Sharp, *Phys. Rev. D* **10** (1974) 1133.
[64] S.M. Blinder, *Int. J. Quantum Chem.* **90** (2002) 144.
[65] E.H. Lieb, M. Loss, Self-energy of electrons in non-perturbative QED, arXiv:math-ph/9908020, v2, 1999.
[66] M. Griesemer, E.H. Lieb, M. Loss, Ground states in non-relativistic quantum electrodynamics, arXiv:math-ph/0007014, v2, 2001.
[67] C. Sulem, P.-L. Sulem, *Nonlinear Schrödinger Equations: Self-Focusing and Wave Collapse, Applied Mathematical Sciences*, vol. 139, Springer-Verlag, 1999.
[68] D.J. Masiello, On the canonical formulation of electrodynamics and wave mechanics, PhD thesis, University of Florida, 2004.
[69] D. Masiello, E. Deumens, Y. Öhrn, *Phys. Rev. A* **71** (2005) 032108.
[70] P.A.M. Dirac, V.A. Fock, B. Podolsky, On quantum electrodynamics, in: J. Schwinger (Ed.), *Selected Papers on Quantum Electrodynamics*, Dover, New York, 1958, pp. 29–40.
[71] D.H. Kobe, *Amer. J. Phys.* **49** (1981) 581.
[72] P. Ring, P. Schuck, *The Nuclear Many-Body Problem*, Springer-Verlag, New York, 1980.
[73] P. Kramer, M. Saraceno, *Geometry of the Time-Dependent Variational Principle in Quantum Mechanics*, *Lecture Notes in Physics*, vol. 140, Springer-Verlag, Berlin, 1981.
[74] J.D. Jackson, *Amer. J. Phys.* **70** (2002) 917.
[75] M. Nowakowski, *Amer. J. Phys.* **67** (1999) 916.
[76] E. Anderson, *et al.*, *LAPACK Users Guide*, Society for Industrial and Applied Mathematics, Philadelphia, 1992.
[77] W.H. Press, B.P. Flannery, S.A. Teukolsky, W.T. Vetterling, *Numerical Recipes*, Cambridge Univ. Press, Cambridge, 1986.
[78] E.P. Wigner, L. Eisenbud, *Phys. Rev.* **72** (1947) 29.
[79] S. Yoshida, S. Watanabe, C. Reinhold, J. Burgdörfer, *Phys. Rev. A* **60** (1999) 1113.
[80] O.I. Tolstikhin, V. Ostrovsky, H. Nakamura, *Phys. Rev. A* **58** (1998) 2077.
[81] E.Y. Sidky, B.D. Esry, *Phys. Rev. Lett.* **85** (2000) 5086.
[82] M. Baertschy, T. Rescigno, W. Isaacs, X. Li, C. McCurdy, *Phys. Rev. A* **63** (2001) 022712.
[83] C. McCurdy, D. Horner, T. Rescigno, F. Martín, *Phys. Rev. A* **69** (2004) 032707.
[84] T.N. Rescigno, M. Baertschy, W.A. Isaacs, C.W. McCurdy, *Science* **286** (1999) 2474.
[85] B. Simon, *Phys. Lett. A* **71** (1979) 211.

This page intentionally left blank

Stopping Power—What Next?

John R. Sabin[1] and Jens Oddershede[2]

[1]*Departments of Physics and Chemistry, University of Florida, Gainesville, FL, USA*
[2]*Kemisk Institut, Syddansk Universitet, Odense, Denmark*

Abstract

The purpose of this chapter is to review the current limits of our understanding of the slowing down of charged particles traversing matter. We discuss some of the effects often omitted in contemporary calculations and interpretation of stopping power data, and we discuss some of the challenging new physics that may be obtained from experimental setups yet to be built. We emphasize the symbiosis between theory and experiment in this endeavor.

Contents

1. INTRODUCTION

From the earliest discussions of the slowing down of charged particles as they traverse matter, there has been a significant interplay among the early experimental and theoretical [1–7] investigations of the phenomenon. As is usual in physics, the effort to compare a calculated to a measured quantity is hampered by the necessity of assuring that the same thing is being calculated as is measured. Otherwise put: "Experiments—what do they measure?" and "Theories—what do they calculate?"

Since these early times, the bulk of the discussion of the energy deposition of a swift particle in matter per unit path length, $-dE/dx$, referred to as the *stopping power* of the material, has been made in the context of a model where energy is transferred from a heavy

ADVANCES IN QUANTUM CHEMISTRY, VOLUME 49
ISSN: 0065-3276 DOI: 10.1016/S0065-3276(05)49007-3

ion projectile to the electrons, and, to a lesser extent, to the nuclei of the target material, leading to excitation and ionization of the target [8,9]. Theories of this sort have been tremendously successful [10,11], as have those which treat energy loss as a continuous slowing down of the projectile in an extended medium [12–16]. In both of the foregoing cases, projectile energy is transferred to the target electrons, and perhaps to target nuclear recoil, leading to a slowing of the projectile.

Parallel to theoretical developments, experiments and their analysis have also progressed rapidly, leading to several very useful compilations of stopping properties [17–22].

Theory typically deals with individual collisions between a projectile and a single atom or molecule or model of a solid while experiment deals typically with measurements following multiple collisions. The connection between the two has been clearly enunciated by Inokuti [23] when he answers the rhetorical question "What do we mean by stopping power?"

His answer [23]: "An experimentalist naturally thinks of the stopping power as the mean energy loss of an energetic particle per unit path length in a given material. Suppose that a particle of given kinetic energy T passes through a thickness Δx and emerges with kinetic energy T'. Repeated trials will result in a distribution of T' values. The mean of $T - T'$ is ΔT, the stopping power is the limit of $\Delta T/\Delta x$ as $\Delta x \to 0$. The limit $\Delta x \to 0$ is an idealization; in practice it means that the length is sufficiently short. We should ask what is meant by "sufficiently short". We should also recognize that the above definition presumes that a particle travels virtually along a straight line, without appreciable deflection. This picture indeed applied to any particle of very high energy, but it becomes progressively more unrealistic with decreasing energy, especially for a light particle such as an electron or a positron.

"A theoretician usually evaluated the stopping power from the cross section for a single collision. Consider a material consisting of n structural units per unit volume. For brevity, let us call the structural unit a molecule. Suppose that $[d\sigma(T, E)/dE]\,dE$ represents the cross section for a collision of a particle with kinetic energy T with a molecule, resulting in energy transfer between E and $E + dE$. Then, the stopping power is evaluated as $n \int dE\, E\, d\sigma(T, E)/dE$.

"Are the definitions of the experimentalist and the theoretician equivalent? The answer is certainly yes, if the material is so thin that a particle collides with a molecule only once at most. Indeed, cross section measurements are carried out for this circumstance, and then a distribution of energy loss is called the energy-loss spectrum. However, when the material is thick enough to cause multiple collisions, the question warrants some discussion." [23]. (There is some discussion of the question of taking the zero thickness limit of a target in Refs. [24], [25], and [26].)

This is the point of view we espouse here.

Both theory and experiment have been most successful at treating stopping at projectile energies above the stopping maximum in the stopping curve (~100 keV/amu), but have been less successful at lower energies. It is the results of calculations and experiments in this energy range that tempt one to say that all there is left to do in the field is to refine the numbers [27].

Several issues now become apparent, in terms of both calculated and measured stopping properties of matter. There are, in fact, many problems which are theoretically open, and many effects which have yet to be experimentally deconvoluted from stopping power measurements. To wit:

- Present day calculations of stopping power, based on cross sections extracted from collision theory, allow much more detailed understanding of the partition of the transferred energy among the available degrees of freedom, in both projectile and target, than do traditional experimental methods. Further, such calculations are not, in principle, restricted to higher projectile energies.
- Traditional methods do not allow for excitation and ionization of a dressed projectile.
- Normally, it is assumed that electron number is separately conserved in both target and projectile, and charge changing events and their consequences are frequently ignored.
- It is difficult to measure low energy stopping, that is, stopping with projectile energies lower than that at the peak in the stopping power curve, or to calculate it using traditional methods.
- Many of the theoretical methods used today have their origins in perturbation theory. It is, however, difficult to treat higher order processes sufficiently accurately with traditional methods. The Barkas effect [28], traceable to polarization effects and proportional to Z_1^3, is a particularly good example.
- Traditionally, gas and liquid targets have been considered as collections of randomly ordered target molecules. With present methods, these molecules can be specifically oriented, and directional effects can be discussed.
- Except for cases where channeling is important, traditional methods generally ignore orientational effects in the target.
- Traditionally, the Bragg Rule [29–31] is assumed when dealing with larger target systems such as those of biological interest. In fact, deviations from the Bragg Rule, arising from molecular bonding, need to be understood more deeply. We note that with the advent of cluster and cluster ion projectiles, a projectile-Bragg-Rule might also be appropriate.
- Traditional methods do not do well with complex or cluster projectiles, as they ignore projectile structure.
- Traditionally, target phase effects are considered small, and ignored [32,33].
- In traditional approaches, negative stopping powers, corresponding to projectile acceleration, are not expected.
- In traditional methods, relativistic effects, both those associated with the speed of the projectile and those associated with the quantum mechanical description of a target containing heavy atoms, are seldom addressed.
- Collision induced radiation, from either projectile or target, is generally ignored.

Considering that knowledge of the details of energy deposition is necessary both in order to understand the details of energy deposition and to design experiments probing specific questions, a desirable situation, especially in the biological arena, the above-mentioned issues need to be understood. These problems are discussed below.

2. WHAT IS STOPPING POWER?

Bohr's early writings on energy deposition are quite clear [6] when he writes "... we shall assume that the atom consists of a central nucleus carrying a positive charge and surrounded by a cluster of electrons kept together by the attractive forces from the nucleus. The nucleus is the seat of practically the entire mass of the atom and has dimensions

exceedingly small compared with the dimensions of the surrounding cluster of electrons. If an α or β particle passes through a sheet of matter it will penetrate through the atoms, and in colliding with the electrons and nuclei it will suffer deflexions from its original path and lose part of its kinetic energy. The deflexions will give rise to the scattering of the rays, and the second effect will produce a decrease in their velocity. On account of the intense field around the nuclei the main part of the scattering will be due to the collisions of the α or β particles with them; but on account of the great mass of the nuclei the total kinetic energy lost in such collisions will be negligibly small compared with that lost in collisions with the electrons. In calculating the decrease of velocity we shall therefore consider only the effect of the latter collisions."

Bohr's view is, then, that the incoming particle collides with a target atom giving up some of its kinetic energy to the atomic electrons which are excited or ionized in the process, with the result that projectile slows down. The result is a conversion of projectile kinetic energy to target electronic energy. This view of the energy loss process has continued to be held over the past hundred years [7], but with an increasingly sophisticated quantum picture initially formulated by Bethe [10,11] supplanting the semi-classical treatment of Bohr. Authors continue to calculate stopping powers from projectile *energy loss*, but energy loss is interpreted to mean kinetic energy loss in most cases (see Refs. [8], [34], and [35] among others).

However, it has long been clear that projectile kinetic energy loss, and by this is meant the kinetic energy of the center of mass of the projectile, is not the only way a projectile can lose energy. Perhaps the most important other process contributing to energy loss is charge exchange between projectile and target, leading to a time dependent projectile charge. This was noticed early on by Bethe [36,37], but, presumably due to computational difficulties, has not been incorporated into most traditional theory.

Other energy loss mechanisms are also possible and include radiation losses, magnetic interactions [38], and transfer of energy to the target nuclei (nuclear stopping). If the target is a molecule, rather than a simple atomic gas, there can be energy transferred to the vibrational and rotational states of the target and target fragmentation as well.

The final complication that we mention here is that the projectile can also be complex: it could be a dressed ion [39] in either the ground or an excited state, or it could be either a molecule or a cluster or cluster ion in a particular electronic, vibrational, and rotational state. In any case, the projectile kinetic energy could be influenced by internal interconversion of kinetic and other sorts of energy.

3. METHODOLOGY

3.1. Theory

In order to discuss stopping power, let us first review several standard formulations of stopping power. In general, the formulas for stopping power are derived from a differential cross section $d\sigma/d\Omega$.

Bohr states [7] that the energy deposited by an ion beam when transiting a target of thickness Δx and with a scattering center density, n_2, is given by

$$-\Delta E = \sum_i^N \Delta E_i n_2 \sigma_i \Delta x, \tag{1}$$

where ΔE_i is the kinetic energy deposited by the projectile (energy loss) for each collision i in the path length Δx with a cross section σ_i. The minus sign on the left-hand side of equation (1) assures a positive energy loss. In the limit when $\Delta x \to 0$, the energy loss per unit path length (stopping power) for a projectile becomes:

$$-\frac{dE}{dx} = n_2 \int \Delta E \, d\sigma = n_2 \int \Delta E \frac{d\sigma}{d\Omega} \, d\Omega. \tag{2}$$

The energy loss per unit path length per scattering center or stopping cross section, which contains all the physics of the process, can then be written:

$$S = -\frac{1}{n_2}\frac{dE}{dx} = \int \Delta E \frac{d\sigma}{d\Omega} \, d\Omega. \tag{3}$$

Note that in the above, the path length, Δx, is the physical path length of the projectile, not the penetration depth. Also, in these equations, the projectile velocity dependence of the stopping has been suppressed.

Stopping power is most commonly understood in the context of perturbation theory. (Many reviews of energy deposition are available such as those found in Refs. [40], [41], [42], [43], and [44] among others, many of which are slanted towards a particular application.) In a time-independent approach based on the First Born Approximation such as that of Bethe [10,11], the scattering cross section is usually obtained through Fermi's golden rule. This formulation leads to the Bethe formula for the stopping:

$$-\frac{\Delta E(v)}{\Delta x} \approx -\frac{dE}{dx} = nS(v) = \frac{4\pi n e^4 Z_1^2 Z_2}{m_e v^2} L_0(v), \tag{4}$$

where Z_1 and Z_2 are the (fixed) projectile charge and target electron number, respectively, and L_0 is the Bethe stopping number (including relativistic terms):

$$L_0^{\text{Bethe}} = \ln \frac{2m_e v^2}{I_0} + \ln\left(\frac{1}{1-\beta^2}\right) - \beta^2 - \delta/2. \tag{5}$$

As usual, $\beta = v/c$, and δ is the a density term [18,45] which corrects for relativistic polarization effects when projectile velocities become comparable to the projectile rest mass. The density correction was first computed by Sternheimer [46,47], and it reduces the Bethe stopping power for relativistically fast projectiles.

Here I_0 is the mean excitation energy of the target system, which is the first energy moment of the dipole oscillator strength distribution of the target [8], written:

$$\ln I_0 = \frac{\int \frac{df}{dE} \ln E \, dE}{\int \frac{df}{dE} \, dE}, \tag{6}$$

where $\{f\}$ is the dipole oscillator strength distribution of the target. I_0 is a materials constant which is a good indicator of the ability of the target to absorb energy. There are several sources of mean excitation energies. A mean excitation energy can be calculated directly from the definition using an atomic or molecular wavefunction [48]. However, the quality of the wavefunction can cause a large effect on the calculated value of I_0 [49], with mean excitation energies varying by nearly 30% between Hartree–Fock and correlated calculations. One can also extract mean excitation energies from experimental data by fitting an ansatz stopping model to the data, and using the mean excitation energies as one of the

fitting parameters *cf. e.g.* Refs. [9,18–20]. Here one must be careful as the mean excitation energy so calculated is no longer the quantity given by equation (6), but will contain contributions from all terms left out of the fitting ansatz [50].

In order to get better agreement with experiment, one normally adds additional terms to the Bethe logarithm to compensate for the approximations introduced in the Bethe derivation. The most egregious of these is that the target electrons are stationary—or at least moving slowly with respect to the projectile. A correction, called the shell corrections [51], written $-C/Z_2$ is thus added before comparing with experiment. If one adds other terms (which is seldom done) one can see that L_0 consists of the sum of terms proportional to the Z_1^2 [45] and one can write a series

$$L_0(v) = \sum_j L_{0j}(v). \tag{7}$$

Thus in the Bethe case $L_{00} = \ln \frac{2m_e v^2}{I_0}$, $L_{01} = -C/Z_2$, *etc.*

A further improvement can be made by avoiding the fast projectile assumption altogether rather than attempting to correct for it, and calculating the entire L_0 directly. In that case, the generalized oscillator strength (GOS) distribution is needed [52,53]. Results are good when compared with experiment, but the method is numerically viable for only the smallest atomic targets.

In the same vein as the foregoing, the energy loss and stopping can be calculated in higher orders of perturbation theory. Going beyond first order perturbation theory, the stopping number can be expanded in a Born series in the fixed projectile charge Z_1:

$$L(v) = \sum_i Z_1^i L_i(v), \tag{8}$$

where i labels both the power of the projectile charge and the order of perturbation theory in each term. Each of the terms L_i has been developed, typically motivated by an experimental observation. Thus, one refers to the Bethe/Born ($i = 0$), Barkas ($i = 1$), and Bloch ($i = 2$) terms. In addition, even higher level and relativistic terms [43] can be included.

While the Bethe approach is best suited for gaseous targets where the projectile can be assumes to interact with a single target atom or molecule at a time, an approach more suitable to study of solid state targets was developed by Lindhard *et al.* [12,54] in the 1950s and 1960s. This method is based on electron gas considerations, but, like the Bethe theory, is a perturbation treatment. Note that many other formulations for stopping power can be cast into the form of equations (4) and (8), but that each has a unique expression for L_0 corresponding to the specific physics of the development. For example, the Bohr theory leads to:

$$L_{00}^{\text{Bohr}} = \ln \frac{C m_e v^3}{Z_1 v_0 \hbar \omega_j} + \ln\left(\frac{1}{1-\beta^2}\right) - \frac{\beta^2}{2} - \delta/2, \tag{9}$$

where $C = 1.1229$ and ω_j is a harmonic oscillator resonant frequency [35]. However, the Lindhard, Scharff and Schiøtt (LSS) [15] formulation does not have a leading term proportional to Z_1^2, and can be brought only formally to this form.

We emphasize that in all of the foregoing formulations, the energy transfer is assumed to be kinetic energy loss of the projectile, and is obtained as the energy gained by the target by conservation of energy in the collision. All other processes such as charge exchange, projectile electronic excitation, vibrational and rotational energy exchange *etc.*, are neglected.

Another approach, which is computationally more intensive, calculates energy deposition properties directly from cross sections obtained from scattering theory.

In this case, one considers the simple case of an ion with some velocity v, not necessarily stripped, impacting on a target at an impact parameter b. For each trajectory, one can calculate the projectile kinetic energy loss and the angle of deflection, θ, leading to a deflection function $\Theta(b)$. For such a system, the stopping power, or energy loss per unit length for a projectile, is given by

$$S(E_\mathrm{p}) = -\frac{1}{n_2}\frac{dE}{dx} = -\int \Delta E(E_\mathrm{p}, \Omega)\frac{d\sigma}{d\Omega}\, d\Omega, \tag{10}$$

where again n_2 is the density of target scattering centers, ΔE is the kinetic energy loss of the projectile, and $d\sigma/d\Omega$ is the direct differential cross section. By using the deflection function, $\Theta(b)$, the integral in equation (10) can be transformed to the impact parameter representation, yielding

$$S(E_\mathrm{p}) = -\int b\, \Delta E(E_\mathrm{p}, b) db\, d\varphi. \tag{11}$$

Such a scheme is non-perturbative and thus includes all the terms in the Born expansion. It has the additional advantage that it restricts neither the projectile trajectory, possible charge exchange, nor energy transfer to and from all energy degrees of freedom in both projectile and target, and thus includes all of these processes. If not artificially restricted, the outcome of the collision is restricted only by quantum mechanics. To include these non-adiabatic effects clearly requires a time dependent analysis of the binary collision. Such schemes are beginning to come into use by various groups, notably those of Schiwietz and Grande [55,56], Arista [57], and Trujillo *et al.* [58–60], among others. Their use encourages the development experimental techniques that can distinguish among all channels for energy transfer.

3.2. Experiment

What is, in fact, measured? In order to compare calculations with experiments, or to design new experiments or calculate new properties, one must be certain that the calculated quantities correspond to those measured. In particular, to calculate a reliable stopping cross section, one must obtain accurate energy losses, ΔE, and scattering cross sections, $d\sigma/d\Omega$, for the collision, and precisely which energies are considered must be clearly defined. Should this energy be the kinetic energy loss of the projectile [61,62] or the energy gained by the target, which, considering the foregoing discussion, can be somewhat different. The purpose to which the stopping power is being put is thus important—clearly the latter in the case of tumor therapy, while it is the former that is important in ion implantation during microelectronics manufacture.

For purposes of this discussion, we consider a model stopping power experiment to begin with the production of a low fluence particle beam with all projectiles having a particular initial charge, in a specific electronic state (normally the ground state), and having a delta-function velocity distribution. The beam impinges on a differentially thin, low density target, and emerges after suffering a single collision with the target system, wherein energy, momentum, and charge may be exchanged. Finally, a measurement is carried out

on the exiting projectile. Although this scenario is certainly oversimplified, it is heuristically useful. In fact, in a measurement, the target will be of finite thickness, which will open the possibilities of charge fluctuation (multiple charge exchanges), multiple scattering and thus energy and charge straggling. Measurement of the energy loss of the projectile and the thickness of the target (usually as areal density), be it solid, liquid, or gas, gives the stopping power directly when extrapolated to zero target thickness [63]. These experiments may then be compared with the theoretical predictions mentioned above which lead to changes in the electronic energy of the projectile.

In fact, there seem to be two approaches in the methods of measurement of energy loss.

The simplest method, at least conceptually, of measuring the energy of the exiting projectile is based on measuring the projectile time-of-flight (TOF). Here, the time necessary for the ion to transit a fixed distance is recorded, giving the laboratory frame center of mass kinetic energy of the projectile directly. Thus the stopping power calculated from this measurement will be purely the kinetic energy version, in consort with the classical definitions. Although giving precise measurements of projectile kinetic energy, TOF based energy loss measurements thus will not take into account changes in non-kinetic energies such as charge exchange, projectile electronic excitation, rovibrational energy changes, or any of the other effects mentioned above.

A similar result is obtained by using a proportional counter, either gas or solid state, to measure the energy of the exiting projectile. In this case, collisions of the projectile ion with the detector produce a current pulse, the magnitude of which is proportional to the projectile kinetic energy. Again, the result is dependent on the projectile kinetic energy only, and on neither either charge or electronic state.

A quite different approach to the measurement of ion energy was proposed by Andersen [64–66] in the 1960s. The method is based in thermometric compensation techniques, where the measured energy is that of an ion brought to rest in a stopping block at liquid helium temperature. In the experiment, the projectile transits the sample foil and then is brought to rest in the stopping block. As the ion energy is converted in macroscopic time to heat energy in the block, which is subsequently measured, it is to be assumed that the projectile comes to rest in its ground, neutral state, and that all of the energy, kinetic and electronic (and rotational and vibrational if the projectile is polyatomic) is deposited in the block. Thus, this method measures something different than does the TOF measurement, namely it measures the sum of the total energy of the projectile above ground. What the method cannot do is to distinguish among the various sorts of energy that are present.

4. OTHER PROCESSES

The question then arises as to what contributions to the energy loss there might be in a stopping power measurement, what the magnitudes of such contributions might be, and whether such contributions might be interesting, useful, or possible to study.

Starting with the ultimate point, it seems clear that it is advantageous to know as much as possible about the details of energy deposition. In terms of nano-fabrication, interaction with biological systems, and radiation hardening of electronics, to name but a few examples, such knowledge might have great significance. For example, the ability to break a specific bond in molecule located deep within a sample is a possibility if the details of energy deposition in chemical bonds were known. It is, in fact, a well-exploited fact that

energy deposition from ions can be carried out with much less ancillary damage with ions than with electro-magnetic radiation due to the shape of the stopping cross section *vs.* projectile energy curve.

4.1. Stopping at low projectile energy

Many of the first principles methods used to study energy deposition invoke the approximation that the projectile is moving much faster than are the target electrons. Such an assumption restricts calculations to projectile velocities corresponding energies above that of the maximum in the stopping power curve, that is, above energies of something like 100 keV/amu. Such restrictions clearly do not apply to the schemes that primarily fit data to an ansatz stopping formula. Other schemes are somewhere in between, for example, that of Sigmund and Schinner [67] which relies on a combination of Bohr and Bethe stopping with added shell corrections, projectile excitation, and relativistic corrections. Although it is not explicitly stated what the lower velocity limit of this scheme is, results are reported for stopping powers down to 1 keV/amu with good agreement for several projectile solid target combinations.

Methods based on scattering theory do not have a low velocity cutoff in their ambit of applicability, and thus may be used down to very low collision energies. Rather, calculations have been made down to proton projectile energies of <10 eV with good agreement with experiment. In fact, the limitation on the projectile velocity is from above, as at high velocity the Dirac rather than the Schrödinger scheme must be used to calculate the scattering.

4.2. Higher order Born terms

The first term in the Born series (equation (8)), L_0, has been the focus of attention since the beginnings of stopping theory. It is, by far, the largest term in the series for projectile energies above the maximum in the stopping curve but below the energies where relativistic effects become important, and produces stopping cross sections which agree with experiments to $\pm 20\%$ in most cases.

The second term in the Born series is L_1, and results from the slight polarization of the target electron cloud under the influence of the projectile. It is proportional to Z_1^3, and is approximately an order of magnitude smaller than L_0 [68]. This is the first term in the Born series that distinguishes the sign of the projectile. It was first reported by Barkas [28] who measured the differences in ranges of $\Sigma^{\pm}$ baryons in emulsion, and is normally referred to as the Barkas term or the Barkas correction. There have been several expositions of L_1, for example, those in Refs. [57,69–74] and [75], all of which give approximately the same value within about a factor of two.

The Lindhard form of the Barkas correction can be written [74]:

$$L_{10} = \frac{3\pi e^2 I_0}{2\hbar m_e v^3} \ln \frac{2m_e v^2}{I_0}. \tag{12}$$

As this formulation is derived with respect to a stationary target electron, there could, presumably, be a shell correction type term, L_{11} to the Barkas correction as well. Although

the complete Barkas correction has been calculated for a spherical harmonic oscillator [76], the shell correction to the Barkas term for an atom or molecule has, to our knowledge, never been investigated.

The term proportional to Z_1^4, L_2, was proposed by Bloch [77], and provides a transition from the semi-classical Bohr formulation to the purely quantum mechanical Bethe formulation. The leading term in Bloch correction can be written:

$$L_{20} = -\sum_{\ell=0}^{\infty}(\ell+1)^{-3}\frac{v_0^2}{v^2} \tag{13}$$

plus higher order corrections in increasing even powers of v^{-1} [74].

The only other term in the Born series that has been investigated, to our knowledge, is L_5, which gives a stopping power contribution proportional to Z_1^7, and has been considered by Ahlen [78]. The effect arises from large velocity close collisions and effects the stopping by a few percent [78].

In any case, in the spirit of the Born expansion, there is much yet to be understood in terms of identifying and understanding terms for L_i, $i > 2$, and calculating and understanding shell corrections for terms with $j > 0$.

4.3. Charge fluctuation

Passage of a charged ion through matter, even if there occurs only a single distant collision, is likely to lead to charge exchange, and the likelihood increases directly with projectile net charge and, on average, inversely with projectile velocity. That is, the projectile can gain or lose electrons by interaction with the target, often several times as the projectile transits the medium. After direct transfer of kinetic energy from a projectile to the electrons in a target atom or molecule, this is probably the most important process in a stopping experiment. As most of the traditional methods for treatment of stopping assume a fixed projectile charge, they cannot address this situation. Dynamic methods, however, especially those that allow unrestricted trajectories and unrestricted charge states, can. The simple case of $He^{q+} \rightarrow Ne$ [79] shown in Fig. 1 gives a graphic representation of charge exchange. As the collision occurs, the quantum mechanical electron hopping in the interaction region is clearly illustrated. Note that the equilibrium charges show a net transfer of one electron from Ne to He^{2+}.

However, a more quantitative description of the exchange process is the charge exchange cross section.

As an example, calculation of the charge exchange cross section [80] for proton projectiles on water shows strong peaks in the exchange cross section in the region of $E_p = 10$ keV/amu [80], as shown in Fig. 2, indicating energy transfer channels that are not accounted in the kinetic energy transfer, if the calculations are to be believed. The experimental numbers of Rudd *et al.* [81] are also included, although they, unfortunately, do not go to lower energies.

A better example of charge exchange is perhaps shown in Fig. 3 for the collision of N^{4+} with H yielding $N^{3+} + H^+$ [82]. In this case, the projectile, however, is not stripped. Under these circumstances it, too, can experience ionization, electron capture, and excitation [39]. Again the illustration here is from a scattering type calculation as described above, done with END [39].

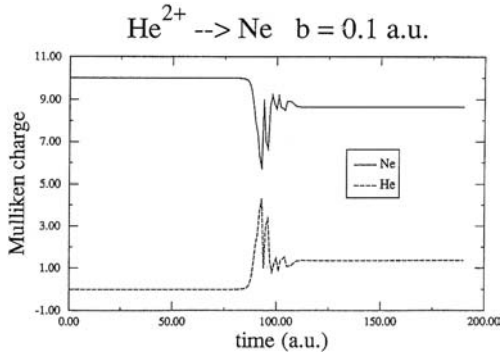

Fig. 1. Mulliken population fluctuation in a $He^{2+} \rightarrow Ne$ collision at 10 keV [79].

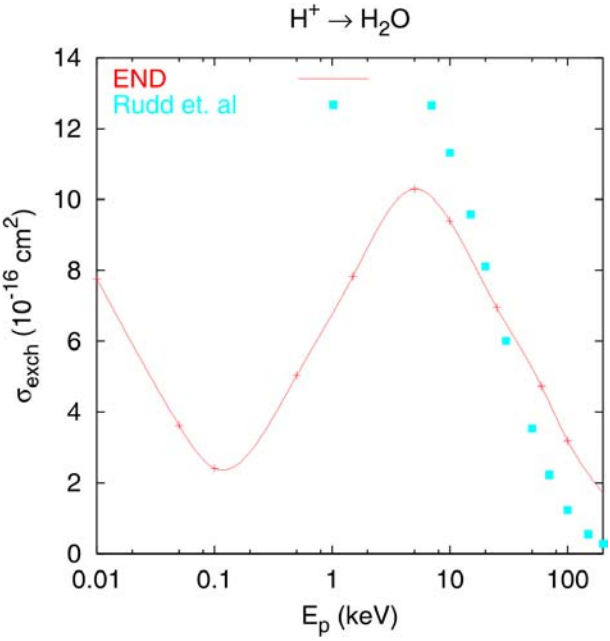

Fig. 2. Charge exchange cross section σ_{exch} for protons impinging on H_2O as a function of proton velocity along with the experimental results of Rudd *et al.* (filled circles) [81].

Figure 3 shows the charge exchange cross section for this process as a function of the projectile energy. First note that the main electron transfer process is electron capture by the projectile. Projectile electron loss has a low probability for the projectile energies of interest in this work, due to the large net charge on the projectile. For larger projectile energies ionization becomes of importance and requires a description using proper continuum states.

The largest contribution to the electron capture cross section comes from impact parameters in the range $b \sim 6$–7 a.u. [82] for all energies. Thus the N^{4+} ion apparently captures

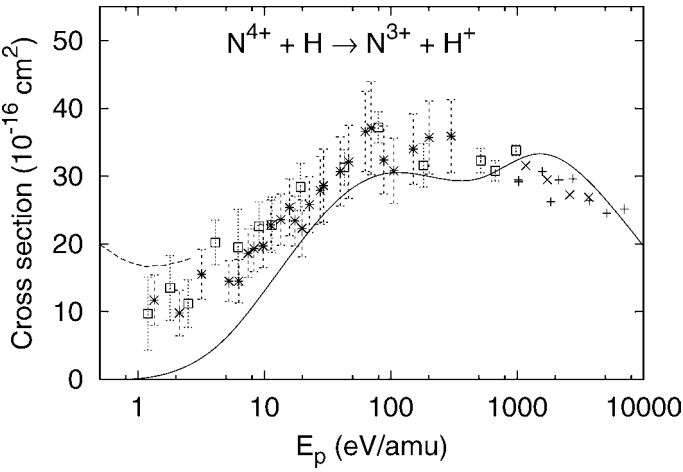

Fig. 3. Total charge exchange cross section for N^{4+} colliding with atomic H as a function of the projectile energy [82]. For comparison, we also show the theoretical coupled channel results (dashed line) from Feickert [83]. The experimental data are from: □ Huq *et al.* [84]; + Crandall *et al.* [85]; × Seim *et al.* [86]; ∗ Folkerts *et al.* [87].

an electron from hydrogen into an orbital approximately 6 to 7 a.u. from its center, thus forming what we denote as a "diffuse ion" with the 3 core electrons having configuration $1s^2 2s$ and the captured electron having highest probability in the 3s, 3p orbitals [87]. There are two maxima in the charge exchange probability as a function of the projectile energy. The first occurs around $E_p \sim 0.1$ keV/amu and the second one around $E_p \sim 2$ keV/amu.

In the same figure we present, for comparison, some experimental results [84–87]. Note that the calculated charge exchange cross section vanishes for low energy projectiles. This seems to agree with the experimental trend. For completeness, we also show the results obtained by Feickert *et al.* [83] by means of a coupled channel theory and a fitted charge exchange potential. Contrary to the results of Trujillo *et al.* [82], their results predict that for lower energies, the charge exchange cross section will increase as the projectile energy decreases; the well known Langevin-type cross section for orbiting. Unfortunately, experiment has nothing to say on the subject.

There has been some discussion of the problems associated with charge changing and projectile excitation from a semi-classical point of view [88], but without concrete examples.

4.4. Projectile excitation and ionization

Traditional methods of calculating stopping properties assume a fixed charge projectile and describe, in one way or another, only the excitation of the target due to collision. Even if the projectile is not stripped, no energy is transferred to the electronic structure of the projectile. That is to say, the mean excitation energy of the projectile is kept at infinity, so that there can be no energy transfer to the projectile (see equation (5)). In fact, this process can be quite important in terms of the details of the stopping process, perhaps second only to charge changes. In the spirit of the Bethe formulation of stopping, it is possible to write down a formalism where both projectile and target have a mean

excitation energy and may be excited [39], but this scheme has not been generally implemented.

Again, methods arising in collision theory should be better suited to treat the problems of projectile excitation. In those methods, the electronic structure of the projectile is not restricted, and excitation is allowed. So far, little attention has been paid to this process. However, it can also be treated by dynamical methods.

Some people use an effective charge to describe the fluxional charge state of a projectile as it transits a target system. Several formulas for effective charge are extant, the most prominent probably being those of Northcliffe [89,90] or of Brandt and Kitagawa [91]. The problem with this approach is that it is an attempt to force the concept of a static, albeit effective, charge on a fundamentally dynamic situation, so that a static charge analysis can be used. It is clear that this approach does not properly represent the physics of the situation: A dynamic approach should be used when projectile and target electron numbers are not separately conserved.

4.5. Nuclear motion

At low projectile velocity energy can be transferred to nuclear motion by a collision. In addition to nuclear stopping, that is, projectile kinetic energy transferred to the center of mass kinetic energy of the target, energy can be transferred to target internal nuclear degrees of freedom such as rotational and vibrational degrees of freedom. As an example, consider the case of proton projectiles on water. The orientationally averaged stopping cross section curve calculated by Cabrera-Trujillo *et al.* [80] is shown in Fig. 4. The curves are calculated within a scattering formalism called Electron Nuclear Dynamics (END), of the type outlined above [59], and they contain all of the non-translational contributions to the energy loss.

Along with the total stopping cross section, the electronic, nuclear, and rovibrational cross sections are included. As expected, the nuclear and rovibrational cross sections are largest at lower projectile energies, where nuclear energy transfer is obviously greatest, and at low projectile energy they make up a considerable fraction of the total stopping cross section. As the projectile in this case is a proton, there cannot be direct electronic excitation of the projectile. However, there is the possibility of capture of an electron into an excited state of the projectile.

4.6. Negative stopping

The possibility of energy gain on collision of a projectile with a target has been speculated upon since the early days of modern stopping theory. Fano, in his classic paper of 1963 [40] notes that "In plasmas or other systems, where many atoms are not in their electronic ground state, a collision may bring these atoms to a lower energy level, with a negative E_{ni}." Although Fano does not specify whether it is the projectile or target atoms to which he refers, the result is the same: An atom or molecule in an excited state can give up electronic energy to projectile kinetic energy, resulting in a larger projectile velocity following the collision than it has before, and thus resulting in a negative stopping power. We note that, in such a collision, both energy and momentum must be conserved.

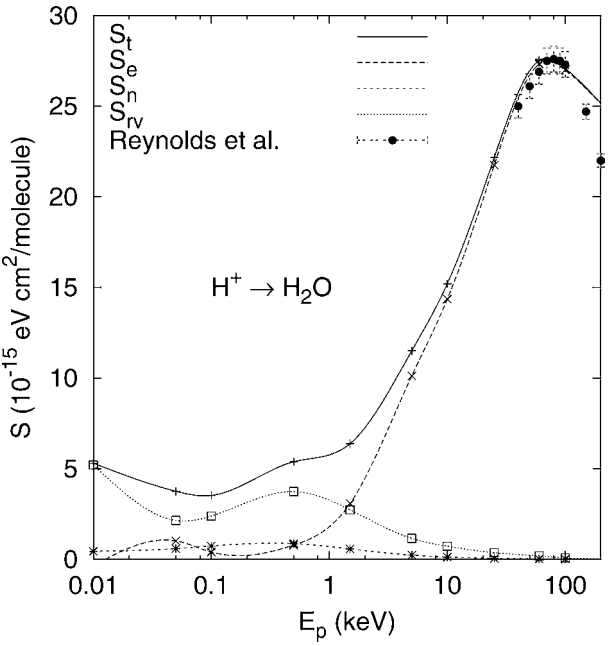

Fig. 4. Orientationally averaged total stopping cross section S_t for protons impinging on H_2O as a function of proton velocity [80] along with the experimental results of Reynolds *et al.* (filled circles) [92]. S_e, S_n, and S_{rv} represent the electronic, nuclear, and rovibrational contributions to the stopping, respectively.

Such a process is not possible in traditional stopping theory, as it requires rather special circumstances which traditional theories do not include, such as negative mean excitation energies which, since they are calculated or measured from a ground state reference, are, by necessity, positive. However, such a process is possible in collision theory based treatments, and, theoretical negative stopping powers have been reported resulting from both END [79,93] and Monte Carlo [94] type calculations. There is some skepticism in the literature that such an acceleration could occur [88], and it should be noted that negative stopping has never been experimentally observed. The process has, however, much in common with superelastic scattering of electrons, which has been observed [95] and with certain studies involving collisions with highly charged ions.

4.7. Orientation

Present day interest in surface physics has led to the fabrication of many new systems which consist of oriented overlayers on surfaces, which lend themselves to being probed by various ion scattering techniques such as those performed in grazing incidence mode. As many of these systems are highly oriented, traditional theories and experiments, which are intended to describe amorphous samples, are not adequate.

There has been a formulation of Bethe stopping theory which considers oriented targets [96] that utilizes mean excitation energies restricted to a particular polarization [97], as

well as some full first Born approximation calculations [52,98] which require directionally specific generalized oscillator strength distributions. However, problems [52] with satisfaction of the Bethe sum rule [10] and computational overhead have kept the latter approach from general use.

The collision theory approach does not suffer from the same problems. Although it is also computationally intensive, it is easy treat oriented samples. As an example, we return to protons on water [80].

In this case, the molecule is fixed in a lab fixed coordinate frame with a specific orientation. The target water molecule was placed with the oxygen atom at the origin of a Cartesian laboratory frame. Orientations are specified by the relation of the dipole moment vector of water to the velocity vector of the incoming beam (along the z-axis).

There are three sets of orientations, each of which is depicted in Fig. 5:

orientation a. The molecule is lined up with the dipole moment vector either parallel or antiparallel to the z-axis. The molecule is rotated about the z-axis.

orientation b. The molecule is aligned with the dipole vector along the x-axis, and the molecule in the xz-plane. The dipole vector is then rotated about the z-axis in the xy plane.

orientation c. The molecule is aligned with the dipole vector along the x-axis and the molecule in the xy-plane. The dipole vector is then rotated about the z-axis with the dipole vector in the xy-plane.

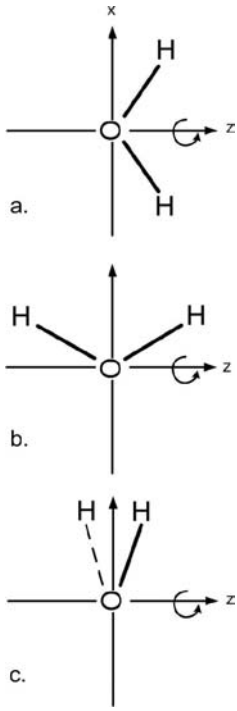

Fig. 5. Orientations of molecules used for determining the stopping power of oriented water.

The total electronic stopping cross sections for the three independent directions in which the water molecule has been oriented with respect to the beam axis are presented in Fig. 6, along with the experimental results of Reynolds *et al.* [92] for comparison.

The total stopping cross section, that which would be expected for a randomly oriented sample such as found in liquid or vapor, would be obtained as an angular average of the directional stopping curves. It should be noted that orientational effects of the same sort would be expected if the projectile beam were of polyatomic particles and such that the projectile were oriented.

The differences in stopping curves as a function of orientation are, again, most pronounced at low projectile energies, and are certainly significant, up to 50%, at the largest difference. Thus energy deposition might be developed into a probe for oriented molecules, for example, on surfaces.

4.8. Fragmentation

When dealing with molecular targets or projectiles, traditional methods of treating stopping have no facility for dealing with fragmentation of either of the collision partners. Collisions at even keV/amu projectile energies can easily lead to fragmentation, which is frequently combined with ionization and/or charge exchange. This is a stopping channel that offers several opportunities.

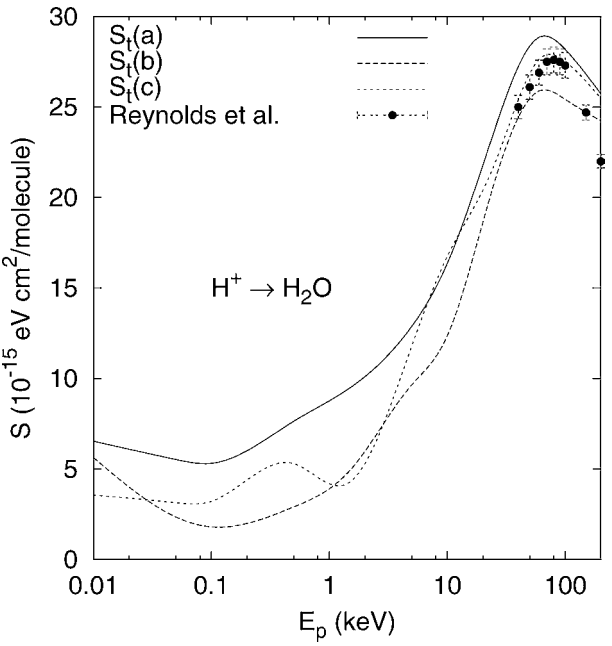

Fig. 6. Stopping cross section for protons impinging on oriented H_2O as a function of proton velocity. See Fig. 5 for the definition of target orientations.

As an example, Fig. 7 shows the fragmentation cross sections as a function of projectile energy for $H^+ \rightarrow C_2H_6$ at projectile energies below the stopping maximum [99], again from calculations using END.

It is apparent here that there are considerable differences in the cross sections for the fragmentation products: The dominant channel in this collision system is the charge exchange or electron capture channel, $H^+ \rightarrow C_2H_6 \Rightarrow (H + C_2H_6)^+$ [100], which has a cross section at $E_p = 10$ eV of approximately 46×10^{-16} cm^2. This compares to the dominant fragmentation cross section, for $H^+ \rightarrow C_2H_6 \Rightarrow (C_2H_5 + 2H)^+$, hydrogen atom abstraction combined with charge exchange, of about 11.5×10^{-16} cm^2, half an order of magnitude less. The cross section is clearly highest at low impact energy and decays at higher impact energies, with a resonance near $E_p = 2$ keV.

The only other fragmentation patterns with non-vanishing probabilities, which have cross sections again an order of magnitude lower, are presented in Fig. 7.

At 10 eV, the channel with highest cross section is $H^+ \rightarrow C_2H_6 \Rightarrow (C_2H_5 + H_2)^+$, similar to the high cross section channel $H^+ \rightarrow C_2H_6 \Rightarrow (C_2H_5 + 2H)^+$, but with a hydrogen molecule formed. The cross section for this channel quickly falls to zero at impact energies over 100 eV.

As the impact energy increases, other fragmentation channels become important, and we see the $H^+ \rightarrow C_2H_6 \Rightarrow (CH_3 + CH_3 + H)^+$, as well as the $H^+ \rightarrow C_2H_6 \Rightarrow (CH_3 + CH_2 + 2H)^+$, and $H^+ \rightarrow C_2H_6 \Rightarrow (CH_3 + C + 4H)^+$ channels appearing at impact energies of 100 eV–10 keV. These involve dissociation of the C–C bond. Channels requiring specific orientations to occur, such as $H^+ \rightarrow C_2H_6 \Rightarrow (CH_3 + CH_4)^+$, have very small cross sections over the entire energy range, but might be accessible in a well-designed experiment. This is presumably because such reactions are highly sensitive to the orientational relations of the collision partners, as well as to the energetics of the process. As the total energy and momentum of the system must be conserved in any collision process, it is

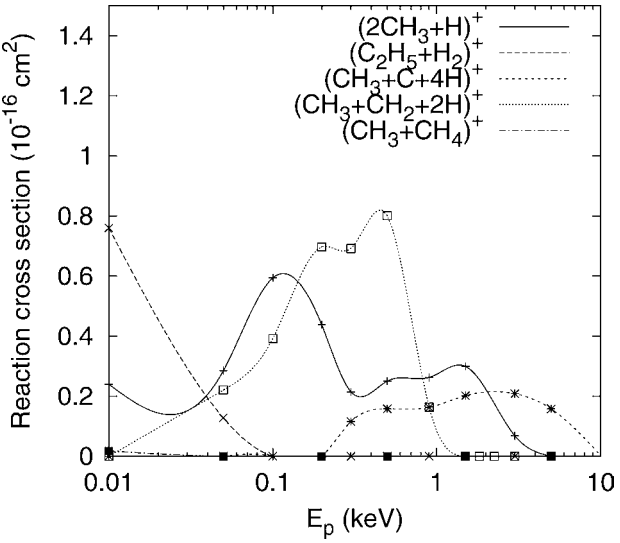

Fig. 7. Energy dependence of the cross sections for several channels observed in the $H^+ \rightarrow C_2H_6$ collision.

more difficult to form new chemical bonds in the process than to fragment a projectile or target and carry excess energy away as fragment kinetic energy.

Many of the fragmentation cross section curves shown in Fig. 7 show some structure. The structure is attributed to a complicated interplay of target orientation, charge exchange and energetic resonance with the chemical bonds. We have not been able to deconvolute these contributions.

4.9. Relativistic considerations

Effects of relativity enter stopping theory at a variety of levels. For the projectile, in the simplest case the relativistic correction to the Bethe L_0 given in equation (5) is included. In addition, the density correction can be added. For close collisions at extreme relativistic velocities, that is, when the projectile kinetic energy is comparable to its rest mass, other corrections such as radiative, kinematic (Mott [101,102]), bremsstrahlung, pair production, nuclear structure and other effects must be introduced. Ahlen [43], and more recently Lindhard and Sørensen [103] have reviewed stopping for relativistic projectiles quite nicely.

However, little has been done with the other aspect of relativity in stopping, namely stopping by heavy atoms that require a relativistic description for their electronic structure. Even if one restricts to slow projectiles and the first few terms in the Born series, then for atoms (or molecules or solids containing atoms) with $Z_2 \gtrapprox 10$, a relativistic description of the target should be used. Considering the well-known shifts of energy levels in heavy atoms [104], one would expect considerable changes from a non-relativistic treatment in the energy level structure and oscillator strength distribution, leading to significant modification of the appropriate mean excitation energies for stopping. Although there are several excellent treatments of the effects of relativity on atomic sum rules (*cf. e.g.* Refs. [105] and [106]), there are few calculations of stopping powers for targets that use relativistic wave functions.

5. SUGGESTIONS

So, where do we go from here? In the foregoing we have discussed several different aspects of stopping theory that are interesting, at least to these authors, and which are yet to be fully investigated. The common thread running through the discussion is that all of these effects are small in magnitude with respect to the total stopping power. Thus we need to measure small changes in large numbers. We set this as a challenge to experimentalists. Can an experiment be designed that can measure all of the following simultaneously:

- Projectile center of mass kinetic energy to $<0.5\%$ over a wide projectile velocity range.
- Projectile and target charge state.
- Projectile and target electronic state.
- Projectile fragmentation patterns.

When such experiments can be made, then there will be impetus to drive theory forward to determine and interpret the quantities discussed above.

It should also be noted that apparently there is no golden method that can be used on all of the various problems discussed here. Although the scattering theoretical methods

are esthetically pleasing, as they do not require the use of several unrelated assumptions, they typically are difficult to apply to solid targets and do not deal well with relativistic problems. A notable exception to the former problem is the method of Arista [107,108]. Similarly, the perturbation methods and those that are based on Bohr theory require use of assumptions regarding calculation of mean excitation energies from schemes not necessarily related to the stopping scheme, projectile charge states [62], as well as other unrelated assumptions and corrections.

ACKNOWLEDGEMENTS

Thanks to Patrick Bourque for help and entertainment on flight 51. This work has been supported in part by an IBM SUR grant to the Quantum Theory Project. This support is gratefully acknowledged.

REFERENCES

[1] E. Rutherford, *Philos. Mag.* **21** (1911) 907.
[2] C.G. Darwin, *Philos. Mag.* **23** (1912) 907.
[3] J.J. Thomson, *Philos. Mag. (6)* **23** (1912) 449.
[4] R. Whiddington, *Proc. Roy. Soc. London* **86** (1912) 360.
[5] N. Bohr, *Philos. Mag.* **25** (1913) 10.
[6] N. Bohr, *Philos. Mag.* **30** (1915) 581.
[7] N. Bohr, *Kgl. Dan. Vidensk. Selsk.: Mat.-Fys. Medd.* **18** (8) (1948).
[8] E. Bonderup, *Penetration of Charged Particles through Matter*, second ed., Fysisk Instituts Trykkeri, Aarhus Universitet, Aarhus, Denmark, 1981.
[9] J.F. Ziegler, J.P. Biersack, U. Littmark, *The Stopping and Range of Ions in Solids*, *The Stopping and Ranges of Ions in Matter*, vol. 1, Pergamon, New York, 1985.
[10] H. Bethe, *Ann. Phys. (Leipzig)* **5** (1930) 325.
[11] H. Bethe, *Z. Physik* **76** (1932) 293.
[12] J. Lindhard, M. Scharff, *Kgl. Dan. Vidensk. Selsk.: Mat.-Fys. Medd.* **27** (15) (1953).
[13] J. Lindhard, *Kgl. Dan. Vidensk. Selsk.: Mat.-Fys. Medd.* **28** (8) (1954).
[14] J. Lindhard, M. Scharff, *Phys. Rev.* **124** (1961) 128.
[15] J. Lindhard, M. Scharff, H.E. Schiøtt, *Kgl. Dan. Vidensk. Selsk.: Mat.-Fys. Medd.* **33** (14) (1963).
[16] J.J. Dorado, O.H. Crawford, F. Flores, *Nucl. Instrum. Meth. B* **93** (1994) 175.
[17] M.J. Berger, S.M. Seltzer, Technical report, U.S. Department of Commerce, National Bureau of Standards (unpublished), publication NBSIR 82-2550-A, 1983.
[18] M.J. Berger, Report Committee Chair, Technical report, International Commission on Radiation and Radiation Measurements (unpublished), ICRU Report No. 49 (1992).
[19] J.F. Janni, *At. Data Nucl. Data Tables* **27** (1982) 147.
[20] H.H. Andersen, J.F. Ziegler, *Hydrogen Stopping Powers and Ranges in All Elements*, *The Stopping and Ranges of Ions in Matter*, vol. 3, Pergamon, New York, 1977.
[21] J.F. Ziegler, *Helium Stopping Powers and Ranges in All Elements*, *The Stopping and Ranges of Ions in Matter*, vol. 4, Pergamon, New York, 1977.
[22] H. Paul, A. Schinner, *At. Data Nucl. Data Tables* **85** (2003) 377.
[23] M. Inokuti, *Int. J. Quantum Chem.* **57** (1996) 173.
[24] S.B. Trickey, J.Z. Wu, J.R. Sabin, *Nucl. Instrum. and Meth. B* **93** (1994) 186; for an opposite viewpoint, see [25].
[25] P. Sigmund, *Nucl. Instrum. and Meth. B* **95** (1995) 477.
[26] S. Trickey, J. Sabin, *Nucl. Instrum. and Meth. B* **95** (1995) 480.

[27] One needs to be careful about making assertions such as this. One is reminded of the statement made by Michelson in 1894: “An eminent physicist has remarked that the future truths of Physical Science are to be looked for in the sixth place of decimals.” Univ. of Chicago Quarterly Calendar, Aug., 1894. The eminent physicist is commonly thought to be Lord Kelvin.
[28] W.H. Barkas, J.N. Dyer, H.H. Heckman, *Phys. Rev. Lett.* **11** (1963) 26.
[29] W.H. Bragg, R. Kleeman, *Philos. Mag.* **10** (1918) 305.
[30] D.I. Thwaites, *Rad. Res.* **95** (1983) 495.
[31] J. Oddershede, J.R. Sabin, *Nucl. Instrum. Meth. B* **42** (1989) 7.
[32] D.I. Thwaites, *Nucl. Instrum. Meth. B* **12** (1985) 84.
[33] J.A. Nobel, J.R. Sabin, S.B. Trickey, *Int. J. Quantum Chem. S* **28** (1994) 283.
[34] H.A. Bethe, *Intermediate Quantum Mechanics*, Benjamin, New York, 1964.
[35] P. Sigmund, *Stopping of Heavy Ions, A Theoretical Approach*, Springer, Karlsruhe, 2004.
[36] M.S. Livingston, H.A. Bethe, *Rev. Mod. Phys.* **9** (1937) 245.
[37] H.A. Bethe, J. Ashkin, in: E. Segre (Ed.), *Experimental Nuclear Physics*, Wiley, New York, 1953.
[38] M. Gryzinski, *Phys. Rev.* **138** (1965) A322.
[39] R. Cabrera-Trujillo, S. Cruz, J. Oddershede, J. Sabin, *Phys. Rev. A* **55** (1997) 2864.
[40] U. Fano, *Ann. Rev. Nucl. Sci.* **13** (1963) 1.
[41] M. Inokuti, *Rev. Mod. Phys.* **43** (1971) 297.
[42] M. Inokuti, Y. Itakawa, J.E. Turner, *Rev. Mod. Phys.* **50** (1978) 23.
[43] S.P. Ahlen, *Rev. Mod. Phys.* **52** (1980) 121.
[44] J.E. Turner, *Health Phys.* **86** (2004) 228.
[45] V.V. Balashov, *Interaction of Particles and Radiation with Matter*, Springer, Berlin, 1997, translated by G. Pontecorvo.
[46] R.M. Sternheimer, *Phys. Rev.* **88** (1952) 851.
[47] R.M. Sternheimer, M.J. Berger, S.M. Seltzer, *At. Data Nucl. Data Tables* **30** (1984) 261.
[48] J. Oddershede, J.R. Sabin, *At. Data Nucl. Data Tables* **31** (1984) 275.
[49] J. Oddershede, J.R. Sabin, *Phys. Rev. A* **39** (1989) 5565.
[50] J.R. Sabin, J. Oddershede, *Nucl. Instrum. Meth. B* **44** (1990) 253.
[51] E. Bonderup, *Kgl. Dan. Vidensk. Selsk.: Mat.-Fys. Medd.* **35** (17) (1967).
[52] R. Cabrera-Trujillo, J.R. Sabin, J. Oddershede, S.P.A. Sauer, *Adv. Quantum Chem.* **35** (1999) 175.
[53] R. Cabrera-Trujillo, J.R. Sabin, J. Oddershede, *Adv. Quantum Chem.* **46** (2004) 121.
[54] J. Lindhard, A. Winther, *Kgl. Dan. Vidensk. Selsk.: Mat.-Fys. Medd.* **34** (4) (1964).
[55] P.L. Grande, G. Schiwietz, *Phys. Rev. A* **58** (1998) 3796.
[56] G. Schiwietz, P.L. Grande, *Nucl. Instrum. Meth. B* **153** (1999) 1.
[57] N.R. Arista, A.F. Lifschitz, *Phys. Rev. A* **59** (1999) 2719.
[58] R. Cabrera-Trujillo, Y. Öhrn, E. Deumens, J.R. Sabin, *J. Chem. Phys.* **116** (2002) 2783.
[59] R. Cabrera-Trujillo, J.R. Sabin, E. Deumens, Y. Öhrn, *Adv. Quantum Chem.* **45** (2004) 99.
[60] R. Cabrera-Trujillo, J.R. Sabin, E. Deumens, Y. Öhrn, *Adv. Quantum Chem.* **47** (2004) 253.
[61] P. Sigmund, L. Glazov, *Nucl. Instrum. Meth. B* **136–138** (1998) 47.
[62] P. Sigmund, *Adv. Quantum Chem.* **48** (2005), in press.
[63] For a caveat concerning the extrapolation to zero of the continuous quantity *thickness* in a system made up of atoms, see S.B. Trickey, J.Z. Wu, J.R. Sabin, *Nucl. Instrum. Meth. B* **93** (1994) 186.
[64] H.H. Andersen, A.F. Garfinkel, C.C. Hanke, H. Sørensen, *Kgl. Dan. Vidensk. Selsk.: Mat.-Fys. Medd.* **35** (4) (1966).
[65] H.H. Andersen, C.C. Hanke, H. Sørensen, P. Vajda, *Phys. Rev.* **153** (1966) 338.
[66] H.H. Andersen, *Studies of Atomic Collisions in Solids by means of Calorimetric Techniques*, Aarhus Univ. Press, Aarhus, Denmark, 1974, doctor’s thesis.
[67] P. Sigmund, A. Schinner, *Nucl. Instrum. Meth. B* **195** (2002) 64.
[68] H.H. Andersen, *et al.*, *Nucl. Instrum. Meth.* **140** (1977) 537.
[69] J.D. Jackson, R.L. McCarthy, *Phys. Rev. B* **6** (1972) 4131.
[70] J.C. Ashley, R.H. Ritchie, W. Brandt, *Phys. Rev. B* **5** (1972) 2393.
[71] J.C. Ashley, R.H. Ritchie, W. Brandt, *Phys. Rev. A* **8** (1973) 2402.
[72] J.C. Ashley, R.H. Ritchie, W. Brandt, *Phys. Rev. A* **10** (1974) 737.
[73] K.W. Hill, E. Merzbacher, *Phys. Rev. A* **9** (1974) 156.
[74] J. Lindhard, *Nucl. Instrum. Meth.* **132** (1976) 1.
[75] N.R. Arista, P.L. Grande, A.F. Lifschitz, *Phys. Rev. A* **70** (2004) 042902.

[76] H.H. Mikkelsen, P. Sigmund, *Phys. Rev. A* **40** (1989) 101.
[77] F. Bloch, *Ann. Phys. (Leipzig)* **16** (1933) 285.
[78] S.P. Ahlen, *Phys. Rev. A* **17** (1978) 1236.
[79] A.C. Diz, Y. Öhrn, J.R. Sabin, *Nucl. Instrum. Meth. B* **96** (1995) 633.
[80] R. Cabrera-Trujillo, J.R. Sabin, E. Deumens, Y. Öhrn, *Adv. Quantum Chem.* **48** (2005), in press.
[81] M.E. Rudd, Y.K. Kim, D.H. Madison, S.T. Manson, *Rev. Mod. Phys.* **64** (1992) 441.
[82] R. Cabrera-Trujillo, J.R. Sabin, E. Deumens, Y. Öhrn, *Phys. Rev. A* **66** (2002) 022706 (7 pages).
[83] A.J. Feicert, R.J. Blint, G.T. Surratt, W.D. Watson, *Astrophys. J.* **286** (1984) 371.
[84] M.S. Huq, C.C. Havener, R.A. Phaneuf, *Phys. Rev. A* **40** (1989) 1811.
[85] D.H. Crandall, R.A. Phaneuf, F.W. Meyer, *Phys. Rev. A* **19** (1979) 504.
[86] W. Seim, A. Müller, I. Wirkner-Bott, E. Salzborn, *Phys. Rev. A* **14** (1981) 3475.
[87] L. Folkerts, *et al.*, *Phys. Rev. A* **51** (1995) 3685.
[88] P. Sigmund, A. Schinner, *Eur. Phys. J. D* **23** (2003) 201.
[89] L.C. Northcliffe, *Phys. Rev.* **120** (1960) 1744.
[90] L.C. Northcliffe, *Ann. Rev. Nucl. Sci.* **13** (1963) 67.
[91] W. Brandt, M. Kitagawa, *Phys. Rev. B* **25** (1982) 5631.
[92] H.K. Reynolds, D.N. Dunbar, W.A. Wenzel, W. Whaling, *Phys. Rev.* **92** (1953) 742.
[93] R. Cabrera-Trujillo, J.R. Sabin, Y. Öhrn, E. Deumens, *Int. J. Quantum Chem.* **94** (2003) 215.
[94] F. Grüner, F. Bell, W. Assmann, M. Schubert, *Phys. Rev. Lett.* **93** (2004) 213201.
[95] P.A. Z'avodszky, *et al.*, *Phys. Rev. Lett.* **87** (2001) 033202 (4 pages).
[96] H.H. Mikkelsen, J. Oddershede, J.R. Sabin, E. Bonderup, *Nucl. Instrum. Meth. B* **100** (1995) 451.
[97] S.P.A. Sauer, J.R. Sabin, J. Oddershede, *Nucl. Instrum. Meth. B* **100** (1995) 458.
[98] E.H. Mortensen, J. Oddershede, J.R. Sabin, *Nucl. Instrum. Meth. B* **69** (1992) 24.
[99] R. Cabrera-Trujillo, J.R. Sabin, E. E. Deumens, Y. Öhrn, *Phys. Rev. A* **71** (2005) 044702 (4 pages).
[100] R. Cabrera-Trujillo, J.R. Sabin, Y. Öhrn, E. Deumens, *J. Elect. Spectrosc.* **129** (2003) 303.
[101] N.F. Mott, *Proc. Roy. Soc. London* **124** (1929) 426.
[102] N.F. Mott, *Proc. Roy. Soc. London* **135** (1932) 429.
[103] J. Lindhard, A.H. Sørensen, *Phys. Rev. A* **53** (1996) 2443.
[104] B. Cresemann (Ed.), *Atomic Inner-Shell Physics, Physics of Atoms and Molecules*, Plenum, New York, 1985.
[105] S.M. Cohen, P.T. Leung, *Phys. Rev. A* **57** (1998) 4994.
[106] S.M. Cohen, *Adv. Quantum Chem.* **46** (2005) 241.
[107] N.R. Arista, *Nucl. Instrum. Meth. B* **195** (2002) 91.
[108] N.R. Arista, A.F. Lifschitz, *Adv. Quantum Chem.* **45** (2004) 47.

This page intentionally left blank

Subject Index

T

This page intentionally left blank